UNIVERSITY OF NAIROBI

BIOGEOCHEMICAL PROXIES OF ENVIRONMENTAL AND CLIMATE CHANGE ON MOUNT KENYA

by

Christine Atieno Omuombo

I80/90241/2013

A Thesis Submitted for Examination in Fulfilment of the Requirements for Award of the Degree of Doctor of Philosophy in Geology of the University of Nairobi.

2020

DECLARATION

a) I understand what Plagiarism is and I am aware of the University's policy in this regard.
b) I declare that this Thesis is my original work and has not been submitted elsewhere for examination, award of a degree or publication. Where other people's work, or my own work has been used, this has properly been acknowledged and referenced in accordance with the University of Nairobi's requirements.
c) I have not sought or used the services of any professional agencies to produce this work.
d) I have not allowed, and shall not allow anyone to copy my work with the intention of passing it off as his/her own work.
e) I understand that any false claim in respect of this work shall result in disciplinary action, in accordance with University Plagiarism Policy.

Signature ..... **Date** .....

Christine Omuombo
I80/90241/2013
Department of Geology
University of Nairobi

This thesis is submitted for examination with our approval as research supervisors:

	Signature	**Date**
Prof. Daniel Olago, Department of Geology, University of Nairobi, P.O Box 30197 – 00100, Nairobi, Kenya dolago@uonbi.ac.ke	.....	.....
Prof. David Williamson Représentant de l'IRD en Afrique de l'Est IRD c/o ICRAF United Nations avenue, P.O. Box 30677-00100 Nairobi Kenya david.williamson@ird.fr	.....	.....

ACKNOWLEDGEMENTS

It is with a sigh of relief that I have finally reached the end, navigating through this chapter of my life over the last couple of years has taken a village to see me through, it is therefore only proper to accord them my gratitude. The biggest thank you is to my project supervisors Prof. Daniel Olago (University of Nairobi) and Prof. David Williamson (IRD). I am indebted to you for all the support throughout my research, for the long drives to Mt. Kenya where we discussed anything and everything, the support and guidance provided throughout the field campaigns, for all the meetings we have had and for all the opportunities you have given me. It was a privilege to be your Ph.D. student.

A special thanks must also go to Prof. Bruno Turcq (IRD - Bondy) for the warm welcome to his lab, lovely lunches and Portuguese conversations. The support provided by your team at the ALYSES lab in Bondy made my laboratory work straightforward.

To Dr. Arnaud Huguet (UPMC - METIS) who welcomed and trained me in his laboratory on the techniques of lipid biomarker extraction and analyses, thank you for invaluable help and forcing me to take lunch breaks and early evening breaks from the lab. I think I could have lived in the laboratory were it not for the strict protocols.

To Dr. Pierre-Etienne Mathé (CEREGE), your hospitality during my visits and support provided during the magnetic susceptibility studies at your lab was invaluable. To Dr. Sylvie Derenne and Dr. Anne-Marie Lézine who ensured that I was assigned the support staff necessary for the completion of this work. To Patricia Turcq, Sandrine Caquineau, Magloire Mandeng-Yogo, Hugues Boucher, Florence Le Cornec, Fethiye Cetin and Thierry Pilorge and Mercedes Mendez who provided technical assistance during the lab work at the ALYSES platform facility at the Institut de Recherche pour le Développement (IRD) in Bondy. To Christelle Anquetil and Sarah Coffinet for their assistance during lab work at the METIS lab in UPMC; you made sure that I was not lost in a new lab. To Francois Demory, your training and assistance during the magnetic susceptibility analysis at CEREGE was invaluable.

My field assistants Marcel Hale and Stephen Warui had it not been for your support to carry the field equipment to the various sites, I do not know how all this would have been possible. To fellow Ph.D. students at UPMC/IRD - Nicolas Duprey, Luciane Moreira, Douglas Lessa, Keila Aniceto and Gabriel Martins, you kept me smiling and discussed with enthusiasm our stay in Paris over dinner and drinks, you were my family away from Home. To Dr. Lydia Olaka your constant encouragement, support and advice kept me going. To Brenda and Patricia thank you for taking time to read gibberish and make sense of my thesis through your proofreading.

Much of this work would have not been possible without the financial support received through L'Agence Inter-établissements de Recherche pour le Developpement (AIRD) and Campus France through the French Embassy in Nairobi. A special thank you to Mme. Felicite Metonou, Sandrine Lerosier, Smahane Hadouche, Sarah-Ayito Nguema and Severine Fogel-Verton who handled my docket at these organizations at various times.

To my husband, daughter and nanny your patience and support especially when I had to work late in the night probably not understanding what it is I am actually doing has been invaluable. I am looking forward to the next chapter and what it holds.

ABSTRACT

The three crater lakes from Mount Kenya (Nkunga, Sacred and Rutundu) were studied to infer Late Holocene climate and environmental changes. These crater lakes are small closed lake basins with well-defined catchments that are sensitive to seasonal, inter-annual and long-term fluctuations. Consequently, they are promising archives for high-resolution reconstruction of climate and environmental change in Kenya. Already published sedimentary records on the palaeoclimatic and palaeoenvironmental history of east Africa show that the region exhibits variability at various timescales, but matching them across space and time has been problematic either because the records were of low resolution or because the chronology has been too coarse. Consequently, the aim of this study was to elucidate the Late Holocene history of climate and environmental changes on Mount Kenya using multi-proxy palaeo-indicators in soil and lake sediments. By using a multi-proxy suite of indicators, coupled with a good chronology based on radiocarbon dating, it was possible to capture a diverse array of climatic and environmental changes that may not be apparent from one or a limited number of the traditionally used indicators, such as pollen. The multi-proxy analysis that was carried out on the Mount Kenya soils and lake sediments comprised traditional sedimentological (XRD, XRF and X_{lf}) and relatively novel organic geochemical analyses (%C, %N, $\delta^{13}C$, $\delta^{15}N$, n-alkanes and GDGT). The occurrence and timing of different events were established by AMS ^{14}C dating of the cores. From these, it was possible to tease out a high-resolution record that reflects both local and regional changes, thus capturing also the spatial heterogeneity that has been observed in the different east African lake records. The results from our crater lakes cover the last 4770 cal yr. BP to present. There are significant changes in lake ecosystems and hydrology that have occurred during the Late Holocene, which are coincident with large sediment and organic matter influx to the lakes. At the millennial scale, a wet early Holocene followed by a drier mid to late Holocene is observed. The Holocene is punctuated by major dry spells separated by abrupt transitions to wet periods. During the Late Holocene two key dry spells at ca. 4200 and 2800 cal yr. BP occur in the shallow lake phases at lakes Rutundu and Sacred. There is also evidence that describes a wet early Little Ice Age (at Lakes Nkunga and Sacred) followed by drier conditions during the late phase of the Little Ice Age (Lake Nkunga). The multiproxy approach has therefore also allowed the identification of local catchment-scale effects on the individual lakes in addition to the observed regional climate effects, reflecting their sensitivity to climate perturbations and related localised environmental responses.

Keywords: Late Holocene, Mount Kenya, Little Ice Age, Paleo-indicators

TABLE OF CONTENTS

DECLARATION ..... **i**
ACKNOWLEDGEMENTS ..... **ii**
ABSTRACT ..... **iii**
TABLE OF CONTENTS ..... **vi**
LIST OF FIGURES ..... **viii**
LIST OF TABLES ..... **xii**
LIST OF ABBREVIATIONS ..... **xiii**
1 INTRODUCTION **14**
1.1 INTRODUCTION 14
1.2 STATEMENT OF THE PROBLEM AND THESIS RATIONALE 15
1.3 OBJECTIVES 17
1.4 JUSTIFICATION AND SIGNIFICANCE OF THE STUDY 17
1.5 LIMITATIONS OF THE STUDY 18
1.6 LAYOUT OF THE THESIS 19
2 STUDY SITE DESCRIPTIONS AND LITERATURE REVIEW **20**
2.1 INTRODUCTION 20
2.2 GENERAL CONTEXT OF THE STUDY AREA 20
2.2.1 Geologic Setting of Mount Kenya **20**
2.2.2 Topography and Characteristics of the Study Lakes **22**
2.2.3 Modern Day Climate and Vegetation of the Study Area **27**
2.2.4 Soils of the Mt. Kenya Area **33**
2.3 THE UTILITY OF MULTIPROXY DATASETS IN PALAEOENVIRONMENTAL RECONSTRUCTION 35
2.3.1 Crater Lakes and Lake Sedimentary Records in Mt. Kenya **35**
2.3.2 Holocene Multiproxy Datasets from the Crater Lakes of Mt. Kenya **36**
2.3.3 Overview of the Late Quaternary in East Africa from Multiproxy Records **38**
2.4 HUMAN IMPACT ON ECOSYSTEMS DURING THE LATE HOLOCENE IN EAST AFRICA .. 44
3 METHODOLOGY **47**
3.1 METHODOLOGY 47
3.1.1 Soil Sample Collection (Surface and Subsurface Samples) **47**
3.1.2 Lake Sediment Sample Collection **48**
3.1.3 Physical Parameters **50**
3.1.4 Grain Size Analysis of Soil Samples **50**
3.1.5 Radiocarbon Chronology **51**
3.1.6 Mineral Magnetic Measurements **51**
3.1.7 X-Ray Fluorescence (XRF) Analyses **56**
3.1.8 X-Ray Diffraction (XRD) Analyses **56**
3.1.9 Elemental Carbon and Nitrogen and Stable Isotopes Analysis **58**
3.1.10 Lipid Biomarker Analyses **59**
3.1.11 Data Processing and Analyses **72**
4 RESULTS AND DISCUSSION **73**
4.1 INTRODUCTION 73
4.2 THE SOILS IN THE STUDY AREA 73
4.2.1 Characteristics of the Soils and Rocks from Nkunga Area **74**
4.2.2 Characteristics of the Soils from Sacred Lake Area **88**
4.2.3 Characteristics of Soils from the Transect **97**
4.2.4 Synthesis of the Characteristics of the Surface and Subsurface Soils **112**
4.3 LAKE NKUNGA SEDIMENTS 117

4.3.1 Bulk Sediment Parameters **117**
4.3.2 Inorganic Geochemistry of Lake Nkunga **125**
4.3.3 Organic Geochemistry and Stable Isotopes **128**
4.3.4 Synthesis of Lake Nkunga Proxy data **135**
4.4 SACRED LAKE SEDIMENTS 142
4.4.1 Bulk Sediment Parameters **142**
4.4.2 Inorganic Geochemistry of Sacred Lake **149**
4.4.3 Organic Geochemistry **151**
4.4.4 Synthesis of Sacred Lake Proxies **158**
4.5 LAKE RUTUNDU SEDIMENTS 165
4.5.1 Bulk Sediment Parameters **165**
4.5.2 Inorganic Geochemistry of Lake Rutundu **169**
4.5.3 Organic Geochemistry of Lake Rutundu **172**
4.5.4 Synthesis of Lake Rutundu Proxies **178**
4.6 DISCUSSION 182
4.6.1 Late Holocene Signal Coherency among the Mt. Kenya lakes 182
4.6.2 The Period 4470 – 3280 cal yr. BP (LR1, LR2, SLK1, SLK2) 184
4.6.3 The Period 3280 - 2500 cal yr. BP (LR3, LR4) 185
4.6.4 The Period 2500 – 2000 cal yr. BP (LR4) 187
The Period 2000 cal yr. BP to Present (LR4, SLK3, SLK4, LNK1, LNK2, LNK3, LNK4) 189
5 CONCLUSIONS AND RECOMMENDATIONS 194
5.1 CONCLUSIONS 194
5.2 RECOMMENDATIONS 196
6 REFERENCES 198
7 APPENDIX 212

LIST OF FIGURES

Figure 1-1: Mechanisms and modes of studying environmental changes over different timescales (redrawn and modified from Roberts 1998). Palaeoenvironmental reconstruction is reliable over the long-term to discern patterns of environmental changes especially where documentary records are not available. The reliability of the documentary records has improved from Mid to Late Holocene whereas present day environmental changes are in most instances observed and/or simulated to provide comprehensive information on the environmental change witnessed. 15
Figure 2-1: A generalized geological map showing the distribution of the Mount Kenya suite (modified after Olago et al. 2000). 22
Figure 2-2: Map displaying the location of the study area in the African continent and in Central Kenya. The lakes that dot the north eastern slopes of the mountain where the current study was carried out at Lakes Nkunga, Sacred and Rutundu. 23
Figure 2-3: Generalized map of the physiographic and drainage features present in the study area. The several rivers and their tributaries present display a radial pattern from the summit of the mountain to the foothills. 24
Figure 2-4: Profile along the north eastern slopes of Mount Kenya showing the selected sampling transect from the hill slope at Lake Nkunga to Sacred Lake to Lake Rutundu. 25
Figure 2-5: Overview of Lake Nkunga (a) generalized view of Lake Nkunga showing the crater wall surrounding the shallow lake at the edge of the montane forest (b) shows the open water area on the lake and (c) presence of reed swamp and floating mats that restrict access to the centre of the lake. 26
Figure 2-6: Overview of Sacred Lake (a) generalized view of Sacred Lake showing the crater wall and the surrounding montane forest (b) field acquisition of sediment core at Sacred Lake (c) shows the coring platform and the piston corer used for the acquisition of the sediment core placed on the floating mats present in the lake 26
Figure 2-7: (a) An overview of Lake Rutundu occupying one of side vents of Mount Kenya (b) provides a generalized vegetation representation of the bushed grassland of the ericaceous zone where Lake Rutundu is found while (c) and (d) are close up pictures of the vegetation encountered in the grasslands. (c) Tussock grass and scattered off-shoot rosettes of Lobelia telekii (d) Representative dense thickets of the ericaceous belt comprising of, among other vegetation, Philippa, Anthospermum and Alchemilla spp. 27
Figure 2-8: Total annual rainfall distribution in the Mount Kenya area. The north eastern region where this study was carried out. Annual rainfall ranges between 1000-1500 mm (Plotted data obtained from WRI 2007) 29
Figure 2-9: The vegetation distribution within the Kenyan highlands (Plotted data obtained from WRI 2007).. 32
Figure 2-10: Generalized soil map of the study area (Data derived from SOFTWIS database 34
Figure 3-1: Samples collected during fieldwork in 2011 and 2013 on the north-eastern slopes of Mount Kenya (red dots). 48
Figure 3-2: Sediment cores from Lake Nkunga comprising two short sediment cores NKG-I-1-2013 an NKG-I-2-2013 each approximately 45 cm. One half of the sample was subsampled every 1 cm for sample preparation and analysis while XRF scanning was carried out on the other half of the core. 49
Figure 3-3: Six short cores of different sizes obtained from Sacred Lake that was analysed during this study. Total length is approximately 65 cm. Similarly, as carried out in the Lake Nkunga core, one half of the sample was subsampled every 1 cm for sample preparation and analysis while XRF scanning was carried out on the other half of the core. 49
Figure 3-4: (a) The MFK1-FA Kappabridge multifunctional susceptibility meter used for frequency dependent magnetic susceptibility and the field dependent magnetic susceptibility measurements (b) The cryogenic magnetometer used to measure the remanent magnetisation. 52
Figure 3-5: Structure of iGDGT and brGDGT adapted from (Tierney 2012) as discussed in this work. The iGDGT (predominantly archaeal origin) nomenclature is derived from the presence of the cyclopentane (zero to two) moieties present in the basic structure assigned as GDGT-x where x denoted the number of cyclopentane moieties present in the alkyl backbone structure. The structure of the brGDGT displays the presence of the cyclopentane moieties (identified as opposite those of iGDGTs through nuclear magnetic resonance (NMR) and stereochemistry studies) and a basic structure containing methyl (four to six) branches usually a 13,16-dimethyloctacosane typical of a bacterial membrane lipid. IS represents the C_{46} synthesized internal standard 62
Figure 3-6: Illustration of dionex cell as prepared for extraction 66
Figure 3-7: Rotary evaporator set up used for drying extracted lipids at near vacuum conditions 66
Figure 3-8: A diagrammatic representation of the processes involved in the extraction, concentration, separation and analysis of the biomarker fractions from the selected samples 67

Figure 4-1: (a) the less than 200 μm grain size distribution and (b) and (c) the bulk mineralogy based on the percentage of diffracted surface of the soil and rock samples from the Nkunga crater. NB: Feld – plag denotes plagioclase feldspar while illite/Muscov denotes the total peak area occupied by Illite and Muscovite which could not be differentiated in the XRD spectrum of the bulk samples. 75
Figure 4-2: (a) Particle size distribution of the <200 μm soils from farms at Nkunga School (b) the bulk mineralogy from the percentage of the diffracted surface in samples from Nkunga. NB: Feld-plag denotes plagioclase feldspar composition in the samples. 76
Figure 4-3: PCA of the elements from Nkunga area surface soils. Green bars represent the positive correlations while red represents negative correlations. The upper and lower panels show PC1 and PC2 respectively. 77
Figure 4-4: PCA of geochemical ratios from the soils in Nkunga area. Green bars represent the positive correlations while red represents negative correlations. The upper and lower panels show PC1 and PC2 respectively 78
Figure 4-5: Description of soil profile sampled from Nkunga park gate showing the two identified horizons ... 79
Figure 4-6: (a) Grain size distribution of <200 μm fraction and (b) bulk mineralogy of the soil profile at Nkunga. NB: Feld-plag denotes plagioclase feldspar composition in the samples 80
Figure 4-7: The relationship between the high and low frequency bulk magnetic susceptibility for selected samples from soil profile at Nkunga park gate. 81
Figure 4-8: Bulk magnetic characteristics % X_{fd} and X_{lf} from the soil samples in the Nkunga area soil profile. 82
Figure 4-9: NRM profiles of the soils from Nkunga area. 82
Figure 4-10: Single element inorganic geochemistry down the Nkunga soil profile 83
Figure 4-11: Ti-normalized elemental variations down the Nkunga soil profile 84
Figure 4-12: Variations down the soil profile from Lake Nkunga of the % C, % N, C/N, $\delta^{13}C$ and $\delta^{15}N$ isotopes. 85
Figure 4-13: n-alkane distribution in the Lake Nkunga soil profile. 86
Figure 4-14: GDGT distribution in the various soil samples from the soil profile at Lake Nkunga area. 87
Figure 4-15: Sacred Lake soil profile showing the identified horizons. 88
Figure 4-16: (a) Grain size distribution of the <200 μm fraction and (b) bulk mineralogy of the soil profile at Sacred Lake. NB: Feld-plag denotes plagioclase feldspar composition in the samples. 89
Figure 4-17: The relationship between the high and low frequency bulk magnetic susceptibility for selected samples from the soil profile at Lake Nkunga park gate. 90
Figure 4-18: The relationship between the high and low frequency bulk magnetic susceptibility for selected samples from soil profile at Sacred Lake. 91
Figure 4-19: NRM profiles of the Sacred Lake soil profile. 92
Figure 4-20: Elemental geochemical profile from Sacred Lake soil profile. 92
Figure 4-21: Normalized elemental variations down the Sacred Lake soil profile 93
Figure 4-22: Variations down the soil profile from Sacred Lake of %C and %N, C/N, $\delta^{13}C$ and $\delta^{15}N$ 94
Figure 4-23: n-alkane distribution on from the Sacred Lake soil profile. 95
Figure 4-24: GDGT distribution in the various soil samples from the soil profile at Sacred Lake area. 97
Figure 4-25: Bulk mineralogy of soils along the Nkunga-Sacred Lake- Rutundu transect 98
Figure 4-26: The high and low frequency bulk magnetic susceptibility for samples collected along the soil transect. 98
Figure 4-27: The susceptibility characteristics dependence(%X_{fd}) and low magnetic susceptibility (X_{lf}). The first panel **(a)** shows the altitudinal variation in %X_{fd}, red represents low altitude & medium %X_{fd}, samples, blue represents mid altitude and medium to high %X_{fd} samples and green represents high altitude and medium %X_{fd} samples. The horizontal line at 10 % X_{fd} marks the border between the mix-SP and coarser non-SP grains and the predominantly high SP ferrimagnetic grains. The second panel **(b)** shows the results of a cluster analysis performed on the two variable X_{lf} and X_{fd} where these three clusters are linked to the corresponding X_{lf}. 99
Figure 4-28: Natural Remanent Magnetism of soil samples from the soil transect, Lake Nkunga and Sacred Lake 100
Figure 4-29: A bi-plot of the PCA of the different magnetic variables of all surface soils (including surface soils collected from Nkunga area) and soil profiles from Sacred Lake and Lake Nkunga (One sample) 101
Figure 4-30: Variations of % C, % N, $\delta^{13}C$ and $\delta^{15}N$ along the soil transect from Lake Nkunga to Lake Rutundu. The red dots mark the outlier samples in the $\delta^{13}C$ and $\delta^{15}N$ dataset 102
Figure 4-31: Stable carbon isotope signature of the soil organic matter along the soil transect from Mt. Kenya area 103
Figure 4-32: n-alkane distribution along the Nkunga-Sacred Lake- Rutundu transect 104
Figure 4-33: GDGT distribution in percent of the samples from the soil transect 106
Figure 4-34: Bivariate plots of brGDGT, iGDGT, pH (the linear relationship is defined from the exclusion of the samples marked in red) and BIT indices along the soils transect in Mt. Kenya 107

Figure 4-35: The relationship of the brGDGT and iGDGT derived indices with pH from the soil samples. 109
Figure 4-36: brGDGT and iGDGT derived proxies. The upper panel shows the reconstructed MAAT from Weijers et al. (2007) in red, Peterse et al. (2012) in black, and Worldclim data (in blue) for the soil transect. The lower panel shows the reconstructed TEX_{86} along the soil transect. 111
Figure 4-37: PCA of the geochemical properties from Nkunga area soils (blue circle), Nkunga soil profile (green triangle) and Sacred Lake soil profile (yellow square). 115
Figure 4-38: The descriptive stratigraphic section and percentage water content of Lake Nkunga cores NKG-I-1-2013 and NKG-I-2-2013. 118
Figure 4-39: Bayesian age depth model constructed with Bacon age-depth model software Bacon for Lake Nkunga sediment core. The bottom panel shows the calibrated ^{14}C dates (transparent blue) and the age-depth model within 95 % confidence intervals. The darker grey areas on the model represent the more likely sections where the model is running through whilst the red curve shows the single 'best' model based on the weighted mean age for each depth. The upper panels show the MCMC iterations: the left represents the stability of the model while the middle and the right represent the prior (green curve) and posterior (grey histograms distributions of accumulation mean and memory properties, respectively. 120
Figure 4-40: A ghost plot for the sediment accumulation rate for Lake Nkunga. The darker the grey shaded areas the more certainty in value obtained while the red line is the weighted mean representation of the accumulation between the different depths along the sediment core. 121
Figure 4-41: The average quantitative mineralogy from the Lake Nkunga core based on the percentage of the diffracted surface of analysed samples 122
Figure 4-42: Down core variation of bulk mass magnetic susceptibility in sediments from Lake Nkunga. 123
Figure 4-43: NRM profile from Lake Nkunga sediment core 124
Figure 4-44: X_{lf}, X_{fd}, Anhysteretic and Isothermal Remanent Magnetisation profiles for Lake Nkunga sediments 125
Figure 4-45: PCA of the elements from Lake Nkunga. Green bars represent the positive correlations while red represents negative correlations. The upper and lower panels show PC1 and PC2 respectively. 126
Figure 4-46: Geochemical proxies for Lake Nkunga. The blue graph displays the normalized values at every one-millimetre interval while the red graph shows the moving average over one-centimetre interval down the sediment core. The grey line marks the boundary between the two core sections for Lake Nkunga. 127
Figure 4-47: Down core variations in the percentage composition of elemental C and N, CN ratios and the $\delta\ ^{13}C$ and $\delta\ ^{15}N$ isotopes composition from Lake Nkunga 129
Figure 4-48: Provenance of the organic component of the Lake Nkunga sediments 130
Figure 4-49: The relative abundances of the n-alkanes derived from samples collected from Lake Nkunga. ... 131
Figure 4-50: The fractional abundance of the brGDGTs and iGDGTs down core in the Lake Nkunga core. The five graphs represent the main (a) the brGDGT and iGDGT abundances while GDGT groups and their moieties are illustrated in (b) GDGT-I, Ib and Ic (c) GDGT-II, IIb and IIc, (d)GDGT-III and IIb & (e) iGDGTs 133
Figure 4-51: Reconstructed MAAT for Lake Nkunga core using MBT/CBT, MbrGDGT and SFS regional calibrations 135
Figure 4-52: A summary of key findings from Lake Nkunga from 1079 cal yr. BP to Present indicating key changes in lake sedimentation and lake level variations 138
Figure 4-53: The stratigraphic section and percentage water content representation sediment cores from Sacred Lake (SAL 11-1, SAL II-2, SAL II-3, SAL II-4, SAL II-5 and SAL II-6). 143
Figure 4-54: Bayesian age depth model for Sacred Lake sediment core. The bottom panel displays the calibrated ^{14}C dates (transparent blue) and the age-depth model within 95% confidence intervals. The upper panels show the MCMC iterations: the left represents the stability of the model while the middle and the right represent the prior (green curve) and posterior (grey histograms) for the distributions of accumulation mean and memory properties, respectively 144
Figure 4-55: The sediment accumulation rate for Sacred Lake. The grey lines envelope 95 % areas of certainty in value obtained while the red line is the weighted mean representation of the accumulation between the different depths along the sediment 145
Figure 4-57: The average quantitative mineralogy of the Sacred Lake sediment samples 146
Figure 4-58: Bulk magnetic susceptibility parameters from Sacred Lake core. 147
Figure 4-59: X_{lf}, Anhysteretic and Isothermal Magnetisation parameters for sediments from Sacred Lake. 148
Figure 4-60: PCA of the elements from Sacred Lake. Green bars represent the positive correlations while red represents negative correlations. The upper and lower panels show PC1 and PC2, respectively. 149
Figure 4-61: Geochemical proxies for Sacred Lake. The blue graph displays the raw and normalized values at every one-millimetre interval while the red graph shows the moving average over one-centimetre interval down the sediment core. The grey areas mark the extent of the 6 cores; SAL II -1, SALII- 2, SALII- 3,

SALII- 4, SAL II – 5 and SAL II – 6 whilst the dotted black and red lines denote the stratigraphic units and hiatus, respectively..... 150
Figure 4-62: Down core variations in the percentage composition of elemental C and N, C/N ratios and the stable $\delta^{13}C$ and $\delta^{15}N$ isotopes composition from Sacred Lake..... 151
Figure 4-63: Provenance of the organic component of the Sacred Lake sediments..... 153
Figure 4-64: n-alkane distribution from Sacred Lake..... 154
Figure 4-65: The relative abundance of the brGDGTs and iGDGTs down core in the Sacred Lake core. The five graphs represent the main (a) brGDGT and iGDGT abundances, while GDGT groups and their moieties are illustrated in (b) GDGT-I, Ib and Ic (c) GDGT-II, IIb and IIc, (d) GDGT-III and IIb & (e) iGDGTs..... 156
Figure 4-66: Reconstructed MAAT for Sacred Lake core using MBT/CBT, MbrGDGT and SFS regional calibrations..... 157
Figure 4-67: A summary of key findings for Sacred Lake from 4425 to 630 cal yr. BP indicating key changes in lake sedimentation and lake level variations..... 161
Figure 4-68: Descriptive stratigraphic section of sediments and percentage water content in sediment cores from Lake Rutundu..... 166
Figure 4-69: Bayesian age depth model for Lake Rutundu sediment core. The bottom panel displays the calibrated ^{14}C dates (transparent blue) and the age-depth model within 95 % confidence intervals. The upper panels show the MCMC iterations: the left panel represents the stability of the model while the middle and the right panels represent the prior (green curve) and posterior (grey histograms) for the distributions of accumulation mean and memory properties, respectively..... 167
Figure 4-70: Sedimentation rate for Lake Rutundu. The darker the grey shaded areas the higher certainty in value obtained while the red line is the weighted mean of the sediment accumulation rate between the different depths along the sediment providing realistic representation in sediment supply..... 168
Figure 4-71: The bulk mineralogy of sediments from Lake Rutundu represented as a percentage of the diffracted surface..... 169
Figure 4-72: Elemental variation from discrete measurements of pellets from Lake Rutundu sediment..... 170
Figure 4-73: Inorganic geochemical composition for Lake Rutundu..... 171
Figure 4-74: Down core variations in the percentage composition of elemental C and N, CN ratios and the Stable $\delta^{13}C$ and $\delta^{15}N$ isotopes composition from Lake Rutundu..... 172
Figure 4-75: Provenance of the organic component of the Lake Rutundu sediments..... 174
Figure 4-76: n-alkane distribution in Lake Rutundu sediments..... 175
Figure 4-77: The relative abundance of the brGDGTs and iGDGTs down core in the Lake Rutundu core. The five graphs represent the main (a) the brGDGT and iGDGT abundances, while GDGT groups and their moieties are illustrated in (b) GDGT-I, Ib and Ic (c) GDGT-II, IIb and IIc, (d) GDGT-III and IIb & (e) iGDGTs. 176
Figure 4-78: Reconstructed MAAT for Lake Rutundu core using MBT/CBT, MbrGDGT and SFS regional calibrations..... 178
Figure 4-79: A summary of key findings for Lake Rutundu from 4770 cal yr. BP to Present indicating key changes in lake sedimentation..... 180
Figure 4-80: Late Holocene palaeoclimatic and environmental reconstruction from the organic matter from Mt. Kenya. The grey areas mark sections where no information was retrieved from the Mt. Kenya proxies due to core length (L. Nkunga and Sacred Lake) and presence of hiatus in Sacred Lake..... 183
Figure 4-81: A generalized chronology of the Late Holocene climatic changes from the three crater lakes..... 186
Figure 4-82: Late Holocene changes in Lake Nkunga derived from Si/Ti ratio representing aeolian dust, Sacred Lake δDwax (Konecky et al. 2014), L. Victoria shallow water diatoms (Stager et al. 2005, Lake Naivasha lake levels (Verschuren et al. 2000) and Lake Edward (Russell and Johnson, 2007). The grey shading represents the century scale-decadal changes in the multiple records..... 188

LIST OF TABLES

Table 1: Summary of the geologic succession of the Mt. Kenya suite in the selected study area (after Baker 1967). 21
Table 2: A summary of previous palaeoenvironmental studies on Mount Kenya based on a range of different proxies..... 37
Table 3: Induced magnetic field on sediment and soil samples using a pulse magnetizer from ARM and IRM measurements. 55
Table 4: Summary of n-alkane indices from Nkunga area soil profile. 87
Table 5: Summary of n-alkane indices from Sacred Lake soil samples 96
Table 6: Summary of n-alkane indices from the soil transect 105
Table 7: brGDGT and iGDGT-derived proxies along Mt. Kenya transect 108
Table 8: Radiocarbon ages from Lake Nkunga sediment core obtained from the AMS (Age ^{14}C yr. BP) and the calibrated radiocarbon ages (Cal yr. BP and their associated errors). The samples marked in bold were identified as probable outliers..... 119
Table 9: Summary of n-alkane indices from Lake Nkunga 131
Table 10: The variations in BIT, 1302/1292 ratio, MBT and CBT proxies from the Lake Nkunga sediment core 134
Table 11: Proxy indicator summary from Lake Nkunga 136
Table 12: Radiocarbon ages from Sacred Lake sediment core obtained from the AMS (Age ^{14}C yr. BP) and their calibrated radiocarbon ages (cal yr. BP) and their associated errors. The samples marked in bold were identified as outliers..... 143
Table 13: Summary of n-alkane indices from Sacred Lake 155
Table 14: The variations in BIT, 1302 (GDGT-0)/1292 (crenarchaeol) ratio, MBT and CBT proxies from the Sacred Lake sediment core 156
Table 15: Proxy indicators summary from Sacred Lake 159
Table 16:Radiocarbon ages from Lake Rutundu sediments from AMS (Age ^{14}C yr. BP) and calibrated radiocarbon ages (cal yr. BP) and their associated errors. 166
Table 17: Summary of n-alkane indices from Lake Rutundu 175
Table 18: The variations in BIT, 1302/1292 ratio, MBT and CBT proxies from the Lake Rutundu sediment core 177
Table 19: Proxy indicators summary from Lake Rutundu..... 179

LIST OF ABBREVIATIONS

Å – Angstrom
ACL - Average Chain Length of n-alkanes
ACL_{lc} - Average Chain Length of long chain n-alkanes
AD -Anno Domino
AF - Alternating Field
AMS - Accelerated Mass Spectrometry
ARM - Anhysteretic Remanent Magnetisation
BC - Before Christ
BIT - Branched to Isoprenoid Tetraether Index
BP - Before Present
BrGDGTs - Branched Glycerol Dialkyl Glycerol Tetraethers
Cal yr. BP – Calendar years before present
CBT - Cyclization Index of Branched Glycerol Dialkyl Glycerol Tetraethers
CPI - Carbon Preferential Index
Cps – Counts per Second
DCM – Dichloromethane
ENSO - El Niño - Southern Oscillation
GDGTs - Glycerol Dialkyl Glycerol Tetraethers
HPLC-MS - High-Performance Liquid Chromatography Mass Spectrometer
iGDGTs - Isoprenoid Glycerol Dialkyl Glycerol Tetraethers
IRM - Isothermal Remanent Magnetisation
ITCZ - Inter Tropical Convergence Zone
LC - liquid chromatography
LGM - Last Glacial Maximum
LST - Lake Surface Temperature
SARM – Saturated Anhysteretic Remanent Magnetisation
MAAT - Mean Annual Air Temperature
MbrGDGTs - Fractional Abundances of major Branched Glycerol Dialkyl Glycerol Tetraethers
MBT - Methylation Index of Branched Glycerol Dialkyl Glycerol Tetraethers
MCMC - Markov Chain Monte Carlo
MDF - Median Destructive Field
MS - Mass Spectrometry
NRM - Natural Remanent Magnetisation
OM - Organic Matter
PC1 - Principal Component 1
PC2 - Principal Component 2
PCA – Principal Component Analysis
P_{aq} – Aquatic Proxy
SD – Single Domain
SFS - Stepwise Forward Selection
SI – The International System of Units
SIRM - Saturation Isothermal Remanent Magnetisation
SP - Super Paramagnetic
SSTs - Sea Surface Temperatures
TAR - Terrestrial – Aquatic Ratio
TEX_{86} - Tetraether Index of Tetraethers consisting of 86 carbon atoms
X_{fd} – Frequency Dependence of Magnetic Susceptibility
X_{hf} - High Frequency Magnetic Susceptibility
X_{lf} - Low Frequency Magnetic Susceptibility
XRD – X-ray Diffraction
XRF – X-ray Fluorescence

1 INTRODUCTION

1.1 Introduction

Understanding past climate regimes is crucial for the prediction of future trends due to increasing concern and awareness of global climate change. Significant 'wet' and 'dry', and 'cold' and 'warm' phases have been documented during the Late Quaternary (last *ca*. 100,000 years) in East Africa from the study of various natural proxies such as pollen, charcoal, diatoms, and stable carbon isotopes from a number of sites (Roberts 1998, Verschuren et al. 2000; Olago 2001; Garcin et al. 2006; Kiage & Liu 2009). Within the Quaternary, the climate dynamics of the Holocene (*ca*. 11 700 cal yr. BP to Present) provides an analogue for modern day climate significant to human populations and ecosystems (Mayewski et al. 2004) and to the management and use of natural resources by the human population. Since the late Holocene (5000 years ago to present), environmental changes have been compounded by human encroachment of the natural ecosystems and their exploitation due to increase in population.

Lake sediments are important archives of allochthonous and autochthonous proxies of historical catchment and lake processes, respectively. Physical, chemical and biological records of these sedimentary records constitute one of the most reliable sources of palaeoclimate and palaeoenvironmental changes through time. These indices are reliable indicators of past environments based on the assumption that their ecological, physical and chemical affinities have not changed through time and that they have modern analogues (Roberts 1998; Smol et al. 2001). These sedimentary deposits from the lakes preserve the inherent geological, chemical and ecological properties of the provenance environment (Smol et al. 2001) and are particularly useful where instrumental and documentary records are missing. Further, modern instrumental records operate on shorter timescales that are not adequate to inform on long-term trends (Figure 1-1; Olago and Odada 2004), therefore, palaeoenvironmental reconstruction from the lake sedimentary records of East Africa where erosion and land use changes tend to obliterate the geomorphological evidences of the past environments (Roberts 1998; Smol et al. 2001) are reliable sources of information.

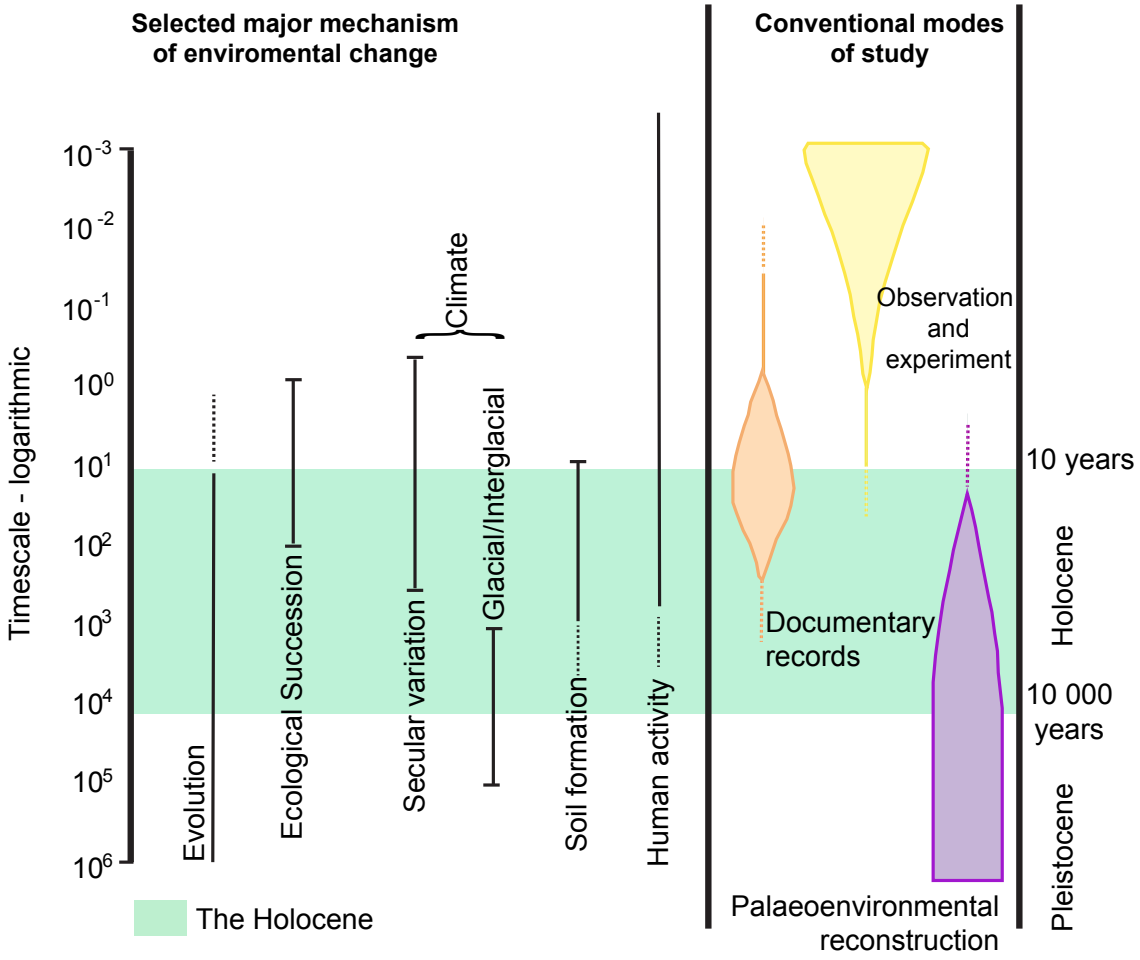

Figure 1-1: Mechanisms and modes of studying environmental changes over different timescales (redrawn and modified from Roberts 1998). Palaeoenvironmental reconstruction is reliable over the long-term to discern patterns of environmental changes especially where documentary records are not available. The reliability of the documentary records has improved from Mid to Late Holocene whereas present day environmental changes are in most instances observed and/or simulated to provide comprehensive information on the environmental change witnessed.

1.2 Statement of the Problem and Thesis Rationale

The chronology of climatic changes in East Africa has been well established with records from several lake sediments (Hamilton 1982; Street-Perrott and Perrott 1993; Olago 1995; Roberts 1998; Verschuren 2003, 2004; Gasse 2005; Verschuren et al. 2009; Kiage and Liu 2009; Rucina et al. 2009; Tierney et al. 2013). However, there are unresolved issues around the spatial resolution, latitudinal gradients and exact timing of the climate change events in relation to the sites on the equator (Gasse 2000) especially in Eastern Africa during the Holocene period.

Generally, the climate of the Holocene is regarded as relatively stable (Dansgaard et al. 1993), but variability is inherent as shown by various researchers (e.g. Coe 1967; Coetzee 1967;

Hamilton 1982; Olago 1995; Verschuren et al. 2000; Alin & Cohen 2003; Cohen et al. 2005; Stager et al. 2005; Russell et al. 2007; Shanahan et al. 2009; Tierney et al. 2013). For example, in contrast to the present-day Sahara Desert, *ca*. 6000 cal yr. BP, the monsoon rains were stronger and spread northward to the Sahara causing a "greening" of the region (deMenocal et al. 2000; deMenocal & Tierney 2012). Severe regional droughts centred at *ca*. 2000, 2750 and 4000 cal yr. BP in Central and East Africa, have been recorded (Coetzee 1967; Gasse 2000, 2005; Verschuren et al. 2000; Russell & Johnson 2005; Garcin et al. 2006; Gasse et al. 2008; Tierney et al. 2013). Other evidences such as that of the relatively wet Little Ice Age (LIA *ca*. 1300 – 1850 AD) display spatial and temporal heterogeneity in East Africa (Verschuren et al. 2000; Tierney et al. 2013).

Precipitation changes over Africa have greater environmental impact than changes in temperature (Olago and Odada 2004). The regional palaeo records especially over the last millennium, show that the easternmost sector of East Africa (closer to the coast) experienced relatively humid conditions as recorded in rising lake levels (Verschuren et al. 2000; Stager et al. 2005; Tierney et al. 2013) whereas, the westernmost sector show wet conditions only at the beginning of the LIA and aridity during its main phase (Alin & Cohen 2003; Cohen et al. 2005; Russell & Johnson 2005; Tierney et al. 2013). This variability in rainfall is closely linked to both El Niño - Southern Oscillation (ENSO) and Sea Surface Temperatures (SSTs) (Nicholson & Kim 1997; Nicholson 2000) and recent present-day model simulations (Tierney et al. 2013) show that wet conditions in coastal east Africa are associated with cool SSTs in eastern Indian Ocean and warm SSTs in western Indian Ocean while the opposite situation causes droughts. This points to the Indian Ocean Circulation as the main driving force behind precipitation changes in East Africa. Unfortunately, the model simulations (Tierney et al. 2013) displaying the west to east gradation of the climatic conditions are based on few lake records and are dominated by records from the westernmost sector of east Africa.

To establish a more comprehensive understanding of the local responses to past climate changes especially during the Late Holocene in east Africa where a climate gradient has been observed from west to east on different sites, the montane ecosystems of Mount Kenya present a unique opportunity to examine responses to climatic and environmental changes during this period. The selected study sites are crater lakes on the north eastern slopes of Mount Kenya. They are located on the eastern most sector of East Africa at different altitudes and are on the windward side. The proxy records obtained from the soils in and around the lake catchment

and sediments of these lakes permit the examination of a large range of palaeoenvironmental indicators thereby providing a better understanding of the Late Holocene pulses in these sites. The questions addressed by this thesis include: Are the crater lakes on Mount Kenya sensitive to Late Holocene climatic and environmental disturbances such as the Medieval Climatic Anomaly (MCA) and LIA? Is there evidence of significant droughts across East Africa during the Holocene? What proxies among those utilized in this study are reliable indicators of precipitation changes and drought during the Late Holocene? Do the results suggest regional heterogeneity or spatial complexity of climatic events across East Africa?

1.3 Objectives

General Objective

The main objective of the study is to elucidate the Late Holocene climate and environmental variability on Mount Kenya over centennial and millennial timescales using multi-proxy palaeo-indicators in soil and lake sediments.

Specific Objectives

The specific objectives are:

I. To establish the Late Holocene sediment chronology of selected Mount Kenya lakes and catchment soils using a multi-proxy analysis of a range of physical, chemical and organic properties in the bulk sediment material;

II. To determine key Late Holocene environmental and climatic events from the sedimentary proxies of the crater lakes;

III. To contribute to the debate surrounding the regional complexity of past regional climate and environmental changes in East Africa.

1.4 Justification and Significance of the Study

Early works on Late Quaternary vegetation and lake level variations in East Africa (Coetzee 1967; Hamilton 1982) presented a relatively stable climate over the last few millennia. This conclusion was derived from low sample resolution and chronology where the last few thousand years were presented by few data points (Verschuren 2004). Recent studies show that the East African lakes have responded to large climatic fluctuations during the Quaternary.

These responses have been linked to extreme rainfall variability (Gasse 2000, 2005) that show a long-term trend of temporal variability controlled by large-scale atmospheric circulation dynamics that generate differences in the seasonal rainfall (Nicholson 2000). The coherent responses obtained from the lake sedimentary archives from the same region gives credibility to the use of lake sediments to evaluate the synchronicity of climatic anomalies in the past (Verschuren 2004). Despite the display of synchronicity in the responses of the various lakes, emerging evidence suggests spatial complexity (Verschuren et al. 2000; Stager et al. 2005; Tierney et al. 2013) pointing to regional heterogeneity of the palaeoenvironments, illustrating local responses to climate conditions such as the LIA (Russell et al. 2007).

Inter-decadal climatic variability and abrupt climate events characterize the short existing instrumental records (Nicholson 2000). Whereas previous research has displayed the dynamism of the African climate at all timescales, there are concerted efforts to reconstruct the continent's climate history with a resolution and precision sufficient enough to separate natural and anthropogenic climate and environmental forcing factors (Verschuren 2004). The current focus of Quaternary research is on understanding comparatively short term (one to two millennia), region specific aspects of climate variability (Verschuren 2003). Such records have the potential to set baselines of natural variations on which long term environmental management plans can be constructed (Olago and Odada 2004) especially if there are major future changes in the hydrological cycle (Christensen et al. 2007).

In most of the regional studies discussed above, the methodology has relied on the sediment cores obtained from the centre of the lakes. This thesis is based on records from one core obtained from the centre of Lake Rutundu and nearshore sediment cores from Sacred Lake and Lake Nkunga. The applicability of the nearshore sediment approach assumes that the strongest evidence of lake level changes is preserved in the shoreline sediments where sufficient accumulations can be used to infer lake level changes and environmental changes (Battarbee 2000).

1.5 Limitations of the Study

Initially in the study design, the assumption was that core samples from Sacred Lake and Lake Nkunga would be retrieved from the centre of the lake. Following field visits, the study had to be modified to retrieve nearshore cores due to limited accessibility. The results presented here from the grain size, mineralogy, XRD and magnetic mineralogy were carried out only on a few

select samples due to laboratory and budgetary constraints. Due to budgetary and time constraints, we were unable to carry out ^{210}Pb and ^{137}Cs dating on recent soil and sediment samples which would have provided a higher resolution chronology of events during the past 150 years as compared to the carbon 14 dating.

1.6 Layout of the Thesis

The importance of the lake sediments as archives of climatically and human-driven changes in the region, and their contribution to the understanding of ecosystem responses, trends and mechanisms, are discussed in **Chapter 1**, alongside the aims, objectives, justification, scope and limitations of the study. **Chapter 2** reviews the general context of the study area, the utility of multiproxy datasets in the study of lacustrine archives and presents the current state of knowledge on the climate and environment of the Quaternary and Holocene periods, with particular focus on eastern Africa, and the causative factors. **Chapter 3** discusses the basis of the methods used in the analysis of the soil and sediment samples collected and details the array of methods used. In **Chapter 4**, the results are presented and discussed, while **Chapter 5** draws out the major conclusions and recommendations.

2 STUDY SITE DESCRIPTIONS AND LITERATURE REVIEW

2.1 Introduction

This chapter consists of three parts. The first part provides a review of the study site from the geologic setting to the topography and characteristics of the study lakes, modern day climate and vegetation and the soils of Mt. Kenya (Section 2.2). The second part presents a review of the utility of multiproxy analyses of lake sediment cores for palaeoenvironmental reconstructions with a focus on the Mt. Kenya lakes and also presents an overview of their use regionally in reconstructions of the Late Quaternary palaeoclimate and palaeoenvironment (Section 2.3). The final part highlights the human impact on ecosystems during the Late Holocene (Section 2.4).

2.2 General Context of the Study Area

2.2.1 Geologic Setting of Mount Kenya

Mt. Kenya is an extinct stratovolcano that was built up by three eruptive events during the Late Pliocene to Quaternary volcanicity (Baker 1967; Olago et al. 2000; Olago 2013). The rocks resulting from the various volcanic eruptions are generally referred to as the Mount Kenya volcanic suite and occupy a circular area of approximately 100km diameter (Table 1). They comprise mainly basalts, phonolites and pyroclastics of similar composition with varying thicknesses. The Thiba basalts (0.8 Ma), basaltic pumice and ashes from parasitic vents are petrologically different and are derived from a different magma chamber (Baker 1967; Coe 1967; Olago 1995; Olago et al. 2000; Veldkamp et al. 2012). Approximately 15 ill-preserved vents and shallow low craters are distributed on the north eastern and northern slopes of the mountain. Some of the cinder cones that appear fresh on the north eastern side can be attributed to the Holocene due to little soil development present (Baker 1967; Olago 1995; Olago et al. 2000). The Mount Kenya volcanics (Figure 2-1) display a general decline in the frequency and intensity of eruption with time during the Quaternary eruptive phase of the satellite vents (Olago et al. 2000).

The main eruptive event from the central plug of the volcano exuded nepheline syenites and porphyritic phonolite, kenytes, trachytes, agglomerates, unexposed basalts and basalts on the

lower slope of the mountain from the parasitic vents deposited during the Late Pliocene *ca*. 3.5 – 3.0 Ma (Baker 1967; Baker et al. 1971) and are distributed in a NW-SE orientation (Baker et al. 1971). Subsequent eruptions are from the parasitic fissures and vents and have resulted in a variety of trachytes (e.g. olivine trachytes, Ithanguni trachytes) and basalts (e.g. Thiba basalts, olivine basalts, mugearites) that are distributed on the mountain slopes on the north eastern and southwestern slopes (Figure 2-1). Late Quaternary volcanicity from the parasitic vents is characterized by Na-K rich alkali pyroclasts with similarity in the geochemical composition and mineralogy of tephras that are rich in Si (60 – 63%; SiO_2), Fe (2.3 – 9.1%; Fe_2O_3) and P (0.4 – 1.8%; P_2O_5) probably derived from a single vent of a highly differentiated magma chamber following an olivine basalt-trachyandesite-trachyte-phonolite series. This explains the morphological differences that can be attributed to each eruption episode (Olago 1995; Olago et al. 2000). Despite an understanding of the mineralogy, chemical composition and morphological differences, a model of the Late Quaternary history of volcanicity does not exist (Olago 1995) and a precise dating of the Mt. Kenya suite has not been done.

Table 1: Summary of the geologic succession of the Mt. Kenya suite in the selected study area (after Baker 1967).

Age	**Eruptive episode**	**Geology**
Recent		Superficial deposits comprising of soils, ashes, moraines and glacial deposits
Pleistocene	Parasitic vents	Basal pumice cones
		Thiba basalts
		Trachytic plugs
		Ithanguni trachytes and tuffs
		Mugi agglomerates
	Parasitic fissure	Riebeckite trachyte
		Olivine basalts
		Mugearites
Late Pliocene	Main eruption	Phonolites and nepheline syenite, porphyritic phonolites, kenytes and agglomerates
		Tuffs, agglomerates, fissile phonolites and alkali trachytes
		Porphyritic phonolites
		Rhomb porphyries
		Unexposed volcanics
		Lower basalts

These phonolitic lava flows from the main vent and successive eruptions overlie the volcanics of the Aberdares range and Laikipia plateau (Laikipian basalts) on the west and southwestern areas that occupy the eastern shoulder of the East African Rift Valley (Baker 1967; Coe 1967;

Olago 1995). To the north, the Mount Kenya suite overlaps with the Nyambeni hills basalts that erupted from a different volcanic centre around the same time as Mt. Kenya and its active phase continued into the Pleistocene (Olago 2013). The remainder of the Mount Kenya suite rests on the Neo-Proterozoic gneisses and schists (Baker 1967; Coe 1967).

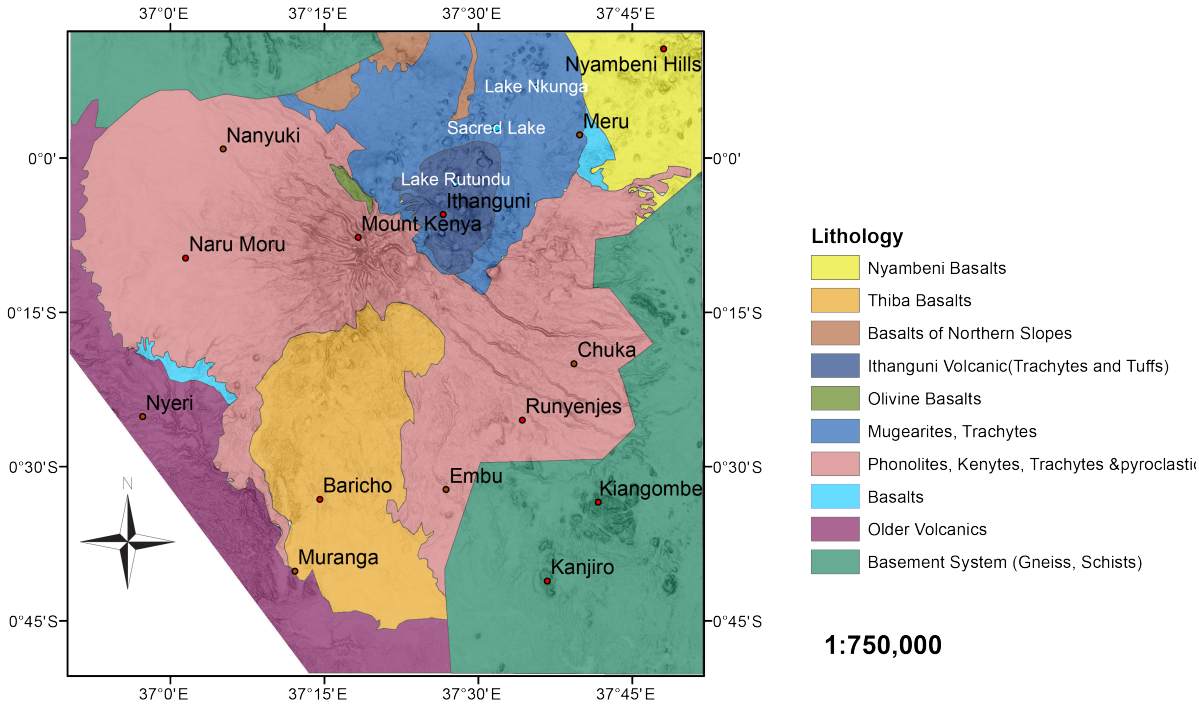

Figure 2-1: A generalized geological map showing the distribution of the Mount Kenya suite (modified after Olago et al. 2000).

2.2.2 Topography and Characteristics of the Study Lakes

Mt. Kenya, located at the equator in East Africa, is an extinct stratovolcano comprising a three peak dome complex; Batian (highest peak 5199 m asl), Nelion (5,188 m asl) and Lenana (4,895 m asl) at the summit (Baker 1967; Figure 2-2). The mountain peak is the plug of an extinct volcano that is accompanied by eroded subsidiary plugs to the north (4676 m) and north east (4669 m) sides of the mountain. It is dissected with deeply cut, radial, youthful valleys that emanate from the mountain peaks (Figure 2-3) that represent at least two periods of intense glacial scouring of the dominantly phonolite rocks. This resulted in the gently eroded slopes and smooth walls of the alpine zone as well as the deeply dissected U-shaped hanging valleys such as Teleki, Burguret, Hausberg, Mackinder, Gorges, Hobley and Hohnel valleys (Baker 1967, Coe 1967).

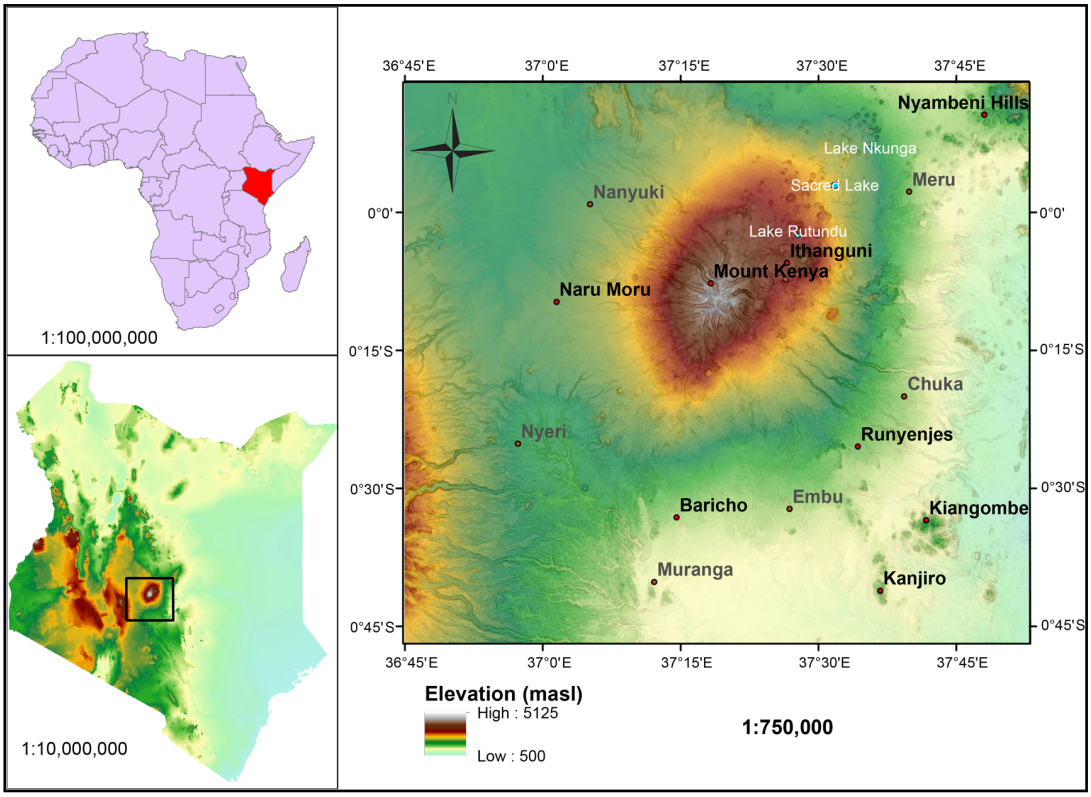

Figure 2-2: Map displaying the location of the study area in the African continent and in Central Kenya. The lakes that dot the north eastern slopes of the mountain where the current study was carried out at Lakes Nkunga, Sacred and Rutundu.

To the east and north, the mountain gently slopes towards the grasslands while to the south and west, the mountain connects to the eastern Kenya highlands (the Aberdares). The north eastern slopes of the mountain are physiographically distinct with gentle undulating narrow steep V-shaped river valleys and its geology comprises of ashes and agglomerates attributed to 5 trachytic necks identified between 2400 – 3300 m asl (Baker 1967). The Ithanguni hills (3576 m asl) are another distinct physiographic feature comprising pyroclastics from the Ithanguni cone to the east (Baker 1967; Olago 1995; Olago et al. 2000; Veldkamp et al. 2007).

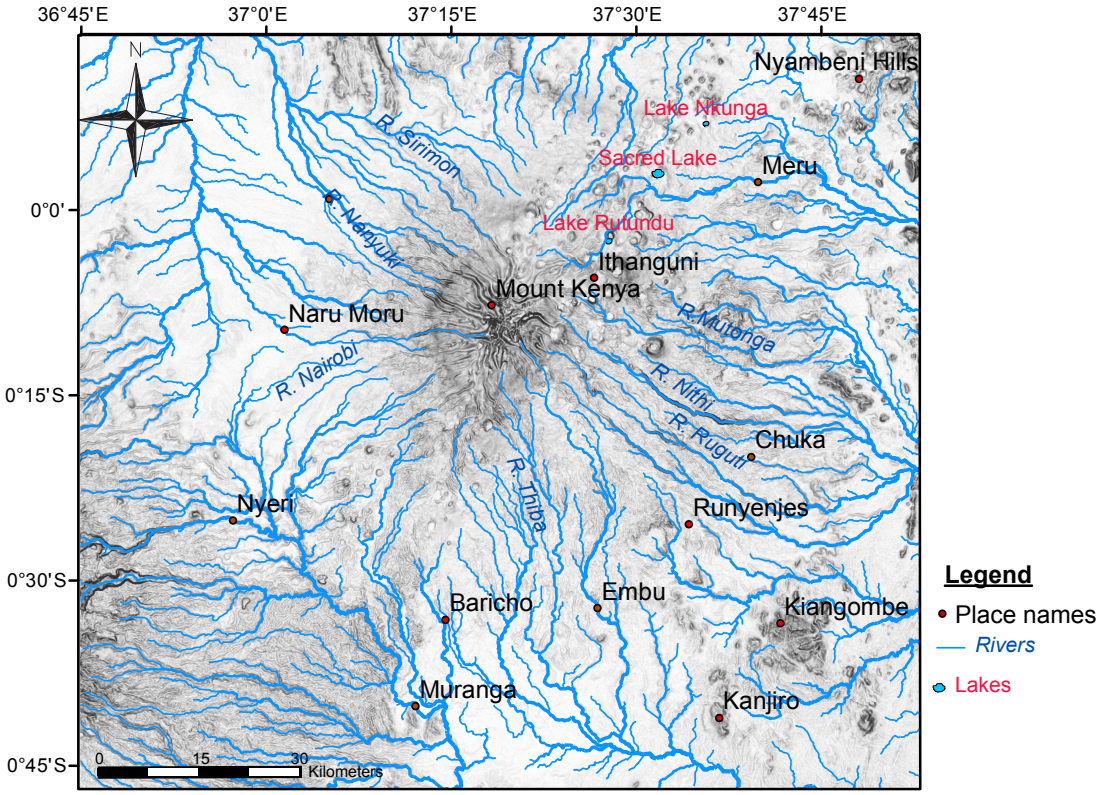

Figure 2-3: Generalized map of the physiographic and drainage features present in the study area. The several rivers and their tributaries present display a radial pattern from the summit of the mountain to the foothills.

Glacial and crater lakes dominate the north eastern slopes of Mount Kenya where a field of parasitic Late Quaternary cones and vents are found (Baker 1967; Olago et al. 2000). Three crater lakes that have been previously studied to provide long term Late Quaternary records for the region (Olago 1995; Ficken et al. 1998; Street-Perrott et al. 2007) were selected for this study on the lower slopes of the north eastern flanks of the mountain along an altitudinal transect (Figure 2-4) as follows: Lake Nkunga (1780 m asl), Sacred Lake (2350 m asl) and Lake Rutundu (3088 m asl). Sacred Lake and Lake Nkunga occupy parasitic craters on the north eastern slopes of Mount Kenya that were likely formed by mid Pleistocene eruptions that extruded small volumes of olivine basalts and pyroclastic rocks younger than the Mount Kenya volcanic suite (Shackleton 1946). The lakes are part of the wider Mt. Kenya forest and therefore the ecosystem around them is a game reserve that serves as a watering point for wildlife such as elephants. The local communities surrounding the forest consider it sacred and therefore little human activity is observed in the vicinity of these lakes.

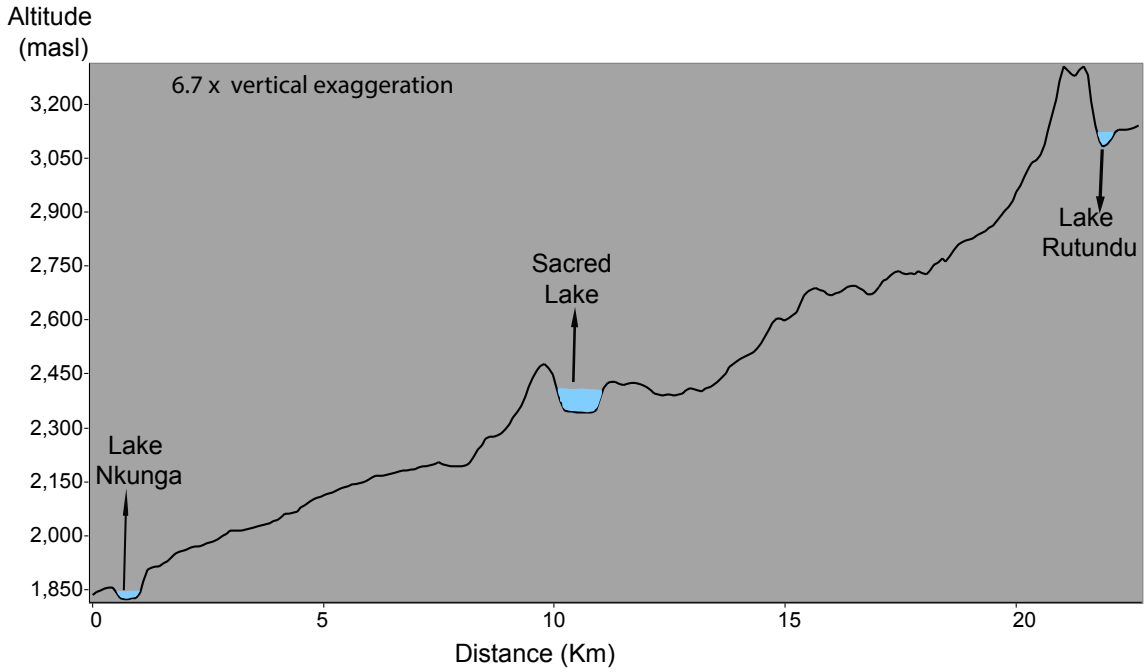

Figure 2-4: Profile along the north eastern slopes of Mount Kenya showing the selected sampling transect from the hill slope at Lake Nkunga to Sacred Lake to Lake Rutundu.

Lake Nkunga is a closed shallow crater lake located at 0.12° N and 37.60° E at an elevation of 1780 m asl with a maximum water depth of 1.9 m. The lake is directly fed by rainfall and cold springs emanating from fissured lava present on the east and west above the lake level (Olago 1995). The lake waters are near anoxic at the top, are acidic with pH ranges of 5.8 – 6.2 and have low diatom productivity (Olago 1995). The lake lies at the border of the dry montane forest and the disturbed vegetation zone. During this study the pH (7.3 and 6.0), temperature (24 °C and 15 °C) and conductivity (320 µs/cm and 201 µs/cm) of near surface waters were recorded in November 2012 and June 2013, respectively. There is restricted access to the lake water due to the presence of reed swamp, floating mats of water lilies, sedges and ferns (Figure 2-5). The lake serves as a water source for the villages around it and wildlife in the Mt. Kenya forest ecosystem.

Figure 2-5: Overview of Lake Nkunga (a) generalized view of Lake Nkunga showing the crater wall surrounding the shallow lake at the edge of the montane forest (b) shows the open water area on the lake and (c) presence of reed swamp and floating mats that restrict access to the centre of the lake.

Sacred Lake is a closed and shallow lake that is located at 0.05°N and 37.53°E at an altitude of 2350 m asl in the humid montane forest zone. It is approximately 1 km across, 5 m deep and receives annual rainfall of about 1780 mm (Olago 1995). Similar to Lake Nkunga, there is restricted access (Figure 2-6) due to the presence of reed swamp and diverse floating mats of sedges, ferns, mosses, and water lilies. During this study, pH (6.3 and 5.0), temperature (27 °C and 18 °C) and conductivity (41.7 µs/cm and 128 µs/cm) of near surface waters were recorded in November 2012 and June 2013, respectively. Located within the Mt. Kenya forest, the lake is isolated from human activities although harvesting of some trees from the catchment was observed during our field work.

Figure 2-6: Overview of Sacred Lake (a) generalized view of Sacred Lake showing the crater wall and the surrounding montane forest (b) field acquisition of sediment core at Sacred Lake (c) shows the coring platform and the piston corer used for the acquisition of the sediment core placed on the floating mats present in the lake

Lake Rutundu is located at 0.04° S and 37.46° E and occupies a side vent on the north eastern slopes of Mount Kenya at an altitude of 3088m asl in the ericaceous zone. The lake is oligotrophic, approximately 0.4 km^2 with a maximum depth of 11 m. During this study pH (4),

temperature (20 °C) and conductivity (39.2 µs/cm) of near surface waters were recorded in June 2013. Lake Rutundu occupies an alkali trachytic neck developed through a phreatic explosion from the contact of ground water with hot thick lava flows (Baker 1967). The adjacent vegetation comprises grassland containing subalpine shrubs of *Artemisia, Cliffortia, Ericaceae* and *Proteaceae* (Figure 2-7). The moorland zone at lake and its catchment is isolated from human population. Adjacent to the lake are log cabins only inhabited by tourists from time to time.

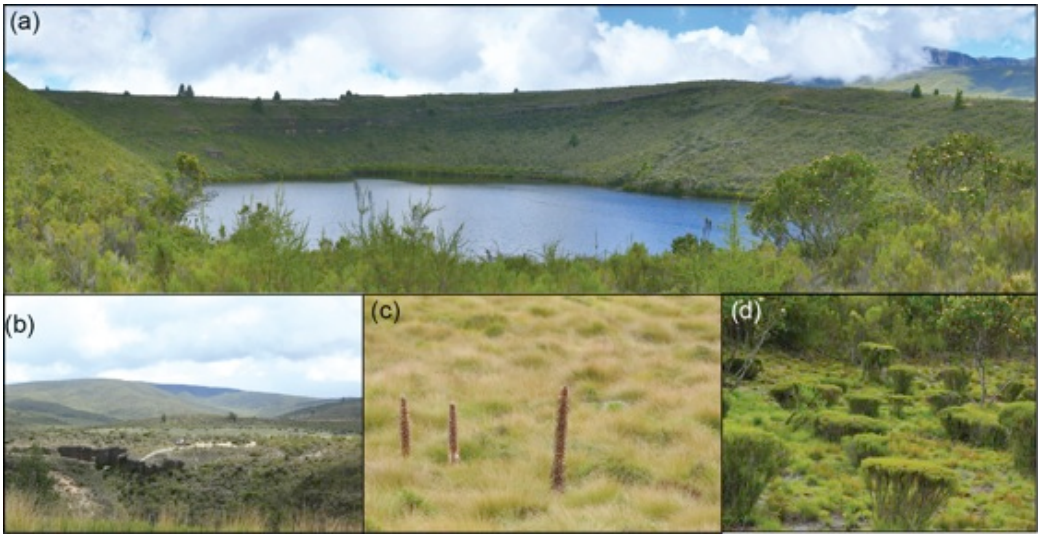

Figure 2-7: (a) An overview of Lake Rutundu occupying one of side vents of Mount Kenya (b) provides a generalized vegetation representation of the bushed grassland of the ericaceous zone where Lake Rutundu is found while (c) and (d) are close up pictures of the vegetation encountered in the grasslands. (c) Tussock grass and scattered off-shoot rosettes of Lobelia telekii (d) Representative dense thickets of the ericaceous belt comprising of, among other vegetation, Philippa, Anthospermum and Alchemilla spp.

2.2.3 Modern Day Climate and Vegetation of the Study Area

Equatorial East Africa is characterized by a bimodal annual rainfall pattern associated with the seasonal interhemispheric change in insolation, and the biannual migration of the Inter Tropical Convergence Zone (ITCZ) across the equator. Three air streams; (i) the humid thermally unstable Congo air, (ii) the dry north east monsoon winds and (iii) the moisture rich south east monsoon winds, are separated by the ITCZ (Nicholson 1996) causing rainfall over East Africa. The seasonal migration of the ITCZ is as a result of pressure differences between the northern and southern hemispheres in response to changes in the location of the solar heating maxima (Nicholson 1996). From October to March (southern hemisphere summer), increasing pressure

over the cold northern hemisphere and low pressure over the warm the southern hemisphere results in the southward migration of the ITCZ. Conversely, from April to September, the low pressure and warm northern hemisphere (especially during the summer) causes the northward migration of the ITCZ (Nicholson 1996). The shifts result in changes in the onset and duration two rainy seasons: the "short rains" from October to December and the "long rains" from March to May rainy. When the ITCZ is in the northernmost position, humid air carried by the southeast monsoon winds rises above East Africa leading to the long rains experienced in the region (Nicholson 1996).

On Mt. Kenya, the topography enhances the effects of the precipitation received during the rainy season (Camberlin et al. 2012). Along the slopes on the windward side (where our study sites are located), the amount of precipitation gradually increases with altitude until about 2000 – 2500 m asl (Figure 2-8) where a decline in rainfall, similar to other East African mountains, is observed (Coe 1967, Camberlin et al. 2009). A further pronounced impact of the topography on the regional microclimate is evidenced on the southern flanks of Mount Kenya which receive approximately 2500 mm rainfall per year and on the northern flank which is much drier receiving approximately 1500 mm rainfall per year (Thompson 1965). There are marked altitudinal variations in the mean annual rainfall values ranging from 1015 mm per year at the foothills to over 2000 mm per year in the montane forest (on the south east) and declining to 1015 mm per year in the alpine zone (Baker 1967; Coe 1967). The top of the southeast monsoon is indicated by a strong inversion at 3600 m asl (Figure 2-8) during the northern hemisphere summer season and leads to higher rainfall especially at the beginning of May (Oettli and Camberlin 2005; Camberlin et al. 2009).

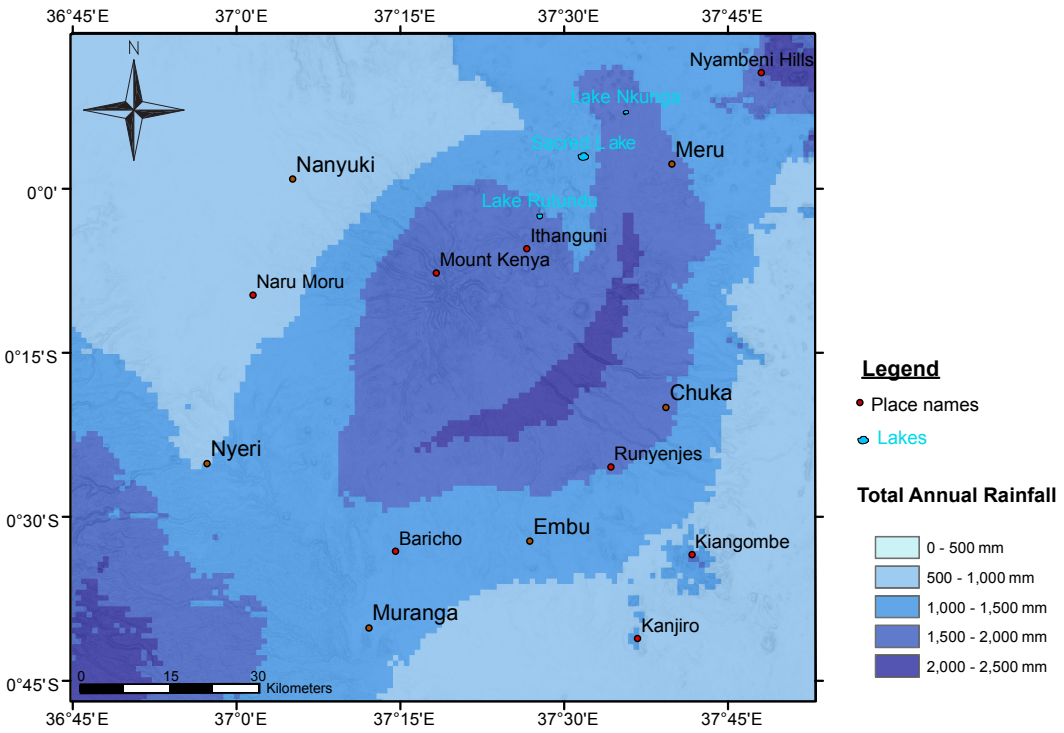

Figure 2-8: Total annual rainfall distribution in the Mount Kenya area. The north eastern region where this study was carried out. Annual rainfall ranges between 1000-1500 mm (Plotted data obtained from WRI 2007)

Most rainfall over the region originates from the Indian Ocean which is considered partly responsible for driving the regional climate variability (Marchant et al. 2006). In such context, one important feature of the intertropical climate, in contrast with climates from mid – and high latitudes, is its strong inter-annual variability linked with sea-surface temperature changes. Both the El Niño Southern Oscillation (ENSO) teleconnections (Nicholson 2001) and the Indian Ocean Dipole (IOD) (Marchant et al. 2006) influence the inter-annual climate variability over East Africa. ENSO oscillations occur at irregular intervals of about 2 – 7 years (Nicholson & Kim 1997; Nicholson 2001); the positive phase of ENSO ("El Niño conditions) tends to be associated with above average precipitation during the short rains (October – December) over Mt. Kenya. Similarly, enhanced precipitation over east Africa occurs during positive IOD events usually associated with cool SSTs in the eastern Indian Ocean and warm SSTs in the western Indian Ocean. This causes alterations in the normal convective atmospheric circulation patterns over the eastern Indian Ocean resulting in heavy rainfall (Nicholson 2001; Marchant et al. 2006; Tierney et al. 2013). Uncertainty still exists on the role of the Indian Ocean in the long-term regional climate dynamics.

In Equatorial Africa, regional temperatures are moderate (around 15 °C – 30 °C) except in areas along the Arid and Semi-Arid regions (ASAL) and the East African coast where a hot and humid climate is witnessed. On Mt. Kenya, the annual-mean maximum temperatures are 26 °C at the foothills decreasing to 2 °C at the nival zone. Diurnal variations in temperature are pronounced with daily temperatures commonly fluctuating between 20 °C at the foothills and 14 °C at the tree line (Camberlin et al. 2012). Generally, the area around Mt. Kenya does not show marked seasonal variations in temperature due to its location at the equator, but does exhibit strong altitudinal gradient (Thompson 1965; Camberlin et al. 2012), up to 1 °C per 100 m (Camberlin et al. 2012).

The present-day vegetation of East Africa covers a wide range of ecological and climatic conditions on the basis of rainfall and altitude. The distribution of the vegetation around Mt. Kenya is influenced by rainfall and temperature regimes. Seven broad ecological zones linked to the annual rainfall timing, altitude, duration and intensity of dry seasons have been identified. These zones are: the alpine zone (alt > 3650 m asl), the highlands (alt 1800 – 3650 m asl; rainfall > 1000 mm), the moist (alt 1100 – 2000 m asl; rainfall > 625 -1000 mm) and dry (alt 760 – 1800 m asl; rainfall 400 – 625 mm) woodland and grassland belts, the dry (alt. < 1060 m asl; rainfall 250 – 400 mm) and arid (alt < 760 m; rainfall < 250 mm) bush lands and the coastal zone (rainfall > 1,000 mm) (Coe 1967; Coetzee 1967; Hamilton 1982; Street-Perrott and Perrott 1993; Olago 2001). Unlike the lowland ecosystems that are extensive and marked by transitional boundaries, mountain ecosystems have different ecozones due to pronounced temperature variations, atmospheric CO_2 concentration, precipitation, soil moisture indices and solar radiation; which are linked to cloud cover, annual rainfall and altitudinal changes (topography and aspect) (Coetzee 1967; Coe 1967; Hamilton 1982; Olago 2001).

A generalized and widely accepted classification of montane ecozones from studies of individual East African mountains identifies three distinct belts: The Montane forest, Ericaceous and Afro alpine belts (in ascending order), however, not all individual zones are necessarily present in each of the East Africa mountains. Broad-leaved hardwood trees and conifers characterize the montane forest, whereas small leaved trees and shrubs are prominent in the ericaceous zone. The Afro-alpine belt is located above the upper limit of the ericaceous belt, and is represented by giant groundsels, shrubs and grasslands (Coe 1967; Coetzee 1967; Hamilton 1982). Although giant groundsels are common in the Afro-alpine belt, they are not

restricted to this zone alone. In some mountains, like the Ruwenzori and Mt. Elgon, they are distributed within the Ericaceous belt as well (Hamilton 1982).

The altitudinal variations in the vegetation assemblages of the Montane ecozones differ considerably on the wet and dry sides of mountains on the basis of moisture availability, presence and extent of vegetation cover, aspect, vegetation disturbance, temperature and human induced or natural competition (Hamilton 1982). Livingstone and Clayton (1980) noted that the grasses present in the high-altitude regions (>2000 m asl) are largely C_3 while those present on the low altitude ranges are C_4 supported by about 10% of C_3 plants, although in exceptional cases C_4 grasses are present up to 3200 m asl and 4000 m asl in select areas of Mt. Kenya (Tieszen et al. 1979; Hamilton 1982; Wooller et al. 2003).

At the foothills, the cultivation/pastoral zone is present between 1000 – 2000 m asl (Figure 2-9). The vegetation of this zone in strongly controlled by land use activities. In its lowest altitude and drier parts, up to ~800 m asl, it consists of *Acacia-commiphora* deciduous bushland and thicket, where the canopy cover is less than 40% (Hamilton 1982). South of the mountain (up to 1400 m asl) evergreen and semi-evergreen bushland dominate the lower altitude while the higher altitudes are dominated by wetter species such as *Juniperus procera*, *Acacia*, *Allophyllus africanus*, *Croton dichogamus*, *Cussiona holstii*, *Euphorbia candelabrum*, *Olea europea*, *Vepris simplicifolia*, *Vernonia brachycalyx* (Coetzee 1967). North of the mountain, *Acacia* wooded grassland (up to ~1800 m asl) is dominant while along the streams trees such as *Syzygium cordatum*, *Podocarpus gracilior* and *Erica arborea* are present (Coetzee 1967).

The montane forest zone lies between 1980 – 3000 m asl and is the dominant vegetation zone on the western, eastern and southern sides of the mountain (protected in the Mt. Kenya National Park). There's a gap on the northern side that is covered by grass, *Ericaceae* and *Protea* scrub and scattered trees (Coetzee 1967). The forest is distinguished into two types; the humid and dry forests (Figure 2-9). The north eastern, eastern and southern slopes comprise *Camphor, Myrica salicifora, Prunus, Macaranga kilimandscharica* and patches of *Podocarpus milanjianus.* The humid forest reaches its maximum development in the southeast sector. The dry montane forest consists of *Cedar, Podocarpus milanjianus, Olea africana,* and *Cassipourea malosana.* The species present at the lower edge of the forest are shorter and less diverse consisting mainly of *Podocarpus milanjianus* and other dry tree species such as *Juniperus procera, Olea hochstetteri* and *Olea chrysophylla* (Baker 1967; Coe 1967; Coetzee 1967; Hamilton 1982).

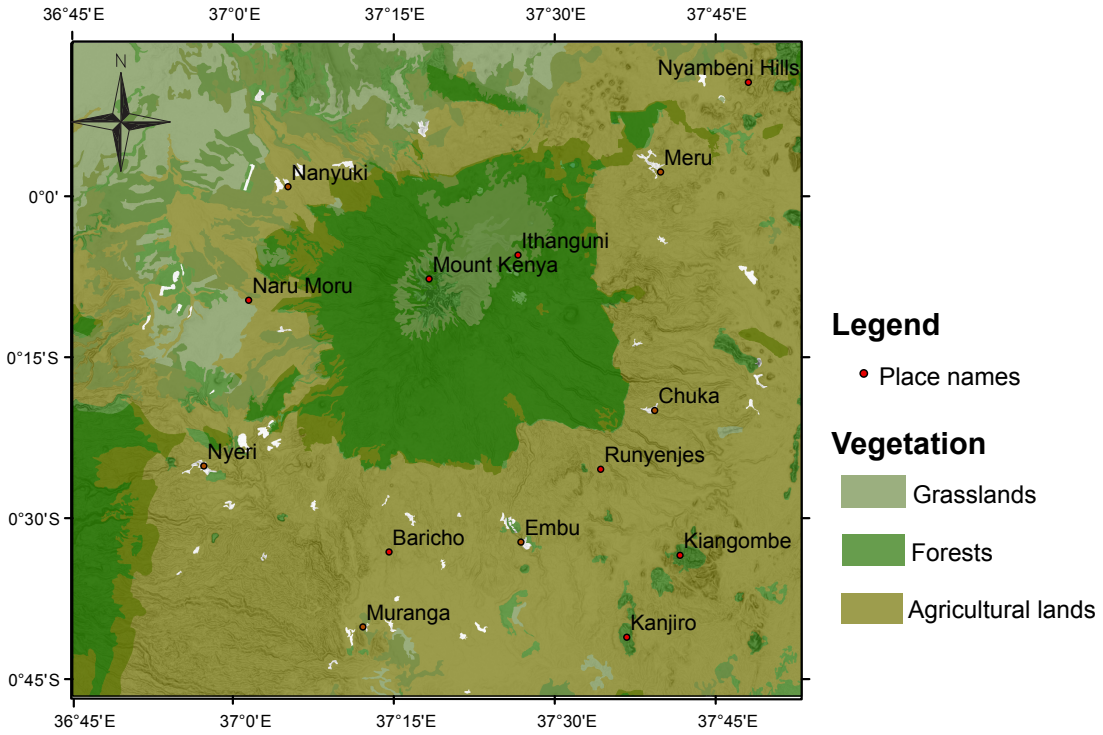

Figure 2-9: The vegetation distribution within the Kenyan highlands (Plotted data obtained from WRI 2007)

At higher altitude, *Arundinaria alpina* (bamboo) is present between 2800 – 3300 m asl on the south eastern slopes while a mosaic of bamboo and *Podocarpus milanjianus* occurs at intermediate intervals. Towards the west and north of the mountain, bamboo becomes less dominant; on the northern slopes there is no bamboo and the montane forest is poorly developed with open gaps. On the western and eastern slopes of the mountain, a well-defined narrow zone of *Hypericum* and *Hagenia abyssinica* is found at 2900 – 3300 m asl (on the east) and 3200 m asl (on the west) of the mountain. Bamboo abundance declines at higher altitude while *Cliffortia nitidula, Afrocrania volkensii, Dombeya goetzenii* and *Agaurea salicifolia* start to emerge (Coetzee 1967).

At 3,000 – 4000 m asl the ericaceous zone is present. The lower part of the zone near the edge of the montane forest comprises *Philippia keniensis, Philippia excelsa, Philippia johnstonii* and *Stoebe kilimandscharia* as the dominant species (Coe 1967; Coetzee 1967). This progresses to the shrubby moorland vegetation characterized by *Philippia trimera*, *Erica sp., Helichrysum sp*. and giant groundsel (Baker 1967). The upper margin of the ericaceous zone is not well defined although patches of 'heather' persist up to *ca.* 4,100 m (Baker 1967).

Notably, the maximum extension of the zone from northeast to the southeast coincides with the highest rainfall recorded above the montane forest (Coe 1967).

Towards the top of the mountain, the Alpine zone marks the thermal limit of plant growth and vegetation transition that culminates in a narrow nival zone. This zone is characteristically marshy and is marked by the presence of *Dendrosenecio* and *Alchemilla* shrubs, *Helichrysum,* and mosses and lichens on the surface of weathered rocks (Baker 1967; Coe 1967; Coetzee 1967). The Alpine zone is divided into two; the upper and lower Alpine zones. The upper Alpine zone represents an area that has undergone solifluction and frost heaving due to climate extremes that have influenced the present-day vegetation composition (Baker 1967; Coe 1967). This upper zone contains sedges, grasses, thistles and species such as *Arabis alpine, Senecio keniophytum, Lobelia telekii and Helichrysum sp.* that persist up to 4600 m asl in scattered patches and damp ground characterized by *Senecio brassica*, *Lobelia keniensis* and tussock grass, whereas *Alchemilla* occupies the drier better-drained areas that characterize the lower Alpine zone (Baker 1967; Coe 1967).

The grasses in the area display altitudinal variations linked to their photosynthetic pathways (Tieszen et al. 1979). Generally, nearly all are associated with C_4 photosynthetic pathways and low moisture content at lower altitudes less than 1500 m asl (Tieszen et al. 1979; Ficken et al. 2002; Wooller & Agnew 2002). A decline in C_4 is encountered with increasing altitude in response to both drought stress and altitude related temperature decline. On Mt. Kenya, this is evidenced at the *Hagenia – Hypericum* zone where a mixed C_4 and C_3 habitat is present on the northern slopes. Below this zone, C_4 plants dominate, and above it, the C_3 grasses are present (Tieszen et al. 1979; Livingstone & Clayton 1980; Ficken et al. 2002; Wooller & Agnew 2002).

2.2.4 Soils of the Mt. Kenya Area

The soils on the slopes of Mount Kenya are derived from volcanic rocks. The distribution of the soils varies with altitude as evidenced by the bare rocks with patches of dry sandy loam soils rich in organic matter on the mountain top; humic silty loam and in some instances, poorly decomposed organic matter on the upper slopes; and clay loam and clays on the lower slopes (Figure 2-10). On the foothills of the mountain, red friable clays (Latosolic soils) have influenced the cultural use of the soil for either crop cultivation or cattle rearing (Speck 1982). The deep humic topsoils of this zone are dark reddish-brown with 3 – 7% carbon in the A horizon which overlies blocky friable clay. Red friable clays, dark clays and brown loams

characterize the montane forest zone while the *Hagenia – Hypericum* and ericaceous zones are predominantly composed of dark peaty loams characteristic of lower rainfall (Olago 1995).

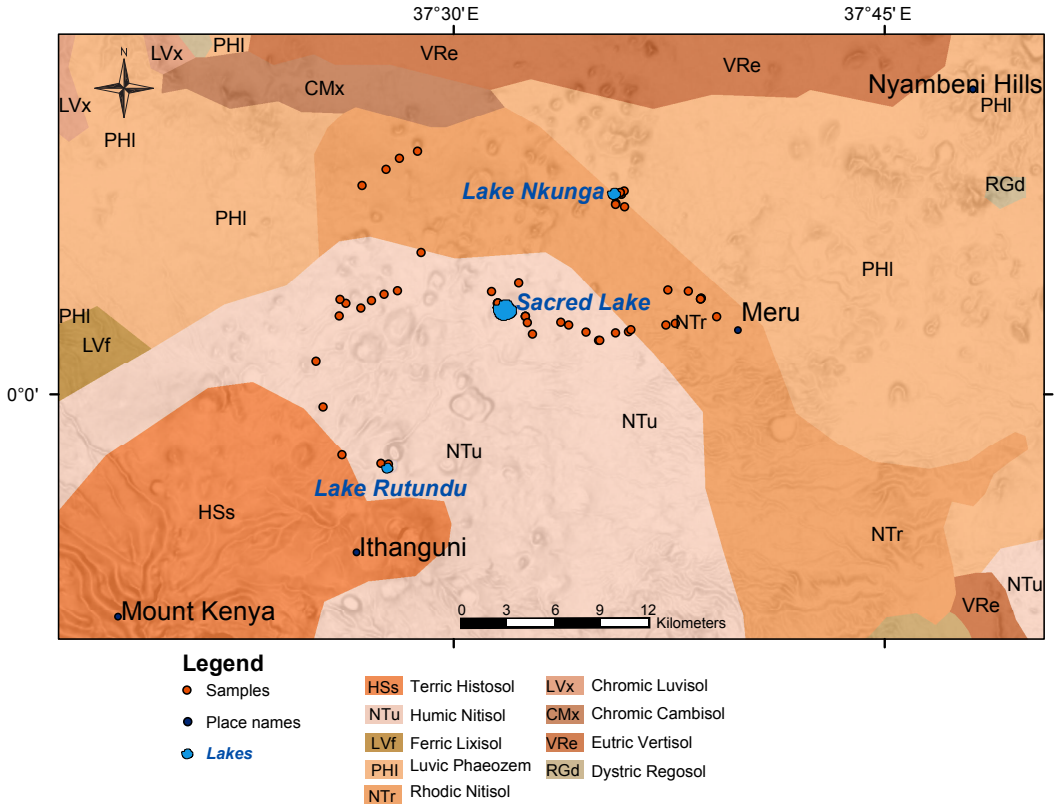

Figure 2-10: Generalized soil map of the study area (Data derived from SOFTWIS database

2.3 The Utility of Multiproxy Datasets in Palaeoenvironmental Reconstruction

2.3.1 Crater Lakes and Lake Sedimentary Records in Mt. Kenya

Widespread proxy records for climate change in East Africa have been obtained from lake sediments. Proxy records from East Africa provide an understanding of climate and environmental dynamics especially in a region where instrumental and documentary histories older than 100 years are lacking or are discontinuous in most cases (Nicholson 2001). These archives have proven vital to palaeoenvironmental reconstruction as they provide continuous chronological records that integrate ecosystem changes for both local and regional environmental changes. They are also the only way to establish a robust "natural background reference signal" to further estimate the magnitude of present-day and future climate and land use impacts on the environment. This thesis examines lake sediments from crater lakes on Mt. Kenya. Crater lakes are a category of lakes formed in an explosion crater or volcanic vent and are fed by rainfall and/or by underground water and springs (most crater lakes originate from phreatomagmatic volcanic activity involving underground aquifer). A newly formed volcanic crater is generally steep-sided and may contain a deep lake with little fringing vegetation. These lakes are short-lived water features and as time passes, sediment is washed from the steep crater walls and the lake becomes shallower. This increases colonization by vegetation thus evolving into a swamp. These lakes have small, closed, well-defined catchments (their surface is typically <1 Km^2) with simple basin morphology, and continuous sedimentation, that act as excellent high-resolution sensors of past climate variability and environmental changes (Battarbee 2000; Lamb et al. 2000). Closed lake basins are hydrologically sensitive to climatic fluctuations. Variations in the lake levels and lake chemistry in response to differences between input (precipitation) and outputs (evaporation and evapotranspiration) during seasonal, inter-annual or long-term climatic fluctuations are reflected in the lake sediments (Gasse et al. 2000). Further, the hydrogeological setting of crater lakes simplifies the relationship between lake hydrology and climate history (Gasse 2000; Verschuren 2001) making the selected sites for this thesis ideal for high resolution palaeoclimate and palaeoenvironmental reconstruction.

2.3.2 Holocene Multiproxy Datasets from the Crater Lakes of Mt. Kenya

Various proxy records from Mt. Kenya exist from swamps, crater lakes, glacial lakes and valleys (Table 2), and provide a good overview of the Quaternary studies in East Africa; however, the data often does not provide detailed and highly resolved records of variability during the Late Holocene which is the focus of this thesis. Much of the previous work conducted on the swamps, glacial and crater lakes, and valleys (Table 2) on Mt. Kenya has been based on vegetation reconstruction through pollen and stable isotope analysis as indicators of climate induced ecosystem changes (Coe 1967; Coetzee 1967; Perrott 1982; Olago 1995; Rucina et al. 2009; Mustaphi et al. 2017).

The early to mid-Holocene transitions (10,560 to 6,000 ^{14}C yr. BP) is marked by a transition from arid to humid conditions with ecosystem changes characterized by increasing forest vegetation including invasion by woody and subalpine shrubs at higher altitudes (Street-Perrott et al. 2007). A decline in ericaceous vegetation at mid-altitude (Sacred Lake) and diminishing grassland fires (Coetzee 1967; Olago 2001; Street-Perrott et al 2007) is also noted. These wetter and warmer conditions are also marked by changes in the $\delta^{18}O_{diatom}$ signal from Simba Tarn and Small Hall Tarn (Barker et al. 2001). Burnt Chloridoid-type (*Acrachne*) grass cuticles in Lake Rutundu (Wooller et al. 2003) point to a very dry episode at 7,980 ^{14}C yr. BP. The warmer and wetter conditions persisted to *ca*. 6,000 to 5,000 ^{14}C yr. BP. There is pronounced resurgence of *Hagenia* and decline in *Gramineae* (characteristic of grasslands) at Sacred Lake where the forest vegetation moved up displacing the bamboo zone to a higher altitudinal range on the mountain reaching a maximum *ca*. 4,000 ^{14}C yr. BP (Coetzee 1967; Street-Perrott & Perrott 1993).

A decline in *Polysica, Ilex, Macaranga, Afrocrania* and *Schefflera,* a rise in *Podocarpus, Hagenia* and *Poaceae,* and large size charcoal classes, mark a transition from the warm and wet conditions to drier conditions from *ca*. 6,500 – 4,000 ^{14}C yr. BP at Rumuiku swamp (Rucina et al. 2009). On Simba and Small Hall Tarn, diatom records indicate minimum $\delta^{18}O_{diatom}$ *ca*. 6,700 – 5,600 ^{14}C yr. BP (Barker et al. 2001) indicative of drying during this period. The expansion of C_4 grasses at Sacred Lake and Lake Rutundu marks the onset of drier conditions *ca*. 4,500 – 4,000 ^{14}C yr. BP (Coetzee 1967; Perrott 1982; Wooller et al. 2000). Generally, drought conditions *ca*. 4,000 ^{14}C yr. BP are observed on Mt. Kenya (Coetzee 1967, Street-Perrott and Perrott 1993) as evidenced by the sharp rise in *Podocarpus* at Sacred Lake and Hohnel Valley Mire shortly after 4,000 yr. BP. At Kiluli swamp relatively dry conditions

characterized by the lack of diatoms and C_3 – C_4 mixed vegetation are recorded *ca*. 3,970 ^{14}C yr. BP (Olago et al. 2003).

Table 2: A summary of previous palaeoenvironmental studies on Mount Kenya based on a range of different proxies.

Site	**Elev. (m asl)**	**Biogeochemical proxies**	**Age range (^{14}C yr. BP)**	**References**
Simba Tarn	4595	Diatoms, O isotopes	8,500 - Present	Barker et al. 2001
Oblong Tarn	4370	Pollen, LOI	5,300 - Present	Mustaphi et al. 2017
Hausberg Tarn	4360	O isotopes	4,000 - 1000	Barker et al. 2001
Hobley Valley Mire	4265	Pollen	5,500 - Present	Perrott 1982
Small Hall Tarn	4070	O isotopes, diatoms, pollen	14,000 - Present	Barker et al. 2001
		C isotopes, biomarkers	14,000 - Present	Street-Perrott et al. 2004, 2007
Lake Rutundu	3088	Pollen	38,300 - Present	Swain 1999
		Diatoms		Barker et al. 2000
		%C, C isotopes, n-alkanes, pollen	38,300 - Present	Ficken et al. 1998, 2002
		Grass cuticles, c isotopes, pollen	38,300 - Present	Wooller et al. 2003
		Biogenic Silica	18,500 - Present	Barão et al. 2015
Sacred Lake	2350	Pollen	33,300 - Present	Coetzee 1967
		Diatoms, mineral magnetics, Stable C, %C, U/Th dating, Mineral magnetics	115,000 - Present	Olago 1995; Olago et al. 1999, 2000.
		Stable C	115,000 - present	Street-Perrott et al. 1997, 2004
		Organic geochemistry	115,000 - present	Huang et al. 1999a, 1999b
		Grass cuticles (~0.93)	40,000 - present	Wooller et al. 2000
		Leaf waxes	2,000 - present	Konecky et al. 2014
		Organic geochemistry		Loomis et al. 2012
Rumuiku Swamp	2160	Pollen, microscopic charcoal	27,000 - Present	Rucina et al. 2009
Lake Nkunga	1780	Organic geochemistry, stable C, pollen	40,000 - Present	Ficken et al. 1998
		Mineral magnetics/IRM, pollen, diatoms, Stable C	130,000 - Present	Olago 1995; Olago et al. 1999, 2001
Kiluli Swamp	1390	Mineral magnetics, %C, %N, stable C	4,000 - Present	Olago et al. 2003

Note: Elev – elevation, ^{14}C yr. BP –^{14}carbon years before present

Alternating wet and dry intervals on Mt. Kenya mark the Late Holocene (5,000 ^{14}C yr. BP to present). Very high values of *Podocarpus* and other montane forest elements (*Olea, Macaranga, Pygeum, Neoboutonia, Galiniera* and *Celtis*) indicate the development of montane rain forest at Sacred Lake *ca*. 3,285 ^{14}C yr. to present (Coetzee 1967; Olago 1995) while at Kiluli swamp, increase in organic matter (OM) inputs from vegetation encroachment and high diatom productivity marks the progressive development of swamp conditions and vegetation encroachment *ca*. 2,245 to 470 ^{14}C yr. BP (Olago et al. 2003). These wetter conditions are interrupted by dry conditions as observed in the substantial decline of the $\delta^{18}O_{diatom}$ at Simba Tarn (3,400, 2,800 and 1,300 ^{14}C yr. BP), Small Hall Tarn (1,900 and 1,300 ^{14}C yr. BP) and Hausberg Tarn (2,500 and 2,400 ^{14}C yr. BP) that imprint pulses of dry periods during the late Holocene (Barker et al. 2001). A decline in montane forest species is observed from 1100 to 415 ^{14}C yr. BP at Oblong Tarn (Mustaphi et al. 2017). The establishment of the true swamp conditions at Kiluli swamp *ca*. 470 ^{14}C yr. BP coincides with arid conditions at Lake Nkunga marked by the appearance of sedge *ca*. 510 ^{14}C yr. BP in the pollen data (Olago et al. 2003). Clear evidence of anthropogenic influence on Mt. Kenya is seen in the pollen records from Rumuiku swamp, where the expansion of grasslands, decline in forest taxa and the high accumulation of charcoal marks the conversion of the montane forest to an open forest (Rucina et al. 2009). These changes in the ecosystem assemblage coincide with the onset of agriculture in the region from *ca*. 500 ^{14}C yr. BP (Rucina et al. 2009). High incidences of charcoal occurrence linked to anthropogenic fires in the Kiluli swamp are recorded from 470 ^{14}C yr. BP to present and there is also a shift in vegetation composition from C_4 to C_3 due to crop cultivation from 130 ^{14}C yr. BP reflecting the impact of human activities on the mountain (Olago et al. 2003). The presence of charcoal in sedimentary records are in most instances associated with forest clearance due to increased frequency of fires.

2.3.3 Overview of the Late Quaternary in East Africa from Multiproxy Records

2.3.3.1 Last Glacial Maximum (LGM) History of East Africa

The palaeovegetation records from high altitude sites in the tropics display synchronous zonal and altitudinal migrations worldwide, implying globally significant impacts of climatic change on these biomes (Taylor 1990; Olago et al. 1999; Olago 2001). The pollen records of the LGM from the East Africa highlands display similar trends to those observed in other high-altitude sites in tropical South America and Australasia. In these areas, significant altitudinal and zonal migrations of vegetation assemblages have been recorded with a maximum depression of

vegetation in the highlands during the last glacial. This trend is concurrent with evidence of tropical glacier advances in high altitude regions linked to changes in atmospheric circulation, surface temperatures and ocean evaporation rates (Taylor 1990; Ficken et al. 1998; Olago et al. 1999; Olago 2001; Ficken et al. 2002; Wooller et al. 2003).

The LGM is an important climate marker as it represents a period when vast ice sheets were present in North America, northern Europe and Asia, reaching their maximum extent before the commencement of deglaciation. The expansion of these ice sheets triggered climatic impacts such as droughts, desertification and a drop in the sea level. These records are well represented in the northern hemisphere where the ice sheets are present. These aridity events are recorded at *ca*. 128,000 ^{14}C yr. BP and between 114,000 ^{14}C yr. BP and 97,000 ^{14}C yr. BP during the Late Quaternary in East Africa (Cohen et al. 2007; Trauth et al. 2007; Gasse et al. 2008; Garcin et al. 2009). The longest palaeovegetation records from the East Africa highlands is from Sacred Lake (Mt. Kenya) and Rukiga highlands (Uganda) that span 115,000 yr. BP and 42,000 yr. BP respectively (Coetzee 1967; Olago 1995; Street-Perrott et al. 1997; Olago et al. 1999). Prior to 42,000 ^{14}C yrs. BP, the records from Sacred Lake imply an unstable vegetation assemblage comprising of ericaceous and humid forest belt taxa displaying shifts of the vegetation zones (Coetzee 1967; Olago 1995; Olago 2001). A *Hagenia and Olea* dominated pollen assemblage marks the transition from relatively dry to humid conditions between 42,000 and 34,000 ^{14}C yr. BP at Sacred Lake (Olago 1995). At the Aberdares range (west of Mt. Kenya), Lake Abiyata (Ethiopia) and the Rukiga highlands (Uganda) dry climatic conditions showing an altitudinal depression of the vegetation between 32,000 and 30,000 ^{14}C yr. BP evidenced by the expansion of C_4 grasses and a decline in the forest taxa until *ca*. 22,000 yr. BP mark the beginning of the LGM (Lezine 1982; Perrott 1982; Bonnefille et al. 1990; Olago 2001; Street-Perrott et al. 2008)

Although the LGM aridity is observed across different sites in East Africa, there are intervals of enhanced moisture transport from the Indian Ocean within this period. This trend is unlike in other parts of continental Africa where dry conditions prevailed throughout the LGM (Street-Perrott & Perrott 1993; Gasse 2000; Garcin et al. 2006; Vincens et al. 2007; Gasse et al. 2008; Tierney et al. 2011). Records of the LGM from East African lakes indicate low stands for most lakes (Victoria, Tanganyika, Malawi and Rukwa) attributed to low sea surface temperatures resulting in less moisture transport to the continent due to reduction in the monsoon effect

(Talbot & Livingston 1989; Gasse 2000; Gasse et al. 2002; Stager et al. 2002; Barker et al. 2003; Barker & Gasse 2003; Cohen et al. 2007; Stager & Johnson 2008; Liu et al. 2013).

Studies from south eastern Africa reveal that this area was not particularly dry during the LGM as their records reflect a consistently moist period with sufficient forest cover that may be as a consequence of the influence of the Indian Ocean (Garcin et al. 2006; Mumbi et al. 2017; Tierney et al. 2013). Synchronous expansion of C_4 grasses and fire tolerant plants is recorded across the tropics in East Africa, West Africa and Southern India during the LGM (22,000 – 14,000 ^{14}C yr. BP). This expansion of the grasslands at the expense of lowland forests (in the lowlands) and the expansion of grasslands, depression and fragmentation of high altitude vegetation zones in the highlands during this period suggests progressive aridity at this interval (Aucour et al. 1994; Huang et al. 1999; Olago 2001; Ficken et al. 2002; Rucina et al. 2009). Several sites exemplify these synchronous changes in the East Africa highlands where large altitudinal migrations of vegetation belts are observed: in Rukiga highlands the dry montane shrub persisted; on Mt. Elgon a decline in the extent of the forest is recorded; from the Cherangani hills the establishment of Afro alpine vegetation is recorded; from Sacred Lake a lowering of altitudinal vegetation is recorded; from Lake Nkunga there is expansion of C_4 plants and other dry forest species; and from Lake Rutundu an expansion of grasslands and ecosystems similar to afro alpine vegetation is observed. Records from Sacred Lake, Lake Rutundu and Rukiga highlands indicate slight increase in humidity marked by expansion of montane forest at *ca*. 14,000 ^{14}C yr. BP during this dry climatic period. The pollen derived temperature estimates from multivariate statistical analysis provides an average temperature depression estimate of 4 °C, 4 °C ± 2 °C and 4.2 °C ± 3.6 °C from Sacred Lake, Kashiru swamp and Lake Tanganyika, respectively, during the LGM (Coetzee 1967; Hamilton 1982; Bonnefille et al. 1990; Taylor 1990; Olago 1995; Olago et al. 1999; Huang et al. 1999; Street-Perrott et al. 2004; Olago 2001; Ficken et al. 2002; Rucina et al. 2009).

2.3.3.2 The Last Glacial – Interglacial Transition: Period between LGM and Holocene

During the deglaciation period, the East African lakes began to fill up from *ca*. 15,000 ^{14}C yr. BP (Gasse 2000; Trauth et al. 2007; Edwards 2013) although records from Lake Victoria mark a desiccation event at between 15,900 and 14,200 ^{14}C yr. BP coinciding with the weakening of the Afro-Asian monsoons, tropical droughts and cooling at higher latitudes (Stager et al. 2002). The LGM-Holocene climatic transition displays stepwise increments in atmospheric CO_2, moisture and temperature. Stable carbon isotope data from Sacred lake mark a transition to

warmer climate *ca*. 14,000 ^{14}C yr. BP while the abundance of *Artemisia* and *Cliffortia* in the pollen record after 14,050 ^{14}C yr. BP imply accentuated dry conditions that reached maximum aridity at 13,500 ^{14}C yr. BP (Coetzee 1967; Street-Perrott & Perrott 1993; Huang et al. 1999; Olago 2001). Temporal correlations are observed in the pollen records of the Burundi highlands where the stable carbon isotope records at *ca*. 15,000 ^{14}C yr. BP and 12,000 ^{14}C yr. BP display shifts from C_4 to C_3 dominated vegetation (Coetzee 1967; Aucour et al. 1994; Olago 1995; Olago et al. 1999; Olago 2001; Huang et al. 1999; Street-Perrott et al. 2004). From *ca*. 12,000 yr. BP – 10,000 ^{14}C yr. BP a period of climatic transition to warmer and wetter conditions is observed across various sites in East Africa (Coetzee 1967; Hamilton 1982; Vincens 1986; Olago 2001). The abundance of *Hagenia* and the spread of C_3 plants especially the sub alpine shrubs in the pollen records from Lake Rutundu mark increases in moisture while at Sacred Lake a reduction in *Poaceae* and montane forest taxa coincides with an increase in the concentration of *Ericaceae* assemblages from Lake Rutundu signifying an increase in atmospheric temperature (Coetzee 1967; Hamilton 1982; Huang et al. 1999; Olago 2001; Ficken et al. 2002; Street-Perrott et al. 2004).

2.3.3.3 The Holocene Period

The conditions of the early Holocene are characterized by progressive humidity recorded in the expansion and diversification of forest in moisture rich assemblages across the various sites in East Africa (Coetzee 1967; Lezine 1982; Vincens 1986; Hamilton 1982; Huang et al. 1999; Olago 2001). Hydrological changes of large amplitude are observed in Lakes Tanganyika, Victoria and Albert that overflowed and supplied the Congo and Nile rivers, respectively (Gasse 2000). Although a general trend of progressive moisture increase was recorded during this period, there were large climatic fluctuations superimposed on the trend, such as short-lived return to arid conditions in sites like Lake Victoria, where a short decline in forest development and diversity is recorded at 10,000 ^{14}C yr. BP. In the highlands, the regression of montane forest and afro-alpine vegetation before attaining their position similar to that observed today is noted (Coetzee 1967; Hamilton 1982; Huang et al. 1999; Olago 2001; Ficken et al. 2002; Street-Perrott et al. 2004).

Tropical forests achieve their maximum extension during the early Holocene period. The regional coherency of the early Holocene climate trends accompanied with progressive forest expansion indicates a transition from dry to wet climatic conditions including in the lowland sites such as in Lake Bogoria where a decline in *Gramineae* and *Cyperaceae* accompanied with

increases in arboreal pollen is observed; in Lake Naivasha where the *Olea – Podocarpus* dominant assemblage is recorded at 12,070 ^{14}C yr. BP and persists until *ca*. 6,500 ^{14}C yr. BP and in lake Tanganyika where *ca*. 12,000 ^{14}C yr. BP the establishment of open forests which achieved maximum species diversity at 10,000 ^{14}C yr. BP is noted (Hamilton 1982; Vincens 1986; Maitima 1991). Records from Sacred Lake indicate that while montane forest pollen becomes dominant from 10,560 ^{14}C yr. BP to *ca*. 6,000 ^{14}C yr. BP, this period is marked by decline in the ericaceous taxa and the establishment of the Afro-alpine grasslands in the pollen assemblage (Coetzee 1967; Hamilton 1982; Street-Perrott & Perrott 1993; Olago 2001).

A reconstruction of the climate regime in East Africa using modern analogues reveals that at *ca*. 6,000 ^{14}C yr. BP the vegetation assemblages north of the 3^{o}S latitude represented a warmer and wetter climate coinciding with the Africa humid Period (Peyron et al. 2017). The Early to Mid-Holocene palaeoclimatic reconstruction paints a wet period with progressive drying events that were not synchronous in the region. Some prominent sites that have yielded transitions to drier conditions include Lake Malawi (10,000 ^{14}C yr. - 7,000 ^{14}C yr. BP), Mount Kenya (9,000 - 6,000 ^{14}C yr. BP) and Lakes Manyara, Magadi, Natron, and Bogoria within the rift valley where low stands are recorded around 6,000 yr. BP (Street-Perrot et al. 1993; Barker et al. 2001; Edwards 2013).

2.3.3.4 The Late Holocene in East Africa

The Late Holocene (~5,000 ^{14}C yr. BP to Present) follows the termination of the Africa humid period. Evidence of synchronous initiation of dry conditions is present in the lowland and highland sites in the East Africa region. The initiation of drier conditions at *ca*. 4,000 ^{14}C yr. BP across the region is marked by the replacement of wet montane taxa by dry montane taxa in the high-altitude regions, and by the abrupt drop of several lakes (e.g. Langano and Abijata in Ethiopia, Nakuru in Kenya). On Mt. Kenya a sharp rise in *Podocarpus* and other dry montane forest elements; more positive δ^{13}C from Sacred lake and the presence of C_4 from Kiluli swamp are observed (Coetzee 1967; Hamilton 1982; Street-Perrott & Perrott 1993; Olago 1995; Olago 2001; Ficken et al. 2002). The regional coherence of this trend is also observed at Kashiru swamp, Burundi *ca*. 4,500 ^{14}C yr. BP where stable isotope record shows increases in C_4 plants (Aucour et al. 1994). The hot and dry condition persisted in the lowlands too where trees are replaced by herbaceous elements. This is marked in some sites e.g. a decline in arboreal pollen at Lake Turkana; the development of *Acacia* woodland at Lake Baringo; and the disappearance of lowland forest pollen assemblages at Lake Naivasha (Owen et al. 1982; Vincens 1986;

Maitima 1991). This abrupt drying event has been linked to the dramatic weakening of monsoon circulation patterns in the tropics (COHMAP 1988).

The records of lake level changes (from the lowlands) and recent glacial retreats in the East African highlands provide evidence of the significant climatic changes during the past two millennia that is characterized as an arid period interrupted by brief wet episodes with rising lake level (Coe 1967; Hamilton 1982; Verschuren et al. 2000; Verschuren 2003, 2004; Konecky et al. 2014). An example is Lake Edward (Uganda) where century – scale droughts centred at 4,100, 2,000, and 850 ^{14}C yr. BP and numerous lesser droughts are present in its record (Russell & Johnson 2005). At the beginning of the second millennium (*ca*. 900 -700 ^{14}C yr. BP), low lake levels are recorded across the lakes in East Africa (Verschuren et al. 2000; Alin & Cohen 2003; Russell & Johnson 2005). Important climatic markers of significance during the Late Holocene are (i) the drier Medieval Climatic Anomaly – MCA (950-680 ^{14}C yr. BP) and (ii) the wetter Little Ice Age – LIA (680-100 ^{14}C yr. BP) which are recorded in the East Africa region (Verschuren et al. 2000; Cohen et al. 2006; Kiage & Liu 2009; Russell et al. 2009).

Precipitation anomalies experienced during the Little Ice Age and the Medieval Climatic Anomaly were controlled by Walker Circulation Anomaly localized over the Indian Ocean where wet conditions linked to cool Sea Surface Temperature (SST) in the eastern Indian Ocean and warm SST in the western Indian Ocean coupled with the atmospheric circulation over the eastern most part in East Africa lead to rainfall while the converse leads to droughts (Tierney et al. 2013). The Little Ice Age represents a wet period pulsed by dry events. The first half of the little Ice Age – LIA (700 - 400 ^{14}C yr. BP) represents the last maximum lake level high stands that are interrupted by an arid interval *ca*. 550 ^{14}C yr. BP. Although the second half is characterized as wet, lake level regressions associated with persistent droughts are recorded in lakes Turkana, Edward, Challa, Baringo, Victoria, Tanganyika and Naivasha (Nicholson 1998; Verschuren et al. 2000; Lamb et al. 2003; Alin & Cohen 2003; Russell & Johnson 2005; Edwards 2013; Kiage & Liu 2009; Verschuren et al. 2009; Edwards 2013). Other important wet intervals across the East African region are centred on 1450, 450, and 80 ^{14}C yr. BP which are linked to the Wolf, Spörer and Maunder minima in solar activity (Alin & Cohen 2003; Verschuren 2004; Kiage & Liu 2009).

The past two centuries have been unusually moist based on the entire record of the late Holocene although an extreme arid event between *ca*. 250 and 150 ^{14}C yr. BP is observed

(Russell & Johnson 2005). Lake level changes across equatorial east Africa display similarity in trends in the 19th and the 20th Centuries. Major lake level transgression is recorded during the 1890s followed by marked low stands in the 1940s – 1950s. An accelerated recovery of the lakes in the early 1960s is noted across the region following unusually heavy rainfall in 1961/1962. Currently, lake levels oscillate between continuously low to intermediate levels reflecting ENSO type cyclicities (Verschuren 2004; Russell & Johnson 2005).

2.4 Human Impact on Ecosystems during the Late Holocene in East Africa

The Late Holocene (5,000 ^{14}C yr. BP to Present) is characterized by changes in the natural environment linked to both climatic changes and human settlement expansion. This section looks at the individual records of human impact from various sites in East Africa where records show progressive changes of ecosystems due increasing population, migration and settlement of various communities that occur simultaneously with the expansion of grasslands and the development of open forests (both lowland and highland) (Kiage & Liu 2009; Rucina et al. 2009, 2010; Russell et al. 2009; Stoof-Leichsenring et al. 2011).

The human-environment interactions during this period are critical in understanding the global cultural impacts of societal development linked to land use changes recorded in soils, sediments and water (Roberts 1998). During this period, human populations progressed from being minor players in ecosystem modification to key influencers of the natural environment (Hamilton 1982; Roberts 1998). In East Africa, the expansion and settlement of the various ethnic groups: Bantus, Nilotes and Cushites into the region (around 2350 ^{14}C yr. BP) played a key role in the modification of the environmental resources at their disposal (Hamilton 1982; Roberts 1998; Kiage & Liu 2009).

Late Holocene records of human settlement and associated impacts on ecosystems in East Africa recorded in pollen, charcoal, spore and sediment geochemistry are linked to major land use changes. However, it is difficult to interpret these palaeoenvironmental records as it is difficult to isolate the climatic from anthropogenic signals in most cases (Lamb et al. 2003; Kiage & Liu 2009; Rucina et al. 2009, 2010), and in most cases the combination of palaeoenvironmental records with archaeological and historical studies is required to assess the impact of land use on ecosystems.

The first large-scale human influence is evidenced around 4000 ^{14}C yr. BP, associated with the introduction of domesticated livestock and the expansion of pastoral communities (Marchant

et al. 2018). However, as shown from a series of records, the first widespread and intensive forest clearances were synchronous with the arrival of iron-using communities around 2500 ^{14}C yr. BP, particularly in productive and easily-cleared mid-altitudinal areas (Marchant et al. 2018). In the Amboseli basin (Kenya), pollen records show progressive development of open forests associated with human settlement and the introduction of domesticated crops such as cereal, *Cannabis sativa* and castor oil plant alongside increases in charcoal from 1670 ^{14}C yr. BP which is recognized as an indicator of landscape modification by human activity (Rucina et al. 2010). In western Uganda, vegetation records from Lake Wakandara indicate a resilient ecosystem from *ca*. 1250 – 950 ^{14}C yr. BP where the lake catchment is surrounded by C_3 plants despite century scale hydroclimatic changes recorded in the C_4 signature. Archaeological evidence from the surrounding catchment has linked this C_4 grassland expansion to forest clearing by the population *ca*. 950 ^{14}C yr. BP which coincides with the establishment of sorghum and millet farming in the arable lands of the catchment (Taylor et al. 1999; Ssemmanda et al. 2005; Russell et al. 2009). The clearing of catchment land cover for settlement and agriculture is recorded in the lake δ^{15}N signal showing its enrichment *ca*. 810 – 770 ^{14}C yr. BP due to siltation derived from the land use changes rather than to climate variability (Taylor et al. 1999; Ssemmanda et al. 2005; Russell et al. 2009). The expansion of trading routes between the interior and the coast, starting around 1300 years ago and intensifying in the eighteenth and nineteenth centuries, played a key process in modifying the land cover in the region, spreading domesticated plants from East Asia such as banana, rice, taro and chicken earlier than *ca*. 800 ^{14}C yr. BP, or more recently south and central American crops such as maize, tomato or avocado (Marchant et al. 2018).

Micro-charcoal and fungal spores from a Lake Baringo record at *ca*. 120 ^{14}C yr. BP are linked to widespread pastoral activities and expansion of agricultural practices by agro-pastoralists (Njemps community) through land practices such burning, slashing or biomass burning to rid livestock of ticks and smoking of bees during honey harvesting is present in the historical records (Anderson 2002; Kiage & Liu 2009). Monitoring of *Glomus* spores (a terrestrial fungi that improves nutrient uptakes and makes crops disease resistant) as an indicator of soil erosion and land degradation implies increased human impact (by mid-19th Century) and improvement in land management practices through the soil conservation efforts introduced during the colonial period (Anderson 2002; Kiage & Liu 2009). Other records from the region that mark human modification of the landscape include Stoof-Leichsenring et al. (2011) who noted that increased sediment flow into Lake Naivasha between *ca*.130 – 54 ^{14}C yr. BP, was largely

influenced by natural climatic events documented in historical records of droughts and rainfall anomaly; however, there may be a minor influence from human activity (Verschuren et al. 2000; Nicholson 2001). A transitional period between *ca*. 54 – 12 ^{14}C yr. BP marked by eutrophication due to increase in total phosphorus concentrations in Lake Naivasha from 50 yr. BP (Verschuren 2004; Stoof-Leichsenring et al. 2011) is largely anthropogenic. In lake Bogoria, increase in clay content and high charcoal abundance from *ca*. 110 ^{14}C yr. BP coincide with land use changes in the catchment (De Cort et al. 2013).

3 METHODOLOGY

3.1 Methodology

This section documents the basis of the materials, techniques and research approaches utilised in this study. It further describes the acquisition of soil and sediment samples, processing of the samples, water content determination, stable isotope analysis, elemental Carbon - Nitrogen analysis, geochemical analysis and mineralogical analysis (carried out at ALYSES facility (IRD-UPMC); magnetic susceptibility analysis (carried out at CEREGE) and lipid biomarker extraction and analysis (carried out at METIS-UPMC). The techniques associated with the establishment of core chronology are also outlined.

3.1.1 Soil Sample Collection (Surface and Subsurface Samples)

80 surface and sub-surface soils were collected from the study sites in two field campaigns, one in 2011 and the other in 2013, from the selected lakes and the surroundings soils (Figure 3-1). The surface soil samples were collected using a spade while the sub surface samples were obtained using an auger. Two vertical soil profiles were sampled for analysis in this study. These profiles were obtained from Lake Nkunga viewpoint gate located at 0°6’ N, 37°35’ E and Sacred Lake area at 0°03’N, 37°31'E. These initial samples were collected in 2011. The Lake Nkunga soil profile and surface soil samples were obtained above the Crater Lake wall in a small clearing of the montane forest and within the crater itself. The soil profile and surface samples for Sacred Lake were obtained from the forest undergrowth north east of the lake, about 20 m from the lakeshore, where an opening to the lake is present.

In 2013 surface soil samples were collected along the Lake Nkunga to Lake Rutundu transect at every 100 m of altitudinal gain. These samples were preserved in resealable plastic bags and initially stored in the cold room at the University of Nairobi and the soil storage facility at ICRAF Soil and Plant laboratories. Later the samples were transported to the IRD laboratory in Bondy, France and stored in the cold room.

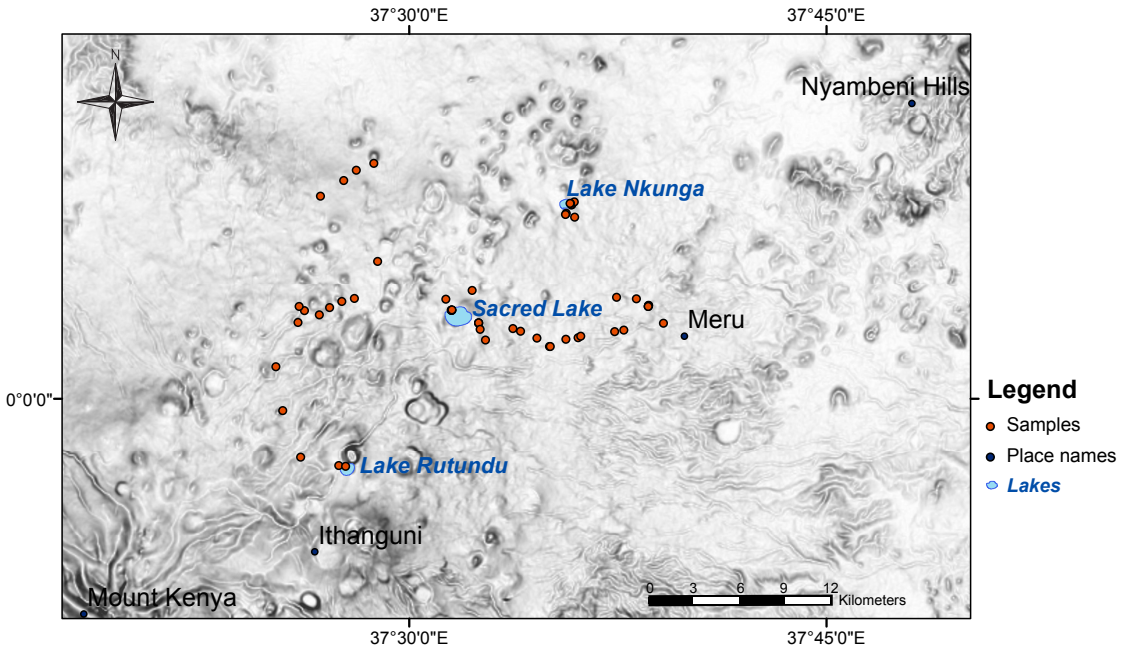

Figure 3-1: Samples collected during fieldwork in 2011 and 2013 on the north-eastern slopes of Mount Kenya (red dots).

3.1.2 Lake Sediment Sample Collection

Fresh sediment cores were obtained from Lake Nkunga (Figure 3-2) and Sacred Lake (Figure 3-3) using a Wright stable piston corer in June 2013 operated from a rubber boat. The sediment cores collected were approximately 1 m below the water surface. The high compaction-level of the sediment led to the recovery of several short sections (two sections of 45 cm and 44 cm at Lake Nkunga, and six sections raging in length from 8 cm to 12 cm at Sacred Lake) taken successively to recover continuous upper sedimentary sequences. From Lake Nkunga, two core sections spanning a total depth of 89 cm (Figure 3-2) were obtained approximately 20 m from the lake shoreline: NKG-I-1 (45 cm) and NKG-I-2 (44 cm) at a water depth of 1.5 m.

Figure 3-2: Sediment cores from Lake Nkunga comprising two short sediment cores NKG-I-1-2013 an NKG-I-2-2013 each approximately 45 cm. One half of the sample was subsampled every 1 cm for sample preparation and analysis while XRF scanning was carried out on the other half of the core.

In Sacred Lake, the six successive core sections; SAL-I, SAL-II, SAL-III, SAL-IV, SAL-V and SAL-VI recovered constitute 63 cm (Figure 3-3) at a water depth of 1m. The cores were stored in the laboratory at 4° C. Once in the laboratory, core splitting was carried out using a clean thin fishing line. One half of the split core was then sub-sampled at every centimetre for the analyses presented in this thesis.

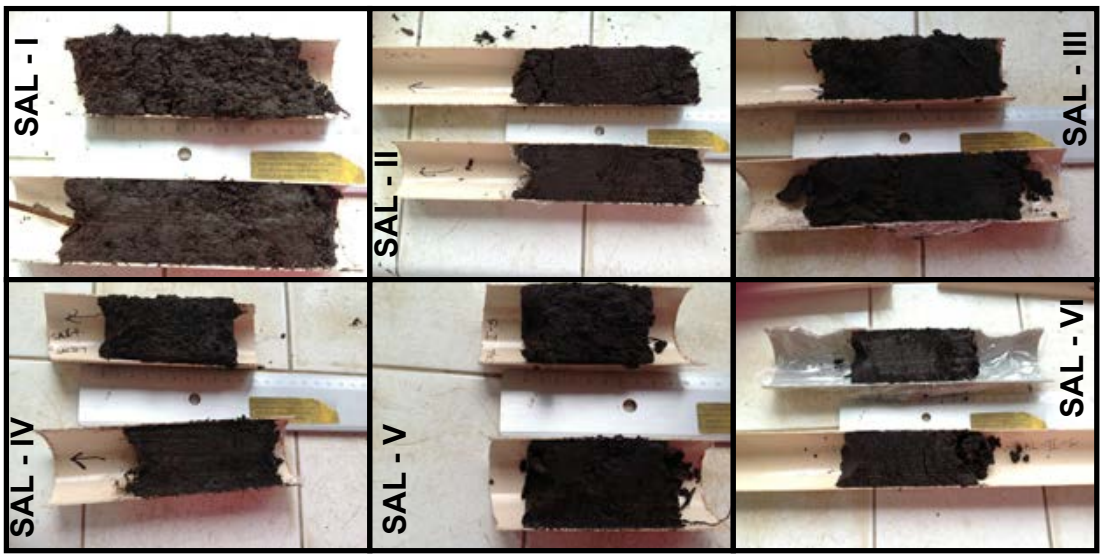

Figure 3-3: Six short cores of different sizes obtained from Sacred Lake that was analysed during this study. Total length is approximately 65 cm. Similarly, as carried out in the Lake Nkunga core, one half of the sample was subsampled every 1 cm for sample preparation and analysis while XRF scanning was carried out on the other half of the core.

A 100 m sediment core RP6 recovered from the centre Lake Rutundu using a gravity corer in 2009 by Prof. Olago (University of Nairobi), Prof. Verschuren (University of Ghent) and their team was also analysed. The core was archived at the University of Nairobi cold storage (4° C) and subsequently sub-sampled at 1 cm interval for the analysis carried out in this study.

3.1.3 Physical Parameters

The lithology of each core was described by colour (using Munsell colour chart) and texture. The samples from Lake Nkunga, Sacred Lake and Lake Rutundu were analysed for water content (W_c), a fundamental parameter linked to the organic matter content. Lacustrine sediments with low water values are usually associated with high inorganic contribution to the bulk sediment. These samples were taken at every 1 cm through the core length, weighed (± 0.001g) and oven dried at 35° C – 40° C for 48 hours until a constant weight was obtained, then allowed to cool at room temperature before being weighed again.

The water content was calculated as follows:

$$W_c = \left(\frac{M_{wet\,(g)} - M_{dry\,(g)}}{M_{wet(g)}} \right) x\ 100\ \%$$

Where W_c is the water content, $M_{wet\,(g)}$ is the mass of wet sediment in grams and $M_{dry\,(g)}$ is the mass of dry sediment in grams.

3.1.4 Grain Size Analysis of Soil Samples

To isolate the terrigenous mineral fraction, organic matter, calcium carbonate and biogenic silica, 100 mg of bulk soil sample was attacked using H_2O_2 (30% at 50 °C for 3 to 4 days), HCl (10% for 12 hrs) and Na_2CO_3 (1M at 90 °C for 3 hrs), respectively. Between each chemical treatment, samples were repeatedly rinsed with deionized water and centrifuged at 4000 rpm until neutral pH. The samples were sieved with a 200 μm mesh in order to recover coarser particles; in this case <1 mg of total soils was recovered in the >200 μm fraction in a few soil samples while in most samples this size fraction was missing. The analysis was carried out using an automated image analysis system (model FPIA3000, Malvern Instruments). The obtained particle sizes from the FPIA method are considered representative following their classification using GRADISTAT version 4.0 (Blott & Pye 2001), a particle size statistics program for laser granulometric data that runs on Microsoft Excel providing the full range of grain sizes in the soils using the Folk and Ward measures that provided a range of frequency and ternary plots of the various class particle sizes.

3.1.5 Radiocarbon Chronology

In order to provide age controls that would enable local, regional and global comparisons of the results of this study, down core ^{14}C measurements were carried out on selected samples from the 3 sediment cores. One gram of 19 bulk sediment samples and one identified charcoal sample were dried in the oven at 40° C for 48 hrs, weighed (± 0.001g) and submitted to "*Laboratoire de Mesure du Carbone 14*" in Gif sur Yvette (France) for ^{14}C AMS dating (± 30 as indicated in sections 4.3.1.2, 4.4.1.2 and 4.5.1.2). The radiocarbon ages obtained were calibrated using IntCal13 calibration curve for the northern hemisphere (Reimer et al. 2013) using Clam version 2.2 (Blaauw 2010), which incorporates IntCal13 ^{14}C calibration curves from Reimer et al. (2013). An age-depth model was fitted through the obtained dates using Bacon software (Blaauw & Christen 2011) version 2.3, a Bayesian statistical program used to construct Bayesian accumulation histories for sediment deposits. Bacon divides the sediment core into several vertical sections and through millions of Markov Chain Monte Carlo (MCMC) iterations generates estimates of sedimentation accumulation rates for each section. The memory/coherency in the sediment accumulation rates along the core is based on how strongly the accumulation rate at each interval depends on the previous section and therefore produces stratigraphically ordered estimates. The selected Bayesian model provided realistic estimates of dates through the reduction of error ranges and removal of outliers from the obtained ages.

3.1.6 Mineral Magnetic Measurements

a) Rationale

One aspect of interest in this study was magnetic susceptibility which is defined as the quantitative measure of the extent to which a material may be magnetized in relation to a given applied field (Oldfield & Robinson 1985). Due to the interaction between subsurface processes and the biogeochemistry of iron and titanium magnetic minerals such as Fe-Ti oxides, sulphides or carbonates, the magnetic susceptibility and other mineral magnetic properties such as artificially imparted remanent magnetisations are applicable in the study of soil formation processes, slope evolution, drainage basin erosion and sedimentation and stratigraphic correlation in both deep sea and lake sediments (Oldfield and Robinson 1985; Olago 1995; Williamson et al. 1999). The main interest of such analytical method is (i) the ultra-high sensitivity of mass specific magnetic parameters (susceptibility and frequency dependence) to the iron content, (ii) the ability to perform non-destructive (and low cost) measurements in most cases, (iii) the short measurement time (a few seconds) enabling to multiply

measurements and to provide high resolution records of soil and sediment changes. The mineral magnetic measurements were carried out at the laboratory facility in CEREGE ("*Centre Europeen de Recherche et d'Enseignement des Geosciences de l'Environnement"*) at Aix-en-Provence, France. The frequency-dependent and low field magnetic susceptibility was measured using the MFK1-FA multifunction Kappabridge by AGICO. Natural or artificially imparted remanent magnetisation was measured using a 2G cryogenic magnetometer which has a has a noise level less than $10^{-12}Am^2$ (Figure 3-4).

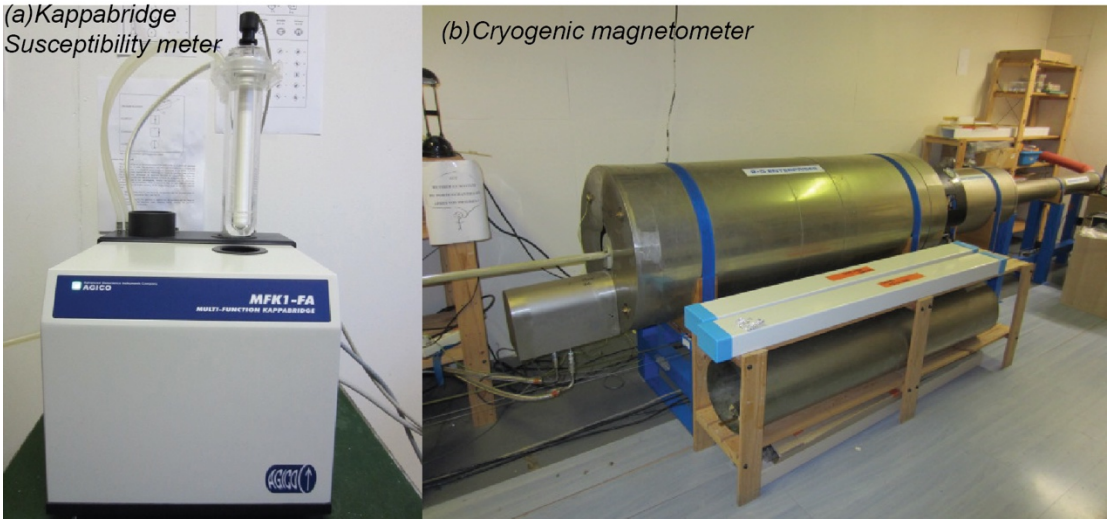

Figure 3-4: (a) The MFK1-FA Kappabridge multifunctional susceptibility meter used for frequency dependent magnetic susceptibility and the field dependent magnetic susceptibility measurements (b) The cryogenic magnetometer used to measure the remanent magnetisation.

The low field magnetic susceptibility is a measure of how easily a material can acquire an induced magnetisation. *Diamagnetic materials* have paired electrons in the electron shell and in the presence of an applied field results in a negative magnetic moment where the electron orbits become aligned anti-parallel to the external field, a common behaviour exhibited in materials rich in quartz, feldspars, calcite and water. *Paramagnetic materials,* unlike diamagnetic substances, are attracted to the applied magnetic field and are dependent on temperature. The magnetisation of these substances is lost when the external magnetic field is removed. Natural-iron bearing minerals such as olivine, pyroxenes, garnets, biotite and manganese exhibit this behaviour. In the case of *ferromagnetic materials,* the unpaired atoms that are present are closely and regularly spaced leading to a strong coupling that produce a permanent magnetisation commonly referred to as spontaneous magnetisation. This occurs

even in the absence of a magnetic field and is lost above a critical temperature known as ***Curie temperature*** which is specific to individual ferromagnetic material and above which the substances display paramagnetic behaviour.

The $\%X_{fd}$ strongly depends on the occurrence of ultrafine (around 10 nm size, depending on the type of crystal) superparamagnetic grains and thus provide a "magnetic grain size and origin" indicator where low values of $\%X_{fd}$ i.e. <2 % represent none or less than 10 % super paramagnetic (SP) grains, median values between 2 - 10 % represent a mixture of SP and coarser non-SP grains whereas high values between 10 - 14 % imply that virtually all the grains are SP ferrimagnets (Dearing 1999). Due to the relatively poor chemical stability of nanometric size minerals in the environment, the frequency dependence therefore strongly depends on specific processes leading to the (bio) precipitation and conservation of iron titanium oxides, such as microbial soil activity and its dependence on temperature, moisture and organic content. When preserved in moderately acidic conditions, it is therefore an excellent early diagenetic climate/paleoclimate proxy in soils and sediments.

The measurement of natural or artificially imparted remanent magnetizations in subsurface materials enables one to identify the occurrence of ferrimagnetic and antiferromagnetic remanence carriers (mostly iron oxides and sulphides) in subsurface materials. The intensity of remanence depends on the concentration of such minerals. Moreover, when combined with low field magnetic susceptibility (which depends on diamagnetic, paramagnetic and ferromagnetic components) and with frequency dependence (which depends on the superparamagnetic content), the natural and artificial remanences are good proxies of the magnetic mineralogy and magnetic grain size.

b) Method for Magnetic Susceptibility

The measurement was carried out using a Kappabridge MFK1-FA multifunctional magnetic susceptibility meter at room temperature with an accuracy range within ± 0.1%. The sensitivity of this apparatus is such that it is able to correct for the errors that arise from the contribution of the plastic holder and container. For each sample, measurements were made at the initial frequency (F1; an operating frequency of 976 Hz), measuring field strength of 2 – 727 A/m (Pokorny et al. 2011). The initial magnetic susceptibility measurement (k) is defined as per unit volume of material and was converted to mass susceptibility (x) using the mass of the samples.

Frequency dependent magnetic susceptibility was carried out using 2 frequencies; F1 (operating frequency of 976 Hz, measuring field strength 2 – 700 A/m, measuring range of 0.9 SI units and a sensitivity of 4 x 10^{-8} SI) and F3 (operating frequency of 15616 Hz, measuring field strength 2 – 200 A/m, 0.7 SI measuring range and a sensitivity of 12 x 10^{-8}) as defined by Pokorny et al. (2011). The frequency dependency was then calculated as a percentage of the low frequency magnetic susceptibility using the formula below (Dearing et al. 1996):

$$x_{fd} = \left(\frac{x_{lf} - x_{fd}}{x_{lf}}\right) x\ 100\ \%$$

Where x_{lf} and x_{hf} are the mass susceptibilities at the lower (F1) and higher (F3) frequencies respectively and x_{fd} is the percentage frequency dependency of the material. Blank samples were analysed at the beginning and after every five samples to monitor the integrity of the results obtained.

c) Method for Magnetic Remanence Measurements

The measurement of the remanent magnetisation was done using the 2G superconducting cryogenic magnetometer on discrete oriented soil and sediment samples. The cryogenic magnetometer is equipped with Superconducting Quantum Interference Device Sensors (SQUIDS) that allows for uniform demagnetisation and measurement of remanent magnetism in the sample through a 3-axis pass on the discrete samples after exposure to the magnetic fields at stepwise increments from 0 to 100 mT (Figure 3-4) with the total magnetic moment noise level less than 10^{-12} Am^2. The parameters that were obtained from this instrument include the Natural Remanent Magnetisation (NRM), Anhysteretic Remanent Magnetisation (ARM) and Isothermal Remanent Magnetisation (IRM) /Saturation Isothermal Remanent Magnetisation (SIRM) at 0 mT, 2.5 mT, 5 mT, 10 mT, 15 mT, 20 mT, 25 mT, 30 mT, 35 mT, 40 mT, 50 mT, 60 mT, 70 mT, 80 mT and 100 mT.

Generally, when a sample becomes magnetized, the magnetisation will remain parallel or very close to the induced fields. In order to determine the ***Natural Remanent Magnetisation (NRM)***, oriented samples were introduced into the SQUIDS detector to enable the measurement of the strength of magnetisation of the natural materials. A magnetic pulse charger was then used to generate strong magnetic fields (at 30 mT and 100 mT), which alter

the magnetic intensity of the samples. After exposure to each successive magnetic field, the remanent magnetisation was measured.

The grain size dependent variables ARM_{30mT}, SARM (ARM_{100mT}) and concentration dependent variables IRM_{-300mT} and SIRM (IRM_{1T}) measurements were carried out on the soil and sediment samples at room temperature. In ***Anhysteretic Remanent Magnetisation (ARM)*** measurements, magnetic grains gradually become anhysteretic following the reduction of the alternating field (AF) in the prevailing direction. In this study ARM was achieved by applying alternating fields (30 mT and 100 mT) gradually decreasing amplitude on oriented samples using the magnetic pulse charger stepwise by saturating the samples with the highest intensity at 100 mT, followed by reversal at -30 mT and a final demagnetisation at -100 mT (Table 3). ***Isothermal Remanent Magnetisation (IRM)*** was carried out by progressively increasing the intensity of the magnetic fields followed by a reversal of this field. In this case, 300 mT field was applied on the samples followed by saturation at 1T and a reversal at -300 mT at room temperature. The assumption in this case is that the value obtained at IRM_{1T} corresponds to a magnetic field strong enough to saturate both "soft" ferrimagnetic spinel in grains such as magnetite and maghemite, and "hard" poorly ferromagnetic, corundum structure magnetic minerals such as hematite or goethite. It is thus referred to as ***Saturation Isothermal Remanent Magnetisation (IRM).*** In contrast, the reversed magnetic field of -0.3 T would preferentially re-saturate the magnetization of soft minerals in a new direction. Duplicate samples were analysed at the beginning and after every 5 samples to monitor the integrity of the results obtained.

Table 3: Induced magnetic field on sediment and soil samples using a pulse magnetizer from ARM and IRM measurements.

Magnetisation	**ARM**	**IRM**
Step 1	100 mT	300 mT
Step 2	-30 mT	1 T
Step 3	-100 mT	-300 mT

3.1.7 X-Ray Fluorescence (XRF) Analyses

a) Rationale

The XRF spectroscopy is a fast, non-destructive method that is widely used to provide high-resolution geochemical profiles of all elements present within a sample in a very short period of time thus its utility as a powerful tool in palaeolimnology and land use processes. In this method, photoelectric fluorescence of characteristic x-rays (generated by accelerating electrons in a tube) from a sample is stimulated by irradiation of a primary source. The secondary energies generated are characteristic of the elements present in the sample. The method can be used to detect the elemental compositions of soil and sediments, which can be used to understand the interactions and linkages of the various elements to environmental changes.

b) Method

In the preparation of 19 discrete soil samples and 12 sediment samples from Lake Rutundu, 500 mg of sediments were homogenized using an agate pestle and mortar and compressed into pellets. On the other hand, whole core scans for the sediment from Sacred Lake and Lake Nkunga, were carried out on the U-channels. The samples were analysed using an ARTAX Brunker AXS x-ray Spectrometer suitable for multi-element analysis which offers a spatial resolution down to 70 µm. The pellets were scanned at a high voltage of 50 kV under a current of 704 µA at 60 seconds per spectrum while the cores were scanned at 1 mm resolution and 20 seconds exposure time per spectrum at 35 kV and a current of 1142 µA. In order to ensure the integrity of the data, two discrete pellets and SAL – V section from the Sacred Lake core were used as duplicates to monitor the whole range of elements (detection limit 6 sigma; results below detection limit = 4 ppm) detected in the samples.

3.1.8 X-Ray Diffraction (XRD) Analyses

Bulk mineralogical analyses were carried out on selected 54 soil and 25 sediment samples that were treated with H_2O_2 (for 3 – 4 days) to eliminate the organic matter content, and with HCl (10 % for 12 h) to eliminate any calcium carbonate present in the samples. The samples were then repeatedly rinsed with deionized water and centrifuged at 4000 rpm until a neutral pH was reached. These samples were then dried at 35° – 40 °C for 24 hrs, sieved at 200 µm and homogenized into fine powder using agate pestle and mortar and 3 mg (± 0.001 mg) mounted in an aluminium holder for analysis.

For clay samples, 17 soil and 10 sediment samples from the inventory were elected for analysis. A drop of sodium metaphosphate was added to each sample to assist in the dispersion of particles; thereafter, the samples were allowed to settle in a 20 cm long tube for 2 hours after which 10 cm of the suspended material was collected. This settling step was repeated several times by adding more deionized water to the samples, which were then agitated, after which the sediments were allowed to settle until there were no suspended particles in the 10 cm section of the tube. The collected material suspended material was dried at 35° – 40° C for 24 – 48 hours. The dry sample was homogenized and mixed with deionized water in 10 mm vials and mounted on a square (1 x 1 cm) slide in triplicate as follows:

a) Untreated XRD mount i.e. normal oriented sample dried at room temperature overnight. This mount was used for identification of the illite group of clays which are distinguished by peaks at 10 Å, 5 Å and 3.33 Å. Overlaps with the peaks of quartz at 3.34 Å and iron rich clays at 5 Å led to the selection of the 10 Å peak as characteristic of the illite clays present;

b) Glycolated XRD mount was dried at room temperature and later glycerol was added to the sample before analysis. This mount was used to identify the kaolinite group of clays which are distinguished by peaks at 3.57 Å and 7.2 Å. Whereas it is possible to have both chlorite (3.53 Å and 7 Å) and kaolinite in one sample, the 7 Å was selected for the identification of dehydrated kaolinite unaffected by glycolation; and

c) Heated XRD mount was oven heated at 500° C for 3 hours. This mount was used to identify the chlorite clays which are distinguished by peaks at 14 Å, 7 Å, 4.72 Å and 3.53 Å due to their diverse properties. During the high heat treatment most of the chlorites collapse and the 14 Å peak was selected to be indicative of this group following the identification of the other groups of clays.

Both bulk and clay mineralogy of soil samples were analysed in 2012 at the IRD laboratory in Bondy using a Siemens D500 diffractometer (with a relative error of 1% corresponding to the counting statistical error) with Ni-filtered Cu Kα radiation at 40 kV and 30 mA. Bulk samples as well as the < 2 mm fraction were scanned from 2° to 70° 2θ, for 2 seconds every 0.02° in a rotating aluminium sample-holder. For the clay mineralogy, the oriented samples were scanned from 2° to 15° 2θ with counting for 2 seconds every 0.02°.

Both bulk and clay mineralogy of the sediment samples were analysed in 2014 at the IRD laboratory in Bondy, using a Panalytical X'Pert Powder diffractometer with Ni-filtered Cu Kα operating at 40 kV and 40 mA with a relative error of 1% corresponding to the counting statistical error. The clay samples were scanned from 2° to 15° 2θ with counting for 2 s every 0.02°. The semi-quantification of the bulk samples was carried out through the determination of the percentage of diffracted surface that can be attributed to individual peak areas of characteristic minerals. For the clay samples, the peak areas, though present, were too small for peak area characterization. In order to ensure the integrity of the data, five laboratory duplicates were mounted to monitor the whole range of mineralogy detected in the bulk and clay samples.

3.1.9 Elemental Carbon and Nitrogen and Stable Isotopes Analysis

a) Rationale

The range of %C in lake sediments can range from <1 to 40% with the higher values reflecting an increase in %C input from OM in the watershed or increase in productivity of a lake (Meyers & Teranes 2001). The changes in %C can also be directly linked to the inorganic matter deposited where a decline in %C can be attributed to an influx of inorganic matter (Meyers and Teranes 2001). Further, microbial processes during sedimentation and burial may alter the amount of carbon present by reducing the %C content. A comparison of the %C to %N or C/N in sediments is a general indicator of OM deposited. Different plants have distinct C/N ratios: vascular land plants have a relatively high C/N ratio (above 20) while algae tend to have lower ratios that are typically below 10 (Meyers & Teranes 2001). By analysing the C/N ratio of lake sediments it is possible to make inferences as to the different OM sources.

$\delta^{13}C$ is another useful proxy for the differentiation of the type of OM deposited in sediments (Meyers & Teranes 2001). There are two isotopes of carbon, $\delta^{12}C$ (99% of all carbon) and $\delta^{13}C$ (1%), whose different atomic masses and their relative abundance in sediments are dependent upon environmental, chemical and biological processes. The $\delta^{13}C$/ $\delta^{12}C$ value of plant material is affected by the concentration of $\delta^{13}C$ in the environment, the photosynthetic pathway (C_3, C_4 or CAM) used and the stomatal conductance of the plant (O'Leary 1988). In general, algae and C_3 vascular plants tend to have similar $\delta^{13}C$ values (-30 to -25‰) compared to C_4 plants, which have values of about -10‰ (Meyers & Teranes 2001). Aquatic macrophytes, on the other hand, have a wide range of $\delta^{13}C$ values from -30 to -10‰ due to the varied environmental

conditions that lead to their production (Meyers & Teranes 2001). Emergent macrophytes tend to have more negative values closer to land plants while the submerged macrophytes tend to have values that are more positive than that of the algae and land plants (Meyers & Teranes 2001).

Nitrogen isotope is an indicator of past palaeoproductivity and availability of nitrogen to aquatic primary producers (Meyers & Teranes 2001). However, in lacustrine environments, nitrogen is less widely used in comparison to carbon isotopes. The $\delta^{15}N$ ratio is representative of the isotopic discrimination of inorganic nitrogen in aquatic and terrestrial plants (Meyers & Teranes 2001) and the values represent the utilization of dissolved inorganic nitrogen by aquatic plants and nitrogen fixation by plants.

b) Method

Sediment and soil samples from the three lakes and along the chosen transect were analysed for elemental C, N and the stable isotopes of C ($\delta^{13}C$) and N ($\delta^{15}N$). For Lakes Nkunga and Sacred, analysis was done on samples at every 1 cm, whereas for Lake Rutundu, the analysis was carried out every 2 cm. The soil and sediment samples were attacked using HCl to eliminate any carbonates that may have been present. These samples were later dried at 40º C for 24 hrs and ground using an agate pestle and mortar, weighed and encapsulated in tin boxes for the subsequent elemental and stable isotopes analyses. A total of 268 samples were analysed using a fully automated isotope analyser, the Thermoscientific Flash 2000 organic elemental analyser (C/N), coupled with Thermoscientific Delta V advantage isotope ratio mass spectrometry for $\delta^{13}C$ and $\delta^{15}N$ measurements. Reference material was used to monitor the accuracy of ranges detected at the beginning, after every 10 samples and at the end of the complete sample analysis.

3.1.10 Lipid Biomarker Analyses

a) Rationale for n-alkanes

n-alkanes are hydrocarbon compounds of straight chain alkanes produced by a broad range of organisms and are relatively stable over time. Usually, higher plant leaf waxes contain C_{27} - C_{33} while algae and plants are dominated by C_{17} - C_{19} (Meyers & Ishiwatari 1993). The sources of sediments, environment of formation and organic matter diagenesis affect the composition of n-alkanes present in a sampled material. This has led to the development of indices such as

the Average Chain Length (ACL) (Maffei 1996) and Carbon Preferential Index (CPI) (Bray & Evans 1961) that are indicators of the source and evolution of organic matter in soils and in the palaeoenvironment (Cranwell 1973; Pancost & Boot 2004). Usually, higher plant leaf waxes contain long chain alkanes (C_{25} - C_{31}) with a strong predominance of odd-over-even carbon number, which is expressed as CPI and reflects a terrestrial origin for organic matter (Collister et al. 1994). The microbial alterations of these shorter alkane compounds rarely preserve the odd-over-even predominance. Bacteria, on the other hand, produce C_{12} - C_{28} with no marked odd-over-even preference. The ACL of alkanes are used to differentiate between predominantly higher plants derived organic matter (OM) (ACL >25) and degraded or microorganism derived OM (ACL <25). This is because long chain n-alkanes are derived from terrestrial vascular plants that show predominance of odd-over-even carbon number, whereas degraded materials or the presence of microorganisms in organic matter display a predominance of even homologues. The odd-over-even predominance of n-alkanes is influenced by the maturity and biodegradation of organic matter leading to an increase or decrease of this index. Generally, high CPI values (>10) are typical of fresh higher plants, while values <10 indicate the degradation of organic matter or biomass rot. CPI values around 1 are characteristic of degraded organic matter and/or the presence of large amounts of microorganisms.

In order to supplement the information obtained from the ACL and CPI values, another index, the Terrestrial – Aquatic Ratio (TAR) (Cranwell 1973), is used to determine the extent of terrestrial and algal input of organic matter. This index compares the relative abundance of long chain n-alkanes derived from terrestrial plants (nC_{27}, nC_{29} and nC_{31}) and short chain n-alkanes (nC_{15}, nC_{17} and nC_{19}). The ratio is defined as:

$$TAR = (nC_{27} + nC_{29} + nC_{31}/nC_{15} + nC_{17} + nC_{19})$$

If this ratio >1, the input is considered as terrestrial and values <1 present a predominance of algal input (Cranwell 1973; Fang et al. 2014; de Souza et al. 2011; Wang et al. 2013).

The relative contributions of terrestrially derived biomass are indicated by the presence of C_{27}, C_{29}, C_{31} and C_{33} alkanes. The enrichment of C_{27} in most cases is an indicator of tree biomass dominance, whereas the enrichment of C_{31} and C_{33} are representative of grass biomass enrichment (Eglinton & Hamilton 1967). A standard ratio that defines this relationship is the C_{27}/C_{31} that provides insights on the terrestrially derived organic matter sources. This is an

indirect indicator of the prevailing environmental conditions during the time of deposition of the n-alkanes in soils and sediments. This ratio has been used to reconstruct the environmental representation of tree (C_{27}) versus grass (C_{31}) dominance in terrestrially derived material (Cranwell 1973; Ficken et al. 2000; Sojinu et al. 2012; Fang et al. 2014).

Possible relationships between n-alkane chain and climate have been investigated indirectly from sediments, atmospheric dust and stratigraphic sections (Castaneda et al. 2009). According to Dodd & Poveda (2003) in a study carried out in the Pyrenees, the ACL appeared to be related to altitude where greatest values were at extreme elevations i.e. the high and low altitudes. This was attributed to the adaptation of plants, in particular *Juniperus communis* during summer (at low elevation), winter (at high elevation) and droughts at low elevation when water is inaccessible to the plants, creating this similarity in effect. Despite the findings, Dodd and Poveda (2003) did not find a significant relationship between the climate data (rainfall and temperature) and ACL values. A further study by Rommerskirchen et al. (2003) has linked an increase in ACL to an increase in latitude. This, although seemingly useful, has not been widely applied.

b) Rationale for GDGTs

Glycerol dialkyl glycerol tetraethers (GDGTs) are membrane lipids of both archaeal and bacterial origin containing two long alkyl chains attached to glycerol anchors at both ends and are found in soils and sediments. Isoprenoid GDGTs (iGDGTs) are derived from archaeal communities (*Thaumarchaeota* and *Euryarchaeota*) in marine environment (Figure 3-5) and consist of cyclopentyl moieties 0 – 3 (i.e. iGDGT 1 – 3) as well as creanarcheol, an iGDGT consisting of 4 cyclopentane rings with an additional cyclohexane moiety (Sinninghe Damsté et al. 2012; Schouten et al. 2013; Pearson & Ingalls 2013). Branched GDGTs (BrGDGTs) are lipids consisting of a straight alkyl chain with 28 C atoms and two additional methyl branches at positions 13 and 16 (i.e. 13, 16-dimethyl octacosane; Figure 3-5).

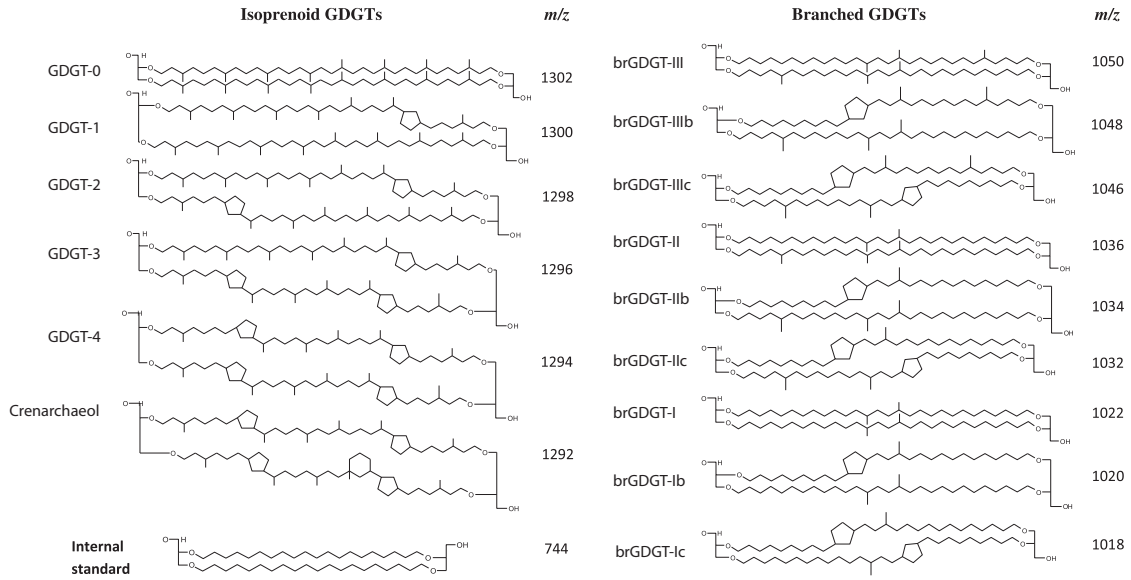

Figure 3-5: Structure of iGDGT and brGDGT adapted from (Tierney 2012) as discussed in this work. The iGDGT (predominantly archaeal origin) nomenclature is derived from the presence of the cyclopentane (zero to two) moieties present in the basic structure assigned as GDGT-x where x denoted the number of cyclopentane moieties present in the alkyl backbone structure. The structure of the brGDGT displays the presence of the cyclopentane moieties (identified as opposite those of iGDGTs through nuclear magnetic resonance (NMR) and stereochemistry studies) and a basic structure containing methyl (four to six) branches usually a 13,16-dimethyloctacosane typical of a bacterial membrane lipid. IS represents the C_{46} synthesized internal standard.

Advances in analytical techniques have played an essential role in the determination of the GDGT biomarker. The recent employment of liquid chromatography (LC) in combination with mass spectrometry (MS) extended the range of detectable molecules to higher molecular weight and high polarity such as the GDGTs (Hopmans et al. 2000; Sachs et al. 2013). The use of these membrane lipids synthesized by archaea and bacteria is built upon the principle that cell membrane structures adjust their rigidity in response to environmental changes by altering the number of double bonds or branches (Tierney et al. 2010; Sachs et al. 2013).

The most common application of the relative abundance of iGDGTs is in the marine environment for the reconstruction of sea surface temperature using the TEX_{86} (Tetraether index of Tetraethers consisting of 86 carbon atoms) proxy (Schouten et al. 2002) that relies on a linear relationship between the number of cyclopentane rings and Sea Surface Temperatures (i.e. the number cyclopentyl rings increases with increase in SST; Schouten et al. 2002). Although this relationship is widely accepted, the dataset by Schouten et al. (2002) recognized the importance of salinity in the relative composition of GDGTs derived from archaea.

The first investigation of iGDGTs in the lacustrine environment and the extended application of the TEX_{86} proxy was carried out by Powers et al. (2004; 2005) where the mean annual Lake Surface Temperature (LST) was reflected in TEX_{86} variations. Later applications of TEX_{86} in large lake systems demonstrated its potential use as a lake surface temperature proxy (Blaga et al. 2009; Bechtel et al. 2010; Tierney et al. 2010b) especially where little terrestrial input exists. However, this proxy is not often applicable to all lacustrine systems where the iGDGTs are frequently low in abundance and the Branched to Isoprenoid Tetraether (BIT) Index is high (Blaga et al. 2009). The BIT index (Hopmans *et al*. 2004) was developed as a proxy of terrestrial input into the marine environment that is dominated by iGDGTs and represents the ratio of brGDGTs to iGDGTs. As a rule of thumb where BIT > 0.3, the use of TEX_{86} as a palaeothermometer is impractical as the results obtained are unreliable due to the high proportion of brGDGTs (Hopmans et al. 2004; Weijers et al. 2006; Blaga et al. 2009). Further the production of iGDGT-2 by sedimentary *Euryarchaeota* through anaerobic oxidation renders the application of TEX_{86}inappropriate leading to the introduction of GDGT-2/crenarchaeol ratio as a control value (Weijers et al. 2007).

Whilst iGDGTs occur mainly in open oceans and lakes, the branched GDGTs (brGDGTs) have been extensively found in soils, peats, hot springs, rivers, seas and lake sediments (Weijers et al. 2006; Liu et al. 2010; Schouten et al. 2002; Wu et al. 2013). The subsequent studies of GDGTs therefore led to their utility in these environments (Powers et al. 2004; Weijers et al. 2006; Peterse et al. 2009; Blaga et al. 2010; Pearson et al. 2011; Loomis et al. 2012). Since the TEX_{86} index displayed disparity in the lacustrine environment due to a relatively high proportion of brGDGTs, some researchers applied the Methylation (MBT) and Cyclization (CBT) indices of brGDGTs to reconstruct lake pH and Mean Annual Air Temperature (MAAT) (Sinninghe Damsté *et al*. 2009; Tierney & Russell 2009; Naeher *et al*. 2014). The controlling factors that affect the relative abundance of the brGDGTs in soil was first investigated by Weijers *et al*. (2007) where from a global dataset the differing abundance and structural differences was found to correlate with pH and air temperature. These relationships were expressed as follows: (i) the number of cyclopentyl moieties displays a positive correlation (R^2 = 0.70) to soil pH through the cyclization of brGDGTs (CBT) and (ii) the number of methyl branches positively correlates (R^2 = 0.62) to Mean Annual Air Temperature (MAAT) and to a lesser extent is negatively correlated to pH (R^2 = 0.37) through methylation of brGDGTs (MBT).

By combining both the MBT and CBT relationships, the MBT/CBT index was developed as a proxy for reconstruction of past MAAT and pH of soil samples. The MBT/CBT proxy developed by Weijers *et al*. (2007) was initially applied in peat bogs and soils (Weijers *et al*. 2007; Peterse *et al*. 2009, 2012; Sinninghe Damsté *et al*. 2000; Huguet *et al*. 2010; Weijers *et al*. 2011) and later applied to the lacustrine environment by Tierney & Russell (2009). However, in the application of this proxy in lake systems, researchers have found that the MBT/CBT proxy underestimates the MAAT and pH values (Zink et al. 2010; Tierney & Russell 2009; Tierney et al. 2010b). This discrepancy has been suggested to be due to simultaneous autochthonous and allochthonous sources of brGDGTs in lakes where the brGDGTs can be derived from soils, river tributaries and within the lake system itself in response to different environmental controls (Tierney & Russell 2009; Peterse et al. 2009).

The suggestion that the brGDGTs are also produced *in-situ* within the water column and in lacustrine sediments (Tierney & Russell 2009; Tierney 2012) meant that implementation of the MBT/CBT proxy as a reliable temperature indicator is dependent upon establishing the source of the brGDGTs. Studies on the *in-situ* lake production of the brGDGTs (Tierney & Russell 2009) evaluated the influence of temperature and pH on their abundances in tropical lake systems. These studies showed that there are complex dramatic changes in the *in-situ* production of GDGTs within one lake system (Tierney & Russell 2009); environmental controls such as temperature, pH and depth have been determined as key influences on the abundance of brGDGT in lakes from east Africa (Tierney et al. 2010). This determination led to the recalibration of the MBT/CBT proxy derived mean air temperature and inferred pH to consider environmental controls (Tierney et al. 2010) for east Africa. The BIT index from the east Africa regions lakes, on the other hand, was found to be an indicator of the production of crenarchaeol which displays a strong correlation with depth rather than the flux of brGDGTs (Tierney et al. 2010).

A new calibration developed using MBT' which is based on the seven most common brGDGTs in soils (Peterse et al. 2012) and their fractional was abundances later developed. This calibration estimates the mean annual air temperature and pH values from distinct localities and environmental settings (Sinninghe Damste et al. 2009; Tierney & Russell 2009; Coffinet et al. 2017) thereby emphasizing the importance of local and regional calibrations. In an aim to improve the accuracy of the MBT/CBT proxy, Peterse *et al*. (2012) added new soil surface samples (126 in number) to the Weijers *et al*. (2007) global dataset, namely, Peterse *et al*.

(2009a) samples from China, Bendle *et al*. (2010) samples from the Amazon fan and Peterse et al. (2009b) samples from Svalbard creating a total sample size of 278 globally distributed soils. This led to the exclusion of brGDGT-IIIb and brGDGT-IIIc from the MBT relationship as they were frequently below the detection limit and comprised <1 % of the total brGDGTs on average. This led to the development of the MBT' index (Peterse *et al*. 2012) that is more directly influenced by the MAAT (since the calibration comprised of surface samples only) and thus the recalibration of the MBT/CBT index using the MBT'. The application of the MBT'/CBT index in both soils and lakes (Yang *et al*. 2013; Woltering *et al*. 2014; Peterse *et al*. 2014) led to the conclusion that the MBT'/CBT over estimated temperatures at high latitudes than the original MBT/CBT proxy (Weijers et al. 2007) and therefore it is more suitable for reconstructions in the tropics.

For east Africa the MBT/CBT and MBT'/CBT calibrations from MAAT have been tested in Sacred Lake (Loomis et al. 2012), Lake Challa (Tierney et al. 2010) and Lake Tanganyika (Tierney & Russell 2009) sediments. Their performance as a palaeothermometer proxy has presented varying ranges of temperature changes from the LGM to the present (Loomis et al. 2012). In order to improve the performance of the palaeotemperature proxy, a new regional lacustrine calibration based on the fractional abundance of brGDGTs and the application of the Stepwise Forward Selection (SFS) method on Tierney et al. (2010) dataset that was expanded by Loomis et al. (2012) from 41 to 111 samples from east African lakes improved the accuracy and reduced the prediction errors across the dataset. This calibration by Loomis et al. (2012) through SFS was able to statistically test the significance between environmental variables and brGDGT data by sequentially adding variables based on the weight of the relationship to the brGDGT data. The application of the SFS calibration on a sediment core from Sacred Lake showed a 6.3° C warming between LGM and mid-Holocene followed by a 1.2°C cooling giving an overall temperature difference of 5.1°C between LGM and present (Loomis et al. 2012). This calibration improved the accuracy of temperature prediction in the regional dataset as well as in the Sacred lake LGM to present (Loomis et al. 2012).

3.1.10.1 Lipid Extraction

Two grams of sediments (10 samples from Lake Nkunga and Sacred Lake, 11 samples from Lake Rutundu) and twenty grams of soils (31 soil samples) were oven dried at 40° C for 48 hrs and then introduced in a Dionex extraction cell with cellulose filter and cotton (Figure 3-6). The extraction of the organic lipids was done using the DIONEX Accelerated Solvent Extractor

(ASE 100) using a 9:1 dichloromethane/methanol solvent mixture. Each sample was extracted over three cycles of 15 minutes each at 100° C using nitrogen gas (100 bar pressure) as illustrated in Figure 3-6.

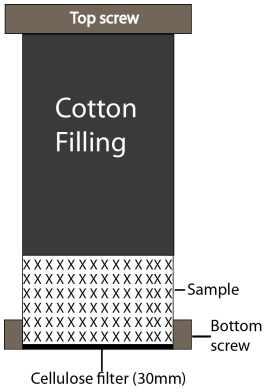

Figure 3-6: Illustration of dionex cell as prepared for extraction

The extracted lipids were dried under near vacuum conditions using a rotary evaporator in a water bath maintained at room temperature (Figure 3-7).

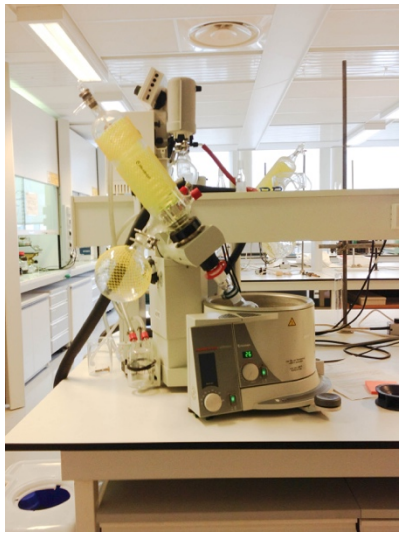

Figure 3-7: Rotary evaporator set up used for drying extracted lipids at near vacuum conditions

3.1.10.2 Lipid Separation

The separation of the total lipid extracts into polar and apolar fractions was carried out using an alumina column. The Al_2O_3 was put in the oven at 150°C for two hours before the separation. The column was conditioned by flushing with *n*-heptane : DCM (9:1, v/v) solvent,

which was then packed with the Al_2O_3. The elution was performed with two mixtures of solvents:

- *n*-heptane : DCM (9:1, v/v) for the apolar fraction (including *n*-alkanes)
- DCM : MeOH (1:1, v/v) for the polar fraction (including GDGTs)

The separated fractions were dried using the rotary evaporator under near vacuum conditions in a water bath at room temperature. These samples were transferred to four ml vials using DCM, after which they were dried under N_2 gas and dissolved in 1000 µl hexane prior to analysis. This process is summarized in Figure 3-8.

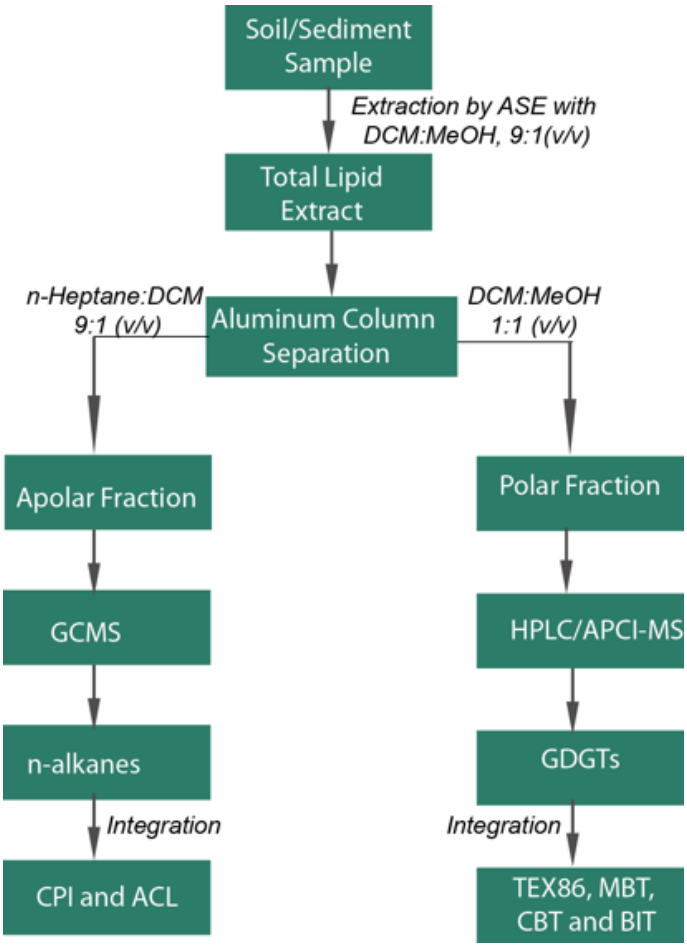

Figure 3-8: A diagrammatic representation of the processes involved in the extraction, concentration, separation and analysis of the biomarker fractions from the selected samples.

3.1.10.3 Analysis and Integration of Polar and Apolar Lipid Fraction

The apolar fraction was analysed using an Agilent 6890N gas chromatograph coupled to an Agilent 5973N mass spectrometer with electron impact at 70 eV. Separation was achieved using a Restek RTX-5 Sil MS silica capillary column (30 m × 0.25 mm ID, 0.50 μm film thickness) with constant flow of He carrier gas of 1 mL/min. The oven temperature was programmed to run from 50° C to 320° C in 20 minutes at a rate of 4° C/min. Samples were injected in splitless mode and the injector temperature was 280° C. Blank samples were used to monitor the precision of the ranges within the retention time of 0.048 seconds obtained after every ten samples. With measurements this precise, small changes in ambient operating conditions can dramatically affect retention time.

The polar fraction was analysed using a Shimadzu LCMS-2020, a High-Performance Liquid Chromatography Mass Spectrometer (HPLC-MS). Separation was achieved with a Prevail Cyano column (2.1 mm x 150 mm, 3 μm; Alltech, Deerfield, IL, USA) thermostat at 30°C, using a mixture of A and B (A= hexane and B= isopropanol) at 0.2 ml/min. Elution began at 99 % A/1 % B for 5 min followed by a linear gradient to 98 % A/2 % B in 45 min. A second linear gradient led to a mixture of 90 % A/10 % B in 10 minutes, maintained for 10 minutes and returned to the initial conditions (99 % A/1 % B) in 14 minutes, then maintained for 10 minutes. The injection volume was 10 μl. Single ion monitoring (SIM) of the $[M+H]^+$ ions were used to detect the GDGTs. Semi-quantification of the GDGTs was performed by comparing the integrated signal of the respective compound with the signal of a C_{46} synthesized internal standard, as described by Huguet et al. (2013). Bases on duplicate samples added after 10 samples, the HPLC/MS analysis error for GDGT quantification with the internal standard was ca. 10%. .

3.1.10.4 Integration of GDGT Results

3.1.10.4.1 Integration of Soil Results

For the soil samples, the MBT and CBT indices were calculated using Weijers et al. (2007)

$$MBT = ([I + Ib + Ic])/([III + IIIb + IIIc] + [II + IIb + IIc] + [I + Ib + Ic])$$

Equation 1

$$CBT = -\log([Ib + IIb])/([I + II])$$

Equation 2

The MBT' was calculated as using the calibration developed by Peterse et al. (2012) as follows:

$$MBT' = ([I + Ib + Ic])/([III] + [II + IIb + IIc] + [I + Ib + Ic])$$

Equation 3

Note I, II and III denote GDGT structures described in Figure 3-5, pg. 62 above.

The MAAT was estimated using the global soil calibration (*Equation 4*) developed by Weijers et al. (2007) and the extended calibration (*Equation 5*) introduced by Peterse et al. (2012) respectively.

$$MAAT = (MBT - 0.122 - 0.187 \times CBT)/0.020$$

Equation 4

$$MAAT = 0.81 - 5.67 \times CBT + 31.0 \times MBT'$$

Equation 5

pH for the soils were calculated using *Equation 6* developed by Weijers et al. (2007) and Peterse et al. (2012, *Equation 7*):

$$pH = (3.33 - CBT)/0.38$$

Equation 6

$$pH = 7.90 - 1.97 \times CBT$$

Equation 7

The BIT index was calculated as follows (Hopmans et al. 2004):

$$BIT = (I + II + III)/(I + II + III + IV)$$

Equation 8

TEX_{86} was calculated as follows:

$$TEX_{86} = (GDGT\,2 + GDGT3 + VI)/(GDGT1 + GDGT2 + GDGT3 + VI)$$ *Equation 9*

3.1.10.4.2 Integration of Sediment Results

The MBT and CBT indices were calculated according to Weijers et al. (2007, *Equation 1* and *Equation 2*). The fractional abundances *f(i)* of each brGDGT *i* is defined as:

$$f(i) = \ i/(I + Ib + Ic + II + IIb + IIc + III + IIIb + IIIc)$$

Equation 10

The pH function of the samples was calibrated through the application for the east Africa *Equation 11* regional calibration developed by Tierney et al. (2010):

$$pH = 10.32 - 3.03 \ \times \ CBT$$

Equation 11

Regional calibrations have the potential to provide more accurate temperature reconstructions in comparison to the existing global calibrations. Here two east Africa calibrations were used to estimate the MAAT. The first estimate was based on the MBT/CBT calibrations developed by Tierney et al. (2010, *Equation 12*) and the second, on the fractional abundance calibration by Loomis et al. (2012, *Equation 13*) and they were calculated as follows:

$$MAAT = 11.84 + 32.54 \ \times \ MBT - 9.32 \ \times \ CBT$$

Equation 12

$$MAAT = 2.54 + 45.28 \times MBT - 5.02 \times CBT$$

Equation 13

For comparison the palaeotemperature calibration based on the fractional abundances of major brGDGTs (MbrGDGTs) developed by Tierney et al. (2010, *Equation 14*) and Loomis et al. (2012, *Equation 15*) were applied as follows:

$$MAAT = 50.47 - 74.18 \times f(III) - 31.60 \times f(II) - 34.69 \times f(I)$$

Equation 14

$$MAAT = 36.90 - 50.14 \times f(III) - 35.52 \times f(II) - 0.96 \times f(I)$$

Equation 15

Finally, the SFS calibration developed by Loomis et al. (2012, *Equation 16*) was used as follows:

$$MAAT = 22.77 - 33.58 \times f(III) - 12.88 \times f(II) - 418.53 \times f(IIc) + 86.43 \times f(Ib)$$

Equation 16

3.1.10.5 Integration of n-Alkane Results

A total mass ion chromatograph typical of all series of compounds present was obtained from the analysis carried out. In order to detect the alkanes of interest, the base peak of the alkanes ion chromatograph m/z = 57 was selected for the identification of the alkanes in the $C_{12} - C_{34}$ range present in the samples. The identification was made based on the mass detected by the relative abundance of the peak area.The following calculations were done:

a) The average length of all n-alkanes (ACL)

$$ACL = \frac{\sum\left[(n_{14-35})*(nC_{14-35})\right]}{\sum(nC_{14-35})}$$

Equation 17

Where

n is the number of carbons in the n-alkane chain.
nC_n is the relative abundance of the n-alkane.

b) The average chain length of long chain n-alkanes (ACL_{lc}) i.e. $C_{25} - C_{33}$

$$ACLlc = \frac{\sum\left[(n_{25-35})*(nC_{25-35})\right]}{\sum(nC_{25-35})}$$

Equation 18

c) The Carbon Preference Index (CPI) describes the relationship of the number of odd number homologues over the sum of the even number homologues. High CPI values are typical for fresh plant biomass (CPI>10) and lower CPI values (CPI<10) indicate the degradation of biomass or can be related to the root biomass. Calculations were

done to determine the overall CPI (Equation 19) and the high alkane chain CPI (Equation 20) as indicated below:

$$OverallCPI = 0.5\left(\frac{\sum Odds\left[nC_{15-33}\right]+\sum Odds\left[nC_{17-35}\right]}{\sum Evens\left[nC_{16-34}\right]}\right) \qquad \textit{Equation 21}$$

$$CPI = 0.5\left(\frac{\sum Odds\left[nC_{25-33}\right]}{\sum Evens\left[nC_{24-32}\right]}+\frac{\sum Odds\left[nC_{25-33}\right]}{\sum Evens\left[nC_{26-34}\right]}\right) \qquad \textit{Equation 22}$$

d) The Terrigenous – Aquatic Ratio (TAR), enables the evaluation of the relative distribution of terrestrial organic matter and that of aquatic algal contribution. This was done using the following equation:

$$TAR = \left(\frac{nC_{27}+nC_{29}+nC_{31}}{nC_{15}+nC_{17}+nC_{19}}\right) \qquad \textit{Equation 23}$$

e) The P_{aq} proxy (Ficken et al. 2000) was used to differentiate the submerged aquatic macrophyte versus emergent and terrestrial plant input into the lakes based on n-alkane data of mid chain length (C_{23},C_{25}) to long-chain length (C_{29}, C_{31}). This was done using the following equation:

$$P_{aq} = \frac{C_{23}+C_{25}}{C_{23}+C_{25}+C_{29}+C_{31}} \qquad \textit{Equation 24}$$

3.1.11 Data Processing and Analyses

All data analysis and statistical tests were performed using in R software (v3.3.2) with Vegan (Oksanen et al. 2013), Rioja (Juggins 2017), Clam (Blaauw 2010) and Bacon (Blaauw & Christen 2011) packages. In order to establish if the results display any significant differences, a student T-test was carried out in R with a confidence interval of 95 % where linear regressions were performed. Figures used in this thesis are either original or redrawn and adapted from literature. Graphs were created in Matlab 2017b student edition and other figures were created using Adobe Illustrator CC 2018. Photographs were taken by the author unless otherwise stated.

4 RESULTS AND DISCUSSION

4.1 Introduction

This section focuses on the results obtained from the soil and sediment samples from the study area. Section 4.2 highlights the characteristic of the soil samples, providing context for the present-day conditions on Mount Kenya. Sections 4.3, 4.4 and 4.5 refer to Lakes Nkunga, Sacred and Rutundu sediments, respectively. These results correspond to objective one and provide a multi proxy representation of the Late Holocene. Section 4.6 addresses objectives 2 and 3. In this section, the evidence of key Late Holocene environmental and climatic events based on the analysed proxies are discussed and the research findings are evaluated in the context of the current knowledge of regional changes in eastern Africa's Late Holocene palaeoclimate and palaeoenvironment.

4.2 The soils in the study area

The surface soils are well-drained, moderately deep nitisols (Figure 2-10, pg. 34), with colour ranging from dark red to dark brown. The soils are friable to firm with a loamy to clayey texture depending on the sampling location (Figure 2-10, pg. 34). A gradation from nitisols to andosols with altitudinal decline is noted; the lower altitude soils are well drained and moderately deep, often derived from the weathered material from the surrounding catchment, unlike the high-altitude soils that are moderately shallow and well drained. At high altitudes (>3000 m) where the slope is steep, the soils are humic nitisols developed on undifferentiated pyroclastic rocks while the mid altitude soils (2000 – 3000 m) overlie the basalts of Mt. Kenya and Nyambeni hills and at low altitude (1600 – 2000 m) these soils cover the younger volcanics. Samples obtained from the high-altitude areas were from the ericaceous belt whilst those of the mid to low altitude slopes were collected from the montane forest and the cultivated foothills, respectively.

4.2.1 Characteristics of the Soils and Rocks from Nkunga Area

4.2.1.1 Surface Soils and Rocks

4.2.1.1.1 Mineralogy and Grain Size

This section describes the characteristics of soils and rocks from within the Nkunga crater, surface soils from Nkunga school farm and the soil profile from Nkunga area. The soils from within the Nkunga crater comprise 60 – 89 % silts, 7 – 38 % fine sands and 1 – 4 % clays (Figure 4-1). The minerals comprise plagioclase feldspars (46.0 – 90.0 %), haematite (0.5 – 21.0 %), diopside (4.8 – 22.0 %), halloysite (4.0 – 11.8 %), quartz (7.1 – 11.8 %), and small quantities of gibbsite (2.0 – 4.1 %) (Figure 4-1). The rocks (Figure 4-1) collected from the inner rim of the crater contain diopside and plagioclase feldspars and minor contributions from hematite and illite/muscovite. Of the feldspars from the rocks and soils, the predominant plagioclase feldspar is labradorite (3.20 Å) while sanidine (3.24 Å) is the most prominent K-feldspar. In the soil samples, the presence of minerals such as gibbsite, halloysite and hematite reflect weathering processes in the crater soils. Quartz is present in the soil samples but absent in the rock samples.

Seven samples from Nkunga school farm, adjacent to the crater, were selected for grain size analysis. These soils are clayey silts (fine sands: 0 % silts: 86 – 92 %, and clays: 8 – 14 %) with the exception of two samples; NKS 4 and NKS 5. These two samples (NKS 4 and NKS 5) display a coarser texture (sandy clays) with a higher proportion of fine sands (36 % & 41 % respectively), lesser amounts of silts (58 % and 53 % respectively) and clays (6 % and 7 % respectively) (Figure 4-2). The mineralogy comprises both weathering products and parent minerals in the surrounding volcanic area. Halloysite (20 – 33 %), plagioclase feldspars (13 – 28 %), quartz (14 – 24 %), magnetite (15 – 19 %) and hematite (14 – 19 %) are the dominant mineralogy of these soils (Figure 4-2). The three groups of clay mineral corresponding to characteristic peaks; illite (10.0 Å), kaolinite (7.3 Å) and chlorite (14.0 Å) were all identified.

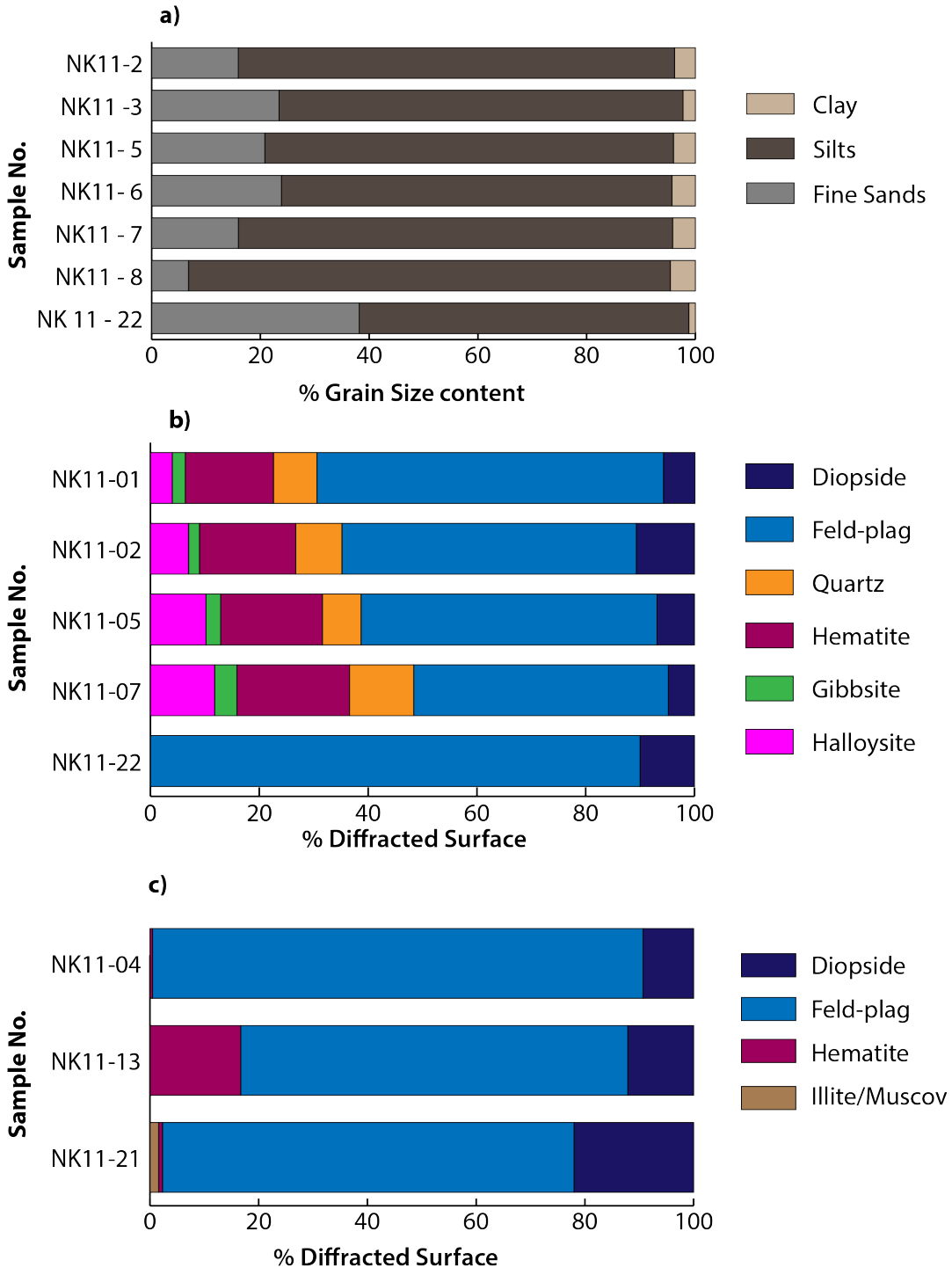

Figure 4-1: (a) the less than 200 µm grain size distribution and (b) and (c) the bulk mineralogy based on the percentage of diffracted surface of the soil and rock samples from the Nkunga crater. NB: Feld – plag denotes plagioclase feldspar while illite/Muscov denotes the total peak area occupied by Illite and Muscovite which could not be differentiated in the XRD spectrum of the bulk samples.

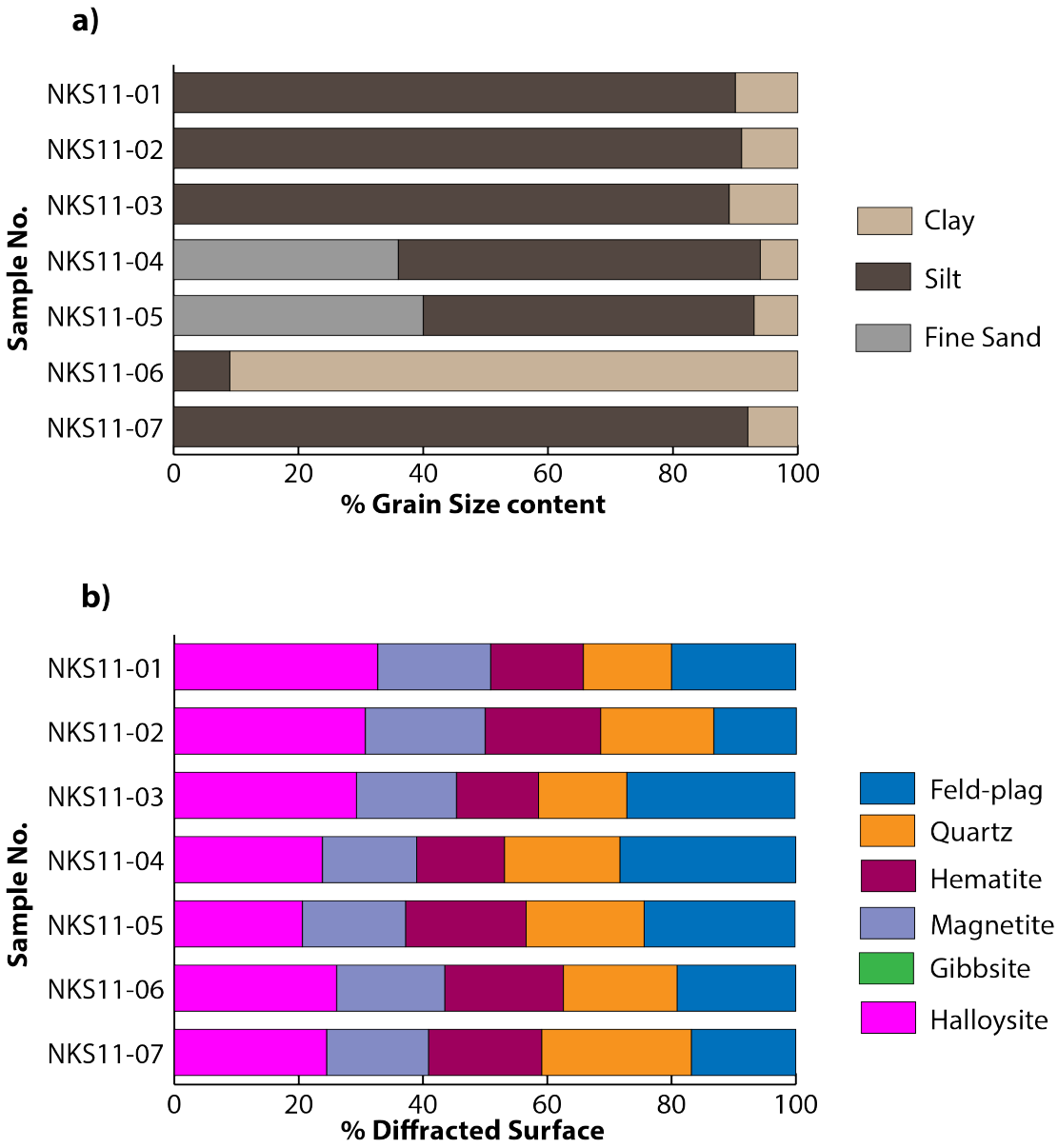

Figure 4-2: (a) Particle size distribution of the <200 µm soils from farms at Nkunga School (b) the bulk mineralogy from the percentage of the diffracted surface in samples from Nkunga. NB: Feld-plag denotes plagioclase feldspar composition in the samples.

Quartz is dominant in the soil samples but absent in the rock samples. Most likely this can be attributed to the aeolian deposition of fine-grained quartz sands from quartz rich neighbouring areas of exposed basement rocks (Mahaney 1990; Olago and Odada 1996).

4.2.1.1.2 Inorganic Geochemistry

The surface samples from the Nkunga area contain 17 detected elements (Al, Si, Ti, Ca, Cl, Cu, Fe, K, Mn, Nb, Ni, P, Rb, S, Sr, Zn, Zr). A principal component analysis of the variations of these elements in the various samples was carried out. The first principal component (PC1) accounts for 74.3 % of the variability while the second principal component (PC2) accounts for 12.7 % of the variability (Figure 4-3). PC1 positively correlates with Al, Cl, Fe, K, Mn, Nb, P, Rb, Ti, Zr and Zn, in relatively equal contributions of these elements that are preferentially mobilized through physical weathering, erosion, transportation and deposition as detrital materials. PC1 negatively correlates with Ca, Cu, Ni, S, Si and Sr, which reflect more likely the in-situ or locally constrained leaching and remobilisation processes (Figure 4-3). Thus, PC1 would be strongly controlled by the intensity of mechanical erosion/transportation processes. PC2, on the other hand, positively correlates with relatively soluble and poorly soluble elements such as Ca, Cl, Cu, K, Mn, Nb, Ni, P, Rb, S, Si, Sr, Zr and Zn. K, Rb, Si and Zn are the main contributors to this component inferring transported aeolian material alongside in-situ secondary chemical weathering and negatively correlates with Al, Fe and Ti (Figure 4-3). High PC2 values would be preferentially observed in accumulation zones, while PC1 high values would be preferentially observed in strongly weathered and leached materials.

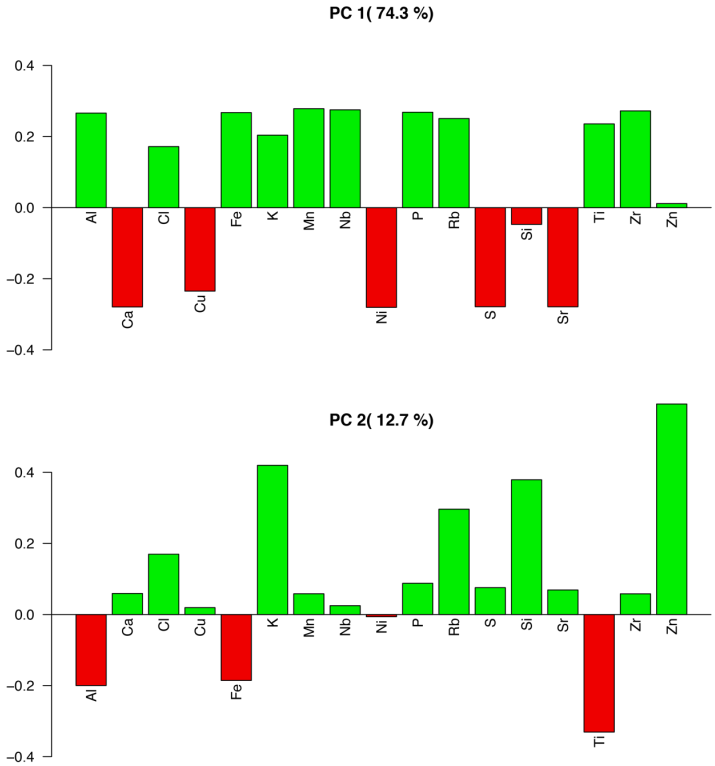

Figure 4-3: PCA of the elements from Nkunga area surface soils. Green bars represent the positive correlations while red represents negative correlations. The upper and lower panels show PC1 and PC2 respectively.

The surface soil geochemistry is characteristic of the siliciclastic origin of the soils which agrees with the mineralogy described in section 4.2.1.1, pg. 74. On the basis of the principal components analysis, Fe, K, Al, and Nb were selected as proxies of subsurface enhancement while Si was selected as representative of biochemical dissolution, remobilisation and enhancement. The selected elements were normalized against Ti. The PCA performed on the resulting ratios show that the first principal component (PC1) accounts for 62.4 % of the variability (Figure 4-4).

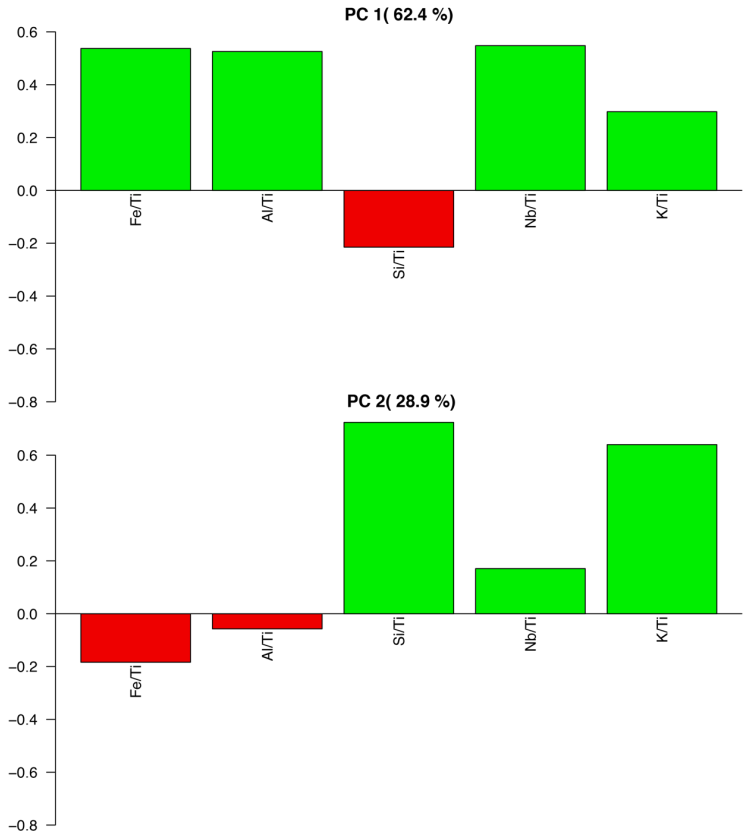

Figure 4-4: PCA of geochemical ratios from the soils in Nkunga area. Green bars represent the positive correlations while red represents negative correlations. The upper and lower panels show PC1 and PC2 respectively

Not surprisingly PC1 positively correlates with Fe/Ti, Al/Ti, Nb/Ti and K/Ti and negatively correlates with Si/Ti (Figure 4-4). These relations describe highly weathered rock, enriched in oxides and clays (K/Ti and Al/Ti). The second principal component (PC2) accounts for 28.9 % of the variability only (Figure 4-4); it positively correlates with Si/Ti, Nb/Ti and K/Ti and negatively correlates with Fe/Ti and Al/Ti (Figure 4-4). PC2 thus illustrates the input of biogeochemical weathering products such as silica, together with the input of strongly refractory aeolian material as suggested by the mineralogy (4.2.1.1, pg. 74).

4.2.1.2 Nkunga Area Soil Profile

4.2.1.2.1 Stratigraphy, Mineralogy and Grain size

In the Lake Nkunga soil profile, two horizons were identified: horizon A0 (0 – 15 cm) is a yellowish brown porous crumbly soil containing a mix of undecomposed and decomposed organic matter. Horizon B (10 – 125 cm) has a well-drained, deep brown and clayey nitisol containing organic plant roots (Figure 4-5).

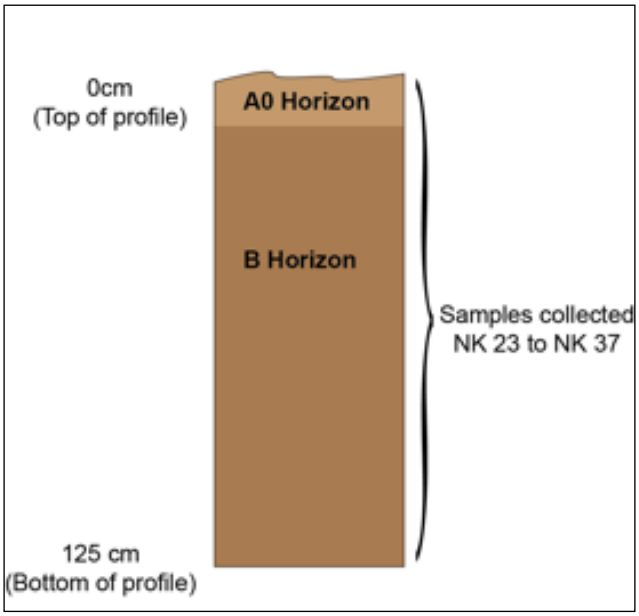

Figure 4-5: Description of soil profile sampled from Nkunga park gate showing the two identified horizons

The <200 µm fraction is texturally homogeneous (Figure 4-6), and comprises clayey-sandy silts (fine sands: 3 – 18 %, silt: 78 – 91 %, clay: 3 – 7 %) with higher content of fine sands in two samples: NK11-26 (18 %) and NK11-34 (17 %).

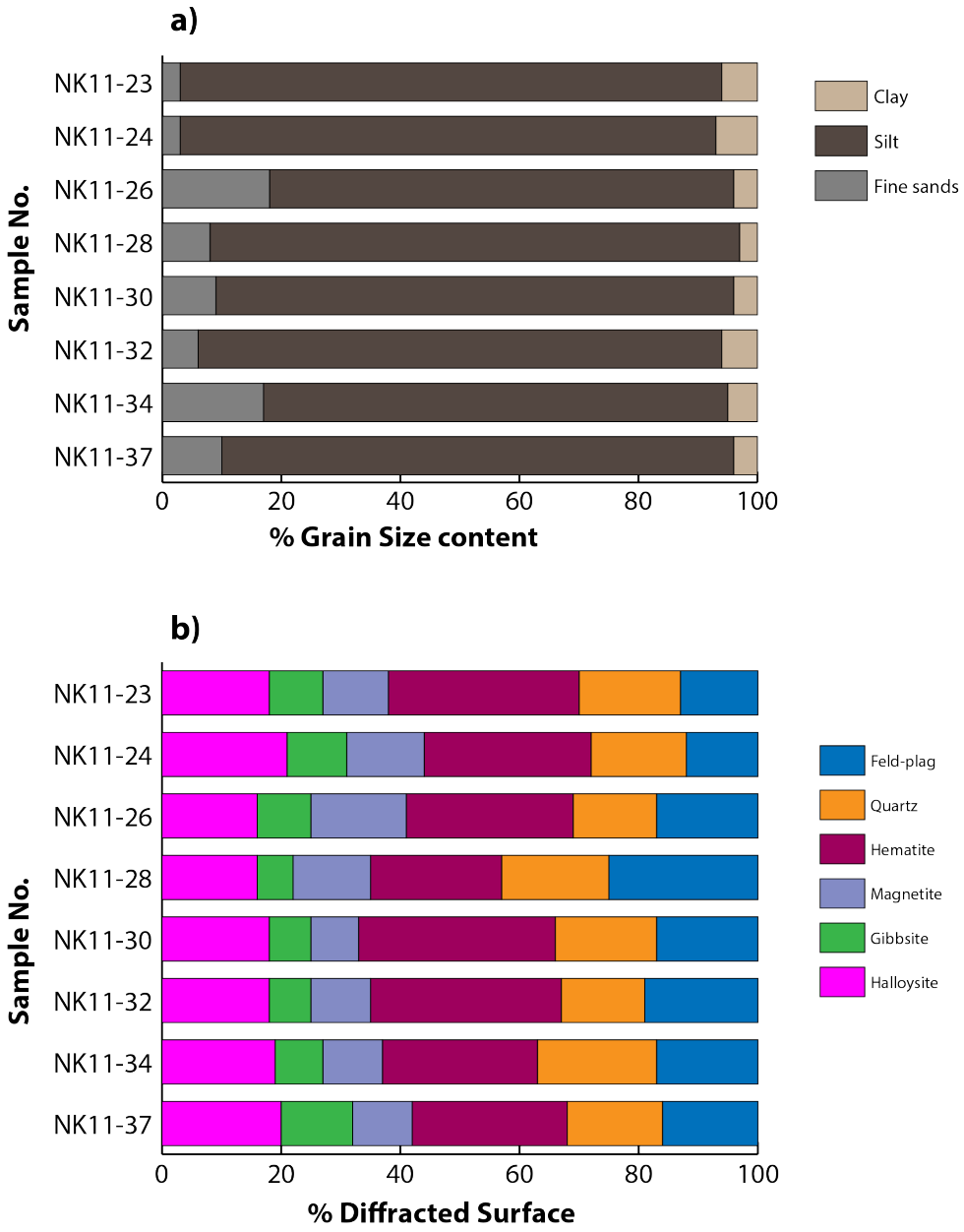

Figure 4-6: (a) Grain size distribution of <200 µm fraction and (b) bulk mineralogy of the soil profile at Nkunga. NB: Feld-plag denotes plagioclase feldspar composition in the samples

The mineralogy comprises plagioclase feldspar (12 – 25 %), hematite (22 – 33 %), halloysite (16 – 21 %), magnetite (8 – 16 %) and gibbsite (6 – 12 %). This bulk mineralogical representation is similar throughout the soil profile with no abrupt changes present. Kaolinite clay was detected throughout the soil profile while illite was detected in the topmost sample only.

4.2.1.2.2 Mineral Magnetics

The magnetic susceptibility displays a progressive increase down the soil profile. The bulk mass magnetic susceptibility values at low frequency (X_{lf}) range from 2.2×10^{-5} m^3kg^{-1} to 3.5×10^{-5} m^3kg^{-1} while at high frequency (X_{hf}) it is between 2.1×10^{-5} m^3kg^{-1} and 3.2×10^{-5} m^3kg^{-1} (Figure 4-7). The associated low and high frequency values of the magnetic susceptibility display a high linear correlation with R^2 value of 0.99 ($p < 0.001$).

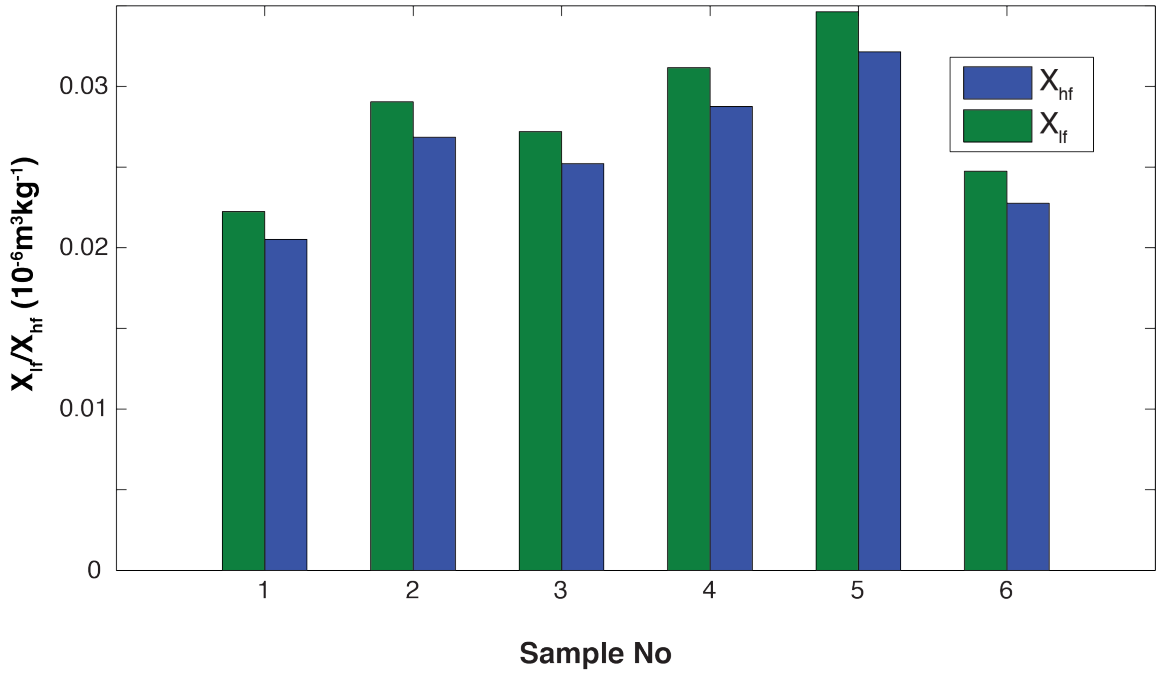

Figure 4-7: The relationship between the high and low frequency bulk magnetic susceptibility for selected samples from soil profile at Nkunga park gate.

The $\%X_{fd}$ shows a relatively high, and more or less constant value of 7 – 8 % along the soil profile. This indicates a remarkable enhancement in superparamagnetic grains, likely maghemite given the colour of the soil (consistent deep brown colour of the B - Horizon). No clear relationship can be observed between the X_{lf} and $\%X_{fd}$ (Figure 4-8), and the poor change of magnetic susceptibility and frequency dependence with depth strongly suggest a remobilisation of iron in the Nkunga forest soil, likely linked with the activity of iron-reducing and iron-oxidizing bacteria, which are the main mediators of organic carbon oxidation in tropical forest soils (Dubinsky et al. 2010).

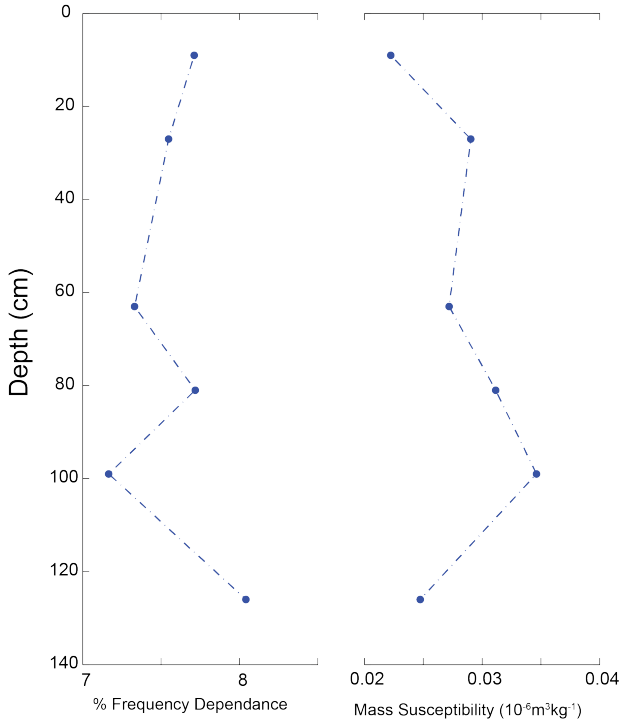

Figure 4-8: Bulk magnetic characteristics % X_{fd} and X_{lf} from the soil samples in the Nkunga area soil profile.

A total of four samples (two each from the surface and the soil profile) were selected for the NRM analysis. The demagnetization curves are generally scattered, suggesting the presence of highly viscous and soft components, as already illustrated by the high frequency dependence of magnetic susceptibility. Still, for the surface samples (NK 7 and NK 10) the MDF values were 22.1 mT and 14.8 mT, respectively, whereas from the soil profile (NK20 – 0 cm and NK37 – 125 cm) an MDF value of 2.5 mT was recorded. This possibly account for a relative enhancement of the surface in titanomaghemite of different grain sizes, seen as a "refractory" fraction compared to smaller unstable grains which would easily translocate into the soil profile. The NRM intensity of the surface sample NK 7 demagnetizes at 30.0 mT whereas the rest of the NRM intensities do not display clear demagnetisation curves (Figure 4-9).

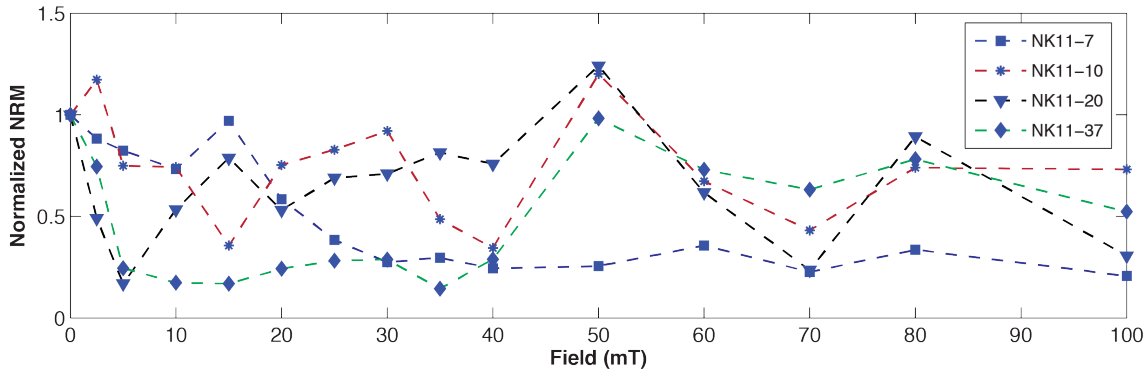

Figure 4-9: NRM profiles of the soils from Nkunga area.

4.2.1.2.3 Inorganic Geochemistry

The five samples selected for inorganic geochemistry, one from the A0 horizon and four from the B-horizon, display minimal variation in the single element abundance profile. The soils of the Nkunga soil profile contain 17 detected elements (Al, Si, Ti, Ca, Cl, Cu, Fe, K, Mn, Nb, Ni, P, Rb, S, Sr, Zn, Zr) and display no vertical variation with the exception of the upper 45 cm where a decline or increase is observed towards the top of the profile. Si, Al, Mn, Ca, K, Fe and Ti were selected as geochemically stable elements present in conservative geochemical environments (Boës et al. 2011). The variations of these elements (Figure 4-10) within the soil profile do not reveal any major change in the weathering regime or detrital inputs.

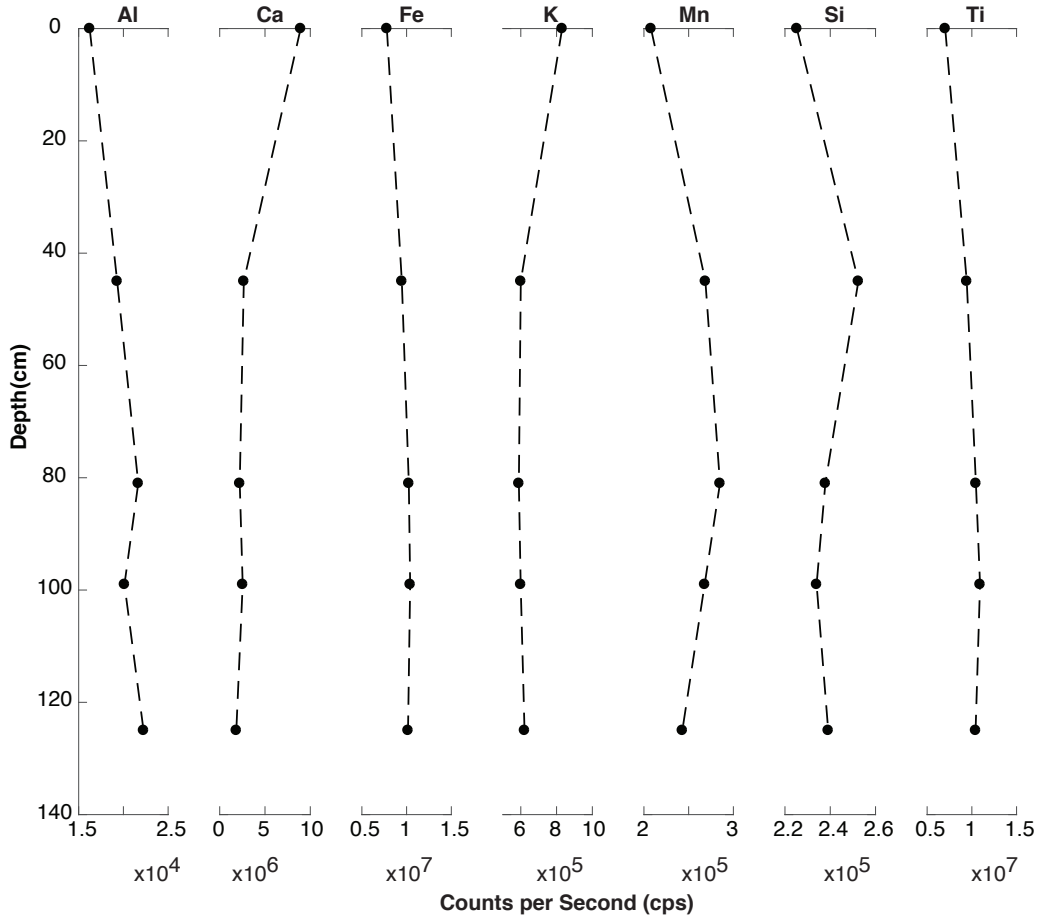

Figure 4-10: Single element inorganic geochemistry down the Nkunga soil profile.

Ca, Fe and K were normalized against Ti as proxies of changes in erosion, *in-situ* weathering and possible burning of vegetation, respectively (Figure 4-11). The Ca/Ti, Fe/Ti and K/Ti profiles display muted changes at the bottom of the soil profile and a relative increase in the upper 45 cm. The Fe/Mn shows a decline from the bottom of the profile to 80 cm where the

ratio stabilizes. In the upper 45 cm, the Fe/Mn ratio rises to the top of the profile (Figure 4-11). Based on the inorganic geochemical data (Figure 4-10 and Figure 4-11), the soil horizons were revised from the stratigraphic description above (Section 4.2.1.2.1, pg. 79). The B-horizon made of accumulated clay from the upper soil layer was designated 125 to 80 cm. This is due to the relative increase in Al in the profile and the decline in the lithogenic ratios (Fe/Ti and K/Ti). A relative increase in Mn and decline in the Fe/Mn ratio in the 45 -80 cm depth likely illustrates the fixation of Mn in a lower pH, organic rich and reducing soil environment. Indeed, this interval is a zone of eluviation and leaching (a possible E horizon) where hardly any change is observed in the all the proxies, while the upper section of the core from 45 to 0 cm represents the A and O horizons characterized by an increase in Fe/Mn (oxidizing environment) and in the geochemical elements of lithogenic origin.

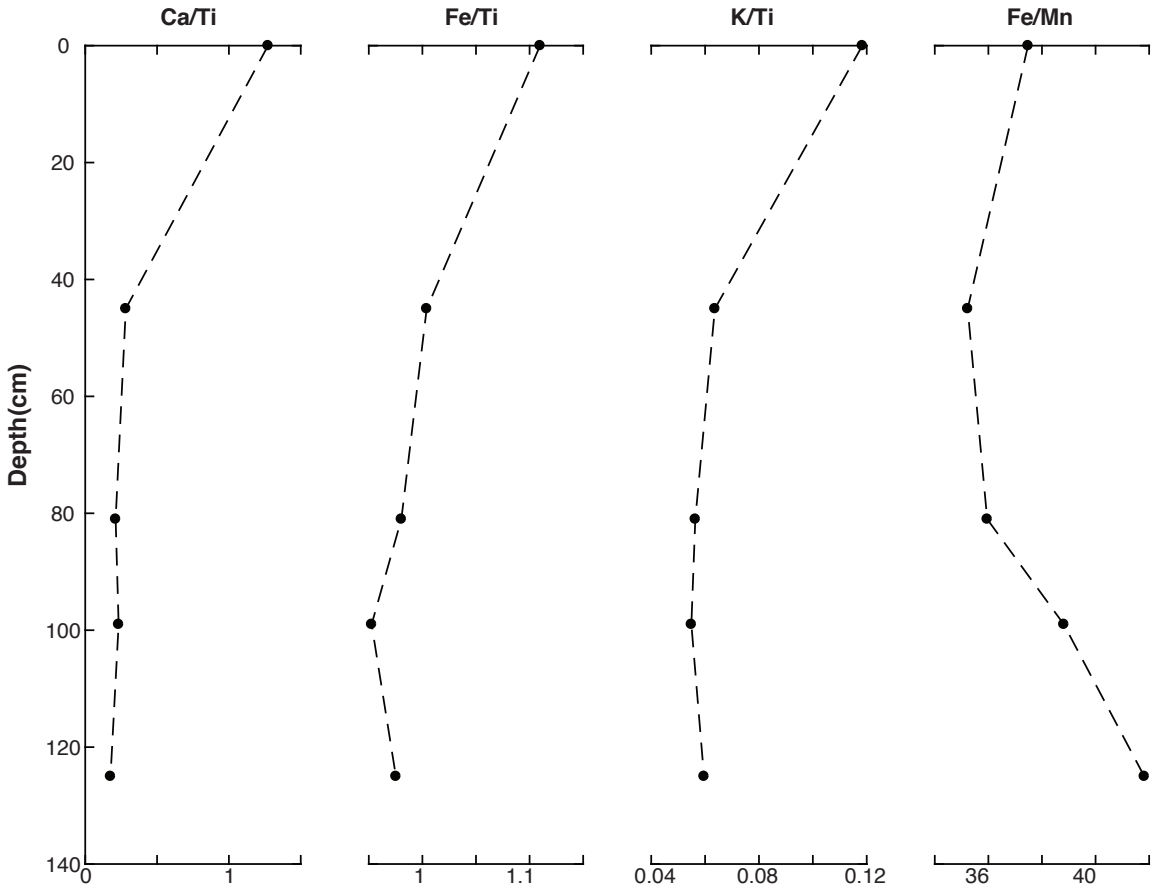

Figure 4-11: Ti-normalized elemental variations down the Nkunga soil profile.

4.2.1.2.4 Organic Geochemistry

4.2.1.2.4.1 Carbon, Nitrogen and their Isotopes

The range of carbon (%C) is from 3.2 % to 4.8 % with an average of 4.2 % and declines steadily down the soil profile from Nkunga area. The %N ranges from 0.2 to 0.4% with an average of 0.35 % (Figure 4-12). The %C and %N, display a strong correlation ($R^2 = 0.97$, $p < 0.001$). The C/N ratio displays a decreasing trend from the bottom of the profile from 15 to 11 at the top with an average value of 12. For the stable isotopes the $\delta^{13}C$ ranges from -19.3‰ to –15.7‰ with an average of -18.2 ‰ showing a decline to more negative values at the top of the soil profile. The range of $\delta^{13}C$ values of the organic matter in the Lake Nkunga profile is characteristic of C_4 – type and $C_3 – C_4$ type vegetation. The $\delta^{15}N$ ranges from 7.6‰ to 9.8‰ with an average of 8.4‰. The $\delta^{15}N$ displays an overall decreasing trend towards the top of the soil profile.

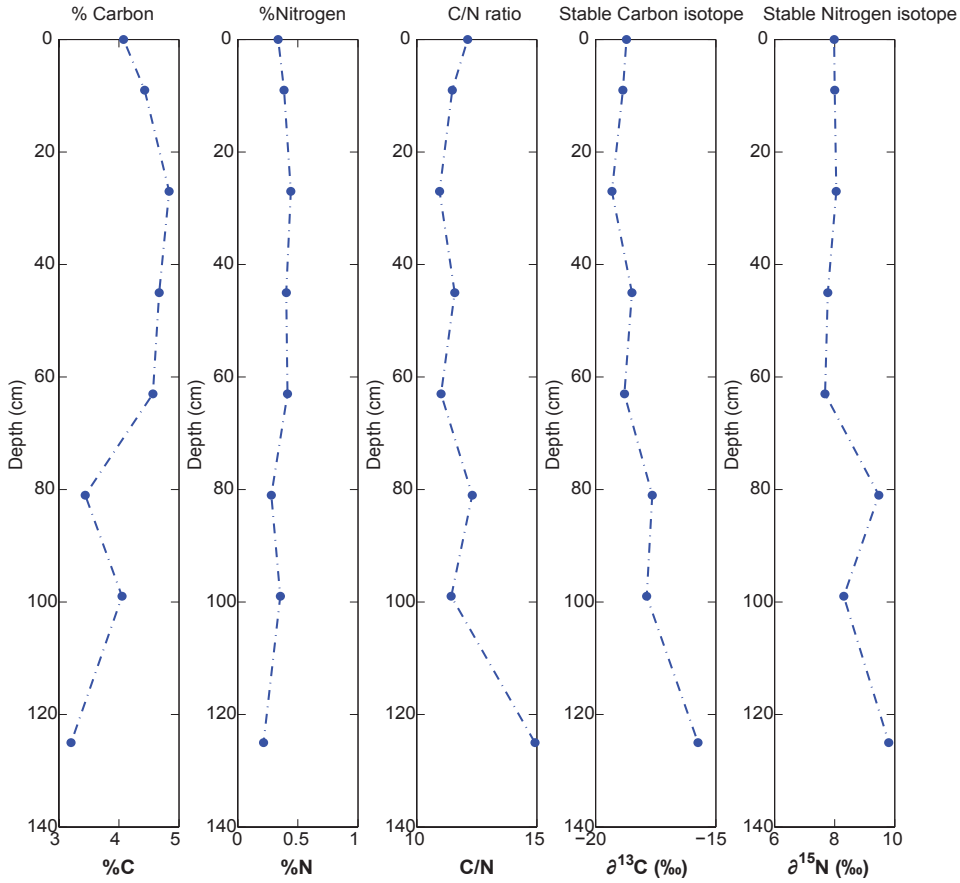

Figure 4-12: Variations down the soil profile from Lake Nkunga of the % C, % N, C/N, $\delta^{13}C$ and $\delta^{15}N$ isotopes.

4.2.1.2.4.2 n-alkanes

The *n*-alkane chain range is C_{14-35} with the most abundant n-alkanes in the samples occurring as either C_{29} or C_{31} along with significant presence of short and mid chain *n*-alkanes C_{15-24}. The distribution of the *n*-alkanes is unimodal, displaying dominance of the long odd chain homologues (C_{25+}) associated with higher plant biomass as the main source of organic matter. The short chain n-alkanes are more abundant in the samples at the bottom of the soil profile and this abundance progressively declines towards the top of the soil profile. The sample at 9 cm displays a bimodal distribution maximising the C_{17} n-alkane.

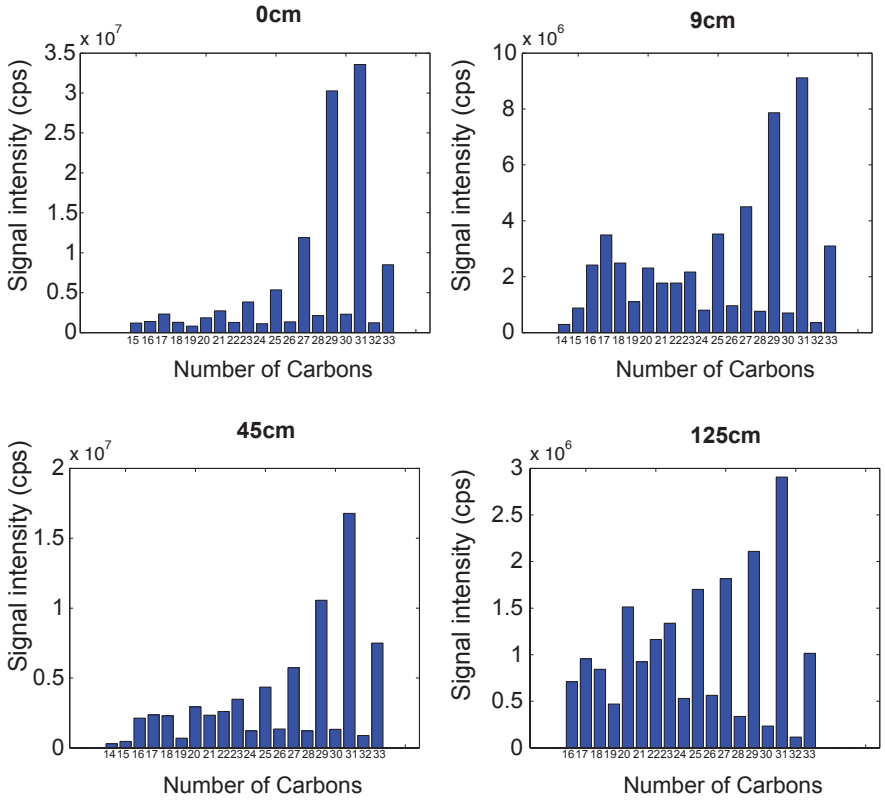

Figure 4-13: n-alkane distribution in the Lake Nkunga soil profile.

The ACL (27.8 – 29.8) and CPI (8.9 – 11.9) values are indicative of terrestrially derived n-alkanes with an odd over even predominance (Table 4). The TAR values range from 2.6 to 17.6 with the highest value at the surface and an intermediate value at 45 cm. The other two samples at 125 cm and 9 cm have low TAR values indicative of microbial/algal activity. These samples show the relatively high abundance of the short to mid-chain *n*-alkanes (Figure 4-13). The terrestrially derived $C_{31} > C_{29} > C_{27}$ and the C_{27}/C_{31} ratio record the highest C_{27}/C_{31} value

at the bottom of the soil profile (2.1) while lower values are recorded in the upper section (0 – 45 cm) of the soil profile where the values range from 0.3 to 0.5.

Table 4: Summary of n-alkane indices from Nkunga area soil profile.

Depth (cm)	C_n range	C_n max	ACL	CPI	C_{27}/C_{31}	TAR
0	15-33	31	29.6	11.9	0.4	17.6
9	14-33	31	29.3	9.0	0.5	3.9
45	14-33	31	29.8	8.4	0.3	9.4
125	14-31	29	27.8	8.9	2.1	2.6

C_n-number of carbon atoms present in the n-alkane chain: ACL-ACL of long chain n-alkanes; CPI-Carbon Preference Index of long chain alkanes; C_{27}/C_{31} ratio; TAR-Terrigenous-Aquatic Ratio.

4.2.1.2.4.3 GDGTs

All the soil samples contain amounts of brGDGTs and iGDGTs ranging from 177 to 1640 µg/g and 32 to 336 µg/g, respectively. The brGDGTs and iGDGTs are most abundant on the surface sample NK11-03. The brGDGT-I is more abundant whereas brGDGT – III is the least abundant. Among the iGDGTs, crenarchaeol is most abundance in all the samples except for the surface sample where GDGT-4 is the most abundant (Figure 4-14). Some iGDGTs (GDGT-0 and GDGT-1) are below detection limits in samples collected at 9 cm and 125 cm.

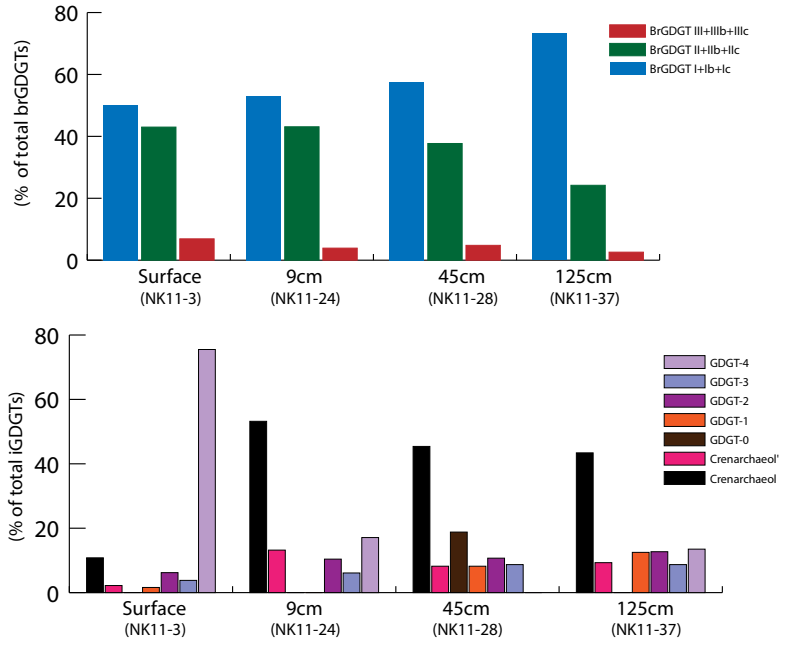

Figure 4-14: GDGT distribution in the various soil samples from the soil profile at Lake Nkunga area.

4.2.2 Characteristics of the Soils from Sacred Lake Area

4.2.2.1 Stratigraphy, Mineralogy and Grain size

Four soil horizons were identified on the basis of colour and textural changes. The A horizon (0 – 80 cm) is a well-developed topsoil comprising of organic litter and coarse fragments of mixed minerals (Figure 4-15). Below this horizon, three B horizons were identified based on the subtle colour and textural changes. B1 horizon (81-144 cm) is deep red at the top and yellowish brown towards the bottom, poor in humus, has a clayey texture, and is rich in mineral and rock fragments. B2 (145 – 184 cm) is poor in humus, rich in volcanic fragments and is persistently yellowish brown in colour. B3 (185 – 224 cm) is reddish brown and poor in humus with gravel sized scoria clasts.

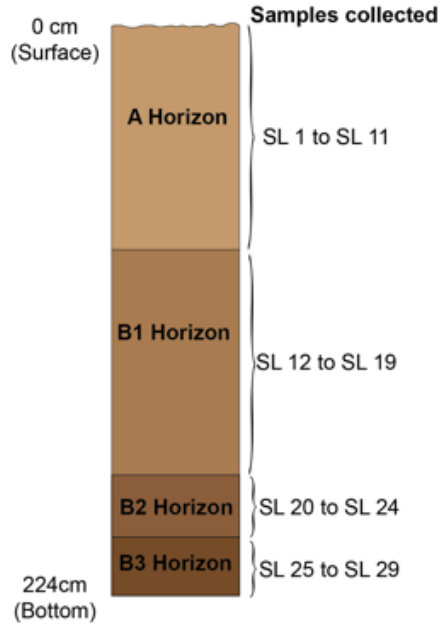

Figure 4-15: Sacred Lake soil profile showing the identified horizons.

Sacred Lake soil profile contains two slightly texturally distinct sections at the top and bottom. At the top of the profile, the soils are clayey-sandy-silts (fine sand: 44.1 – 49.1 %, silt: 55.5 – 50.8 % clay: 0.0 – 0.6 %) whilst at the bottom; the soils are clayey-silty-sands (fine sands are 50.6 – 55.5 %) (Figure 4-16). Plagioclase feldspars and quartz are the dominant peaks detected (70 – 80 %) and reflect parent rock mineralogy with notable contributions of gibbsite (2 – 10 %), halloysite (1 – 4 %) and illite (1 – 8 %) that suggest weathering of K-feldspars from catchment rocks. Illite and kaolinite were the identified clay minerals down the soil profile,

with contributions of hematite and magnetite at the bottom (Figure 4-16). The large contribution of quartz (and to a lesser extent, the occurrence of illite) does suggest a significant contribution of remote aeolian dust in the soil as previously observed in Lake Nkunga (see 4.2.1.1.1).

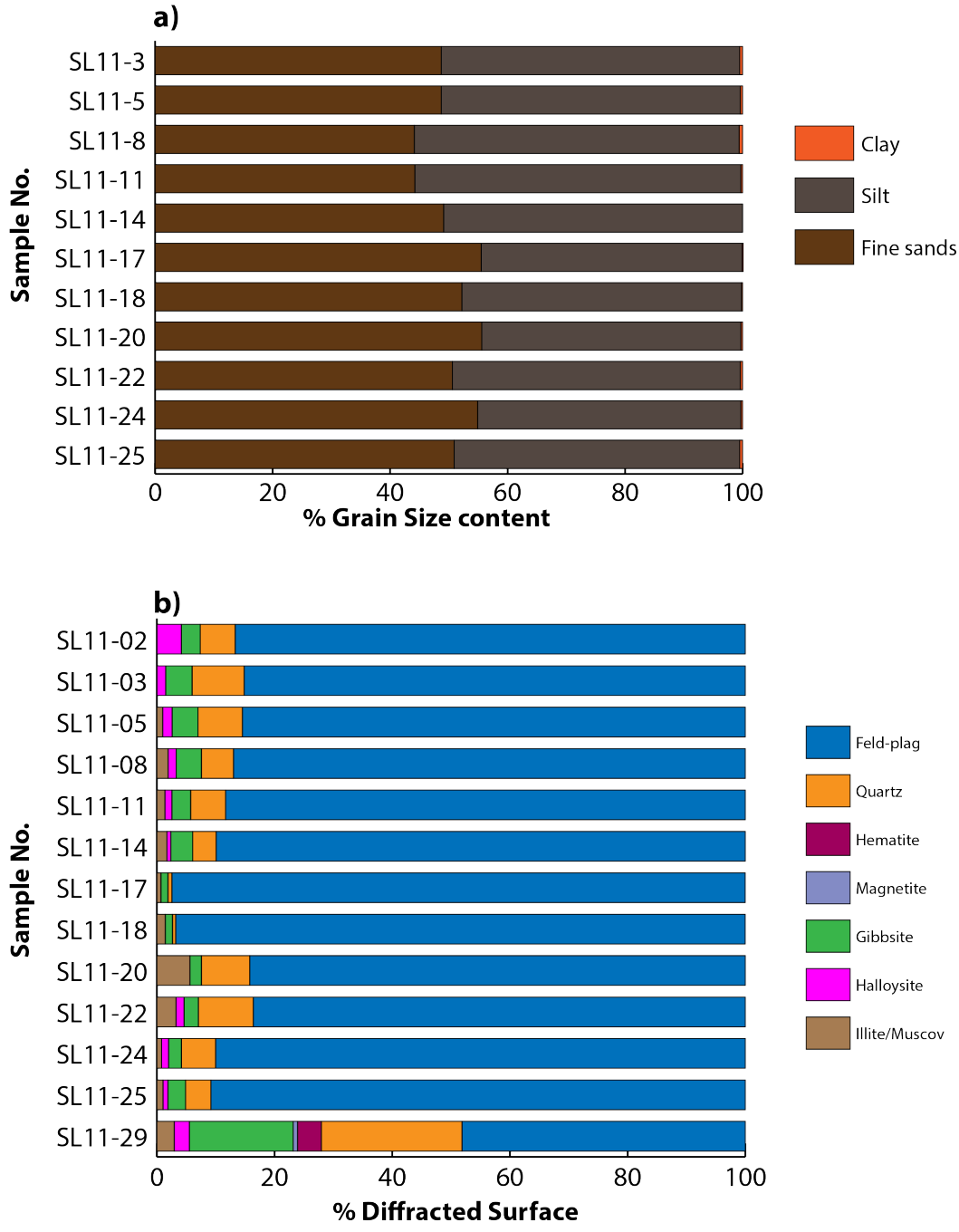

Figure 4-16: (a) Grain size distribution of the <200 µm fraction and (b) bulk mineralogy of the soil profile at Sacred Lake. NB: Feld-plag denotes plagioclase feldspar composition in the samples.

4.2.2.2 Mineral Magnetics

The bulk magnetic susceptibility values at low frequency (X_{lf}) range from 0.25 × 10^{-6} m^3kg^{-1} to 7.3 × 10^{-6} m^3kg^{-1} while high frequency (X_{hf}) oscillates between 0.22 × 10^{-6} m^3kg^{-1} and 6.6 × 10^{-6} m^3kg^{-1}. Not surprisingly, the low and high frequency magnetic susceptibility values are strongly correlated (Figure 4-17). The associated low and high frequency values display a good linear correlation with $R^2 = 0.99$ ($p < 0.001$). A marked increment in the magnetic susceptibility values is encountered at 200 cm, likely indicating a polygenic soil profile (Figure 4-17).

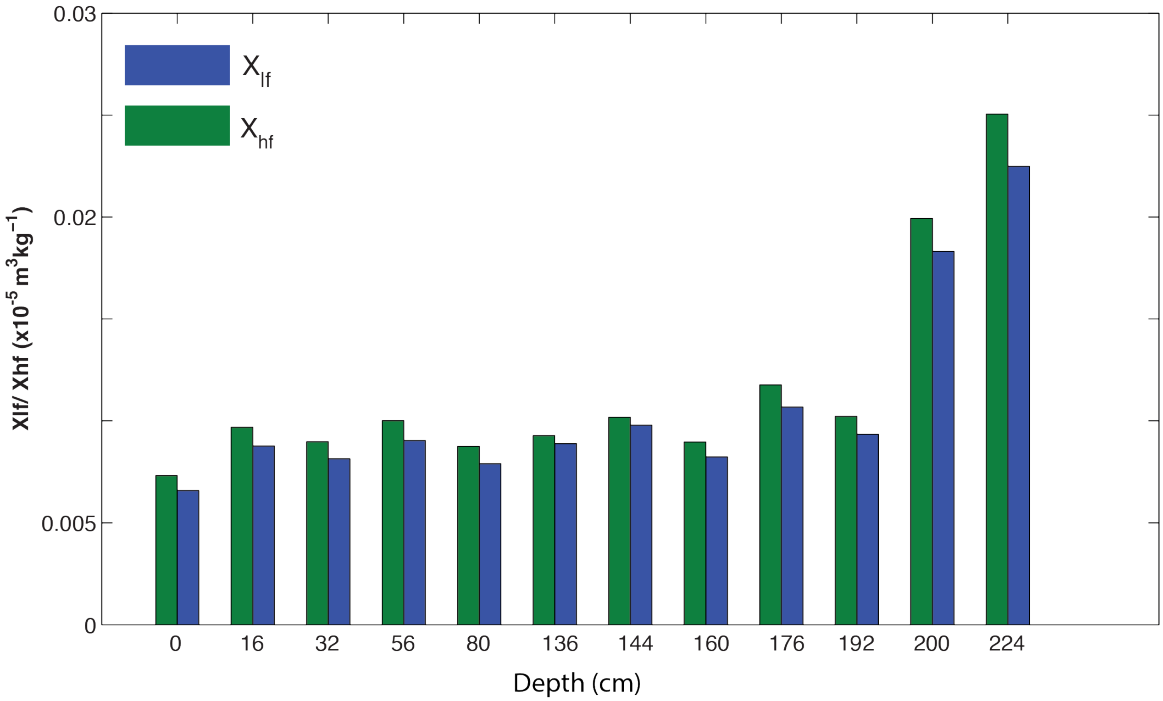

Figure 4-17: The relationship between the high and low frequency bulk magnetic susceptibility for selected samples from the soil profile at Lake Nkunga park gate.

The $\%X_{fd}$ values ranges from 4 to 10 %, the latter value indicating a strong contribution of ultrafine superparamagnetic grains in the magnetic susceptibility signal. However, there is no clear relationship between the X_{lf} and $\%X_{fd}$ (Figure 4-18), suggesting the probable contributions of paramagnetic clays as well as ferrimagnetic Fe-Ti oxides. From the bottom of the soil profile, a decline in X_{lf} and corresponding decline in $\%X_{fd}$ until 150 cm. After 10 cm, the $\%X_{fd}$ increases towards the top of the profile while the X_{lf} is relatively stable. The X_{fd} values level off after 80 cm. The decline in the X_{fd} values from the bottom of the profile corresponds to an increase in coarse grain fragments observed noted by the decline in clay/silt

fragments incorporating non – SP ferrimagnetic grains as the corresponding X_{lf} value is not markedly different.

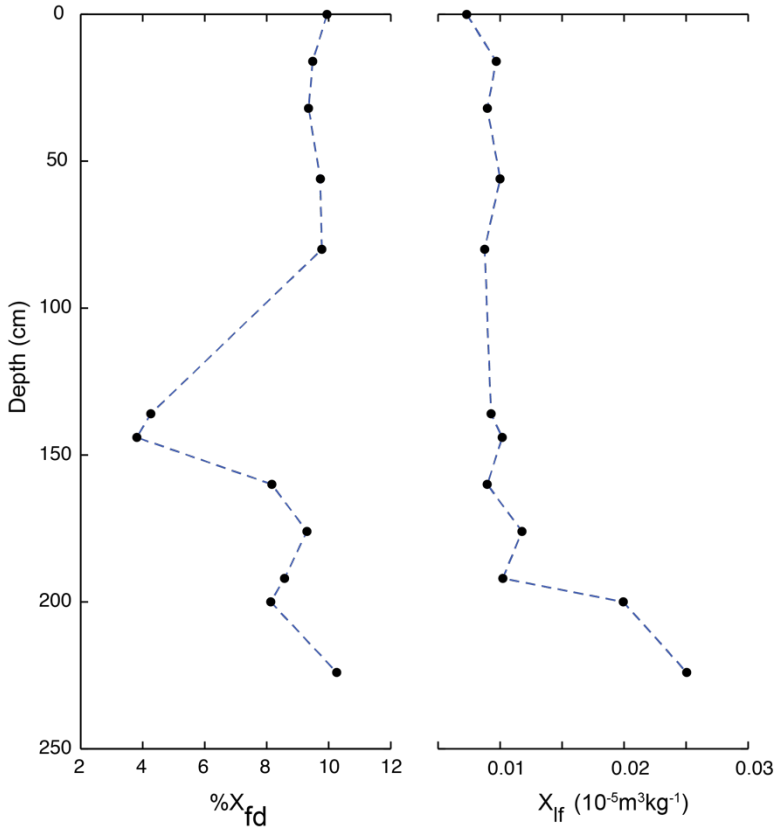

Figure 4-18: The relationship between the high and low frequency bulk magnetic susceptibility for selected samples from soil profile at Sacred Lake.

Six samples selected from the Sacred Lake soil profile display low MDF values between 4.8 – 6.8 mT with the exception of one sample at 136 cm where an MDF value of 24.1 mT is observed. The NRM intensities are almost completely demagnetized at about 10 mT for all the samples (Figure 4-19). Such relatively low MDF values are consistent with highly viscous and soft mineral magnetic assemblages, primarily dominated by soft multi-domain titanomagnetite grains and/or by thermally unstable, easily demagnetized ultrafine oxides lying near the superparamagnetic state similar to the observations at Lake Nkunga.

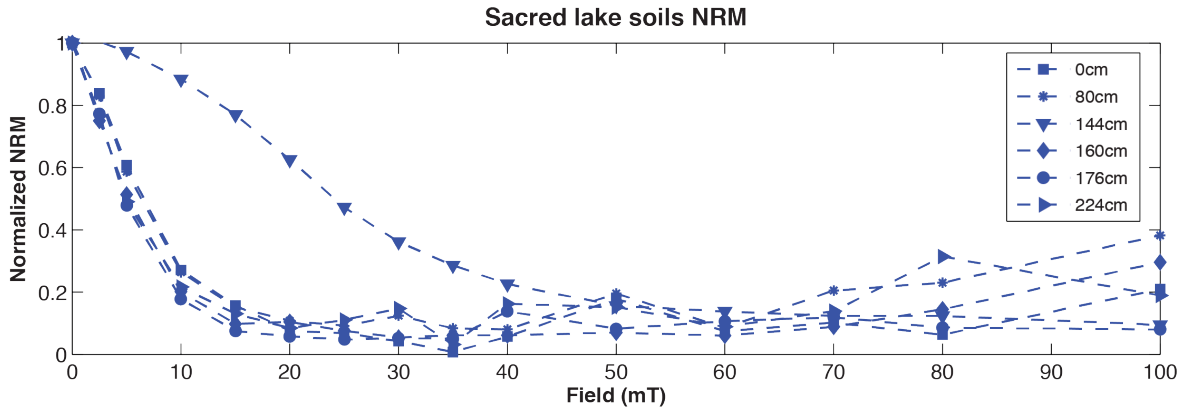

Figure 4-19: NRM profiles of the Sacred Lake soil profile.

4.2.2.3 Inorganic Geochemistry

The Sacred Lake area soils contain 17 detected elements (Al, Si, Ti, Ca, Cl, Cu, Fe, K, Mn, Nb, Ni, P, Rb, S, Sr, Zn, Zr), showing only little variation along the soil profile (Figure 4-20). Si, Al, Mn, Ca, K, Fe and Ti were selected as geochemical elements representative of the conservative indicators of environmental processes (Boës et al. 2011). The variations of these elements within the soil profile were used to define detrital and *in-situ* changes due to weathering processes within the profile (Figure 4-21).

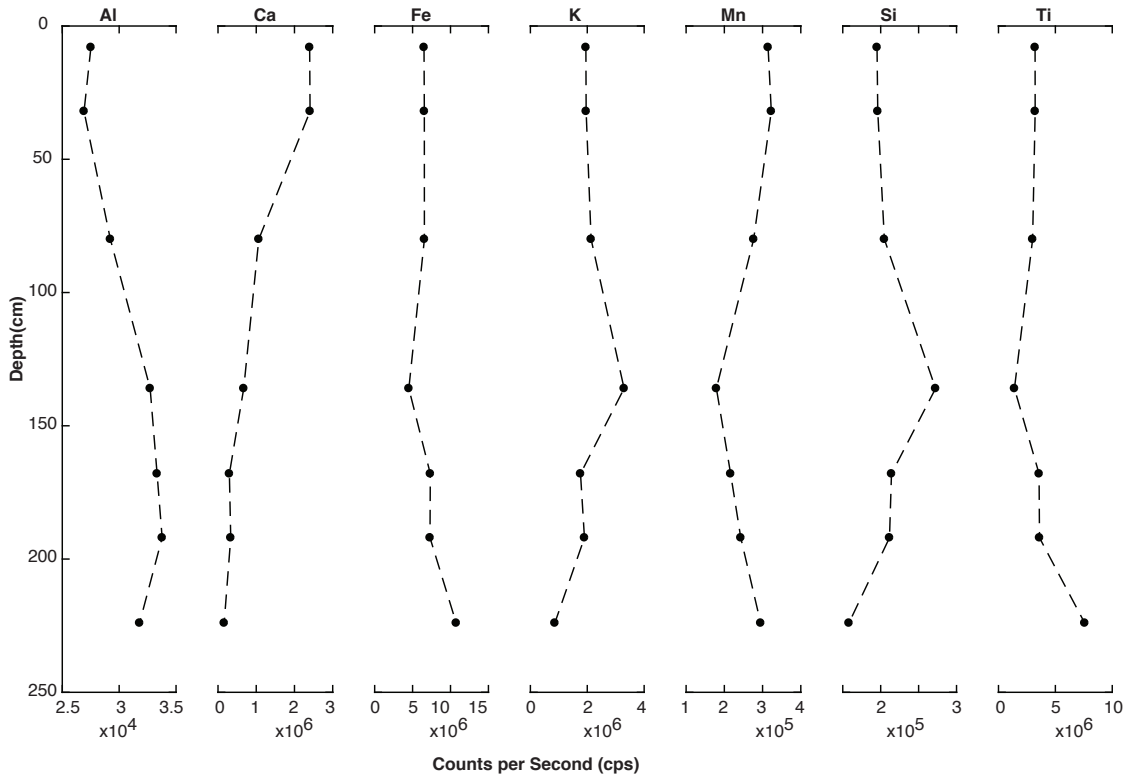

Figure 4-20: Elemental geochemical profile from Sacred Lake soil profile.

The Ca/Ti, Fe/Ti and K/Ti (Figure 4-21) profiles, potentially illustrate the respective signature of combined deposition process and soil weathering as well as biomass input. The three parameters show a rise in these ratios up to 150 cm. Above 150 cm, the proxies exhibit continuous declines that stabilise at the top of the soil profile. In contrast, the Fe/Mn ratio declines from the bottom of the profile and stabilises at about 150 cm to the top of the soil profile, likely indicating a fixed higher value of Mn concentration in the upper layers of the profile with limited variation (Figure 4-20) and thus the observed changes correspond to changes in Fe. This is verified by the similarity of the Fe/Mn (Figure 4-21) and Fe (Figure 4-20) graphs from 150 cm to 0 cm depth. The soil profile was revised from the stratigraphic section in 4.2.2.1 (pg. 88) to horizons based on the geochemical proxies where the B horizon (224 to 160 cm) is dominated by the weathering of aluminosilicates (evidenced by the high Al in this section), smaller grain sizes (increase in Fe/Ti) and higher Fe/Mn.

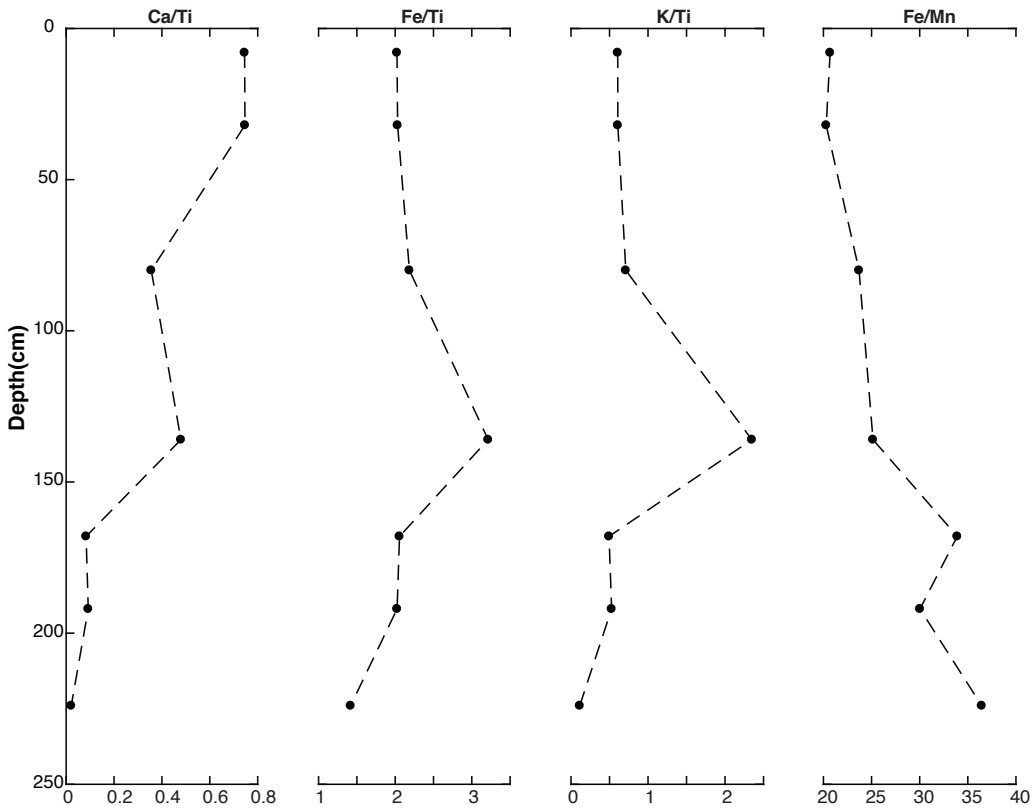

Figure 4-21: Normalized elemental variations down the Sacred Lake soil profile.

A major change occurs between 160 and 140 cm where predominantly lithogenic indicators such as Fe/Ti show a rapid increase while the Fe/Mn value show a major decrease. This suggests a zone of Mn accumulation, possibly linked with temporarily water logging at the limit between the weathering E horizon and the accumulation B horizon. The E horizon (140

– 80 cm) is characterized by increasing titanium content at the expense of other mobile or soluble components. The content in aluminosilicates is lower, but the minimum Fe/Mn values near the top of the profile illustrate the accumulation of Mn in relatively oxidising and organic rich conditions. Similarly, the upward increase of Ca/Ti likely illustrates the uptake of soil Ca by vegetation and its further deposition and burial in litter biomass. The A horizon is observed between 80 and 40 cm while O horizon is above it.

4.2.2.4 Organic Geochemistry

4.2.2.4.1 Carbon, Nitrogen and their Isotopes

The % C ranges from 0.6 % to 8.3 % with an average of 3.3 %. %C displays a steady decline down the soil profile. On the other hand, %N ranges from 0.05 to 0.80 % with an average of 0.30 %. The %N values are relatively constant with minimal to no change down the soil profile (Figure 4-22). The %C and %N display a strong correlation, $R^2 = 0.99$ ($p < 0.001$). The C/N ratio displays a decrease from the bottom of the profile (8.7- 11.5) with an average value of 10.3.

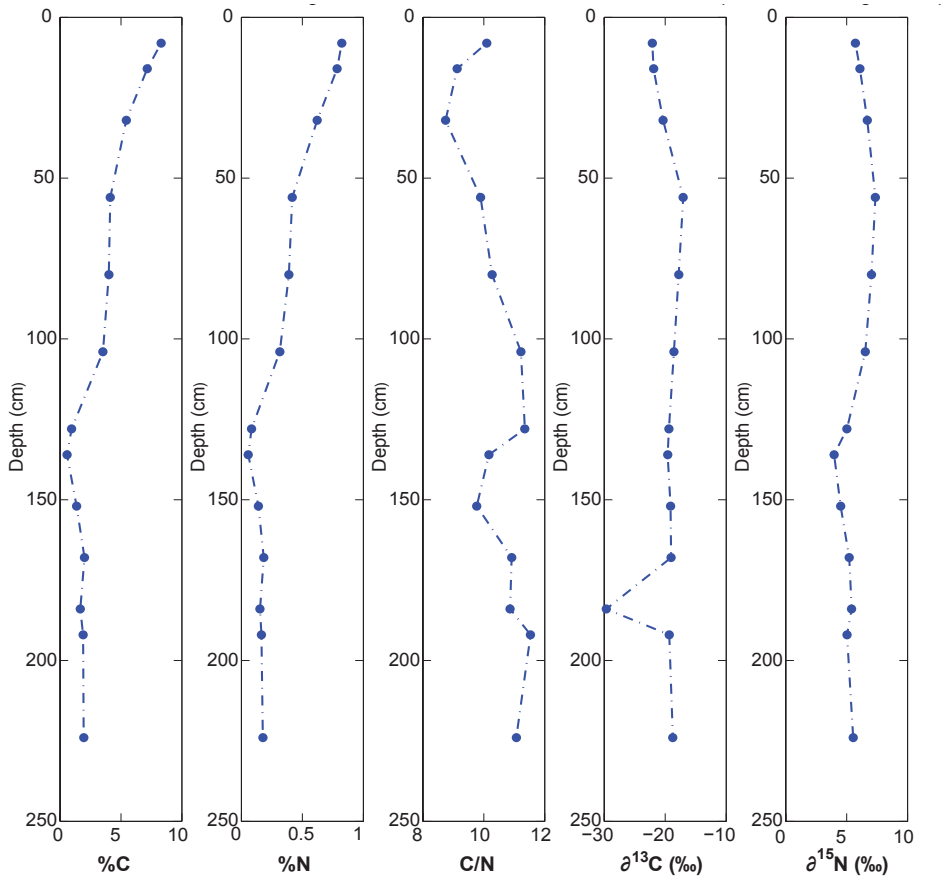

Figure 4-22: Variations down the soil profile from Sacred Lake of %C and %N, C/N, $\delta^{13}C$ and $\delta^{15}N$.

The $\delta^{13}C$ ranges from -29.7‰ to –17.0‰ with an average of -20.2‰ whilst the $\delta^{15}N$ ranges from 4.0 ‰ to 7.4‰ with an average of 5.7‰. The $\delta^{13}C$ displays a sharp excursion to the most negative value at 184 cm while at 150 cm a slight increase in $\delta^{15}N$ towards the top of the profile occurs; the $\delta^{13}C$ and $\delta^{15}N$ are relatively constant. The ranges of OM $\delta^{13}C$ values from the Sacred Lake profile are characteristic of C_3 - C_4 type vegetation.

4.2.2.4.2 n-alkanes

The *n*-alkane chain range is C_{14-35} with the most abundant n-alkanes in the samples occurring at C_{29} and C_{31} along with significant presence of short and mid chain *n*-alkanes C_{15-24} (Figure 4-23). The distribution of the *n*-alkanes is unimodal, displaying dominance of the long odd chain homologues (C_{25+}) associated with higher plant biomass as the main source of organic matter. The short chain n-alkanes are more abundant in the sample at the bottom of the soil profile and this abundance progressively declines towards the top of the soil profile. The sample at the bottom of the profile (224 cm) displays bimodal distribution with the C_{18} *n*-alkane as the most predominant.

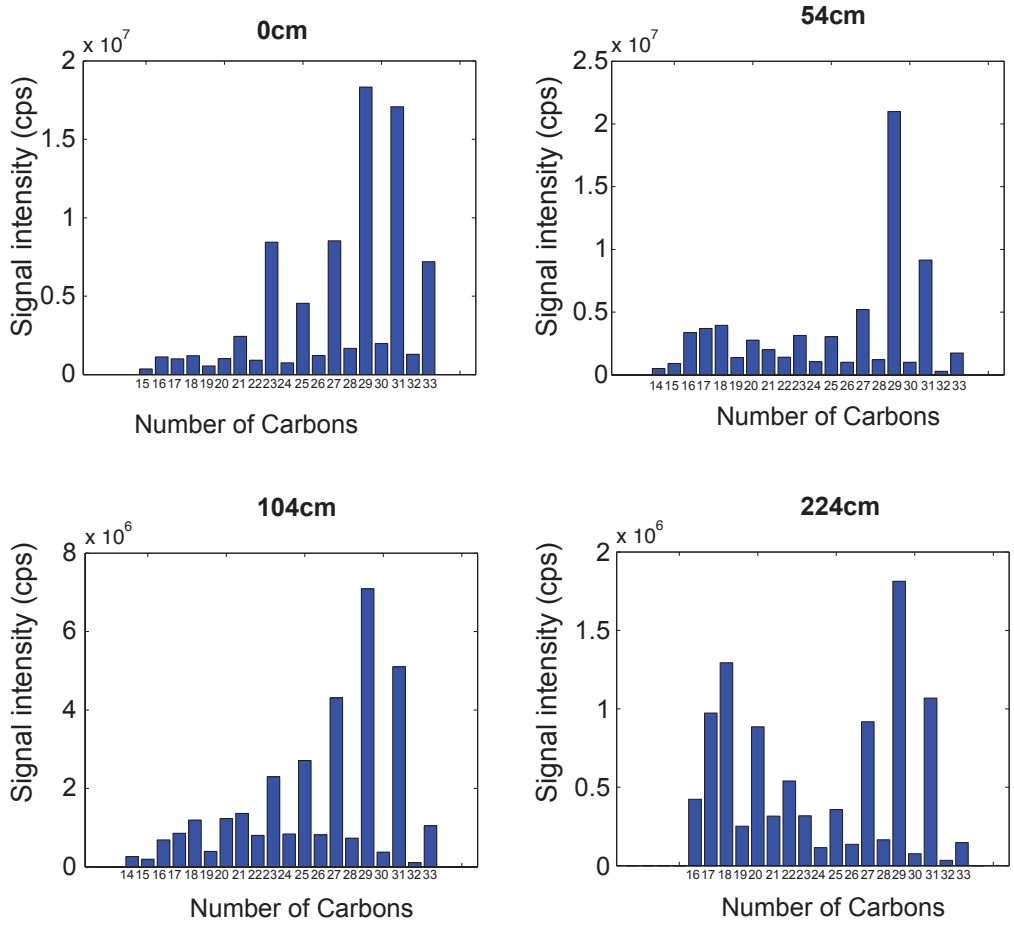

Figure 4-23: n-alkane distribution on from the Sacred Lake soil profile.

These samples show the relatively high abundance of the short to mid-chain *n*-alkanes (Figure 4-23). Among the long chains n-alkanes, the higher plants terrestrial n-alkanes C_{29} is the most abundant, followed by C_{31} and lastly C_{27}. The C_{27}/C_{31} ratio (0.5 – 0.9) has the highest value at the bottom (0.9) and declines towards the top (0.5) of the profile.

The ACL (28.7 – 29.5) and CPI (8.5 – 10.1) are indicative of terrestrially derived *n*-alkanes with an odd over even predominance (Table 5). The TAR values (3.1 – 22.9) display higher values in the surface and at 104 cm while two other samples at 54 cm and 224 cm display low TAR values indicative of microbial/algal activity.

Table 5: Summary of n-alkane indices from Sacred Lake soil samples

Depth (cm)	C_n range	C_n max	ACL	CPI	C_{27}/C_{31}	TAR
0	15-33	29	29.5	8.6	0.5	22.9
54	14-33	29	29.1	10.1	0.6	5.9
104	14-33	29	28.7	8.5	0.8	11.5
224	14-33	29	28.9	9.3	0.9	3.1

C_n-number of carbon atoms present in the n-alkane chain: ACL-ACL of long chain n-alkanes; CPI-Carbon Preference Index of long chain alkanes; C_{27}/C_{31} ratio; TAR-Terrigenous-Aquatic Ratio

4.2.2.4.3 GDGTs

BrGDGT-I is the most abundant in the samples from the subsurface while GDGT-II is the most abundant in the sample from the surface. Among the iGDGTs, there are some changes in the profile where crenarchaeol is more abundant on the surface and at 54 cm whereas GDGT-0 is more abundant at 104 cm and GDGT-2 is the most abundant of the iGDGTs at 224 cm (Figure 4-24).

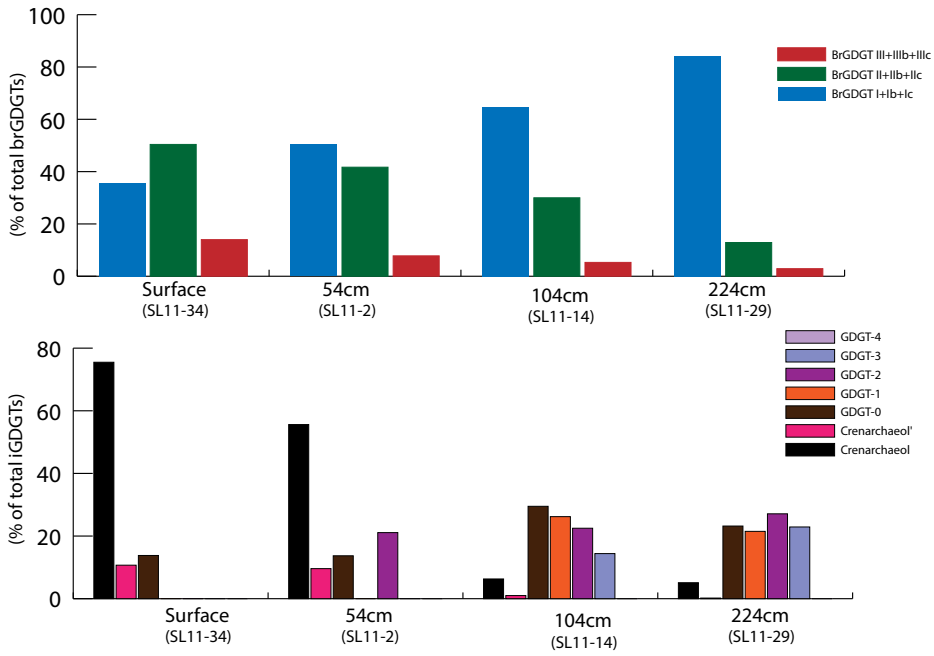

Figure 4-24: GDGT distribution in the various soil samples from the soil profile at Sacred Lake area.

There are several iGDGTs that are below detection limits in the samples e.g. GDGT-1 to GDGT-4 were not detected on the surface sample, GDGT-1, GDGT-3 and GDGT-4 were below detection in the sample at 54 cm, GDGT-4 was not detected in the sample at 104 cm and at 224 cm the crenarchaeol regio isomer and GDGT-4 were below detection limits (Figure 4-24).

4.2.3 Characteristics of Soils from the Transect

4.2.3.1 Mineralogy

The mineralogy of the transect soils is dominated by feldspars (70 – 95 %) and secondly by quartz (2 – 15 %) (Figure 4-25). At the lower altitudes between 1800 – 2100 m asl, the soils are dominated by halloysite, hematite and magnetite which are weathering products. Above 2500 m asl, chlorite is detected in small quantities (Figure 4-25) whereas diopside that was present in the lower altitudes is absent. Quartz, gibbsite and plagioclase feldspars appear in all samples along this transect. The plagioclase feldspars are more abundant above 2000 m asl while the abundance of quartz declines from the lower to higher altitudes. Among the clay minerals, kaolinite, illite and chlorite are present. Not surprisingly, the lower altitude, warmer and wetter surface soils from show significant enhancement in silicate and iron weathering products, together with a probable input from atmospheric dust.

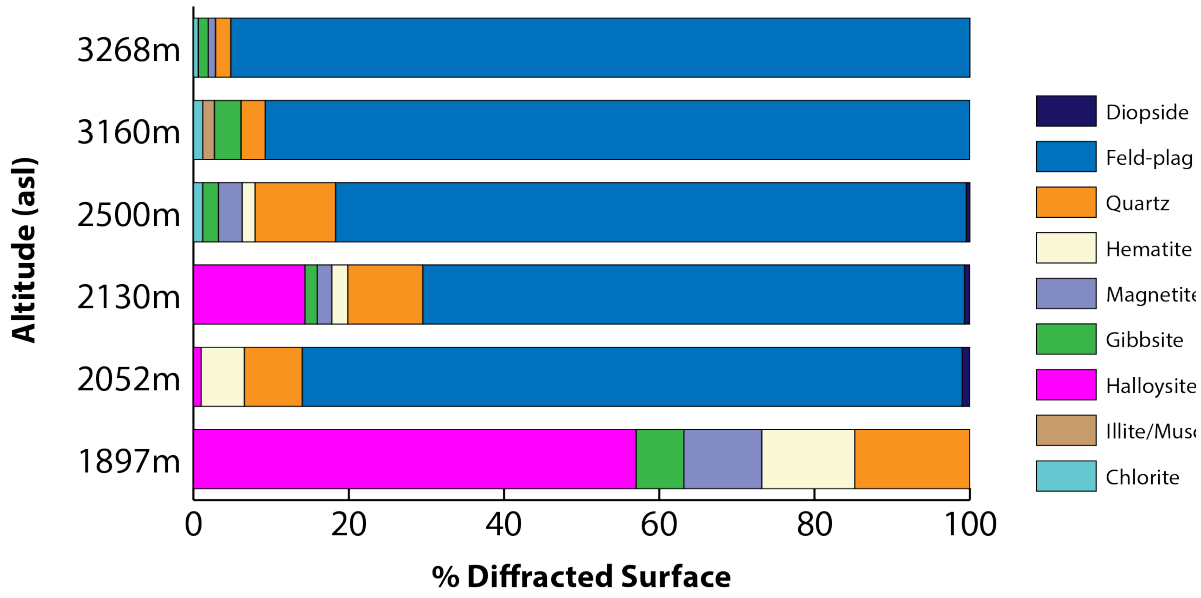

Figure 4-25: Bulk mineralogy of soils along the Nkunga-Sacred Lake- Rutundu transect.

4.2.3.2 Magnetic Susceptibility

The mass specific magnetic susceptibility values at low frequency (Xlf) ranges from 0.2 × 10^{-6} m^3kg^{-1} to 1.9 × 10^{-6} m^3kg^{-1} while at high frequency (X_{hf}) it ranges from 0.2 × 10^{-6} m^3kg^{-1} to 1.7 × 10^{-6} m^3kg^{-1} (Figure 4-26). The associated low and high frequency values display a good linear correlation (R^2 = 0.99, p < 0.001). Three susceptibility clusters can be identified along the transect; (i) soils with the highest magnetic susceptibility values (1800 – 2000 m) are mainly from the Nkunga crater and its surroundings; (ii) soils with intermediate susceptibility values (2300 – 2700 m) are found around Sacred Lake, and; (iii) soils with generally low susceptibility values occur above 3000 m and have large fluctuations in the low frequency magnetic susceptibility values (Figure 4-27).

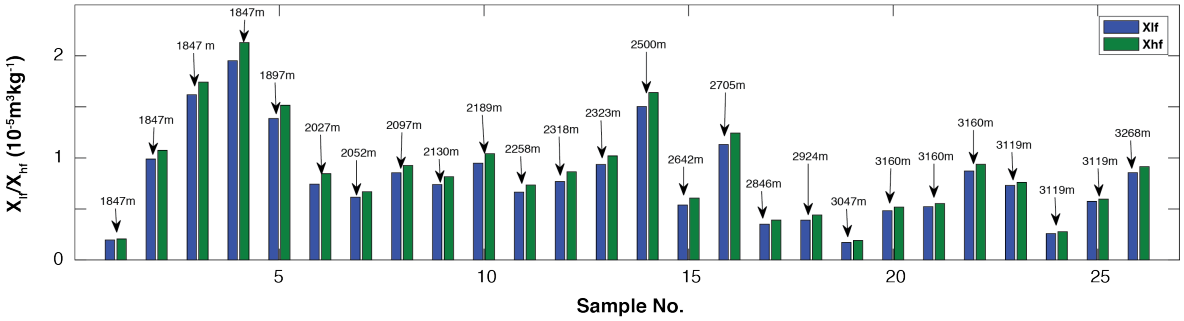

Figure 4-26: The high and low frequency bulk magnetic susceptibility for samples collected along the soil transect.

The frequency dependency ($\%X_{fd}$) varies from 3 to 12 %, implying that the samples collected along the soil transect represent a mixture of SP and coarser non-SP ferrimagnetic grains (Figure 4-27). Three clusters are observed in $\%X_{fd}$ trends: the low altitude (1500 – 2000 m asl) medium $\%X_{fd}$ (5 – 6 %) values; the mid altitude (2500 – 3000 m asl) with medium to high $\%X_{fd}$ (7 – 12 %) values and the high altitude (> 3000 m asl) with medium $\%X_{fd}$ (3 – 7 %) values. Interestingly, the maximum $\%X_{fd}$ values are observed in soils from the Afromontane forest, in the higher rainfall zone.

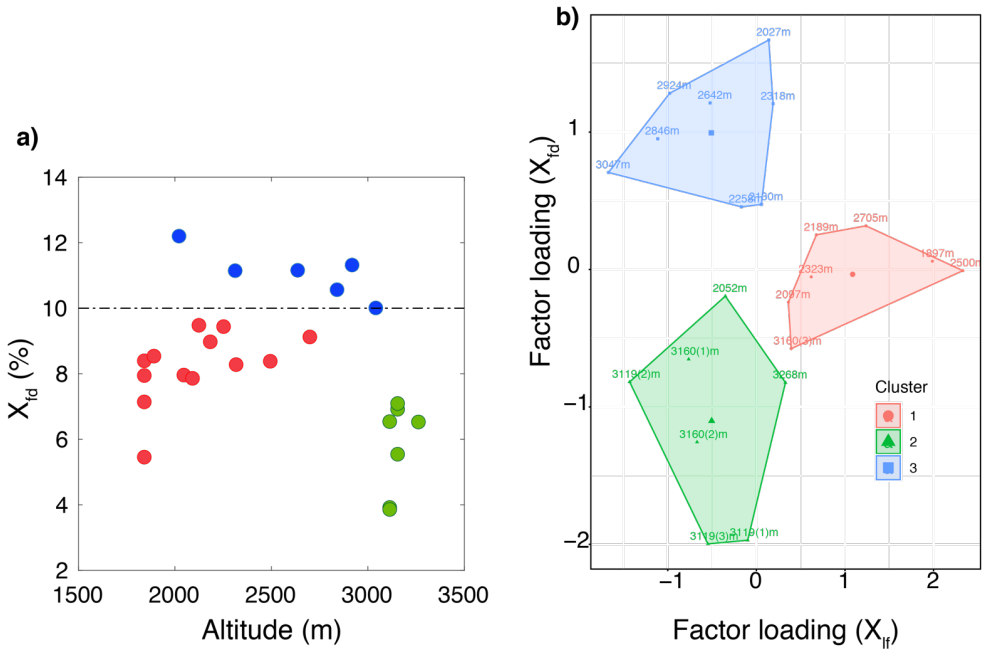

*Figure 4-27: The susceptibility characteristics dependence($\%X_{fd}$) and low magnetic susceptibility (X_{lf}). The first panel **(a)** shows the altitudinal variation in $\%X_{fd}$, red represents low altitude & medium $\%X_{fd}$, samples, blue represents mid altitude and medium to high $\%X_{fd}$ samples and green represents high altitude and medium $\%X_{fd}$ samples. The horizontal line at 10 % X_{fd} marks the border between the mix-SP and coarser non-SP grains and the predominantly high SP ferrimagnetic grains. The second panel **(b)** shows the results of a cluster analysis performed on the two variable X_{lf} and X_{fd} where these three clusters are linked to the corresponding X_{lf}.*

The Median Destructive Field (MDF) was calculated from the normalized Natural Remanence Magnetism (NRM) intensities. The soils displayed low MDF values (4.5 – 12.2 mT) and the demagnetisation of the samples was achieved at about 10 mT (Figure 4-28). These results imply that the bulk of the magnetic signal of the samples is carried by coarse-grained fraction. The similarities in the shape of the demagnetisation curves of the soil samples point to a single source origin of the magnetic minerals along the altitudinal transect. The NRM intensities for the high-altitude soils (>3000 m asl) display magnetisation after 40 mT. Generally, the soils

along the transect are derived from the same parent material with the exception of the high-altitude soils that are probably palaeosols.

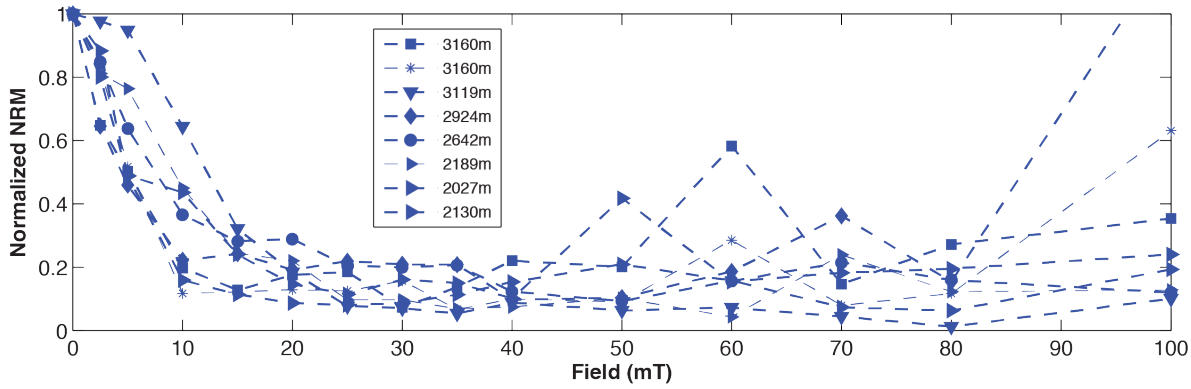

Figure 4-28: Natural Remanent Magnetism of soil samples from the soil transect, Lake Nkunga and Sacred Lake

Using the NRM results, the average MDF of 30 mT was selected for the Anhysteretic Remanence Magnetism (ARM) and Isothermal Remanence Magnetisation (IRM) measurements on the assumption that at 300 mT the saturation of the fine-grained ferrimagnetic minerals will have occurred. X_{lf}, ARM_{30mT}, SARM, IRM_{300mT} and SIRM have low correlation coefficients (R^2 ranges from 0.2 – 0.6) and do not display any clear trends in the soils (Figure 4-29).

IRM_{300mT} ranges from 0.3×10^{-5} to 2.8×10^{-5} Am^2kg^{-1} whilst the SIRM values range from 0.35×10^{-5} to 2.9×10^{-5} Am^2kg^{-1}. The S-ratio of these samples fluctuates between 0.6 and 1 with an average of 0.8. The samples generally display low coercivity suggesting the dominance of ferrimagnetic minerals (e.g. magnetite); however, the detection of S-ratio below 0.8 implies co-existence of anti-ferromagnetic minerals (e.g. goethite and hematite) in these soils possibly due to redox processes.

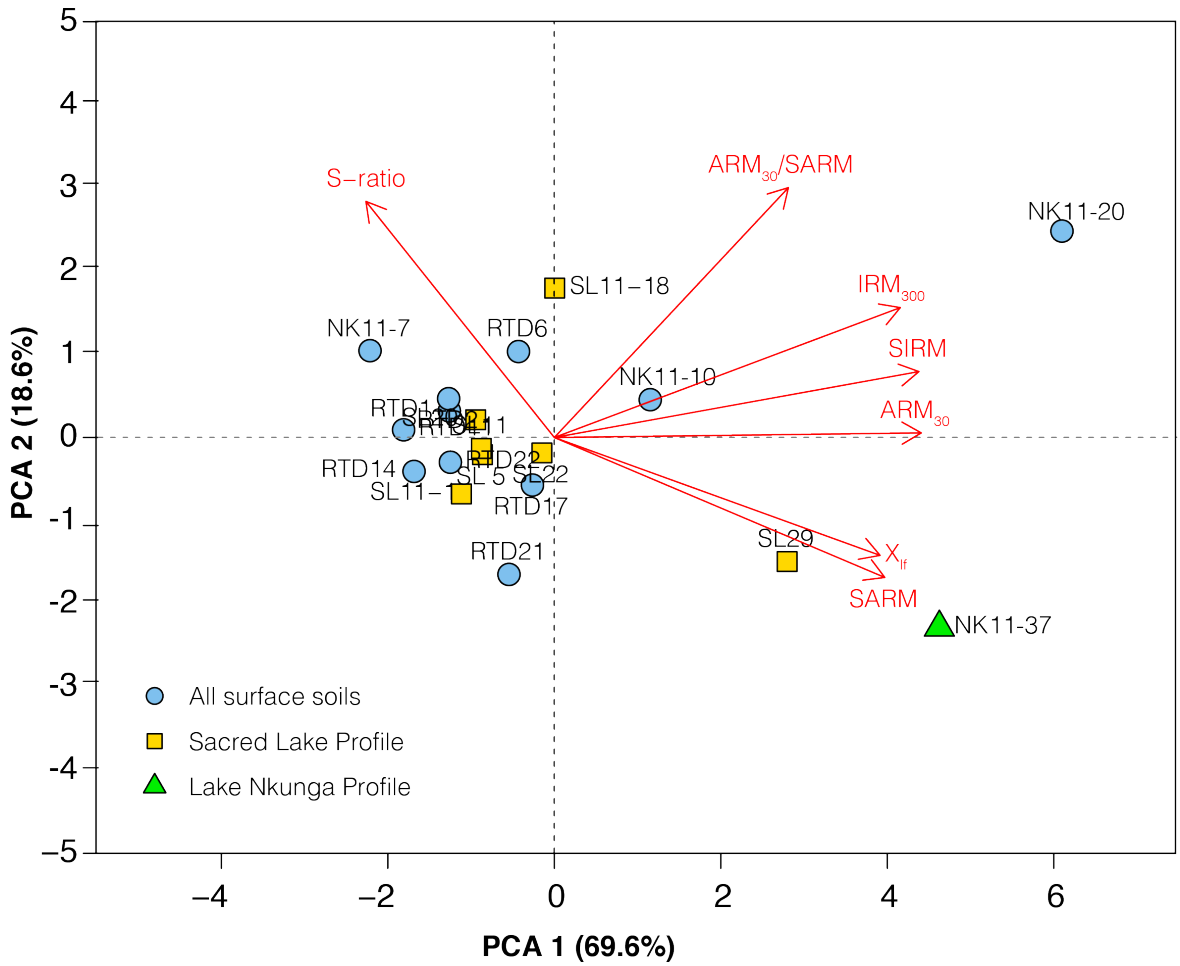

Figure 4-29: A bi-plot of the PCA of the different magnetic variables of all surface soils (including surface soils collected from Nkunga area) and soil profiles from Sacred Lake and Lake Nkunga (One sample).

The intensity of the ARM_{30mT} ranges from 0.31×10^{-4} to 2.1×10^{-4} Am^2kg^{-1} whilst those of the SARM (ARM_{100mT}) range from 0.8×10^{-4} to 7.8×10^{-4} Am^2kg^{-1}. The ARM_{30mT}/SARM ratio ranges between 0.1 and 0.45. This low value generally characterizes the dominant state of the remanence-carrying component of the soil samples as soft multi-domain viscous grains. However, the values of the $\%X_{fd}$ previously discussed (up to 10 %) shows that there is probably a considerable influence of ultrafine SP ferrimagnetic grains from the catchment soils. Consequently, the magnetic grain assemblages of the catchment contain two dominant sources of particles: one SP component likely of pedogenic origin, and soft and coarse detrital titanomagnetite component inherited from the volcanic bedrock.

4.2.3.3 Organic Geochemistry

4.2.3.3.1 Carbon, Nitrogen and their Isotopes

The %C, %N, $\delta^{13}C$ and $\delta^{15}N$ were measured along the transect and do not display any unique trends with elevation. %C has a wide range from 1.0 % to 29.9 % with an average of 7.8 %, whilst the %N ranges from 0.0 to 2.3 % with an average of 0.7 % (Figure 4-30). The R^2 value of %N and %C is 0.91 ($p < 0.001$) displaying a good a linear relationship between these two variables. The C/N ratio ranges from 7.3 to 20.1 with an average value of 12.3 while the $\delta^{13}C$ ranges from –60.7 ‰ to –14 ‰ although most of the values oscillate around the average concentration of –23.6 ‰ and $\delta^{15}N$ range from –1.3 ‰ to 12.8 ‰ with an average of 7.2 ‰. Three outliers are observed in the $\delta^{13}C$ values of the surface samples NK11-4, NK11-2 and NKS11-3. Although during sampling, effort was made to ensure that fresh roots from the vegetation was not collected, the high values from these samples point to fresh terrestrial samples. The linear relationship between $\delta^{13}C$ and $\delta^{15}N$ is defined by $R^2 = 0.20$ ($p < 0.002$) with the exclusion of the three outlier samples.

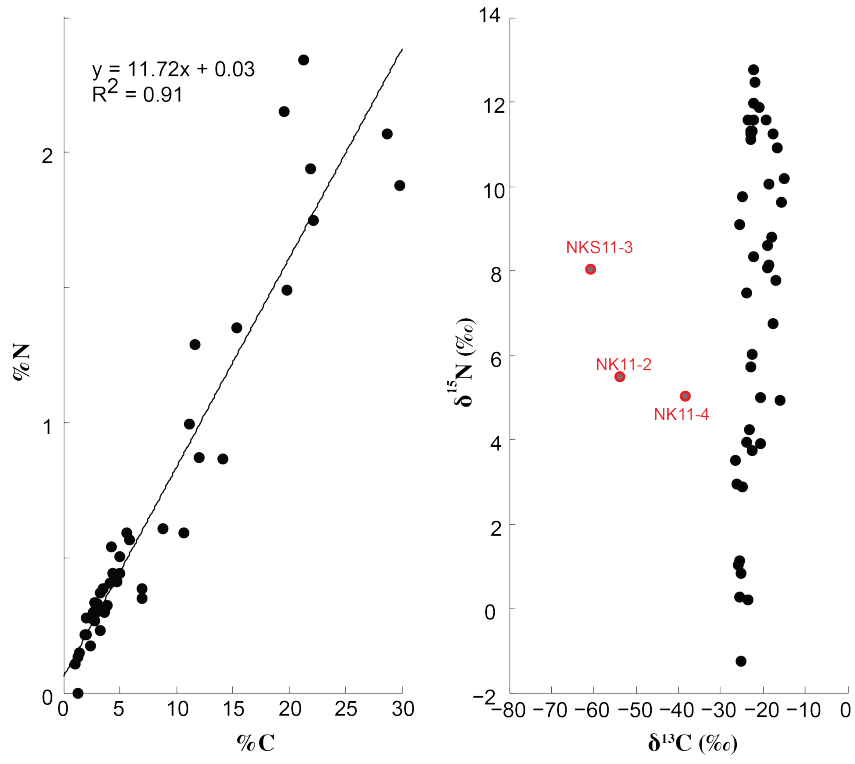

Figure 4-30: Variations of % C, % N, $\delta^{13}C$ and $\delta^{15}N$ along the soil transect from Lake Nkunga to Lake Rutundu. The red dots mark the outlier samples in the $\delta^{13}C$ and $\delta^{15}N$ dataset

Based on the C/N and the $\delta^{13}C$, the OM of the soils along the transect reflect C_3 and C_4 type vegetation . This is not surprising as the soil samples are collected from the montane forest and cultivated slopes of the mountain. From 1800 to 2500 m asl, a mix of C_3 and C_4 type vegetation are the main sources of OM while from 2500 to 3500 m asl, the OM is predominantly derived from C_3-type vegetation (Figure 4-31).

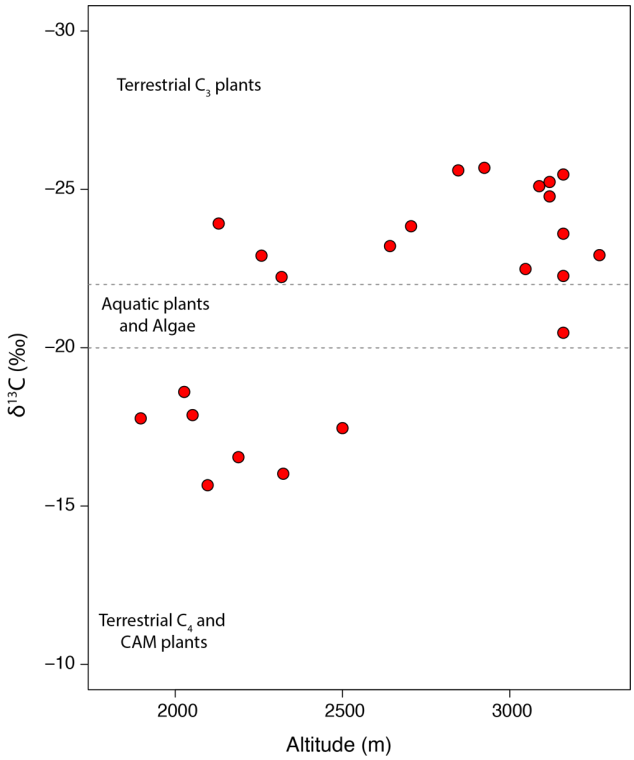

Figure 4-31: Stable carbon isotope signature of the soil organic matter along the soil transect from Mt. Kenya area

4.2.3.3.2 n-alkanes

The distribution of n-alkanes from the surface soils of the Nkunga-Sacred Lake-Rutundu transect is unimodal in samples above 2500 m asl and bimodal in samples below this altitude. The samples below 2500 m display bimodal distribution of mid and long *n*-alkane chains indicating a mix of terrestrial and microbial input into the soils. Above 2500 m the unimodal distribution reflects the abundance of the long chain odd homologues C_{25+} associated with higher plant biomass which indicates that terrestrial plant materials are the main source of organic matter (Figure 4-32). The n-alkane chain range is C_{14-35} with the most abundant n-alkanes in the samples being either C_{29} or C_{31} and with a substantial presence of short chain n-alkanes C_{15-24}. The C_{27}/C_{31} ratio (0.1 – 2.0) generally implies a grassland-dominated ecosystem.

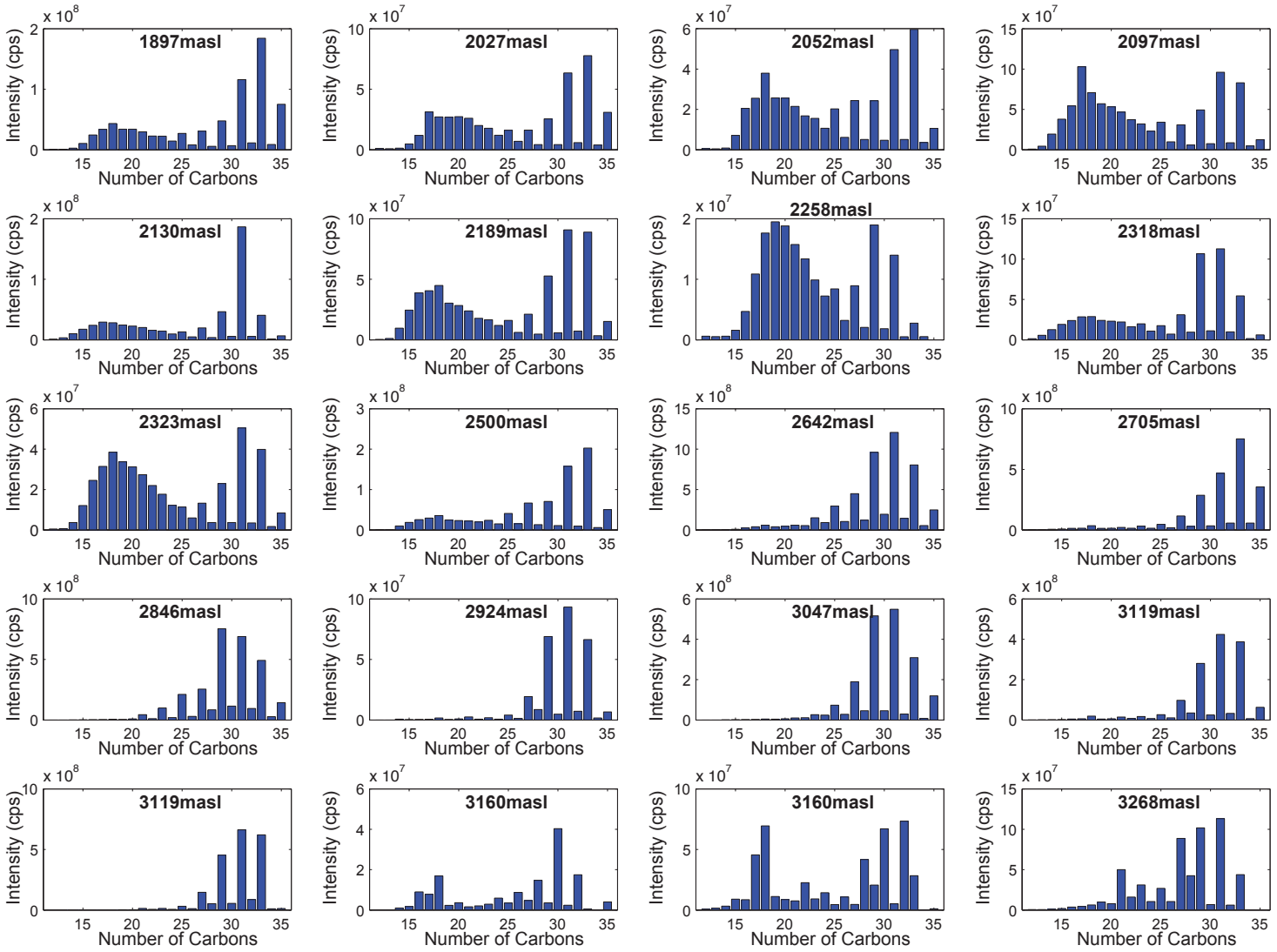

Figure 4-32: n-alkane distribution along the Nkunga-Sacred Lake- Rutundu transect

The ACL varies from 27.8 – 29.8 along the transect (Table 6) indicative of predominantly higher plant terrestrial OM sources. The CPI (6.9 – 11.9) values affirm the terrestrial source origin of the soil organic matter.

Table 6: Summary of n-alkane indices from the soil transect

Altitude (m)	C_n range	C_n max	ACL	CPI	C_{27}/C_{31}	TAR
1897	12-35	33	31.0	9.3	0.3	2.5
2027	12-35	33	30.7	6.9	0.3	1.7
2052	12-35	33	30.2	6.4	0.5	1.7
2097	12-35	17	30.1	6.6	0.3	0.9
2130	12-35	31	30.4	12.2	0.1	3.6
2189	12-35	31	30.6	8.7	0.2	1.7
2258	12-34	29	28.8	5.0	0.6	1.3
2318	12-35	31	30.0	7.4	0.3	3.5
2323	12-35	31	30.4	6.1	0.3	1.1
2500	14-35	33	30.5	9.0	0.4	4.1
2642	15-35	31	30.0	5.8	0.4	29.4
2705	14-35	33	31.1	9.7	0.2	23.8
2846	14-35	29	29.8	6.9	0.4	168.1
2924	14-35	31	30.6	10.8	0.2	118.5
3047	14-35	31	30.0	9.9	0.3	141.0
3119	14-35	31	30.7	10.9	0.2	62.9
3119	14-35	31	30.6	8.0	0.3	99.1
3119	14-35	31	30.8	8.9	0.2	274.5
3160	14-35	30	27.9	0.2	2.0	0.9
3160	12-35	32	30.5	0.3	0.9	0.5
3268	12-33	31	29.3	5.3	0.8	18.6

C_n-number of Carbon present in n-alkane chain: ACL- total Average alkane Chain Length; CPI-Carbon Preference Index of long chain alkanes; TAR-Terrigenous-Aquatic Ratio.

4.2.3.3.1 GDGTs

4.2.3.3.1.1 GDGT Distribution and Concentration

All the soil samples contain abundant amounts of brGDGTs and iGDGTs ranging from 93 to 3157 µg/g (57.0 - 99.7 %) and 2 to 156 µg/g (0.3 – 43.0 %), respectively. On average the iGDGT constitutes 12 % of the total GDGTs, which agrees with values obtained by Weijers et al. (2006) where the average relative abundances are 10 %. The samples are dominated by brGDGT-I and its moieties while brGDGT-III is the least abundant from 1800 – 2500 m asl.

Between 2500 m asl and 3000 m asl brGDGT-II becomes the most abundant among the samples (Figure 4-33). Among the iGDGTs, a similar trend is observed where relatively higher crenarchaeol is observed below 2500 m asl and GDGT – 0 is more abundant above 2500 m asl.

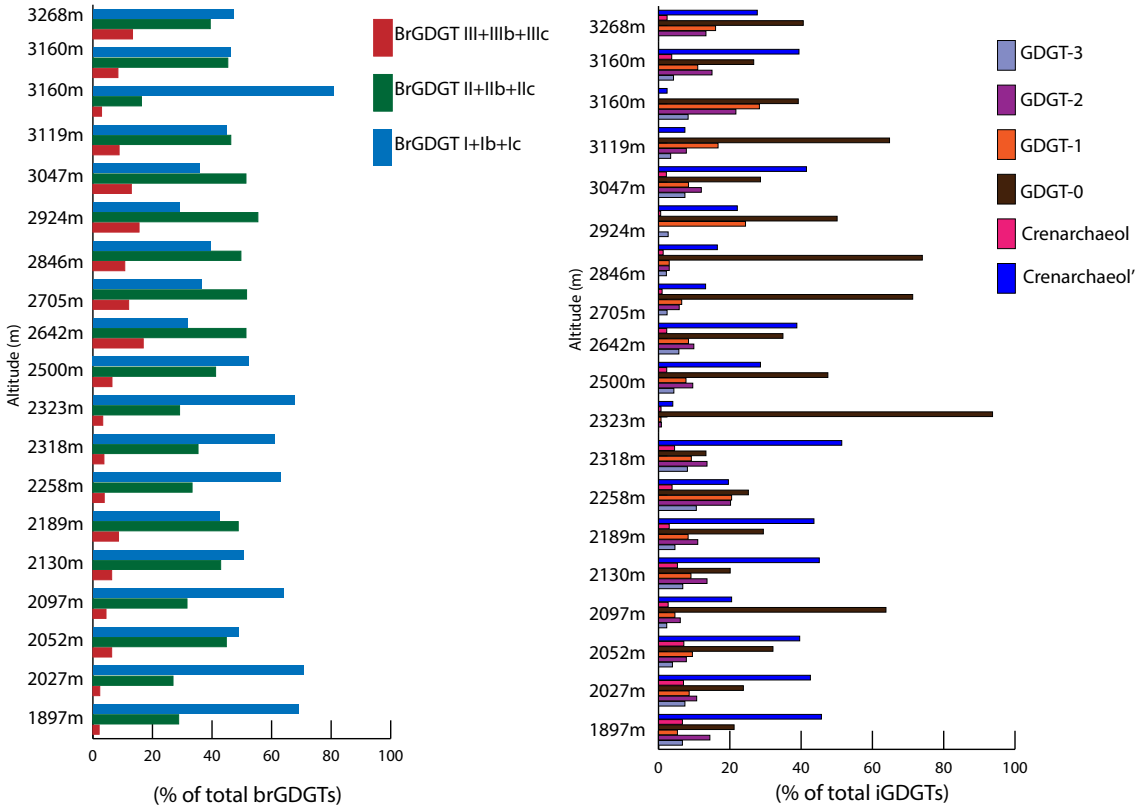

Figure 4-33: GDGT distribution in percent of the samples from the soil transect

The BIT values <1 (see *Equation 8*, pg. 69 for BIT calculations) imply that the methanogenic archaea are only a minor component of the microbial community in these soils. Above 3119 m asl the BIT index less than 0.5 due to significant contributions of iGDGTs and a decline in the relative abundance of brGDGT (Figure 4-34). In the samples below 3119m asl, a relative decline in the total GDGTs is observed alongside the relative abundance of brGDGT-II and GDGT-0 (Figure 4-33). The BIT index demonstrates a strong linear relationship with altitude where R^2=0.70 ($p < 0.001$). Although this value displays a good linear relationship, the index is dependent on other factors such as pH where an increase in soil pH favours the concentration of iGDGT that leads to a decline in the BIT values (Weijers et al. 2007).

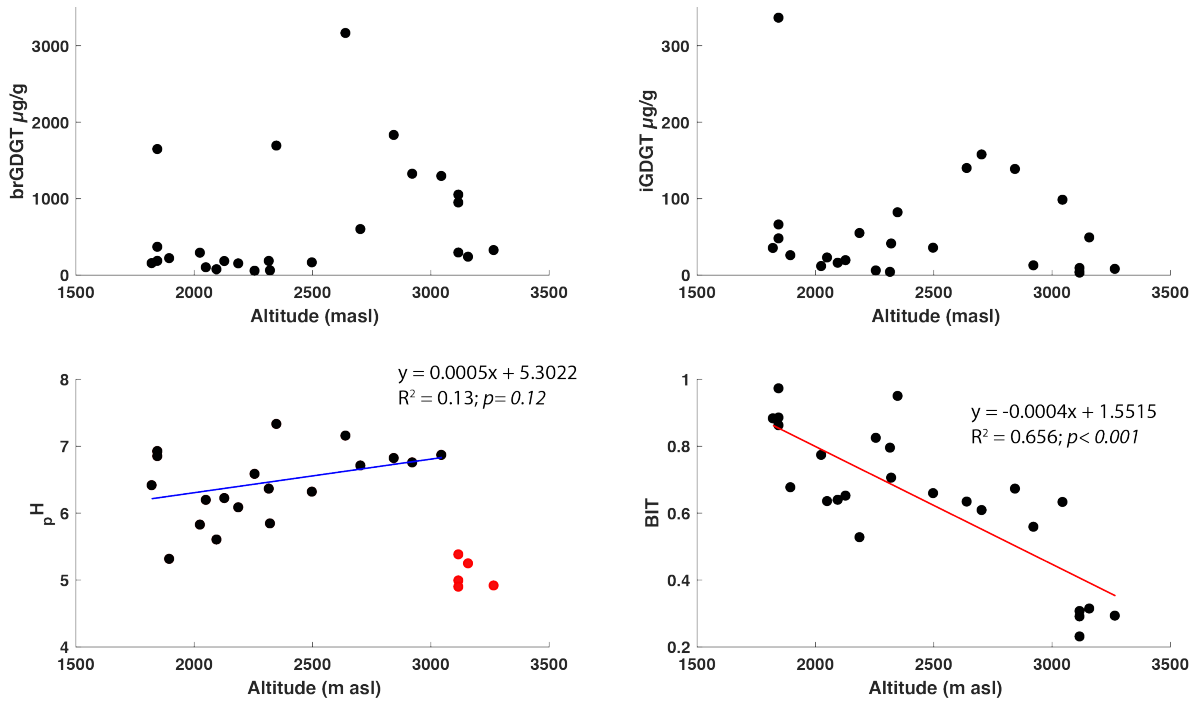

Figure 4-34: Bivariate plots of brGDGT, iGDGT, pH (the linear relationship is defined from the exclusion of the samples marked in red) and BIT indices along the soils transect in Mt. Kenya

4.2.3.3.1.2 brGDGT – derived proxies

pH, MBT, MBT' and CBT were calculated for all the soil samples from the altitudinal transect (Table 7). The reconstructed pH along the soil transect derived from calibrations by Peterse et al. (2012) and Weijers et al. (2007) display similarity in distribution with a weak correlation ($R^2 = 0.15$, $p = 0.05$, not shown in the figure). This relationship is weakened by the effect of the sample cluster above 3000 m asl where the pH values (4.5 – 5.0 pH units) are lower (Figure 4-34). The exclusion of these values provides a relationship defined by $R^2 = 0.130$; $p = 0.12$.

Table 7: brGDGT and iGDGT-derived proxies along Mt. Kenya transect

No.	Altitude (m asl)	BIT	MBT	MBT'	CBT	pH Weijers	pH Peterse	T Peterse	T Weijers	1302/1292	TEX86
1	1823	0.88	0.62	0.62	0.76	6.77	6.41	15.64	17.66	0.44	0.77
2	1847	0.97	0.50	0.50	0.50	7.45	6.92	13.58	14.29	7.00	n.d
3	1847	0.88	0.53	0.53	0.50	7.44	6.91	14.41	15.73	0.32	0.79
4	1847	0.86	0.58	0.58	0.54	7.35	6.84	15.60	17.64	0.41	0.77
5	1897	0.68	0.69	0.69	1.32	5.30	5.31	14.76	16.14	0.46	0.84
6	2027	0.77	0.71	0.71	1.06	5.98	5.82	16.76	19.42	0.56	0.74
7	2052	0.63	0.49	0.49	0.87	6.48	6.19	11.04	10.22	0.81	0.67
8	2097	0.64	0.64	0.64	1.17	5.69	5.60	14.15	14.97	3.11	n.d
9	2130	0.65	0.51	0.51	0.86	6.51	6.22	11.72	11.27	0.45	0.74
10	2189	0.53	0.43	0.43	0.93	6.33	6.08	8.75	6.52	0.68	0.69
11	2258	0.82	0.63	0.63	0.67	7.00	6.58	16.57	19.06	1.29	0.63
12	2318	0.79	0.61	0.61	0.78	6.70	6.36	15.33	17.09	0.26	0.74
13	2323	0.70	0.68	0.68	1.05	6.01	5.84	15.84	17.93	23.20	n.d
14	2350	0.95	0.36	0.36	0.29	7.99	7.32	10.39	8.98	0.18	1.00
15	2500	0.66	0.52	0.52	0.81	6.64	6.31	12.49	12.57	1.66	0.68
16	2642	0.63	0.32	0.32	0.38	7.76	7.15	8.66	6.16	0.90	0.68
17	2705	0.61	0.36	***0.37***	0.61	7.16	6.70	8.72	6.42	5.42	n.d
18	2846	0.67	0.40	0.40	0.55	7.31	6.81	10.09	8.57	4.47	n.d
19	2924	0.56	0.29	***0.30***	0.58	7.22	6.75	6.64	3.02	2.26	n.d
20	3047	0.63	0.36	0.36	0.53	7.37	6.86	9.02	6.82	0.69	0.72
21	3119	0.29	0.49	0.49	1.48	4.87	4.98	7.52	4.43	3.54	n.d
22	3119	0.31	0.40	0.40	1.28	5.39	5.37	6.04	2.08	1.49	0.65
23	3119	0.23	0.45	0.45	1.53	4.74	4.89	6.06	2.06	8.80	n.d
24	3160	0.31	0.46	0.46	1.35	5.21	5.24	7.49	4.40	0.68	0.68
25	3268	0.29	0.47	***0.48***	1.52	4.77	4.91	7.20	3.31	1.46	0.50

The CBT values range from 0.38 to 1.58 and are strongly correlated with reconstructed pH values ($R^2 = 1$, $p < 0.001$). On the other hand, the CBT values (Table 7, Figure 4-35) display a weaker relationship with altitude (R^2=0.14, p = 0.12).

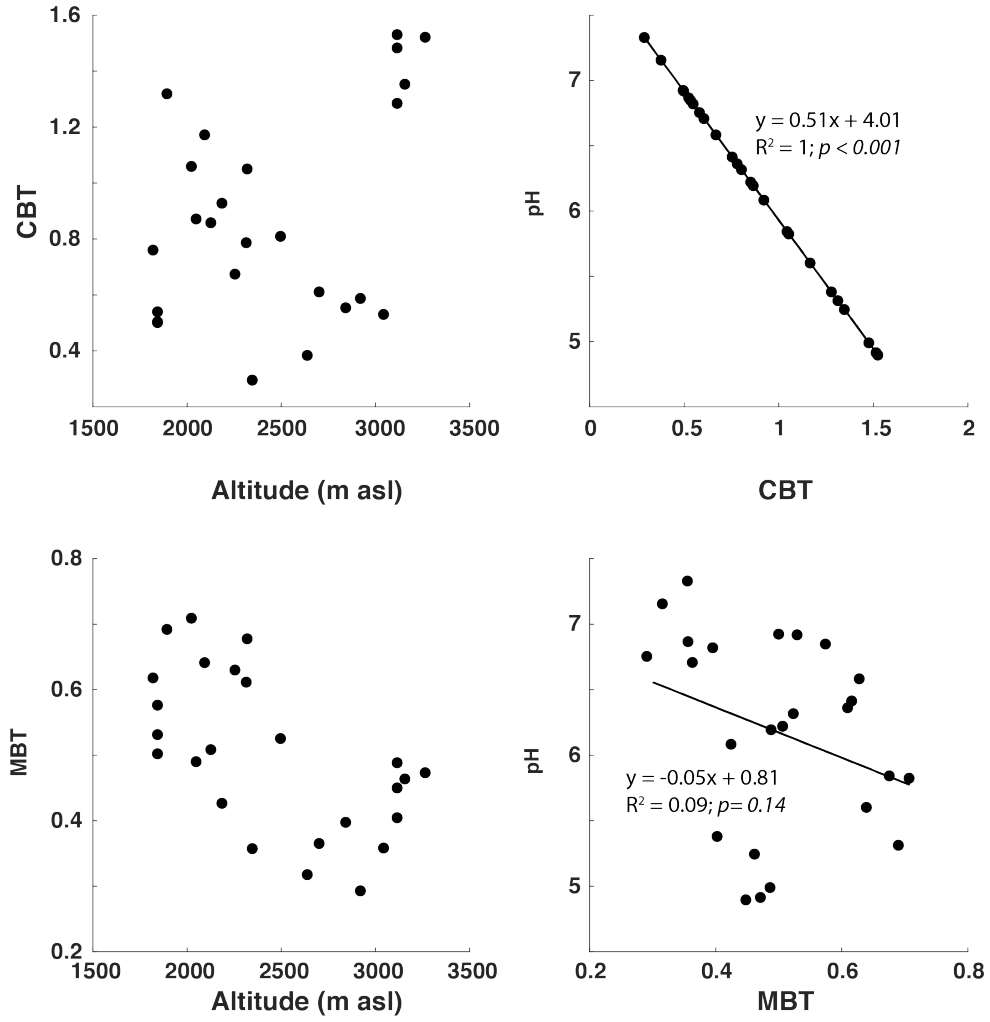

Figure 4-35: The relationship of the brGDGT and iGDGT derived indices with pH from the soil samples.

The samples above 3000 m asl deviate from the linear regression. Globally, CBT is negatively controlled by pH of the soils and this cluster of high altitude (>3000 m asl) acidic soils (pH 4.9 – 5.4) shows this coherency. Weijers et al. (2007) proposed that a decrease in the number of cyclopentyl moieties is associated with the permeability of bacterial cell membranes that regulate internal pH conditions within acidic soils. From our dataset, it is evident that the pH controls the cyclization of the brGDGTs as suggested by Weijers et al. (2007).

The MBT and MBT' values are identical in most cases with the exception of three samples (Table 7, pg. 108). A weak linear trend is observed between MBT and altitude ($R^2 = 0.37$, $p > 0.001$) as displayed by the large scatter of the dataset. MBT does not display a significant trend with pH ($R^2 = 0.09$, $p = 0.14$, Figure 4-35). This relationship is weakened by the pH of the samples above 3000 m asl; the exclusion of these samples improves the relationship between pH and MBT ($R^2 = 0.5$, $p = 0.0005$). In this case the acidity of the soils from Mt. Kenya increases the scatter in the pH – MBT relationship.

MAAT was reconstructed from the MBT, MBT' and CBT indices (Table 7, Figure 4-35) using calibrations defined by *Equation 4* and *Equation 5* (see pg. 69). The MBT/CBT derived MAAT ranges from 4° C to 16° C using the Weijers et al. (2007) calibration and 7° C to 14° C using the Peterse et al. (2012) calibration. The difference in temperature estimates from the two calibrations display a wide range from 0.82° C to 4.00° C along the altitudinal transect.

The MAAT and altitude along the transect in both cases display a strong linear relationship (Figure 4-36). The lapse rate of the reconstructed MAAT is 0.90° C / 100 m and 0.50° C / 100 m based on the Weijers et al. (2007) and Peterse et al. (2012) calibrations, respectively. Estimates from Worldclim data (Fick and Hijman 2017) provide a lapse rate of 0.55° C / 100 m (Figure 4-36). The temperature estimates from Peterse et al. (2012) are more consistent with temperature estimates from the Worldclim data than those based on the Weijers et al. 2007 calibrations. The application of the Peterse et al. (2012) calibration on Mt. Kenya presents realistic values and therefore this brGDGT-derived temperature proxy is applicable on this mountain.

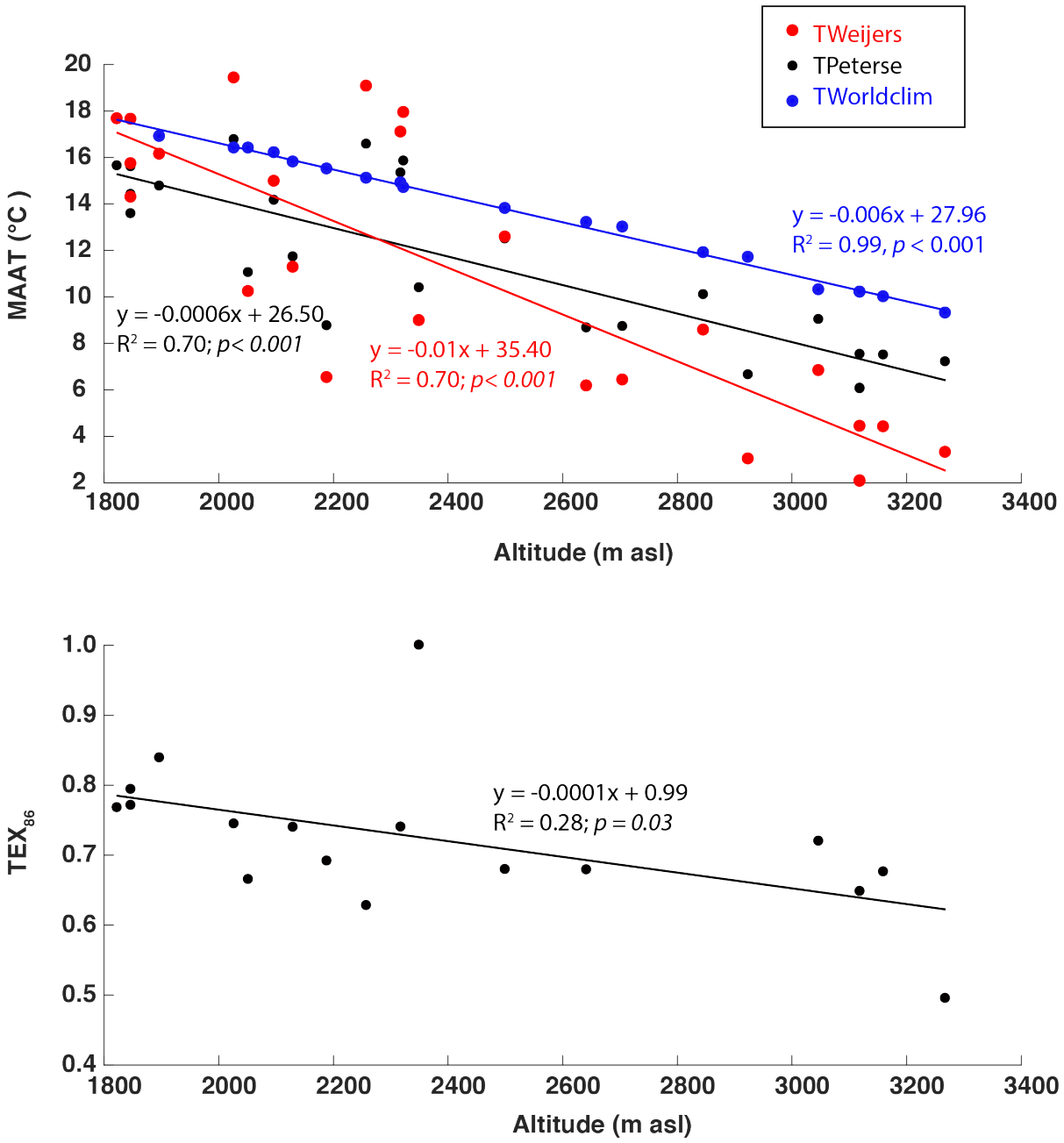

Figure 4-36: brGDGT and iGDGT derived proxies. The upper panel shows the reconstructed MAAT from Weijers et al. (2007) in red, Peterse et al. (2012) in black, and Worldclim data (in blue) for the soil transect. The lower panel shows the reconstructed TEX_{86} along the soil transect.

4.2.3.3.1.3 iGDGT – derived proxies

The TEX_{86} was calculated for 19 of the 28 samples, as more than one of the iGDGTs necessary for this calculation were below detection limits (i.e. GDGT-3, GDGT-2 and GDGT1 were missing in various samples from the transect). A proper application of TEX_{86} requires that all the iGDGTs derived from *Thaumarchaeota* be present in the samples (Schouten et al. 2013).

This is not the case in these samples and therefore care must be taken in the interpretation of the results. The calculation of the caldarchaeol (GDGT-I) ratio to crenarchaeol ratio where this value is >2 are considered as an indicator of the dominance of the *Euryarchaeota* among the archaeal community (Blaga et al. 2009). This was not the case for some of the soil samples derived from the surface as the ratio was much lower than 2, ranging from 0.4 to 1.6 with the exception of 8 samples out of the 25 analysed in the transect (Table 7, pg. 108). From this ratio, 17 samples derived from *Thaumarchaeota* and therefore it is meaningful to calculate the TEX_{86} proxy for the samples. The TEX_{86} values (Figure 4-36) display a weak relationship with altitude (R^2 = 0.28, p = 0.03). In spite of the fact that the calculated TEX_{86} was reasonable, its applicability as a palaeoelevation calibration for the soil samples on Mt. Kenya is questionable due to the low R^2 value obtained that is lower than 0.50.

4.2.4 Synthesis of the Characteristics of the Surface and Subsurface Soils

The samples from the Nkunga area are predominantly weathered soils with the characteristic minerals being halloysite, gibbsite, magnetite and haematite. The presence of these weathered products has been associated with the weathering of older Quaternary palaeosols on Mt. Kenya through leaching of volcanic glass (Mahaney & Vortisch 1989) and therefore, is indicative of hot and humid conditions on the lower slopes of the mountain. The coexistence of gibbsite and halloysite in the surface soils reflects possible interaction with water (Parfitt et al. 1983; Parfitt & Wilson 1985; Mahaney & Vortisch 1989) from both precipitation and the lake itself during high stands. This is because, during chemical weathering of the volcanic tuff ring surrounding the lake, silica may be released in the pore solution and therefore, due to lower permeability and higher clay content there is the transformation of gibbsite to halloysite (Mahaney & Vortisch 1989).

From the Nkunga soil profile, the grain size and mineralogy provide a context of the physical characteristics and origin of the soils. The inorganic geochemistry (Fe and Mn) links potential redox and low pH zones within the soil profile. These zones are aligned with the magnetic mineralogy and %C composition as follows: (i) declining %C and increasing %C (ii) Slight localized enhancements in the magnetic susceptibility (at 100 cm) within the soil profile correspond to decline in $\%X_{fd}$ indicating the iron re-deposition (or the inclusion) of less weathered granules the soil profile within this section (Maher 1986). Multiple sources of the magnetic component are implied by the NRM from Nkunga area and the soil profile is representative of erosion, deposition and the *in-situ* changes in the soil profile.

The Sacred Lake soil profile displays an abundance of plagioclase feldspars with halloysite and gibbsite. Gibbsite and halloysite coexist in this soil profile, which is not surprising as the site is in a relatively moist and humid area where leaching processes can easily occur. This reflects weathering of aluminosilicates as observed in the Al profile where high Al values are detected at the bottom of the soil profile. Haematite and magnetite are observed at the bottom of the soil profile only and correspond to relatively higher magnetic susceptibility, as well as a decline in $\%X_{fd}$. This could be attributed to the incorporation of the non-SP grains in the soils as the corresponding X_{lf} is markedly low (Maher 1986). The relatively low X_{lf} values from Sacred Lake profile correspond to measurable $\%X_{fd}$ probably due to the presence of superparamagnetic inclusions in a mostly clayey and paramagnetic matrix. The Sacred Lake soils display a uniform trend in the NRM that can be linked to a single source of the magnetic minerals. The $\%X_{fd}$ of all the samples points to the mix of SP and coarser soft grains, probably coarse-grained titanomaghemite. On the other hand, the low values centred at 144 cm point to the presence of haematite, which is observed in these samples. The reducing environment at the bottom of the profile is further supported by the low %C and a bimodal n-alkane distribution. A progressive increase in %C is observed towards the top of the profile when oxidizing conditions are observed with accompanying unimodal n-alkane distribution of terrestrial vegetation.

Along the soil profile, the mineralogy comprises plagioclase feldspars, magnetite, gibbsite and diopside. Subtle changes are observed with altitude where the lowest altitude sample (1897 m asl) lacks plagioclase feldspars while in the samples above 2500 m asl, the presence of chlorite is observed. At mid to high altitudes sanidine and labradorite (not shown in the graphs) are present, reflecting the parent rock mineralogy. The bulk susceptibility of soils generally declines with increase in altitude. Localized peaks that could be linked to detrital matter inputs derived from catchment erosion punctuate this general trend. The greatest scatter of the magnetic susceptibility is observed in the samples above 3000 m asl. The coercivity S-ratio is the main controlling factor of the magnetic component. In all the soil samples, the S-ratio is very high showing the resistance of the magnetic components present in the soil at the -300_{mT} backfield at nearly 80 – 90 % of the initial forward magnetisation. This is characterized as canted antiferromagnetic behaviour that is present where there are significant quantities of hematite especially below 2500 m asl. Quartz is dominant in all the soils samples but absent in the rock samples. This is likely due to aeolian enrichment of fine-grained quartz sands from quartz rich areas transported by NE and SE monsoon winds that blow over regions dominated

by units derived from basement rocks (Mahaney 1990; Olago and Odada 1996). A mix of C_3 – C_4 type vegetation is encountered along the transect. The C_3 type is found above 2500 m asl while C_3 – C_4 mix is present between 1800 and 2500 m asl. Below 2000 m asl, the n-alkanes distribution is bimodal while it is unimodal in the upper reaches of the mountain.

PCA was used to assess the dominant geochemical signal of the different indicators in order to elucidate the relationships between the soil from Nkunga area and Sacred Lake. The analysis was carried out on the geochemical elements normalized against Ti: Fe/Ti, Al/Ti, Cl/Ti, Si/Ti, S/Ti, Nb/Ti and K/Ti. The first PC axis (PC1) accounts for 80.0 % of the total variance and is positively correlated to all ratios except Cl/Ti (Figure 4-37). The correlation of Al/Ti and Fe/Ti suggests that the positive values on this axis represents varying inputs from the sources and the axis reflects the influence of weathering and erosional processes on the soil samples from the catchment. On the other hand, PC2 explains 14.5 % of the total variance and positively correlate to Al/Ti, Si/Ti and K/Ti (in-situ erosional process) while negatively correlates to the rest of the ratios (concentration of the lithogenic residue following chemical erosional processes). Significant correlation is seen in the S/Ti and Cl/Ti ratios and reflects aeolian transport and deposition that plays a key role. The samples from the upper sections of the soil profile from Sacred Lake (SL-02, SL-05) and surface samples from Nkunga crater (NK11-02 and NK11-07) are most affected by the aeolian deposition (Figure 4-37).

The craters on the north eastern slopes of Mt. Kenya are composed of ash or ash and lava (Mason 1953; Baker 1967) from the Nyambeni volcanics which have not been well investigated. From the field observations, the exposures from the Nkunga crater wall are made up of tuffs and alkali trachyte. Since the samples were largely collected within the crater, these samples present the signature of the Nyambeni parasitic eruptions (Mason, 1953). The Sacred Lake crater wall, on the other hand, is not well exposed and could not be sampled during the field studies. The samples analysed were collected outside the crater and it is therefore possible that the source of the magnetic carrying component in Sacred Lake is associated with titaniferous olivine basalts from the upper Mt. Kenya basalts based on the geology of the lake catchment (Mason, 1953). The differences in the inorganic geochemistry point to the different geology of the parasitic eruptions from Nyambeni volcanics and the main volcanic event from the eruption of Mt. Kenya.

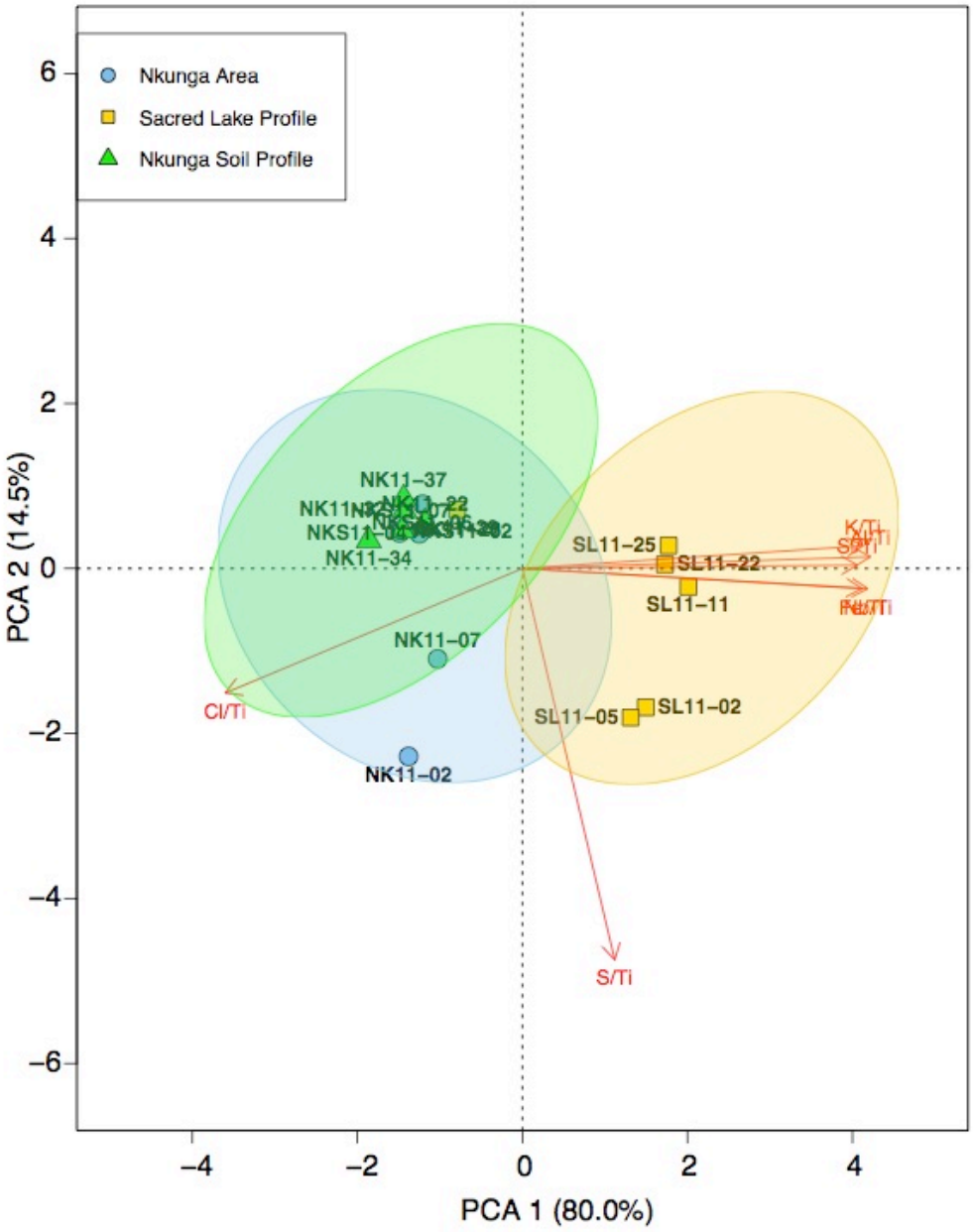

Figure 4-37: PCA of the geochemical properties from Nkunga area soils (blue circle), Nkunga soil profile (green triangle) and Sacred Lake soil profile (yellow square).

In addition, field observations indicate that the morphology of Lake Nkunga crater rim is better preserved than the Sacred Lake crater rim, consistent with a more recent age for the Lake Nkunga crater. Still, contrasted erosion and weathering state of the two craters are evidenced. This is further strongly supported by Figure 4-37, where the PCA axis 2 formerly interpreted as a "chemical weathering index" shows positive and higher values in Sacred Lake soils.

Generally, in the soil profiles, increased inputs of minerogenic inputs, as observed in the geochemistry and magnetic susceptibility in the catchment are accompanied by decreased %C values. The predominant source of OM in the soils is from terrestrial origin as seen in the abundance of brGDGTs and from the supporting n-alkane data. The reconstructed brGDGT derived proxies for MAAT show a decline with altitude consistent with previous observations (Peterse et al. 2009, Weijers et al. 2006, Sinnighe Damsté et al. 2008) and thus is coherent with the use of brGDGTs as indirect indicators of changes in temperature with altitude. The samples from the higher altitudes above 3000 m asl, deviate from the brGDGT derived proxies, perhaps pointing to their palaeosol nature as they were collected in a dry patch of the ericaceous forest zone. The weak linear trend observed between MBT and altitude ($R^2 = 0.37$) is weaker than those obtained from Mt. Xiangpi, China where the $R^2 = 0.69$ (Liu et al. 2013) and closer to values from Mt. Rungwe, Tanzania where $R^2 = 0.39$ (Coffinet et al. 2014). These differences could be partly linked to the pH differences in the soils, 7.0 ± 0.2 and 6.0 ± 0.5 for Mt. Xiangpi and Mt. Rungwe, respectively.

The iGDGT derived temperature proxy TEX_{86} is linked to the distribution of *Thaumarchaeota* in the soils (Schouten et al. 2007, Kim et al. 2010, Sinnighe Damsté et al. 2012). In this study, there is no clear trend in the TEX_{86} ($R^2 = 0.28$). This is unlike the values obtained from a much shorter transect (Coffinet et al. 2014) from 500 – 2500 m on Mt. Rungwe, Tanzania and a higher altitude transect (Liu et al. 2013) from 3250 – 4100 m on Mt. Xiangpi, China where a stronger linear correlation ($R^2 > 0.5$) was obtained. The application of the TEX_{86} along our altitudinal transect as a temperature variable is not reliable and therefore it is not suitable as a palaeoelevation proxy. The poor correlation of the TEX_{86} with altitude implies a possible contribution of iGDGTs derived from Thaumarchaeota as the predominant source of variability. This is comparable to observations in other locations such as Mt. Rungwe (Coffinet et al. 2014), Mt. Xiangpi (Liu et al. 2013) and the global soils database described by Weijers et al. (2006) where such organisms are present. This further explains the inability to calculate the TEX_{86} proxy for some of the samples as the Thaumarchaea in soils have been observed to synthesize crenarchaeol and its regio isomer (Sinninghe Damsté et al. 2012).

4.3 Lake Nkunga Sediments

4.3.1 Bulk Sediment Parameters

4.3.1.1 Stratigraphic Description

Two core sections (top section NKG-I-1-2013; 45 cm and bottom section NKG-I-2-2013; 44 cm) were recovered from Lake Nkunga, spanning a combined total depth of 89 cm at a water depth of 1 m (Figure 4-38) approximately 20 m from the lakeshore. Generally, the cores obtained were in good condition with no visible deformation from the extraction process. At the base of the core, olive black (Munsell colour - 5Y 2/1) sediments comprising a mix of coarse detrital material such as sand and pebbles, with fragments of macroscopic plant remains, were identified from 89 to 77 cm (Figure 4-38). At 79 cm, this unit ends abruptly with the introduction of reworked volcaniclastic material contained in an ill-preserved ash horizon, thus cannot be used as a stratigraphic marker. From 77 to 58 cm brownish black sediments (Munsell colour - 5YR 2/1) comprising clayey silts with a few pebble clasts are present while between 58 – 17 cm greyish brown (Munsell colour - 5YR 3/2) clayey silts are observed.

A section of reworked ash/pumice and charcoal like particles (ranging in size from 0.5 to 2.0 cm) are present between 32 and 37 cm. The uppermost layer comprises a homogeneous dusky yellowish brown (Munsell colour – 10YR 2/2) silty clay at 17- 0 cm (Figure 4-38). The water content (W_c) values range from 29 % – 54 % throughout the core with an average of 39 % for the 89 samples collected at 1 cm intervals. Generally, W_c increases from the bottom to the top of the core with a sharp positive excursion at 35 cm.

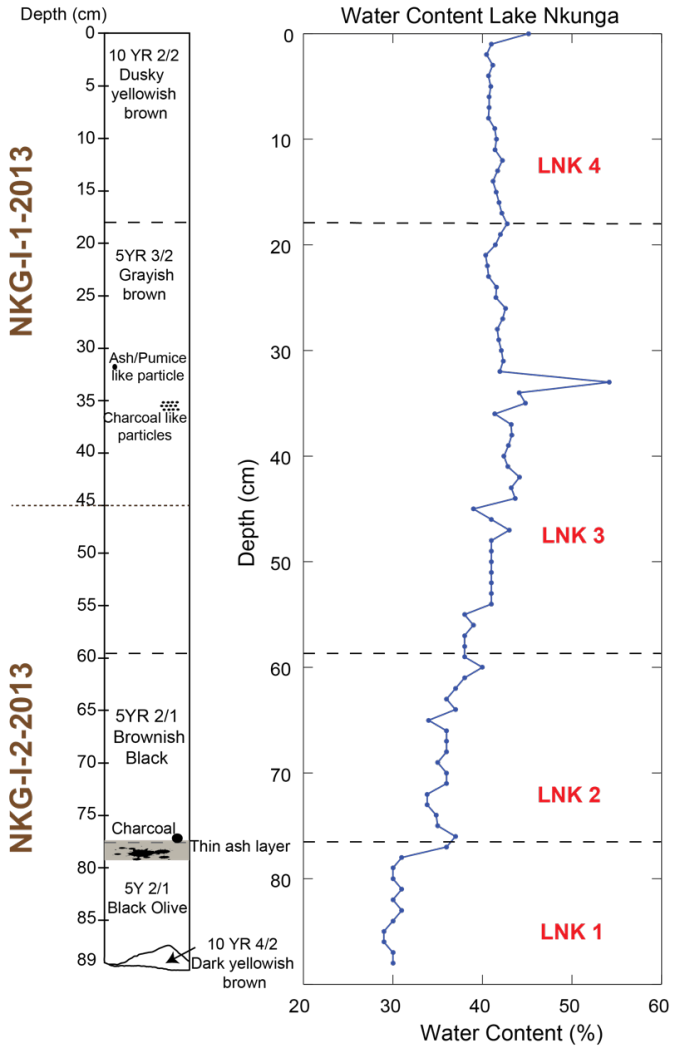

Figure 4-38: The descriptive stratigraphic section and percentage water content of Lake Nkunga cores NKG-I-1-2013 and NKG-I-2-2013.

Although different lithologies are present in this core, they do not define distinct stratigraphic or sedimentological indicators (such as banding). A stratigraphically constrained hierarchical cluster analysis was therefore carried out using the Rioja (Juggins 2017), a statistical package in R for the analysis of Quaternary data. The hierarchical clustering was carried out on the combined compositional variation of the OM based on %C, %N, $\delta^{13}C$ and $\delta^{15}N$ and led to the identification of four significant stratigraphic zones: low OM in LNK1 (89 – 77 cm), increasing OM in LNK2 (77-58 cm), oscillating changes in OM within LNK3 (58-13 cm) and insignificant OM changes in LNK4 (13-0 cm).

4.3.1.2 Radiocarbon Chronology

Ten radiocarbon dates were obtained from bulk sediment samples with the exception of one sample, which was a charcoal sample, retrieved at 78 cm depth (Table 8). The calibration of the individual ages (cal yr. BP) obtained using the intCal13 (Reimer et al. 2013) are presented in Table 8 below.

Table 8: Radiocarbon ages from Lake Nkunga sediment core obtained from the AMS (Age ^{14}C yr. BP) and the calibrated radiocarbon ages (Cal yr. BP and their associated errors). The samples marked in bold were identified as probable outliers

Lab No	Sample	Depth (cm)	Age ^{14}C yr. BP	cal yr. BP
SacA34944*	**NKG- 8-2013**	**8**	**465 ± 30**	**495±88**
SacA34945*	**NKG-18-2013**	**18**	**430 ± 30**	**483±79**
SacA34946	NKG-28-2013	28	380 ± 30	466±61
SacA34947	NKG- 38-2013	38	445 ± 30	488±85
SacA34948	NKG- 45-2013	45	455 ± 30	492±89
SacA34949	NKGII-5-2013	50	525 ± 30	533±45
SacA34950	NKGII-15-2013	60	635 ± 30	609±82
SacA34951	NKGII-25-2013	70	775 ± 30	723±86
SacA34952*	**NKGII-Charcoal**	**78**	**470 ± 30**	**498±86**
SacA34953	NKGII-43-2013	88	1230 ± 30	1069±82

The obtained radiocarbon ages displayed strong age reversal in the top 30 cm. These reversals in the selected samples are thought to be probable artefacts of mechanical sediment mixing by bioturbation (SacA34944 and SacA34945). Previous studies (Olago 1995) have shown that there is a feasible contamination of the water and sediments in this lake by old carbon. Bacon v2.3 (Blaauw & Christen 2011) was used to generate a robust age-depth model to provide chronological coherency against the outlying ages shown in Table 8 (Figure 4-39).

This age-depth modelling technique estimates the calibrated radiocarbon ages of the sections of the core that were not dated (see section 3.1.5) and generates values that are chronologically ordered at 1 cm interval for the entire sediment core (Figure 4-39). The dated charcoal sample SacA34952 yielded an age close to the general bulk dates that point to a distinct sedimentation event around 500 – 400 cal yr. BP (Figure 4-40).

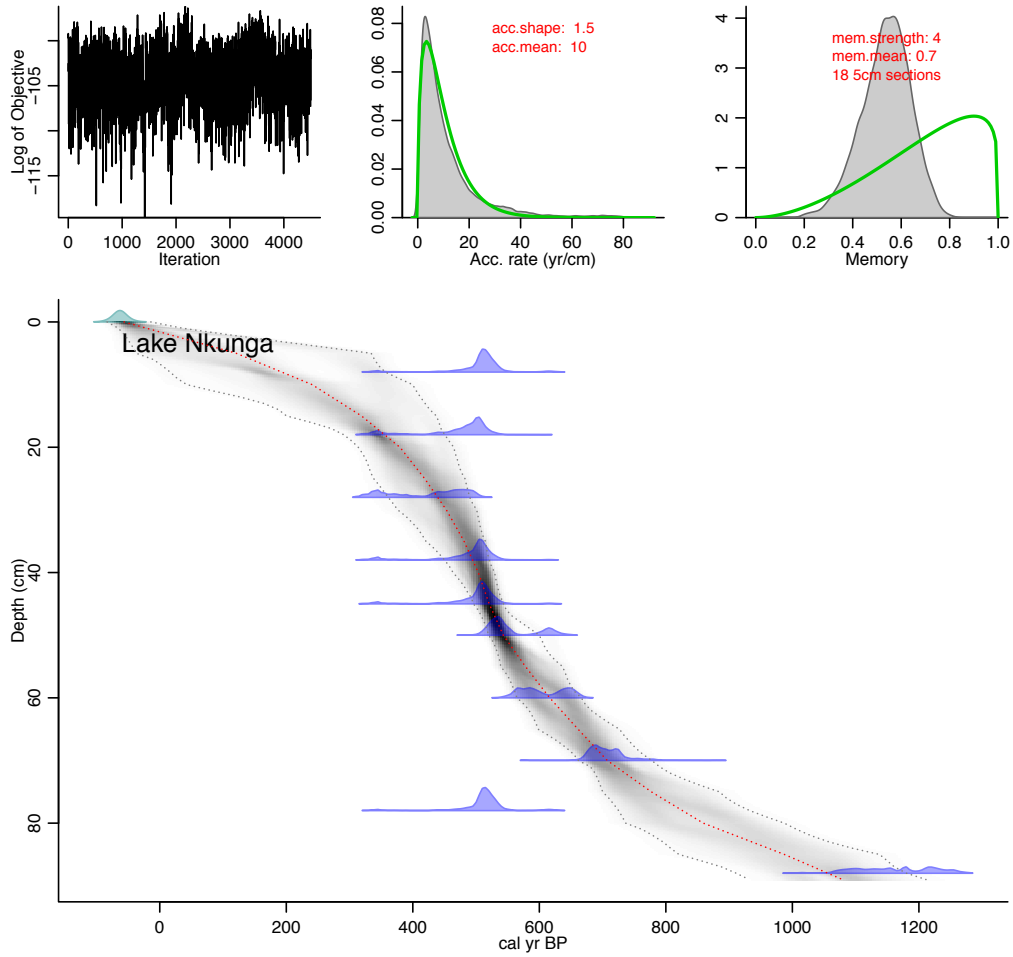

Figure 4-39: Bayesian age depth model constructed with Bacon age-depth model software Bacon for Lake Nkunga sediment core. The bottom panel shows the calibrated ^{14}C dates (transparent blue) and the age-depth model within 95 % confidence intervals. The darker grey areas on the model represent the more likely sections where the model is running through whilst the red curve shows the single 'best' model based on the weighted mean age for each depth. The upper panels show the MCMC iterations: the left represents the stability of the model while the middle and the right represent the prior (green curve) and posterior (grey histograms) distributions of accumulation mean and memory properties, respectively.

The top of the sediment core was fixed to the year the core was collected (2013) as previous test runs of the age-depth model produced large uncertainties in the upper section. The age-depth model generated shows that the sediments for Lake Nkunga cover 1079 ±140 cal yr. BP to Present. The sedimentation rate ranges from 0.03 to 0.6 cm/yr. (Figure 4-40). The sedimentation rate increases from the bottom of the core to about 40 cm (Figure 4-40). After 40 cm, a rapid decline in sedimentation is observed to the top of the sediment core.

Since the sediment core obtained is near shore, the rate of change in the sedimentation implies periods of shallow and deep lake intervals where there are periods of increased sedimentation in the lower section (deep lake phase) and a decline in sedimentation in the upper section (shallow lake phase) of the core. Due to the chronological ordering from the age model (Figure 4-39) and the accompanying sedimentation rate (Figure 4-40), the charcoal sample dated at 78 cm (SacA34952) was treated as a "dropstone" from the layer between 43 – 37 cm on account of density differences between it and loose sediment matrix at the time of deposition.

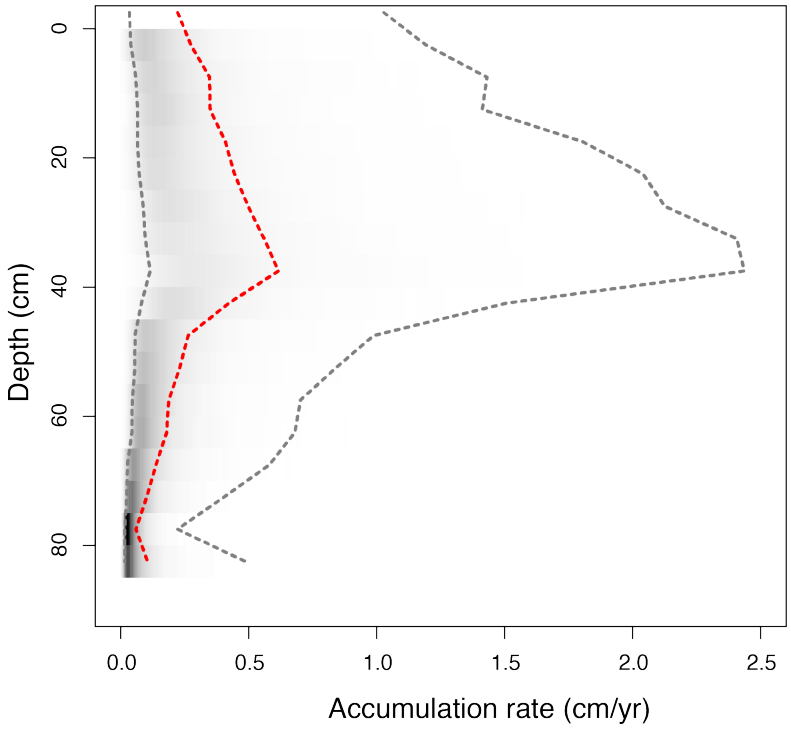

Figure 4-40: A ghost plot for the sediment accumulation rate for Lake Nkunga. The darker the grey shaded areas the more certainty in value obtained while the red line is the weighted mean representation of the accumulation between the different depths along the sediment core.

4.3.1.3 Bulk Mineralogy and Mineral Magnetics

Plagioclase and potash feldspar (60 – 70 %), quartz (10 %), haematite (10 %), gibbsite (1 %), halloysite (10 – 20 %), diopside (10 %) and illite (1 %) are the major mineral peaks detected in the sediment core samples (Figure 4-41). Feldspars are abundant, comprising labradorite and sanidine, with minor contributions from the other plagioclase feldspars and quartz throughout the sediment core. The presence of illite, intermittently alongside quartz (samples collected at 86 cm, 77 cm, 58 cm, 24 cm and 1 cm) could be attributed to aeolian deposition. Illite is the

dominant clay present in the samples but kaolinite was also identified. This not surprising as illite and kaolinite are derived from feldspar rich volcanic rocks (felsic silicates), which constitute the rocks of Mt. Kenya.

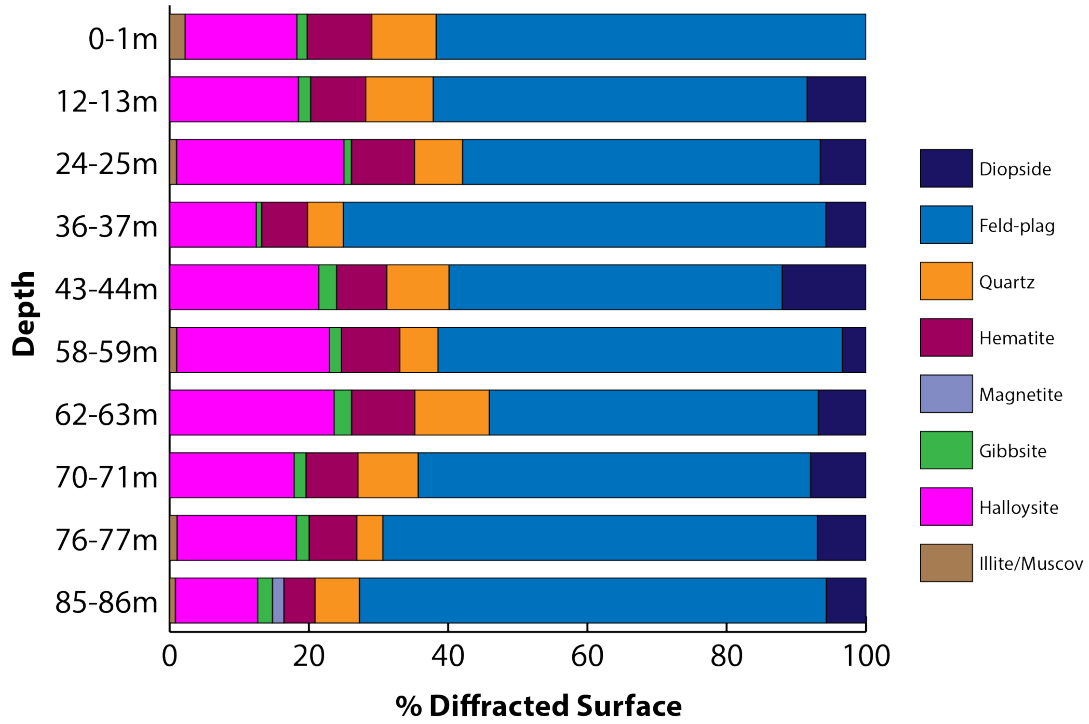

Figure 4-41: The average quantitative mineralogy from the Lake Nkunga core based on the percentage of the diffracted surface of analysed samples

Low X_{lf} values displaying progressive decline up core ranging from 1.7×10^{-6} m^3kg^{-1} to 8.0×10^{-6} m^3kg^{-1} characterize the magnetic mineralogy of these sediments. Relatively higher peaks at 59 cm, 45 cm, 11 cm and the last 5 cm of the sediment core interrupt the trend and represent localized increases in ferrimagnetic concentration. During the initial lake rejuvenation and deep lake phases, higher X_{lf} values are recorded (LNK1 and LNK2). The shallowing phase of the lake is characterized by lower X_{lf} values. Despite the low X_{lf} values, the presence of paramagnetic grains, based on measurable $\%X_{fd}$, is noted (Figure 4-42). The $\%X_{fd}$ range of all the samples points to a source with a mix of SP and coarser non-SP grains. The $\%X_{fd}$ values display two distinct patterns in the lower and upper sections of the core characterizing the deep and shallow lake phases.

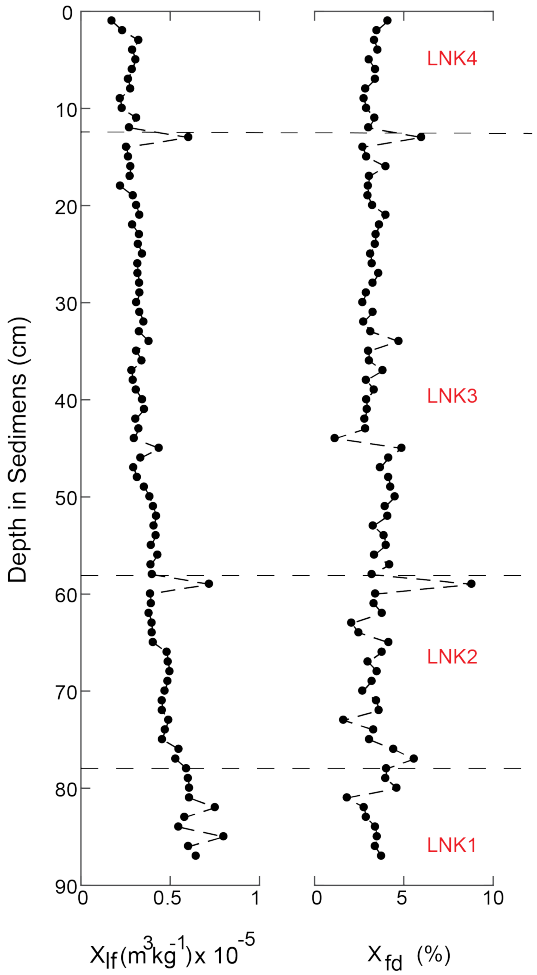

Figure 4-42: Down core variation of bulk mass magnetic susceptibility in sediments from Lake Nkunga.

The results of Alternating Field (AF) demagnetisation of the sediment samples give MDF values between 17 and 38 mT with the exception of samples at 9 cm (52.3 mT), 11 cm (55.9 mT) and 13 cm (95.6 mT), which have distinctly different values (Figure 4-43). These samples are from the upper section of the core, linked to the shallowing of the lake and perhaps characterising episodes of increased terrestrial input. The unique curves of the NRM point to a single source of magnetic minerals for the samples. The NRM intensities are almost completely demagnetized at about 50 mT although a few samples display subsequent magnetisation above this AF value (Figure 4-43).

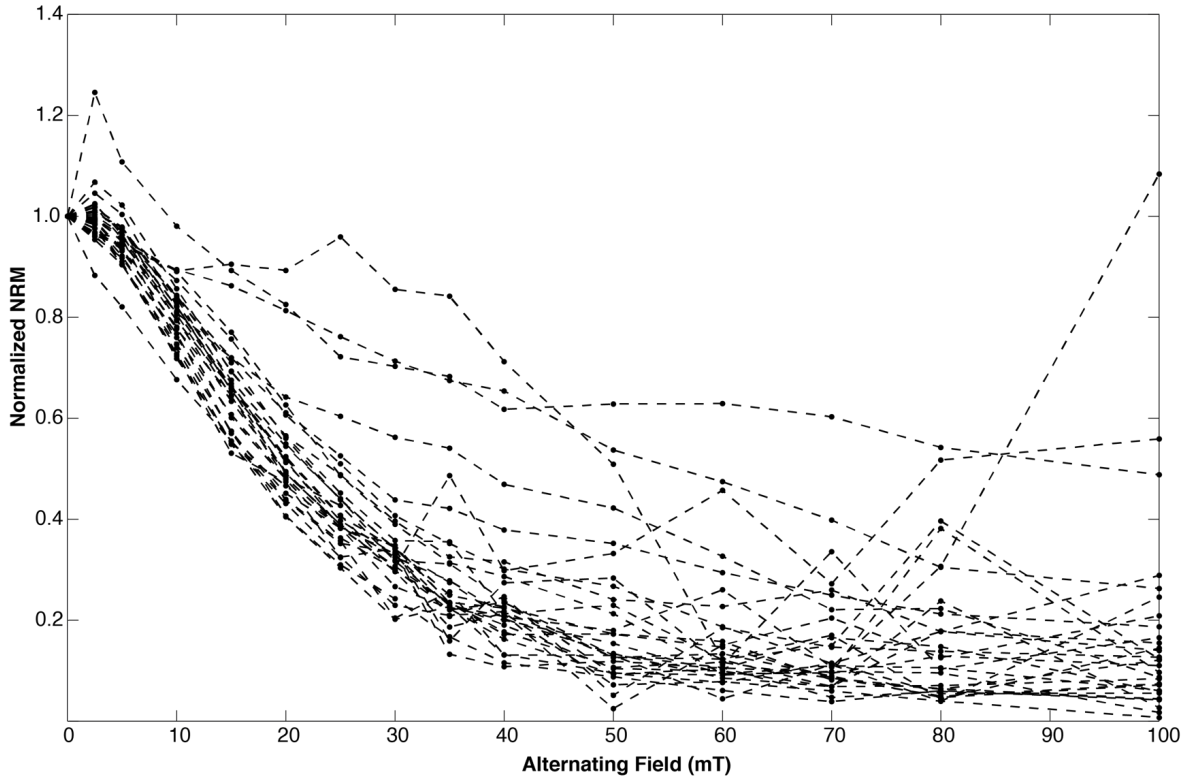

Figure 4-43: NRM profile from Lake Nkunga sediment core

The results indicate a mix of fine and coarse-grained magnetite or titanomagnetite with the exception of samples with higher MDF that implies the presence of haematite/goethite. Progressive decline of ARM_{30mT} and IRM_{-300mT} is observed from the bottom to the top of the sediment core (Figure 4-44). The S-ratio points to high coercivity ranging from 0.98 to 1.2 with higher values during the rejuvenation and deep lake phases and lower values during the shallow lake phase. ARM_{30mT}, IRM_{-300mT}, SIRM and SARM display similar trends where the lake rejuvenation and deep lake phase display minimal variations while the upper section of the core shows a decline in these values. The range of ARM_{30mT} varies from 0.5 $x10^{-4}$ Am^2kg^{-1} to 2.2 x 10^{-4} Am^2kg^{-1} with correspondingly low SARM values whereas that of IRM_{-300mT} varies from 0.014 – 0.05 Am^2kg^{-1}. The ARM_{30mT}/SARM varies from 0.1 – 0.3 where 0.1 represents a prominent dip in the ratio. At the IRM_{-300mT} backfield nearly 98 % – 102 % of the initial forward magnetisation is present and is thus characterized as canted antiferromagnetic behaviour representing significant quantities of haematite/goethite. On the other hand, the low ARM_{30mT}/SARM ratio characterizes the dominant state of the remanence carrying component of the sediments as soft multi-domain viscous grains.

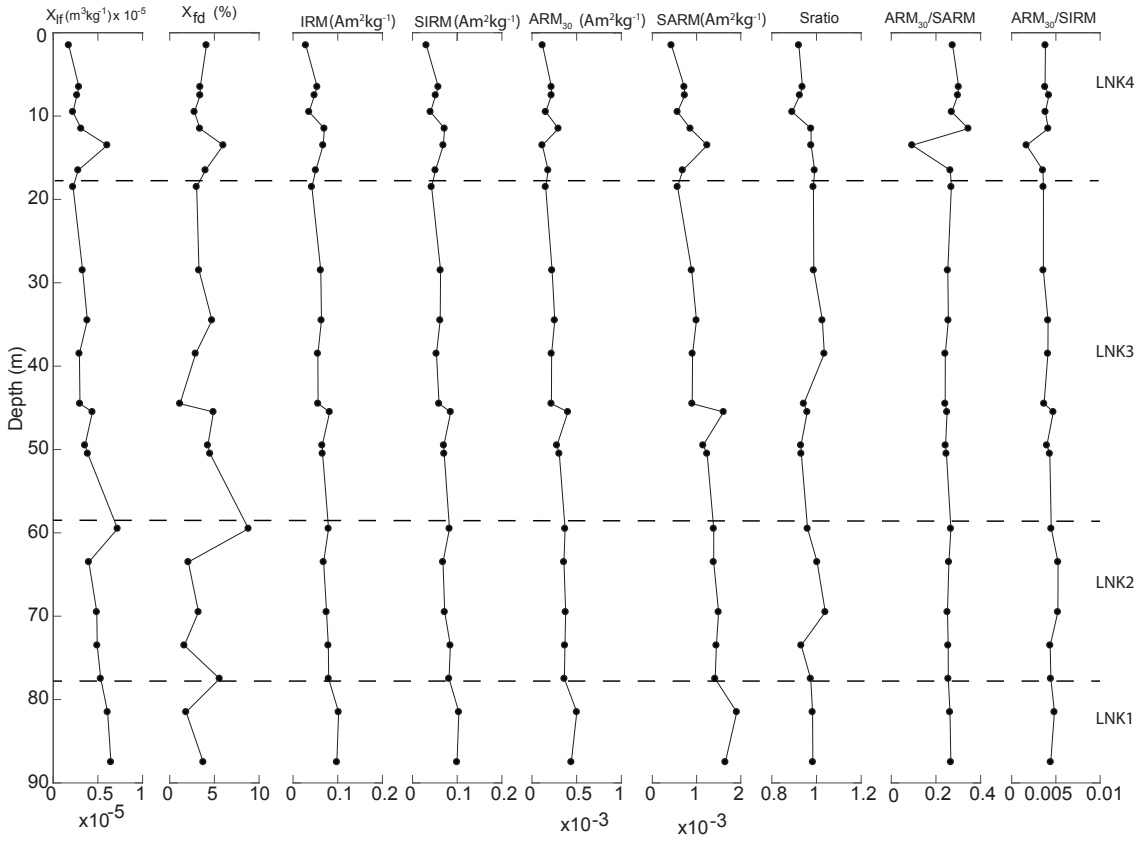

Figure 4-44: X_{lf}, X_{fd}, Anhysteretic and Isothermal Remanent Magnetisation profiles for Lake Nkunga sediments

4.3.2 Inorganic Geochemistry of Lake Nkunga

Lake Nkunga contains 18 detected elements (Al, Si, Ti, Ca, Cl, Cu, Fe, K, Mn, Nb, Ni, P, Rb, S, Sr, V, Zn, Zr). The peak area (cps) for Al signal after data correction displays a dramatic jump in values between the upper and lower sections of the retrieved core. This inconsistency in the Al spectrum between the two sections of the core meant that the dataset from this particular element is not a reliable indicator of the sediment source changes and is therefore excluded in our results interpretation. Of importance to lakes are the weathering and erosion indicators such as Si, K, Ti, Fe, Rb and Zr that are known to be geochemically stable and conservative in most geochemical environments (Boës et al. 2011). Caution is exercised in our interpretation of Si as in some cases Si is linked to authigenic production.

The second group of elements of importance are Fe and Mn usually linked to in-lake redox processes (Boyle 2001). These selected elements were subjected to principal component

analysis. The first principal component (PC1) accounts for 42.4 % of the variability while the second principal component (PC2) accounts for 24.9 % of the variability (Figure 4-45). PC1 positively correlates with Fe, Mn, Fe/Ti and Fe/Mn that are representative of redox processes in the lake and negatively correlates with K, Rb, Si, Sr, Ti, Zr, Si/Ti, K/Ti and Rb/Zr that are representative of a clastic phase derived from the catchment weathering and erosion processes. PC2 positively correlates with Mn, Rb, Zr and Rb/Zr representing in-lake redox conditions as well as grain size variation within the sediment core and negatively correlates with Fe, K, Si, Sr, Ti, Si/Ti, Fe/Ti, Fe/Mn and K/Ti representing enrichment in the clastic phase once more mobile elements are removed. From the PCA, it is evident that the weathering, erosion and deposition processes of geochemically stable elements are as important as the *in-situ* lake processes.

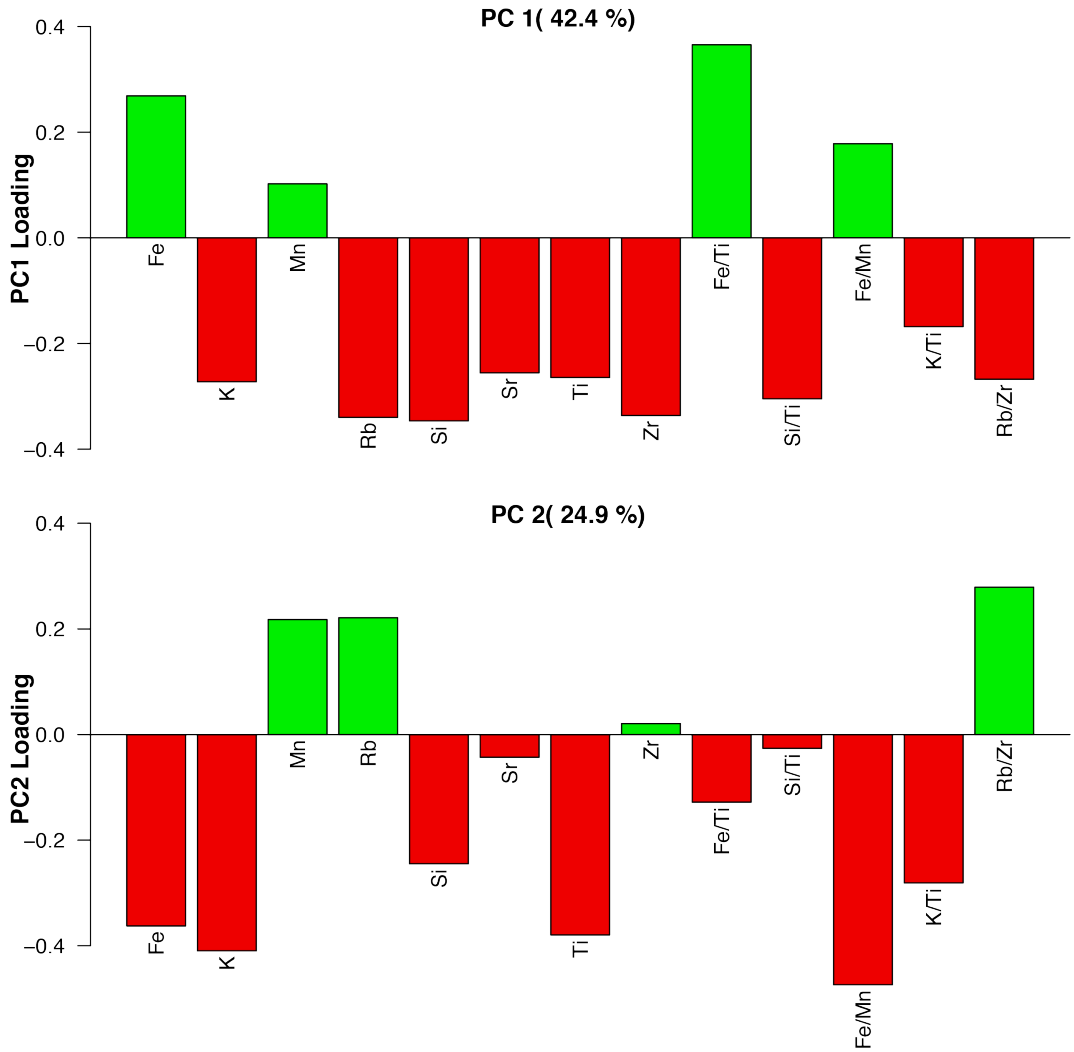

Figure 4-45: PCA of the elements from Lake Nkunga. Green bars represent the positive correlations while red represents negative correlations. The upper and lower panels show PC1 and PC2 respectively.

In order to examine the variations along the core further, Fe, Mn, Ti, Si/Ti and Fe/Ti were selected as proxies of sediment characterization and in-lake processes. Most of the variations along the sediment core are observed within LNK1 where Fe, Mn, Ti, Si/Ti and Fe/Ti profiles (Figure 4-46) display fluctuations. The Si/Ti displays an increasing trend within LNK2 followed by indistinct oscillations within LNK3 while in the upper section of LNK4 a decrease is observed. From the PCA, the Si/Ti ratio is linked to the clastic component, these changes can be attributed to the aeolian transportation of quartz rich fragments from the basement rocks as the catchment rocks from the Mt. Kenya suite are derived from sodic potash rich magma (Shackleton 1946, Baker 1967).

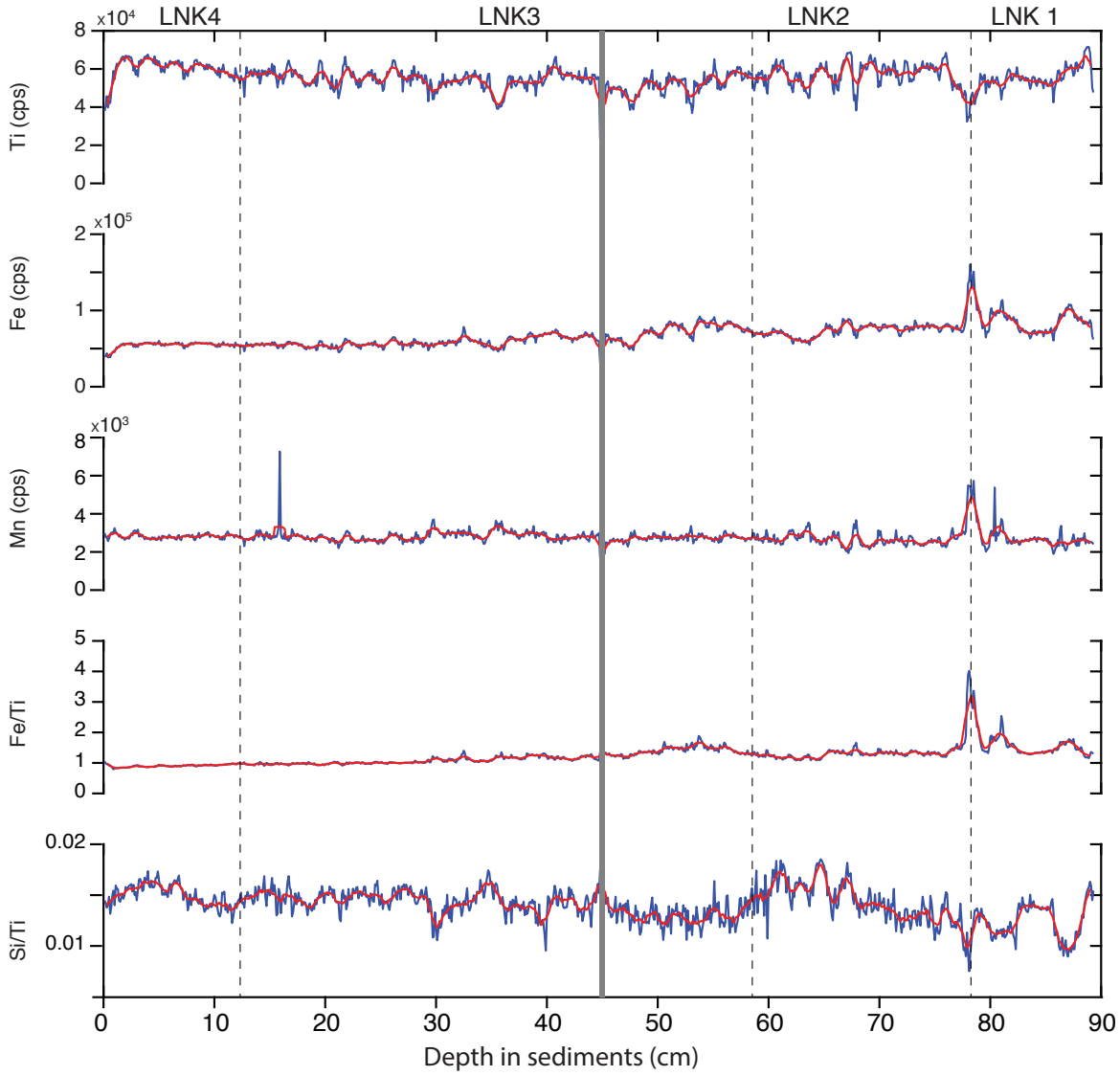

Figure 4-46: Geochemical proxies for Lake Nkunga. The blue graph displays the normalized values at every one-millimetre interval while the red graph shows the moving average over one-centimetre interval down the sediment core. The grey line marks the boundary between the two core sections for Lake Nkunga.

Initially, indistinct oscillations in the Fe/Ti profile are observed from the bottom of the core to 30 cm after which, the profile does not display any changes. Fe/Ti is often used as an indicator of grain size (Marshall et al. 2012) where increases in the ratio are representative of smaller/finer grains incorporation in the sediment. This is evident from the various ash-like horizons observed in section 4.3.1.1, pg. 117. The Fe and Mn profiles show similar patterns along the sediment core and are therefore used to interpret the redox conditions within the core. The Fe and Mn oscillate at the bottom of the core (within LNK1), detailing changes in the oxic and anaerobic conditions. Within LNK2 and LNK3 these shifts are not as pronounced as the profiles begin to stabilize. In LNK4, the profiles are stable with low Mn and Fe values pointing to a relatively oxygenated environment.

4.3.3 Organic Geochemistry and Stable Isotopes

4.3.3.1 Total Carbon, Total Nitrogen and C/N Ratios of Organic Matter

The total carbon content in the sediments is generally low to moderate with increase from the bottom to the top of the core ranging from 1.28 % to 7.85 % (mean 4.44 %) (Figure 4-47). The %C minimum is between 89 – 80 cm (mean; 1.50 %) and corresponds to LNK1 whose upper boundary is marked by the presence of an ash layer. It is most likely that this low %C is the result of a dilution effect caused by the incorporation of inorganic ash material and detrital input rather than a genuine drop in the organic matter flux. The %C begins to gradually rise at 76 cm and this increase continues until its peak of 7.80 % at *ca*. 34 – 36 cm. The %C remains relatively high through LNK4 with a mean %C content of 5.00 %.

The %N values range from 0.11 to 0.61 % (mean 0.4%; Figure 4-47). As seen in the %C variation, the minimum %N value is recorded between 89 and 80 cm (0.11 to 0.13 %), which correspond to LNK1. The %N gradually rises from 76 cm until its highest peak of 0.61 % between 34 and 36 cm. The C/N ratios span 11.6 to 14.3 and are centred at 12.2. The C/N values between 89 – 77 cm are generally higher than in the rest of the core. The maximum peak (14.3) corresponds to the ash horizon corresponding to higher values at the bottom of the sediment core. This is indicative of increased terrestrial organic matter and detrital influx. The C/N value does not change significantly in the remaining section of the core.

4.3.3.1 Bulk $\delta^{13}C$ and $\delta^{15}N$

The $\delta^{13}C$ ranges from -24.28 ‰ to -17.69 ‰ with a mean concentration of -19.10 ‰. This value steadily rises up core between *ca*. -20 ‰ and -18 ‰ with a pronounced depletion (-21 ‰) at 78-80 cm (located above the ash layer at the interface between LNK1 and LNK2). Above this, the $\delta^{13}C$ values are between – 24.90 and -17.70 ‰ with pronounced fluctuation at 51 cm (-21.70‰) and 14 cm (-24.30‰). Within LNK3 at the interval between 35 and 36 cm, a small shift to less negative values (*ca*. -17‰) is observed (Figure 4-47).

The $\delta^{15}N$ values observed in Lake Nkunga vary from 4.80 to 8.01 ‰ over the whole record. In the oldest part of the record (LNK 1) there is a slight depletion with the values ranging from 6.00 – 7.50 ‰ (Figure 4-47). Above LNK 2, a notable enrichment of 1.50 ‰ occurs producing $\delta^{15}N$ values in the range of 6.20 to 8.01 ‰. In LNK3 and LNK4 the $\delta^{15}N$ values generally fluctuate between 5.00 and 6.50 ‰ with the top most sample representing the minimum $\delta^{15}N$ value of 4.77 ‰ (Figure 4-47).

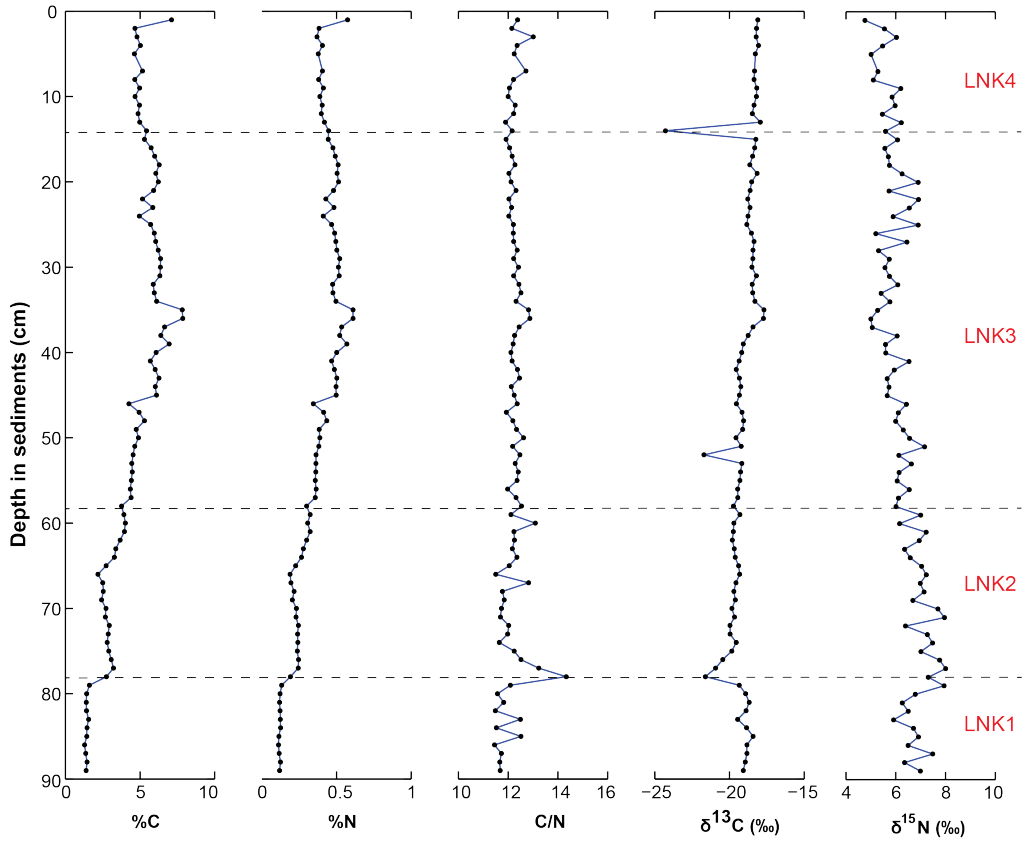

Figure 4-47: Down core variations in the percentage composition of elemental C and N, CN ratios and the $\delta^{13}C$ and $\delta^{15}N$ isotopes composition from Lake Nkunga

4.3.3.1 Provenance of OM based on $\delta^{13}C$ and C/N

The $\delta^{13}C$ values and C/N ratio coupling of the Lake Nkunga results imply C_4-type plants (Figure 4-48) are the major contributors to the OM component of the sediments although a few samples in this sediment core are linked to possible terrestrial input of C_3-type and aquatic plants (Figure 4-48).

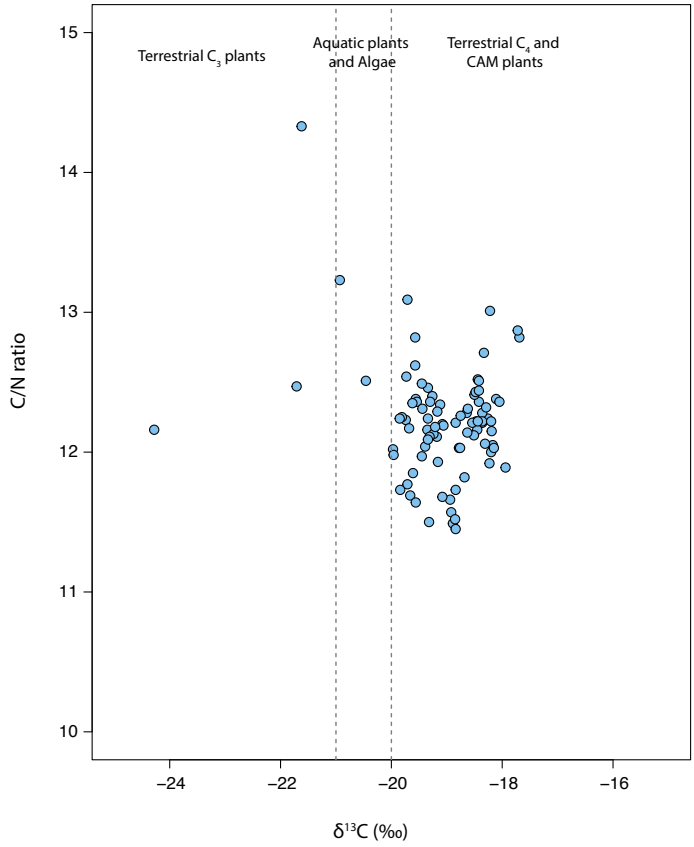

Figure 4-48: Provenance of the organic component of the Lake Nkunga sediments

4.3.3.2 Distribution of n-Alkane Lipids

The *n*-alkanes from Lake Nkunga sediments range from C_{12} to C_{35} (Figure 4-49), peaking at C_{18} and C_{31} with the exception of the sample at 75 cm depth, which displays a unimodal distribution of short chain n-alkanes (C_{14} to C_{23};Figure 4-49). The terrestrially derived odd long chain *n*-alkanes C_{29}, C_{31} and C_{33} are abundant throughout the core (with the exception of the sample at 75 cm). Among these *n*-alkanes, C_{31} is the most abundant followed by $C_{33} > C_{29} > C_{27}$ (Figure 4-49). The short chain *n*-alkanes do not display a strong odd-over-even carbon number preference and are dominated by C_{18}.

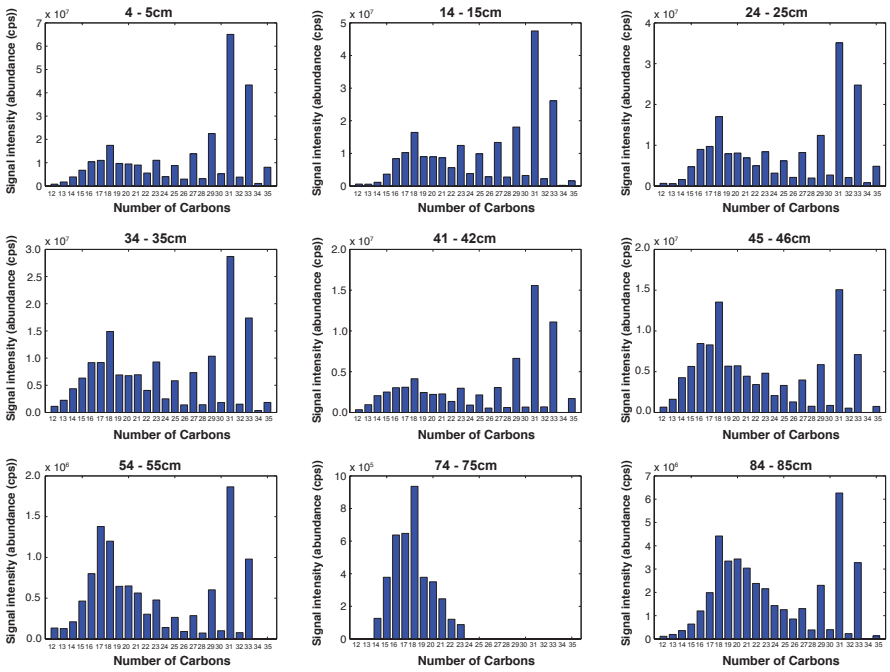

Figure 4-49: The relative abundances of the n-alkanes derived from samples collected from Lake Nkunga.

A distinct odd-over-even predominance is observed throughout the sediment core (CPI 6.0 – 13.4) except for the sample at 75 cm where long chain n-alkanes C_{23} - C_{33} are absent. The ACL values range from 30.1 – 30.6 (Table 9). The C_{27}/C_{31} ranges from 0.2 to 0.3 while the $C_{15\text{-}21}/C_{22\text{-}33}$ ranges from 0.4 to 17.0 where the sample at 75 cm recorded the highest value due to missing long *n*-alkane chains. For the majority of the samples this value ranges from 0.4 to 1.2 (Table 9). The range of the TAR varies from 1.1 to 3.7 whereas the P_{aq} values display slight variations from 0.18 to 0.27.

Table 9: Summary of n-alkane indices from Lake Nkunga

Depth (cm)	C_n range	C_n max	ACL	ACL_{lc}	CPI	Overall CPI	C_{27}/C_{31}	TAR	P_{aq}
4-5	12-35	31	26.5	30.6	8.7	3.2	0.2	3.7	0.18
14-15	12-35	31	25.7	30.2	9.0	2.9	0.3	3.4	0.25
24-25	12-35	31	25.4	30.5	8.1	2.4	0.2	2.5	0.23
34-35	12-35	31	24.4	30.3	9.3	2.4	0.3	2.1	0.27
41-42	12-35	31	25.9	30.6	13.4	3.6	0.2	3.1	0.18
45-46	12-35	31	22.7	30.1	8.3	1.6	0.3	1.3	0.28
54-55	12-33	31	23.1	30.5	10	2.1	0.2	1.1	0.23
74-75	14-23	18	17.8	n.d	n.d	0.8	n.d	n.d	n.d
84-85	12-35	31	23.8	30.3	6	1.7	0.2	1.7	0.20

C_n-number of Carbon present in n-alkane chain: ACL – total Average alkane Chain Length; ACL_{lc} – ACL of long chain n-alkanes; CPI – Carbon Preference Index of long chain alkanes; Overall CPI – CPI for all alkane chains; TAR – Terrigenous-Aquatic Ratio; P_{aq} – Aquatic macrophyte input proxy.

4.3.3.3 Distribution of Glycerol Dialkyl Glycerol Tetraethers

Ten samples were selected for GDGT analysis. All the sediment samples contain abundant amounts of brGDGTs and iGDGTs. The brGDGTs range from 713 to 5901µg/g, comprising 80.9 – 87.9 % of total GDGTs, whilst the iGDGTs are less abundant and range from 167 to 955 µg/g, which makes 12.1 – 19.1 % of total GDGTs (Figure 4-50). Among the iGDGTs the GDGT-0 is the most abundant (35 – 66 % of the total iGDGTs) while the crenarchaeol (10 – 37 % of the total GDGTs) is the second most abundant. The relative abundance of the iGDGTs decreases up core in samples collected at 56 cm (least abundance of iGDGT), 46 cm and 42 cm. All the other iGDGTs display little variation in their relative abundance up core while iGDGT-4 is missing from the samples. The brGDGTs without cyclopentyl moieties, i.e. GDGT-I (30 – 48 % of the total brGDGTs) and brGDGT-II (30.0 to 36.9 % of the total brGDGTs), are more abundant than the pentyl rings. GDGT-IIIc is absent throughout the core (was below the detection limit; Figure 4-50). Of all the brGDGTs, GDGT-I and its moieties are the most abundant (on average 52.6 % of all brGDGTs) followed by GDGT-II and its moieties.

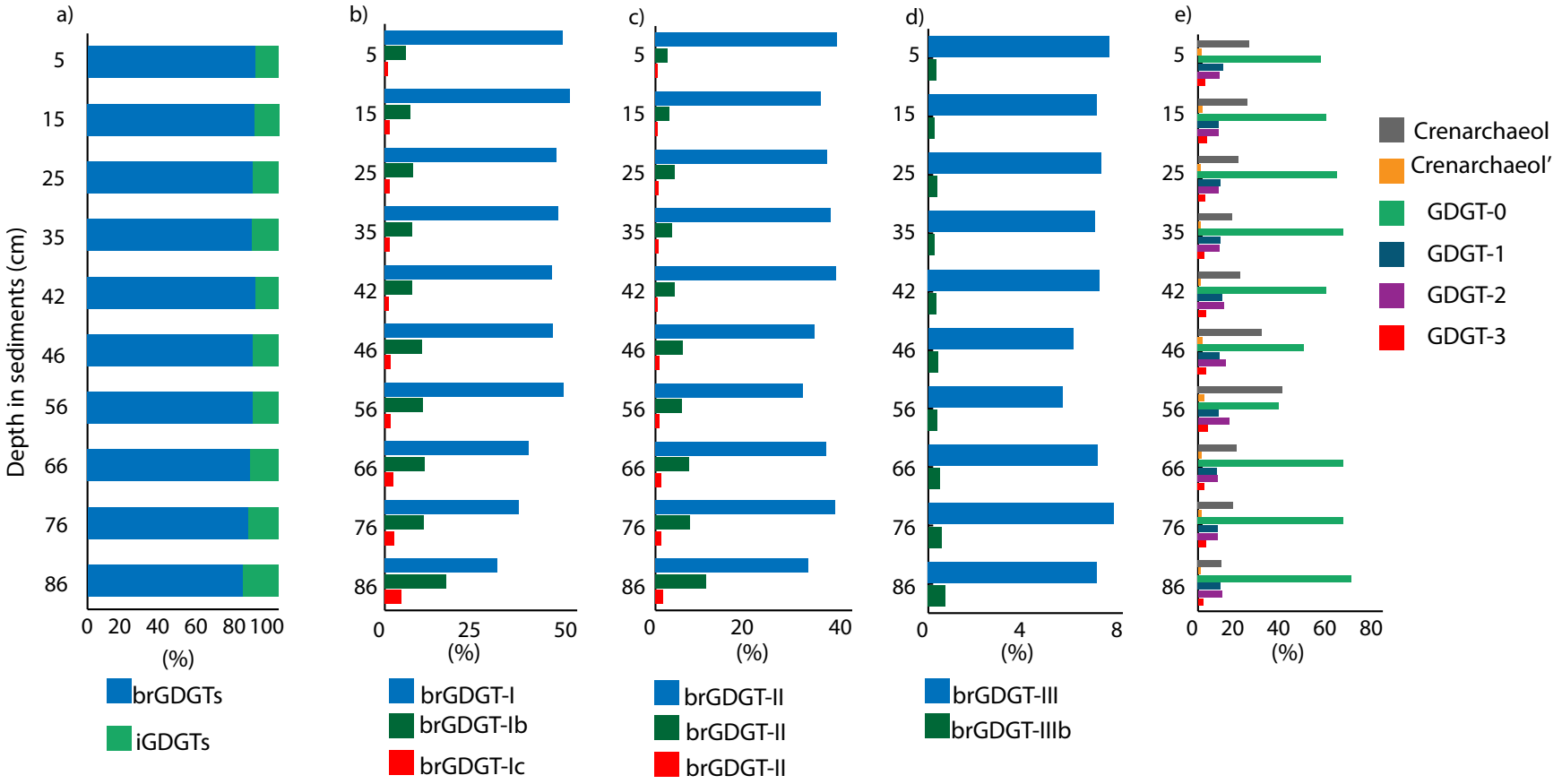

Figure 4-50: The fractional abundance of the brGDGTs and iGDGTs down core in the Lake Nkunga core. The five graphs represent the main (a) the brGDGT and iGDGT abundances while GDGT groups and their moieties are illustrated in (b) GDGT-I, Ib and Ic (c) GDGT-II, IIb and IIc, (d)GDGT-III and IIb & (e) iGDGTs

The reconstructed pH (Equation 10) values range from 7.2 to 9.2 pH units thereby displaying a decreasing trend from the bottom to the top of the core (Table 10). The Branched vs. Isoprenoid Tetraether (BIT) index is high (0.94 – 0.97) throughout the core indicating the dominance of the terrestrially derived brGDGTs in the lake sediments (Table 10). The calculated MBT and CBT values range from 0.47 – 0.58 and 0.36 – 1.01, respectively. The MBT displays little coherency with depth while the CBT displays an increasing trend from the bottom of the core to the top.

Table 10: The variations in BIT, 1302/1292 ratio, MBT and CBT proxies from the Lake Nkunga sediment core

Depth (cm)	BIT	1302/1292	MBT	CBT	pH
5	0.97	2.39	0.52	1.01	7.2
15	0.97	2.63	0.56	0.94	7.5
25	0.97	3.49	0.53	0.85	7.8
35	0.97	4.30	0.53	0.89	7.6
42	0.97	3.05	0.52	0.87	7.7
46	0.95	1.67	0.55	0.70	8.2
56	0.94	0.95	0.58	0.70	8.2
66	0.96	3.76	0.50	0.62	8.4
76	0.96	4.13	0.47	0.62	8.4
86	0.97	6.51	0.49	0.36	9.2

The high BIT index coupled with the GDGT-0/crenarchaeol (1302/1292) ratio >2 eliminated the potential application of the TEX_{86} proxy as a meaningful proxy for palaeotemperature (Weijers et al. 2007). The application of GDGT as a palaeotemperature proxy was carried out using equations 12, 13, 14, 15 and 16 (Section 3.1.10.5, pg. 70 and pg. 71) as described above. The reconstructed palaeotemperature (Figure 4-51) from the various calibrations represents progressive cooling from the bottom of the core. The resulting temperature reconstructions are generally highest using the MBT/CBT calibrations from both Tierney et al. (2010) and Loomis et al. (2012) with the values ranging from 19.5 - 24.5° C and 20.8 - 25.3° C, respectively (Figure 4-51). The MbrGDGT calibrations range from 17.3 - 25.3° C (Tierney et al. 2010) and 19.6 - 23.0° C (Loomis et al. 2012) while the SFS calibration ranges from 18.6 - 23.6° C (Loomis et al. 2012). The MbrGDGT ranges represent the maximum (8.0° C; Tierney et al. 2010) and minimum (3.4° C; Loomis et al. 2012) temperature variations in the core (Figure 4-51). There is a slight increase in the reconstructed temperatures between 66 and 42 cm with the graphs

displaying a peak at *ca*. 56 cm, however, this peak is not present in the MbrGDGT calibration by Tierney et al. (2010).

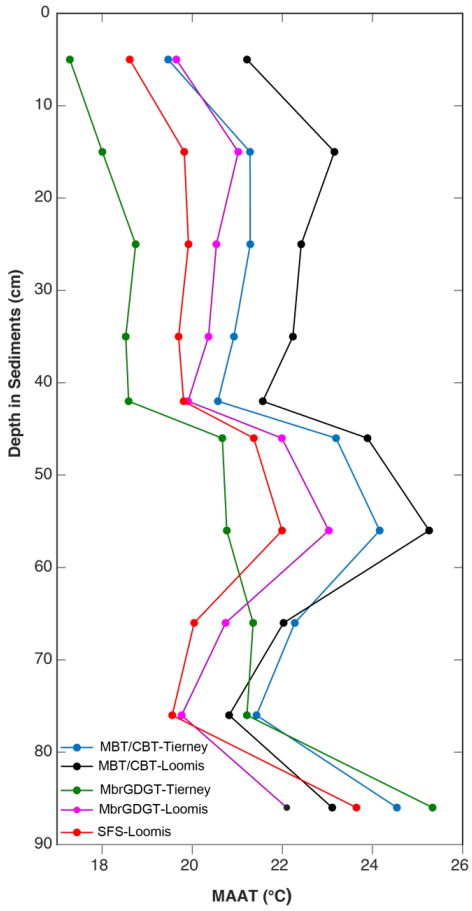

Figure 4-51: Reconstructed MAAT for Lake Nkunga core using MBT/CBT, MbrGDGT and SFS regional calibrations

4.3.4 Synthesis of Lake Nkunga Proxy data

The 89 cm of the sediments from Lake Nkunga cover approximately 1079 cal yr. BP to present (Table 11). The sedimentation rate is lowest within LNK1 (89 – 77 cm), above which the rate slowly rises until its peak at 40 cm. Some of the samples dated represent a rapid sedimentation event between 529 and 380 cal yr. BP as seven out of the ten dated samples yield ages within this range. The age-depth model and sedimentation rates show deep and shallow lake phases that are also reflected by the X_{lf} values, where higher values at the bottom of the core correspond to a deeper lake phase with catchment in-wash of sediments and the lower values at the top of the core correspond to a shallower lake phase where the trends stabilize. The lake has therefore gotten shallower over the last 1000 cal yr. BP with a notable increase in sediment influx from about 500 cal yr. BP.

Table 11: Proxy indicator summary from Lake Nkunga

Stratigraphic Unit	Proxy information
LNK 1: 89 – 77 cm 1079 – 810 cal yr. BP (879 – 1152 AD)	▪ %C and %N are low reflecting minerogenic inputs of detrital material as seen in the stratigraphy and the associated mineralogy. ▪ Changes present in the mineralogy denoted by the co-existence of magnetite and hematite in this section are attributed to redox conditions linked to possible changes in the lake level. ▪ The average C/N value (12.0) points to plankton/algae and aquatic plants as the main source of the OM of the sediments. The $\delta^{13}C$ values within this unit (average -19.16 ‰) also imply that the dominant influence on the $\delta^{13}C$ signature is plankton/algae with secondary inputs from aquatic macrophytes and terrestrial plants derived from C_3-type vegetation. ▪ The slight positive trend in the $\delta^{13}C$ values observed in this unit probably reflects increased aquatic macrophyte contributions and a concomitant increase in C_4–type plants (*Cyperacea*e and grasses) within the catchment. ▪ The C_{27}/C_{31} (0.2) of the sole sample analysed from this unit imply significant contributions of grass- over tree-derived organic matter from the catchment. The CPI value (6) is indicative of the dominance of long chain *n*-alkanes with odd over even predominance implying a modern terrestrial plant source of organic matter (Cranwell, 1982; Cranwell et al. 1987). ▪ The other *n*-alkane parameters, ACL (23.8), P_{aq} (0.29) and TAR (1.7) point towards a mix of aquatic macrophytes and terrestrial input of OM into the lake from the catchment (Eglinton et al. 1962; Kolattukudy et al. 1976; Cranwell 1982; Cranwell et al. 1987; Meyers 1997).
LNK 2: 77 – 58 cm 810 – 600 cal yr. BP (1152 – 1341 AD)	▪ A slight increase in the average %C (3.04 %) and %N (0.25 %) reflects a probable increase in aquatic macrophyte productivity since the average C/N value (12.17) does not change significantly (Tyson 1995; Meyers & Teranes 2001). ▪ The minerogenic composition does not change significantly. ▪ Limited variations in the C_{27}/C_{31} (0.2), ACL (23.1), P_{aq} (0.23) and TAR (1.1) values from sediment samples in the upper section of this unit implies a mixture of OM source from aquatic macrophytes and terrestrial input (Eglinton et al. 1962; Kolattukudy et al. 1976; Cranwell 1982; Cranwell et al. 1987; Meyers 1997). ▪ The absence of long chain *n*-alkane at 75 cm depth did not allow for the calculation of ACL, CPI and P_{aq} parameters although the dominance of the long chain *n*-alkane could imply the predominance of degraded/microbially derived OM.
LNK 3: 58 – 13 cm 600 – 290 cal yr. BP (1341 – 1688 AD)	▪ The average %C (5.62 %) and %N (0.46 %) are higher than in the underlying units. There is a slight increase in the concentration of %C and %N in this section alongside the presence of reworked ash and sediments. ▪ Evidence of the commencement of leaching can be derived from the coexistence of halloysite and gibbsite. ▪ The X_{lf} values are fairly invariant in this section of the core. ▪ A progressive replacement of the C_3-type vegetation by C_4-type plants especially grasses and *Cyperaceae* is implied by the dominance of the C_{31} over C_{27} *n*-alkane homologues. ▪ This period reflects a stable catchment and water table level with little terrestrial-derived material inputs to the lake. ▪ The inorganic geochemistry points to increased aeolian deposition of sand grains derived from the basement rocks which do not occur within this catchment.
LNK 4: 13 – 0 cm 290 – (-86) cal yr. BP (1688 AD to present)	▪ The mean %C (5.18 %) and %N (0.42 %) are similar to those of the underlying unit and do not show any significant increase or decrease with the exception of the top-most sample that has a relatively higher %C (7.11 %) and %N (0.57 %) content. ▪ Oscillations in the geochemistry (%C, %N and their stable isotopes) imply a period lake development leading to periods of oxic and anoxic conditions where the lake shore is covered by well mixed waters and other periods where anoxic conditions occur.

The sediments from Lake Nkunga are mainly of terrigenous origin as seen in the sediment chemistry (siliciclastic material represented by the presence of Si, Ti, Fe and K) as well as the organic geochemistry of the n-alkanes (presence of long chain alkane and high TAR ratios, representing terrestrial origin of OM). These terrigenous sediments are largely derived from a small catchment and do not show any major stratigraphic changes (although there are subtle colour changes observed down the sediment profile). The magnetic mineralogy, sedimentation rate and the geochemical ratios constrain the sediment source to detrital material derived from the preferential weathering of the volcanic crater walls plus *in-situ* formation of Fe-Mn oxyhydroxides. In the core descriptions (Section 4.3.1.1), two sediment influx events marked by the presence of pebbles, volcanic ash and charcoal particles are prominent. The upper limit of LNK1 is marked by a detrital influx of finer grained clastic material. Quartz, although intermittent in the mineralogy, originates from the weathered material derived from the exposed Precambrian basement and demonstrates the importance of the dry NE monsoon winds in erosion, transportation and deposition processes within the catchment especially during the period 801 – 600 cal yr. BP where an increase in the Si/Ti ratio is observed.

The samples dated provide the lower age limit of the sediments *ca.* 1079 cal yr. BP. LNK 1 represents a lake rejuvenation phase (Figure 4-52) where redox processes dominate (co-existence of magnetite and hematite), a decline in Fe/Ti (implying increase in detrital input), and increase in Si/Ti (authigenic input). There is an ash layer in the sediment matrix mixed together with lake muds probably during the settling of clastic and aeolian (high Si/Ti) material.

LNK2 represents a period of increased sediment supply from the lake catchment marked by increased minerogenic input (predominantly quartz and plagioclase feldspar), increase in Si/Ti ratio and relatively higher sedimentation rates. This core section represents a deeper lake phase as can be seen in the oscillating changes in X_{lf} which are centred at 0.5 m^3kg^{-1} x 10^{-5} except for the top most sample in this unit where the highest value of X_{lf} is recorded (Figure 4-52).

In LNK3 the Si/Ti ratios display positive and negative excursions, perhaps pointing to seasonal aeolian input into the lake, while the Fe/Ti ratio displays an initial increase that levels off in the upper section of this period. The presence of pumice-like clasts, charcoal particles as well as plant materials and declining X_{lf} values imply that the source of the ash and charcoal are related to erosional changes from the restricted catchment.

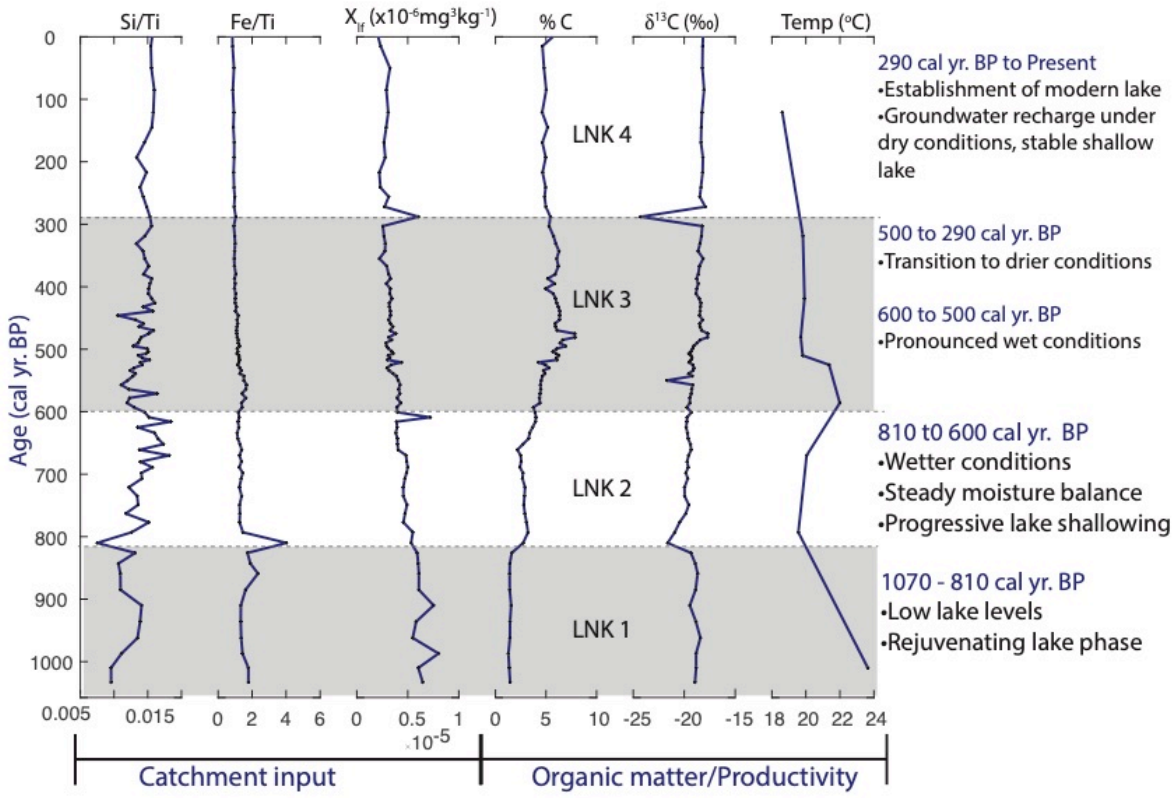

Figure 4-52: A summary of key findings from Lake Nkunga from 1079 cal yr. BP to Present indicating key changes in lake sedimentation and lake level variations

The presence of SP minerals with the accompanying presence of hematite and magnetite supports the terrestrial origin of the sediment from the soils within the lake's catchment (Thompson and Oldfield, 1986). There are no significant changes in the sedimentation, mineral magnetics and geochemical proxies in the upper section (LNK4), pointing to a stable shallow lake (Figure 4-52). There are slight increases in the Si/Ti to present day, suggesting that aeolian deposition is a minor but significant sediment source for this lake.

The observed values for %N and %C, although generally low, display similar variations throughout the sediment core that are linked to changes in catchment supply processes and display significant correlation where $R^2 = 0.99$, $p < 0.001$. The extrapolated intercept of the %C and %N relationship reveals a slightly positive intercept on the %N axis (0.006 %). This suggests that inorganically bound nitrogen is negligible and has little influence on C/N ratios thus deducing an organic origin of the lake sediments. This is to be expected in lacustrine sediments where the large majority of total N is derived from organic matter sources (Talbot & Brendeland 2001).

The C/N values vary from 11.6 to 14.3 pointing to OM contribution from primary production (aquatic macrophytes). Although there are subtle changes in this record they are not significant enough to imply a shift in the OM sources for this lake. The coupling of $\delta^{13}C$ values and the C/N ratio imply a mix C_3 /C_4-type vegetation from the catchment. Within LNK1 and LNK2, the influx of material from the catchment is represented by the oscillating C/N and $\delta^{13}C$ values. LNK 3 and LNK 4, on the other hand, display a stable trend indicative of mixed OM sources from within the catchment although dominated by C_4. The bulk $\delta^{15}N$ gives two contrasting zones; LNK1 and values above LNK1 (i.e. LNK 2, 3 & 4 combined). As discussed earlier, LNK1 represents a lake rejuvenation phase with relatively low $\delta^{15}N$ ranging from 6.0 to 7.5 ‰. Above LNK1 a deeper lake phase, followed by progressive lake shallowing, is implied by the slight enrichment of $\delta^{15}N$ (6.20 to 8.01 ‰) that covers periods of intense aquatic productivity (deep lake phase) and shallow lake phase as well. Although an attempt has been made to interpret the $\delta^{15}N$ values, there is no discernible relationship between $\delta^{15}N$ and C/N or $\delta^{15}N$ and $\delta^{13}C$ suggesting that the isotopic variability is largely independent of the OM source contributions of aquatic and terrestrial origin. From the inorganic chemistry above, it is evident that there are redox zones within the sediment core. Although the effect of diagenesis on the $\delta^{15}N$ of OM in lacustrine systems is inconclusive, minor alterations are observed due to preferential degradation of OM. Denitrification of OM is a significant factor in $\delta^{15}N$ composition (Talbot & Brendeland 2001). Under anoxic conditions denitrifying bacteria causes the reduction of NO^{-3} to gaseous N_2 in the water column (Talbot & Brendeland 2001). It is therefore safe to assume that the changes in redox conditions cause slight variations in $\delta^{15}N$ in the sediment core.

The *n*-alkane record displays a bimodal distribution (short and long homologues) representative of mixed origin of the *n*-alkanes (terrestrial and algal input). Generally, the number of carbon atoms present in the *n*-alkane chains range from $C_{12\text{-}35}$. The range of total ACL ranges from 30.1 – 30.6. These values represent a dominance of long chain alkanes in the samples. The distribution of n-alkane homologues shows a strong odd-over-even preference that is a characteristic of higher plants, as reflected by the high CPI values (6.0-13.4) in the samples (Cranwell 1982; Cranwell et al. 1987). The odd long chain n-alkanes C_{29}, C_{31} and C_{33}, characteristic of higher plant sources is abundant in the samples. Presently, Lake Nkunga contains emergent, floating and submerged macrophytes. Ficken et al. (1998), found that the present-day submerged plants in Lake Nkunga show dominance of C_{23} or C_{25} alkanes whereas C_{29} or C_{31} alkanes are more abundant in the emergent macrophytes and terrestrial plants. The

emergent/terrestrial macrophytes are a dominant *n*-alkane source in our sediments. Both CPI and ACL are indicative of higher plants and the C_{31} alkane (characteristic of grasses and herbaceous plants) is more abundant than the C_{27} (representative of forest vegetation) leading to a low C_{27}/C_{31} ratio (0.2 – 0.3). This suggests an open vegetation watershed such as an open forest. The $C_{15\text{-}21}/C_{22\text{-}33}$ value ranges, with the exception of the sample at 75 cm, are indicative of contributions from higher plants. The sample at 75 cm, on the other hand, displays the dominance of microorganisms such as bacteria and algae.

The use of TAR to evaluate the relative inputs of OM types provided two contrasting zones with lower values at the bottom (1.1 – 1.7) and relatively high values (2.1 – 3.7) in the upper sections of the sediment core. This points to a change in the OM sources for this core that was initially characterized by increased *in-situ* aquatic production during the development of the deep lake phase followed by significant terrigenous OM inputs during the shallow lake phase. The TAR values in the upper section generally represent a relatively stable environment that affirms the existence of a shallow lake from around 500 cal yr. BP. The low P_{aq} (0.18 – 0.27) values reveal the influence of higher plant/emergent macrophyte waxes as the main OM source throughout the late Holocene. The various n-alkane proxies from this lake are consistent with a mixed origin of OM from both terrestrial and aquatic sources and are indicative of a transition from a transient shallow lake to deep lake to a shallow lake phase.

All samples from Lake Nkunga display a distinct pattern in the variation of the short chain n-alkane where C_{18} is most abundant in the samples. The C_{18} abundance has been linked to the combustion of non-woody biomass from agricultural lands (Eckmeier & Wiesenberg 2009). The evidence of charcoal and charcoal-like particles in the sediment stratigraphy indicate that fires were important in the lake catchment. Since the lake is within a crater surrounded by montane forest, the presence of burnt non-woody biomass affirms aeolian transport as a contributing source to the lake sediments, perhaps from biomass burning activities within the wider Mt. Kenya catchment over the past 1000 cal yr. BP.

The most abundant iGDGTs in the Lake Nkunga samples are GDGT-0 and crenarchaeol. The crenarchaeol is a highly specific biomarker of ammonia oxidizing *Thaurmarchaeota* (Sinninghe Damsté et al. 2012, Pearson and Ingalls 2013). Even with the relative abundance of the GDGT-0, the elevated 1302/1292 ratio (>2) implies the dominance of methanogenic *Euryarchaea* under anoxic OM rich conditions in the lacustrine deposits (Blaga et al. 2009). The fractional abundances of the iGDGTs display a small contribution from GDGT-1, 2, 3 and

in some places the GDGT-VI regio isomer (crenarchaeol'). This has implications on the high BIT index throughout the core as the value most likely reflects the covariance of GDGT-0 and the crenarchaeol thereby yielding similar BIT values.

The brGDGTs are dominant in all the sediment samples in comparison to the iGDGTs affirming catchment erosion processes as the main source of sediments. Among the brGDGTs, those without cyclopentyl moieties are more abundant than those with one or two cyclopentyl moieties while the brGDGT-IIIc was not detected in all the samples. Generally, the presence of brGDGTs indicates anoxic conditions as these lipids are likely synthesized by anaerobic heterotrophic acidobacteria (Hopmans et al. 2004, Weijers et al. 2006). There is an observed increase of brGDGTs up core that correlates with the general trend of increasing %C and a decline in the reconstructed pH values that can be attributed to the deepening of the lake. This relationship affirms the linkage of anoxic conditions to the production and preservability of the brGDGTs (Weijers et al. 2006).

The palaeotemperature calibrations (Tierney et al. 2010 and Loomis et al. 2012) display coherency in the changes experienced during the Late Holocene. Small disparities between the palaeotemperature calibrations result in different magnitudes of change during this Late Holocene period. The SFS and MbrGDGT (Tierney et al. 2010) temperature calibrations result in cooler temperatures (Figure 4-51) than the MBT/CBT temperature calibrations. A general cooling trend is observed from the bottom of the core to the top. The records show a cooling trend from 1070 cal yr. BP to 800 cal yr. BP when a temperature rise of 1.5 ± 0.5° C is observed in all the calibrations. This warming persists until *ca*. 600 cal yr. BP when the temperatures drop to values close to present day temperatures. The coherency of the warming *ca*. 800 – 600 cal yr. BP coincides with widespread drought deduced at Sacred Lake from *ca*. 900 to 500 cal yr. BP (Konecky et al. 2014).

4.4 Sacred Lake Sediments

4.4.1 Bulk Sediment Parameters

4.4.1.1 Stratigraphic Description

A total of six successive core sections spanning a total depth of 63 cm were recovered from Sacred Lake, approximately 20 m at a water depth of 1m. The core sections acquired; SAL II -1, SAL II – 2, SAL II – 3, SAL II – 4, SAL II – 5 and SAL II – 6 are of varying lengths ranging from 8 cm – 12 cm. Macroscopic plant rootlet remains are present in all six of the acquired core sections and there are no identifiable tephra layers. The sediment colour ranges from brownish black to olive black, indicative of high organic matter content. Generally, the cores were in good condition with no visible deformation from the extraction process. The water content (W_c) determined from the sediment is displayed in Figure 4-53 and ranges from 35 % to 65 % with an average of 50 % for the 63 samples analysed. The higher peaks that are seen along the profile correspond to the top of some of the cores retrieved i.e. SAL II – 3, SAL II – 4 and SAL II – 6. These peaks could be linked to slight compression of the upper section of these cores during extraction. The subtle lithological changes and lack of distinct stratigraphic markers led to the use of the compositional variation of %C, %N and the stable isotopes of C and N to identify significant stratigraphic zones using constrained hierarchical clustering in Rioja (Juggins 2015): low OM in SLK1 (63 – 41 cm), rapid increase in OM in SLK2 (41 – 35 cm), stable OM supply within SLK3 (35 – 14 cm) and declining OM in SLK4 (14 – 0 cm).

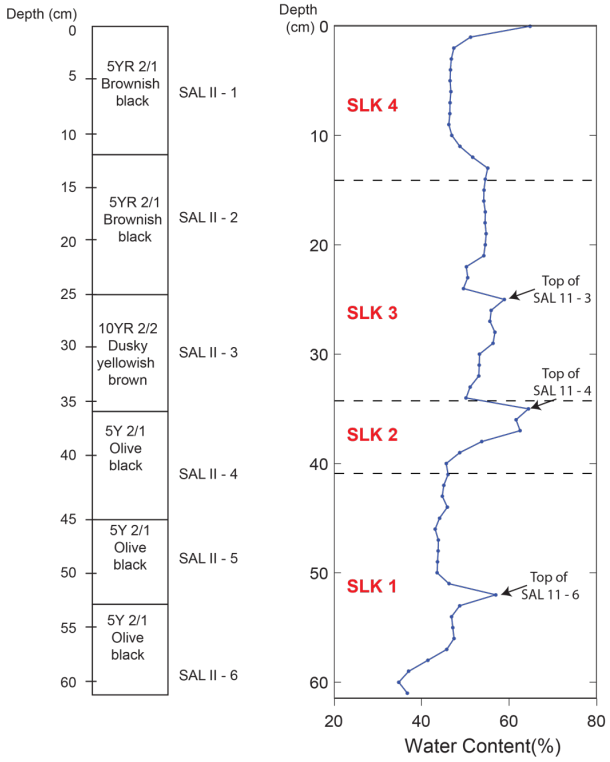

Figure 4-53: The stratigraphic section and percentage water content representation sediment cores from Sacred Lake (SAL 11-1, SAL II-2, SAL II-3, SAL II-4, SAL II-5 and SAL II-6).

4.4.1.2 Radiocarbon Chronology

The six radiocarbon ages obtained were calibrated using Reimer et al. (2013) calibration curve (Table 12). The lab sample (SacA34954) collected from 6 cm most likely reflects the mixing of recent and possible contamination by older carbon, a phenomenon postulated to occur in this lake (Olago 1995).

Table 12: Radiocarbon ages from Sacred Lake sediment core obtained from the AMS (Age ^{14}C yr. BP) and their calibrated radiocarbon ages (cal yr. BP) and their associated errors. The samples marked in bold were identified as outliers

Lab No	Sample	Depth (cm)	Age ^{14}C yr. BP	Cal yr. BP
SacA34954*	**SAL -I-6**	**6**	**1060 ± 30**	**990±84**
SacA34955	SAL-II-7	19	1020 ± 30	953±58
SacA34956	SAL-III-5	30	1510 ± 30	1369±55
SacA34957	SAL-IV-6	42	3500 ± 30	3784±99
SacA34958	SAL-V-4	49	3775 ± 30	4176±116
SacA34959*	**SAL-VI-5**	**58**	**3730 ± 30**	**4075±107**

The AMS ^{14}C ages were used to generate an age-depth model for Sacred Lake as described in sections 3.1.5 and 4.3.1.2, using Bacon v2.3 (Blaauw & Christen 2011). The values generated are chronologically ordered at 1 cm interval for the entire sediment core (Figure 4-54). Several test runs within the software produced large uncertainties when the top most age of the sediment core was fixed to the year the core was acquired thus for this core, therefore the age uppermost age was not fixed hence the upper age corresponding to the Bayesian model (630 cal yr. BP) was considered reliable.

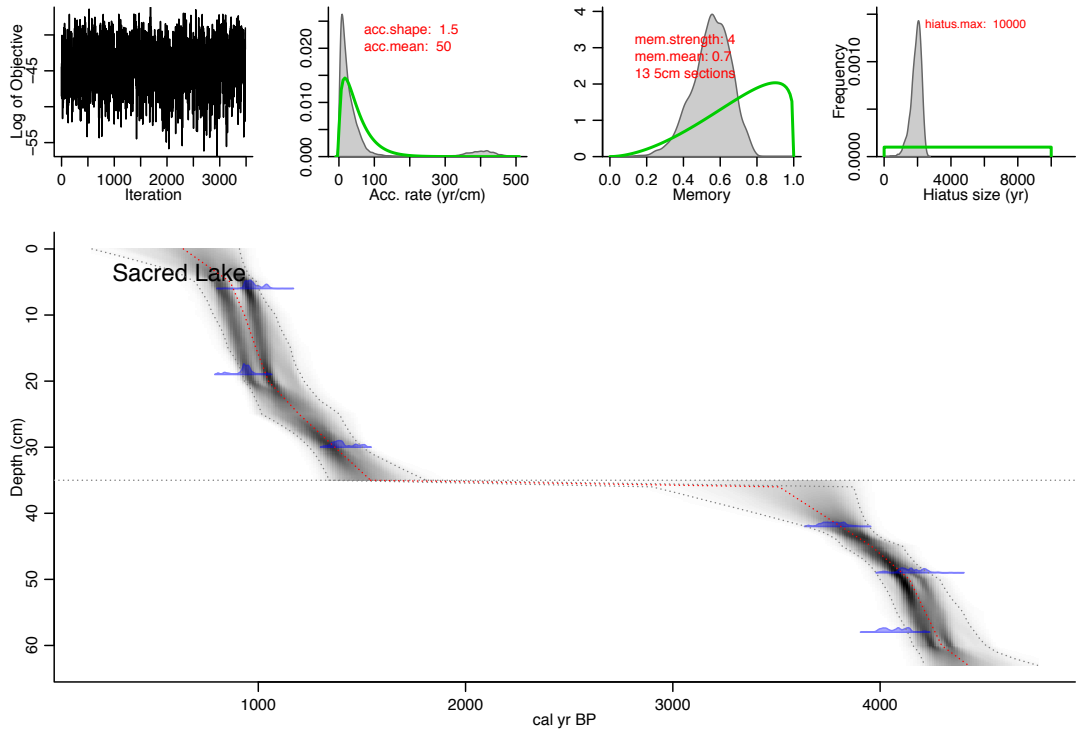

Figure 4-54: Bayesian age depth model for Sacred Lake sediment core. The bottom panel displays the calibrated ^{14}C dates (transparent blue) and the age-depth model within 95% confidence intervals. The upper panels show the MCMC iterations: the left represents the stability of the model while the middle and the right represent the prior (green curve) and posterior (grey histograms) for the distributions of accumulation mean and memory properties, respectively

Previous visits to Sacred lake before the coring revealed that the lake dried out and therefore the top section of this core could have been disturbed by wildlife (such as elephants) hence the mixing of the dates since the cores were collected close to the shoreline. A possible hiatus was identified at 35 cm for this age-depth relationship. From the age-depth model generated, the sediments for Sacred Lake covers 4425 to 630 cal yr. BP. The sediments are characterized in two sections (i) 4425 – 3515 and (ii) 1542 – 630 cal yr. BP corresponding to before and after the hiatus, respectively. The hiatus covers the period 3515 to 1524 cal yr. BP. The sedimentation rate for Sacred Lake is low, ranging from 0.0 to 0.2 cm/yr. (Figure 4-55). The

sedimentation characteristics of this core can be divided into 2 where before the hiatus a decrease in sedimentation (4425 – 3515 cal yr. BP) is observed and above this (1542 – 639 cal yr. BP) there is a steady rise in the sedimentation rate (Figure 4-55). Since this core was obtained in a nearshore zone of the lake, the sedimentation rate and age-depth model imply periods of deeper and shallow lake episodes. Initially, the high sedimentation rate points to a deeper lake interval, followed by a shallow lake interval before the hiatus, soon after the hiatus, there is a relative increase in sedimentation alluding to a deeper lake while the uppermost section of the lake points to a shallow lake interval.

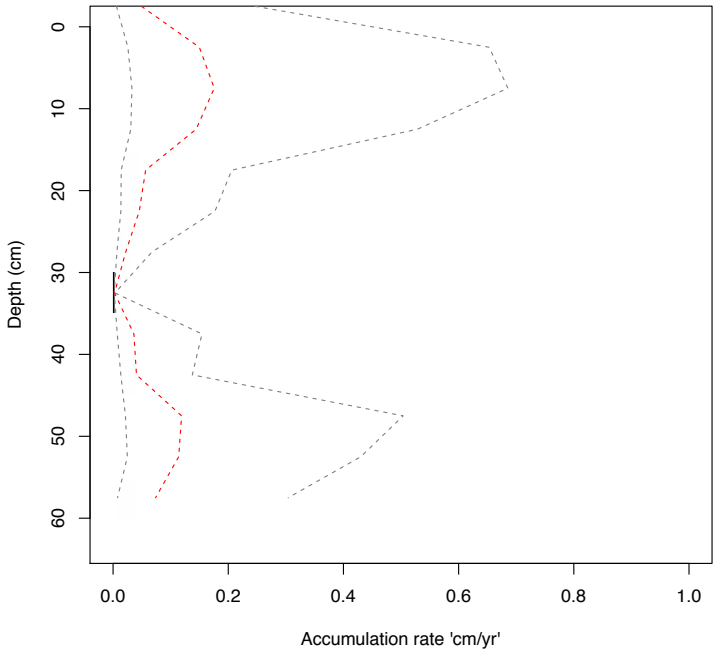

Figure 4-55: The sediment accumulation rate for Sacred Lake. The grey lines envelope 95 % areas of certainty in value obtained while the red line is the weighted mean representation of the accumulation between the different depths along the sediment

4.4.1.3 Mineralogy and Mineral Magnetics for Sacred Lake

The mineralogy is closely linked to the parent geology of the area, comprising plagioclase and potash feldspars (65 – 70 %), quartz (18 – 20 %), halloysite (10 %) and gibbsite (2 %). Weathering products such as chlorite, halloysite and gibbsite are present throughout the core (Figure 4-56) Kaolinite and illite clays were also identified.

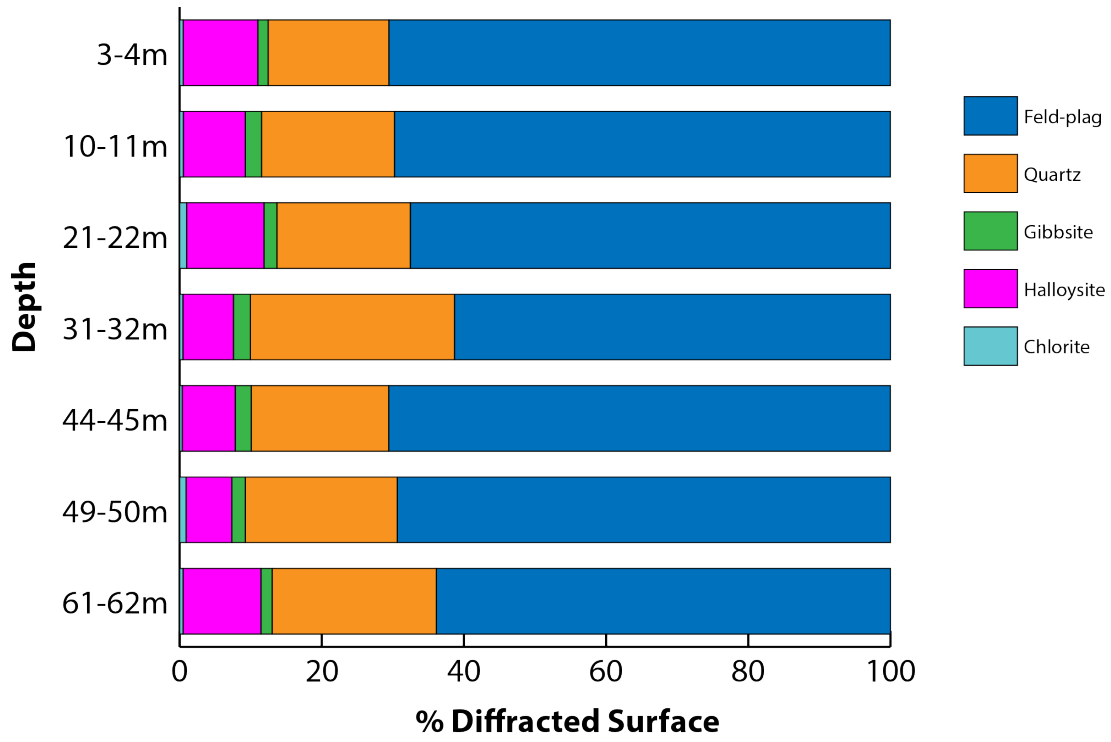

Figure 4-56: The average quantitative mineralogy of the Sacred Lake sediment samples

The X_{lf} values are very low ranging from 7.5 x 10^{-9} to 5.3 x10^{-8} m^3kg^{-1}, reflecting the general dissolution ("cut off") of ferrimagnetic minerals under peat-bog and acidic conditions. Still, the steady decline in X_{lf} shows the hiatus is followed by a relatively low value (in SLK3) that steadily rises in the upper section of the core (SLK4) (Figure 4-57). The negative $\%X_{fd}$ values of the sediments are likely due to instrumental noise involving the response of diamagnetic material to the high frequency inducing field. Due to the low detected susceptibility values, the NRM, a measure of magnetisation retained in material after deposition was not carried out. Instead anhysteretic and isothermal remanence measurements were performed to characterize the magnetic carrying particles in the sample.

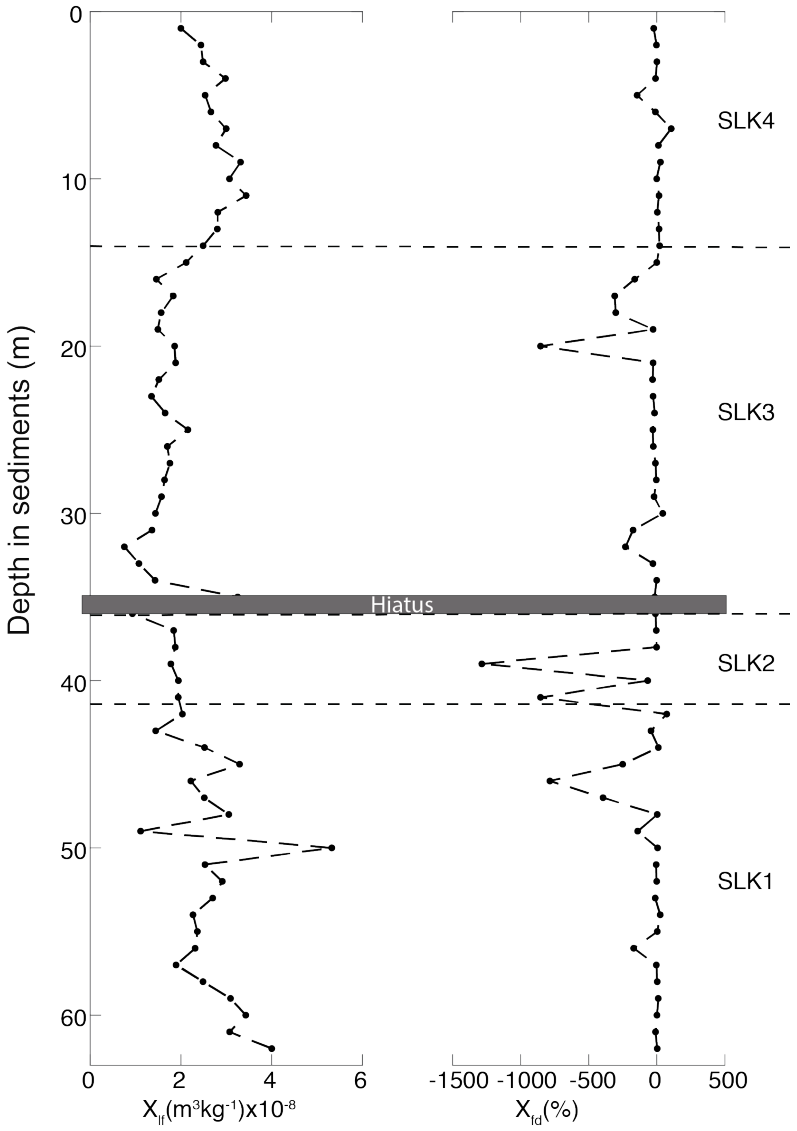

Figure 4-57: Bulk magnetic susceptibility parameters from Sacred Lake core.

The values of ARM_{30mT}, IRM_{-300mT}, S-ratio and ARM_{30mT}/SARM are relatively constant throughout the sediment core (Figure 4-58). Most of the ARM_{30mT} values are centred at 4.1 x 10^{-6} Am^2kg^{-1} with the highest deviation at 20 cm (in SLK3) providing a maximum value of 1.1 x 10^{-5} Am^2kg^{-1} that corresponds to a deep lake phase. A similar trend is observed in the ARM_{30mT}/SARM ratio where the values lie between 3.0 x 10^{-1} Am^2kg^{-1} and 7.4 x 10^{-1} Am^2kg^{-1}. Before the hiatus, high coercivity is noted from the S-ratio that ranges from 0.9 – 1.2 while above the hiatus, low coercivity is reflected by the steady decline in the S-ratio from 1.0 to 0.5 at the top of the sediment core.

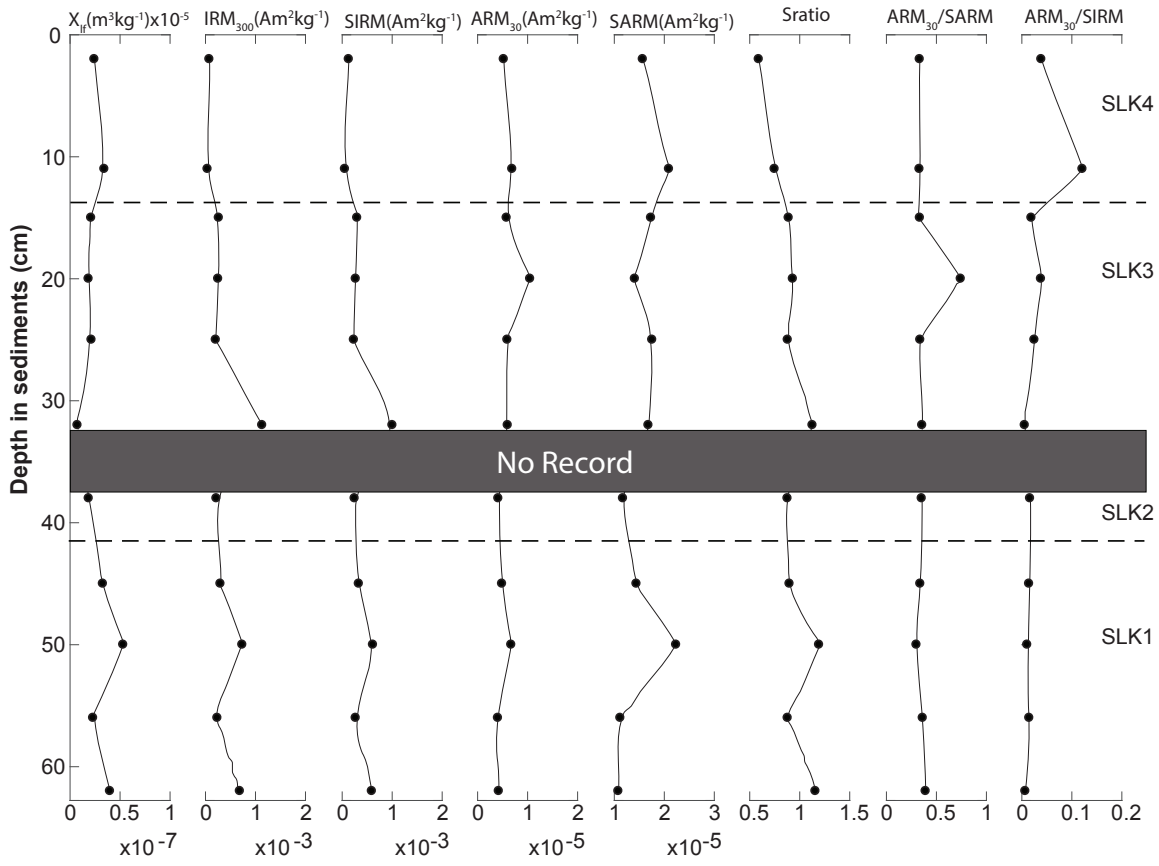

Figure 4-58: X_{lf}, Anhysteretic and Isothermal Magnetisation parameters for sediments from Sacred Lake

The SARM displays a similar trend to the S-ratio. The IRM$_{-300mT}$ values are low ranging from 4.3 x 10^{-5} to 1.1 x 10^{-3} Am^{2}kg^{-1}. The IRM$_{-300mT}$ and SIRM are relatively constant with the exception of the period immediately after the hiatus where peaks in the values are recorded. The ARM$_{30}$/SARM and ARM$_{30}$/SIRM are not diagnostic of any changes in the sediment profile. As shown from the low S-ratio values the preserved magnetization carriers show a dominant "hard" canted antiferromagnetic component, suggesting contributions of hematite/goethite. From the S-ratio and ARM$_{30}$/SARM profiles, the relatively hard remanence contributions show a slight upward increase, consistent with better preservation near the top of the sequence. Superimposed on this signal, the maximum ARM$_{30}$/SARM value observed in SLK3 at 20 cm downcore likely indicates a layer enriched in SD-like maghemite.

4.4.2 Inorganic Geochemistry of Sacred Lake

Sacred Lake contains 15 detected elements (Al, Si, Ti, Ca, Cl, Cu, Fe, K, Nb, Ni, Rb, S, Sr, Zn, Zr). Unlike Lake Nkunga, Mn, P and V were not detected in these samples. Geochemically stable elements and those representative of redox processes were selected for PCA (See section 0, pg. 124). The first principal component (PC1) accounts for 54.40 % of the variability while the second principal component (PC2) accounts for 16.26 % of the variability (Figure 4-59). PC1 positively correlates with indicators of detrital input into the lake and negatively correlates with Fe/Ti and Rb/Zr representative of grain size variation. PC2 positively correlates with K, Si, Si/Ti, K/Ti and Rb/Zr indicating these elements are more tightly held within the structure of aluminosilicates pointing to the enrichment of the clastic phase once the mobile elements are removed and negatively correlates with Fe, Rb, Sr, Ti, Zr and Fe/Ti reflecting changes in the grain size of the clastic phase.

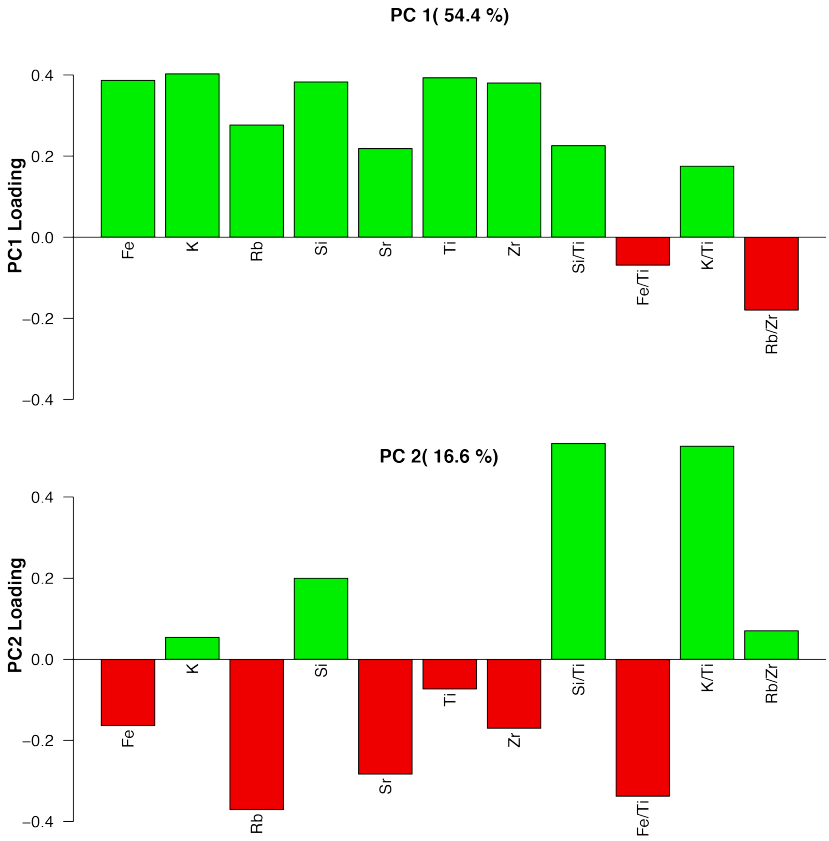

Figure 4-59: PCA of the elements from Sacred Lake. Green bars represent the positive correlations while red represents negative correlations. The upper and lower panels show PC1 and PC2, respectively.

Variations in Fe/Ti, Si/Ti, Ti and Fe were used to observe any significant changes in the sediment core. The Fe and Ti profiles represent subtle variations without any clear trends. On the other hand, for the Fe/Ti ratio, changes are observed in the upper 5 cm within SLK4 where an increase in this ratio is observed (Figure 4-60), indicating an increase in smaller grain size material at the top of the core.

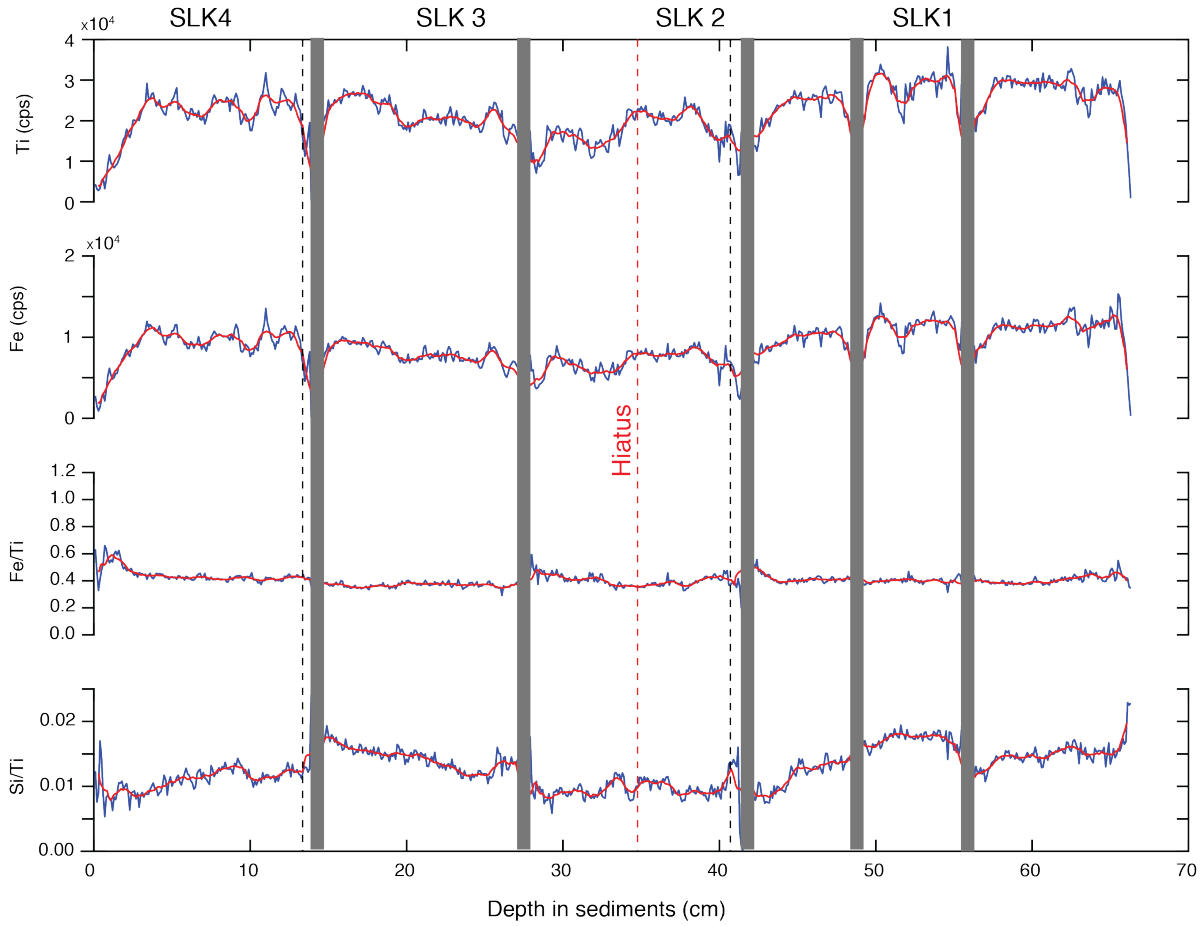

Figure 4-60: Geochemical proxies for Sacred Lake. The blue graph displays the raw and normalized values at every one-millimetre interval while the red graph shows the moving average over one-centimetre interval down the sediment core. The grey areas mark the extent of the 6 cores; SAL II -1, SALII- 2, SALII- 3, SALII- 4, SAL II – 5 and SAL II – 6 whilst the dotted black and red lines denote the stratigraphic units and hiatus, respectively.

The Si/Ti ratios show a general decline until the hiatus. After the hiatus, the Si/Ti does not show any significant changes until 27 cm where a relative rise is observed followed by a decline in the upper section of the core in SLK4. Since the Si/Ti in our PCA is linked to lithogenic input, the source is likely aeolian and therefore the changes recorded represent different states of the lake from shallow to deep lake phases (Figure 4-60)

4.4.3 Organic Geochemistry

4.4.3.1 Total Carbon, Total Nitrogen and C/N Ratios of Organic Matter

The total carbon content of the Sacred Lake sediments at the basal unit of the core (SLK1) is the lowest in the whole core, ranging from 6.4 % to 10.0 %. There is a pronounced peak at 54 cm (15.4 %). SLK2 is characterized by increase in %C from 12.0 % to 17.0 %, with a notable peak at 37 cm (19.6 %) just before the hiatus. Above the hiatus, in SLK 3, the values are fairly constant between 16.0 % and 17 % (Figure 4-61) while within the upper unit SLK4, 4.0 % in %C is observed followed by a notable increase in the uppermost section of the core where the highest value of 26.0 % is observed. The %N values range from 0.36 to 2.10 % (mean 1.06 %; Figure 4-61) and mirrors %C variations along the core. The %N minimum is observed before the hiatus at the bottom of the sediment core in SLK1 while a notable rise in the values is observed in SLK2. The %N remains relatively constant in SLK3 (centred at 1.00 ± 0.50 %) above the hiatus while in SLK4, an initial decline followed by a rise in %N to its maximum value is observed.

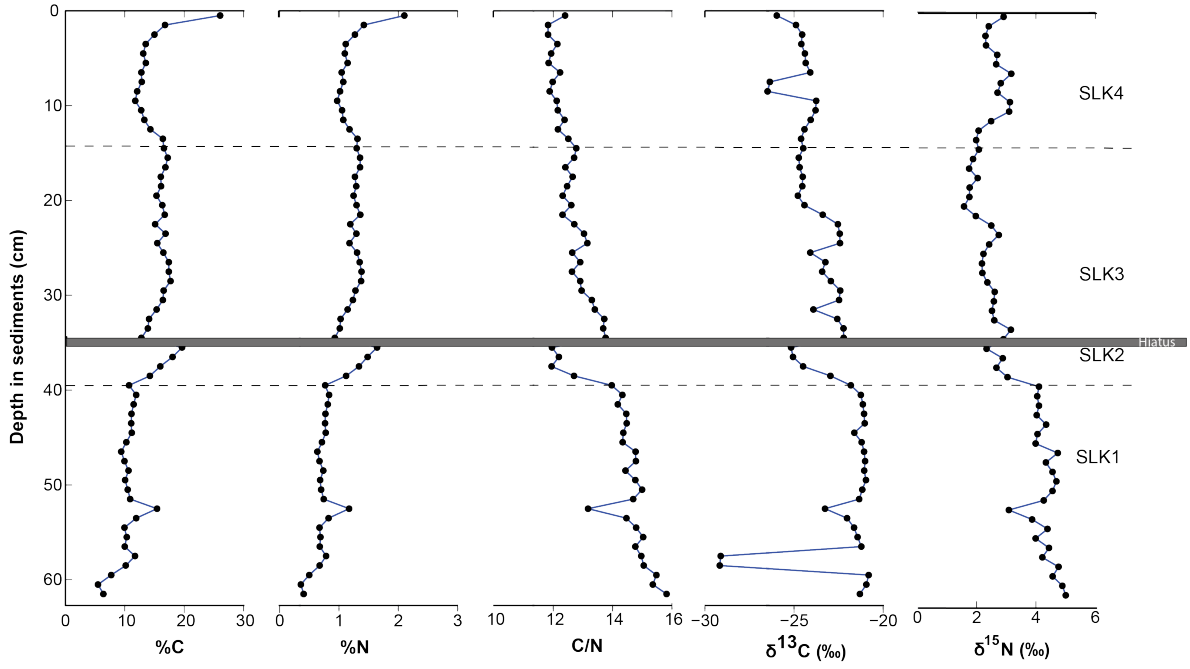

Figure 4-61: Down core variations in the percentage composition of elemental C and N, C/N ratios and the stable $\delta^{13}C$ and $\delta^{15}N$ isotopes composition from Sacred Lake

The C/N ranges from 11.82 to 15.82 with the highest ratio at the bottom of the core in SLK 1 (Figure 4-61). A large decline is present at 54 cm (13.10) within SLK 1 that corresponds to an increase in both %C and %N. Just before the hiatus within SLK2 there is a synchronous rise in %C and %N, and a decline in C/N. Above the hiatus, the C/N values display a relative decline to the top of the sediment core.

4.4.3.1 Bulk $\delta^{13}C$ and $\delta^{15}N$

The $\delta^{13}C$ ranges from -29.16 ‰ to -20.81 ‰ with notable peaks at 57-58 cm (-29 ‰) and 54 cm (-23 ‰) within SLK1. The second negative excursion at 54 cm corresponds to an increase in %C and %N (Figure 4-61). Within SLK2, a general decline in $\delta^{13}C$ is observed before the hiatus. After the hiatus in SLK3, shifts in the bulk $\delta^{13}C$ superimposed on a decreasing (more negative) trend are observed. In SLK 4, a pronounced depletion in bulk $\delta^{13}C$ is present at 8 – 9 cm.

The observed $\delta^{15}N$ values vary from 1.58 to 5.00 ‰. In the oldest part of the record (SLK1) the highest $\delta^{15}N$ values ranging from 3.04 – 5.00 ‰ display multiple fluctuations (Figure 4-61). In SLK2 the bulk $\delta^{15}N$ displays a dramatic decline that is synchronous with a decrease in $\delta^{13}C$ and C/N and an increase in %C and %N perhaps due to the shallowing of the lake before the hiatus. Above the hiatus in SLK3, the bulk $\delta^{15}N$ is centred at 2.00 ± 0.50 ‰ while slight indistinct increases in the $\delta^{15}N$ values are observed in SLK4.

4.4.3.2 Provenance of OM based on $\delta^{13}C$ and C/N

The $\delta^{13}C$ values and C/N ratio coupling in Sacred Lake imply that C_3-type plants (Figure 4-62) are the major contributors to the OM component of the sediments throughout the core, with bulk $\delta^{13}C$ range of -25.2 to -22.0 ‰.

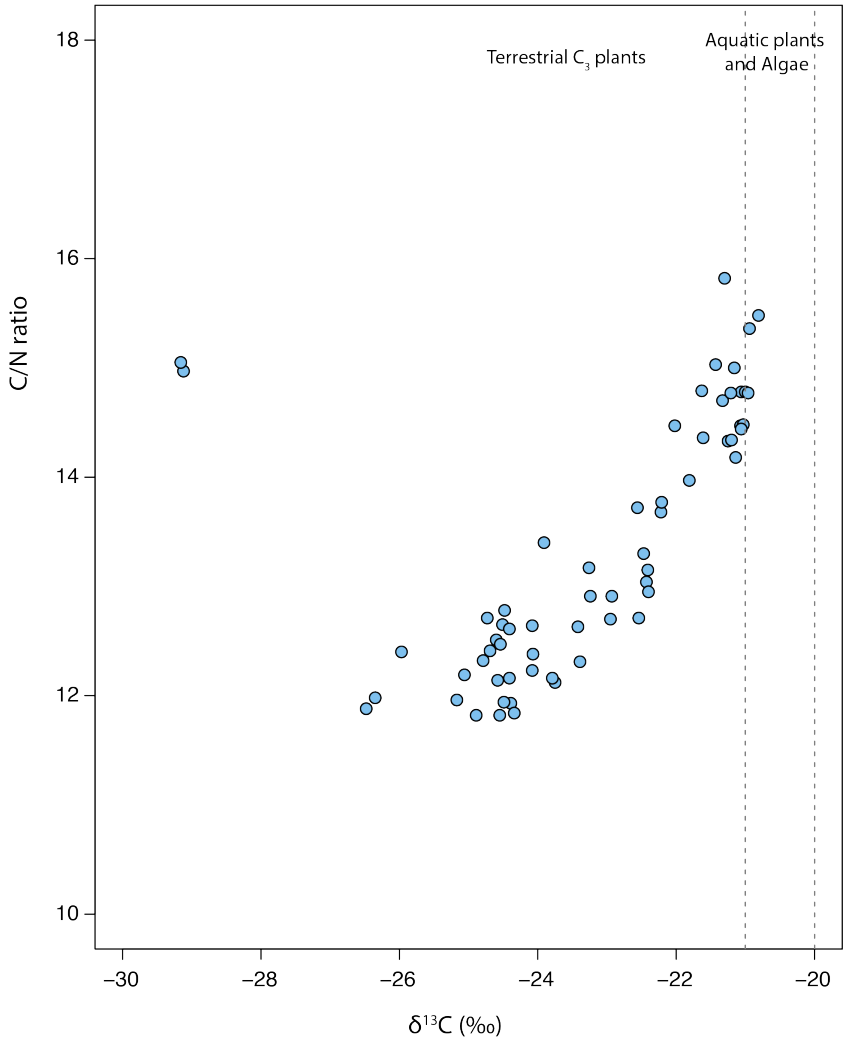

Figure 4-62: Provenance of the organic component of the Sacred Lake sediments

4.4.3.1 Distribution of n-Alkanes

The distribution of n-alkane from Sacred Lake is bimodal in the mid to bottom sections of the core (before the hiatus) and unimodal at the top (above the hiatus). The number of carbon atoms present in the n-alkane chains range from C_{12-35} (Figure 4-63). The samples from the bottom of the core display enrichment in the short to mid-chain n-alkanes while those collected above show a decline in the abundance of these short to mid-chain length *n*-alkanes with the exception of the uppermost sample.

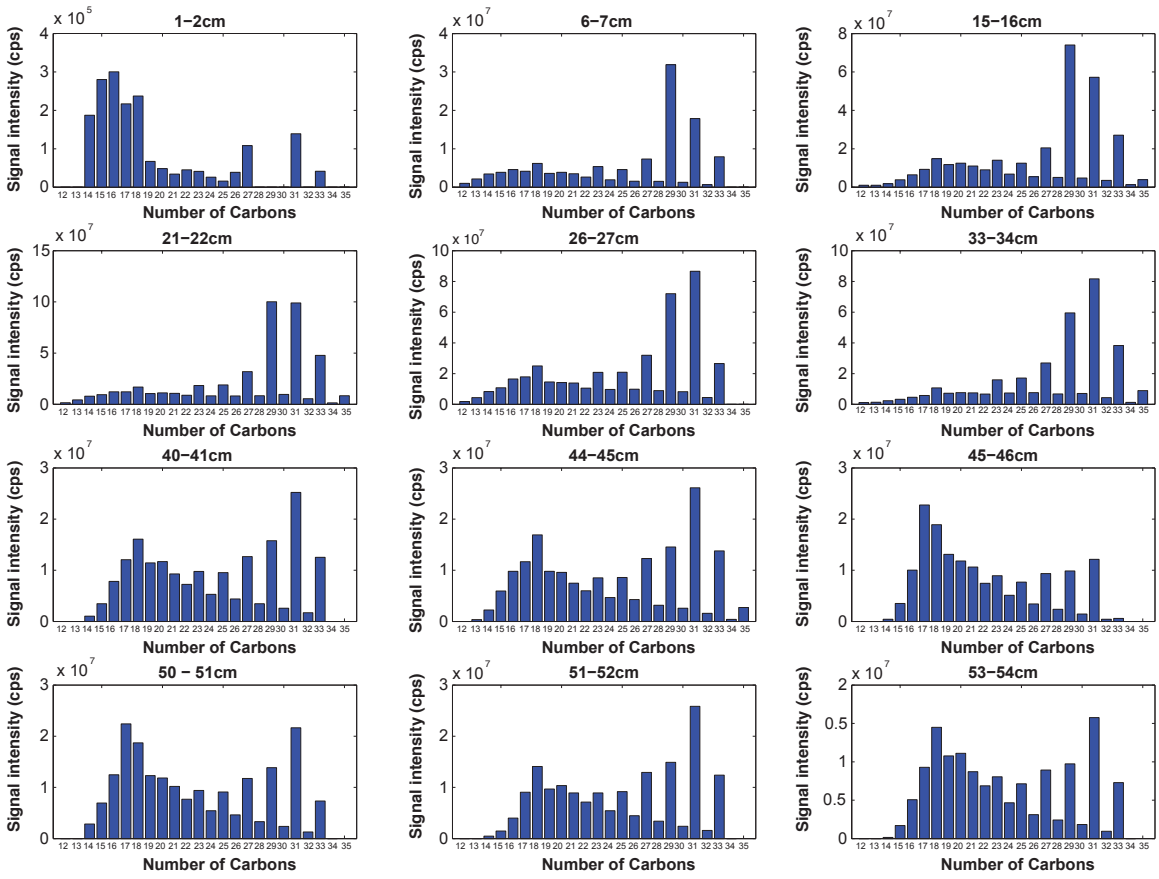

Figure 4-63: n-alkane distribution from Sacred Lake

The terrestrially derived odd long chain *n*-alkanes C_{29}, C_{31} and C_{33} are abundant in most of the samples from the core. There are slight variations in the relative abundance of these *n*-alkanes along the core. Before the hiatus, $C_{31} > C_{29}$ while C_{33} and C_{27} are equally abundant. Above the hiatus, $C_{31} > C_{29}$ while an increase in the relative abundance of C_{33} is accompanied by a decline in C_{27} abundance and vice versa. In the uppermost unit SLK 4, $C_{29} > C_{31} > C_{33} > C_{27}$ while in the sample at the top interval, $C_{31} > C_{27} > C_{33}$ and C_{29} is missing. The short chain *n*-alkanes do not display a strong odd-over-even number preference and are dominated by C_{18} or C_{17}.

The terrestrial indicators ACL (28.4 – 29.8), CPI (4.1 – 11.8), TAR (0.4 – 10.4) and P_{aq} (0.17 – 0.43) (Table 13) show odd-over-even predominance. The ACL, TAR and CPI values from samples before the hiatus are lower than those observed after the hiatus. The P_{aq} values are high before the hiatus and decline after the hiatus. These changes before and after the hiatus are indicative of changes in terrestrial OM sources of the lake sediment. The C_{31} alkane is more abundant than the C_{27} leading to lower C_{27}/C_{31} ratios with values <1, ranging from 0.3 – 0.8,

while the C_{15-21}/C_{22-33} range is from 0.23 to 2.60, with the values generally higher before the hiatus and lower after the hiatus with the exception of the uppermost sample.

Table 13: Summary of n-alkane indices from Sacred Lake

Depth (cm)	C_n range	C_n max	ACL	CPI	C_{27}/C_{31}	TAR	P_{aq}
1-2	14-33	16	29.5	6.3	0.8	0.4	0.29
6-7	12-33	29	29.5	11.8	0.4	5.0	0.17
15-16	12-35	29	29.7	8.4	0.4	6.1	0.17
21-22	12-35	29	29.8	8.2	0.3	7.2	0.16
26-27	12-33	31	29.6	6.6	0.4	4.4	0.21
33-34	12-35	31	29.9	7.4	0.3	10.4	0.19
40-41	14-33	31	29.5	5.3	0.5	2.0	0.32
44-45	13-35	31	29.6	5.4	0.5	2.0	0.30
45-46	14-33	17	28.4	4.1	0.8	0.8	0.43
50-51	14-33	17	29.2	4.6	0.5	1.1	0.34
51-52	14-33	31	29.5	5.3	0.5	2.7	0.31
53-54	14-33	31	29.3	4.8	0.6	1.6	0.37

C_n-number of Carbon atoms present in n-alkane chain: ACL – total Average alkane Chain Length; CPI – Carbon Preference Index of long chain alkanes; TAR – Terrigenous-Aquatic Ratio; P_{aq} – Aquatic macrophyte input proxy

4.4.3.2 Distribution of Glycerol Dialkyl Glycerol Tetraethers (GDGTs)

The brGDGTs range from 4000 to 12648 µg/g, constituting 77.5 – 90.9 % of the total GDGTs, and are more abundant than the iGDGTs (857 to 1248 µg/g) which amount to 9.1 – 22.5 % of total GDGTs (Figure 4-64). Among the iGDGTs, GDGT-0 is the most abundant (67.0 – 50.0 %) while the crenarchaeol is the second most abundant (5.6 – 27.0 %). For the iGDGTs the relative abundance of GDGT-0 decreases while the crenarchaeol increases up core while GDGT-4 is missing throughout the core. The total brGDGTs increase up core, peaking *ca*. 27 cm. GDGT-I (68 – 61 % of total brGDGTs) is the most abundant while GDGT-II (31 – 20 % of total brGDGTs) is the second most abundant (*Figure 4-46*). Two brGDGTs with cyclopentyl moieties GDGT-IIIb and GDGT-IIIc are recorded in the lower section of the core until *ca*. 40 cm when these two disappear. The Branched vs. Isoprenoid Tetraether (BIT) index is high (0.97 – 0.98) throughout the core (Table 14), affirming the dominance of the terrestrially derived brGDGTs in the lake sediments (Figure 4-64).The calculated MBT and CBT values range from 0.63 – 0.72 and 1.51 – 1.71, respectively (Table 14). The MBT displays a decreasing trend up core while the CBT does not display any.

Table 14: The variations in BIT, 1302 (GDGT-0)/1292 (crenarchaeol) ratio, MBT and CBT proxies from the Sacred Lake sediment core

Depth (cm)	BIT	1302/1292	MBT	CBT	pH
2	0.97	1.9	0.63	1.71	5.1
7	0.98	2.3	0.66	1.61	5.4
16	0.97	2.4	0.68	1.68	5.2
22	0.97	2.8	0.70	1.71	5.1
27	0.98	5.1	0.70	1.68	5.2
34	0.98	6.9	0.70	1.65	5.3
41	0.98	10.4	0.72	1.51	5.7
45	0.98	9.8	0.71	1.47	5.9
50	0.98	10.9	0.72	1.42	6.0
54	0.98	11.5	0.73	1.43	6.0

The reconstructed pH (*Equation 11*, pg. 70) values range from 5.1 to 6.0 pH units (Figure 4-64). The high BIT index coupled with the GDGT-0/crenarchaeol (1302/1292) ratio > 2 eliminated the potential application of the TEX_{86} proxy as a meaningful proxy for palaeotemperature. This ratio is higher in the lower section of the core where the value is < 5 and declines in the upper section with values centred at 2.

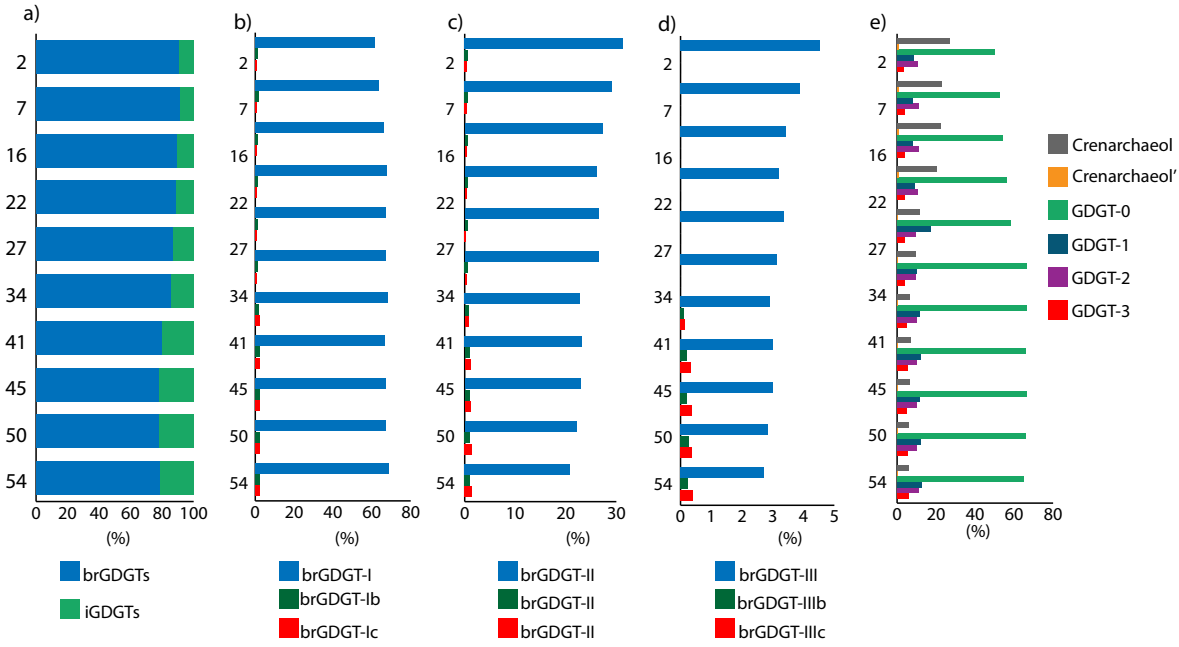

Figure 4-64: The relative abundance of the brGDGTs and iGDGTs down core in the Sacred Lake core. The five graphs represent the main (a) brGDGT and iGDGT abundances, while GDGT groups and their moieties are illustrated in (b) GDGT-I, Ib and Ic (c) GDGT-II, IIb and IIc, (d) GDGT-III and IIb & (e) iGDGTs

The reconstructed MAAT from the various calibrations (Figure 4-65) represents progressive cooling from the bottom of the core. The resulting temperature reconstructions are generally highest using the MBT/CBT calibrations from both Tierney et al. (2010) and Loomis et al. (2012) with the values ranging from 16.5 – 22.4° C and 22.5 – 28.6° C, respectively (Figure 4-65). The values from the two calibrations show a *ca.* 6.0° C shift but absolute values are distinctly different due to the fact that the Loomis et al. (2012) calibration uses the statistical significance of the brGDGT data in the prediction of the temperature.

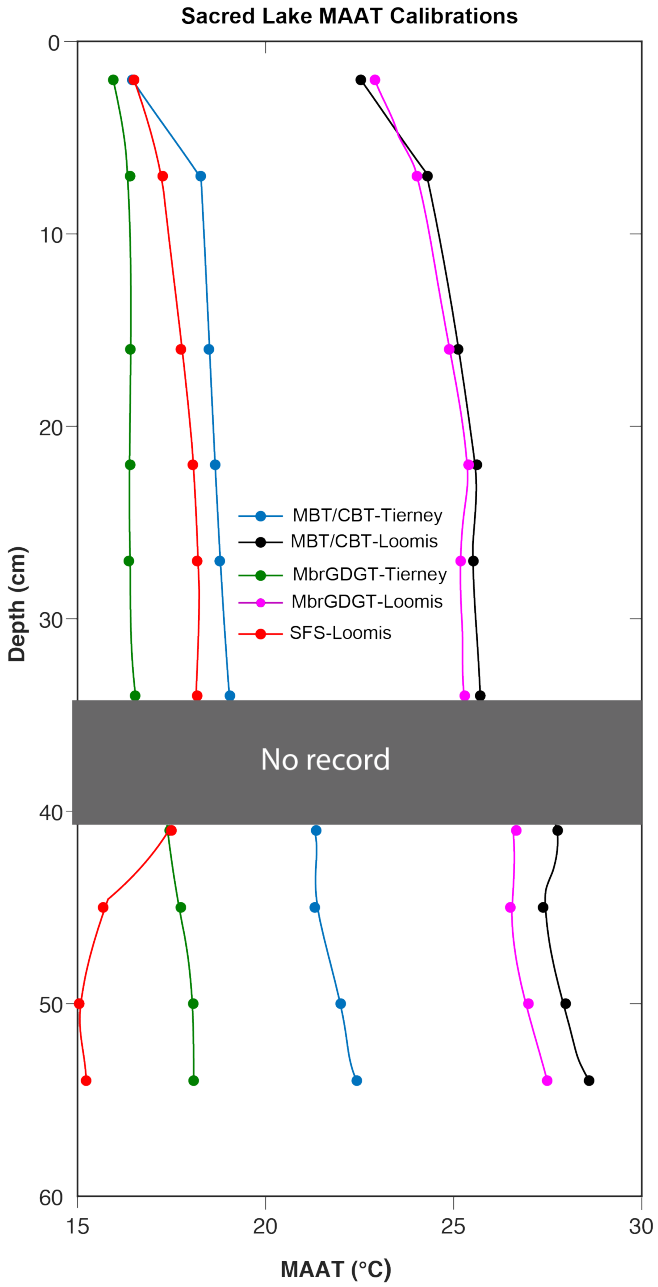

Figure 4-65: Reconstructed MAAT for Sacred Lake core using MBT/CBT, MbrGDGT and SFS regional calibrations

The MbrGDGT calibrations range from 15.95 – 18.10° C (Tierney et al. 2010) and 22.9 – 27.5° C (Loomis et al. 2012) while the SFS calibration ranges from 15.0 – 18.18° C (Loomis et al. 2012). The ranges of MBT/CBT and MbrGDGT derived MAAT by Tierney et al. (2010) represent the maximum (5.9° C) and minimum (2.1° C) temperature variations in the reconstructions from this core (Figure 4-65). The reconstructed MBT/CBT and MbrGDGT (Loomis et al. 2012) are higher with minimum variation (0.3 - 1.1° C) down core while the reconstructed MBT/CBT and MbrGDGT (Tierney et al. 2010) produce lower values with a large variation (0.50 – 4.34° C). Generally, both MBT/CBT and MbrGDGT variations are large with a gap of 6.0 – 7.0° C and 7.0 – 9.4° C, respectively. The reconstructed temperature using the SFS calibration displays an opposite trend to the MBT/CBT and MbrGDGT calibrations in the lower section of the core with a slight increase in temperature until the hiatus where the values become relatively constant with very minimal variations less than 1.0° C (Figure 4-65).

4.4.4 Synthesis of Sacred Lake Proxies

The 63 cm of sediments from Sacred Lake covers approximately 4425 – 639 cal yr. BP. The upper limit of the age of the sediments (639 cal yr. BP) is acceptable as the samples dated in the upper sections of the core collectively show an age that is not close to present day. Fixing the upper section of this core to zero skews the age-model and therefore this was not done for Sacred Lake. A notable hiatus at 36 cm points to missing sediment history during the interval 3515 to 1542 cal yr. BP according to the age model. This hiatus could be attributed to the fact that the sediment core was not obtained at the centre of the lake. The lake levels were relatively low during this period exposing the area where the core was acquired to erosion processes hence the missing sedimentation record. The apparent sedimentation rate (ASR) in this lake is unusually low for a permanent lake environment. The ASR values ranging from 0.008 – 0.240 cm/yr. likely indicate a constant, high frequency and non-detected alteration of deposition /erosion processes near the shore unlike the linear sedimentation rates obtained by Olago (1995) from the centre of this lake. A relative decline in sedimentation rate is observed before the hiatus while an increase in the sedimentation rate is modelled for the period after the hiatus. The magnetic signal supports the alteration of open water and marsh/peat bog environments, the latter being favourable to the dilution and dissolution of iron oxides. The preserved magnetic minerals present are mostly as canted antiferromagnetic and correlate with significant quantities of hematite/goethite that are associated with minor softer spinel (likely titanomaghemite) grains.

A summary of the results from the Sacred Lake proxies is presented in Table 15. The sediments in Sacred Lake are largely derived from a restricted crater catchment, which in the present-day is surrounded by forest vegetation. Limited variations are observed in the stratigraphy, sediment chemistry, mineralogy and mineral magnetics affirming a small-restricted catchment as the main source of materials.

Table 15: Proxy indicators summary from Sacred Lake

Stratigraphic Unit	**Proxy information**
SLK1 63– 41 cm 4425 - 3660 cal yr. BP	▪ Total %C ranging from 6.4 % to 10.0 %. ▪ The mean $\delta^{13}C$ (-22.27‰) points to a predominantly C_3 type vegetation source of OM that could be linked to the montane forest surrounding the catchment ▪ High X_{lf} values recorded in the sediment core are found, indicating a well-preserved fraction of terrigenous iron minerals ▪ The Ca/Ti, K/Ti and Fe/Ti ratios peak at the bottom of the sediment core before they appear relatively constant throughout the rest of the core. ▪ This C_3 type ecosystem supported by C_4 grasses could be attributed to the <1 value of the C_{27}/C_{31} that denotes the expansion of grasslands in an ecosystem that suggests an *n*-alkane origin from grass biomass. ▪ The reconstructed MAAT points to a 3°C warming during this period which could potentially support the expansion of these grasslands.
SLK2 41 – 35 cm 3660 - 3515 cal yr. BP	▪ Total %C ranging from 12 % to 17 %. ▪ Fluctuating X_{lf} and geochemical parameters (Ca/Ti, Fe/Ti and K/Ti) peaks could support postulated input from the catchment. ▪ The bulk $\delta^{13}C$ (-22 to – 25.2‰; mean: -23.70‰) values are within the range of C_3 - type vegetation where bulk $\delta^{13}C$ ranges from -20 to -40‰ which is the range of values for most trees, shrubs and herbs ▪ The C_{27}/C_{31} (<1) of the samples from this unit indicates significant contributions of grass over tree.
SLK3 35 – 14 cm 1542 - 980 cal yr. BP	▪ Total %C ranging from 16 % to 17 %. ▪ The C_{27}/C_{31} (<1) of the samples from this unit indicates significant contributions of grass over tree. ▪ Fluctuating X_{lf} and geochemical parameters (Ca/Ti, Fe/Ti and K/Ti) peaks
SLK 4 14 – 0 cm 980 - 639 cal yr. BP	▪ Total %C ranging from 4 % to 26 %. ▪ The synchronous rise of X_{lf}, Ca/Ti, K/Ti and Al/Ti during this period points to partly anthropogenic input of detrital material from the catchment to the lake. ▪ The C_{27}/C_{31} (<1) values in this unit could be linked to grasslands usually C_4 type grasses present in the Mt. Kenya area. ▪ The CPI (>5), ACL (19.2 – 26.5), P_{aq} (0.17 – 0.29) and TAR (0.4 – 6.1) values display a mix of terrestrial and aquatic OM source

The general linear upward trends in most biogeochemical proxies of the sedimentary environment point to linear evolution of the lake environment across time, likely linked with the filling process by aquatic vegetation under shallow environments. Superimposed on this trend, the Si/Ti ratio seems to be the main diagnostic proxy that displays synchronicity in trends with the sedimentation rate. The relative changes of the Si/Ti values before and after the hiatus seems to be the most significant in this lake (Figure 4-66). The Si/Ti in this lake is an indicator

of aeolian dust transport from the basement (metamorphic rock terrain areas to the east of the mountain) into the lakes. Before the hiatus there is a general decline in the Si/Ti ratio perhaps points to decreasing aeolian input and soon after the hiatus, the rise of the Si/Ti ratio denoting increase in aeolian input and possible biogenic input although it is not possible to discriminate the aeolian and biogenic signal from our results (Figure 4-66).

The coexistence of halloysite and gibbsite imply chemical weathering is a significant process while the presence of feldspars and quartz alongside these weathering products affirm an extra-catchment aeolian influence on the lake. In Sacred Lake, C/N ratios throughout the core (11.0 – 15.9) reflect OM contribution from primary production with a substantial contribution from vascular plants surrounding the catchment (Meyers & Teranes, 2001). The low %C content in SLK1 reflects little or no productivity within the lake. The mean $\delta^{13}C$ (-22.27‰) points to a predominantly C_3-type vegetation source of OM from the catchment (Meyers & Teranes 2001). This period terminated at the hiatus. In SLK 2, higher %C (15 – 19 %) and %N (1.1 – 1.6 %) values are recorded reflecting lake recovery with an influx of OM corresponding to the relative increase in sediment supply. SLK3, on the other hand, has lower values of %C (16 – 17 %) and %N (1.2 %) which are similar to values within SLK4 with mean %C (15 %) and %N (1.2 %), although not significant enough to be linked to a different OM source (Figure 4-66).

There is a strong correlation between %C and %N ($R^2 = 0.97$) with a positive intercept on the %N axis (2 %) suggesting that the total nitrogen is of purely organic origin. This is to be expected in lacustrine sediments where the large majority of total N is derived from organic matter sources. The $\delta^{13}C$ and $\delta^{15}N$ have a strong correlation with C/N ($R^2 = 0.8$ and $R^2 = 0.7$, respectively) perhaps pointing to significant influence of cyanobacteria and probable diagenetic processes in this sediment core (Meyers & Teranes 2001). This is validated by the correlation between %N and $\delta^{15}N$ ($R^2 = 0.7$). The persistence of the very low %N has been used to classify the lake as oligotrophic (Street-Perrott et al. 2007).

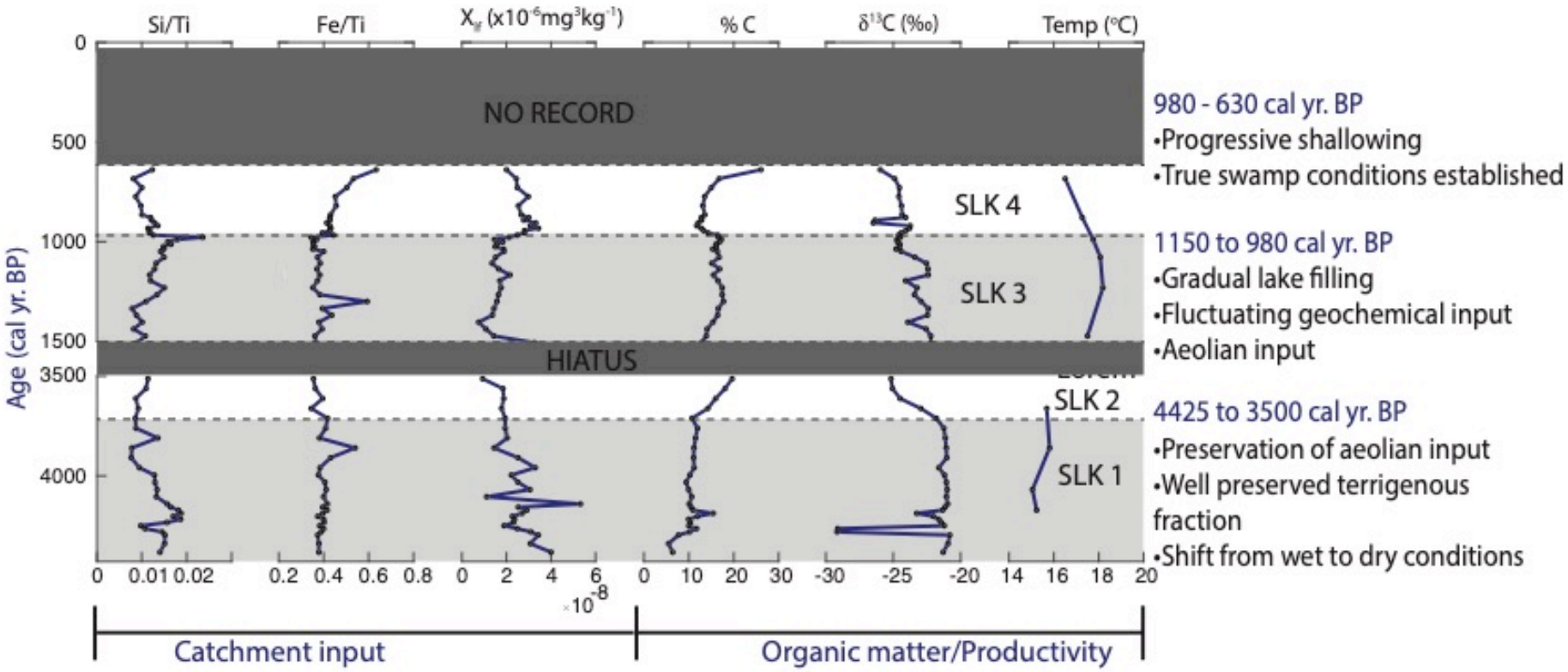

Figure 4-66: A summary of key findings for Sacred Lake from 4425 to 630 cal yr. BP indicating key changes in lake sedimentation and lake level variations

The distribution of n-alkane is unimodal for the samples at the top of the core and bimodal for samples located in the mid to bottom sections of the core. These variations within the core can be attributed to algal, terrestrial and mixed input of OM into the lake sediments with the algal input predominant in the upper sections of the core after the hiatus. The number of carbon atoms present in the n-alkane chains range from $C_{12\text{-}35}$. The odd long chain n-alkanes C_{29}, C_{31} and C_{33} are abundant, indicative of terrestrial input, whereas the most abundant short chain n-alkane is C_{18}.

Throughout the entire core, the C_{31} alkane is more abundant than the C_{27} leading to C_{27}/C_{31} (<1) of the samples throughout the core, pointing to significant contributions of grass over tree possibly due to the expansion of grasslands (Maffei 1996, Schwark et al. 2002). Despite this general trend there are subtle changes in this ratio before and after the hiatus. Before the hiatus, the C_{27}/C_{31} ranges between 0.5 and 0.8 while the values after the hiatus are between 0.3 and 0.4 with the exception of the uppermost sample (0.8). These subtle changes imply changes in dominant catchment vegetation with the lower sections of the core suggesting an open-forest watershed before the hiatus and a grass/herb dominated ecosystem after the hiatus, associated with the establishment of emergent macrophytes in the lake as reflected in the P_{aq} values. Further it is evident that the C_{31} alkane is abundant before the hiatus, while the C_{29} alkane is abundant after the hiatus; this supports changes in ecosystem composition of the emergent/terrestrial plants providing the OM in this lake. The $C_{15\text{-}21}/C_{22\text{-}33}$ before the hiatus is higher implying increase in microbial contributions while after the hiatus, there is an increase in terrestrial input into the lake. The uppermost sample records the highest $C_{15\text{-}21}/C_{22\text{-}33}$ ratio, which reflects the current status of the lake, dominated by emergent plants. Before the hiatus, the short chain n-alkane C_{18} is more abundant. This is attributed to the combustion of non-woody biomass in the catchment (Eckmeier & Wiesenberg 2009). The Late Holocene at Sacred Lake has been characterized by fire incidences marked by the coexistence of panicoid and pooid type grasses (Wooller & Agnew 2002). In the uppermost sample, the short chain n-alkanes (C_{14-18}) are dominant with a maximum at C_{16} alkane. The dominance of these even numbered n-alkanes points to possible partial diagenesis of the odd chained shorter alkanes (Ficken at al. 1998) coupled with thermal degradation of OM due to temperature increase (Eckmeier & Wiesenberg 2009).

The CPI, ACL and TAR values also display differences before and after the hiatus. The lower CPI (4.1 – 5.3), ACL (21.7 – 24.2) and TAR (0.8 – 2.7) values are recorded before the hiatus.

This contrast implies that terrestrial input, although important in Sacred Lake before the hiatus, becomes a significant source for n-alkanes after the hiatus. Since both ACL and CPI values are derived from n-alkane signatures of higher plants, it is expected that these two values would display a high correlation. This is not the case for Sacred Lake where $R^2 = 0.01$; implying different n-alkane sources for the higher plants. This pattern is mirrored in the TAR ratio. The n-alkane proxies for this lake point towards a mix of aquatic macrophytes and terrestrial input of OM into the lake from a moist forest regime with larger plant diversity in the catchment (Eglinton et al. 1962, Kolattukudy et al. 1976, Cranwell 1982, Cranwell et al. 1987, Meyers 1997). Before the hiatus, mixed input from aquatic and terrestrial OM sources play an equal role in their OM contribution whereas after the hiatus, terrestrial input is the predominant OM source. These differences in OM could as well be linked to diagenetic processes implied by the strong correlation of $\delta^{13}C$ and $\delta^{15}N$ with C/N observed in the sediment core as well as the presence of microbial activity as seen in the *n*-alkane data.

The most abundant iGDGT in the Sacred Lake samples is the GDGT-0. The crenarchaeol is relatively abundant in the sediments in the upper sections of the core and is most abundant in the topmost sample. In the lower sections of the core, the GDGT-1 and GDGT-2 are relatively more abundant than the crenarchaeol. The variability in abundance of these two iGDGTs (GDGT-0 and crenarchaeol) has led to elevated (GDGT-0/Crenarchaeol) ratios where the values in the lower sections of the core before the hiatus are higher than values above the hiatus. These values imply methanogenic conditions in the lower sections of the core under anoxic lacustrine conditions (Blaga et al. 2009). The BIT index yields high and similar values (0.97-0.98), which is not surprising as the values probably reflect the variability in the GDGT-0 content.

The terrestrial origin of the brGDGTs in the lake sediment profile is supported by the high BIT ratio. The discrepancy in the relative abundance of the brGDGTs in the sediment up core is the relative abundance of the cyclic compounds of the penta-methylated brGDGTs (GDGT Ib, Ic, IIb, and IIc). In the brGDGT-III group, the cyclopentyl moieties are only present in the samples from the lower sections of the core. This has implications on the CBT index and the complementary pH proxy that has yielded very little variability in its values, which range from 5.1 – 6.0.

A comparison of the brGDGTs and the sediment chemistry (Fe/Ti) does not show any covariation implying *in-situ* production of the brGDGTs. The evidence of diagenetic processes

as seen in section 4.4.3 can therefore be attributed to this stipulated *in-situ* production of the brGDGTs. The CBT/MBT palaeothermometer reconstructions yield MAAT estimates biased towards cooler mid to late Holocene conditions and therefore are considered reliable for this site. The MbrGDGTs and SFS calibrations, on the other hand, display similar trends with the exception of the lower section of the core (before the hiatus) where cyclopentyl moieties of brGDGT III are present. In this section of the core, eutrophication, anoxic conditions, and a strong methane cycle in the lake could influence the brGDGT producing organisms leading to changes in their distribution thus leading to some disparities in the accuracy of the reconstructed temperatures. Previous applications of the SFS calibrations by Loomis et al. (2012) on a sediment core from Sacred Lake yielded a 1.2° C cooling from Mid Holocene to Present (Loomis et al. 2012). Using the SFS calibration on our data, we derive a 2.6° C warming from 4425 to 3515 cal yr. BP followed by a 3.1°C cooling from 1542 – 639 Cal yr. BP. The cooling from 1542 – 639 postulated in our record coincides with a period of widespread drought at Sacred Lake from *ca*. 900 to 500 cal yr. BP (Konecky et al. 2014). The applications of all the calibrations are biased towards the cooling during this period. Further, our record yields an average temperature change of 0.5° C cooling from mid-Holocene to Present, a value lower than estimates by Loomis et al. (2012) and Loomis et al. (2017) by 0.6° C and 1.0° C, respectively.

4.5 Lake Rutundu Sediments

4.5.1 Bulk Sediment Parameters

4.5.1.1 Stratigraphic Description

The sediments from Lake Rutundu are homogenous and have a soft fine-grained consistency throughout (Figure 4-67). The sediment colour ranges from black (5Y 2.5/1) in the bottom to olive grey (5Y 4/2) in upper sections of the core. The bottom section, from 100 – 82 cm, comprises black silty clays with a muddy and fibrous consistency and is overlain by homogeneous olive grey sediments with a soft fibrous (due to the presence of 'root like' fibres) consistency. There are no visible tephra layers or characteristic stratigraphic markers that can be used to distinguish the different sediment units. The core has high W_c ranging from 70- 87 % with an average of 79 %. The W_c progressively declines from a comparatively saturated bottom to the top of the sediment core.

The lithological changes are subtle and lack distinct stratigraphic markers. The compositional variation of %C, %N and their stable isotopes were analysed using constrained hierarchical clustering in Rioja (Juggins 2015) to identify significant stratigraphic zones. Four significant stratigraphic zones were identified as follows: declining OM concentration in LR1 (100 – 84 cm), increase in OM in LR2 (84 – 58 cm), stable OM concentration in LR3 (58 – 48 cm) and a decline in OM within LR4 (48 – 0 cm).

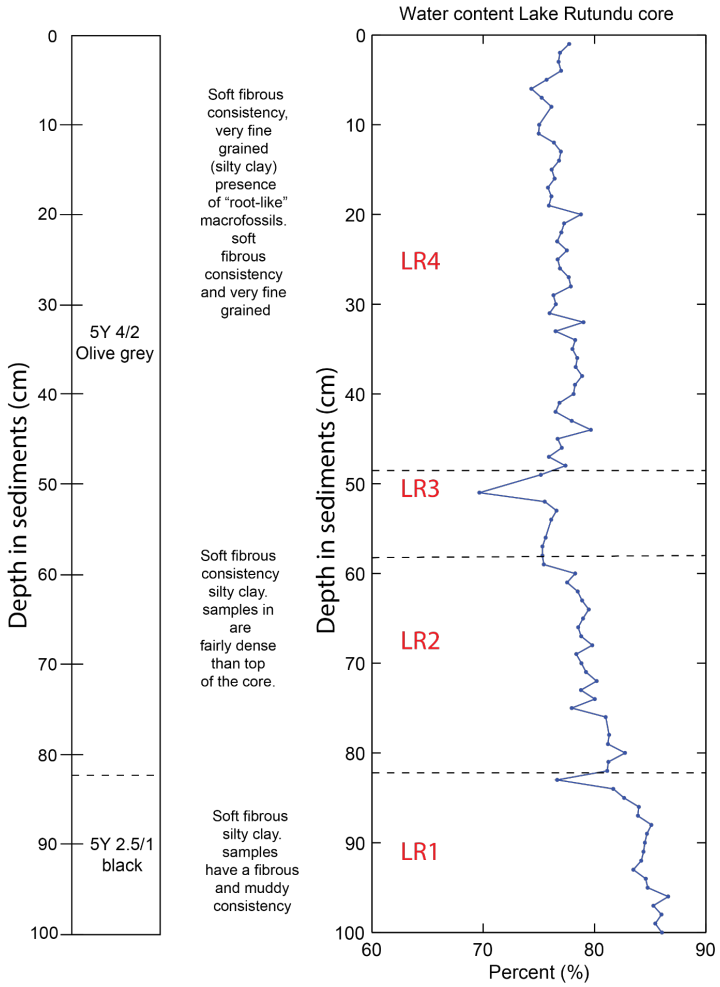

Figure 4-67: Descriptive stratigraphic section of sediments and percentage water content in sediment cores from Lake Rutundu.

4.5.1.2 Radiocarbon Chronology

The radiocarbon ages from four samples and their calibrated equivalents (cal yr. BP) obtained using the intCal13 (Reimer et al. 2013) are presented in Table 16 below.

Table 16:Radiocarbon ages from Lake Rutundu sediments from AMS (Age ^{14}C yr. BP) and calibrated radiocarbon ages (cal yr. BP) and their associated errors.

Lab No	Sample	Depth (cm)	Age ^{14}C yr. BP	Cal yr. BP
SacA34960	RC/22/10	22	1650 ± 30	1566±57
SacA34961	RC/49/10	49	2825 ± 30	2928±77
SacA34962	RC/78/10	78	3530 ± 30	3804±88
SacA34963	RC/99/10	99	4170 ± 30	4689±78

The AMS ^{14}C ages were used to generate an age-depth model for Lake Rutundu using Bacon V2.3 (Blaauw & Christen 2011). The year the sediment core was collected was added as the most recent age at the top sediments with an error of ±10 years. The resulting age-model (Figure 4-68) is internally consistent and is therefore considered representative for Lake Rutundu. The sediments from Lake Rutundu therefore cover 4770 cal yr. BP to Present.

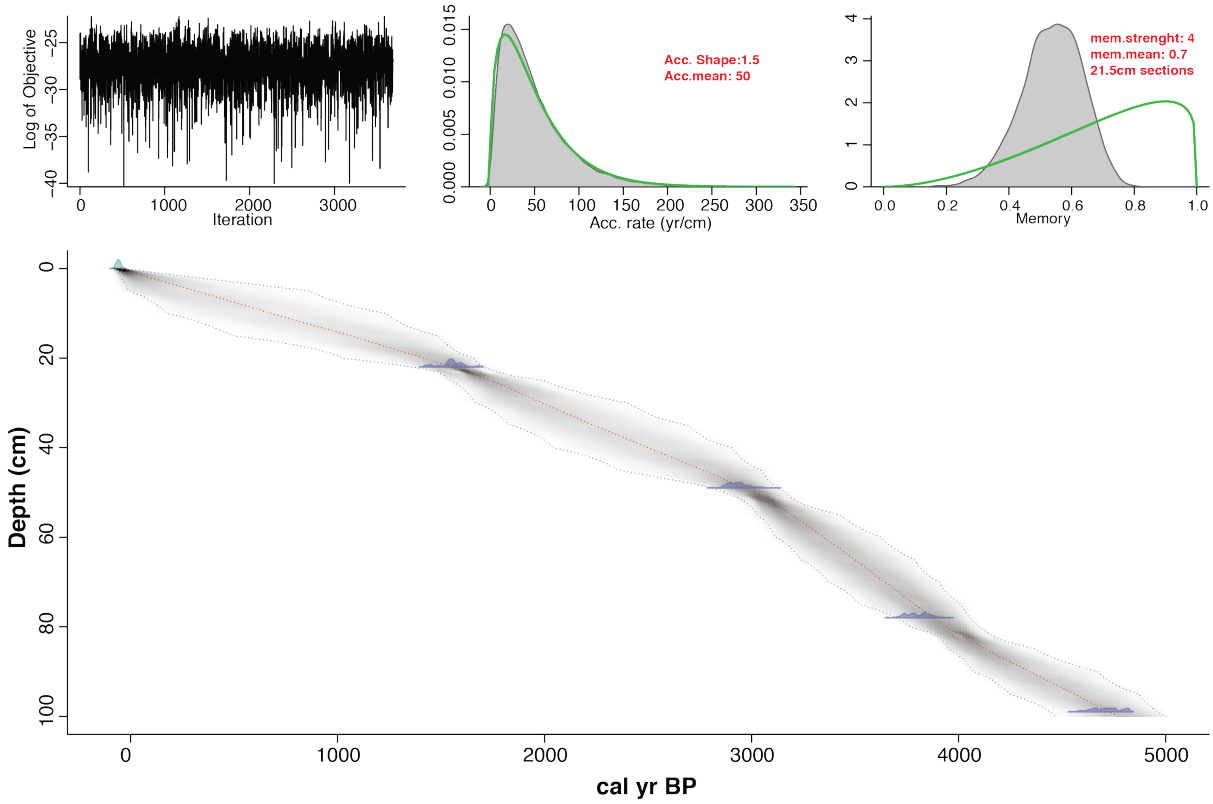

Figure 4-68: Bayesian age depth model for Lake Rutundu sediment core. The bottom panel displays the calibrated ^{14}C dates (transparent blue) and the age-depth model within 95 % confidence intervals. The upper panels show the MCMC iterations: the left panel represents the stability of the model while the middle and the right panels represent the prior (green curve) and posterior (grey histograms) for the distributions of accumulation mean and memory properties, respectively.

The sedimentation rate (Figure 4-69) is low; between 0.03 – 0.07 cm/yr. comparable with values obtain in Lake Nkunga. Generally, the sedimentation rate declines from the bottom to the top of the core but with a notable increase between 80 and 44 cm that slowly declines towards the top of the sediment core.

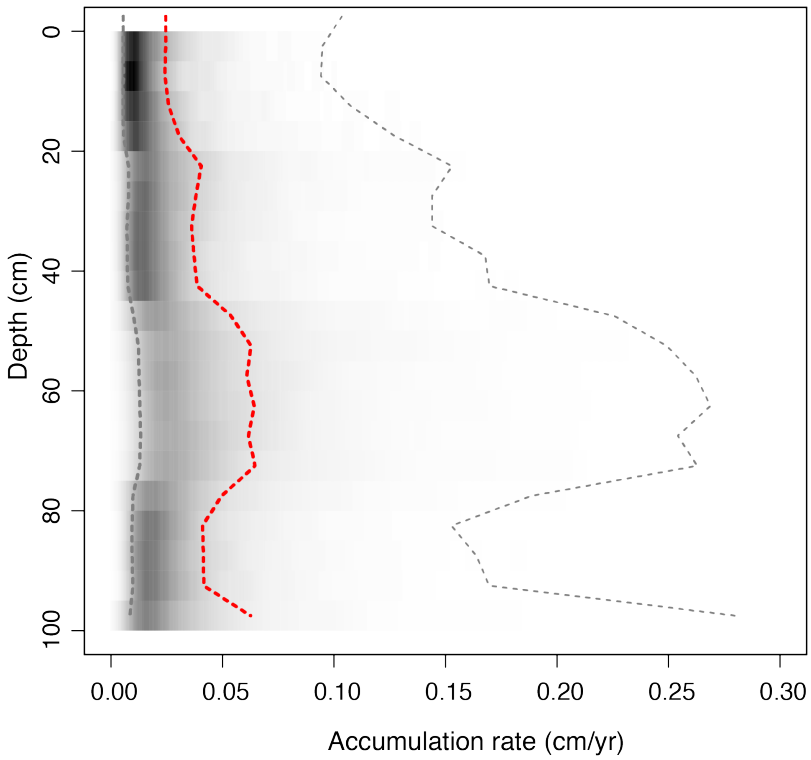

Figure 4-69: Sedimentation rate for Lake Rutundu. The darker the grey shaded areas the higher certainty in value obtained while the red line is the weighted mean of the sediment accumulation rate between the different depths along the sediment providing realistic representation in sediment supply.

4.5.1.3 Mineralogy

The mineralogy of this lake comprises plagioclase and potash feldspars (95 %) dominated by sanidine with small amounts of labradorite, quartz (3 – 5 %) and gibbsite (1 – 2 %). Gibbsite is below detection in two samples from the bottom section of the core (Figure 4-70).

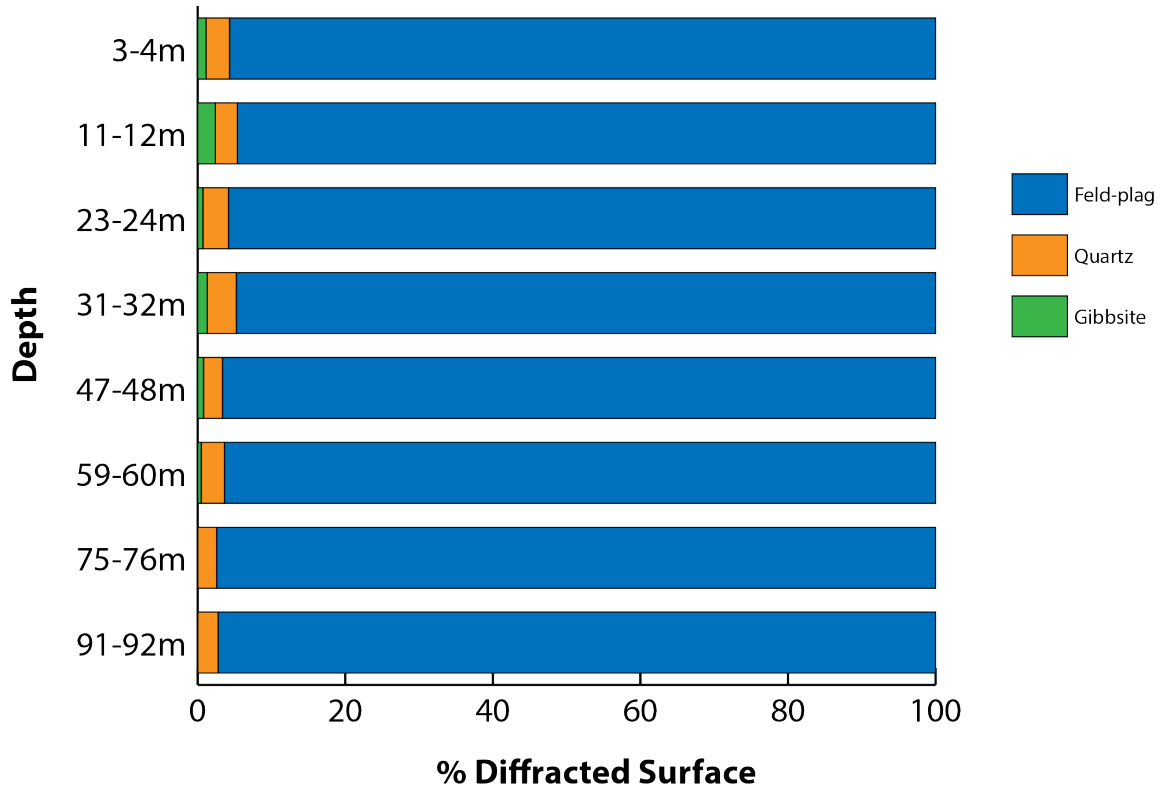

Figure 4-70: The bulk mineralogy of sediments from Lake Rutundu represented as a percentage of the diffracted surface.

4.5.2 Inorganic Geochemistry of Lake Rutundu

Sixteen elements (Al, Si, Ti, Ca, Mn, Cu, Fe, P, K, Nb, Ni, Rb, S, Sr, Zn, Zr) were detected in discrete pellet samples collected at about 8 cm. Geochemically stable elements and those representative of redox processes were selected for PCA.

The first principal component (PC1) accounts for 39.4 % of the variability while the second principal component (PC2) accounts for 30.8 % of the variability (Figure 4-71). The relatively poor and similar scores of PC1 and PC2 do not indicate any dominant processes explaining the biogeochemical signature of the lake environmental change: the whole set of proxies depend on strongly interacting processes which control the general response of the coupled climate-lacustrine environment system.

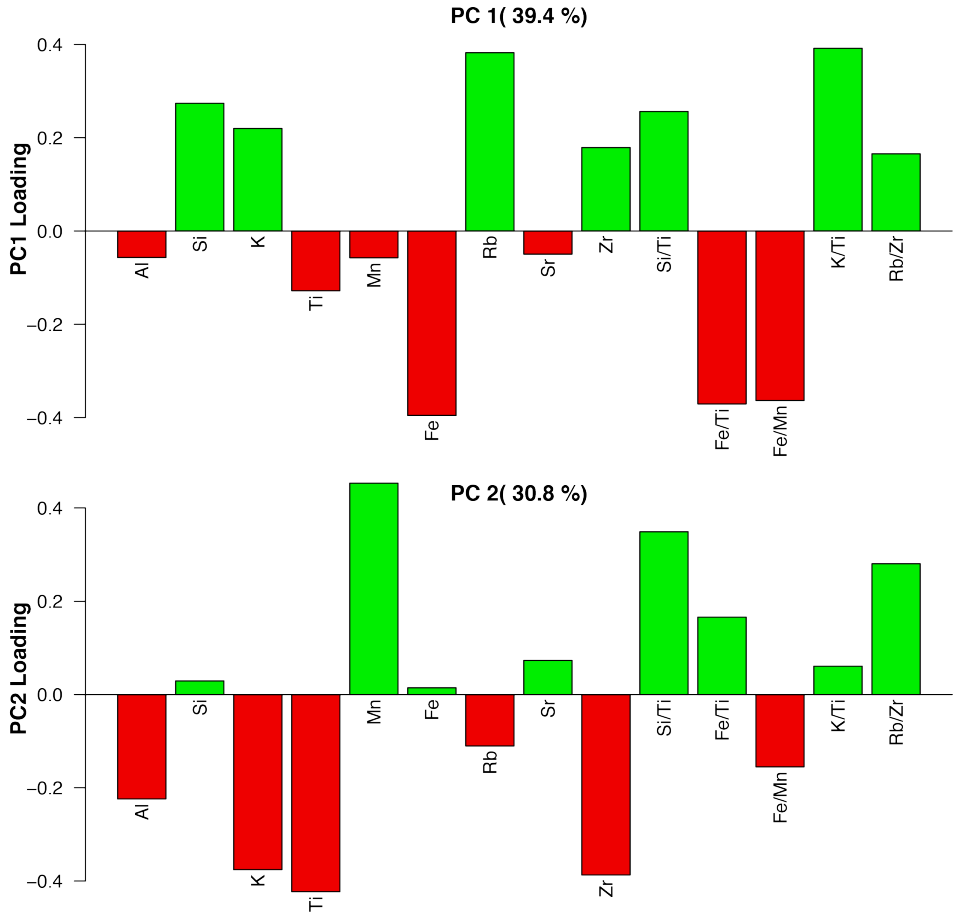

Figure 4-71: Elemental variation from discrete measurements of pellets from Lake Rutundu sediment.

PC1 has positive loading for Si, K, Rb, Zr, Si/Ti, K/Ti and Rb/Zr. It is indicative of autochthonous and allochthonous inputs such as biogenic silica production (Si/Ti), chemical weathering (K/Ti) and terrigenous sources (Rb, Zr, and Rb/Zr are proxies of grain sizes). It has negative loading for Al, Ti, Sr, Fe/Ti and Fe/Mn which is indicative of local clayey inputs. PC2 positively correlates with Si, Mn, Fe, Sr, Si/Ti, Fe/Ti, K/Ti and Rb/Zr, illustrating that the most likely local changes in lake biogeochemistry are associated with biogenic silica production and the dissolution of soluble elements (such as Zr, Fe, K). It negatively correlates with Al, K, Ti, Rb, Zr, and Fe/Mn, which are linked to the clastic phase once more mobile elements are removed under redox conditions, similar to the process in Lake Nkunga.

Despite some differences, PC1 and PC2 likely depend on similar environmental end-members, where the general sediment composition would be either controlled by (i) the primary biogenic production, eutrophication, oxygen deficiency and turnover of lake nutrients, or (ii) runoff and terrigenous inputs and water column mixing. At first glance, such end members would strongly

depend on seasonality and the associated changes in temperature and rainfall distribution and intensity, as well as changes in lake water depth.

Al, Fe, S, Si and Nb were normalized against Ti (Figure 4-72). Of the normalized values, the Fe/Ti ratios are the highest while the Al/Ti values are the lowest with intermediate values of proxies Si/Ti, S/Ti and Nb/Ti (Figure 4-72). Al/Ti is strongly sensitive to the relative clay terrigenous input and would increase in low deposition energy environments. It displays a decline from the bottom of the core to LR3 after which it rises briefly then stabilizes in the upper section of the core. The Si/Ti profile shows a decline in lower sections of the core (LR1, LR2 and LR3). LR4 marks a recovery stage displaying an increase in biogenic silica. Minimal changes are observed in the Fe/Ti profile in the lower sections (LR1, LR2 and LR3).

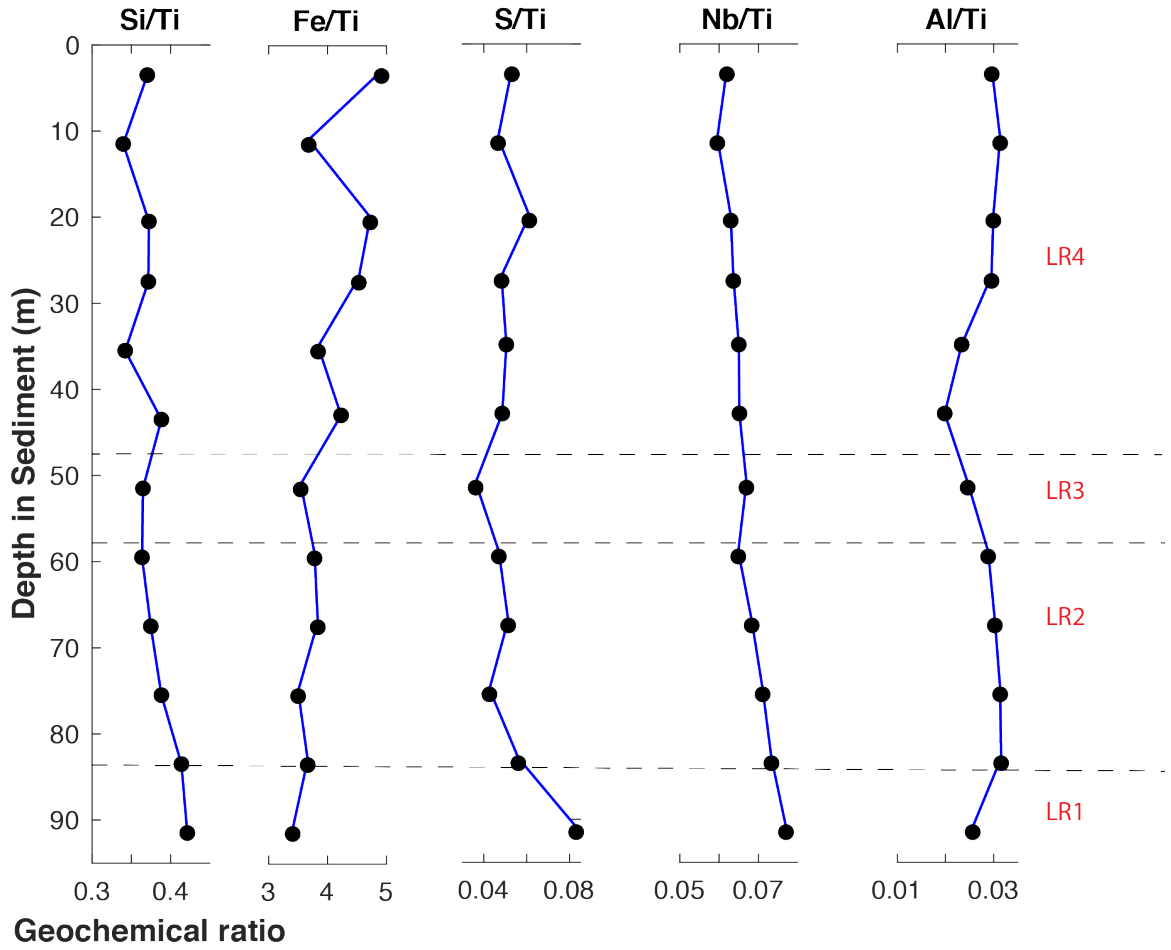

Figure 4-72: Inorganic geochemical composition for Lake Rutundu.

4.5.3 Organic Geochemistry of Lake Rutundu

4.5.3.1 Total Carbon, Total Nitrogen and C/N of Organic Matter

The total %C from the Lake Rutundu sediments is moderate to high, ranging from 12.96 % to 20.96 %, with the highest values recorded at the base of the core in LR1 (Figure 4-73). Above this, the %C displays a steady decrease up core from 20 % to ca.15 % at the boundary between LR2 and LR3 (58 cm). LR3 is characterized by minimal variation with the %C values centred at 15 ± 0.4 %. In LR4, the %C slightly increases and stabilizes in the upper sections of the sediment core. The uppermost sample at 4 cm represents a significant increase of the values in this top section (Figure 4-73).

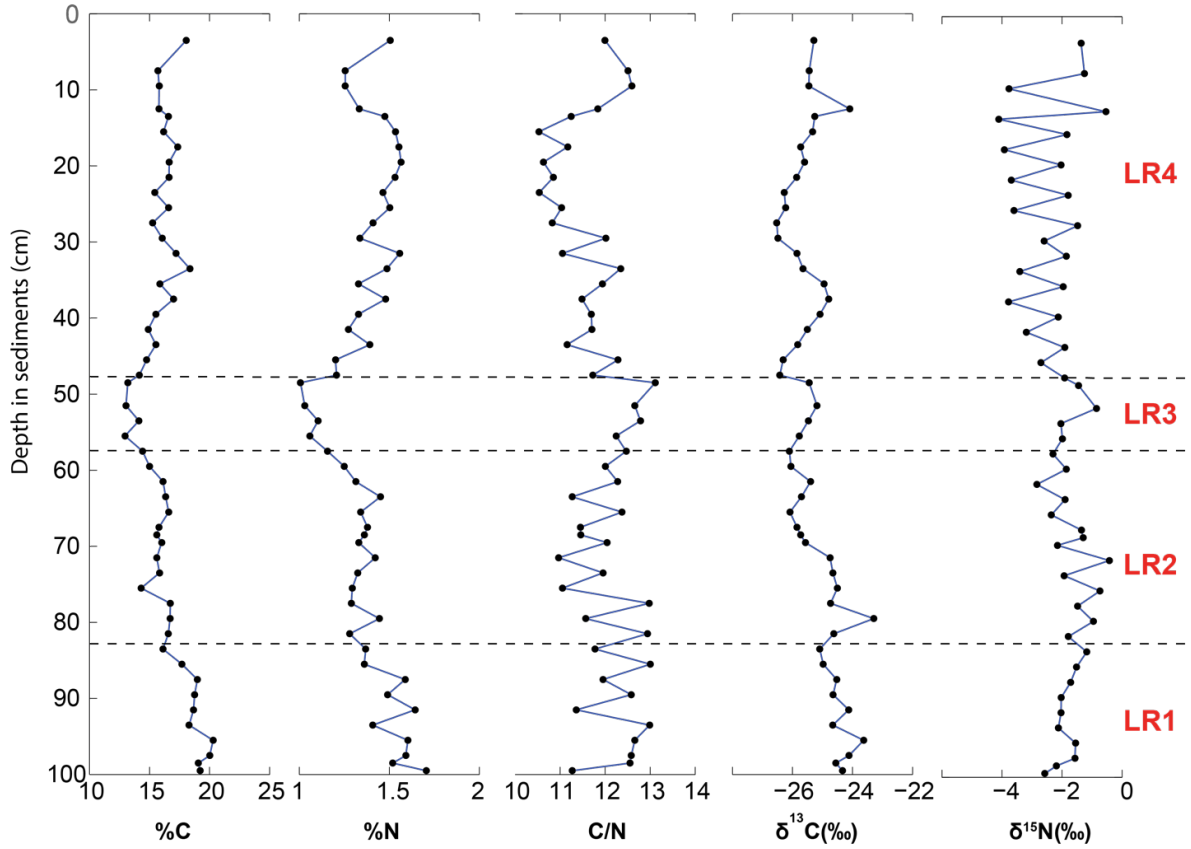

Figure 4-73: Down core variations in the percentage composition of elemental C and N, CN ratios and the Stable $\delta^{13}C$ and $\delta^{15}N$ isotopes composition from Lake Rutundu

The %N trends mirror that of %C with significant correlation between these two parameters (R^2 = 0.71). The line of best fit exhibits a slightly positive intercept on the %N axis (0.09 %) suggesting an organic origin of the nitrogen present in the sediments. The %N values range

from 1.01 to 1.71 % (mean of 1.38 %). A notable steady increase followed by a decline in the %N values is present between 30 – 10 cm, a departure from the relatively stable %C dataset.

The C/N values, on the other hand, range from 10.53 to 13.11 and display oscillations throughout the entire core. There are no clear trends in the lower section of the core. This only becomes apparent in LR3 where C/N displays an increasing trend. Above this, the C/N values decline between 47 and 15 cm. The last 15 cm is characterised by an increase in the C/N ratio and a decline in the %N probably due to post-depositional decomposition of nitrogen bearing OM.

4.5.3.1 Bulk $\delta^{13}C$ and $\delta^{15}N$

The $\delta^{13}C$ values range from -26.52 ‰ to -23.29 ‰, displaying a general decline up core. In the lower sections of the core within LR1 and LR2, the $\delta^{13}C$ displays a general decline to more negative values from -24.5 ‰ to -26.1 ‰, with a few excursions, such as a negative excursion at 80 cm ($\delta^{13}C$ -23.3 ‰). Within LR3, there are fewer negative values that persist to the lower section of LR4. The bulk $\delta^{13}C$ within LR4 shows only slight variations (-25 ‰ ± 0.4 ‰) with the exception of one sample at 12 cm depth (-24 ‰).

The observed $\delta^{15}N$ ranges from -0.43‰ to -4.10 ‰, displaying a general. The only clear trend seen in LR1 is where an increase in the bulk isotopic composition from the bottom of the core is recorded. There is an increase in bulk $\delta^{15}N$ in LR3 although no distinct trend can be seen in the remaining sections of the core.

4.5.3.1 Provenance of OM based on $\delta^{13}C$ and C/N

The $\delta^{13}C$ displays a trend towards more negative values with a mean value of -24.97 ‰ that points to the predominance of C_3 – type vegetation (Figure 4-74). Slight changes in the average %C (16.38 %) and %N (1.36 %) in the upper section of the core are noted with a corresponding mean isotopic $\delta^{13}C$ signature (-25.11 ‰) that points to C_3 type plant (the OM source similar to the underlying units).

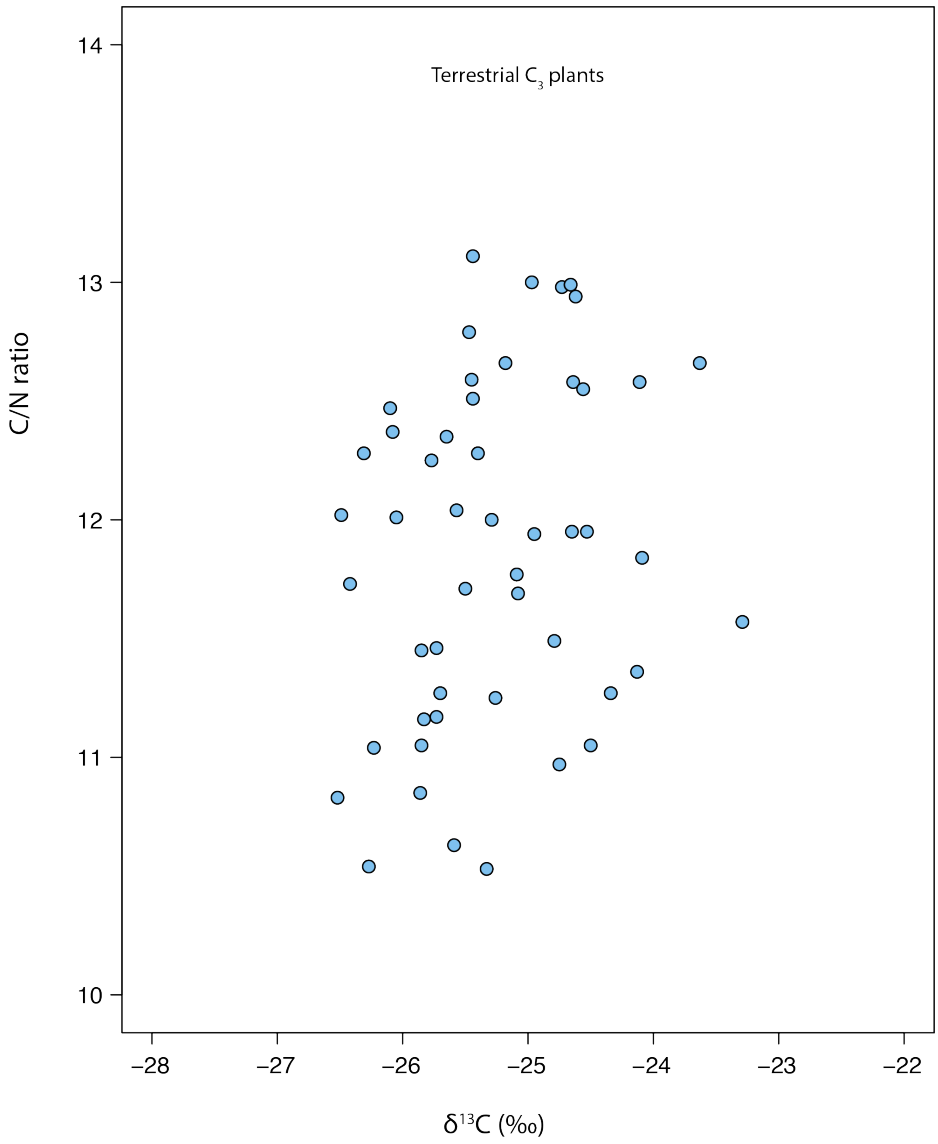

Figure 4-74: Provenance of the organic component of the Lake Rutundu sediments

4.5.3.1 Distribution of n-Alkanes

The distribution of n-alkanes in Lake Rutundu sediments is unimodal with the predominance of long chain odd homologues (> C_{25}). The terrestrially derived odd long chain n-alkanes C_{29}, C_{31} and C_{33} are abundant in all of the samples from the core. The C_{27} and C_{29} n-alkanes are roughly as or more abundant than the C_{31} homologue in all samples (Figure 4-75). The C_{27}/C_{31} ratio values are between 0.9 and 2.2 while the $C_{15\text{-}21}/C_{22\text{-}33}$ values range from 0.08 to 0.38. The short chain *n*-alkanes do not display a strong odd-over-even carbon number preference and are dominated by C_{18}.

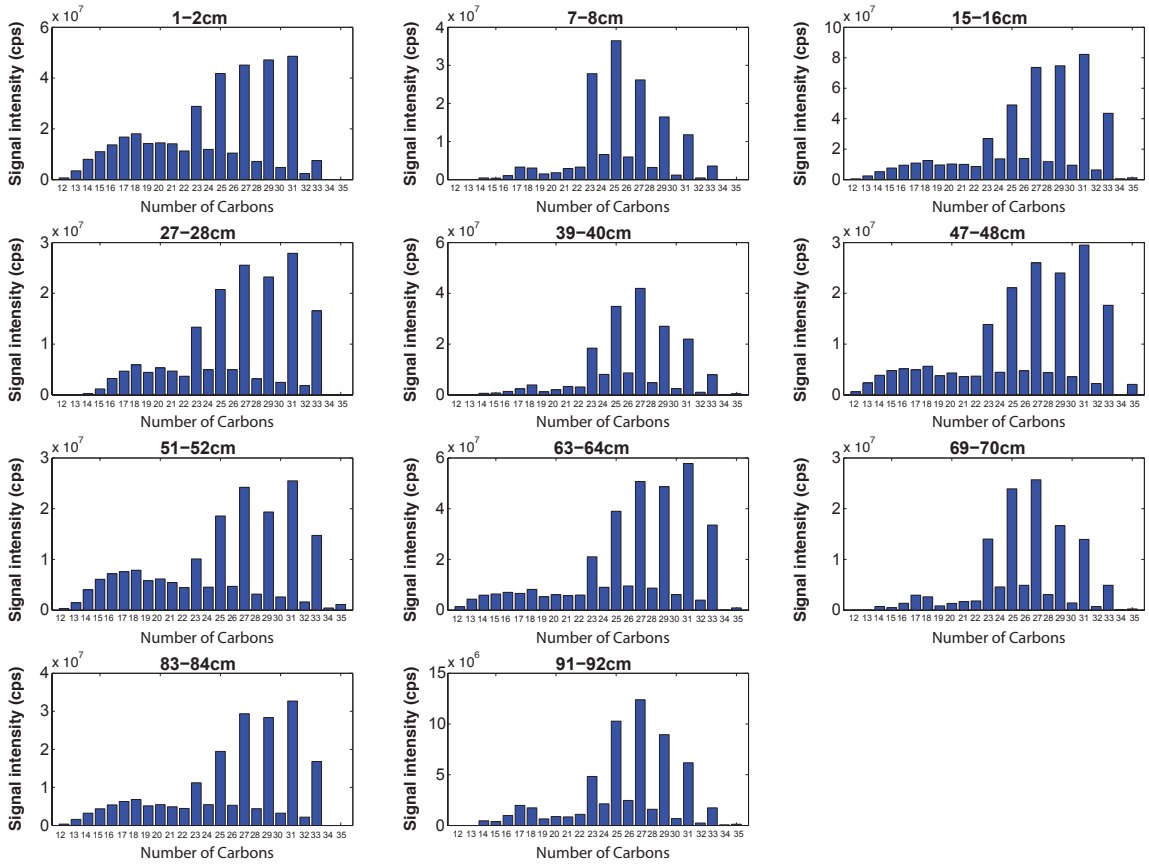

Figure 4-75: n-alkane distribution in Lake Rutundu sediments

The range of the ACL values (27.3 – 29.0), CPI (6.0 – 7.9) and TAR (>1) affirm the odd over even predominance with material derived from higher plants from the lake's watershed (Table 17). Higher values of TAR are observed in three samples (7-8 cm, 39-40 cm and 71-72 cm) where correspondingly very low abundance of short to mid-chain n-alkanes is observed. P_{aq} values (0.33 – 0.69), on the other hand, point to a mixed OM source for Lake Rutundu.

Table 17: Summary of n-alkane indices from Lake Rutundu

Depth (cm)	C_n range	C_n max	ACL	ACL_{lc}	CPI	Overall CPI	C_{27}/C_{31}	TAR	P_{aq}
1-2	12-33	31	24.5	28.3	6.4	2.9	0.9	3.4	0.42
7-8	14-33	25	25.5	27.3	7.1	4.9	2.2	10.5	0.69
15-16	12-35	31	26.7	29.0	6.8	4.0	0.9	8.2	0.33
27-28	14-33	31	26.4	29.0	7.9	4.0	0.9	7.5	0.40
39-40	14-35	27	26.4	27.9	6.6	4.5	1.9	20.7	0.52
47-48	12-35	31	26.1	28.9	7.0	3.9	0.9	5.9	0.40
51-52	12-35	31	25.2	28.9	7.2	3.2	1.0	3.5	0.39
63-64	12-35	31	26.6	29.0	7.1	4.2	0.9	8.6	0.36
71-72	14-35	27	26.1	27.8	7.1	4.8	1.8	13.1	0.55
83-84	12-33	31	26.0	29.0	7.3	3.7	0.9	5.7	0.33
91-92	14-35	27	25.8	27.8	6.7	4.1	2.0	9.1	0.50

4.5.3.2 Distribution of Glycerol Dialkyl Glycerol Tetraethers

All the sediment samples contain abundant amounts of brGDGTs and iGDGTs from 20359 to 39535 µg/g (85.3 – 90.0 % of total GDGTs) and from 2432 to 5388 µg/g (9.7 – 15.0 % of total GDGTs), respectively (

Figure 4-76). Among the iGDGTs, the GDGT-0 is the most abundant (70 – 88 % of the total iGDGTs) while the GDGT-1 is the second most abundant in the samples from this core. The crenarchaeol (0.24 % – 0.63 % in 7 out of 11 samples) and it's regio isomer (0.32 % in only one sample) are the least abundant of the iGDGTs and in some instances were below the detection limits in the samples from this site. GDGT 4 is present in only 3 out of 11 samples. The brGDGTs without cyclopentyl moieties GDGT-1 (22 – 29 % of the total brGDGTs), GDGT-II (30 – 53 % of the total brGDGTs), and GDGT-III (9 – 19 % of the total brGDGTs) are the most abundant (

Figure 4-76). Among the brGDGTs, GDGT-IIIc is absent in 4 out of 11 samples where the crenarchaeol was recorded as below detection limit.

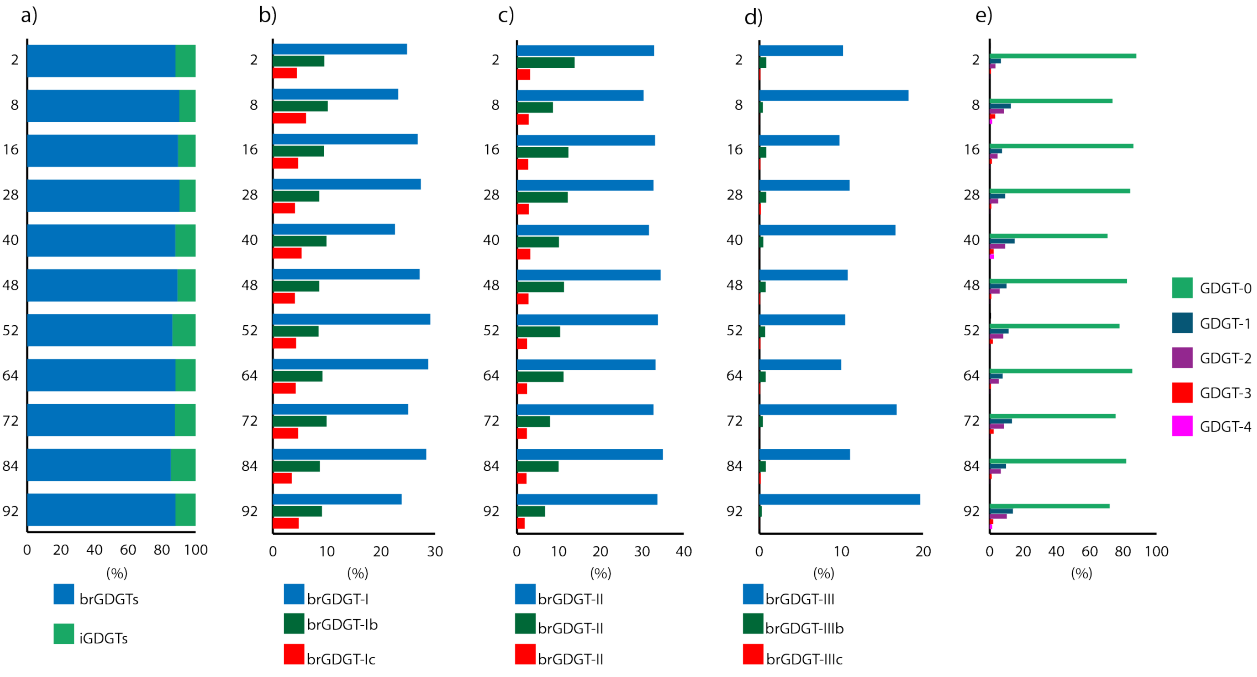

Figure 4-76: The relative abundance of the brGDGTs and iGDGTs down core in the Lake Rutundu core. The five graphs represent the main (a) the brGDGT and iGDGT abundances, while GDGT groups and their moieties are illustrated in (b) GDGT-I, Ib and Ic (c) GDGT-II, IIb and IIc, (d) GDGT-III and IIb & (e) iGDGTs.

The Branched vs. Isoprenoid Tetraether (BIT) index is high (0.96 – 1.00) throughout the core, further affirming insignificant concentration of the crenarchaeol in this lake (Table 18). The calculated MBT and CBT values range from 0.38 – 0.42 and 0.39 – 0.56, respectively. These values display minimal biases with depth while the reconstructed pH values range from 8.62 to 9.13 pH units and display an increasing trend towards the top of the core (Table 18).

Table 18: The variations in BIT, 1302/1292 ratio, MBT and CBT proxies from the Lake Rutundu sediment core

Depth (cm)	BIT	1302/1292	MBT	CBT	pH
2	0.96	195.37	0.39	0.39	9.13
8	1.00	n.d	0.39	0.45	8.94
16	0.98	359.29	0.41	0.44	8.99
28	0.98	291.71	0.40	0.46	8.92
40	1.00	n.d	0.38	0.43	9.01
48	0.99	334.36	0.40	0.49	8.83
52	0.97	123.33	0.42	0.52	8.73
64	0.98	265.38	0.42	0.48	8.86
72	1.00	n.d	0.40	0.51	8.78
84	0.98	262.84	0.41	0.53	8.72
92	1.00	n.d	0.38	0.56	8.62

The high BIT index coupled with the very high GDGT-0/crenarchaeol (1302/1292) ratios that are over a hundred times higher (123 – 359) in these sediments in comparison to Sacred Lake and Lake Nkunga affirm the dominance of the GDGT-0. The resulting temperature reconstructions using the MBT/CBT calibrations from both Tierney et al. (2010) and Loomis et al. (2012) display similarity in trends resulting in 18.8 – 21.0° C and 16.8 – 19.2° C, respectively, with a general gap of approximately 2.0° C throughout the core (Figure 4-77). The MbrGDGT calibrations also display similar trends with values ranging from 16.9 – 23.8° C (Tierney et al. 2010) and 14.8 – 19.9° C (Loomis et al. 2012). Noteworthy of the MbrGDGT calibrations are prominent dips at depths 8 cm, 40 cm, 72 cm, and 92 cm, which correspond to core sections where crenarchaeol is absent in the sediment samples. The SFS calibrations provide the lowest temperature values of 8.1 – 12.7°C (Figure 4-77). The minimum values from this calibration correspond to a depth of 40cm where crenarchaeol is below detection limit

whilst in the other depths where this GDGT is below detection limit a similar decline is not observed.

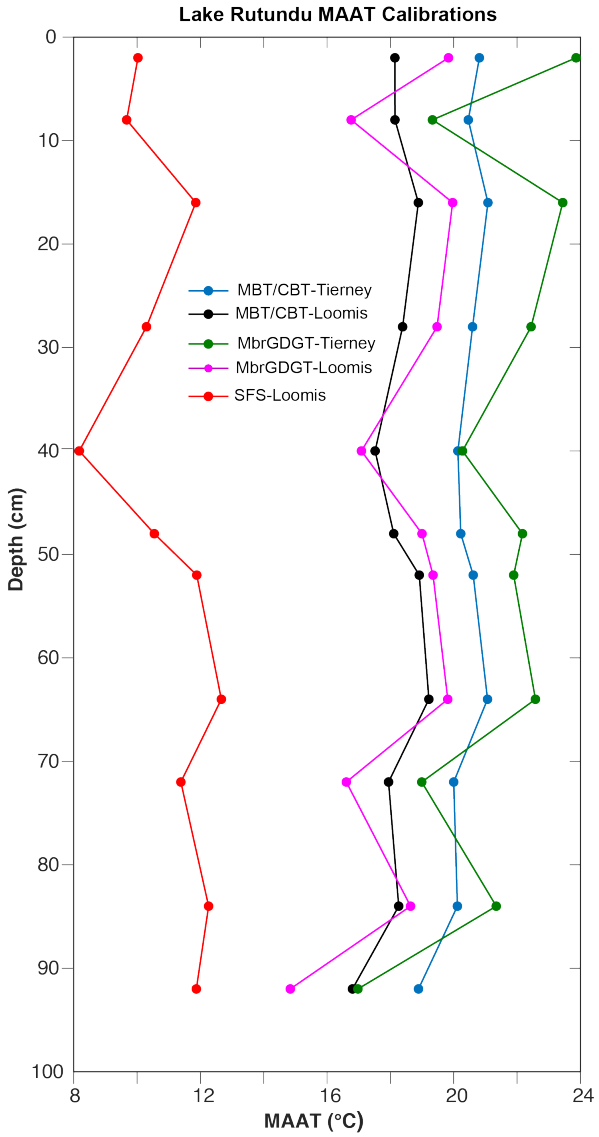

Figure 4-77: Reconstructed MAAT for Lake Rutundu core using MBT/CBT, MbrGDGT and SFS regional calibrations.

4.5.4 Synthesis of Lake Rutundu Proxies

The 100 cm of the sediments of Lake Rutundu cover approximately 4770 cal yr. BP to present. The upper age limit of the sediments is generally acceptable as constrained in the age model developed. The accompanying sedimentation rate is low, ranging from 0.03 – 0.07 cm/yr. The bulk inorganic proxies (geochemical ratios, mineralogy and sedimentation), indicate subtle changes in the detrital sediment supply from the catchment (Table 19).

Table 19: Proxy indicators summary from Lake Rutundu

Stratigraphic Unit	Proxy Information
LR1 100 – 84 cm 4770 – 4069 cal yr. BP	▪ The %C displays a steady decrease up core from 20 % to 15 %. ▪ Synchronous decline in Ca/Ti, Fe/Ti and Fe/Mn with an increase in K/Ti reflect the decrease in inputs from the lake catchment. ▪ The range of the C_{27}/C_{31} ratio point to the contribution from terrestrial trees over grasslands in the OM biomass.
LR2 58 – 84 cm 3254 - 4069 cal yr. BP	▪ The %C further decline from 15 % to 13 %. ▪ $\delta^{15}N$ is maximum in reflecting increased denitrification in the soils. ▪ $\delta^{13}C$ shows higher C_3 values and there is more clay from the Al/Ti and less biogenic silica deducing a relatively warm climate ▪ Synchronous decline in Ca/Ti, Fe/Ti and Fe/Mn with an increase in K/Ti reflect the decrease in inputs from the lake catchment. ▪ The range of the C_{27}/C_{31} ratio point to contribution from terrestrial trees over grasslands in the OM biomass.
LR3 48 – 58 cm 2887 - 3254 cal yr. BP	▪ Minimal variation with the %C values centred at 15 ± 0.4 %. ▪ Synchronous decline in Ca/Ti, Fe/Ti and Fe/Mn with an increase in K/Ti reflect the decrease in inputs from the lake catchment. ▪ The range of the C_{27}/C_{31} ratio point to contribution from terrestrial trees over grasslands in the OM biomass.
LR4 0 – 48 cm 2887 cal yr. BP to Present	▪ The %C slightly increases to 18 % and stabilizes in the upper sections. ▪ The geochemical proxies (Ca/Ti, Fe/Ti, K/Ti and Fe/Mn) and X_{lf} generally fluctuate during this period. ▪ The range of ACL, CPI, P_{aq} and TAR values point to a mixed input from terrestrial and aquatic OM sources into the lake sediments.

At the bottom of the core within LR1 and LR2, a slight increase in the sedimentation rate is observed alongside a synchronous rise in Fe/Ti and decline in Si/Ti ratios (Figure 4-78). The presence of trace amount of quartz and gibbsite (in the lower section) as sedimentation rate increases could be indicative of aeolian input. In the higher altitudes of Mount Kenya, Mahaney (1991) noted that the silica in the volcanic glass from the catchment undergoes aggressive leaching leading to the production of abundant gibbsite in the soils of the upper catchment. From 50-0 cm, a decrease in sedimentation rate to near constant values is noted. The relative decrease in Si/Ti and increase in Fe/Ti throughout suggests that these sediments are more affected by chemical weathering than physical transportation processes (Figure 4-78).

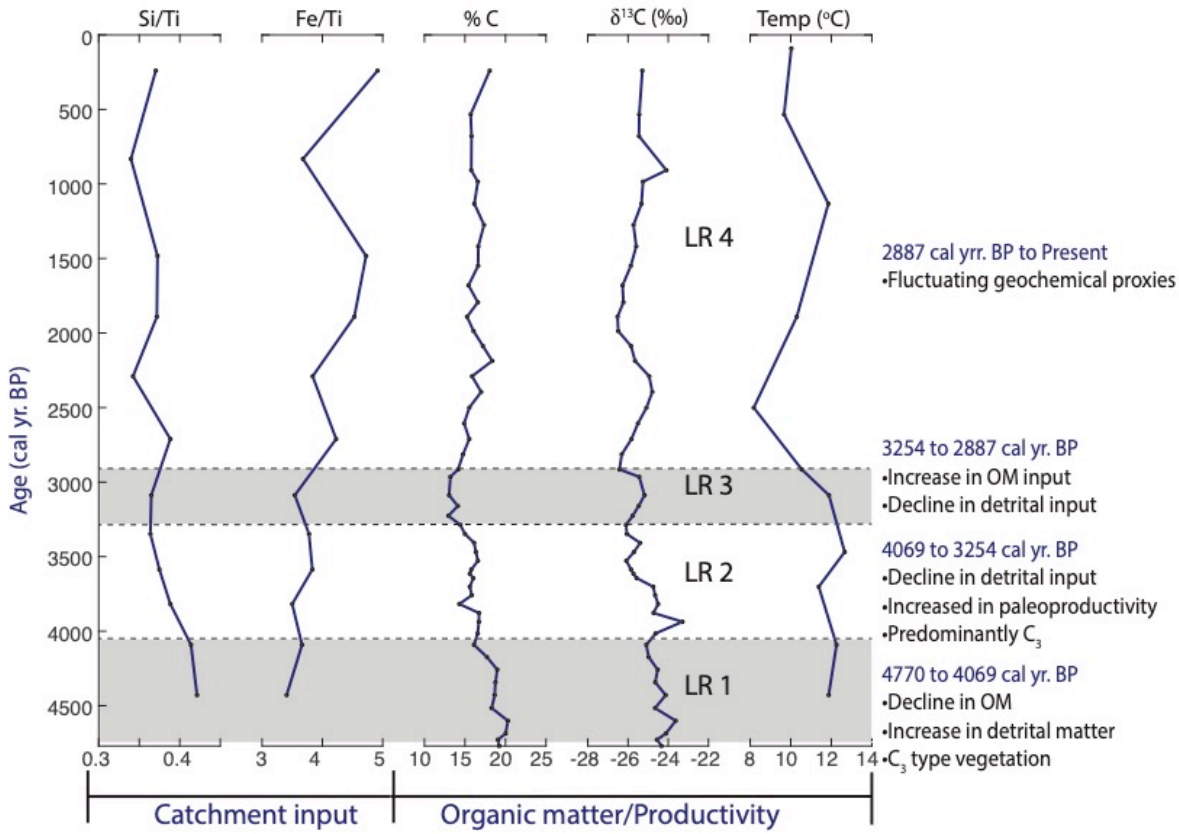

Figure 4-78: A summary of key findings for Lake Rutundu from 4770 cal yr. BP to Present indicating key changes in lake sedimentation

The C/N ratio points to a mix of aquatic (primary production) and terrestrial plants from the lake catchment (Meyers & Teranes 2001). Within this core, there are slight variations in the mean %C and %N with a notable initial decline of these values from the basal section to 50 cm that is followed by an increase in the upper section of the core. The deposition of the organic matter in this core is independent of the sedimentation rate since a decline in the sedimentation rate accompanies an increase in the %C and %N content and *vice versa*, pointing to a change in OM source instead. Nevertheless, the values from the lower section of the core (100 – 50 cm) reflect OM contributions from both vascular plants and primary productivity. The organic proxies point to three contrasting periods: (i) a period described by increase in sedimentation rate and prominent decline in %C and %N (ii) a period of nearly constant %C and %N and (iii) a period of decrease in sedimentation rate accompanied by increase in %C and %N. The synchronicity in the trends of %C and %N and limited degree of variation of $\delta^{15}N$ and $\delta^{13}C$ imply a relatively small catchment influencing the OM production.

The distribution of n-alkanes in the samples from Lake Rutundu is unimodal with some variations from the mid to short chain n-alkanes. The OM reflects a mix of primary production/aquatic sources and terrestrial higher plants in the catchment of the lake ecosystem. The CPI indicates a predominance of the long chain *n*-alkane odd homologues, which is seen in the ACL values that have been generated for this lake. The number of carbon atoms present in the n-alkane chains range from $C_{12\text{-}35}$. The odd mid to long chain n-alkanes C_{25}, C_{27}, C_{29}, and C_{31} are abundant in the samples. These *n*-alkanes abundances differ in the various samples thereby pointing to different relative contributions from emergent macrophytes, terrestrial plants and submerged macrophytes. Among the short chain alkanes, the C_{18} is relatively abundant and may relate to fire incidences (Wooller et al. 2000) at varied times in the lake's catchment. An open forest ecosystem is inferred from the C_{27}/C_{31} ratio (0.9 – 2.0) (Eglinton et al. 1962, Kolattukudy et al. 1976, Cranwell 1982, Cranwell et al. 1987, Maffei 1996, Meyers 1997, Schwark et al. 2002). The TAR is generally >1 with three samples (7-8 cm, 39-40 cm and 69 -70 cm) displaying extremely high TAR values (>10). These values have correspondingly high P_{aq} values affirming the relative importance of the submerged/floating macrophytes and terrestrial leaf waxes as OM sources. Terrestrial higher plants as well as the submerged/floating macrophytes play an important role in the OM contributions to the lake.

The most abundant iGDGT in Lake Rutundu is the GDGT-0. The crenarchaeol is below detection limit in some samples and where present was the least abundant. This variability in the abundance has led to elevated values of the 1302/1292 ratio implying methanogenic conditions in the core under anoxic lacustrine conditions (Blaga et al. 2009). The BIT index yields high values (0.97 – 0.98), which is not surprising as the values probably reflect the variability in the GDGT-0 content relative to the crenarchaeol. Notably, the brGDGT- IIIc is below detection limit in the Lake Rutundu samples; nevertheless, the brGDGT-III seems to display the most amount of variability down core. The CBT/MBT and MbrGDGTs calibrations display similar trends in palaeotemperature reconstructions, with the CBT/MBT reconstructed MAAT yielding estimates biased towards warmer mid to late Holocene conditions than the SFS calibration. The MbrGDGT calibrations display significant dips in temperatures that correspond to sections in the core with high TAR and P_{aq} ratios. On the other hand, the SFS calibrations presents the lowest temperature estimates for Lake Rutundu. From the bottom of the core the temperature is fairly constant centred at 12° C followed by a 4° C decline to 8° C at 40 cm, followed by an increase to 12° C and finally stabilising at 10° C. The 2° C decline

from the mid-Holocene to Present in samples from this site is close to the estimate of 1.5° C suggested by Loomis et al. (2017) for Lake Rutundu.

4.6 Discussion

The results presented in sections 4.3, 4.4 and 4.5 above are hereby discussed and synthesised with the aim to evaluate research findings from this study in the context of the regional palaeo-changes during the Late Holocene. The proxy records are evaluated in the context of other published palaeoclimatic and palaeoenvironmental records from eastern Africa. The three lakes analysed in this study are located on the north eastern slopes of Mt. Kenya within close proximity of each other. These lakes are located in a region of similar geology (section 2.2.1) and climate (Section 2.2.3) and thus broad trends in climate and environmental changes would be expected to manifest in similar ways in the environmental records, with the lake ecosystems responding similarly to the drivers. The difference in altitudes may play a role in the variations observed: for example, the lakes are surrounded by different types of vegetation and receive different quantities of rainfall (Section 2.2.3).

4.6.1 Late Holocene Signal Coherency among the Mt. Kenya lakes

The combined sediment history from the three lakes defines four distinct periods of development of the Crater Lake basins over the last 4770 cal yr. BP to present (Figure 4-79), covering the periods (i) 4470 to 3280 cal yr. BP, (ii) 3280 to 2500 cal yr. BP, (iii) 2500 to 2000 cal yr. BP and (iv) 2000 cal yr. BP to Present. The palaeoclimatic interpretations related to Figure 4-79 are discussed in the subsequent sub-sections.

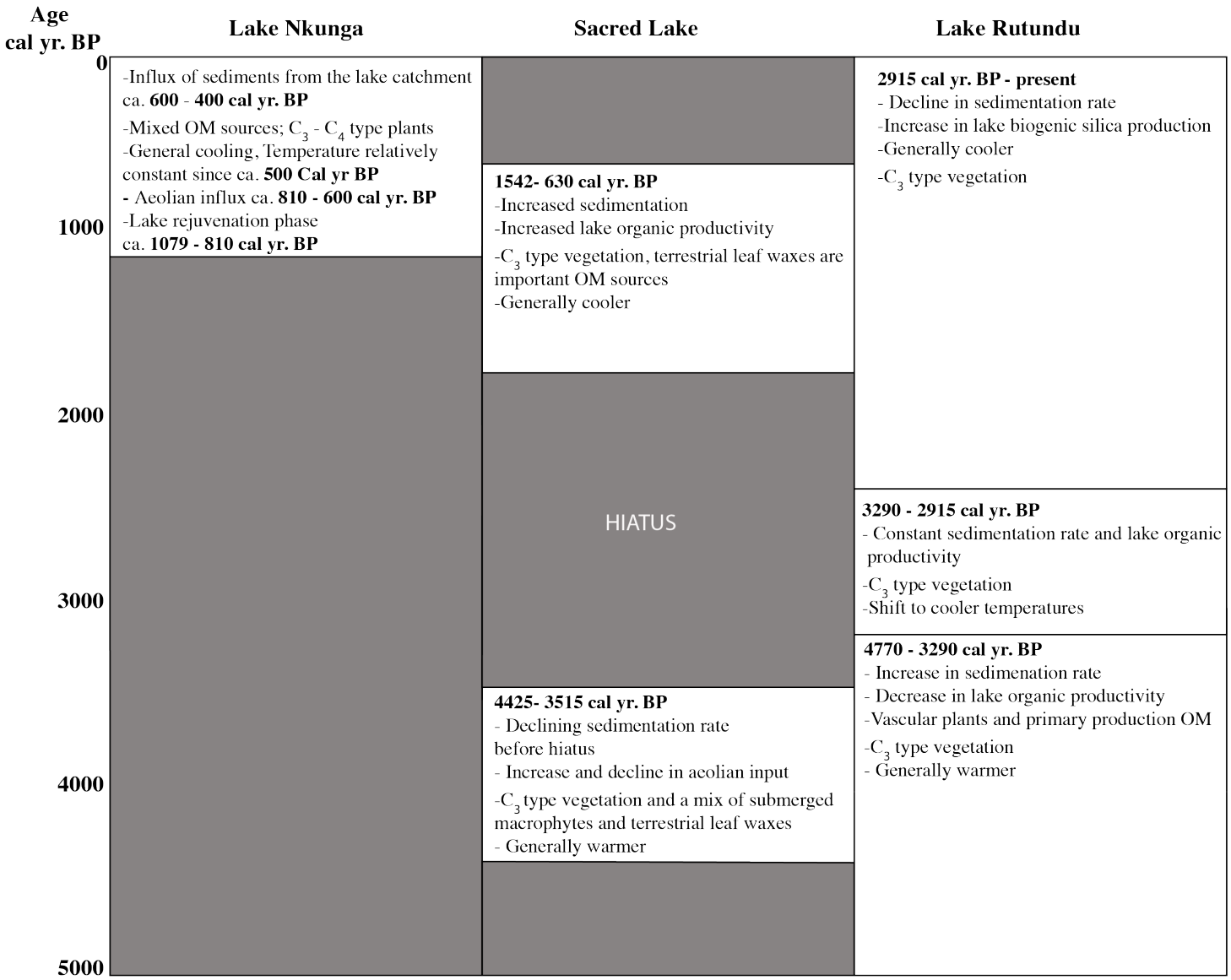

Figure 4-79: Late Holocene palaeoclimatic and environmental reconstruction from the organic matter from Mt. Kenya. The grey areas mark sections where no information was retrieved from the Mt. Kenya proxies due to core length (L. Nkunga and Sacred Lake) and presence of hiatus in Sacred Lake.

4.6.2 The Period 4470 – 3280 cal yr. BP (LR1, LR2, SLK1, SLK2)

During this period, the biogeochemical proxies indicate a shift towards dry conditions. The $\delta^{13}C$ record shows that both lake catchments were occupied by C_3-type woody vegetation with C_3 grasses as seen in the C_{27}/C_{31} ratio that suggests an open forest ecosystem around Sacred Lake and a transition to grasslands for Lake Rutundu where shrub dominated by C_3 pooid grasses occur in the pollen record associated with decline in moisture during the Holocene (Ficken et al. 2002). The C/N ratios which range from 11-14 and display a slight decline in values from the onset of the period are coeval with a decline in Si/Ti and dominance of long odd chain n-alkanes, and therefore generally point to the catchment as an important source of terrestrial OM. Despite the dominance of odd over even long chain n-alkanes, the C_{18} alkane is relatively abundant in both lakes and is sometimes used as an indicator thermal alteration of the vegetation in catchments by natural fires. There is no known history of human occupation on Mount Kenya during this time period; although, this biomass burning could be due to natural fires on the sub alpine zone (*Hagenia-Podocarpus zone*) on Mount Kilimanjaro and Mt. Kenya (Wooller et al. 2000, Hemp 2005, Rucina et al. 2009). Multiproxy evidence from Sacred Lake and Lake Rutundu indicates that fires influenced the vegetation at these sites during the Late Holocene through the persistence of fire tolerant species such as *Stoebe* and *Hagenia* that are present at all times during this period despite the loss and invasion of other montane and ericaceous vegetation (Wooller et al. 2000).

During this time period, the sedimentary records from several sites in the east Africa region show evidence of lake desiccation, decline in lake levels, oxidation of pollen as well as a decline in pollen diversity (Marchant et al. 2018 and the references therein). The lake records in this study are consistent with the wider east African record that shows an abrupt transition to arid conditions during the 4200 cal yr. BP event. However, the extent to which the drying event affected the hydrological balance of our crater lakes seem minor although the proxies from the lakes suggest a progressive lake shallowing and decline in OM influx into the two lakes discussed here.

Previous studies from Mount Kenya have marked this drought event *ca*. 4500 – 3500 cal yr. BP by a sharp rise in *Podocarpus* and low abundance of Panicoid grass cuticles at Sacred Lake, an increase in C_3 grasses in Lake Rutundu and the presence of C_4 vegetation at Kiluli swamp (Coetzee 1967; Olago 1995; Wooller et al. 2000; 2003; Ficken et al. 2002). However, in terms of local water availability, C_3 grasses and *Podocarpus* forest do not point to major local

hydrological stress as recorded at lower altitudes. Other regional records from the region that display pronounced aridity include for example; a visible 30 mm dust layer coupled with less vegetation on the Mt. Kilimanjaro (Thompson et al. 2002); a sharp rise in *Podocarpus* on Lake Kimilili, Mt. Elgon Kenya (Hamilton 1982); declining lake levels and disappearance of lowland forest pollen taxa in Lake Naivasha, Kenya (Butzer et al. 1972; Street & Grove 1976; Maitima 1991), and; a decline in high altitude pollen taxa from Lake Bogoria, Kenya, accompanied by a relative increase in drought tolerant taxa such as *Podocarpus, Juniperus, Acacia* and *Dodonaea* (Kiage & Liu 2006). Evidence of the hot and dry conditions have also been observed in Lakes Turkana and Baringo where a decline in arboreal pollen and the development of *Acacia* forest, respectively, are observed (Owen et al. 1982, Vincens 1986). Further afield, a reduction in the baseflow of the White Nile (Talbot & Brendeland 2001) and a Sr signature reflecting flows originating from Lake Edward during this dry period implies that Lake Victoria may have been isolated from Lake Albert that provides a critical link between flows from Lake Victoria and the White Nile (Talbot & Brendeland 2001).

The regional environmental history describes a period of climatic shift towards drier conditions characterized by reduced rainfall (deMenocal et al. 2000) where the migration of the ITCZ southwards (Gasse 2000; Marchant and Hooghiemstra, 2004; Mayewski et al. 2004) and the suppression of the monsoon circulation in the tropics (COHMAP 1988) have been hypothesized as the cause of the severe droughts centred at *ca*. 4200 cal yr. BP during the Late Holocene.

4.6.3 The Period 3280 - 2500 cal yr. BP (LR3, LR4)

At the onset of this period, there is a hiatus in our Sacred Lake record (see section 4.4.1.1) that is suggestive of a dry period. This hiatus seems to be caused by the lowering of the lake water level perhaps controlled by climate because the closed crater lake has a simple hydrology where input relies on rainfall and the output is through evaporation. The lake, therefore, is able to amplify the climate signal and is an excellent indicator of the lake water budget during a drier period that covers the hiatus. The Lake Rutundu record is therefore the only representative palaeo-record for this period. Initially dry conditions are exemplified by a low sedimentation rate and a correspondingly low OM supply (derived mainly from C_3 type vegetation but reflecting a mix of aquatic and terrestrial OM sources as indicated by the C/N values and the n-alkane composition) from 3287 to 2915 cal yr. BP. However, the biogeochemical markers suggest that the dry phase may have started a bit earlier as observed in the rapid decline of OM

from ca. 4000 cal yr. BP (see Figure 4-73). Its termination is generally coeval with the drought event recorded at ca. 2800 cal yr. BP in Lake Edward by Russell & Johnson (2005), a desiccation in the Mt. Satima mire (Kenya) peat record (Street-Perrott and Perrott, 1990), the interruption of the outflow from Lake Kivu to Lake Tanganyika (Haberyan & Hecky 1987), and the expansion of grasslands at Lake Albert (Ssemmanda & Vincens, 1993). After 2915 cal yr. BP, the rise in OM content, biogenic silica productivity and predominant C_3-type catchment vegetation in the Lake Rutundu record reflect the termination of this dry phase. The initial dry phase transitions from a warm and dry period at the end of the period between 4470 – 3280 cal yr. BP to a warm and relatively moist period that is seen in the relative increase in sedimentation in Lake Rutundu by 2500 cal yr. BP (Figure 4-80).

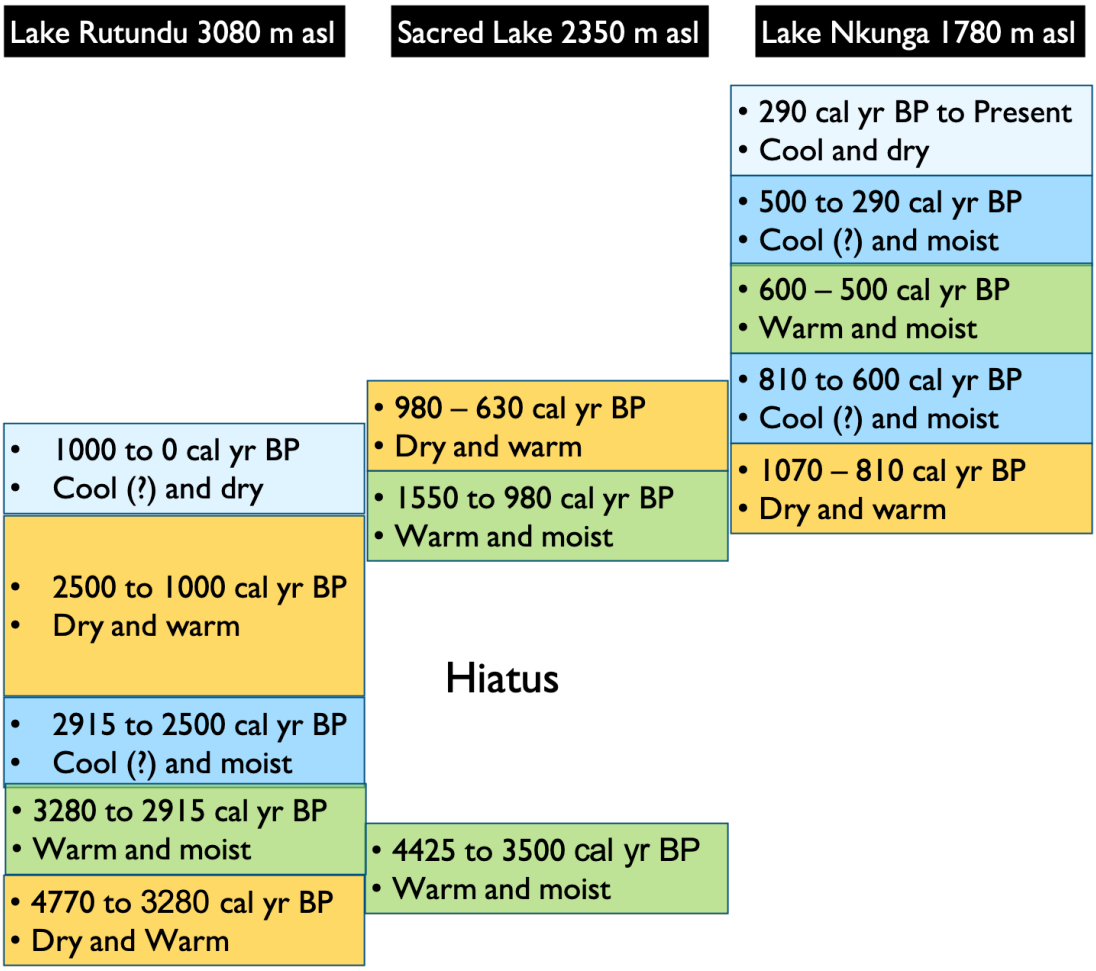

Figure 4-80: A generalized chronology of the Late Holocene climatic changes from the three crater lakes.

The MAAT from Lake Rutundu suggests stepwise cooling from 12° C at 3280 cal yr. BP to 10° C at 2915 cal yr. BP where relatively dry but initially warm and then progressively cooler (8° C by 2500 cal yr. BP) conditions are recorded by the MAAT proxy, and the lake levels were likely sustained by glacial meltwater due to the glacial advances on Mt. Kenya (Karlén et al. 1999). This temperature decline further corresponds to the wetter conditions inferred by the rejuvenation of sediment input and increasing organic matter input into the lake. The decline in estimated temperatures from Lake Rutundu is synchronous with regional records of a "cold Holocene" estimated at 3300 cal yr. BP to 2500 cal yr. BP (Wanner et al. 2011) in Lakes Malawi (Powers et al. 2005), Tanganyika (Tierney et al. 2008), Victoria (Berke et al. 2012), Turkana (Berke et al. 2012b) and Challa (Sinninghe Damsté et al. 2012), indicating that this cooling event affected the entire eastern Africa region.

This cooling also correlates with the advancement of glaciers on Mt. Kenya between 3500 to 3300 and 3200 to 2300 cal yr. BP (Karlén et al. 1999). Whereas the East African records show that after 3000 cal yr. BP there is coherency in low temperatures, the records are too temporally short to be forced by orbital parameters. The forcing mechanism for this cooling is not well understood, as emerging evidence shows low solar forcing, weak monsoons and reduced precipitation for this period (Wanner et al. 2011; Russell and Johnson 2005).

4.6.4 The Period 2500 – 2000 cal yr. BP (LR4)

The sediment influx record for Lake Rutundu (from 2500 to 2000 cal yr. BP) describes a lake rejuvenation phase at the beginning of this time period characterized by an influx of sediments and terrestrial OM and detrital material. Although our nearshore core site on Sacred Lake has a hiatus during the beginning of this period corresponding to a low lake water level in the closed lake basin. A transition to slightly wetter conditions was documented at Sacred Lake in a core recovered from a deeper part of the lake (Konecky et al. 2014), as well as in Lake Naivasha (Verschuren 2001), Lake Edward (Russell and Johnson 2005) and Lake Tanganyika (Stager et al. 2009) (Figure 4-81). The hiatus at our coring site suggests that the lake level rise (cf. Konecky et al. 2014) was not substantially significant during this period and perhaps the increase in precipitation caused erosion of the nearshore sediments to the centre of the lake. The relative importance of submerged macrophytes and planktonic algae, restricted clastic input (low magnetic susceptibility) coupled with a general decline in C/N especially in Lake Rutundu indicates improved preservation of organic matter during this time.

Following this, widespread regional droughts *ca*. 2000 cal yr. BP (Verschuren & Charman 2008) have been recorded from Sacred Lake (Konecky et al. 2014), Lake Edward (Russell & Johnson 2005), Lake Tanganyika (Alin & Cohen 2003), Lake Wakandara (Russell et al. 2007) and Lake Naivasha (Verschuren 2004). The biomarkers from Lake Rutundu record a relatively smooth transition to a dry phase.

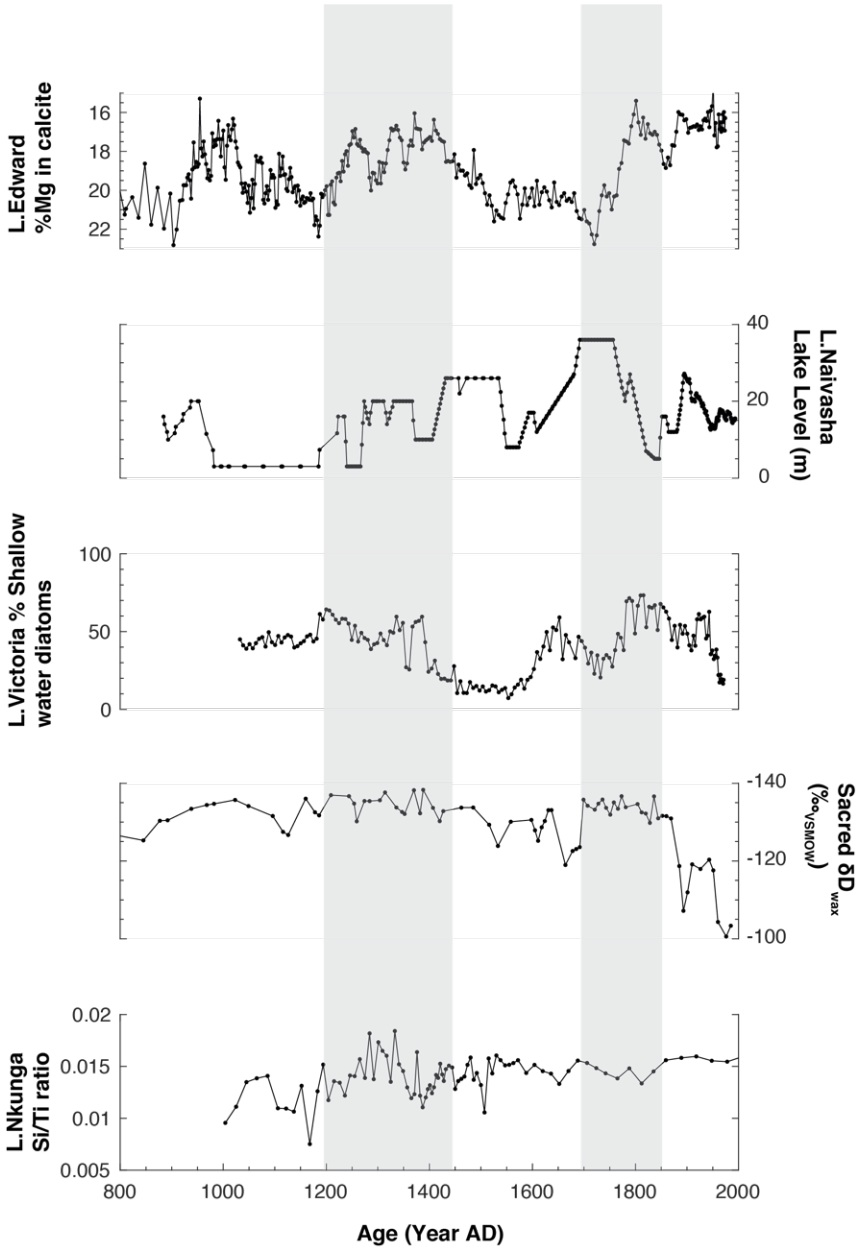

Figure 4-81: Late Holocene changes in Lake Nkunga derived from Si/Ti ratio representing aeolian dust, Sacred Lake δD_{wax} (Konecky et al. 2014), L. Victoria shallow water diatoms (Stager et al. 2005, Lake Naivasha lake levels (Verschuren et al. 2000) and Lake Edward (Russell and Johnson, 2007). The grey shading represents the century scale-decadal changes in the multiple records.

The MAAT from Lake Rutundu suggests a warming from 8°C at 2500 cal yr. BP to *ca*. 10°C by 2000 cal yr. BP. This is reminiscent of the globally warm Late Holocene where the atmospheric humidity is considered more stable and the regional palaeohydrological records indicate a drier late Holocene (Otto-Bliesner et al. 2014).

4.6.4 The Period 2000 cal yr. BP to Present (LR4, SLK3, SLK4, LNK1, LNK2, LNK3, LNK4)

4.6.4.1 2000 cal yr. BP to 950 cal yr. BP (50 BC to 1000AD)

The Lake Rutundu record displays a transition to a wetter period from 2000 – 1000 cal yr. BP (50 BC to 950 AD) that stabilizes by 600 cal yr. BP (1350 AD). Gradual filling by lake sediments *ca*. 1550 – 980 cal yr. BP (400 – 970 AD) in Sacred Lake marks the return to humid conditions with the lake ecosystem comprising terrestrial/emergent macrophytes. Increase in the sedimentation rate associated with relative increases in OM and Si/Ti characterize this time period. The sediments are slightly more acidic than before the hiatus and the dominance of the odd numbered long chain *n*-alkanes become eminent indicating predominantly catchment-derived inputs. Olago (1995) showed that the stratigraphy of Lake Nkunga engulfs a long-lived hiatus from 30,935 to 1430 cal yr. BP when sedimentation resumes. The oldest part of our record from lake Nkunga does not captures this lake rejuvenation phase. The MAAT from Lake Rutundu indicates warming from 10° C at 2000 cal yr. BP to 12° C by 1000 cal yr. BP.

At 2000 cal yr. BP regional records show possibly the driest period of the Late Holocene. The lowest lake levels were recorded at Lake Edward (Russell & Johnson 2005) and Lake Tanganyika (Alin & Cohen 2003), and a complete desiccation is recorded in Crescent Island Crater, Lake Naivasha (Verschuren 2001). These records indicate regional widespread aridity at the beginning of this period. During the period 2000 to 1000 cal yr. BP (50 BC to 950 AD), the biogeochemical proxies present a muddled picture of alternating dryer and wetter phases. From Lake Tanganyika, sediment lamina thickness indicates a pronounced wet period from 1750 to 1450 cal yr. BP (200 to 500 AD) and its ostracod record shows a rising lake from 1800 to 1000 cal yr. BP (150 to 950 AD) supported by stromatolites which indicate a high-stand centred at 1500 cal yr. BP (450 AD; Alin & Cohen 2003). This record corroborates the records from Crescent Island Crater, Lake Naivasha where a lake rejuvenation phase is recorded from 1840 cal yr. BP (110 AD) followed by a relatively high-stand that lasted until 1350 cal yr. BP (600 AD; Verschuren 2001). On the other hand, Lakes Turkana (Ricketts and Johnson 1996)

and the Bogoria record (De Cort et al. 2013) show a negative water balance *ca*. 450 AD while the carbonate flux from Lake Turkana shows higher lake levels during the same period when the Omo river inflows are recorded as high (Halfman et al. 1994). The contradiction in the lake Turkana record is attributable to the morphology and sediment sources of the lake basin itself. The stable $\delta^{18}O$ isotopic measurements by Ricketts and Johnson (1996) was done on authigenic calcites south of Lake while the Halfman et al. (1994) carbonate flux data is from the entire lake. These features of the palaeoclimate record are probably not sufficient enough to accept definite broad and synchronised regional changes.

At Sacred Lake the plant leaf wax record indicates increased aridity before 1650 cal yr. BP (300 AD) that was followed by gradual recovery to reach a maximum wet phase at 1000 cal yr. BP (950 AD; Konecky et al. 2014). This perhaps explains the hiatus captured by our record and the subsequent recovery of the lake observed from 1550 cal yr. BP (400 AD) after the hiatus. The lake rejuvenation phase in Lake Nkunga in the oldest part of the record capture this warm and moist phase.

4.6.4.2 The Medieval Climate Anomaly: 950 to 700 cal yr. BP (1000 – 1250 AD)

From 980 – 630 cal yr. BP (970 - 1320 AD) a decline in sedimentation rate and OM supply point to the establishment of swamp conditions comprising emergent and submergent macrophytes at Sacred Lake. This result is consistent with the findings of Konecky et al. (2014) from the same lake using leaf waxes, which indicates a drought period from *ca*. 900 – 550 cal yr. BP (1050 to 1400 AD; Konecky et al. 2014) that is coincident with the Medieval Climate Anomaly (MCA).

Relatively low but increasing %C, initial increase in X_{lf} followed by a decline, oscillating C/N, Si/Ti and increasing Fe/Ti ratio record a lake filling phase in Lake Nkunga *ca*. 1070 – 620 cal yr. BP (880 – 1340 AD). The sediments are alkaline (pH 8 – 9) and predominantly comprise terrestrial and emergent macrophytes punctuated with a few mid chain n-alkanes marking an increase in detrital input during this lake phase. The relative abundance of C_{18} among the short and mid chain *n*-alkanes in some samples is perhaps indicative of persistent biomass burning. It is not clear whether at this elevation the fires would be climate induced or anthropogenic although C_{18} abundance is connected with the combustion of non-woody biomass from agricultural lands (Eckmeier & Wiesenberg 2009), perhaps indicative of early forest clearing for cultivation.

The MAAT from Lake Rutundu declines from 12° C to 10° C at 500 cal yr. BP (1450 AD). On the other hand, there are no significant changes in the MAAT record from Sacred Lake which remains constant at *ca*. 16° C perhaps due to the development of open forest with delayed feedback of the archaeal community to the temperature changes. Although, it is not clear which of the MAAT calibrations are valid for Lake Nkunga (due to similarity in trends as observed in Figure 4-51, pg. 135), the general trend of MAAT indicates an initial cooling phase by 0.5 – 1.5°C (depending on the selected calibration) from 1070 to 800 cal yr. BP followed by warming that persists to 600 cal yr. BP (1350 AD).

The regional records from equatorial East Africa show broad coherency during the MCA. Pronounced droughts have been recorded in Lake Turkana (900 – 1200 AD; Halfman et al. 1994), Lake Naivasha (1000 – 1250 AD; Verschuren 2001), Lake Edward (at 1050 AD and 1150 Ad and 1200 AD; Russell & Johnson 2005), Lake Tanganyika (1150AD; Alin &Cohen 2003) and Lake Challa (1150 AD and 1200 – 1300AD; Buckles et al. 2016).

4.6.4.3 The Little Ice Age 700 – 100 cal yr. BP (1250 – 1850 AD)

The leaf wax record from Sacred Lake suggests a relatively wet and stable water body at 550 cal yr. BP (1400 AD; Konecky et al. 2014) probably coinciding with a pluvial period in our Lake Nkunga record (Figure 4-81). This provides evidence for a wet early Little Ice Age (LIA). The absence of younger sediments in Sacred Lake points to subsequent removal of exposed lake sediments from its nearshore responsible for this hiatus and suggests that the lake might have never recovered fully after several drought events. The current swamp conditions and extent of Sacred Lake were probably established *ca*. 600 cal yr. BP (1350 AD).

The biogeochemical markers from Lake Rutundu and Lake Nkunga show a gradual transition to wetter conditions *ca*. 500 cal yr. BP (1450 AD) and 620 – 410 cal yr. BP (1330 – 1540 AD) respectively. Notably, all the bulk ages obtained from the Lake Nkunga samples including the sampled charcoal particles, yielded dates within this time period. Detrital input from the catchment is implied by the presence of pumice fragments, charcoal and ash-like sediment. The inferred humid conditions coincide with wet conditions in Lake Naivasha (Verschuren et al. 2000), Lake Tanganyika (Alin & Cohen 2003), Lake Edward (Russell et al. 2007) and Sacred Lake (Konecky et al. 2014) and have been related to the northward displacement of the ITCZ (Huang et al. 2001) during the first half of the LIA. Increased detrital input in Lake Nkunga during this time coincides with a period of increased anthropogenic activities in the

neighbouring Kiluli swamp (Olago 1995), and may suggest that the increased influx is in part related to anthropogenic activities, such as vegetation clearance for cultivation, in the Lake Nkunga catchment. At Lake Rutundu, the reconstructed MAAT displays a 0.2 °C rise in temperature. The easternmost parts of East Africa experienced wetter conditions during the Late LIA (Tierney et al. 2013, Russell et al. 2007). The timing of a wetter phase in Sacred Lake *ca*. 200 cal yr. BP (1750 AD; Konecky et al. 2014), the overflow at Lake Naivasha 280 – 180 cal yr. BP (1670 – 1770 AD; Verschuren et al. 2000) and the rising lake levels at Lake Victoria *ca*. 250 cal yr. BP (1700 AD; Stager et al. 2005) indicate coherency in the events of the LIA. The record from Lake Nkunga fail to mark this second phase of the LIA and instead show a decline in detrital input and OM sediment supply as well as the X_{lf}. This interval *ca*. 250 – 100 cal yr. BP (1700 – 1850AD) represents a wetter period evidenced by the leaf wax time series from Sacred Lake where rising lake levels are present *ca*. 1700 and 1870 AD (Konecky et al. 2014).

The first documented population expansion around Mount Kenya is *ca*. 200 cal yr. BP (1750 AD) when a group known as the proto-Meru settled at the foothills of the mountain (Ndichu 2009), although the extent of their invasion into the montane forest region is not well known. From 200 to 65 cal yr. BP (1750 to 1885 AD), several severe droughts led to conflicts over natural resources and civil wars among the communities neighbouring the mountain (the Meru, Embu, Kikuyu, Chuka and Maasai) leading to their displacement and further intrusion into the montane region (Ndichu 2009). Tales exist of the extent of the regional droughts such as the Lapanarat *ca*. 190 – 158 cal yr. BP (1760 to 1792 AD) and Nvalaganu ca. 140 – 135 cal yr. BP (1810 – 1815 AD) among communities such as the Chuka who also recall the Kiverio famine *ca*. 104 cal yr. BP (1846 AD; Ndichu 2009). These early droughts coincide with the Lapanarat – Mahlatule drought that coincides with a low stand at Lake Naivasha from 1760 – 1840 AD (Verschuren 2000).

Assuming that drying trend commenced regionally around 1750 AD this may have forced the occupation of population in areas around the mountain. There is a broad agreement with data from other sites that display a drier late phase of the LIA, which ended in aridity. Such records from Lake Victoria (Stager et al. 2005), Lake Baringo (Kiage & Liu 2009) and Lake Challa (Buckles et al. 2016) show that these lakes were shallower or more saline (as seen in Lake Naivasha) at the end of the LIA (Verschuren et al. 2000)

4.6.4.4 The Modern era: 100 cal yr. BP to Present (1850 AD to Present)

Although Lakes Nkunga and Rutundu cover this time period, the palaeo-record from Lake Nkunga provides a higher resolution of the changes in the modern era. From 1850 AD to Present the L. Nkunga record shows a constant %C, Si/Ti and a decrease in the X_{lf} values pointing to dropping lake levels. The evidence of this decline has become apparent over the past two decades where the lakeshores seem to retreat towards the centre of the lake while the lake catchment has remained largely unaltered (Olago 2013, personal communication). Several aridification events have been recorded on Mount Kenya from *ca*. 80 – 55 cal yr. BP (1870 – 1895 AD) and from 1950 to present (Konecky et al. 2014). Most notably, Sacred Lake has seen lake levels drop to a point of desiccation in recent times (Konecky et al. 2014). The "drought of the necklaces" at 66 cal yr. BP (1884 AD) witnessed by the Mahaguya age set of the Embu, also known as the *Kibatau* famine by the Meru and the "battle of famine" known as *Ngoko* by the Chuka at 65 cal yr. BP (1885 AD; Ndichu 2009), and drought events observed in the leaf wax record from Sacred Lake (Konecky et al. 2014), are some of the main climatic events that forced populations to move up Mount Kenya in search of resources.

Although it has been suggested that east Africa became wetter around 1840 AD (Nicholson et al. 2012), with near average rainfall in 1850s and 1860s, historical and lake records point towards multiple severe drought events. For example, Lake Naivasha was at a very low water level and was saline between 1870 and 1890 AD (Verschuren 2000, Verschuren 2001) while lakes Nakuru and Elementaita were completely dry during this period (De Cort et al. 2013).

In the most recent times from 1950 to present, there has been region wide anomalies in rainfall relative to the determined long-term averages (Nicholson 2001). Notably, from 1950 above average rainfall was observed in equatorial east Africa marked by extremely high precipitation, peak river discharge and peak lake levels between 1963 – 1964 (Nicholson 2001).

5 CONCLUSIONS AND RECOMMENDATIONS

5.1 CONCLUSIONS

One of the key issues from literature is how can the interpretation of climate and environmental conditions over East Africa during the Late Holocene be improved? The biogeochemistry of lake sediments provides a wealth of information about landscape changes from which climate and environmental conditions can be inferred. However, the interpretations of climate from the regionally fragmented records displays some contradictions as observed in the east-west regional hydroclimatic gradient (Verschuren et al. 2000; Stager et al. 2005; Tierney et al. 2013). But still the question remains, do these biogeochemical records reflect regional climate signals or a very local signal?

What is really driving the disparity in the climate interpretations form the multiple proxies? Do these proxies account for all the possible factors? Changes in sedimentation in lake basis area all too often interprets as direct and indirect changes in lake level as a consequence of changing precipitation or temperature but perhaps this is too simplistic. This thesis has presented a multiproxy approach from mineral magnetics, geochemistry, and biogeochemistry evidence of past climate and environmental changes on Mt. Kenya over the last 4700 cal yr. BP to Present.

This study has sought to advance the application of geochemical techniques in soils and sediments from the north eastern slopes of Mt. Kenya with the intention to resolve the regional Late Holocene palaeoclimate and palaeoenvironment. Combinations of traditional sedimentological (XRD, XRF and X_{lf}) and organic geochemical analyses (%C, %N, $\delta^{13}C$, $\delta^{15}N$, n-alkanes and GDGT) were carried out to provide high-resolution records of the Late Holocene. The combined information from these three crater lakes has allowed us to define climate-driven changes on the north eastern slopes of Mount Kenya. The AMS ^{14}C ages provided a chronological framework to contextualize our results. All of the lakes demonstrate individual responses to late Holocene climatic events. However, despite the individual variations, there is a regional coherency within our sediment archives with the lakes responding to the same drivers through time and at similar times within the limits of our dating technique. As a result, the sedimentary record from this study is a reliable indicator of regional changes in climate and environment.

The comparison of this work with previous palaeolimnological work across East Africa suggests that indeed the crater lakes on Mt. Kenya are sensitive to climate perturbations such as the regional droughts at ca. 4200 cal yr. BP and 2500 cal yr. BP, the MCA and the LIA though the latter is also characterized by fluctuating lake levels. The trends from the individual lakes support the hypothesis of a regionally complex relationship during the Late Holocene. There are minor discrepancies in our records that can be attributed to (i) chronological issues where a higher resolution chronology could be gotten for the 19^{th} – 20^{th} century through the use of other dating methods such as ^{210}Pb and ^{137}Cs, but this method was not applied due to cost constraints (ii) the regional complexity of the climatic perturbations in East Africa (especially in the records of the last millennia) and (iii) the individual buffering of a lake's response. For example, the record from Sacred Lake captures two key erosional periods at 3500 cal yr. BP to 1150 cal yr. BP and 630 cal yr. BP to Present implying shifts in low and high lake levels and the progressive shallowing of the lake establishing the current swamp conditions from ca. 630 cal yr. BP. The sedimentary record from Sacred Lakes shows almost immediate and abrupt responses to climatic drivers while the records from Lake Rutundu suggest a time-lag in responses.

Coherency in our record with regional lakes shows a prolonged region-wide Medieval Climate Anomaly and century-scale LIA droughts. Our record, therefore, captures the hydrological variability although sensitivities to decadal-scale changes is not well recorded. Other regional reconstructions from the east African lakes (Gasse 2000, Verschuren et al. 2000, Kiage & Liu 2006; 2009, Russell & Johnson 2005; Russell et al. 2007; Vincens et al. 2007; Tierney et al. 2010) have shown subtle decadal and/or centennial scale changes in their sedimentary and hydrological records (Tierney et al. 2013) capturing heterogeneities especially during the early and late phases of the LIA. Lastly, whereas it is also possible to infer anthropogenic influence on the catchment from the Lake Nkunga record, the proxy signal of the human impact over a climate record is not clear. In the East African region, climate fluctuations are the principal drivers of observed limnological changes and, therefore, the overprint of human activity on the sediment-climate record is not fully understood.

Our record succeeds to provide valuable insights on climate proxies and relevant interpretations from each of the selected lakes that are considered to be "climatically sensitive". These lakes have simple hydrology that reflects a straightforward lake history – climate relationship. This therefore means that any changes in the sedimentation system is largely linked to changes in

climate parameters, status of the catchment processes, activities and potentially, their altitudinal location on the mountain slopes. Whereas the human imprint is not clear in our study, these lakes are located in the Mt. Kenya ecosystem and outside the national park. Over the recent years with the decentralization in the management of natural resources, local tourism to such sites is becoming increasingly popular. This, therefore, demands the monitoring and perhaps management of the lakes to understand the sediment loading from their wider catchments. Even in the absence of climatic factors, increasing population trends and the reliance on forest resources for tourism developments, agricultural expansion and timber; monitoring of these lakes is crucial to allow a better understanding of how the lakes function.

The successful analysis of near shore sediment records has provided a beneficial record to the climatic events during the late Holocene (Sacred Lake and Lake Nkunga) that could have not been captured in a continuous sediment core from the centre of the lake (Lake Rutundu) that are considered ideal sites for sedimentation studies. It would be beneficial to apply this methodology to some other lakes in the region to assess the performance of the sedimentary records during the Late Holocene especially in closed lake basins.

5.2 RECOMMENDATIONS

The following are the recommendations that derive from this research:

a) Although this biogeochemical evidence has been used to support the conclusions with respect to precipitation and temperature there is need to integrate vegetation changes (from mainly pollen studies) and seasonal climatic drivers to provide a comprehensive outlook.
b) The human question is still not resolved on the Late Quaternary landscapes. Did humans really impact the environment and change the landscape? This remains an open question in the montane regions in East Africa. Further research is needed as it may be crucial to understanding our palaeoenvironmental records.
c) To carry out analysis of the of the $\delta D_{leafwax}$, compound specific $\delta^{13}C$ of n-alkanes and $\delta^{18}O$ that are sensitive to precipitation changes in order to provide a more comprehensive dataset on the environmental controls for the biomarker distribution.
d) To carry out ^{210}Pb and ^{137}Cs dating in the upper sediments from the crater lakes enable chronological constraints for the identification of century and decadal scale changes in the climate and environment.

e) To synthesize and reanalyse the existing late Holocene dataset from both the proxies and models in order to present a better picture of the Late Holocene spatial coherency and heterogeneity.
f) Even though the existing regional calibration for the GDGTs were applied in our dataset, there is need to further evaluate the utility of this proxy. An understanding of the environmental controls and seasonality, could resolve the applicability of these calibrations in the occurrence and distribution of the GDGTs.

6 REFERENCES

Alin, S.R., Cohen, A.S. (2003). Lake-level history of Lake Tanganyika, East Africa, for the past 2500 years based on ostracod-inferred water-depth reconstruction. *Palaeogeography, Palaeoclimatology, Palaeoecology*. **199** (1-2). pp. 31–4.

Anderson, D. (2002). Eroding the commons: the politics of ecology in Baringo, Kenya 1890 – 1963, *E.A.E.P publishers*, Nairobi, 336pp.

Aucour, A., Hillaire-Marcel, C., Bonnefille, R. (1994). Late Quaternary biomass changes from ^{13}C measurements in a highland peatbog from equatorial Africa (Burundi). *Quaternary Research,* **41**, 225-233.

Baker, B.H., (1967). Geology of the Mount Kenya Area. *Geological Survey of Kenya,* Rep. 79, Nairobi.

Baker, B.H., Williams, L.A.J., Miller, J.A., Fitch, F.J. (1971). Sequence and geochronology of the Kenya rift volcanics. *Tectonophysics,* **11**, 191–215.

Barker, P., Street-Perrott, F.A., Leng, M.J., Greenwood, P.B., Swain, D.L., Perrott, R.A., Telford, R.J., Ficken, K.J. (2001). A 14,000-Year Oxygen Isotope Record from Diatom Silica in Two Alpine Lakes on Mt. Kenya. *Science*, **292**, 2307-2310.

Barker, P., Williamson, D., Gasse, F., Gibert, E. (2003). Climatic and volcanic forcing revealed in a 50,000-year diatom record from Lake Massoko, Tanzania. *Quaternary Research*, **60**, 368-376.

Barker, P., Gasse, F. (2003). New evidence for a reduced water balance in East Africa during the Last Glacial Maximum: implication for model-data comparison. *Quaternary Science Reviews,* **22**, 823-837.

Battarbee, R.W. (2000). Palaeolimnological approaches to climate change, with special regard to the biological record. *Quaternary Science Reviews,* **19**, 107-204.

Bechtel, A., Smittenberg, R. H., Bernasconi, S. M., Schubert, C.J. (2010). Distribution of branched and isoprenoid tetraether lipids in an oligotrophic and a eutrophic Swiss lake: Insights into sources and GDGT-based proxies. *Organic Geochemistry*, **41** (8), 822 – 832, DOI:10.1016/j.orggeochem.2010.04.022.

Bendle, J. A., Weijers, J. W. H., Maslin, M. A., Sinninghe Damsté, J. S., Schouten, S., Hopmans, E. C., Boot, C. S., Pancost, R. D. (2010). Major changes in glacial and Holocene terrestrial temperatures and sources of organic carbon recorded in the Amazon fan by tetraether lipids. *Geochemistry, Geophysics, Geosystems*, **11** (12) DOI:10.1029/2010GC003308.

Berke, M.A., Johnson, T.C., Werne, J.P., Grice, K., Schouten, S., Sinninghe Damasté J.S. (2012). Molecular records of climate variability and vegetation response since the Late Pleistocene in Lake Victoria basin, East Africa. *Quaternary Science Reviews*, **55**, 59-74.

Berke, M.A., Johnson, T.C., Werne, J.P., Schouten, S., Sinninghe Damsté J.S. (2012b). A mid Holocene thermal maximum at the end of the African Humid Period. *Earth and Planetary Science Letters*, **351 – 352**, 95 – 104.

Blaauw, M. (2010). Methods and code for 'classical' age-modelling of radiocarbon sequences. *Quaternary Geochronology,* **5**(5), 512- 518, https://doi.org/10.1016/j.quageo.2010.01.002.

Blaauw, M., Christen, J.A. (2011). Flexible paleoclimate age-depth models using an autoregressive gamma process. *Bayesian Analysis.* **6**, 457- 474.

Blaga, C. I., Reichart, G. J., Heiri, O., Sinninghe Damsté, J. S. (2009). Tetraether membrane lipid distributions in water-column particulate matter and sediments: a study of 47 European lakes along a north–south transect. *Journal of Palaeolimnology*. **41** (3) 523–540. DOI:10.1007/s10933-008-9242-2.

Blaga, C.I., Reichart, G.-J., Schouten, S., Lotter, A.F., Werne, J.P., Kosten, S., Mazzeo, N., Lacerot, G., Damsté, J.S.S. (2010). Branched glycerol dialkyl glycerol tetraethers in lake sediments: Can they be used as temperature and pH proxies? *Organic Geochemistry*. **41** (11), 1225–1234.

Blott, S.J., Pye, K. (2001) Gradistat: A Grain Size Distribution and Statistics Package for the Analysis of Unconsolidated Sediments. *Earth Surface Processes and Landforms,* **26**, 1237-1248. http://dx.doi.org/10.1002/esp.261.

Boës, X., Rydberg, J., Martinez-Cortizas, A., Bindler, R., Renberg, I., (2011). Evaluation of conservative lithogenic elements (Ti, Zr, Al, and Rb) to study anthropogenic element enrichments in lake sediments. *Journal of Palaeolimnology*, **46**, 75 – 87.

Bonnefille, R., Hamilton, A.C., Linder, H.P., Riollet, G. (1990). 30, 000-Year-Old Fossil Restionaceae Pollen from Central Equatorial Africa and Its Biogeographical Significance. *Journal of Biogeography,* **17** (3), 307 – 314.

Boyle, J. (2001). Redox remobilization and the heavy metal record in lake sediments: a modelling approach. *Journal of Palaeolimnology*, **26,** 423–431. https://doi.org/10.1023/A:1012785525239

Bray, E.E., Evans, E.D. (1961). Distribution of *n*-paraffins as a clue to the recognition of source beds. *Geochimica et Cosmochimica Acta,* **22**, 2-15.

Buckles, L.K., Weijers, J.W.H., Verschuren, D., Cocquyt, C., Sinninghe Damste, J.S. (2016). Short-term variability in the sedimentary BIT index of Lake Challa, East Africa over the past 2200 years: validating the precipitation proxy. *Climate of the Past*, **12**, 1243 – 1262.

Butzer, K.W., Isaac, G.L., Richardson, J.L., Washburn-Kamau, C. (1972). Radio- carbon Dating of East African Lake Levels. *Science*, **175**, 1069 - 1076.

Camberlin, P., Moron, V., Okoola, R., Philippon, N., Gitau, W. (2009). Components of rainy seasons' variability in Equatorial East Africa: onset, cessation, rainfall frequency and intensity. *Theoretical and Applied Climatology,* **98**, 237-249.

Camberlin, P., Boyard-Micheau, J., Philippon, N., Baron, C., Leclerc, C., Mwongera, C., (2012). Climatic gradients along the windward slopes of Mount Kenya and their implication for crop risks. Part 1: climate variability. *International Journal of Climatology,* DOI: 10.1002/joc.3427.

Castañeda, I.S., Mulitza, S., Schefuß, E., dos Santos, R.A.L., Sinninghe Damsté, J.S., Schouten, S. (2009). Wet phases in the Sahara/Sahel region and human migration patterns in North Africa. *PNAS*, **106** (48), 20159-20163, https://doi.org/10.1073/pnas.0905771106.

Christensen J.H., Hewitson B., Bulsuioc A., Chen A., Gao X., Held I., Jones R., Kolli R.K., Laprise R., Magaña Ruenda R., Mearns L., Menéndez C.G., Rinke A., Sarr A., Whetton P. (2007). Regional climate projections in: climate change 2007: The Physical Science Basis. Contribution of working group 1 to the fourth assessment report of the intergovernmental panel on climate change [Solomon S., Qin D., Manning M., Chen Z., Marquis M., Averyt K.B., Tignor M., and Miller H.L. (eds)] Cambridge University Press Cambridge, United Kingdom and New York, NY, USA, 989 pp.

Coe, M.J. (1967). The ecology of the Alpine zone of Mount Kenya. *The Hague, Dr. W. Junk,* 136 pp.

Coetzee, J.A. (1967). Pollen analytical studies in East and Southern Africa. *Palaeoecology of Africa,* **3**, 1 -146.

Coffinet, S., Huguet, A., Williamson, D., Fosse, C., Derenne, S. (2014). Potential of GDGTs as a temperature proxy along an altitudinal transect at Mount Rungwe (Tanzania). *Organic Geochemistry*, **68**, 82 – 89.

Coffinet, S., Huguet, A., Pedentchouk, N., Bergonzini, L., Omuombo, C., Williamson, D., Anquetil, C., Jones, M., Majule, A., Wagner, T., Derenne, S. (2017). Evaluation of branched GDGTs and leaf wax n-alkane δ^2H as (paleo) environmental proxies in East Africa. *Geochimica et Cosmochimica Acta*, **198**, 182–193. DOI: 10.1016/j.gca.2016.11.020.

Collister, J., Rieley, G., Stern, B., Elington, G., Fry, B. (1994). Compound-specific $\delta^{13}C$ of leaf lipids from plants with differing carbon dioxide metabolisms. *Organic Geochemistry,* **21** (6/7), 619 – 627.

Cohen, A.S., Palacios-Fest, M.R., Msaky, E.S., Alin, S.R., McKee, B., O'Reilly, C.M., Dettman, D.L., Nkotagu, H., Lezzar, K.E. (2005). Paleolimnological investigations of anthropogenic environmental change in Lake Tanganyika: IX. Summary of paleorecords of environmental change and catchment deforestation at Lake Tanganyika and impacts on the Lake Tanganyika ecosystem. *Journal of Palaeolimnology,* **34**,125–145.

Cohen, A.S., Stone, J.R., Beuning, R.M., Park, L.E., Reinthal, P.N., Dettman, D., Scholz, C., Johnson, T.C., King, J.W., Talbot, M.R., Brown, E.T., Ivory, S.J. (2007). Ecological consequences of early Late Pleistocene megadroughts in tropical Africa. *PNAS.* **104** (42), 16422–16427.

Cohen, A.S., Lezzar, K.E., Cole, J., Dettman, D., Ellis, G.S., Gonneea, M.E., Plisnier, P.-D., Langenberg, V., Blaauw, M., Zilifi, D. (2006). Late Holocene linkages between decade–century scale climate variability and productivity at Lake Tanganyika, Africa. *Journal of Palaeolimnology*, **36** (2), 189–209.

COHMAP (1988). Climatic Changes of the Last 18,000 years: Observations and Model Simulations. *Science*, **241** (4869), 1043 - 1052.

Cranwell, P.A. (1973). Chain-length distribution of n-alkanes from lake sediments in relation to post-glacial environmental change. *Freshwater Biology,* **3**, 259–265.

Cranwell, P.A., (1982). Lipids of aquatic sediments and sedimenting particulates. *Progress in Lipid Research,* **21**, 271 - 308.

Cranwell, P.A., Eglinton, G., and Robinson, N. (1987). Lipids of aquatic organisms as potential contributors to lacustrine sediments - II. *Organic Geochemistry,* **6**, 513 - 527.

Dansgaard W., Johnsen S.J., Clausen H.B., Dahl-Jensen D., Gundestrup N.S., Hammer C.U., Hvidberg C.S., Steffensen J.P., Sveinbjornsdottir A.E., Jouzel J., Bond G. (1993). Evidence for general instability of past climate from a 250-kyr ice-core record, *Nature*, **364** (6434), 218–220, doi:10.1038/364218a0.

De Cort, G., Bessems, I., Keppens, E., Mees, F., Cumming, B., Verschuren, D. (2013). Late-Holocene and recent hydroclimatic variability in the central Kenya Rift Valley: the sediment record of hypersaline lakes Bogoria, Nakuru and Elementeita. *Palaeogeography, Palaeoclimatology, Palaeoecology*, **388**, 69 - 80.

De Souza, D.B., Machado, K.S., Froehner, S., Scapulatempo, C.F., Bleninger, T. (2011). Distribution of n-alkanes in lacustrine sediments from subtropical lake in Brazil. *Chemie der Erde – Geochemistry,* **71** (2), 171–176.

Dearing J.A., Dann R.J.L., Hay K., Lees J.A., Loveland P.J., Maher B.A, O'Grady K. (1996). Frequency Dependent Susceptibility Measurements of Environmental Materials. *Geophysical Journal International*, **124**, 228 – 240.

Dearing, J.A. (1999). Holocene environmental change from magnetic proxies in lake sediments. In: Maher, B.A., Thompson, R. (Eds.), Quaternary Climates, Environments and Magnetism, pp. 231–278.

deMenocal P., Ortiz J, Guilderson T., Adkins, J., Sarnthein, M., Baker, L., Yarusinsky, M. (2000). Abrupt onset and termination of the African Humid Period: rapid climate responses to gradual insolation forcing. *Quaternary Science Reviews,* **19**, 347-361.

deMenocal P.B., Tierney, J.E. (2012). Green Sahara: Africa Humid Periods Paced by Earth's Orbital Changes. *Nature Education Knowledge,* **3** (10), 12.

Dodd, R., Poveda, M. (2003). Environmental gradients and population divergence contribute to variation in cuticular wax composition in *Juniperus communis*. *Biochemical Systematics and Ecology*, **31**, 1257-1270.

Dubinsky, E.A., Whendee, L.S., Firestone, M.K. (2010). Tropical forest soil microbial communities couple iron and carbon biogeochemistry. *Ecology*, **91** (9), 2604-2612.

Eckmeier, E., Wiesenberg, G.L. (2009). Short-chain *n*-alkanes (C_{16-20}) in ancient soil are useful molecular markers for prehistoric biomass burning. *Journal of Archaeological Sciences*, **36**(7), 1590-1596.

Edwards, M.E. (2013). Africa during the Late Quaternary. 2nd Ed., Elsevier B.V.

Eglinton, G., Gonzalez, A.G., Hamilton, R.J., Raphael, R.A. (1962). Hydrocarbon constituents of the wax coatings of plant leaves: a taxonomic survey. *Phytochemistry*, **1**, 89–102.

Eglinton, G., Hamilton, R.J. (1967). Leaf epicuticular waxes. *Science*, **156**, 1322-1335.

Fang, J., Wu, F., Xiong, Y., Li, F., Du, X., An, D., Wang, L. (2014). Source characterization of sedimentary organic matter using molecular and stable carbon isotopic composition of n-alkanes and fatty acids in sediment core from Lake Dianchi, China. *Science of the Total Environment*, **473–474**, 410–421, https://doi.org/10.1016/j.scitotenv.2013.10.066.

Fick, S.E., Hijman, R.J. (2017). Worldclim 2: New 1-km spatial resolution climate. http://worldclim.org/version2.

Ficken, K.J., Street-Perrott, F.A., Perrott, R.A., Swain, D., Eglinton, G. (1998). Glacial/interglacial variations in carbon cycling revealed by molecular and isotopic stratigraphy of Lake Nkunga, Mt. Kenya. *Organic Geochemistry*, **29**, 1701–1719.

Ficken, K.J., Li, B., Swain, D.L., Eglinton, G. (2000). An *n*-alkane proxy for the sedimentary input of submerged/floating freshwater aquatic macrophytes. *Organic Geochemistry*, **31**, 745-749.

Ficken, K.J., Wooller, M.J., Swain, D.L., Street-Perrott, F.A., Eglinton, G. (2002). Reconstruction of a subalpine grass-dominated ecosystem, Lake Rutundu, Mount Kenya: a novel multi-proxy approach. *Palaeogeography, Palaeoclimatology, Palaeoecology*, **177**, 137–149.

Gasse, F. (2000). Hydrological changes in the African tropics since the Last Glacial Maximum. *Quaternary Science Reviews*, **19** (1-5), 189–211.

Gasse, F., Barker, P., Johnson, T.C. (2002). A 24,000 yr. diatom record from the northern basin of Lake Malawi. In: Odada, E.O., Olago, D.O. (Eds). *East African Great Lakes: Limnology, Palaeolimnology and Biodiversity. Advances in Global Change Research*, Kluwer Academic, Dordrecht.

Gasse, F. (2005). Continental palaeohydrology and palaeoclimate during the Holocene. *Comptes Rendus Geoscience*, **337** (1-2), 79–86.

Gasse, F., Chalié, F., Vincens, A., Williams, M.A.J., Williamson, D. (2008). Climatic patterns in equatorial and southern Africa from 30,000 to 10,000 years ago reconstructed from terrestrial and near-shore proxy data. *Quaternary Science Reviews*, **27** (25-26), 2316–2340.

Garcin, Y., Williamson, D., Taieb, M., Vincens, A., Mathé, P.-E., Majule, A. (2006). Centennial to millennial changes in maar-lake deposition during the last 45,000 years in tropical Southern Africa (Lake Masoko, Tanzania). *Palaeogeography, Palaeoclimatology, Palaeoecology*. **239** (3-4), 334–354.

Garcin, Y., Junginger, A., Melnick, D., Olago, D.O., Strecker, M.R., Trauth, M.H. (2009). Late Pleistocene - Holocene rise and collapse of Lake Suguta, northern Kenya Rift. *Quaternary Science Reviews,* **28**, 911-925.

Hamilton, A.C. (1982). Environmental History of East Africa: A Study of the Quaternary. *Academic Press, London,* 328pp.

Haberyan, K.A., Hecky, R.E. (1987). The Late Pleistocene and Holocene stratigraphy and palaeolimnology of Lakes Kivu and Tanganyika. *Palaeogeography, Palaeoclimatolology, Palaeoecology,* **61**, 169–197.

Halfman, J.D., Johnson, T.C., Finney, B.P. (1994). New AMS dates, stratigraphic correlations and decadal climatic cycles for the past 4 ka at Lake Turkana, Kenya. *Palaeogeography, Palaeoclimatology, Palaeoecology*, **111**, 83 – 98.

Hemp. A. (2005). Climate change-driven forest fires marginalize the impact of ice cap wasting on Kilimanjaro. *Global Change Biology*, **11**(7), 1013-1023.

Hopmans, E. C., Schouten, S., Pancost, R. D., Van der Meer, M. T., Sinninghe Damsté, J. S. (2000). Analysis of intact tetraether lipids in Archaeal cell material and sediments by high performance liquid chromatography/atmospheric pressure chemical ionization mass spectrometry. *Rapid communications in mass spectrometry*, **14** (7) 585– 589.

Hopmans, E.C., Weijers, J.W.., Schefuß, E., Herfort, L., Sinninghe Damsté, J.S., Schouten, S. (2004). A novel proxy for terrestrial organic matter in sediments based on branched and isoprenoid tetraether lipids. *Earth and Planetary Science Letters*, **224**, 107**–**116.

Huang, Y., Street-Perrott, F.A., Perrott, R.A., Metzger, P., Eglinton, G. (1999). Glacial–interglacial environmental changes inferred from molecular and compound-specific ∂13C analyses of sediments from Sacred Lake, Mt. Kenya. *Geochimica et Cosmochimica Acta*, **63** (9), 1383–1404.

Haug, G., Hughen, K., Sigman, D., Peterson, L., Rohl, U. (2001). Southward migration of the intertropical convergence zone through the Holocene. *Science*, **293**, 1304**-**1308.

Huguet, A., Fosse, C., Laggoun-Défarge, F., Toussaint, M. L., Derenne, S. (2010). Occurrence and distribution of glycerol dialkyl glycerol tetraethers in a French peat bog. *Organic Geochemistry*, **41** (6), 559–572. DOI:10.1016/j.orggeochem.2010.02.015.

Huguet, A., Fosse, C., Laggoun-Défarge, F., Delarue, F., Derenne, S., 2013. Effects of a short-term experimental microclimate warming on the abundance and distribution of branched GDGTs in a French peatland. *Geochimica et Cosmochimica Acta*, **105**, 294–315.

Juggins, S. (2017). Rioja: Analysis of Quaternary Science Data, R package version (0.9-15.1). http://cran.r-project.org/package=rioja.

Karlén, W., Fastook, J.L., Holmgre, K., Malmström, M., Matthews, J.A., Odada, E., Risberg, J., Rosqvist, G., Sandgren, P., Shemesh, A., Westerberg, L. (1999). Glacier fluctuations on Mount Kenya since 6000 Cal. Years BP: Implication for Holocene Climatic Change in Africa. *Ambio*, **28** (5), 409 – 418.

Kiage, L. M., Liu, K. B. (2006). Late Quaternary paleoenvironmental changes in East Africa: a review of multiproxy evidence from palynology, lake sediments, and associated records. *Progress in Physical Geography*, ***30*** (5), 633–658, http://doi.org/10.1177/0309133306071146.

Kiage, L.M., Liu, K.-B. (2009). Palynological evidence of climate change and land degradation in the Lake Baringo area, Kenya, East Africa since AD 1650. *Palaeogeography, Palaeoclimatology, Palaeoecology*, **279** (1-2), 60–72.

Kim, J.-H., van der Meer, J., Schouten, S., Helmke, P., Willmott, V., Sangiorgi, F., Koç, N., Hopmans, E.C., Sinninghe Damsté, J.S. (2010). New indices and calibrations derived from the distribution of crenarchaeal isoprenoid tetraether lipids: implications for past sea surface temperature reconstructions. *Geochimica et Cosmochimica Acta*, **74**, 4639–4654.

Kolattukudy, P.E., Croteau, R., Buckner, J.S., (1976). Biochemistry of plant waxes. In: Kollatukudy, P.E. (Ed.), Chemistry and Biochemistry of Natural Waxes. Elsevier, Amsterdam, pp. 290–347.

Konecky, B., Russell, J., Huang, Y., Vuille, M., Cohen, L., Street-Perrott, F.A. (2014). Impact of monsoons, temperature, and CO_2 on the rainfall and ecosystems of Mt. Kenya during the Common Era. *Palaeogeography, Palaeoclimatology, Palaeoecology*, **396** (C), 17–25.

Lamb, A. L., Leng, M.J., Lamb, H.F., Mohammed, M.U. (2000). A 9000-year oxygen and carbon isotope record of hydrological change in a small Ethiopian crater lake. *The Holocene,* **10**, 167-177.

Lamb, H., Darbyshire, I., Verschuren, D. (2003). Vegetation response to rainfall variation and human impact in central Kenya during the past 1100 years. *Holocene,***13** (2), 285-292.

Lézine, A.M. (1982) Etude palynologique des sediments Quaternaires du Lac Abiyata (Ethiopie). *Palaeoecology of Africa,* **14**, 93–98.

Liu, X.-L., Leider, A., Gillespie, A., Gröger, J., Versteegh, G.J.M., Hinrichs, K.-U. (2010). Identification of polar lipid precursors of the ubiquitous branched GDGT orphan lipids in a peat bog in Northern Germany. *Organic Geochemistry*, **41**, 653–660.

Liu, W., Wang, H., Zhang, C.L., Liu, Z., He, Y. (2013). Distribution of glycerol dialkyl glycerol tetraether lipids along an altitudinal transect on Mt. Xiangpi, NE Qinghai-Tibetan Plateau, China. *Organic Geochemistry*, **57** (C), 76–83.

Livingstone, D.A., Clayton, W.D. (1980). An altitudinal cline in tropical African grass floras and its paleoecological significance. *Quaternary Research,* **13** (3)*,* 392-402*,* DOI: 10.1016/0033-5894(80)90065-4.

Loomis, S. E., Russell, J., Bethany, L., Street-Perrott, F. A., Damsté, J. S. (2012). Calibration and application of the branched GDGT temperature proxy on East African lake sediments. *Earth and Planetary Science Letters*, **357-358**, 277–88.

Loomis, S. E., Russell, J., Verschuren, D., Morrill, C., De Cort, G., Sinninghe Damsté, J. S., Olago, D., Eggermont, H., Street-Perrott, F.A., Kelly, M. (2017). The tropical lapse rate steepened during the Last Glacial Maximum. *Science Advances*, **3**(1), https://doi.org/10.1126/sciadv.1600815.

Maffei, M. (1996). Chemotaxonomic significance of leaf wax n-alkanes in the Gramineae. *Biochemical Systematics and Ecology*, **24**, 53-64.

Mahaney, W.C., Vortisch, W. (1989). Scanning electron microscopy of feldspar and volcanic glass weathering and neoformation of clay minerals in Quaternary paleosol sequence, Mount Kenya, East Africa. *Journal of African Earth Sciences*, **9** (3/4), 729 – 737.

Mahaney, W.C. (1990). Ice on the Equator. Ellison Bay, Wisconsin, USA: Wm Caxton press, 386 pp.

Mahaney, W.C., (1991). Distribution of halloysite-metahalloysite and gibbsite in tropical mountain paleosols: relationship to Quaternary paleoclimate. *Palaeogeography Palaeoclimatology Paleoecology*, **88** (3-4), 219 – 230.

Maher, B.A. (1986). Characterisation of soils by mineral magnetic measurements. *Physics of the Earth and Planetary Interiors*, **42** (1-2), 76 – 92.

Maitima, J.M. (1991). Vegetation response to climatic change in Central Rift Valley, Kenya. *Quaternary Research*, **35**, 234–245.

Marchant, R., Hooghiemstra, H. (2004). Rapid environmental change in Africa and South America tropics around 4000 years before present: a review. *Earth-Science Reviews*, **66** (3-4), 217 – 260.

Marchant, R., Mumbi, C., Behera, S., Yamagata, T. (2006). The Indian Ocean dipole – the unsung driver of climatic variability in East Africa. *African Journal of Ecology,* **45**, 4-16.

Marchant, R., Richer, S., Boles, O., Capitani, C., Courtney-Mustaphi, C., Lane, P., Prendergast, M., Stump, D., De Cort, G., Kaplan, J.O., Phelps, L., Kay, A., Olago, D., Petek, N., Platts, P.J., Punwong, P., Widgren, M., Wynne-Jones, S., et al. (2018). Drivers and trajectories of land cover change in East Africa: Human and environmental interactions from 6000 years ago to present. *Earth-Science Reviews*, **178**, 322–378.

Marshall, M., Schlolaut, G., Nakagawa, T., Lamb, H., Brauer, A., Staff, R., Ramsey, C., Tarasov, P., Gotanda, K., Haraguchi, T., Yokoyama, Y., Yonenobu, H., Tada, R., (2012). A novel approach to varve counting using μXRF and X-radiography in combination with thin-section microscopy, applied to the Late Glacial chronology from Lake Suigetsu, Japan. *Quaternary Geochronology*, **13**, 70 – 80. doi:889 10.1016/j.quageo.2012.06.002.

Mason, P. (1953). Geology of the Meru – Isiolo Area. *Geological Survey of Kenya,* Rep. 31, Nairobi.

Mayewski, P.A., Rohling, E.E., Curt Stager, J., Karlen, W., Maasch, K.A., David Meeker, L., Meyerson, E.A., Gasse, F., van Kreveld, S., Holmgren, K., Lee-Thorp, J., Rosqvist, G., Rack,

F., Staubwasser, M., Schneider, R.R., Steig, E.J. (2004). Holocene climate variability. *Quaternary Research,* **62**, 243-255. https://doi.org/10.1016/j.yqres.2004. 07.001.

Meyers P.A., Ishlwatari R. (1993). The early diagenesis of organic matter in lacustrine sediments. In Organic Geochemistry (Edited by Engel M. and Macko S. A.), pp 185-209, Plenum, New York.

Meyers, P.A. (1997). Organic geochemical proxies for paleooceanographic, paleolimnologic and paleoclimatic processes. *Organic Geochemistry* 27: 213-250.

Meyers P.A., Terranes J.L. (2001). *Sediment Organic Matter. In: Tracking environmental Change using Lake Sediments* (Last, W.M. and Smol J.P, Eds)*,* **2**, 239 - 269, Dordrecht.

Mumbi, C.T., Marchant, R., Hooghiemstra, H., Wooller, M.J. (2017). Late Quaternary vegetation reconstruction from the Eastern Arc Mountains, Tanzania. *Quaternary Research*, **69** (02), 326–341.

Mustaphi, C.J.C., Gajewski, K., Marchant, R., Rosqvist, G. (2017). A Late Holocene pollen record from proglacial Oblong Tarn, Mount Kenya. PLoS ONE, **12** (9): e0184925. https://doi.org/10.1371/journal.pone.0184925.

Naeher, S., Peterse, F., Smittenberg, R. H., Niemann, H., Zigah, P. K. and Schubert, C. J. (2014). Sources of glycerol dialkyl glycerol tetraethers (GDGTs) in catchment soils, water column and sediments of Lake Rotsee (Switzerland) – Implications for the application of GDGT-based proxies for lakes. *Organic Geochemistry*, **66**, 164–173. DOI:10.1016/j.orggeochem.2013.10.017.

Ndichu, R. W. (2009). The most devastating Famines in East Africa in the last 1700 years, Sanctified Publishers, Nairobi, 340pp.

Nicholson, S. E. (1996). A review of climate dynamics and climate variability in eastern Africa. In T. C. Johnson, & E. Odada (Eds.), *The limnology, climatology and paleoclimatology of the East African lakes,* pp. 25-56, Amsterdam: Gordon and Breach.

Nicholson, S.E., Kim, J. (1997). The relationship of the El Niño-Southern Oscillation to African rainfall. *International Journal of Climatology,* **17**, 117-135.

Nicholson, S. E., (1998). Inter-annual and inter-decadal variability of rainfall over the African continent during the last two centuries, in *Water Resources Variability in Africa During the XXth Century*. edited by M. Servat, E and Hughes, D and Fritsch, JM and Hulme, pp. 107–116.

Nicholson, S.E. (2000). The nature of rainfall variability over Africa on time scales of decades to millennia. *Global and Planetary Change,* **26**, 137-158.

Nicholson, S.E. (2001). Rainfall Conditions in Equatorial East Africa during the Nineteenth Century as Inferred from the Record of Lake Victoria. *Climatic Change,* **48**, 387-398.

Nicholson, S.E., Dezfuli, A.K., Klotter, D. (2012). A two-century precipitation dataset for the continent of Africa. *American Meteorological Society*, **93**(8), 1219-1231.

Oksanen, J., Blanchet, F.G., Kindt, R., Legendre, P., Minchin, P.R., O'Hara R.B., Simpson, G.L., Solymos, P., Stevens, M.H.H., Wagner, H. (2013). Package 'vegan' - Community ecology package, version2.2-1, **2** (9), 1-295.

O'Leary, M. H. (1988). Carbon isotopes in photosynthesis. *Bioscience,* **38**, 328- 336.

Oettli, P., Camberlin, P. (2005). Influence of topography on monthly rainfall distribution over East Africa. *Climate Research,* **28**, 199-212.

Olago, D.O. (1995). Late Quaternary lake sediments of Mount Kenya, Kenya. DPhil thesis, University of Oxford.

Olago, D.O., Street-Perrott, F.A., Perrott, R.A., Ivanovich, M., Harkness, D.D. (1999). Late Quaternary glacial-interglacial cycle of climatic and environmental change on Mount Kenya, Kenya. *Journal of African Earth Sciences,* **29** (2),1–26.

Olago, D.O., Street-Perrott, F. A., Perrott, R. A., Ivanovich, M., & Harkness, D.D. (2000). Late Quaternary primary tephras in Sacred Lake sediments, northeast Mount Kenya, Kenya. *Journal of African Earth Sciences*, ***30*** (4), 957–969.

Olago, D. O. (2001). Vegetation changes over palaeo-time scales in Africa. *Climate Research*, **17**, 105–121.

Olago, D.O., Street-Perrott, F.A., Perrott, R.A., Odada, E.O. (2003). Late Holocene sedimentology and palaeoenvironment of Kiluli Swamp, Mount Kenya. *African Journal of Science and Technology,* **4,** 12-23.

Olago, D.O., Odada, E.O. (2004). Palaeo-research in Africa: relevance to sustainable environmental management and significance for the future. In: R. Battarbee, F. Gasse and C. Stickley (Eds.) *Past Climate Variability through Europe and Africa*. Kluwer Academic Publishers, Dordrecht, The Netherlands, pp. 551-565.

Olago, D.O., Odada, E.O. (1996). Some aspects of the physical and chemical dynamics of a large rift lake: the Lake Turkana North Basin, northwest Kenya. In: T.C Johnson and E.O Odada (Eds.) *The Limnology, Climatology and Paleoclimatology of the East African Lakes*. Gordon and Breach Science Publishers, South Africa, pp. 413-430.

Olago, D.O., (2013). Quaternary Evolution. In P. Paron, D.O. Olago and C.T Omuto (Eds.) *Kenya: A Natural Outlook Geo-Environmental Resources and Hazards*. Development in earth Science processes 16. Elsevier B.V, pp 31 – 37.

Oldfield, F., Robinson, S.G. (1985). Geomagnetism and paleoclimate. In *The Climatic Scene*, M.J. Tooley and G. Sheil (eds). London. George Allen & Unwin.

Otto-Bliesner, B.L, Russell, J.M., Clark, P.U., Liu, Z., Overpeck, J.T., Konecky, B., deMenocal, P., Nicholson, S.E., He, F., Lu, Z. (2014). Coherent changes of southeastern equatorial and northern African rainfall during the last deglaciation. *Science*, **346**, 1223–1227.

Owen, R.B., Barthelme, J.W., Renaut, R.W., Vincens, A. (1982). Palaeolimnology and archaeology of Holocene deposits north-east of Lake Turkana, Kenya. *Nature,* 298:523–529.

Parfitt, R.L., Wilson, A.D. (1985). Estimation of allophane and halloysite in three sequences of volcanic soils, New Zealand. In: E. Fernandez Caldas and D.H. Yaalon (Editors), Volcanic Soils. *Catena Suppl.,* **7**, 1-8.

Parfitt, R.L., Russell, M., Orbell, G.E., 1983. Weathering sequence of soils from volcanic ash involving allophane and halloysite. *Geoderma*, **29**, 41-57.

Pancost, R.D., Boot, C.S. (2004). The palaeoclimatic utility of terrestrial biomarkers in marine sediments. *Marine Chemistry*, **92** (1-4), 239 – 261, https://doi.org/10.1016/j.marchem.2004.06.029.

Pearson, E. J., Juggins, S., Talbot, H. M., Weckstrom, J., Rosen, P., Ryves, D. B., Roberts, S. J., Schmidt, R. (2011). A lacustrine GDGT-temperature calibration from the Scandinavian Arctic to Antarctic: Renewed potential for the application of GDGT- paleothermometry in lakes. *Geochimica et Cosmochimica Acta*, **75** (20) 6225–6238, DOI:10.1016/j.gca.2011.07.042.

Pearson, A., Ingalls, A.E. (2013). Assessing the Use of Archaeal Lipids as Marine Environmental Proxies. *Annual Review of Earth and Planetary Sciences*, **41**, 359 – 384.

Perrott, R.A., (1982). A high altitude pollen diagram from Mount Kenya: its implications for the history of glaciation. *Palaeoecology of Africa,* **14**, 77–83.

Peterse, F., Schouten, S., van der Meer, J., van der Meer, M.T.J., Sinninghe Damsté, J.S. (2009). Distribution of branched tetraether lipids in geothermally heated soils: Implications for the MBT/CBT temperature proxy. *Organic Geochemistry,* **40** (2) 201 – 205, DOI:10.1016/j.orggeochem.2008.10.010.

Peterse, F., van der Meer, J., Schouten, S., Jia, G., Ossebaar, J., Blokker, J., Sinninghe Damsté, J. S. (2009a). Assessment of soil n-alkane δD and branched tetraether membrane lipid distributions as tools for paleoelevation reconstruction. *Biogeosciences Discuss*, **6**, 8609–8631.

Peterse, F., Kim, J-H., Schouten, S., Kristensen, D. K., Koç, N., Sinninghe Damsté, J. S. (2009b). Constraints on the application of the MBT/CBT palaeothermometer at high latitude environments (Svalbard, Norway). *Organic Geochemistry*, **40** (6), 692–699. DOI:10.1016/j.orggeochem.2009.03.004.

Peterse, F., van der Meer, J., Schouten, S., Weijers, J. W. H., Fierer, N., Jackson, R. B., Kim, J-H. Sinninghe Damsté, J. S. (2012). Revised calibration of the MBT–CBT paleotemperature proxy based on branched tetraether membrane lipids in surface soils. *Geochimica et Cosmochimica Acta*, **96**, 215 – 229, DOI: 10.1016/j.gca.2012.08.011.

Peterse, F., Vonk, J., Holmes, M., Giosan, L., Zimov, N., Eglinton, T.I. (2014). Branched glycerol dialkyl glycerol tetraethers in Arctic lake sediments: Sources and implications for paleothermometry at high latitudes. *Journal of Geophysical Research*: *Biogeosciences*, **119**, 1738 – 1754, DOI:10.1002/2014JG002639.

Peyron, O., Jolly, D., Bonnefille, R., Vincens, A., Guiot, J. (2017). Climate of East Africa 6000 14C Yr. B.P. as Inferred from Pollen Data. *Quaternary Research*, **54** (01), 90 – 101.

Pokorny, J., Pokorny, P., Suza P., Hrouda, F. (2011). A Multi-Function Kappabridge for High Precision Measurement of the AMS and the Variations of Magnetic Susceptibility with Field, Temperature and Frequency. In E. Petrovsky, D. Ivers, T. Harinarayana, E. Herrero-Bervera (eds), *Earth's Magnetic Interior.* IAGA Special Sopron Book Series 1. pp 293 - 301. DOI 10.1007/978-94-007-0323-0_20.

Powers, L.A., Werne, J.P., Johnson, T.C., Hopmans, E.C., Damsté, J.S.S., Schouten, S. (2004). Crenarchaeotal membrane lipids in lake sediments: A new paleotemperature proxy for continental paleoclimate reconstruction? *Geology*, **32** (7), 613–616, DOI:10.1130/G20434.1.

Powers, L.A., Johnson, T.C., Werne, J.P., Castañeda, I.S. (2005). Large temperature variability in the southern African tropics since the Last Glacial Maximum. *Geophysical Research Letters,* **32** (L08706). DOI:10.1029/2004GL022014.

Reimer, P.J., Bard, E., Bayliss, A., Beck, J.W., Blackwell, P.G., Bronk Ramsey, C., Buck, C.E., Edwards, R.L., Friedrich, M., Grootes, P.M., Guilderson, T.P., Haflidason, H., Hajdas, I., Hatté, C., Heaton, T.J., Hoffmann, D.L., Hogg, A.G., Hughen, K.A., Kaiser, K.F., Kromer, B., Manning, S.W., Niu, M., Reimer, R.W., Richards, D.A., Scott, E.M., Southon, J.R., Turney, C.S.M., van der Plicht, J. (2013). IntCal13 and Marine13 radiocarbon age calibration curves, 0-50,000 years cal BP. *Radiocarbon,* **55**, 1869 – 1887.

Ricketts, R.D., Johnson, T.C. (1996). Climate change in the Turkana basin as deduced from a 4000 year long d18O record. *Earth and Planetary Science Letters,* **142**, 7–17.

Roberts N. (1998). The Holocene: An Environmental History. 2nd Edition, Blackwell publishing, 316 pp.

Rommerskirchen, F., Eglinton, G., Dupont, L., Gunter, U., Wenzel, C., Rullkötter, J. (2003). A north to south transect of Holocene southeast Atlantic continental margin sediments: relationships between aerosol transport and compound-specific $\delta^{13}C$ land plant biomarker and pollen records. *Geochemistry Geophysics Geosystems,* **4**, 1 – 29.

Rucina, S.M., Muiruri, V.M., Kinyanjui, R.N., McGuiness, K., Marchant, R. (2009). Late Quaternary vegetation and fire dynamics on Mount Kenya. *Palaeogeography, Palaeoclimatology, Palaeoecology*, **283** (1-2), 1–14.

Rucina, S.M., Muiruri, V.M., Downton, L., Marchant, R. (2010). Late-Holocene savanna dynamics in the Amboseli Basin, Kenya. *The Holocene*, **20** (5), 667 – 677.

Russell, J.M., Johnson, T.C. (2005). A high-resolution geochemical record from Lake Edward, Uganda Congo and the timing and causes of tropical African drought during the late Holocene. *Quaternary Science Reviews*, **24** (12-13), 1375 – 1389.

Russell, J.M., Verschuren, D., Eggermont, H. (2007). Spatial complexity of 'Little Ice Age' climate in East Africa: sedimentary records from two crater lake basins in western Uganda. *Holocene,* **17**, 183 – 193, https://doi.org/10.1177/ 0959683607075832.

Russell, J.M., McCoy, S.J., Verschuren, D., Bessems, I., Huang, Y. (2009). Human impacts, climate change, and aquatic ecosystem response during the past 2000 yr. at Lake Wandakara, Uganda. *Quaternary Research*, **72** (3), 315–324.

Sachs, J.P., Pahnke, K., Smittenberg, R., Zhang, Z. (2013). Biomarker indicators of past climate. In: *Elias, S.A. (Ed.), The Encyclopaedia of Quaternary Science*. Elsevier, Amsterdam, pp. 775-782.

Schouten, S., Hopmans, E.C., Schefuß, E., Sinninghe Damste, J.S. (2002). Distributional variations in marine crenarchaeotal membrane lipids: a new tool for reconstructing ancient sea water temperatures? *Earth and Planetary Science Letters* 204, 265 – 274.

Schouten, S., Forster, A., Panoto, F.E., Sinninghe Damsté, J.S. (2007). Palaeothermometer for tropical sea surface temperatures in ancient greenhouse worlds. *Organic Geochemistry*, **38**, 1537 – 1546.

Schouten, S., Hopmans, E.C., Sinninghe Damsté, J.S. (2013). The organic geochemistry of glycerol dialkyl glycerol tetraethers: a review. *Organic Geochemistry,* **54**, 19-61.

Schwark, L., Zink, K., Lechterbeck, J. (2002). Reconstruction of postglacial to early Holocene vegetation history in terrestrial Central Europe via cuticular lipid biomarkers and pollen records from lake sediments. *Geology* 30:463–466.

Shackleton (1946). Geology of the country between Nanyuki and Maralal. *Geological Survey of Kenya,* Rep. 11, Nairobi.

Shanahan, T.M., Overpeck, J.T., Anchukaitis, K.J., Beck, J.W., Cole, J.E., Dettman, D.L., Peck, J.A., Scholz, C.A., King, J.W. (2009). Atlantic forcing of persistent drought in West Africa. *Science,* **324**, 377–380.

Sinninghe Damsté, J. S., Hopmans, E. C., Pancost, R. D., Schouten, S., Geenevasen, J. A. J. (2000). Newly discovered non-isoprenoid glycerol dialkyl glycerol tetraether lipids in sediments. *Chemical Communications*, **17**, 1683 – 1684. DOI:10.1039/B004517I.

Sinninghe Damsté, J.S., Ossebaar, J., Schouten, S., Verschuren, D. (2008). Altitudinal shifts in the branched tetraether lipid distribution in soil from Mt. Kilimanjaro (Tanzania): Implications for the MBT/CBT continental palaeothermometer. *Organic Geochemistry*, **39**, 1072-1076.

Sinninghe Damsté, J. S., Ossebaar, J., Abbas, B., Schouten, S., Verschuren, D. (2009). Fluxes and distribution of tetraether lipids in an equatorial African lake: Constraints on the application of the TEX86 palaeothermometer and BIT index in lacustrine settings. *Geochimica et Cosmochimica Acta*, **73** (14), 4232 – 4249, DOI:10.1016/j.gca.2009.04.022.

Sinninghe Damste, J.S., Ossebaar, J., Schouten, S., Verschuren, D. (2012). Distribution of tetraether lipids in the 25-ka sedimentary record of Lake Challa: extracting reliable TEX_{86} and MBT/CBT palaeotemperatures from an equatorial African lake. *Quaternary Science Reviews,* **50**, 43-54. https://doi.org/10.1016/j.quascirev.2012.07.001.

Smol, J.P., Birks, H.J.B., Last, W.M., (eds.) (2001). Using biology to study long-term environmental change. In: *Tracking Environmental Change Using Lake Sediments, Volume 3: Terrestrial, Algal, and Siliceous Indicators, 1-3,* Kluwer Academic Publishers, Dordrecht, The Netherlands.

Sojinu, O.S., Sonibare, O.O., Ekundayo, O.O., Zeng, E.Y. (2012). Assessment of organochlorine pesticides residues in higher plants from oil exploration areas of Niger Delta, Nigeria. *Science of the Total Environment*, **433,** 169 - 177, https://doi.org/10.1016/j.scitotenv.2012.06.043.

Speck, H., (1982). Soils of the Mount Kenya area, their formation ecological, and agricultural significance. *Mountain Research and Development,* **2** (2), 201 - 221.

Ssemmanda, I., Vincens, A. (1993). Végétation et climate dans le Bassin du lac Albert (Ouganda, Zaïre) depuis 13,000 ans BP. *Apport de la Palynologie. C. R.,* Acad. Sci. Paris, **316** (2), 561 **–** 567.

Ssemmanda I., Ryves D.B., Bennike O., Appleby P.G. (2005). Vegetation history in west Uganda during the last 1200 years: a sediment-based reconstruction from two crater lakes. *The Holocene,* **15**, 119 – 132.

Stager, J.C., Mayewski, P.A., Meeker, L.D. (2002). Cooling cycles, Heinrich event 1, and the desiccation of Lake Victoria. *Palaeogeography, Palaeoclimatology, Palaeoecology,* **183**, 169 - 178.

Stager, J. C., Ryves, D., Cumming, B.F., Meeker, L.D., Beer, J. (2005). Solar variability and the levels of Lake Victoria, East Africa, during the last millennium. *Journal of Palaeolimnology,* **33**, 243 - 251.

Stager, J.C., Johnson, T.C. (2008). The Late Pleistocene desiccation of Lake Victoria and the origin of its endemic fauna. *Hydrobiologia,* **596**, 5 - 16.

Stager, J., Cocquyt, C., Bonnefille, R., Weyhenmeyer, C., Bowerman, N. (2009). A late Holocene paleoclimatic history of Lake Tanganyika, East Africa. *Quaternary Research,* **72**(1), 47-56. doi:10.1016/j.yqres.2009.04.003.

Street, F.A. and Grove, A.T. (1976). Environmental and climatic implications of late Quaternary lake-level fluctuations in Africa. *Nature*, **261**, 385 **–** 390.

Street-Perrott F.A., Perrott R.A. (1990). Abrupt climate fluctuations in the tropics: the influence of Atlantic Ocean Circulation. *Nature*, **343** (6259), 607 – 612.

Street-Perrott F.A., Perrott R.A. (1993). Holocene vegetation, lake levels and climate of Africa. *In: Wright HE, Kutzbach JE, Webb T III, Ruddiman WF, Street-Perrott FA, Bartlein PJ (eds) Global climates since the last glacial maximum*. University of Minnesota Press, Minneapolis, 318 – 356.

Street-Perrott, F.A., Huang, Y., Perrott, R.A., Eglinton, G., Barker, P., Khelifa, L.B., Harkness, D.D., Ivanovich, M., Olago, D.O. (1997). Impact of lower atmospheric CO_2 on tropical mountain ecosystems: carbon-isotope evidence. *Science*, **278**, 1422 - 1426.

Street-Perrott, F.A., Ficken, K.J., Huang, Y., Eglinton, G. (2004). Late Quaternary changes in carbon cycling on Mt. Kenya, East Africa: an overview of the δ13C record in lacustrine organic matter. *Quaternary Science Reviews*, **23** (7-8), 861 – 879.

Street-Perrott, F.A., Barker, P.A., Swain, D.L., Ficken, K.J., Wooller, M.J., Olago, D.O., Huang, Y. (2007). Late Quaternary changes in ecosystems and carbon cycling on Mt. Kenya, East Africa: a landscape-ecological perspective based on multi-proxy lake-sediment influxes. *Quaternary Science Reviews*, **26** (13-14), 1838 – 1860.

Street-Perrott, F.A., Barker, P.A., Leng, M.J., Sloane, H.J., Wooller, M.J., Ficken, K.J. Swain, D.L. (2008). Towards an understanding of late Quaternary variations in the continental biogeochemical cycle of silicon: multi-isotope and sediment-flux data for Lake Rutundu, Mt Kenya, East Africa, since 38 ka BP. *Journal of Quaternary Science*, **23** (4), 375–380.

Stoof-Leichsenring, K.R., Junginger, A., Olaka, L.A., Tiedemann, R., Trauth, M.H. (2011). Environmental variability in Lake Naivasha, Kenya, over the last two centuries. *Journal of Paleolimnology*, **45** (3), 353 – 367.

Talbot, M.R., Livingston, D.A. (1989). Hydrogen index and carbon isotopes of lacustrine organic matter as lake-level indicators. *Palaeogeography, Palaeoclimatology, Palaeoecology,* **70**, 121–137.

Talbot, M.R., Brendeland, K.I. (2001). Strontium isotopes as palaeohydrological tracers in the White Nile headwater lakes, East Africa. In: *AGU Fall Meeting Abstracts*, **1**, 05.

Taylor, D. (1990). Late Quaternary pollen diagrams from two Ugandan mires: evidence for environmental change in the Rukiga Highlands of southwest Uganda. *Palaeogeography, Palaeoclimatology, Palaeoecology,* **80**, 283 - 300.

Taylor, D., Marchant, R., Robertshaw, P. (1999). Late Glacial-Holocene history of lowland rain forest in central Africa: a record from Kabata Swamp, Ndale volcanic field, Uganda. *Journal of Ecology,* **87**, 303 - 315.

Thompson, B.W. (1965). The climate of Africa. Oxford University Press, Nairobi, 132 pp.

Thompson, R., Oldfield, F. (1986). Environmental Magnetism. Springer, Dordrecht, 277 pp.

Thompson, L.G., Mosley-Thompson, E., Davis, M.E., Henderson, K.A., Brecher, H.H., Zagorodnov, V.S., Mashiotta, T.A., Lin, P-N., Mikhalenko, V.N., Hardy, D., Beer, J. (2002). Kilimanjaro Ice Core Records: Evidence of Holocene Climate Change in Tropical Africa. *Science*, **298** (5593), 589 – 593.

Tierney, J. E., Russell, J. M. and Huang, Y., Sinninghe Damsté, J. S., Hopmans, E. C., Cohen, A.S. (2008). Northern Hemisphere controls on tropical southeast African Climate during the past 60,000 years. Science, **322**, 252 – 255.

Tierney, J.E., Russell, J.M. (2009). Distributions of branched GDGTs in a tropical lake system: Implications for lacustrine application of the MBT/CBT paleoproxy. *Organic Geochemistry*, **40** (9), 1032–1036.

Tierney, J. E., Russell, J. M., Eggermont, H., Hopmans, E. C., Verschuren, D., Damsté, J. S. S. (2010). Environmental controls on branched tetraether lipid distributions in tropical East African lake sediments, *Geochimica et Cosmochimica Acta,* **74** (17), 4902–18, DOI: 10.1016/j.gca.2010.06.002.

Tierney, J. E., Russell, J. M., Huang, Y. (2010b). A molecular perspective on Late Quaternary climate and vegetation change in the Lake Tanganyika basin, East Africa. *Quaternary Science Reviews*, **29** (5–6), 787 – 800, DOI:10.1016/j.quascirev.2009.11.030.

Tierney, J.E., Russell, J.M., Damsté, J.S.S., Huang, Y., Verschuren, D. (2011). Late Quaternary behaviour of the East African monsoon and the importance of the Congo Air Boundary. *Quaternary Science Reviews*, **30** (7-8), 798 – 807.

Tierney, J. E. (2012). GDGT Thermometry: Lipid tools for reconstructing paleotemperatures. *In: Reconstructing Earth's Deep Time Climate. The Paleontological Society Papers*. **18**, 115 – 131.

Tierney, J.E., Smerdon, J.E., Anchukaitis, K.J., Seager, R. (2013). Multidecadal variability in East African hydroclimate controlled by the Indian Ocean. *Nature*, **493** (7432), 389 – 392.

Tieszen, L.L., Senyimba, M.M., Imbamba, S.K., Troughton J.H., (1979). The distribution of C_3 and C_4 grasses and carbon isotope discrimination along an altitudinal and moisture gradient in Kenya. *Oecologia*, **37** (3), 337 – 350.

Trauth, M.H., Maslin, M.A., Deino, A.L., Strecker, M.R., Bergner, A.G.N., Dühnforth, M. (2007). High- and low-latitude forcing of Plio-Pleistocene East African climate and human evolution. *Journal of Human Evolution*, **53** (5), 475 – 486.

Tyson, R.V., 1995. Sedimentary Organic Matter: Organic Facies and Palynofacies. Chapman & Hall, London.

Veldkamp, A., Buis, E., Wijbrans, J.R., Olago, D.O., Boshoven, E.H., Marée, M., van den Berg van Saparoea, R.M. (2007). Late Cenozoic fluvial dynamics of the River Tana, Kenya, an uplift dominated record. *Quaternary Science Reviews,* **26**, 2897 – 2912.

Veldkamp, A., Schoorl, J.M., Wijbrans, J.R., Claessens, L., (2012). Mount Kenya volcanic activity and the Late Cenozoic landscape reorganisation in the upper Tana fluvial system. *Geomorphology*, **145-146**, 19 – 31, doi:10.1016/j.geomorph.2011.10.026

Verschuren, D. (2003). Lake-based climate reconstruction in Africa: progress and challenges. In *Aquatic Biodiversity*. **500** (1-3), 315 – 330. http://doi.org/10.1007/978-94-007-1084-9_22.

Verschuren, D. (2004). Decadal and century-scale climate variability in tropical Africa during the past 2000 years. In *Past Climate Variability through Europe and Africa*. **6**, 139 – 158, http://doi.org/10.1007/978-1-4020-2121-3_8.

Verschuren, D. (2001). Reconstructing fluctuations of a shallow East African lake during the past 1800yrs from sediment stratigraphy in a submerged crater basin. *Journal of Paleolimnology.* **25**, 297-311.

Verschuren, D., Laird, K. R., Cumming, B. F. (2000). Rainfall and drought in equatorial east Africa during the past 1,100 years. *Nature*, **403** (6768), 410 – 414.

Verschuren, D., Charman, D.J. (2008). Latitudinal Linkages in Late Holocene Moisture-Balance Variation. In: R.W. Battarbee & H.A. Binney (Eds.) *Natural Climate Variability and Global Warming: A Holocene Perspective*. Blackwell Publishing, pp 189-231.

Verschuren, D., Damsté, J.S.S., Moernaut, J., Kristen, I., Blaauw, M., Fagot, M., Haug, G.H.,

Members, C.P. (2009). Half-precessional dynamics of monsoon rainfall near the East African Equator. *Nature*, **462** (7273), 637 – 641.

Vincens, A., Garcin, Y., Buchet, G. (2007). Influence of rainfall seasonality on African lowland vegetation during the Late Quaternary: pollen evidence from Lake Masoko, Tanzania. *Journal of Biogeography*, **34** (7), 1274 – 1288.

Vincens, A. (1986). Diagramme pollinique d'un sondage Pleistocene superieur-Holocene du Lac Bogoria (Kenya). *Review of Paleobotany and Palynology,* **47** (1–2), (169–179 and 183–192).

Wang Y-H, Yang H, Chen X, Zhang J-X, Ou J, Xie B, Huang C-C (2013). Molecular biomarkers for sources of organic matter in lacustrine sediments in a subtropical lake in China. *Journal of Environmental Pollution*, **176**, 284–291.

Wanner, H., Solomina, O., Grosjean, M., Ritz, S.P., Jetel, M. (2011). Structure and origin of Holocene cold events. *Quaternary Science Reviews*, **30**, 3109– 3123.

Weijers, J.W.H., Schouten, S., Spaargaren, O.C. and Sinninghe Damsté, J.S. (2006). Occurrence and distribution of tetraether membrane lipids in soils: Implications for the use of the TEX86 proxy and the BIT index. *Organic Geochemistry*, **37** (12) 1680 – 1693, DOI:10.1016/j.orggeochem.2006.07.018.

Weijers, J.W.H., Schouten, S., Van den Donker, J.C., Hopmans, E.C., Sinninghe Damsté, J.S. (2007). Environmental controls on bacterial tetraether membrane lipid distribution in soils. *Geochimica et Cosmochimica Acta,* **71** (3) 703 – 713, DOI:10.1016/j.gca.2006.10.003.

Weijers, J. W. H., Steinmann, P., Hopmans, E. C., Schouten, S., Sinninghe Damsté, J.S. (2011). Bacterial tetraether membrane lipids in peat and coal: Testing the MBT-CBT temperature proxy for climate reconstruction. *Organic Geochemistry*, **42** (5) 477 – 486, DOI:10.1016/j.orggeochem.2011.03.013.

Williamson, D., Jackson, M.J., Banerjee, S.K., Marvin, J., Merdaci, O., Thouveny, N., Decobert, M., Gibert-Massault, E., Massault, M., Mazaudier, D., Taieb, M. (1999). Magnetic signatures of hydrological change in a tropical Maar-lake (Lake Massoko, Tanzania): preliminary results. *Physics and Chemistry of the Earth Part a—Solid Earth and Geodesy*, **24**, 799 – 803.

Woltering, M., Atahan, P., Grice, K., Heijnis, H., Taffs, K., Dodson, J. 2014. Glacial and Holocene terrestrial temperature variability in subtropical east Australia as inferred from branched GDGT distributions in a sediment core from Lake McKenzie. *Quaternary Research*, **82** (1), 132 – 145, DOI:10.1016/j.yqres.2014.02.005.

Wooller, M., Street-Perrott, F.A., Agnew, A.D.Q. (2000). Late Quaternary fires and grassland paleoecology of Mount Kenya, East Africa: evidence from charred grass cuticles in Lake sediments. *Palaeogeography, Palaeoclimatology, Palaeoecology,* **164**, 207 – 230.

Wooller, M.J., Agnew, A.D.Q. (2002). Changes in graminoid stomatal morphology over the last glacial/interglacial transition: evidence from Mount Kenya, East Africa. *Palaeogeography, Palaeoclimatology, Palaeoecology*, **177**, 123 – 136.

Wooller, M.J., Swain, D.L., Ficken, K.J., Agnew, A.D.Q., Street-Perrott, F.A., Eglinton, G. (2003). Late Quaternary vegetation changes around Lake Rutundu, Mount Kenya, East Africa: evidence from grass cuticles, pollen and stable carbon isotopes. *Journal of Quaternary Science*, **18** (1), 3 – 15.

WRI (2007). World Resource Institute; Department of Resource and Remote Sensing, Ministry of Environment and Natural Resources Kenya; Central Bureau of Statistics, Ministry of Planning and National Development Kenya; and International Livestock Research Institute. Nature's Benefits in Kenya, An Atlas of Ecosystems and Human Well-Being. Washington DC and Nairobi, 148pp.

Wu, X., Dong, H., Zhang, C. L., Liu, X., Hou, W., Zhang, J., Jiang, H. (2013). Evaluation of glycerol dialkyl glycerol tetraether proxies for reconstruction of the paleo- environment on the Qinghai-Tibetan Plateau. *Organic Geochemistry*, **61**, 45 – 56, DOI:10.1016/j.orggeochem.2013.06.002.

Yang, G., Zhang, C. L., Xie, S., Chen, Z., Gao, M., Ge. Z., Yang, Z. (2013). Microbial glycerol dialkyl glycerol tetraethers from river water and soil near the Three Gorges Dam on the Yangtze River. *Organic Geochemistry*, **56**, 40 – 50. DOI:10.1016/j.orggeochem.2012.11.014

Zink, K. G., Vandergoes, M. J., Mangelsdorf, K., Dieffenbacher-Krall, A. C., Schwark, L. (2010). Application of bacterial glycerol dialkyl glycerol tetraethers (GDGTs) to develop modern and past temperature estimates from New Zealand lakes. *Organic Geochemistry*, **41** (9), 1060–1066, DOI:10.1016/j.orggeochem.2010.03.004.

7 APPENDIX

A. APPENDIX

A.1 Soil samples dataset

A.1.1 Nkunga area surface soils samples

Table A-1: Percentage of detected minerals from XRD measurements (%)

Sample	Illite/Muscov	Halloysite	Gibbsite	Hematite	Quartz	Feld-plag	Diopside
NK11-01	0	4	2	16	8	64	6
NK11-02	0	7	2	18	8	54	11
NK11-04	0	0	0	0	0	90	9
NK11-05	0	10	3	19	7	54	7
NK11-07	0	12	4	21	12	47	5
NK11-13	0	0	0	17	0	71	12
NK11-21	**2**	0	0	1	0	76	22
NK11-22	0	0	0	0	0	90	10

Table A-2: Magnetic Susceptibility measurements from Nkunga area (SI)

Sample	Weight (g)	F1	F3
NK11-7	6.0639	1.25E-03	1.19E-03
NK11-10	6.1628	6.62E-03	6.10E-03
NK11-14	5.9336	1.03E-02	9.61E-03
NK11-20	6.7948	1.45E-02	1.33E-02

Table A-3: Carbon and Nitrogen values from surface samples Nkunga area

Sample	%N	%C	$\delta^{15}N$ (‰)	$\delta^{13}C$ (‰)
NK11-1	0.56	5.84	6.01	-22.49
NK11-7	1.29	11.70	5.00	-20.51
NK11-22	0.23	3.23	2.95	-26.19
NKS11-1	0.44	4.99	7.78	-17.10
NKS11-2	0.30	3.63	8.08	-18.77
NKS11-5	0.32	3.84	8.60	-18.99
NKS11-6	0.17	2.37	10.17	-14.94
NKS11-7	0.30	3.63	8.13	-18.73

A.1.2 Nkunga area soil profile samples

Table A-4: Mineralogy from Nkunga area soil profile from XRD measurements (%)

Sample	Illite/Muscov	Halloysite	Gibbsite	Magnetite	Hematite	Quartz	Feld-plag	diopside
NK11-23	0	18	9	11	31	17	13	0
NK11-24	0	21	10	13	28	16	12	0
NK11-26	0	16	9	16	28	14	17	0
NK11-28	0	16	6	13	22	18	25	0
NK11-30	0	18	7	8	33	17	17	0
NK11-32	0	18	7	10	32	14	19	0
NK11-34	0	19	8	10	26	21	17	0
NK11-37	0	20	12	10	26	15	16	0

Table A-5: Low (F1) and High (F3) frequency Magnetic Susceptibility (SI); Carbon, Nitrogen and their respective isotopes

		Magnetic Susceptibility (SI)				Organic Chemistry			
Depth (cm)	**weight (g)**	**F1**	**F3**	**Depth (cm)**	**Weight (mg)**	**%N**	**%C**	**$\delta^{15}N$ (‰)**	**$\delta^{13}C$ (‰)**
9	7.35	1.63E-02	1.51E-02	**0**	15.05	0.34	4.08	7.98	-18.71
27	5.88	1.71E-02	1.58E-02	**9**	16.60	0.39	4.43	8.00	-18.87
63	6.27	1.71E-02	1.58E-02	**27**	17.14	0.44	4.84	8.05	-19.32
81	5.86	1.83E-02	1.69E-02	**45**	15.05	0.40	4.67	7.77	-18.49
99	5.32	1.84E-02	1.71E-02	**63**	20.31	0.41	4.57	7.68	-18.80
126	6.58	1.63E-02	1.50E-02	**81**	15.79	0.28	3.44	9.47	-17.64
				99	18.36	0.35	4.05	8.30	-17.87
				125	19.55	0.21	3.21	9.80	-15.74

Table A-6: Inorganic geochemistry (XRF) from Nkunga soil profile (cps)

	Depth (cm)				
Elements	**0**	**45**	**81**	**99**	**125**
Al	16232	19302	21662	20120	22253
Ca	8934562	2662113	2212068	2536605	1832975
Cl	2826	4325	4326	6293	4316
Cu	14135	11552	11251	11607	10073
Fe	7792233	9466555	10248762	10398578	10159762
K	831083	599981	589201	599304	620788
Mn	207901	268722	285035	267897	242951
Nb	7756	21897	23127	23861	24363
Ni	17783	10397	11896	10878	11617
P	7543	13935	14246	14231	12836
Rb	9374	17855	17659	17223	17752
S	3296	4196	2798	3441	1009
Si	225245	252413	237839	233972	239097
Sr	219199	64774	57679	60954	51270
Ti	7021436	9428723	10453845	10915615	10417182
Zr	50954	103298	109092	106170	108987
Zn	14755	26903	23398	25118	22480

Table A-7: n-alkane measurements from Nkunga area soil profile (signal intensity cps)

No. of Carbons	Depth (cm)			
	0	**9**	**45**	**125**
12	0	0	0	0
13	0	0	0	0
14	0	292300	298681	708928
15	1185376	876927	456044	955891
16	1397094	2415467	2128582	842684
17	2313689	3491274	2358471	469811
18	1296332	2487073	2286616	1512158
19	806998	1105109	690128	922361
20	1864269	2313156	2937162	1162436
21	2721333	1772079	2332023	1337141
22	1274271	1771851	2600332	530137
23	3832953	2166312	3475779	1701244
24	1110692	800727	1216438	563630
25	5356088	3529253	4345325	1814984
26	1351624	965164	1350202	336663
27	11892770	4505438	5732075	2108223
28	2127752	761433	1219042	234692
29	30267175	7866816	10565830	2905277
30	2305644	701645	1324856	115031
31	33565312	9113444	16775922	1014338
32	1227779	358958	882247	0
33	8495875	3098104	7493611	0
34	0	0	0	0
35	0	0	0	0

Table A-8: GDGT measurements from the Nkunga soil profile (μg)

GDGT type	Depth (cm)			
	0	9	45	125
brGDGT-Ic	51.00	13.49	7.01	13.13
brGDGT-Ib	238.89	50.03	24.78	42.84
brGDGT-I	531.49	127.86	70.12	193.16
brGDGT-IIc	9.14	4.45	2.03	1.02
brGDGT-IIb	114.29	28.86	11.15	7.74
brGDGT-II	581.42	122.30	53.57	73.38
brGDGT - IIIc	0.00	0.00	0.00	0.00
brGDGT - IIIb	6.59	0.00	0.00	0.00
brGDGT - III	106.80	13.95	8.51	8.77
Crenoarchaeol VI	36.21	34.72	21.39	13.68
Crenoarchaeol VI'	7.33	8.59	3.89	2.93
GDGT-4	0.00	0.00	0.00	0.00
GDGT-3	5.37	0.00	4.10	3.95
GDGT-2	20.73	6.82	5.04	4.01
GDGT-1	12.64	4.00	3.87	2.73
GDGT-0	253.42	11.17	8.86	4.24

A.1.3 Sacred Lake soil profile samples

Table A-9: Mineralogy from Sacred Lake soil profile from XRD measurements (%)

Sample	Minerals							
	Illite/Muscov	Halloysite	Gibbsite	Magnetite	Hematite	Quartz	Feld-plag	Diopside
SL11-02	0	4	3	0	0	6	87	0
SL11-03	0	1	4	0	0	9	85	0
SL11-05	1	2	4	0	0	8	85	0
SL11-08	2	1	4	0	0	5	87	0
SL11-11	1	1	3	0	0	6	88	0
SL11-14	2	1	4	0	0	4	90	0
SL11-17	1	0	1	0	0	1	97	0
SL11-18	1	0	1	0	0	1	97	0
SL11-20	6	0	2	0	0	8	84	0
SL11-22	3	1	2	0	0	9	84	0
SL11-24	1	1	2	0	0	6	90	0
SL11-25	1	1	3	0	0	4	91	0
SL11-29	3	3	18	1	4	24	48	0
SL11-34	1	2	3	0	0	30	64	0

Table A-10: Inorganic geochemistry (XRF) from Sacred Lake soil profile (cps)

Elements	Depth (cm)						
	8	32	80	136	168	192	224
Al	27517	26913	29226	32724	33333	33778	31794
Ca	2396996	2407760	1066624	672566	297217	332848	161071
Cl	1234	1474	899	1	735	601	3100
Cu	6621	6819	4589	2738	4555	4391	6142
Fe	6507488	6549229	6557148	4507567	7336953	7296637	10749736
K	1951397	1960266	2134799	3294896	1762321	1900783	859372
Mn	314438	322801	276669	179223	216423	242975	294974
Nb	63244	63645	69326	65399	68485	66538	52700
Ni	4225	4017	3766	149	4500	4280	9568
P	9062	8492	7191	1407	3118	3483	4138
Rb	26773	26675	26775	19948	23675	21541	17756
S	9870	9801	4631	1198	5153	4603	1702
Si	195187	196135	204862	272364	214239	211617	158114
Sr	70874	72071	43393	53023	23470	18176	10922
Ti	3216024	3223741	2999999	1402808	3567712	3603857	7578433
Zr	283883	283688	317338	320871	299067	310410	228252
Zn	39248	39769	31820	38803	31386	25205	19667

Table A-11: Low (F1) and High (F3) frequency Magnetic Susceptibility (SI); Carbon, Nitrogen and their respective isotopes

		Magnetic susceptibility (SI)			Organic Chemistry			
Depth (cm)	**Weight (g)**	**F1**	**F3**	**Depth (cm)**	**%N**	**%C**	**$\delta^{15}N$ (‰)**	**$\delta^{13}C$ (‰)**
0	4.29	3.14E-03	2.83E-03	**8**	5.72	-22.12	0.82	8.31
16	6.04	5.85E-03	5.30E-03	**16**	6.09	-21.90	0.79	7.17
32	7.15	6.42E-03	5.82E-03	**32**	6.70	-20.34	0.62	5.44
56	6.85	6.86E-03	6.19E-03	**56**	7.36	-17.05	0.42	4.13
80	7.56	6.62E-03	5.97E-03	**80**	7.04	-17.78	0.39	4.00
136	7.46	6.92E-03	6.63E-03	**104**	6.54	-18.56	0.31	3.53
144	7.83	7.98E-03	7.67E-03	**128**	5.02	-19.38	0.08	0.95
160	8.06	7.23E-03	6.64E-03	**136**	3.97	-19.61	0.06	0.58
176	7.82	9.20E-03	8.34E-03	**152**	4.51	-19.12	0.14	1.36
192	7.75	7.92E-03	7.24E-03	**168**	5.21	-19.02	0.18	2.01
200	3.73	7.44E-03	6.84E-03	**184**	5.41	-29.66	0.15	1.66
224	5.68	1.42E-02	1.28E-02	**192**	5.03	-19.34	0.16	1.90
				224	5.53	-18.73	0.18	1.95

Table A-12: n-alkane measurements from Sacred Lake profile (signal intensity cps)

No. of carbons	**Depth (cm)**			
	8	**104**	**224**	**0**
12	0	0	0	0
13	0	0	0	0
14	504085	261600	0	0
15	909446	193899	0	365898
16	3359904	684844	423190	1125273
17	3698789	855161	972841	1005778
18	3952082	1193108	1294058	1207937
19	1385082	391867	251503	551074
20	2768238	1229621	885599	1010614
21	2007620	1361912	316100	2435840
22	1403377	799534	540426	914531
23	3141239	2298898	317819	8444753
24	1045406	837248	115363	753681
25	3044438	2708968	357488	4540114
26	1004545	812944	136045	1212641
27	5212695	4310212	917724	8530503
28	1207437	731250	165184	1675549
29	20984670	7089868	1812641	18334037
30	1011938	377275	76417	1976071
31	9144525	5099612	1067713	17078263
32	290983	108841	34231	1293177
33	1737469	1046328	146908	7201764
34	0	0	0	0
35	0	0	0	0

Table A-13: GDGT measurements from Sacred Lake soil profile (µg)

	Depth (cm)			
GDGT type	**8**	**104**	**224**	**0**
brGDGT-Ic	61.43	23.93	8.52	38.77
brGDGT-Ib	222.89	56.62	17.91	249.32
brGDGT-I	344.57	201.28	150.11	311.98
brGDGT-IIc	9.48	5.33	3.36	17.11
brGDGT-IIb	109.97	22.55	1.99	220.95
brGDGT-II	400.73	102.65	21.64	610.90
brGDGT - IIIc	0.00	1.86	0.00	0.00
brGDGT - IIIb	0.00	1.77	0.00	29.10
brGDGT - III	97.70	19.43	6.10	206.24
Crenoarchaeol VI	35.57	7.16	1.98	61.35
Crenoarchaeol VI'	6.14	1.19	0.08	8.68
GDGT-4	0.00	0.00	0.00	0.00
GDGT-3	0.00	16.40	8.81	0.00
GDGT-2	13.51	25.68	10.44	0.00

GDGT-1	0.00	29.88	8.29	0.00
GDGT-0	8.78	33.68	8.94	11.23

A.2 Sediment dataset

A.2.1 Lake Nkunga sediment measurements

Table A-14: Mineralogy XRD measurements (%)

Depth (cm)	Chlorite	Illite/Muscov	Halloysite	Gibbsite	Magnetite	Hematite	Quartz	Feld-plag	diopside
1	0	2	16	1	0	9	9	62	0
13	0	0	18	2	0	8	10	54	8
25	0	1	24	1	0	9	7	51	7
37	0	0	12	1	0	7	5	69	6
44	0	0	21	3	0	7	9	48	12
59	0	1	22	2	0	8	5	58	3
63	0	0	24	2	0	9	11	47	7
71	0	0	18	2	0	7	9	56	8
77	0	1	17	2	0	7	4	62	7
86	0	1	12	2	2	4	6	67	6

Table A-15: Low (F1) and High (F3) frequency Magnetic Susceptibility (SI); Carbon, Nitrogen and their respective isotopes

Magnetic Susceptibility (SI)					Organic Chemistry Parameter			
Depth (cm)	**wt sample (g)**	**F1**	**F3**	**Depth (cm)**	**$\delta^{15}N$ (‰)**	**$\delta^{13}C$ (‰)**	**%N**	**%C**
1	0.4284	7.47E-05	7.16E-05	**1**	4.77	-18.11	0.57	7.11
2	0.4897	1.15E-04	1.11E-04	**2**	5.55	-18.19	0.38	4.65
3	0.5043	1.64E-04	1.58E-04	**3**	6.03	-18.22	0.37	4.8
4	0.4377	1.27E-04	1.22E-04	**4**	5.47	-18.05	0.41	5.02
5	0.5727	1.77E-04	1.71E-04	**5**	5.01	-18.26	0.38	4.62
6	0.4676	1.35E-04	1.30E-04	**6**	5.66	-18.24	0.6	4.57
7	0.4292	1.14E-04	1.11E-04	**7**	5.29	-18.33	0.41	5.16
8	0.5757	1.61E-04	1.56E-04	**8**	5.1	-18.36	0.38	4.64
9	0.5225	1.15E-04	1.12E-04	**9**	6.2	-18.17	0.41	4.97
10	0.504	1.17E-04	1.13E-04	**10**	5.85	-18.2	0.39	4.66
11	0.5213	1.63E-04	1.57E-04	**11**	5.98	-18.36	0.4	4.96
12	0.5201	1.42E-04	1.37E-04	**12**	5.46	-18.47	0.4	4.86
13	0.4689	2.84E-04	2.67E-04	**13**	6.22	-17.94	0.42	4.98
14	0.6348	1.62E-04	1.58E-04	**14**	5.59	-24.28	0.45	5.43
15	0.6163	1.64E-04	1.60E-04	**15**	6.07	-18.23	0.44	5.3
16	0.5183	1.45E-04	1.39E-04	**16**	5.56	-18.31	0.48	5.74
17	0.5654	1.56E-04	1.51E-04	**17**	5.71	-18.45	0.49	5.97
18	0.4781	1.06E-04	1.03E-04	**18**	5.75	-18.64	0.51	6.28
19	0.5351	1.57E-04	1.52E-04	**19**	6.26	-18.15	0.5	6.06
20	0.5513	1.72E-04	1.67E-04	**20**	6.9	-18.51	0.51	6.22
21	0.4544	1.50E-04	1.44E-04	**21**	5.73	-18.62	0.48	5.91
22	0.5028	1.46E-04	1.41E-04	**22**	6.92	-18.78	0.43	5.17
23	0.6633	2.18E-04	2.10E-04	**23**	6.55	-18.63	0.48	5.85
24	0.5201	1.68E-04	1.62E-04	**24**	5.9	-18.76	0.41	4.95
25	0.6738	2.33E-04	2.25E-04	**25**	6.9	-18.84	0.47	5.71
26	0.5049	1.61E-04	1.56E-04	**26**	5.2	-18.54	0.49	5.95
27	0.4349	1.39E-04	1.34E-04	**27**	6.45	-18.36	0.49	6.05
28	0.5382	1.77E-04	1.71E-04	**28**	5.31	-18.42	0.5	6.21
29	0.5109	1.69E-04	1.64E-04	**29**	5.74	-18.44	0.52	6.37
30	0.5681	1.78E-04	1.73E-04	**30**	5.57	-18.5	0.51	6.36
31	0.5451	1.80E-04	1.74E-04	**31**	5.75	-18.2	0.52	6.33
32	0.5968	2.11E-04	2.05E-04	**32**	6.08	-18.48	0.47	5.89
33	0.5422	1.78E-04	1.72E-04	**33**	5.41	-18.44	0.48	5.95
34	0.587	2.24E-04	2.14E-04	**34**	5.76	-18.29	0.5	6.11
35	0.4872	1.52E-04	1.47E-04	**35**	5.27	-17.69	0.61	7.83
36	0.4375	1.50E-04	1.45E-04	**36**	5	-17.72	0.61	7.86
37	0.5298	1.51E-04	1.46E-04	**37**	5.06	-18.42	0.53	6.65
38	0.5524	1.62E-04	1.57E-04	**38**	6.06	-18.75	0.52	6.39
39	0.5109	1.59E-04	1.53E-04	**39**	5.58	-19.08	0.57	6.95
40	0.5058	1.75E-04	1.70E-04	**40**	5.6	-19.18	0.5	6.07
41	0.5801	2.07E-04	2.01E-04	**41**	6.53	-19.35	0.47	5.69
42	0.6577	2.02E-04	1.97E-04	**42**	5.94	-19.56	0.49	6.01

43	0.5052	1.64E-04	1.60E-04	**43**	5.66	-19.34	0.5	6.26
44	0.4644	1.39E-04	1.37E-04	**44**	5.73	-19.24	0.5	6.02
45	0.433	1.90E-04	1.81E-04	**45**	5.66	-19.34	0.5	6.1
46	0.5302	1.78E-04	1.71E-04	**46**	6.43	-19.54	0.34	4.25
47	0.5035	1.49E-04	1.44E-04	**47**	6.11	-19.16	0.41	4.94
48	0.4873	1.54E-04	1.48E-04	**48**	6	-19.06	0.43	5.3
49	0.4941	1.76E-04	1.68E-04	**49**	6.3	-19.12	0.38	4.74
50	0.5041	1.95E-04	1.86E-04	**50**	6.55	-19.57	0.39	4.89
51	0.4788	1.95E-04	1.87E-04	**51**	7.16	-19.21	0.38	4.65
52	0.4369	1.85E-04	1.78E-04	**52**	6.13	-21.71	0.36	4.53
53	0.6012	2.46E-04	2.38E-04	**53**	6.63	-19.17	0.36	4.45
54	0.6158	2.60E-04	2.49E-04	**54**	6.13	-19.26	0.36	4.48
55	0.4735	1.87E-04	1.79E-04	**55**	6.06	-19.3	0.36	4.42
56	0.6215	2.68E-04	2.59E-04	**56**	6.54	-19.45	0.36	4.35
57	0.4958	1.95E-04	1.87E-04	**57**	6.11	-19.44	0.36	4.4
58	0.5347	2.14E-04	2.07E-04	**58**	6.01	-19.73	0.3	3.75
59	0.4394	3.17E-04	2.89E-04	**59**	7	-19.31	0.32	3.91
60	0.4794	1.87E-04	1.81E-04	**60**	6.16	-19.71	0.31	4.02
61	0.5015	1.98E-04	1.91E-04	**61**	7.22	-19.74	0.32	3.95
62	0.5388	2.06E-04	1.98E-04	**62**	6.94	-19.81	0.3	3.67
63	0.53	2.11E-04	2.07E-04	**63**	6.35	-19.68	0.28	3.38
64	0.5342	2.13E-04	2.08E-04	**64**	6.58	-19.62	0.27	3.28
65	0.5271	2.14E-04	2.05E-04	**65**	7.04	-19.39	0.23	2.72
66	0.4923	2.38E-04	2.29E-04	**66**	7.23	-19.32	0.19	2.17
67	0.4981	2.44E-04	2.36E-04	**67**	6.98	-19.57	0.2	2.5
68	0.6458	3.22E-04	3.11E-04	**68**	7.14	-19.71	0.22	2.54
69	0.6045	2.95E-04	2.85E-04	**69**	6.69	-19.61	0.2	2.42
70	0.3141	1.48E-04	1.44E-04	**70**	7.69	-19.84	0.23	2.72
71	0.6128	2.79E-04	2.70E-04	**71**	7.96	-19.66	0.23	2.67
72	0.4545	2.07E-04	2.00E-04	**72**	6.39	-19.97	0.24	2.93
73	0.5224	2.57E-04	2.53E-04	**73**	7.27	-19.96	0.24	2.87
74	0.5486	2.60E-04	2.51E-04	**74**	7.48	-19.56	0.24	2.8
75	0.5115	2.34E-04	2.27E-04	**75**	7.01	-19.85	0.24	2.91
76	0.5087	2.80E-04	2.67E-04	**76**	7.77	-20.46	0.25	3.07
77	0.4678	2.49E-04	2.35E-04	**77**	8.01	-20.93	0.24	3.22
78	0.4728	2.80E-04	2.69E-04	**78**	7.31	-21.62	0.19	2.74
79	0.4663	2.81E-04	2.70E-04	**79**	7.94	-19.34	0.13	1.61
80	0.4484	2.73E-04	2.60E-04	**80**	6.79	-18.92	0.12	1.42
81	0.439	2.67E-04	2.62E-04	**81**	6.26	-18.68	0.12	1.4
82	0.3535	2.66E-04	2.59E-04	**82**	6.51	-18.89	0.12	1.41
83	0.4266	2.48E-04	2.41E-04	**83**	5.91	-19.45	0.12	1.55
84	0.4436	2.43E-04	2.35E-04	**84**	6.72	-18.85	0.13	1.44
85	0.533	4.27E-04	4.12E-04	**85**	6.91	-18.42	0.11	1.43
86	0.4918	2.97E-04	2.87E-04	**86**	6.5	-18.84	0.11	1.28
87	0.371	2.40E-04	2.31E-04	**87**	7.49	-18.84	0.12	1.36
88	-	-	-	**88**	6.36	-18.94	0.12	1.45
89	-	-	-	**89**	6.99	-19.08	0.12	1.39

Table A-16: n – alkane measurements (signal intensity cps)

	Depth (cm)								
No. of Carbon	**5**	**15**	**25**	**35**	**42**	**46**	**55**	**75**	**85**
12	804589	605751	646160	1124345	342257	649513	133248	0	116028
13	1723336	576710	554881	2231806	946582	1612594	126788	0	191253
14	3917126	1149170	1585877	4378293	2057883	4270490	210316	126290	359071
15	6765456	3656264	4722412	6321260	2507938	5642613	464703	378264	640014
16	10387050	8376053	8969875	9172830	3032560	8449744	801037	637169	1203547
17	11007812	10258916	9703319	9177068	3091814	8281232	1378640	647545	1986678
18	17468519	16439954	16997175	14885060	4130018	13534883	1199335	936083	4418144
19	9691793	9010377	7903461	6906260	2450745	5679798	645680	378412	3343952
20	9472439	8953555	8093546	6760638	2209041	5722562	649752	350559	3430864
21	9007143	8665872	6890303	6938915	2273927	4442212	563583	245993	3038963
22	5590255	5627818	4971314	4054269	1343583	3424756	303507	120505	2382696
23	11035854	12439767	8397560	9288523	2973289	4812367	477805	87980	2157743
24	4027420	3813600	3152993	2503236	904913	2073163	140079	0	1432048
25	8780436	9859183	6147286	5835805	2151549	3308338	264476	0	1257330
26	2955604	2845843	2116604	1395627	542373	1288410	91288	0	857833
27	13783679	13357939	8212792	7328755	3061149	3975146	285529	0	1301423
28	3149792	2761239	1956830	1417663	600225	761777	73238	0	388218
29	22484698	18075531	12418537	10351522	6628132	5863825	602243	0	2303532
30	5250332	3222728	2689755	1830163	663579	857928	100036	0	397874

31	65051935	47510948	35082917	28692243	15570741	15050814	1865633	0	6262428
32	3822414	2240205	2085598	1526343	684846	527962	77545	0	227451
33	43347157	26120413	24754311	17373225	11091069	7101726	978980	0	3278274
34	1113620	200122	813771	361481	0	0	0	0	0
35	8042362	1560495	4845781	1841034	1700152	743084	0	0	131121

Table A-17: GDGT measurements from Lake Nkunga sediments (µg)

	Depth (cm)									
GDGT type	**5**	**15**	**25**	**35**	**42**	**46**	**56**	**66**	**76**	**86**
brGDGT-Ic	25.46	50.79	69.19	73.80	66.54	47.26	56.77	41.14	56.40	30.36
brGDGT-Ib	181.76	286.61	389.99	415.26	418.60	302.10	367.55	198.79	238.70	113.26
brGDGT-I	1527.74	2084.18	2333.16	2624.48	2560.57	1358.51	1722.62	720.63	820.00	209.07
brGDGT-IIc	13.18	20.85	30.20	32.46	28.14	26.94	32.16	22.33	26.45	11.11
brGDGT-IIb	83.80	119.52	201.76	195.51	226.16	171.46	196.23	130.35	163.60	73.11
brGDGT-II	1217.47	1456.09	1825.20	2084.15	2166.94	1007.53	1111.31	666.24	862.24	221.75
brGDGT - IIIc	0.00	0.00	0.00	0.00	0.00	0.00	0.00	0.00	0.00	0.00
brGDGT - IIIb	10.25	10.67	18.08	13.68	18.65	11.94	13.87	9.20	12.42	5.03
brGDGT - III	245.59	299.02	372.40	399.04	415.69	185.41	204.56	133.83	179.85	49.41
Crenoarchaeol VI	104.04	133.00	140.74	139.18	147.43	136.08	210.35	55.94	69.10	17.11
Crenoarchaeol VI'	7.73	11.09	9.62	10.53	9.28	10.00	14.72	4.60	6.44	1.72
GDGT-4	0.00	0.00	0.00	0.00	0.00	0.00	0.00	0.00	0.00	0.00
GDGT-3	15.04	23.01	24.57	26.86	26.59	17.69	23.27	9.13	15.39	3.88
GDGT-2	43.70	56.21	72.81	89.20	91.73	59.05	77.04	28.65	38.97	17.43
GDGT-1	50.06	56.11	78.16	90.71	84.97	45.04	49.93	27.34	38.37	16.36
GDGT-0	248.35	349.21	491.35	598.18	449.84	227.08	200.62	210.13	285.59	111.42

A.2.2 Sacred Lake sediment measurements

Table A-18: Mineralogy XRD measurements (%)

Depth (cm)	**Chlorite**	**Illite/Muscov**	**Halloysite**	**Gibbsite**	**Magnetite**	**Hematite**	**Quartz**	**Feld-plag**	**diopside**
4	1	0	11	1	0	0	17	71	0
11	1	0	9	2	0	0	19	70	0
22	1	0	11	2	0	0	19	68	0
32	0	0	7	2	0	0	29	61	0
45	0	0	7	2	0	0	19	71	0
50	1	0	6	2	0	0	21	69	0
62	0	0	11	2	0	0	23	64	0

Table A-19: Low (F1) and High (F3) frequency Magnetic Susceptibility (SI); Carbon, Nitrogen and their respective isotopes

Magnetic Susceptibility (SI)			**Organic chemistry**				
Depth (cm)	**F1**	**F3**	**Depth (cm)**	**$\delta^{15}N$ (‰)**	**$\delta^{13}C$ (‰)**	**%N**	**%C**
1	8.22E-07	1.01E-06	2	2.41	-24.89	1.42	16.77
2	1.34E-06	1.38E-06	3	2.3	-24.55	1.27	15
3	9.00E-07	8.93E-07	4	2.32	-24.58	1.11	13.52
4	1.52E-06	1.67E-06	5	2.69	-24.39	1.1	13.11
5	1.05E-06	2.58E-06	6	2.66	-24.34	1.14	13.56
6	6.31E-07	6.96E-07	7	3.17	-24.08	1.05	12.8
7	1.39E-06	-8.00E-08	8	2.81	-26.35	1.07	12.85
8	1.28E-06	1.13E-06	9	2.71	-26.48	1.02	12.1
9	1.56E-06	1.14E-06	10	3.12	-23.75	0.97	11.76
10	1.29E-06	1.30E-06	11	3.1	-23.79	1.05	12.79
11	1.77E-06	1.48E-06	12	2.49	-24.07	1.07	13.28
12	1.14E-06	1.10E-06	13	2.07	-24.41	1.18	14.31
13	1.27E-06	1.06E-06	14	1.98	-24.6	1.31	16.4
14	1.25E-06	9.91E-07	15	2.07	-24.48	1.3	16.59
15	7.20E-07	7.24E-07	16	1.88	-24.73	1.36	17.24
16	5.63E-07	1.48E-06	17	1.75	-24.69	1.36	16.83
17	8.04E-07	3.29E-06	18	2.04	-24.51	1.27	16.07
18	6.55E-07	2.63E-06	19	1.76	-24.54	1.29	16.11
19	5.68E-07	7.24E-07	20	1.76	-24.79	1.24	15.34
20	8.89E-07	8.48E-06	21	1.58	-24.41	1.29	16.33
21	9.84E-07	1.25E-06	22	1.97	-23.39	1.36	16.73

22	6.66E-07	8.74E-07	23	2.49	-22.54	1.19	15.12
23	6.61E-07	8.44E-07	24	2.74	-22.43	1.29	16.85
24	8.67E-07	1.01E-06	25	2.42	-22.41	1.18	15.48
25	1.06E-06	1.37E-06	26	2.23	-24.08	1.3	16.49
26	6.24E-07	7.85E-07	28	2.18	-23.24	1.35	17.42
27	5.56E-07	6.14E-07	29	2.19	-23.42	1.38	17.43
28	5.80E-07	6.02E-07	30	2.36	-22.93	1.37	17.72
29	4.93E-07	5.93E-07	31	2.61	-22.4	1.28	16.56
30	5.12E-07	2.89E-07	32	2.58	-22.47	1.23	16.42
31	5.37E-07	1.47E-06	33	2.52	-23.91	1.15	15.36
32	1.97E-07	6.52E-07	34	2.59	-22.56	1.03	14.08
33	3.62E-07	4.67E-07	35	3.16	-22.22	1.01	13.89
34	5.07E-07	5.12E-07	36	2.9	-22.21	0.93	12.79
35	1.12E-06	1.29E-06	37	2.34	-25.17	1.64	19.65
36	5.41E-07	5.97E-07	38	2.88	-25.06	1.48	18.06
37	8.93E-07	9.29E-07	39	2.67	-24.49	1.34	15.98
38	9.02E-07	9.19E-07	40	3.04	-22.95	1.12	14.23
39	5.14E-07	7.12E-06	41	4.1	-21.81	0.77	10.71
40	5.36E-07	8.94E-07	42	4.04	-21.25	0.83	11.92
41	4.51E-07	4.31E-06	43	4.1	-21.14	0.81	11.49
42	9.93E-07	2.69E-07	44	4.02	-21.07	0.77	11.14
43	6.88E-07	9.85E-07	45	4.34	-21.03	0.76	11.07
44	1.32E-06	1.17E-06	46	4.05	-21.61	0.78	11.17
45	1.59E-06	5.57E-06	47	3.99	-21.2	0.71	10.24
46	1.13E-06	9.99E-06	48	4.73	-21.06	0.64	9.41
47	1.27E-06	6.28E-06	49	4.33	-21	0.67	9.96
48	1.53E-06	1.48E-06	50	4.56	-21.06	0.74	10.64
49	4.35E-07	1.05E-06	51	4.69	-20.96	0.68	10.07
50	2.20E-06	2.09E-06	52	4.56	-21.16	0.7	10.51
51	1.21E-06	1.27E-06	53	4.26	-21.33	0.74	10.91
52	1.52E-06	1.54E-06	54	3.09	-23.26	1.17	15.43
53	1.23E-06	1.37E-06	55	3.87	-22.02	0.82	11.92
54	9.28E-07	6.94E-07	56	4.39	-21.63	0.67	9.94
55	9.22E-07	8.92E-07	57	3.99	-21.43	0.69	10.33
56	1.37E-06	3.71E-06	58	4.44	-21.21	0.68	10
57	8.95E-07	9.29E-07	59	4.21	-29.12	0.78	11.72
58	1.13E-06	1.10E-06	60	4.76	-29.16	0.68	10.16
59	1.69E-06	1.52E-06	61	4.56	-20.81	0.5	7.71
60	2.11E-06	2.09E-06	62	4.89	-20.94	0.36	5.49
61	1.84E-06	2.02E-06	63	5	-21.3	0.41	6.41
62	2.53E-06	2.45E-06					

Table A-20: n – alkane measurements (signal intensity cps)

No. of Carbon	**Depth (cm)**											
	2	**7**	**16**	**22**	**27**	**34**	**41**	**45**	**46**	**50**	**52**	**54**
12	0	996119	1021242	1534688	1816142	1088473	0	0	0	0	0	0
13	0	2147066	1043623	4310619	4379697	1336268	0	363210	0	0	0	0
14	187422	3448263	1807376	7983490	8324515	2320084	1040513	2226378	428272	2842633	485071	146509
15	280223	3883620	3865110	9423525	10771525	3245354	3477293	5935690	3501447	6950506	1470056	1698749
16	300478	4593799	6463836	12222112	16483501	4605578	7834833	9789077	10017581	12458569	3997718	5056222
17	216929	4157849	9307309	12181001	17838472	5756166	12077056	11682728	22766047	22413225	9062194	9287335
18	237339	6181048	14850901	16839397	25008824	10711504	16080118	16922279	18906022	18709390	14080266	14496369
19	67131	3596219	11799107	10526484	14546555	7200204	11443806	9791939	13117700	12302621	9678409	10759100
20	48374	3874214	12517497	11218020	14144087	7626674	11704744	9594782	11801918	11840479	10352143	11100496
21	34141	3498486	11057864	10770864	13897026	7475641	9283461	7480616	10632314	10180988	8920699	8705735
22	45360	2628422	9034266	8822254	10502179	6682239	7250975	5997219	7463106	7692851	7126273	6867492
23	41088	5367659	14047135	18406691	20823596	15920431	9774915	8511559	8937467	9398245	8904707	8045006
24	26220	1933887	6813971	8285855	9702384	7347635	5295950	4676988	5116466	5438980	5436995	4661839
25	15887	4578271	12525914	18916978	20856030	17081729	9549080	8593886	7689056	9088375	9173366	7128668
26	38672	1553578	5464441	8109730	9863680	7609542	4391333	4282643	3426032	4635032	4451704	3110629
27	108139	7330417	20455315	31958209	31939192	26889306	12678085	12289797	9348510	11741764	12923595	8930130
28	0	1541713	5121912	8356640	8922643	6774086	3462216	3165284	2375592	3306410	3385586	2422680
29	0	31885171	74046004	100109906	71971555	59468938	15786062	14553600	9857595	13843978	14902017	9730976
30	0	1290111	4766267	9664992	8231281	7100517	2587452	2591749	1459365	2382938	2397423	1836801
31	139060	17873897	57260115	99027086	86580399	81685899	25214987	26106956	12130825	21644013	25839134	15762517
32	0	673756	3536717	5446258	4430606	4346558	1694033	1598655	433603	1275214	1583135	949018
33	41674	7907915	27097909	47823790	26518999	38256025	12527345	13775909	580633	7346864	12396988	7286404
34	0	0	1309009	1426747	0	1283695	0	411584	0	0	0	0
35	0	0	3936169	8356484	0	8944045	0	2733922	0	0	0	0

Table A-21:GDGT measurements from Sacred Lake (μg)

GDGT type	Depth (cm)									
	2	7	16	22	27	34	41	45	50	54
GDGT-Ic	80.83	76.81	96.15	108.82	142.33	99.01	133.18	100.12	97.47	113.63
GDGT-Ib	148.10	134.83	149.26	154.98	227.72	155.00	120.82	95.09	92.46	105.67
GDGT-I	7748.58	5443.02	6861.20	7912.91	10872.63	7035.05	4006.10	2980.21	2689.75	3144.08
GDGT-IIc	51.97	37.31	39.88	39.76	49.28	35.35	43.90	52.57	56.67	65.05
GDGT-IIb	82.01	59.34	55.04	59.21	91.74	63.61	44.81	41.90	42.80	48.20
GDGT-II	3962.83	2493.70	2825.84	3047.07	4285.04	2775.73	1343.99	1036.16	884.51	954.03
GDGT-IIIc	0.00	0.00	0.00	0.00	0.00	0.00	9.31	14.59	15.20	18.84
GDGT-IIIb	0.00	0.00	0.00	0.00	0.00	0.00	7.09	9.80	10.64	10.64
GDGT-III	574.16	331.79	355.84	373.34	544.39	327.40	171.70	134.50	113.28	124.84
Crenarcheol	356.06	197.68	273.63	301.89	283.28	174.48	95.74	85.78	70.19	70.46
Crenarcheol'	9.69	7.62	9.21	9.24	11.64	8.45	7.19	5.91	5.35	5.12
GDGT-4	0.00	0.00	0.00	0.00	0.00	0.00	0.00	0.00	0.00	0.00
GDGT-3	46.53	34.75	47.91	58.42	97.65	72.70	75.40	66.33	62.11	70.51
GDGT-2	139.49	95.71	133.95	154.78	233.11	173.10	153.09	126.91	118.73	135.44
GDGT-1	113.87	69.79	96.23	137.18	425.23	183.53	170.44	151.12	142.29	157.29
GDGT-0	661.56	452.36	664.96	840.56	1452.24	1207.38	998.85	843.68	761.80	809.71

A.2.3 Lake Rutundu sediment measurements

Table A-22: Mineralogy XRD measurements (%)

Depth (cm)	Illite/Muscov	Halloysite	Gibbsite	Magnetite	Hematite	Quartz	Feld-plag	diopside
4	0	0	1	0	0	3	96	0
12	0	0	2	0	0	3	95	0
24	0	0	1	0	0	3	96	0
32	0	0	1	0	0	4	95	0
48	0	0	1	0	0	3	97	0
60	0	0	0	0	0	3	96	0
76	0	0	0	0	0	3	97	0
92	0	0	0	0	0	3	97	0

Table A-23:Carbon and Nitrogen measures

Samples	Depth (cm)	$\delta^{15}N$ (‰)	$\delta^{13}C$ (‰)	%N	%C
RC/4/10	4	-1.36	-25.29	1.50	18.05
RC-8-10	8	-1.25	-25.44	1.26	15.70
RC/10/10	10	-3.77	-25.45	1.26	15.81
RC-12-10	12	-0.54	-24.09	1.33	15.78
RC/14/10	14	-4.10	-25.26	1.47	16.58
RC-16-10	16	-1.84	-25.33	1.53	16.16
RC/18/10	18	-3.92	-25.73	1.55	17.35
RC-20-10	20	-2.03	-25.59	1.57	16.64
RC/22/10	22	-3.69	-25.86	1.53	16.62
RC-24-10	24	-1.79	-26.27	1.47	15.44
RC/26/10	26	-3.60	-26.23	1.50	16.59
RC/28/10	28	-1.48	-26.52	1.41	15.26
RC/30/10	30	-2.60	-26.49	1.34	16.06
RC-32-10	32	-1.86	-25.85	1.56	17.21
RC/34/10	34	-3.40	-25.65	1.49	18.36
RC-36-10	36	-1.96	-24.95	1.33	15.87
RC/38/10	38	-3.78	-24.79	1.48	16.99
RC-40-10	40	-2.12	-25.08	1.33	15.53
RC/42/10	42	-3.19	-25.50	1.27	14.90
RC-44-10	44	-1.91	-25.83	1.39	15.53
RC/46/10	46	-2.70	-26.31	1.20	14.76
RC/48/10	48	-1.92	-26.42	1.21	14.15
RC/49/10	49	-1.45	-25.44	1.01	13.20
RC-52-10	52	-0.85	-25.18	1.03	13.04
RC/54/10	54	-2.04	-25.47	1.10	14.11
RC-56-10	56	-1.99	-25.77	1.06	12.96
RC/58/10	58	-2.30	-26.10	1.16	14.42
RC-60-10	60	-1.85	-26.05	1.25	15.00
RC/62/10	62	-2.84	-25.40	1.31	16.13

RC-64-10	64	-1.90	-25.70	1.45	16.35
RC/66/10	66	-2.36	-26.08	1.34	16.59
RC-68-10	68	-1.35	-25.85	1.38	15.79
Rc/69/10	69	-1.29	-25.73	1.36	15.60
RC/70/10	70	-2.15	-25.57	1.33	16.02
RC-72-10	72	-0.43	-24.75	1.42	15.60
RC/74/10	74	-1.93	-24.65	1.32	15.84
RC-76-10	76	-0.74	-24.50	1.29	14.30
RC/78/10	78	-1.48	-24.73	1.29	16.73
RC-80-10	80	-0.95	-23.29	1.44	16.72
RC/82/10	82	-1.79	-24.62	1.28	16.56
RC/84/10	84	-1.18	-25.09	1.37	16.12
RC/86/10	86	-1.51	-24.97	1.36	17.69
RC/88/10	88	-1.71	-24.53	1.59	18.98
RC/90/10	90	-2.02	-24.64	1.49	18.76
RC-92-10	92	-2.03	-24.13	1.64	18.66
RC/94/10	94	-2.12	-24.66	1.41	18.29
RC/96/10	96	-1.55	-23.63	1.60	20.29
RC/98/10	98	-1.57	-24.11	1.59	20.02
RC/99/10	99	-2.18	-24.56	1.52	19.07
RC/100/10	100	-2.57	-24.34	1.71	19.22

Table A-24: n – alkane measurements (signal intensity cps)

No. of Carbon	**Depth (cm)**										
	2	**8**	**16**	**28**	**40**	**48**	**52**	**64**	**70**	**84**	**92**
12	680860		503937	0	0	614353	324848	1378475	0	364246	0
13	3434903		2450136	0		2351498	1481952	4339814	0	1591005	0
14	7979269	444195	5179624	253696	622810	3865213	4031947	5928350	723694	3242757	454776
15	11019569	371919	7626746	1176805	771072	4777650	6083778	6370757	489282	4382627	390711
16	13697583	1044450	9423218	3242788	1369545	5129156	7174642	7037837	1357227	5409426	980877
17	16753706	3300984	10823554	4664988	2404374	4950904	7567047	6586416	2945018	6289518	1973241
18	18026150	3031464	12523336	5921318	3918070	5631391	7863027	8199149	2639177	6811567	1729918
19	14207502	1505944	9586091	4436011	1219394	3753309	5813622	5300420	856025	5157200	647027
20	14495958	1819230	10234297	5322337	2011634	4315449	6155027	6077632	1328708	5446595	880259
21	14098681	2914542	9988994	4698941	3317024	3594410	5434883	5731405	1677377	4914159	841179
22	11294425	3294054	8587886	3680458	3108148	3703929	4442527	5970270	1824576	4472542	1096300
23	28846834	27827842	27001311	13337723	18439225	13856021	10094440	21019313	14025198	11212858	4825532
24	11890787	6584731	13666449	4972886	8078526	4455312	4540224	9029954	4579712	5463860	2123292
25	41772529	36458342	48962068	20752471	34844272	21085573	18552752	38990681	23911376	19443731	10273936
26	10445267	5958538	13836904	4966027	8655915	4726752	4701490	9546101	4896195	5314518	2465149
27	45113711	26181076	73647700	25543707	41973269	26006783	24210051	50684057	25706288	29359318	12391761
28	7140423	3206806	11791479	3162694	4781825	4387356	3158434	8704804	3067966	4403285	1588521
29	47153969	16450826	74740353	23231341	27057767	24000828	19342790	48649791	16666356	28376446	8941488
30	4814683	1187694	9478124	2470899	2472166	3578024	2619039	6131861	1434316	3235437	676316
31	48571528	11798004	82189967	27873599	21966971	29504919	25500975	57794063	13934784	32678520	6176882
32	2403817	455555	6338202	1823724	1040323	2239308	1646019	3986303	702848	2172371	234719
33	7476794	3561786	43530331	16558812	7895722	17633223	14742023	33562988	4910121	16812036	1727443
34	0	0	586048	0	156037	0	418063	0	96286	0	63520
35	0	0	1207326	0	412545	2084006	1125265	906951	247711	0	116244

Table A-25: GDGT measurements from Lake Rutundu (μg)

GDGT type	**Depth (cm)**										
	2	**8**	**16**	**28**	**40**	**48**	**52**	**64**	**72**	**84**	**92**
GDGT-Ic	986.36	1390.91	1691.27	1252.19	1469.04	1345.20	884.09	1470.94	1486.89	959.14	1899.08
GDGT-Ib	2115.72	2295.92	3413.03	2605.69	2740.56	2827.99	1724.77	3184.47	3166.05	2388.25	3594.68
GDGT-I	5505.03	5235.67	9668.56	8298.54	6221.81	8938.21	5933.55	9985.87	7959.99	7780.00	9416.26
1GDGT-Iic	705.27	640.04	994.55	867.71	890.06	911.92	502.43	862.82	770.36	642.54	738.20
GDGT-Iib	3071.13	1956.31	4465.79	3702.44	2777.59	3722.23	2116.86	3899.77	2525.15	2749.79	2663.40
GDGT-II	7302.76	6863.46	11955.72	9929.87	8725.30	11343.58	6888.51	11534.30	10425.47	9598.74	13338.76
GDGT-IIIc	30.58	0.00	45.50	56.86	0.00	36.90	28.14	39.57	0.00	42.88	0.00
GDGT-IIIb	191.68	96.57	309.29	257.08	133.32	253.16	146.72	268.43	135.87	215.98	118.70
GDGT-III	2269.51	4112.00	3528.91	3342.45	4584.14	3550.17	2134.16	3469.21	5332.49	3037.28	7765.87
GDGT-VI	13.66	0.00	10.13	9.40	0.00	9.79	20.61	15.28	0.00	14.76	0.00
GDGT-VI'	9.64	0.00	0.00	0.00	0.00	0.00	0.00	0.00	0.00	0.00	0.00
GDGT-4	0.00	38.62	0.00	0.00	97.22	0.00	0.00	0.00	0.00	0.00	85.22
GDGT-3	25.80	82.14	56.88	33.19	92.49	42.59	62.58	41.80	110.47	59.46	119.39
GDGT-2	108.38	207.73	200.39	167.33	353.71	243.32	269.71	259.77	383.91	318.96	552.77
GDGT-1	207.13	311.59	316.35	302.08	567.82	405.28	372.21	369.67	603.69	467.91	752.85
GDGT-0	2669.45	1791.79	3637.88	2740.79	2678.00	3274.94	2542.09	4055.01	3381.23	3879.54	3877.28

A.3 XRF core scan datasets

Table A-26: Lake Nkunga XRF scan

	Chemical Elements (cps)																
Depth (cm)	Al	Ca	Fe	K	Mn	Si	Ti	Cl	Nb	Ni	P	Rb	S	Sr	V	Zn	Zr
0.1	-18	-5545	-17099	-397	225	-72	-5859	-291	79	83	12	139	39	472	2261	153	497
0.2	-27	-5205	-17202	-244	8	-48	-3304	-272	77	85	19	162	43	484	2245	163	553
0.3	-14	-3495	-13414	89	31	7	1866	55	96	97	12	161	46	529	2409	207	591
0.4	-10	-5203	-18862	-297	-197	-61	-4075	686	74	83	15	154	39	494	2140	162	541
0.5	-5	-4048	-17616	-38	-56	15	-867	2039	57	80	15	156	53	483	2292	168	548
0.6	-27	-3671	-18475	-111	150	-68	-1699	1735	89	90	10	154	53	507	2347	178	594
0.7	-10	-2700	-14707	290	241	40	4029	766	59	83	16	169	55	548	2550	184	596
0.8	11	-809	-12238	-650	255	-181	-8127	-41	117	80	14	167	50	609	2708	189	690
0.9	7	2136	-10501	-239	280	-80	-2936	-16	83	119	21	175	54	662	2864	222	671
1	-17	1603	-11813	-584	481	-225	-7294	-20	109	92	19	180	57	672	2856	220	652
1.1	-3	2276	-7459	-28	275	-26	-1484	-10	118	104	13	195	47	705	2950	213	693
1.2	10	2911	-5182	-37	231	-8	839	-36	75	92	14	165	49	715	3080	220	682
1.3	-10	1303	-5729	-41	129	-31	-380	-18	106	102	22	158	42	750	2990	231	670
1.4	-2	1753	-4462	8	39	-74	1461	-5	85	99	13	181	30	745	3061	225	649
1.5	-6	1595	-3072	-6	128	-74	1902	1	107	116	15	168	42	725	3009	224	690
1.6	-17	2120	-1540	157	-19	-27	3573	-2	94	111	16	185	37	762	3116	227	711
1.7	-1	1831	-1565	302	-44	15	4428	1	52	116	17	175	42	750	3099	231	704
1.8	2	895	-389	348	-21	-16	4600	0	133	94	17	196	29	778	3083	222	722
1.9	0	857	-3009	176	-130	-25	2164	8	119	110	18	181	36	747	3083	231	709
2	10	2114	-1041	442	-71	68	5032	15	113	90	27	174	29	752	3157	230	699
2.1	10	2613	-393	365	-57	41	4810	2	93	122	22	195	36	780	3060	240	679
2.2	-1	2487	-1197	201	-2	55	4453	13	138	109	19	191	34	809	3082	234	711
2.3	-2	2882	-155	415	-76	72	4798	0	115	117	17	173	40	795	3134	232	709
2.4	14	2257	-395	196	33	67	4207	7	87	92	27	176	52	773	3107	220	661
2.5	22	2872	79	332	201	72	4135	-12	117	96	24	175	46	827	3071	224	703
2.6	3	2018	-763	61	96	-13	1762	-4	111	107	21	159	43	800	3038	230	685
2.7	7	-511	-4852	-231	329	-43	-2803	-3	99	111	20	166	45	710	2974	217	670
2.8	-6	-408	-1209	-160	356	-75	-952	-22	99	101	16	162	35	740	3065	217	705
2.9	-11	-960	-5162	-459	350	-118	-4900	-15	107	111	17	176	28	750	2997	225	661
3	15	-171	-2651	-299	268	-130	-2578	-35	110	113	17	197	36	746	3034	232	704
3.1	-11	-1038	-5020	-445	407	-118	-5827	-11	103	95	10	178	29	707	2903	205	652
3.2	5	1810	-858	175	42	70	2163	-7	120	102	11	168	34	784	3043	228	701
3.3	-4	1135	-1640	85	161	45	488	-19	94	94	12	209	39	782	3012	218	749
3.4	-4	1596	-483	185	40	65	2981	-10	98	103	14	177	50	774	3065	216	697
3.5	-1	828	-1716	75	140	-18	1174	1	111	101	19	152	39	764	3072	207	702
3.6	-3	1018	-621	107	29	3	2084	-2	107	99	23	169	30	759	3095	220	699
3.7	1	1968	732	292	-99	120	4487	14	91	103	26	188	32	786	3102	217	703
3.8	-21	2088	78	318	25	93	4067	10	124	98	22	198	42	821	3056	225	690
3.9	17	3683	609	446	-80	119	5103	18	94	114	22	151	49	790	3109	200	704

4	9	2899	767	527	-62	183	5651	32	97	105	31	192	50	773	3030	214	719
4.1	-6	2455	-433	272	-53	53	3425	15	109	109	16	185	29	760	3084	245	693
4.2	19	2239	768	264	-125	44	3738	18	92	96	16	171	34	756	3094	237	713
4.3	3	1702	-685	277	-114	75	2947	35	133	123	23	193	38	784	3042	224	718
4.4	-1	1585	-389	287	6	32	2899	12	117	116	21	192	31	781	3068	225	706
4.5	9	777	-2323	66	-103	2	1124	17	125	91	17	172	36	730	2997	205	670
4.6	9	1365	582	251	-4	69	4786	15	115	100	17	189	46	758	3105	215	701
4.7	-6	433	-2110	-23	-133	49	289	18	107	106	13	182	39	731	2927	211	664
4.8	16	1561	-85	324	-136	89	2684	18	97	108	22	169	36	751	2991	217	698
4.9	13	1373	-156	163	-105	83	-10	8	109	137	26	174	33	749	2840	217	713
5	9	1893	3044	303	48	65	2152	2	120	154	17	199	47	789	2966	221	718
5.1	-8	638	-316	-99	-73	-16	-340	-23	115	110	23	174	39	756	2936	208	682
5.2	-4	-104	-3422	-325	-167	-58	-3649	-17	95	106	15	180	33	744	2824	212	697
5.3	5	309	-2325	-185	88	-85	-1658	-6	113	108	17	181	37	749	2893	200	702
5.4	3	699	-2497	-312	8	-89	-2572	-7	104	105	26	193	43	749	2950	204	682
5.5	7	163	-3773	-298	54	-115	-3730	0	118	102	18	126	44	710	2873	207	680
5.6	-3	918	-487	27	17	-14	1218	20	82	101	12	178	40	808	2958	221	704
5.7	-3	561	-1931	-114	-36	-62	-100	25	119	96	20	169	40	705	2997	213	680
5.8	7	470	-2542	-188	-60	-93	-1292	21	133	93	13	193	33	720	2885	216	703
5.9	10	1884	-1872	73	128	-1	837	35	94	105	12	184	38	823	2913	204	667
6	2	2210	-621	277	84	45	2352	38	82	108	15	177	42	743	3026	230	712
6.1	-7	1790	-2091	147	-15	-33	1299	34	97	102	23	166	36	785	3015	220	667
6.2	3	1386	-1255	106	-8	30	1649	32	118	117	27	168	44	783	3067	225	683
6.3	0	1611	-1115	109	25	40	1693	33	92	108	9	163	40	723	2997	236	690
6.4	0	928	-927	-14	-67	33	236	27	85	98	25	166	40	670	2995	210	678
6.5	3	590	1008	173	-100	58	2048	45	95	90	18	158	36	700	2992	201	658
6.6	-8	327	-1273	-69	-119	24	869	35	100	108	16	175	52	728	2940	216	676
6.7	-2	2020	503	326	97	79	2510	48	115	109	23	201	37	782	3050	239	703
6.8	4	2639	830	394	118	99	2464	22	113	122	16	174	40	729	3005	232	717
6.9	-3	1428	-2280	182	-83	7	626	16	94	109	12	177	41	762	2980	212	664
7	12	1132	-2046	48	-151	-24	25	10	99	103	21	167	63	777	2898	216	656
7.1	6	2429	-32	67	57	2	1696	0	119	121	30	175	32	786	2986	234	698
7.2	8	-800	-6416	-362	70	-196	-7178	-2	111	96	25	172	43	704	2672	216	654
7.3	3	253	-6970	-516	82	-165	-7119	2	98	124	15	168	48	699	2649	196	695
7.4	-5	619	-3541	-194	74	-80	-2540	13	109	109	18	173	39	744	2938	213	702
7.5	3	358	-3899	-303	122	-127	-4264	13	117	102	18	181	33	766	2894	216	688
7.6	-3	-1079	-4720	-472	81	-232	-5725	17	84	107	20	174	39	716	2839	202	646
7.7	-8	516	-1010	-221	141	-144	-2035	36	49	121	16	146	47	794	2958	216	649
7.8	-5	1105	-2036	-208	12	-83	-1772	37	84	94	18	168	32	804	2938	203	607
7.9	0	425	481	-197	46	-127	-345	37	78	105	26	147	47	776	3048	209	702
8	4	930	-36	-58	137	-99	-1275	36	104	93	27	157	39	755	2988	212	696
8.1	-3	-1607	-1830	-264	-26	-139	-3268	42	118	104	20	186	31	733	2905	212	693
8.2	11	428	16	217	-149	-38	2214	55	105	106	27	174	50	708	2988	217	710
8.3	14	1019	1315	264	-110	20	2757	53	112	110	16	182	33	721	2978	223	674
8.4	11	1100	-69	81	62	-49	2853	111	91	108	24	181	44	698	3017	236	660
8.5	8	345	298	133	60	-85	1240	44	102	96	15	168	32	731	2984	225	677
8.6	-4	550	447	-48	239	-114	68	50	102	101	20	185	28	744	2983	217	701

8.7	16	919	385	153	-36	-63	1489	80	102	102	24	189	32	759	2995	217	687
8.8	3	-498	-437	-88	52	-108	611	52	115	109	15	183	37	703	3013	223	694
8.9	-6	150	-539	-96	84	-84	-73	53	79	112	19	203	61	697	3032	223	701
9	-10	-1183	-93	-122	77	-129	-20	63	146	104	18	160	38	704	3048	238	704
9.1	-13	-669	-820	-245	137	-191	-2135	55	100	104	24	177	39	735	2965	234	673
9.2	-16	-842	-638	-292	223	-182	-2113	46	125	116	24	187	38	773	3017	217	717
9.3	5	162	324	-74	207	-112	522	52	100	105	25	186	36	765	3055	228	672
9.4	9	218	-1412	-296	281	-173	-2067	38	109	102	24	142	22	710	2916	207	669
9.5	16	-479	-161	-140	252	-128	408	62	123	96	19	179	27	761	3002	228	686
9.6	12	-434	317	-134	6	-116	-149	52	103	104	20	152	41	731	3009	205	709
9.7	-12	-982	22	-237	109	-161	-1914	41	92	104	24	185	39	712	2969	224	694
9.8	0	-94	-399	-63	122	-140	-693	47	97	102	24	174	44	708	3047	218	676
9.9	5	-892	-1836	-231	103	-121	-1854	39	97	100	15	162	37	706	2857	222	668
10	0	-466	-2516	-187	53	-91	-2073	38	99	101	13	184	32	724	2894	235	686
10.1	-17	-825	-4299	-338	3	-130	-3854	30	88	98	18	159	36	705	2874	217	692
10.2	-1	-1332	-4793	-442	37	-172	-4271	37	105	105	18	173	48	701	2823	223	654
10.3	-9	-1893	-4894	-497	88	-220	-5180	50	111	94	21	183	45	726	2859	220	700
10.4	-12	74	-640	-229	75	-199	-1224	47	101	103	19	169	47	720	3047	242	668
10.5	-5	-1677	-4719	-599	-115	-274	-6438	47	95	113	16	180	59	747	2756	203	635
10.6	11	-296	-1485	-222	-12	-193	-2329	51	111	115	19	190	59	756	2843	222	676
10.7	-1	812	-1740	-112	-131	-81	-2329	57	88	180	25	147	35	732	2824	227	638
10.8	1	1714	1569	41	-13	-47	452	68	94	198	28	158	60	742	2980	231	705
10.9	30	300	-1822	-208	-121	-92	-3396	48	113	131	16	161	34	752	2961	209	629
11	4	-158	-2385	-303	138	-209	-4276	52	95	98	26	183	28	729	2965	196	660
11.1	-10	691	-2696	-507	212	-183	-3624	60	92	90	22	163	34	736	2930	223	690
11.2	-2	-416	-829	-108	313	-214	-3519	58	109	109	18	201	50	745	2940	223	682
11.3	-3	-1376	-2991	-587	202	-213	-5576	41	89	103	19	156	47	714	2903	236	666
11.4	-13	-573	-4385	-513	84	-206	-6364	47	112	109	10	168	30	727	2818	210	634
11.5	5	-632	-1654	-459	137	-202	-4787	31	105	101	36	185	36	688	2859	218	693
11.6	-8	-1918	-2649	-658	121	-312	-6536	33	111	94	17	160	37	732	2859	217	679
11.7	-13	-1789	-2525	-652	102	-278	-6524	30	97	107	11	183	33	678	2841	206	675
11.8	0	-2857	-5830	-789	-15	-263	-8402	30	83	96	22	189	29	702	2696	201	659
11.9	-8	-775	781	-118	123	-133	-1410	40	129	102	30	200	50	690	2911	228	705
12	-3	-1351	-2984	-491	111	-207	-4829	28	115	102	14	191	30	725	2837	219	668
12.1	-8	-1108	-2087	-487	24	-181	-5499	42	101	116	24	169	43	668	2701	214	669
12.2	-1	-1993	-2520	-550	32	-192	-7060	20	78	106	21	165	47	658	2766	214	655
12.3	2	-1872	-4370	-667	41	-224	-9540	14	86	117	17	177	30	696	2588	207	647
12.4	-1	-1464	-2420	-405	41	-130	-5480	21	96	107	30	168	38	666	2750	207	656
12.5	4	-2386	-4585	-558	1	-219	-7568	11	95	119	18	194	34	674	2794	202	648
12.6	-14	-2668	-3538	-601	-87	-219	-7907	-2	75	125	18	184	31	720	2719	208	614
12.7	-11	-4663	-10693	-1232	-460	-366	-16530	14	72	137	19	137	31	665	2276	177	547
12.8	-19	-25	-4821	-384	-95	-173	-7231	55	99	91	22	139	38	813	2751	192	585
12.9	5	1148	901	-84	-80	-86	-991	45	95	106	22	176	35	894	2921	218	653
13	6	-1130	-2929	-268	-101	-105	-4154	53	100	97	9	146	41	694	2743	220	671
13.1	-2	-1112	-2419	-236	-131	-127	-3767	45	94	97	27	201	44	654	2787	213	650
13.2	7	-848	-2634	-220	-50	-128	-3717	56	89	112	15	148	40	672	2842	213	655
13.3	11	-959	-1255	-82	-89	-99	-2496	40	83	106	16	160	32	674	2865	205	652

13.4	1	-2369	-4735	-406	-58	-169	-5606	51	97	99	24	169	34	660	2774	202	618
13.5	4	-1935	-4693	-396	-167	-196	-5648	51	103	87	17	194	33	749	2828	206	647
13.6	-6	-225	-2452	-213	-106	-132	-1943	68	93	88	29	141	42	691	2880	194	632
13.7	-5	0	-1040	-138	84	-60	-3107	66	95	87	27	154	43	718	2861	198	667
13.8	3	-1155	-376	-341	360	-105	-3458	55	105	102	25	160	44	669	2970	215	680
13.9	2	-2722	-2306	-565	324	-187	-6462	75	92	89	18	182	38	687	2847	193	661
14	4	-534	-1052	-126	21	-48	-2546	74	104	96	28	184	37	665	2904	211	662
14.1	-3	-1079	-3157	-691	387	-189	-9675	65	92	131	20	173	32	662	2771	203	628
14.2	14	-1670	-1945	-400	312	-147	-7389	73	86	113	27	158	38	780	2761	199	620
14.3	10	591	333	-109	53	-85	-2524	68	88	94	15	184	39	761	2933	216	614
14.4	2	-58	-2090	-282	92	-73	-3820	64	81	103	29	167	48	733	2929	191	645
14.5	23	602	-3928	-104	-146	3	-3040	61	111	98	21	172	37	787	2754	197	589
14.6	2	456	-1402	-437	134	-117	-3039	62	64	88	20	136	31	733	2975	216	622
14.7	1	-1305	-678	-592	281	-203	-5413	69	65	99	37	147	37	731	2955	206	653
14.8	-11	-480	-1378	-433	153	-121	-5573	75	97	103	19	174	38	743	2783	216	637
14.9	-1	502	-594	-219	-43	-56	-1664	81	77	99	24	168	51	743	2887	232	649
15	-10	-922	-2047	-385	164	-130	-4434	63	91	90	25	191	44	697	2845	208	645
15.1	8	-1301	-2935	-366	-101	-79	-3367	69	90	95	26	181	38	724	2831	197	641
15.2	5	955	1147	3	-28	56	726	67	87	107	20	139	46	746	2985	215	663
15.3	1	-1662	-2509	-416	31	-114	-4672	74	124	103	25	187	39	698	2883	207	663
15.4	15	-111	1319	58	-14	-5	-350	67	98	101	21	200	39	705	2929	226	674
15.5	3	-1415	-350	-444	80	-117	-4894	50	92	103	29	200	40	724	2870	206	632
15.6	3	-2058	-3479	-737	22	-277	-7136	59	132	92	21	170	39	718	2757	205	664
15.7	-3	-2976	-6770	-948	210	-329	-11662	60	122	95	18	147	39	722	2649	190	621
15.8	-8	-1770	-6235	-578	558	-151	-8167	66	133	93	15	168	43	715	2678	196	645
15.9	8	386	-2247	-152	4501	-115	-4450	65	133	118	11	166	38	773	2837	192	675
16	-7	-1882	-2591	-691	183	-265	-7064	65	93	94	21	152	37	710	2831	184	668
16.1	-12	-1021	-1960	-435	-45	-165	-5251	53	81	97	18	189	39	692	2791	200	662
16.2	-10	-1063	-6895	-727	-79	-207	-9771	57	93	99	21	161	50	670	2649	197	646
16.3	7	-1978	-4136	-582	200	-196	-7025	75	80	110	20	169	36	749	2767	194	617
16.4	5	-2265	-3535	-593	-93	-199	-5990	70	109	91	13	172	43	744	2765	196	662
16.5	-1	-254	-233	-149	31	-82	-1703	62	83	87	31	173	48	696	2854	201	662
16.6	16	830	1542	113	-153	36	1008	76	110	99	19	130	44	716	2908	191	667
16.7	12	2348	1682	201	-185	97	2533	66	118	84	24	188	51	685	2966	212	659
16.8	8	2263	1765	44	26	-14	195	70	101	116	26	159	55	721	2912	199	656
16.9	8	2097	231	-150	-59	-48	-1186	62	80	112	25	172	47	770	2901	199	615
17	-1	883	-1932	-575	433	-270	-6100	63	84	110	18	151	37	713	2814	194	615
17.1	-9	228	-1151	-558	309	-241	-5677	76	119	104	-97	162	42	655	2856	182	632
17.2	3	868	818	-332	114	-150	-2886	76	98	101	29	181	44	705	2919	185	676
17.3	-2	2730	445	-243	71	-86	-2327	74	100	123	20	172	45	658	2862	210	638
17.4	10	1182	-369	-369	53	-171	-3807	58	110	98	20	156	40	662	2878	188	651
17.5	-13	436	-195	-461	188	-158	-5176	65	-72	93	20	140	34	676	2919	213	661
17.6	4	101	-3413	-583	114	-145	-6457	66	92	93	19	168	38	635	2817	201	650
17.7	1	1714	-1251	-384	95	-163	-4820	75	91	107	16	197	41	687	2828	197	667
17.8	-3	2265	-2215	-470	67	-166	-5880	76	73	100	25	160	49	680	2746	200	641
17.9	-12	712	-1562	-526	101	-201	-5446	74	107	114	24	195	52	658	2838	216	714
18	-2	-275	-4354	-767	-60	-238	-9430	74	108	102	25	188	50	675	2609	219	658

18.1	-12	-334	-6711	-763	-83	-245	-9860	51	97	114	29	153	45	612	2612	206	655
18.2	0	-1433	-7068	-795	-130	-268	-11292	57	86	101	26	173	43	601	2512	201	672
18.3	2	-955	-8406	-794	-80	-274	-10393	53	94	108	14	185	50	606	2624	210	665
18.4	-11	-1324	-5325	-833	73	-306	-9341	62	87	111	24	210	45	591	2739	219	644
18.5	-4	-1213	-4135	-838	-69	-286	-10509	51	116	131	22	169	41	566	2640	206	693
18.6	-6	-1664	-7265	-887	-104	-266	-10860	75	114	120	29	151	55	554	2599	208	672
18.7	-9	-1788	-6201	-814	-209	-281	-9976	51	86	104	21	164	44	591	2590	221	668
18.8	-7	-728	-5064	-905	-36	-272	-8561	62	76	93	19	164	43	572	2729	223	662
18.9	0	-1357	-5578	-689	-58	-232	-7490	46	112	97	25	161	40	587	2753	215	643
19	-4	-868	-5132	-766	-103	-274	-9352	46	110	107	25	177	36	618	2707	205	658
19.1	-3	495	-4109	-496	-213	-174	-5802	53	110	93	18	182	51	630	2770	198	632
19.2	-6	-1792	-9491	-907	-217	-273	-10995	48	100	94	21	173	39	565	2614	193	614
19.3	-3	-1200	-8260	-722	14	-208	-8785	49	89	78	19	190	45	585	2681	194	641
19.4	-6	779	-445	-255	69	-85	-484	66	93	95	30	189	46	603	2978	221	715
19.5	-4	2076	2815	-53	131	-2	2546	49	83	119	18	139	42	664	3032	236	663
19.6	5	2443	2267	310	142	-40	2322	42	115	92	13	184	44	692	3122	228	718
19.7	6	2478	2253	68	142	14	1263	54	115	121	25	167	44	671	2982	225	693
19.8	2	-397	-4733	-596	27	-154	-7239	51	80	106	32	168	40	643	2695	210	645
19.9	-4	1039	-4389	-377	2	-173	-4475	60	100	110	27	176	44	648	2808	213	658
20	-12	1215	-3729	-360	-6	-138	-5439	58	106	123	31	187	48	649	2704	214	658
20.1	2	2555	-3020	-434	-3	-136	-5570	55	117	123	19	209	51	635	2742	199	708
20.2	7	1334	-4062	-391	-51	-171	-7437	53	101	108	23	241	43	627	2683	189	681
20.3	-12	454	-7206	-644	-149	-199	-9141	64	117	103	24	170	63	636	2561	194	689
20.4	1	-184	-5579	-664	-287	-158	-9464	64	127	113	24	165	58	632	2475	213	644
20.5	-7	-867	-7959	-849	-212	-219	-12393	56	109	97	20	176	50	617	2501	210	652
20.6	-4	1272	-936	-364	-21	-108	-5334	47	100	115	26	160	43	691	2776	216	678
20.7	-4	-651	-7046	-854	-53	-266	-12779	54	91	99	26	179	60	604	2482	210	637
20.8	-2	-1160	-7352	-832	-69	-246	-14038	68	116	103	19	158	46	677	2393	210	649
20.9	-7	-1133	-6390	-876	-326	-276	-12501	61	104	94	25	192	38	650	2453	211	647
21	-1	171	-2653	-494	-177	-213	-7532	68	75	108	26	185	51	688	2656	229	661
21.1	-1	-915	-5030	-840	-251	-267	-11618	57	107	92	15	176	39	609	2533	206	641
21.2	-14	-2992	-11823	-1302	-565	-356	-17313	43	73	84	14	150	39	578	2312	186	580
21.3	-16	-2030	-11829	-1194	-422	-392	-14756	50	85	84	25	160	40	720	2395	187	578
21.4	-17	-1463	-8945	-935	-241	-366	-11627	53	111	89	21	148	35	735	2559	193	607
21.5	-14	733	-7953	-393	-271	-179	-8271	25	96	90	23	120	46	996	2633	202	589
21.6	7	4347	-477	509	-88	-35	-299	-3	92	87	38	142	46	1248	2910	203	641
21.7	9	3584	1621	50	93	-75	618	-7	131	99	29	184	59	842	3025	215	751
21.8	7	3622	5914	219	151	3	4549	-16	106	103	22	161	65	635	3178	243	755
21.9	11	2100	4978	-131	322	-155	-489	7	126	117	34	169	62	614	3042	221	715
22	-6	433	3120	-347	343	-154	-2386	31	93	105	38	188	56	593	2977	203	714
22.1	13	1438	1638	-127	231	-37	-848	21	128	107	35	158	49	589	2943	212	730
22.2	-5	462	3374	-239	238	-126	-2509	41	79	109	19	175	57	561	2923	209	708
22.3	4	-1112	-385	-442	-117	-145	-5265	56	91	94	23	174	41	589	2764	211	711
22.4	13	-1324	-2970	-536	-127	-182	-6477	57	113	95	16	159	46	596	2710	192	658
22.5	11	-191	518	-209	-111	-73	-3233	55	118	110	30	183	48	605	2763	230	693
22.6	13	-622	-687	-320	-145	-123	-5048	79	94	107	18	191	43	637	2708	210	674
22.7	6	-2011	-1268	-487	-278	-152	-7192	60	108	103	25	182	36	590	2581	194	663

22.8	0	-1849	-4537	-671	-194	-177	-10229	53	134	97	18	169	27	601	2515	201	674
22.9	14	-989	-2115	-509	-271	-137	-7914	60	126	107	35	165	45	616	2584	186	696
23	-8	-2598	-6292	-865	-281	-255	-11842	47	116	90	21	172	28	554	2473	187	680
23.1	10	-756	-2028	-551	-214	-147	-6888	74	124	100	22	172	39	761	2718	193	659
23.2	3	-475	-7883	-768	-145	-223	-11286	46	99	98	17	150	42	650	2569	184	642
23.3	0	587	-2261	-579	-18	-187	-8083	47	64	111	20	184	52	632	2613	200	694
23.4	-4	944	-1861	-480	84	-170	-7782	57	116	99	29	157	45	675	2754	194	669
23.5	3	1229	-1876	-245	-125	-104	-5903	59	143	101	32	185	46	655	2669	198	701
23.6	13	-182	-2960	-400	-261	-99	-5671	44	95	104	26	164	42	618	2624	211	671
23.7	6	93	-1700	-451	-137	-147	-5082	56	130	112	25	155	49	602	2771	200	695
23.8	-11	-172	-1631	-408	-203	-133	-4567	56	111	91	21	120	42	598	2794	215	696
23.9	5	97	302	-202	-58	-135	-3415	48	87	103	26	166	49	607	2830	205	668
24	-4	-72	-2157	-447	-116	-209	-5724	39	129	86	21	161	37	587	2799	192	675
24.1	9	2065	-997	-240	-165	-105	-3503	38	96	113	20	160	55	589	2812	225	710
24.2	-4	374	634	-136	-136	-95	-2384	27	89	111	28	167	33	636	2898	213	709
24.3	-6	-1128	-3300	-654	-193	-215	-8047	35	122	95	22	168	36	623	2686	201	671
24.4	-2	-21	1344	-343	-87	-173	-4926	38	129	115	28	185	46	625	2743	241	715
24.5	-3	896	2663	-143	-85	-65	-4301	51	127	109	25	189	38	650	2799	212	711
24.6	-14	-309	-2793	-514	-229	-154	-9405	51	120	95	19	160	42	675	2554	202	709
24.7	-6	-1316	-2196	-493	-307	-116	-8709	43	103	89	24	194	34	586	2542	205	698
24.8	8	-1650	-5288	-712	-355	-212	-9807	68	59	99	24	166	33	568	2492	188	631
24.9	-9	-425	-2558	-526	-124	-226	-7394	70	120	109	28	161	51	611	2635	210	641
25	3	478	-4495	-749	-262	-248	-9596	70	93	103	29	125	38	688	2545	184	639
25.1	1	-471	-2314	-528	-106	-187	-8770	61	86	108	22	155	42	639	2643	217	644
25.2	-16	-2522	-8888	-1049	-326	-330	-13507	52	89	89	13	139	33	558	2468	186	600
25.3	-2	-1522	-8186	-972	-304	-276	-12379	50	101	97	28	164	51	548	2485	183	609
25.4	-10	89	-3220	-605	-193	-206	-6876	36	116	93	28	177	43	572	2701	189	668
25.5	-9	27	-1773	-361	-136	-194	-6339	48	113	103	26	164	51	597	2732	192	660
25.6	8	1238	-757	-248	-59	-144	-3330	10	104	92	26	187	52	639	2824	191	676
25.7	-4	1041	417	-270	44	-188	-3853	14	113	94	29	157	45	832	2868	194	675
25.8	-1	551	2805	-203	295	-201	-3637	9	92	101	28	205	41	887	2880	187	692
25.9	1	1135	3966	-206	209	-121	-1460	1	107	103	34	182	66	574	3017	181	682
26	-1	2144	5353	-165	186	-112	-1162	-7	92	95	44	165	71	555	2980	188	712
26.1	-1	2952	7505	137	104	15	2495	-2	86	97	35	198	65	551	3101	205	744
26.2	14	3336	7995	355	88	29	2708	-3	124	109	28	184	57	583	3058	203	703
26.3	10	2155	7120	146	197	-8	1840	1	117	98	32	167	53	569	3088	206	705
26.4	9	1682	3368	-173	239	-95	-1261	31	78	106	35	155	44	617	2943	221	681
26.5	-2	3267	2002	-169	39	-127	-2529	50	104	110	21	195	53	674	2895	205	635
26.6	5	1044	-1412	-408	85	-93	-5608	43	100	110	27	193	39	707	2730	200	681
26.7	-1	309	-1910	-310	-137	-121	-5950	46	101	89	16	169	47	597	2697	184	656
26.8	-5	1151	-1487	-323	95	-163	-5119	47	111	111	18	188	47	693	2856	214	686
26.9	11	1955	2340	-17	148	-50	-2549	57	125	112	18	162	50	663	2854	217	680
27	-4	-1343	-9161	-956	-354	-229	-13817	57	107	86	27	171	47	656	2388	164	634
27.1	15	686	-1170	-229	-99	-90	-5859	76	88	105	27	161	49	620	2688	200	672
27.2	1	425	-1638	-499	-230	-140	-7137	65	106	118	29	187	50	662	2614	185	703
27.3	4	316	-2749	-445	-178	-120	-7685	54	119	107	23	179	46	579	2604	191	641
27.4	2	51	-3163	-461	-244	-160	-8776	55	76	114	30	154	52	565	2555	175	646

27.5	8	-93	-1198	-196	-117	-146	-5596	64	106	104	27	153	39	606	2693	185	688
27.6	11	1046	-84	-230	-144	-101	-5371	66	110	112	17	191	57	611	2699	213	648
27.7	-5	-1130	-5752	-627	-209	-178	-10813	61	116	97	33	166	56	584	2525	182	634
27.8	9	1315	1473	-46	-4	-85	-2755	65	107	125	27	150	56	598	2768	183	627
27.9	-9	-570	-3321	-370	-288	-184	-7704	58	90	81	22	154	48	581	2713	183	635
28	15	1155	5568	89	-49	-55	-369	51	90	98	35	165	50	639	3008	186	699
28.1	5	424	4436	-329	52	-169	-4635	69	138	98	32	206	45	667	2877	194	685
28.2	-3	389	2557	-416	275	-187	-5033	68	121	105	24	142	39	641	2869	182	665
28.3	-2	-70	-919	-553	-23	-222	-7616	64	119	96	24	159	49	648	2745	193	665
28.4	-3	1813	1577	-266	104	-144	-3420	62	98	99	25	179	43	644	2814	209	661
28.5	-1	801	-1275	-304	-135	-176	-6480	57	119	94	26	184	41	641	2649	208	649
28.6	6	1527	748	-165	-328	-139	-6125	56	109	98	28	185	42	656	2648	222	636
28.7	8	1225	823	-275	-151	-108	-5097	69	81	105	25	170	48	613	2734	215	656
28.8	-1	-717	-4677	-642	-265	-206	-9264	52	89	101	20	157	48	595	2523	209	600
28.9	-7	-280	-4843	-708	-130	-229	-9660	68	95	96	27	172	43	637	2628	191	629
29	-19	1495	-13	-294	-22	-129	-5069	69	123	104	29	158	45	678	2766	200	635
29.1	4	1343	492	-365	-12	-100	-5504	74	120	100	27	159	63	646	2769	200	669
29.2	2	-1012	-1395	-847	313	-226	-10420	68	113	98	29	150	40	632	2675	187	625
29.3	-12	-3418	-9410	-1431	359	-417	-18878	49	81	84	17	147	36	635	2493	199	603
29.4	-9	-1132	-6488	-878	13	-263	-12277	56	79	81	20	156	48	635	2615	188	599
29.5	-1	46	-1727	-703	226	-206	-7409	70	111	76	26	177	57	633	2812	201	682
29.6	-1	-1474	86	-1010	638	-305	-10450	64	67	81	18	164	53	627	2892	213	654
29.7	-19	-3808	-3330	-1627	904	-512	-17818	58	91	77	20	171	29	632	2706	209	646
29.8	-7	-3688	-5340	-1498	937	-507	-17656	61	116	76	15	155	37	638	2721	192	642
29.9	-9	-2249	-786	-1076	417	-341	-13170	70	84	68	26	206	39	632	2708	207	696
30	-9	-2729	-2302	-1290	440	-428	-14669	72	96	93	14	160	34	628	2766	194	623
30.1	-9	-3059	-909	-1252	388	-492	-14722	68	100	90	18	167	49	617	2700	175	607
30.2	-4	-1116	-340	-969	400	-418	-12366	69	87	79	32	166	41	635	2783	170	622
30.3	-13	1338	2697	-765	238	-325	-8432	62	87	107	21	167	50	672	2877	179	603
30.4	-13	-1375	-540	-1133	205	-402	-11956	60	104	95	20	164	41	694	2992	169	663
30.5	0	-99	1213	-863	160	-354	-9530	59	99	95	24	162	33	643	2843	171	637
30.6	-13	1571	2833	-425	191	-210	-4452	72	85	94	23	167	52	689	2925	186	625
30.7	-16	61	-2444	-859	-8	-306	-9466	59	109	80	26	173	37	621	2735	165	626
30.8	1	28	-3645	-783	-25	-267	-10088	57	81	99	16	126	52	640	2656	185	616
30.9	0	-609	-2980	-977	208	-324	-11487	61	72	91	29	148	44	652	2674	170	563
31	-3	1307	-1130	-644	276	-174	-7691	56	105	85	21	156	50	642	2725	186	605
31.1	-6	125	3461	-722	378	-274	-7667	65	97	104	30	154	45	602	2855	200	636
31.2	-16	-1126	3723	-766	225	-314	-8725	74	92	87	28	162	60	628	2805	184	679
31.3	2	-775	1199	-763	94	-256	-9172	63	87	86	20	163	52	537	2782	189	644
31.4	-14	-1711	849	-873	284	-353	-10421	53	110	101	17	152	48	561	2792	176	630
31.5	-16	-1207	3193	-665	291	-226	-7876	63	84	115	28	149	67	566	2856	196	676
31.6	0	-229	150	-600	256	-193	-8138	60	104	96	25	147	52	572	2772	181	678
31.7	9	283	2491	-428	244	-158	-4805	56	-94	109	25	168	49	575	2876	206	664
31.8	-4	-240	-3045	-621	-38	-208	-8296	65	88	87	24	154	52	625	2722	173	636
31.9	3	100	1700	-536	208	-229	-7448	60	75	91	25	153	45	591	2857	191	640
32	2	-944	843	-851	406	-262	-9603	62	123	90	30	177	55	635	2814	186	671
32.1	0	-922	3910	-760	288	-224	-8584	57	116	84	20	161	47	621	2786	200	654

32.2	0	-1891	1786	-852	124	-272	-10507	62	73	91	20	195	48	522	2681	198	626
32.3	-23	-1438	9814	-799	336	-311	-9455	52	79	93	31	189	42	580	2721	196	605
32.4	-5	-740	11623	-769	69	-276	-8797	45	79	96	52	142	48	505	2684	167	582
32.5	-2	509	21272	-548	382	-182	-5850	54	90	92	62	145	51	492	2788	189	580
32.6	-9	717	16425	-485	281	-202	-5888	47	107	92	35	168	56	563	2844	180	602
32.7	-7	343	8356	-244	146	-124	-3408	50	104	100	32	149	44	605	2918	180	679
32.8	3	1139	7642	-225	122	-74	-3503	51	99	95	27	166	54	614	2905	191	647
32.9	0	28	5527	-386	127	-206	-5818	54	72	94	24	160	48	612	2901	185	602
33	-18	-1917	3471	-976	592	-290	-9907	61	83	95	21	144	57	603	2845	202	647
33.1	-17	-184	2292	-636	300	-257	-8489	54	113	102	24	137	33	563	2876	203	625
33.2	7	192	4017	-495	124	-188	-6145	72	75	93	31	180	61	593	2833	164	632
33.3	0	579	3908	-338	136	-167	-4614	70	83	84	26	203	53	640	2821	195	627
33.4	16	235	1817	-397	-98	-146	-5579	60	111	80	35	183	50	593	2833	194	639
33.5	0	594	3920	-284	-20	-124	-2683	61	122	98	24	160	44	632	2915	192	673
33.6	-9	-69	2732	-540	93	-185	-5091	61	77	110	39	173	52	610	2906	195	644
33.7	-7	418	1494	-397	157	-130	-5868	59	92	97	28	132	58	617	2823	201	630
33.8	7	-77	-371	-527	-36	-151	-6724	64	84	91	27	144	49	604	2759	192	639
33.9	1	55	722	-360	58	-132	-5546	57	90	101	30	144	50	607	2853	201	644
34	5	647	5324	-254	9	-49	-4879	59	91	118	33	175	37	629	2832	206	666
34.1	4	-1283	-3116	-751	-69	-197	-11881	46	99	89	20	174	49	580	2554	179	610
34.2	-13	2	244	-657	-165	-159	-8699	22	67	103	-4	179	45	600	2583	193	607
34.3	-10	-1957	-5186	-1065	-348	-282	-13910	-3	73	80	23	127	43	575	2452	173	562
34.4	1	-1087	-4401	-904	-322	-232	-12383	27	67	93	22	157	47	671	2543	169	555
34.5	6	-1001	-5232	-828	-132	-185	-11836	33	52	95	20	109	62	598	2517	175	572
34.6	5	28	-825	-481	-21	-83	-7691	60	109	91	27	178	62	544	2748	208	630
34.7	18	1167	1926	-272	53	11	-4533	52	101	111	21	188	54	568	2754	220	667
34.8	10	999	3468	-291	352	1	-4396	43	85	106	23	156	56	557	2831	224	669
34.9	-9	-997	-3808	-971	315	-203	-13608	53	96	104	23	208	67	559	2591	214	629
35	-12	-1309	-7118	-1008	427	-222	-14916	37	71	104	16	158	85	561	2594	204	629
35.1	-19	-1998	-7765	-1207	418	-313	-17258	31	92	111	20	152	71	527	2522	170	636
35.2	-10	-2721	-9176	-1384	400	-360	-18775	52	91	115	25	170	71	537	2511	205	607
35.3	-10	-1962	-7395	-1326	477	-301	-18722	31	92	97	25	178	75	547	2413	195	655
35.4	14	-542	-5499	-1402	875	-318	-20335	44	98	111	27	213	98	539	2508	192	630
35.5	-11	-1264	-8959	-1569	746	-364	-22713	24	92	84	15	129	79	473	2389	158	595
35.6	1	-2510	-11145	-1660	355	-396	-22867	39	78	83	19	159	77	482	2378	164	613
35.7	3	-1650	-7000	-1375	726	-378	-20311	42	53	92	21	167	76	489	2515	177	576
35.8	-18	-2761	-8498	-1532	559	-422	-21773	29	86	101	13	179	63	515	2357	162	602
35.9	-17	-828	-2412	-1575	846	-407	-21417	41	72	102	20	160	96	525	2442	183	589
36	-3	-1495	-4250	-1346	620	-360	-19433	23	72	93	19	177	85	541	2451	157	567
36.1	-13	-3136	-9066	-1356	145	-391	-19167	36	81	85	18	148	65	516	2363	165	577
36.2	-3	-1996	-4552	-1155	316	-390	-15788	46	111	80	21	129	66	510	2524	196	627
36.3	-12	-1954	2191	-985	332	-389	-12515	50	73	87	23	166	56	561	2779	184	599
36.4	-8	-1542	3288	-869	269	-289	-10743	65	91	75	19	152	53	558	2713	179	618
36.5	-13	-633	6820	-498	226	-248	-6596	62	111	81	27	161	61	598	2874	180	676
36.6	-8	-1259	8164	-371	275	-214	-5661	54	93	82	41	146	50	559	2865	167	664
36.7	8	-1101	9100	-316	207	-180	-5556	60	106	99	28	175	54	560	2801	169	668
36.8	4	-2600	6148	-942	463	-376	-11857	56	108	105	31	156	55	544	2686	158	658

36.9	-1	-1190	8041	-440	221	-173	-5826	50	109	90	33	148	72	545	2850	179	666
37	2	-1622	6050	-628	147	-219	-8589	39	91	94	22	150	53	541	2740	168	689
37.1	0	-1649	4221	-680	337	-273	-9963	30	96	89	29	149	54	525	2808	180	654
37.2	-7	-1968	2518	-704	255	-232	-10941	21	75	105	26	149	50	513	2648	167	609
37.3	-11	-2738	4473	-705	30	-259	-10034	17	94	94	46	145	45	557	2660	161	672
37.4	-11	-2333	4969	-539	12	-246	-8042	35	110	101	39	136	46	571	2725	191	639
37.5	-9	-2104	4206	-433	-85	-231	-7245	50	90	93	37	142	60	605	2767	179	622
37.6	-11	-1235	5605	-437	24	-235	-5808	48	98	93	37	154	45	587	2835	191	635
37.7	0	-1665	4104	-563	68	-214	-6640	28	90	74	35	166	53	562	2747	191	640
37.8	-5	-1772	3756	-696	187	-259	-8675	48	119	95	36	171	55	549	2778	186	696
37.9	-15	-1676	2538	-700	29	-238	-9556	26	104	101	25	180	55	557	2737	190	651
38	-15	-2444	-927	-963	181	-341	-12080	33	83	77	31	152	64	510	2714	170	628
38.1	-8	-2655	4709	-684	321	-279	-9570	45	93	71	31	148	64	571	2809	169	631
38.2	-20	-2453	6233	-1119	420	-357	-13721	53	89	95	16	147	71	493	2712	159	647
38.3	-12	-2229	11670	-767	264	-273	-8403	62	115	87	35	122	68	533	2883	172	640
38.4	-13	-1996	11694	-575	99	-218	-7744	56	113	99	53	163	54	536	2840	161	659
38.5	-4	-153	14337	-364	286	-176	-5083	43	94	81	46	168	66	566	2865	181	679
38.6	0	-1159	11933	-436	218	-202	-6373	27	114	86	51	153	37	566	2828	177	708
38.7	-12	-725	11955	-517	333	-204	-7878	14	105	85	67	174	70	535	2791	156	670
38.8	-12	-1400	7332	-777	591	-262	-10597	0	111	96	64	152	82	503	2714	171	658
38.9	-16	-1428	8422	-700	110	-228	-8875	5	82	80	62	145	71	507	2765	163	630
39	-18	-4174	563	-1205	-40	-428	-16029	28	115	71	33	147	59	487	2491	138	636
39.1	-14	-2529	8715	-923	267	-324	-9984	42	82	78	59	164	74	476	2830	140	670
39.2	-5	-3264	9014	-847	143	-355	-9054	45	76	81	48	167	55	570	2830	177	631
39.3	1	-1884	10960	-345	56	-162	-3140	45	114	83	34	171	68	547	2899	184	647
39.4	-5	-3680	11132	-647	179	-303	-5640	45	121	94	40	123	57	532	2908	189	674
39.5	-18	-4089	10677	-922	237	-343	-8264	34	98	80	30	155	47	504	2857	173	657
39.6	-12	-4706	8851	-969	258	-347	-10763	29	103	84	49	163	51	487	2779	161	653
39.7	-13	-4691	11544	-948	299	-356	-9628	37	110	75	32	163	53	494	2798	161	673
39.8	7	-4734	13522	-883	135	-393	-7723	40	131	92	34	172	53	576	2882	167	655
39.9	-13	-4532	12797	-962	246	-468	-7217	35	115	95	33	176	40	539	2959	186	659
40	-6	-3255	11445	-449	-106	-236	-3965	39	83	96	36	131	51	503	2919	180	687
40.1	5	-2023	12473	-36	-270	-69	-98	47	82	90	52	148	62	552	2940	189	646
40.2	-13	-1981	13216	-154	-79	-102	-1592	51	108	65	49	177	52	572	2932	179	656
40.3	1	-3510	11320	-408	-43	-191	-4106	41	125	87	59	170	46	533	2857	178	673
40.4	-20	-2747	12586	-439	-144	-182	-4897	45	124	79	62	177	62	460	2825	170	650
40.5	1	-2271	15587	-267	-69	-137	-1601	53	105	63	59	162	57	515	2916	166	648
40.6	7	-1179	14016	21	-257	-53	668	51	127	97	39	154	55	575	2906	179	650
40.7	-9	-613	14594	237	-231	50	3426	64	95	92	39	159	67	584	3071	180	649
40.8	16	-889	17988	271	-248	39	4537	56	93	71	58	188	66	564	3029	168	707
40.9	-1	-2244	16480	-150	154	-135	-1059	42	115	78	54	156	49	561	3043	179	692
41	5	-2591	15375	-261	123	-159	-2339	42	101	89	56	165	49	554	3024	179	702
41.1	-4	-2345	8992	-237	-91	-126	-4618	32	106	88	61	168	59	553	2756	183	698
41.2	5	-1232	11863	80	-229	-31	-419	18	95	114	60	144	68	560	2882	188	647
41.3	8	-2514	5588	-330	-332	-137	-6220	25	64	80	63	137	37	562	2652	183	656
41.4	-6	-2643	7581	-548	30	-208	-7193	11	82	71	56	170	63	523	2759	176	683
41.5	-16	-3239	7904	-575	-117	-243	-7652	19	94	74	68	151	42	512	2721	174	682

41.6	-6	35	9143	-399	150	-212	-5200	22	131	94	67	166	45	570	2919	177	712
41.7	12	-1481	6694	-443	-9	-212	-5562	10	112	88	25	159	45	587	2770	202	724
41.8	-3	-1429	8871	-241	32	-184	-3585	-7	89	80	54	171	56	551	2867	210	679
41.9	-8	-1513	7412	-247	-188	-140	-3968	-10	92	97	64	189	41	549	2783	193	668
42	5	-1465	5584	-284	-129	-97	-5314	-15	97	90	44	147	59	530	2740	192	695
42.1	-8	-1266	6932	-236	-28	-138	-4089	-15	79	89	46	166	64	564	2875	176	703
42.2	1	-836	5867	-214	-31	-89	-3885	-22	99	74	41	181	54	566	2832	180	681
42.3	4	-1903	958	-441	-4	-166	-7366	-20	110	73	28	173	46	538	2642	184	708
42.4	20	-2466	4852	-380	-74	-148	-5705	14	74	86	30	168	71	521	2796	178	646
42.5	5	-2128	7219	-372	23	-197	-5469	2	88	91	51	146	50	541	2871	182	668
42.6	-2	-2049	5077	-407	-103	-181	-5588	-7	81	82	28	178	55	563	2779	182	688
42.7	-17	-2795	4406	-486	-35	-223	-7020	-1	105	87	42	166	59	549	2700	172	653
42.8	-3	-2945	5351	-586	155	-289	-7434	-1	78	63	37	161	53	530	2819	173	658
42.9	-6	-1302	9424	-255	84	-184	-2980	-10	91	94	58	169	63	542	2919	211	657
43	-8	-2432	7105	-649	-56	-270	-7990	-18	111	94	62	172	59	527	2703	193	649
43.1	-5	-2427	10226	-459	32	-243	-6953	-5	111	94	79	193	68	557	2752	192	643
43.2	-8	-3323	7624	-787	159	-336	-9319	-12	79	83	70	164	66	538	2817	176	637
43.3	-6	-2817	8530	-641	291	-292	-7736	-2	89	91	60	166	66	521	2883	181	643
43.4	-1	-1325	12626	-508	111	-217	-5457	-19	113	101	54	131	67	550	2854	197	657
43.5	-6	-841	14303	-78	-10	-105	-1325	-27	99	97	58	147	82	534	2891	194	672
43.6	-8	-1587	12772	-322	-101	-160	-6496	-23	80	80	49	184	71	543	2716	182	663
43.7	-10	-1622	10750	-325	-127	-187	-7130	-37	100	90	78	186	62	534	2723	177	657
43.8	-2	-2302	8150	-543	-222	-249	-7931	-31	88	94	60	151	62	509	2629	182	633
43.9	-17	-2436	8570	-704	56	-314	-9986	-31	94	101	58	144	54	502	2646	193	624
44	-17	-1327	10048	-769	189	-370	-9684	-17	119	99	63	158	55	637	2794	185	647
44.1	-2	-292	13325	-308	326	-177	-4748	-30	96	105	65	173	57	590	2885	200	676
44.2	8	54	8463	-296	-51	-144	-5509	-84	105	100	64	155	66	599	2761	202	703
44.3	-9	304	6954	123	2	-120	-4855	-114	101	99	45	148	52	615	2779	200	710
44.4	7	-347	5091	-399	34	-200	-6541	-116	97	109	45	171	48	583	2840	200	679
44.5	-3	-94	3594	-528	147	-161	-7387	-124	104	105	25	183	70	595	2753	194	703
44.6	-1	223	3280	-396	103	-90	-6070	-194	76	112	25	178	52	574	2797	195	662
44.7	5	91	2034	-562	228	-156	-7073	-261	84	112	27	156	51	550	2808	201	680
44.8	-5	-10279	-24857	-2796	-1050	-573	-38046	28613	61	46	26	50	177	249	1356	142	272
44.9	-11	-11909	-33602	-3212	-1424	-685	-45077	31692	50	38	24	36	169	180	966	140	240
45	-6	-6911	-9658	-1897	-677	-376	-25878	32549	67	56	43	82	216	378	1873	186	448
45.1	-9	-5118	-2724	-1259	-736	-336	-19058	411	101	73	58	101	37	436	2097	152	500
45.2	1	-5100	-2630	-1284	-869	-348	-19877	162	78	56	61	105	32	412	2037	138	517
45.3	-10	-1775	11905	-740	-256	-262	-10436	165	97	91	76	106	48	459	2556	171	649
45.4	7	-909	9108	-716	-300	-243	-9656	297	102	101	75	123	46	502	2635	168	588
45.5	0	-1178	11195	-581	-280	-200	-8362	232	117	89	74	122	51	495	2626	179	615
45.6	-2	-3244	7232	-1002	-354	-339	-13034	11	103	81	71	134	44	461	2519	152	643
45.7	2	-3340	5037	-999	-150	-332	-12836	347	91	92	43	90	42	499	2585	175	600
45.8	-1	-4679	639	-1221	-149	-386	-14780	524	102	87	37	105	47	465	2582	167	596
45.9	11	-4540	4331	-1085	-202	-347	-12263	1051	98	80	65	116	65	467	2584	165	606
46	-3	-4096	6285	-936	-52	-313	-11188	1648	100	85	48	119	60	482	2692	181	604
46.1	1	-4354	3955	-965	-233	-290	-11534	461	96	72	55	118	55	438	2628	168	605
46.2	-9	-4474	2521	-950	-167	-254	-12326	224	115	75	39	109	55	445	2553	181	589

46.3	-7	-4317	4065	-1056	-143	-387	-12674	400	92	74	42	120	53	471	2569	173	561
46.4	-6	-3785	6722	-891	-93	-331	-11362	-9	95	85	56	110	62	485	2657	160	590
46.5	5	-3821	5750	-857	-241	-292	-11131	-9	96	76	60	115	56	456	2614	178	587
46.6	-9	-3617	6393	-842	-227	-270	-11204	68	90	85	65	113	42	454	2539	172	565
46.7	1	-3798	7228	-855	-112	-297	-12102	123	101	78	83	137	48	492	2556	172	632
46.8	-4	-4808	62	-1361	-86	-432	-16846	1557	87	79	47	114	49	486	2450	177	589
46.9	-7	-4614	-4352	-1173	-364	-335	-15233	1890	88	87	40	120	50	467	2390	182	600
47	10	-4439	-722	-1020	-220	-322	-13763	214	81	78	42	130	46	486	2529	181	606
47.1	0	-3847	157	-876	-153	-289	-12446	52	118	81	39	132	43	498	2544	177	616
47.2	-4	-3852	-1236	-1121	-310	-356	-14620	71	91	91	38	122	45	492	2370	175	586
47.3	-1	-4680	-4057	-1215	-484	-326	-16045	81	85	76	22	128	41	598	2362	168	587
47.4	-3	-5814	-7648	-1434	-293	-418	-19325	86	90	79	31	119	43	461	2261	165	638
47.5	-16	-5554	-7764	-1783	48	-546	-23377	283	95	75	24	97	45	486	2300	182	669
47.6	-1	-4346	-4082	-1620	260	-486	-20721	983	94	87	19	116	55	534	2477	174	599
47.7	3	-5553	-5070	-1583	-21	-452	-20375	1937	109	83	35	96	59	455	2364	185	583
47.8	-6	-5562	-9431	-1635	78	-499	-23147	820	80	80	17	99	55	425	2204	160	553
47.9	-4	-4696	-1356	-1462	355	-463	-18998	1698	121	85	27	117	49	510	2443	182	607
48	-10	-3872	1651	-1201	77	-337	-15224	1937	82	76	30	142	57	516	2524	164	610
48.1	-1	-4693	1629	-1260	-5	-394	-16051	1991	96	64	40	113	39	467	2456	157	607
48.2	-7	-5017	3004	-1199	7	-375	-16026	596	93	65	40	120	41	482	2451	149	578
48.3	-5	-5204	5873	-1364	-114	-442	-16589	997	79	62	40	111	43	473	2474	150	578
48.4	-6	-4441	-7772	-1124	-19	-450	-13296	1165	87	81	50	111	47	502	2621	160	557
48.5	-15	-2533	-7690	-982	-24	-428	-12546	837	112	70	42	111	36	455	2638	155	615
48.6	-1	-3823	-5999	-872	-120	-344	-10191	1525	103	72	41	136	56	515	2699	164	609
48.7	-1	-2891	-4505	-643	-119	-290	-8718	2391	87	74	32	129	50	530	2699	158	602
48.8	8	-2463	-120	-449	-36	-252	-6623	366	93	91	54	131	44	534	2779	162	628
48.9	10	-3531	-4901	-770	-149	-344	-9597	323	123	76	41	129	46	521	2646	166	608
49	3	-2744	-1238	-517	-193	-315	-6766	359	109	90	42	112	42	500	2750	157	594
49.1	-10	-2717	-1873	-633	-13	-321	-7973	353	106	78	63	131	40	550	2707	161	626
49.2	-7	-3976	-5904	-903	78	-383	-12277	347	112	83	49	111	37	549	2637	179	644
49.3	-2	-2577	-1579	-639	-92	-279	-8036	360	112	111	56	112	41	576	2702	146	609
49.4	-10	-2191	2572	-433	16	-203	-5640	367	106	73	62	131	36	520	2770	152	610
49.5	-8	-788	1634	-170	-96	-112	-2447	377	82	91	55	96	41	558	2869	175	630
49.6	5	-3955	-5364	-955	223	-360	-12710	359	107	78	53	104	47	544	2652	166	660
49.7	1	-3022	-2025	-747	190	-331	-9414	376	113	84	65	124	41	533	2740	173	660
49.8	3	-2816	-7131	-734	135	-269	-10690	346	123	80	52	103	38	541	2650	160	643
49.9	6	-2795	-4559	-670	-46	-243	-8110	347	87	93	54	132	38	566	2738	176	627
50	-5	-3647	-9679	-934	100	-387	-12109	345	96	102	32	103	47	533	2651	191	628
50.1	-10	-3504	-11225	-869	-45	-331	-11940	321	89	75	19	109	37	513	2588	166	622
50.2	0	-3402	-5592	-852	34	-307	-9185	308	90	87	36	117	44	500	2663	169	632
50.3	-7	-5148	-11376	-1320	-205	-454	-16136	279	76	79	40	113	36	460	2403	140	615
50.4	-1	-4664	-12174	-1171	-122	-435	-15196	325	121	85	34	101	41	509	2479	150	599
50.5	7	-4759	-2494	-1324	259	-502	-15812	355	81	76	47	114	34	510	2612	146	597
50.6	-12	-4141	770	-1222	296	-459	-16980	363	85	91	38	111	36	484	2532	141	596
50.7	-15	-3386	306	-930	-113	-389	-13055	382	101	65	69	105	39	487	2626	139	575
50.8	6	-2790	6654	-503	-78	-271	-6235	405	83	76	66	119	42	555	2745	141	602
50.9	1	-3636	5447	-656	-5	-362	-9022	419	113	75	62	111	45	511	2788	136	617

51	-1	-1724	9365	-280	-104	-183	-3951	426	81	66	63	118	51	488	2817	142	608
51.1	-3	-2711	10541	-298	157	-264	-5253	429	76	92	83	130	49	583	2797	144	573
51.2	-3	-3621	9429	-567	8	-381	-7565	396	86	82	70	106	28	564	2791	154	595
51.3	4	-3535	4145	-731	-126	-278	-9747	397	121	70	63	110	43	531	2659	137	595
51.4	-9	-2074	4957	-324	-48	-239	-5744	421	123	86	45	107	40	516	2708	142	597
51.5	15	-2815	9138	-437	-86	-242	-5966	420	112	86	74	110	52	504	2777	157	622
51.6	3	-3212	7496	-502	-4	-249	-6945	419	85	74	70	117	38	527	2719	137	585
51.7	3	-2798	5670	-406	-181	-216	-7389	393	78	99	74	128	35	509	2660	140	591
51.8	-6	-3427	4451	-743	-103	-307	-9146	403	110	64	67	117	40	512	2670	140	618
51.9	-10	-3457	-1984	-763	-133	-311	-10946	415	79	79	53	99	35	507	2617	139	568
52	1	-3010	5883	-610	34	-293	-7565	452	110	89	46	137	27	533	2810	155	627
52.1	-3	-3204	5422	-753	107	-349	-8577	451	88	92	50	85	42	502	2693	145	592
52.2	-4	-3401	7618	-601	94	-304	-7165	433	124	100	57	136	40	550	2807	164	668
52.3	5	-3107	-43	-579	-130	-231	-7721	383	126	83	58	116	47	530	2627	143	649
52.4	-12	-2971	1715	-683	14	-252	-6869	391	124	89	78	123	52	493	2737	172	649
52.5	8	-3262	-453	-581	-3	-237	-6984	352	111	100	55	136	41	532	2780	160	653
52.6	-11	-6907	-6391	-1629	187	-543	-19724	310	120	74	46	126	22	491	2432	156	618
52.7	-9	-4589	-6251	-1004	-196	-331	-13138	319	97	89	55	140	40	511	2517	145	610
52.8	1	-5944	-6343	-1447	166	-468	-16523	281	107	76	43	112	37	496	2543	169	608
52.9	-7	-6535	-11118	-1646	281	-497	-20017	284	127	77	50	113	27	491	2478	141	575
53	-8	-6386	-7659	-1578	595	-484	-20024	276	83	77	65	119	29	473	2505	165	633
53.1	0	-7275	-13572	-1884	203	-582	-25049	269	86	66	47	105	39	488	2268	138	597
53.2	-10	-6438	-15599	-1486	-318	-461	-21204	326	81	63	45	98	34	453	2254	136	506
53.3	3	-2638	1793	-794	-158	-332	-8117	360	84	76	41	120	50	546	2716	158	556
53.4	-5	-3673	4545	-978	-97	-369	-11255	375	111	72	73	126	40	539	2613	152	561
53.5	-2	-2804	6678	-563	-142	-257	-9022	380	108	62	108	127	40	501	2706	154	575
53.6	7	-3122	12147	-696	19	-315	-9786	397	77	67	107	98	33	463	2681	150	570
53.7	-6	-4081	13666	-1152	208	-419	-14768	400	88	66	108	97	15	472	2524	128	534
53.8	-13	-3551	16913	-942	158	-400	-12137	405	74	72	109	118	23	511	2655	129	560
53.9	-4	-4208	12636	-922	67	-447	-11834	412	91	60	98	112	27	509	2704	137	576
54	7	-3387	13108	-691	213	-386	-9717	409	89	85	116	97	42	483	2702	134	630
54.1	3	-3856	8840	-847	44	-362	-10326	400	96	73	82	106	26	479	2688	137	596
54.2	3	-1927	11429	-277	-73	-184	-3383	414	95	75	103	116	43	509	2803	152	614
54.3	0	-3663	4937	-843	29	-323	-9901	409	97	77	87	130	31	539	2681	161	638
54.4	-2	-3868	2127	-866	74	-339	-10041	422	87	81	73	115	36	522	2679	145	605
54.5	-4	-2628	4550	-521	-52	-219	-5709	419	97	78	78	126	39	555	2816	159	629
54.6	-6	-3142	2277	-662	-57	-322	-8919	435	80	82	59	104	29	485	2638	139	561
54.7	6	-2155	8922	-332	-30	-192	-4975	454	124	87	71	139	33	523	2795	162	604
54.8	-3	-2863	11220	-576	-13	-324	-7617	466	85	79	66	122	28	490	2756	148	550
54.9	-10	-2098	11574	-369	-189	-242	-5383	449	97	78	65	115	15	532	2786	150	581
55	2	-1756	12830	-165	-153	-217	-4037	473	101	80	80	105	17	591	2831	142	578
55.1	8	55	16078	623	-228	77	3209	468	104	91	86	114	28	625	2974	148	628
55.2	-10	-1771	9485	0	13	-192	-2246	400	94	87	63	116	29	569	2863	144	613
55.3	9	-956	6968	-205	-73	-167	-3770	377	101	78	71	140	45	572	2835	156	577
55.4	-15	-3313	-2933	-854	-86	-310	-12383	322	103	77	75	110	35	547	2540	139	561
55.5	10	-2626	-2190	-521	-292	-215	-7835	340	87	73	48	101	43	522	2732	138	591
55.6	-1	-4372	2924	-920	96	-407	-12774	336	85	79	64	118	30	588	2636	139	563

55.7	-7	-4665	-498	-890	-249	-362	-12753	338	99	83	82	94	42	503	2518	147	580
55.8	3	-3429	204	-686	-120	-359	-10627	401	80	78	54	113	42	648	2555	142	562
55.9	0	-2104	5367	-625	51	-344	-9498	458	81	79	55	121	32	701	2654	126	554
56	-10	-2998	8212	-834	296	-395	-11859	473	96	102	53	118	38	658	2623	141	582
56.1	-12	-1704	7133	-700	346	-367	-11359	501	86	112	62	126	57	622	2819	135	610
56.2	-9	-951	6817	-438	190	-182	-7733	510	110	82	67	125	47	567	2787	145	616
56.3	0	-1180	11052	-97	96	-109	-3093	503	70	78	74	119	35	525	2911	137	600
56.4	4	-2089	8089	-427	116	-269	-5617	497	111	81	51	111	43	573	2899	156	616
56.5	-2	-2245	10570	-429	100	-341	-4425	535	129	96	74	115	29	529	2969	144	655
56.6	7	-2107	9822	-276	-37	-251	-3214	483	117	85	82	158	23	545	2850	171	657
56.7	-11	-3037	7454	-442	30	-308	-4531	488	120	102	71	113	27	526	2916	154	653
56.8	5	-1824	7097	-254	241	-226	-2662	495	97	88	62	116	31	534	2981	166	668
56.9	3	-2092	3035	-255	39	-254	-3559	450	114	93	58	107	39	575	2857	170	671
57	15	-2523	3326	-517	132	-350	-5515	451	120	85	55	115	39	588	2899	187	651
57.1	0	-1989	6043	-200	3	-285	-2846	446	89	93	47	126	38	525	2924	164	627
57.2	-2	-1233	5330	-54	-39	-231	-721	419	108	72	48	96	39	529	2962	172	699
57.3	8	-1449	4290	-220	-9	-198	-2017	388	119	84	59	118	36	566	2954	165	646
57.4	12	-1624	3376	-105	-43	-95	-858	339	109	99	54	142	25	581	2861	177	632
57.5	0	-1694	2282	-112	-53	-105	-1847	318	115	90	75	137	37	567	2849	167	658
57.6	-4	-3282	-3030	-571	17	-292	-8007	270	115	76	44	128	29	527	2755	168	627
57.7	-1	-3202	-3218	-586	-31	-294	-7287	274	116	84	49	143	35	534	2757	178	719
57.8	0	-3134	-4131	-562	-70	-250	-6852	267	111	76	51	126	35	536	2761	172	661
57.9	-6	-1724	-1707	-141	-208	-131	-3816	276	85	82	52	100	35	521	2801	168	629
58	2	-2583	3	-313	-137	-168	-5054	238	76	78	51	114	28	499	2732	146	637
58.1	-16	-2264	2288	-547	-55	-276	-6858	217	101	74	67	117	25	519	2673	166	591
58.2	1	-1439	152	-216	-74	-136	-3114	247	91	66	56	113	43	523	2765	166	610
58.3	-3	-2074	-126	-314	-90	-203	-4087	244	93	85	68	103	42	520	2835	185	607
58.4	11	-2876	-3040	-162	-122	-137	-5141	198	121	91	62	153	39	518	2768	145	641
58.5	14	-2709	-4358	-263	-21	-85	-4235	169	106	84	52	124	35	491	2795	164	643
58.6	4	-4614	-8013	-794	233	-232	-10371	159	116	93	65	144	32	520	2731	172	635
58.7	0	-5213	-8861	-1047	201	-355	-13254	157	118	73	53	129	29	513	2614	174	676
58.8	11	-3792	-7214	-680	-116	-182	-9796	137	131	74	61	133	36	474	2678	155	651
58.9	8	-2218	-4099	-274	-120	2	-4959	152	111	73	83	127	40	484	2772	165	637
59	-4	-4199	-4566	-795	178	-290	-9047	115	113	85	59	134	33	523	2757	172	641
59.1	0	-2418	-5924	-259	-163	-144	-3788	107	123	81	59	119	45	516	2834	176	681
59.2	8	-2780	-5176	-371	-131	-152	-4939	122	91	71	80	130	35	528	2833	172	655
59.3	16	-2383	-3830	-206	-155	-88	-4156	150	147	73	65	115	42	498	2857	172	655
59.4	2	-2329	-2784	-120	-178	-93	-2801	152	134	95	77	118	31	536	2752	177	684
59.5	-6	-2857	-9233	-391	-283	-142	-6985	149	86	85	37	149	36	501	2645	169	627
59.6	-11	-4120	-10390	-936	32	-327	-10845	162	96	68	35	133	29	549	2673	168	655
59.7	5	-1853	-7346	-192	-90	-24	-4998	172	129	76	47	153	41	548	2719	190	663
59.8	4	-4704	-5297	-914	385	-244	-12531	148	108	92	73	101	31	485	2700	167	665
59.9	-8	-5130	-9036	-1360	158	-486	-14911	124	91	71	33	118	31	519	2677	174	623
60	3	-2154	-5103	-278	-239	-110	-5278	147	133	85	45	112	30	507	2689	162	608
60.1	-3	-1674	-7307	-447	-141	-152	-6778	172	80	83	48	126	35	556	2682	155	625
60.2	11	617	-7208	-258	-241	-151	-5720	182	93	86	70	101	42	645	2736	165	576
60.3	-1	-1463	-2903	31	-167	-21	-2548	192	107	68	71	98	45	656	2773	131	597

60.4	3	-826	1387	205	-131	96	110	200	119	89	86	147	42	537	2862	162	638
60.5	-2	-1882	105	19	149	6	-2317	198	102	78	68	133	32	525	2832	169	647
60.6	5	-515	-1688	221	-334	88	928	213	92	88	59	104	41	549	2877	162	630
60.7	3	430	-2318	492	-305	207	3243	179	92	85	56	133	53	520	2879	172	676
60.8	-1	-2046	-5502	-285	-40	-98	-3623	169	126	82	47	135	32	497	2803	167	655
60.9	8	-2231	-5157	-85	-186	-37	-2710	156	120	97	65	123	51	514	2783	161	637
61	28	-1018	-4576	-50	-208	28	-2589	157	104	85	76	145	39	523	2769	160	639
61.1	20	-618	-560	328	-392	185	1910	167	106	90	73	114	37	552	2827	166	643
61.2	4	-130	-2722	348	-338	129	2491	122	86	96	58	119	41	571	2873	192	669
61.3	10	-105	-3526	392	-361	179	2727	109	101	94	49	139	36	501	2904	178	658
61.4	12	-1752	-6050	-154	-53	56	-3091	80	99	84	40	140	32	528	2793	176	654
61.5	17	-1416	-7783	-73	-121	30	-2831	46	91	100	54	128	34	531	2829	185	642
61.6	-7	-2429	-8403	-368	52	-120	-4820	22	144	96	43	112	46	538	2828	170	686
61.7	10	-1862	-6145	-163	-52	-23	-3606	8	140	97	51	140	42	579	2855	187	722
61.8	-3	-3493	-9210	-676	273	-117	-10043	1	102	77	84	143	44	552	2734	163	635
61.9	-4	-4092	-10103	-851	362	-220	-10405	-55	104	81	77	119	36	513	2755	183	657
62	2	-3295	-8573	-798	280	-242	-8765	-69	77	86	72	149	46	554	2827	171	694
62.1	2	-5096	-15187	-1126	391	-322	-12533	-74	98	83	37	126	36	507	2735	181	691
62.2	5	-4681	-19104	-1125	384	-258	-14169	-106	97	110	42	133	51	433	2631	161	678
62.3	8	-3629	-14835	-751	163	-197	-8243	-77	101	90	49	123	52	527	2799	175	685
62.4	-3	-2728	-13369	-468	-27	-82	-5603	-73	124	94	40	121	42	496	2841	176	688
62.5	13	-2391	-12203	-327	-83	-46	-3912	-60	118	99	32	141	39	511	2832	176	693
62.6	3	-2415	-13408	-419	-161	-76	-5497	-64	112	100	50	134	49	500	2767	168	659
62.7	-7	-3179	-14679	-652	190	-141	-8610	-59	131	112	45	117	35	447	2719	181	681
62.8	5	-2437	-11368	-229	-44	-16	-3736	-78	78	100	49	129	55	533	2820	192	664
62.9	7	-2828	-14338	-388	-31	-71	-5630	-70	122	88	40	153	48	579	2788	180	692
63	6	-4066	-17194	-600	213	-168	-10779	-58	107	89	28	150	35	511	2721	172	670
63.1	10	-3586	-15178	-491	8	-134	-8499	-52	91	79	44	105	35	519	2771	169	676
63.2	2	-3207	-16735	-849	334	-207	-13600	-60	93	102	57	131	33	476	2646	155	625
63.3	6	-3540	-13872	-842	309	-216	-11718	-58	112	73	39	120	41	497	2707	161	653
63.4	2	-4975	-17791	-974	563	-228	-14399	-50	102	79	73	120	38	440	2644	168	661
63.5	-2	-5100	-15855	-1134	552	-281	-14797	-40	78	85	71	128	38	468	2608	175	622
63.6	-5	-5701	-18076	-1272	782	-341	-17193	-44	98	86	51	108	41	490	2629	161	614
63.7	6	-6046	-20259	-1377	683	-366	-17017	-48	94	71	44	96	32	470	2615	167	615
63.8	-4	-2669	-13385	-345	-231	-97	-5071	-17	98	92	48	157	42	490	2789	172	646
63.9	16	-2670	-10991	-425	-35	-98	-5117	7	109	90	40	135	45	508	2839	169	654
64	-9	-3899	-13934	-757	102	-193	-8521	12	140	89	46	141	41	505	2713	164	671
64.1	15	-2491	-8971	-344	-122	-44	-4568	13	99	78	60	147	33	521	2845	177	646
64.2	0	-2797	-11942	-360	0	-35	-6088	25	102	82	38	124	45	511	2731	168	664
64.3	23	-1125	-9914	74	-268	90	-1708	56	98	90	53	132	58	492	2732	160	655
64.4	6	-1659	-9514	-15	-153	98	-1941	40	124	89	44	138	43	541	2764	169	662
64.5	7	-2197	-8942	-133	-128	59	-3264	49	103	85	47	112	54	539	2790	163	667
64.6	26	-1479	-8425	331	-342	130	-624	51	145	85	40	138	42	543	2818	155	669
64.7	8	-244	-4988	419	-392	180	1247	60	101	89	52	130	41	525	2868	164	645
64.8	13	-1317	-3922	194	-344	136	-713	77	129	88	59	120	49	528	2809	181	653
64.9	-1	-1527	-1135	148	-208	109	-1304	42	110	100	69	118	41	575	2843	170	634
65	12	-1975	-1253	132	-47	83	-1848	32	113	86	70	124	39	540	2806	158	622

65.1	5	-2451	94	-95	-134	24	-3390	9	104	88	70	110	30	501	2802	160	593
65.2	-6	102	7693	330	-375	117	1998	10	106	98	93	129	38	598	2920	158	617
65.3	-6	-2576	2944	-316	-41	-127	-4248	-14	135	85	76	111	35	564	2874	158	641
65.4	7	-3432	2908	-452	50	-110	-6278	-32	99	112	80	147	34	484	2777	174	614
65.5	3	-2910	6050	-405	-26	-132	-5103	-48	100	91	101	124	37	493	2780	169	606
65.6	6	-3907	2240	-562	-32	-203	-6245	-58	127	87	75	122	20	584	2882	175	617
65.7	-8	-4429	3634	-630	-170	-256	-5344	-67	90	103	81	107	38	535	2906	159	672
65.8	0	-6423	-5555	-1156	255	-371	-12432	-59	100	86	65	111	30	578	2759	150	621
65.9	0	-5852	-10067	-1158	320	-299	-15029	-65	103	70	59	105	42	654	2642	140	628
66	0	-3350	14	-318	-51	-93	-4665	-56	117	96	62	131	34	538	2793	162	636
66.1	3	-4762	-2604	-840	60	-266	-9352	-43	117	84	69	115	33	626	2770	166	623
66.2	6	-5636	-6031	-1124	137	-317	-12727	-34	99	66	69	119	28	638	2650	151	635
66.3	8	-5993	-7478	-1191	281	-305	-13317	-35	87	63	69	106	26	469	2637	158	609
66.4	6	-3161	-591	-263	-204	-80	-5076	-4	99	71	68	101	25	511	2778	160	654
66.5	-2	-2688	-4340	-381	-259	-147	-7853	24	94	62	97	118	25	525	2639	124	553
66.6	25	-1105	4765	219	-538	11	-1121	78	88	70	97	97	35	547	2829	148	551
66.7	36	521	13817	250	-476	55	804	139	94	83	109	115	35	627	2818	142	537
66.8	0	158	12645	371	-535	20	2633	154	113	83	98	120	25	709	2836	166	588
66.9	14	-294	8968	275	-613	10	1972	165	103	85	86	109	40	610	2886	164	589
67	21	334	11002	639	-727	147	4293	182	86	92	90	118	34	572	2913	160	585
67.1	2	1288	10771	905	-664	253	6446	196	119	92	81	94	36	691	2897	168	602
67.2	11	377	13652	812	-827	160	6414	185	95	88	68	111	40	622	2910	157	599
67.3	-4	238	12785	745	-571	165	6521	161	89	129	78	127	47	630	2885	172	642
67.4	16	417	12030	876	-617	191	6925	139	108	101	89	107	30	603	2936	177	623
67.5	17	-557	8691	535	-468	67	5067	113	117	79	78	121	42	532	2926	168	639
67.6	-9	-4166	211	-534	226	-200	-8173	49	99	68	60	142	31	532	2749	166	632
67.7	-3	-6819	-7587	-1278	695	-375	-18363	10	111	76	60	119	30	555	2535	157	622
67.8	-6	-6091	-2588	-1065	469	-286	-15590	11	93	71	88	118	25	506	2679	146	607
67.9	-7	-8451	-11601	-1781	901	-427	-23650	-14	91	78	51	120	19	502	2515	156	634
68	0	-7050	-10396	-1381	400	-379	-17085	-24	105	70	58	110	20	483	2600	136	601
68.1	-1	-4952	-302	-649	-46	-231	-7266	-27	88	72	80	122	17	566	2858	159	622
68.2	-2	-4732	-327	-557	-108	-287	-6897	-22	120	81	80	122	25	538	2809	155	626
68.3	21	-2388	4847	67	-387	-60	1579	-14	116	90	95	114	48	524	2990	161	609
68.4	-3	-3292	4567	-87	-416	-150	-1543	11	100	116	81	97	33	502	2847	157	604
68.5	6	-1824	1590	79	-483	-109	34	20	97	80	85	116	37	524	2884	157	598
68.6	-11	-2480	3347	-61	-365	-170	-543	39	98	80	90	106	40	530	2862	160	607
68.7	-13	-2188	3295	17	-464	-171	-554	59	108	82	79	105	34	540	2864	159	602
68.8	-9	-295	3710	-177	-507	-212	-2326	60	99	77	95	113	33	675	2773	145	622
68.9	1	-2347	2947	-19	-429	-144	-1942	90	90	84	70	112	35	547	2907	152	577
69	8	-1163	5403	183	-531	-63	1104	103	95	108	65	112	34	536	2884	136	588
69.1	4	-1616	7065	543	-625	51	4386	103	111	85	73	125	37	474	2884	167	641
69.2	5	-569	8546	704	-534	34	5478	80	89	74	88	128	47	546	2951	165	620
69.3	4	-1721	7116	254	-399	-133	2370	64	113	88	87	136	30	520	2997	171	677
69.4	-6	-1851	3694	24	-345	-151	602	46	104	103	62	132	26	545	2926	168	633
69.5	-7	-2127	6019	154	-484	-114	2214	14	89	86	85	127	32	533	2966	174	627
69.6	11	-1938	6344	383	-366	2	3866	-9	113	92	85	126	27	580	2907	169	641
69.7	-7	-2762	3131	-108	-286	-139	15	-23	104	80	67	116	23	513	2906	158	647

69.8	1	-3345	2119	-316	-322	-188	-2904	-44	97	86	67	112	23	483	2898	160	647
69.9	-9	-5545	-1171	-1004	369	-311	-11526	-54	79	67	62	125	29	496	2746	155	666
70	-4	-4676	-2691	-596	93	-174	-8310	-60	112	67	74	115	30	466	2773	153	698
70.1	5	-5162	-1225	-795	327	-272	-10855	-79	102	76	71	124	35	516	2778	160	688
70.2	3	-3719	503	-308	-108	-177	-4441	-82	103	81	85	122	39	535	2882	177	625
70.3	9	-2784	6287	-71	-287	-102	-34	-71	89	73	111	113	44	518	2921	157	660
70.4	-12	-2964	6080	-1	-414	-69	765	-77	115	78	96	144	37	542	2956	170	616
70.5	-8	-3267	6573	-120	-379	-169	-348	-71	124	75	91	140	25	523	2971	169	669
70.6	-4	-4376	3084	-548	-184	-295	-5009	-73	96	73	77	112	39	468	2915	168	662
70.7	-9	-3967	1748	-469	-145	-245	-5049	-64	116	76	81	134	40	480	2957	149	658
70.8	-3	-2722	3980	35	-293	-95	-541	-77	108	88	101	115	39	498	2961	137	645
70.9	-2	-3450	3554	-202	-298	-175	-1561	-67	82	85	89	134	28	517	2992	152	664
71	5	-4297	3488	-439	-114	-276	-5279	-62	97	73	77	124	39	483	2863	150	655
71.1	6	-2503	5181	-202	-216	-153	-2657	-55	90	85	87	129	35	499	2915	165	655
71.2	5	-3053	5400	10	-269	-152	-1718	-51	111	81	108	109	31	515	2918	150	660
71.3	7	-2101	5520	313	-300	17	2557	-66	117	77	73	139	43	526	2999	173	676
71.4	-1	-2178	6012	-49	-129	-172	470	-104	111	113	77	130	34	602	3088	179	643
71.5	-2	-5086	3521	-795	376	-355	-6397	-148	121	103	41	134	28	565	3051	174	696
71.6	-3	-4083	4201	-256	-113	-247	-2897	-217	90	88	85	129	34	539	2935	165	654
71.7	-3	-4807	-3781	-615	-180	-269	-6740	-226	87	70	61	122	40	527	2806	164	647
71.8	-9	-5482	-8786	-881	-219	-304	-10500	-207	92	70	48	95	32	574	2658	155	642
71.9	9	-3985	-9087	-897	-64	-358	-10073	-174	122	72	39	115	31	546	2764	152	644
72	0	-4643	-4869	-937	29	-391	-8894	-158	117	75	68	126	26	528	2821	166	647
72.1	8	-3597	-3130	-397	-223	-288	-4306	-136	114	75	49	134	30	532	2861	164	642
72.2	8	-3572	-2003	-261	-369	-301	-3831	-104	125	80	48	112	30	542	2930	163	648
72.3	-3	-2732	3285	137	-347	-117	2482	-93	109	83	68	130	40	481	2998	172	698
72.4	-8	-2700	4175	111	-516	-117	1958	-65	131	79	83	112	31	543	3003	165	642
72.5	3	-2470	3907	113	-405	-124	1762	-71	109	87	73	115	39	579	2989	166	651
72.6	-2	-3898	3274	-368	-147	-241	-2166	-71	134	94	54	103	31	518	2891	167	659
72.7	5	-5413	-3245	-829	75	-321	-8587	-75	105	92	58	113	29	477	2830	155	622
72.8	-7	-5077	1120	-561	82	-352	-7053	-81	103	67	59	121	31	500	2901	169	685
72.9	-8	-5263	437	-858	35	-344	-8577	-79	107	68	71	115	32	513	2841	147	648
73	5	-4742	-1113	-519	-49	-261	-7522	-78	-28	67	81	127	30	551	2786	162	627
73.1	-3	-3862	-275	-443	-382	-262	-7684	-62	69	72	91	89	26	480	2703	140	599
73.2	-2	-2774	11705	94	-313	-147	539	-51	94	82	101	116	21	502	2906	161	598
73.3	-1	-3776	8849	-114	-262	-239	-1737	-61	115	72	72	125	38	555	2982	162	624
73.4	-12	-3530	4250	-371	-313	-290	-3550	-57	109	85	61	135	33	548	2937	158	646
73.5	10	-3396	1360	-292	-347	-195	-2810	-59	109	84	48	115	30	550	2844	171	602
73.6	-4	-3255	3475	-364	-335	-240	-3551	-59	86	90	58	118	27	636	2879	163	576
73.7	5	-2487	3951	-330	-444	-278	-2488	-56	58	83	44	117	30	805	2887	143	526
73.8	0	-2534	4026	-3	-430	-159	-564	-62	118	88	69	124	39	643	2924	157	632
73.9	7	-2190	5600	210	-363	-39	2171	-80	117	89	86	106	34	498	2937	177	692
74	-10	-3205	-806	-78	-458	-136	-1359	-93	96	107	63	133	35	532	2848	172	695
74.1	1	-2328	1972	-55	-302	-160	-785	-62	138	88	57	115	30	544	2960	176	642
74.2	2	-2806	3569	-68	-371	-165	-1583	-80	109	96	96	118	33	593	2886	173	619
74.3	-2	-2607	8612	-9	-311	-189	1125	-65	122	84	92	119	32	547	2949	162	674
74.4	3	-2844	7810	-308	-188	-279	-1818	-63	100	81	87	115	29	510	3002	164	635

74.5	0	-3087	1453	-299	-170	-285	-2493	176	108	79	64	126	29	691	2964	166	611
74.6	13	-2096	3716	143	-263	-49	1105	4	115	94	52	126	35	570	3010	170	660
74.7	10	-3090	6141	-139	-74	-130	-1556	-65	100	93	75	133	31	729	2970	167	646
74.8	-4	-2539	5638	11	-286	-173	380	-93	107	90	88	123	32	579	2959	174	679
74.9	0	-3465	5860	-240	-163	-289	-1781	-84	86	76	87	110	38	507	2972	162	639
75	-2	-3178	4249	-380	-158	-374	-3598	-90	123	90	58	130	19	594	2996	174	627
75.1	-1	-3004	3182	-267	-214	-272	-821	-78	104	105	67	114	35	586	3036	167	672
75.2	-9	-3205	3638	-255	-280	-275	-1733	-79	89	77	86	114	36	580	2971	168	646
75.3	0	-4188	420	-610	-20	-354	-5432	-75	98	74	52	108	27	514	2931	165	630
75.4	-8	-4779	-3690	-782	7	-386	-7856	-77	96	82	46	110	25	602	2842	161	637
75.5	-8	-3661	-3020	-523	-180	-318	-4221	-65	79	97	54	123	28	559	2897	159	603
75.6	-6	-1306	-255	98	-460	-137	27	-38	118	76	51	128	30	696	2918	158	585
75.7	10	-355	3633	354	-476	-66	3597	-37	101	85	59	113	29	712	3017	160	591
75.8	6	-1369	4118	345	-427	-108	3951	-22	92	86	64	119	37	751	2992	177	623
75.9	10	-859	5205	308	-413	-22	4475	-18	99	92	63	117	38	731	2953	158	612
76	23	-1002	6516	529	-525	58	6589	-33	122	83	61	138	29	603	3023	167	680
76.1	0	-1734	7155	321	-427	0	3341	-47	102	106	71	129	24	578	2972	186	615
76.2	-8	-3435	6754	-272	-192	-193	-1703	-67	102	80	82	125	26	585	2896	166	620
76.3	-6	-3630	5082	-377	-187	-239	-3221	-82	97	79	93	113	37	568	2863	161	622
76.4	-3	-4920	4812	-662	-81	-285	-6069	-74	96	70	106	125	31	508	2854	154	627
76.5	-3	-3635	1392	-755	291	-360	-8779	-73	90	76	81	125	26	480	2789	150	600
76.6	0	-5163	-3114	-1084	485	-407	-13116	-62	81	75	89	88	39	448	2666	154	577
76.7	6	-4406	242	-701	78	-352	-8147	-75	104	82	79	117	39	506	2753	164	626
76.8	-4	-5261	1424	-943	-79	-362	-11041	-57	92	88	100	131	27	503	2586	166	588
76.9	-10	-4353	2851	-790	-79	-381	-10124	-43	85	75	116	92	28	539	2741	153	604
77	-5	-4118	5144	-1036	-93	-391	-12465	-54	85	92	154	118	23	526	2664	142	567
77.1	0	-4056	472	-814	56	-335	-9934	-62	93	64	88	103	23	550	2677	139	564
77.2	1	-5036	-880	-1041	187	-380	-12793	-48	73	65	75	98	31	462	2651	129	530
77.3	-2	-1105	-180	-528	156	-249	-9652	-48	57	73	82	103	36	484	2678	155	545
77.4	-4	-3382	-3795	-882	138	-379	-13405	-53	91	66	64	113	30	540	2553	132	571
77.5	-11	-4976	-3451	-1264	265	-510	-16911	-38	72	82	69	104	30	446	2505	146	572
77.6	-4	-5047	-544	-1264	306	-549	-15889	-16	110	64	74	120	30	464	2596	139	569
77.7	-9	-3103	5297	-1045	168	-512	-13401	2	111	77	77	108	23	495	2632	125	599
77.8	0	-4487	12933	-1303	321	-570	-15180	21	77	72	92	119	19	570	2659	142	510
77.9	-5	-4845	31007	-2004	-409	-623	-29534	12	53	47	143	87	36	448	2136	72	401
78	-4	-33	60365	-1937	622	-670	-27154	-34	54	44	121	95	27	430	2243	93	358
78.1	-10	63	63359	-2017	592	-731	-27440	-18	47	47	69	79	19	369	2196	81	354
78.2	-4	4976	85241	-1356	554	-594	-19076	-40	50	54	102	63	28	418	2408	88	378
78.3	-8	5527	64066	-866	-80	-505	-15594	-62	92	63	42	77	21	465	2348	111	430
78.4	-2	5076	57460	-868	181	-442	-14322	-68	66	67	40	77	37	450	2460	103	404
78.5	-5	8083	75597	-1014	860	-426	-17051	-110	86	69	68	96	25	445	2294	105	395
78.6	2	3769	50533	-1298	-235	-429	-20395	-187	53	50	69	72	37	398	2214	100	413
78.7	2	2506	39692	-1146	-770	-388	-17362	-212	64	50	69	70	32	440	2316	109	434
78.8	6	2619	16252	-1067	1010	-357	-15745	-244	89	84	67	99	32	496	2305	132	480
78.9	-3	1234	20959	-816	1083	-345	-13616	-260	77	70	59	81	31	462	2434	115	489
79	-10	239	12321	-853	635	-380	-12540	-249	91	75	49	109	26	464	2523	111	542
79.1	-2	2234	14794	-375	643	-235	-4405	-126	84	71	58	83	27	509	2756	145	569

79.2	-3	-356	1327	-484	132	-228	-6172	2149	86	77	54	101	43	562	2752	141	599
79.3	5	-1990	-7910	-713	-162	-293	-7834	1715	87	81	44	107	42	523	2635	142	576
79.4	-5	-1613	-4928	-565	-197	-258	-5668	2191	98	81	42	103	47	587	2745	147	615
79.5	2	-1998	-6203	-437	-248	-269	-4912	2695	90	79	47	92	37	536	2784	145	577
79.6	-3	-3462	-19691	-1120	-528	-395	-14634	1001	68	70	48	73	27	644	2368	124	525
79.7	1	284	-11878	-774	-446	-369	-9371	-143	73	78	33	90	27	807	2585	134	487
79.8	6	-39	-12927	-584	-351	-323	-7779	-166	76	77	57	102	28	718	2646	148	538
79.9	3	-629	-9785	-848	-273	-374	-11621	-102	85	85	52	86	20	569	2534	127	507
80	-10	1093	12462	-755	399	-375	-9565	-78	89	77	53	87	18	550	2570	129	496
80.1	-7	1102	18733	-578	570	-413	-7707	-63	75	73	57	97	15	626	2697	142	486
80.2	-4	1293	10905	-484	352	-403	-5937	-92	86	92	41	84	19	661	2867	168	542
80.3	-3	-819	13109	-636	300	-416	-9527	-112	71	81	54	108	27	579	2720	135	516
80.4	-9	-637	9562	-699	2832	-394	-8348	-154	92	86	51	92	31	577	2662	133	585
80.5	0	-107	8935	-545	30	-410	-7675	-163	70	90	55	90	17	587	2778	127	522
80.6	-5	1222	14431	-428	486	-343	-6091	-186	90	68	93	89	34	561	2751	132	507
80.7	3	219	12982	-622	308	-387	-8335	-187	74	85	64	100	23	564	2679	130	491
80.8	-5	-465	12185	-859	414	-400	-10315	-154	83	68	81	88	22	531	2673	135	524
80.9	-7	691	15753	-949	717	-412	-11767	1173	94	78	68	71	28	499	2605	140	487
81	-6	1801	27360	-1440	1184	-479	-17977	1599	66	77	82	97	29	427	2370	119	472
81.1	1	1726	29376	-1092	1066	-459	-13359	2059	86	73	75	99	38	607	2619	127	553
81.2	6	-860	11561	-965	481	-405	-11868	3215	70	85	86	105	39	586	2602	132	521
81.3	-3	-1556	6756	-1115	466	-449	-11967	2467	90	68	56	92	31	559	2709	145	562
81.4	-6	-619	8109	-757	304	-388	-7075	1520	87	78	51	124	32	631	2878	156	635
81.5	-7	-185	2980	-122	-61	-354	-4896	-149	114	90	64	112	23	608	2847	144	603
81.6	4	1731	5126	141	-103	-282	-2549	-178	80	82	66	129	23	595	2912	145	597
81.7	1	1104	9224	71	33	-300	-1997	-172	65	94	66	100	19	647	2974	148	580
81.8	-2	-314	6209	38	-14	-264	-3250	-178	87	91	90	108	35	610	2820	144	588
81.9	-9	-827	2972	-244	-123	-351	-8075	-175	96	81	90	99	23	613	2667	133	554
82	0	1802	4293	-370	-95	-369	-7797	-136	77	92	58	101	21	553	2663	147	536
82.1	-5	2705	6985	-135	229	-371	-5460	-134	90	116	53	109	30	546	2780	170	576
82.2	-2	-304	3436	-105	-69	-378	-4635	-126	105	108	52	90	26	602	2886	153	580
82.3	-8	-684	1545	-424	22	-442	-5269	-132	110	112	47	135	18	694	2858	149	606
82.4	-1	886	3629	260	88	-220	-996	-228	116	101	47	122	34	753	2988	167	648
82.5	-6	87	-7293	-31	-36	-209	-4740	-290	91	97	51	127	27	713	2784	159	649
82.6	-5	-1053	-10631	97	-177	-210	-6967	-319	94	107	40	116	33	578	2674	146	640
82.7	5	-1875	-13251	-420	-144	-258	-8096	-319	107	87	57	111	25	540	2643	155	635
82.8	-5	-1374	-10351	-324	35	-255	-7579	-325	92	101	62	106	32	571	2733	161	645
82.9	-3	-565	-7900	96	63	-157	-5534	-309	104	116	70	126	33	609	2715	161	634
83	1	-2211	-10382	-167	19	-217	-6742	794	105	82	71	117	38	566	2734	161	626
83.1	0	-1558	-12242	-353	43	-231	-8024	1362	99	75	66	117	40	557	2685	161	631
83.2	-1	-2165	-10898	-268	122	-236	-6333	-445	100	82	60	107	33	540	2767	156	609
83.3	-2	-2569	-13008	-328	41	-258	-7218	-428	91	80	66	115	34	558	2732	157	595
83.4	-2	-1900	-13173	-200	51	-256	-6858	-415	113	79	59	131	31	573	2800	157	638
83.5	-2	-2647	-16830	-14	12	-257	-9339	-373	145	82	54	200	29	511	2654	154	710
83.6	-3	-3146	-21035	2249	170	-244	-12353	-362	214	78	54	355	31	446	2600	184	871
83.7	-5	-2382	-18083	921	85	-281	-10335	-372	199	84	56	311	29	433	2653	173	830
83.8	1	-1284	-11778	131	140	-214	-6323	-412	163	94	58	234	29	513	2815	178	752

83.9	0	-2117	-11411	227	143	-184	-5987	-435	120	85	65	164	38	551	2786	172	658
84	2	-2496	-10302	-285	239	-224	-6502	-453	102	82	69	109	32	546	2786	160	614
84.1	1	-3444	-14574	-495	116	-263	-9482	-453	100	80	63	114	36	525	2640	156	595
84.2	1	-3687	-16435	-591	-22	-286	-10845	-440	100	74	68	112	32	505	2568	151	597
84.3	1	-3076	-12772	-401	219	-247	-8466	-442	95	83	63	111	33	532	2719	164	592
84.4	3	-2687	-10875	-315	172	-236	-6879	-453	101	83	72	114	37	555	2758	162	620
84.5	4	-2731	-11392	-319	172	-246	-7274	-452	105	80	68	117	33	547	2757	159	629
84.6	3	-3137	-12556	-412	120	-263	-8284	-441	98	83	73	111	36	531	2707	153	636
84.7	2	-3051	-11846	-438	82	-262	-9306	-433	96	83	62	101	34	509	2654	157	625
84.8	0	-3887	-18385	-631	40	-310	-12053	-425	87	64	59	106	36	488	2537	144	576
84.9	1	-2878	-13737	-357	179	-256	-8407	-435	94	78	58	125	32	515	2700	155	605
85	3	-2480	-9522	-306	122	-243	-7532	-432	93	82	74	136	38	556	2713	166	624
85.1	-1	-3427	-14603	-517	154	-297	-10540	-425	94	71	64	105	33	519	2641	151	597
85.2	4	-2658	-12936	-484	125	-284	-10982	-413	92	79	54	116	32	524	2593	145	607
85.3	-3	-2728	-13100	-505	-103	-290	-10395	-382	96	71	54	112	31	498	2622	145	609
85.4	-4	-1943	-9870	-302	-10	-272	-9256	-368	101	74	55	99	30	518	2645	140	591
85.5	0	-780	-7320	-215	-152	-208	-7224	-339	98	67	54	90	35	579	2664	143	633
85.6	-5	-1794	-15757	-343	-392	-230	-9955	-317	87	77	47	99	35	524	2512	130	582
85.7	-8	-5215	-23804	-1006	-651	-423	-19459	-215	87	67	45	77	20	469	2143	119	508
85.8	2	-2691	-11615	-658	-521	-443	-12380	-100	110	95	43	88	26	628	2518	138	548
85.9	-2	-3036	-10053	-701	-343	-417	-10006	-49	91	90	55	104	21	713	2577	130	557
86	-5	-915	-6465	-78	-266	-359	-7083	-10	117	74	55	107	14	872	2749	134	604
86.1	-6	1948	233	115	88	-334	-2932	30	94	96	49	122	18	898	2855	143	596
86.2	0	477	6452	143	-234	-399	-2651	45	93	119	67	95	18	660	2844	148	550
86.3	-8	-142	11337	-224	631	-446	-5258	28	189	101	82	87	15	650	2845	135	491
86.4	-12	-1338	5699	-433	823	-464	-8130	24	94	101	60	86	16	618	2700	120	515
86.5	-5	992	8454	-327	-211	-393	-6760	25	74	82	59	95	19	732	2754	110	498
86.6	-12	-1039	8587	-248	-85	-497	-7244	48	74	94	103	82	12	643	2693	107	504
86.7	1	1500	8520	117	-356	-420	-4036	75	69	91	76	95	13	682	2812	119	509
86.8	20	2274	17748	425	-478	-313	2004	88	59	97	42	82	18	715	2886	155	519
86.9	-4	879	19550	356	-391	-415	-610	112	83	104	52	85	19	857	2875	130	508
87	1	1773	18395	64	-99	-450	-1728	102	77	82	46	101	16	795	2958	139	512
87.1	5	2643	23707	227	-130	-410	-1350	106	71	81	61	82	23	817	2862	129	487
87.2	-5	1808	22893	480	-99	-393	-992	77	90	80	61	110	15	678	2879	130	516
87.3	-8	1408	22868	370	-21	-407	97	31	79	91	90	97	27	582	2970	133	494
87.4	11	-158	15877	-94	106	-389	-2238	-14	61	102	60	110	12	605	2924	129	499
87.5	-9	190	16388	-190	373	-444	-5681	-31	107	98	53	66	22	667	2847	126	544
87.6	-6	-592	6456	-205	93	-435	-4629	-67	76	74	53	97	30	641	2883	138	547
87.7	-8	2397	7168	495	-137	-270	1135	-67	96	107	59	107	29	842	2948	143	571
87.8	-3	2263	6285	431	-232	-266	1367	-90	85	88	40	100	18	723	2962	152	580
87.9	-5	1246	2124	164	177	-352	-3151	-91	109	107	39	92	25	692	2870	151	577
88	-3	2386	5374	338	-221	-302	280	-122	89	116	37	95	33	650	2955	157	545
88.1	-1	2046	6013	426	156	-308	-824	-143	103	120	45	103	29	701	3022	176	575
88.2	-6	2471	7658	336	126	-254	-1442	-184	80	108	49	110	25	682	2952	185	593
88.3	6	1929	824	281	175	-201	-1659	-211	87	138	46	119	32	683	2945	168	581
88.4	-2	1872	-1928	562	124	-191	588	-222	114	118	44	116	28	710	3047	160	618
88.5	14	4710	-98	838	435	-8	7342	-216	83	142	37	120	26	719	3108	176	633

88.6	-6	6064	-1777	1063	-108	36	7940	-228	118	116	36	145	31	678	3215	173	656
88.7	3	5670	154	1207	48	100	9303	-256	92	118	44	112	25	745	3238	182	643
88.8	13	3729	-144	1080	30	127	9532	-272	126	106	48	104	26	672	3301	183	683
88.9	13	4233	-1555	1272	-86	141	9409	-260	123	138	48	104	33	613	3237	166	697
89	7	2786	3014	839	-26	130	6425	-241	111	125	58	128	38	645	3085	180	643
89.1	-2	715	-879	318	-30	-12	-666	62	103	91	64	126	35	592	2817	180	592
89.2	-1	-3913	-17848	-677	-52	-263	-12067	7452	93	75	66	106	60	492	2484	161	483
89.3	1	-4212	-22310	-913	-145	-251	-14350	20243	88	73	55	104	119	465	2378	163	455

Table A-27: XRF core scan for Sacred Lake

	Chemical Elements (cps)														
Depth (cm)	**Al**	**Ca**	**Cl**	**Cu**	**Fe**	**K**	**Nb**	**N**	**Rb**	**S**	**Si**	**Sr**	**Ti**	**Zn**	**Zr**
0.1	1	1447	21	102	2772	872	-4	91	20	73	54	81	4374	104	203
0.2	1	514	4	33	1459	664	17	40	27	42	24	12	3154	52	140
0.3	1	547	11	28	914	631	4	30	8	36	25	13	2782	44	101
0.4	8	662	15	23	1386	736	1	19	31	33	57	27	3357	39	164
0.5	1	1061	4	25	2515	1050	28	17	30	23	74	51	5232	67	255
0.6	1	1085	9	38	3001	994	14	18	50	33	50	60	5722	83	197
0.7	2	788	13	30	2130	712	0	10	25	24	17	33	3227	39	123
0.8	7	857	11	37	3474	951	8	26	57	38	46	89	5472	117	293
0.9	1	1269	24	17	5285	1902	36	30	57	52	81	77	9339	121	434
1	2	1264	14	33	6179	1821	37	42	71	46	94	85	11607	181	467
1.1	9	1169	17	32	5316	1572	33	23	76	52	78	94	9615	151	455
1.2	2	1122	12	26	4850	1312	22	24	79	47	57	78	9008	115	366
1.3	4	1163	22	59	5025	1437	33	19	63	52	70	84	8390	132	336
1.4	4	1221	13	40	5514	1451	28	38	49	52	71	60	8929	120	401
1.5	1	1317	26	47	5542	1656	7	34	70	68	86	82	9388	115	398
1.6	8	1409	14	27	6472	1909	29	18	58	67	109	79	10357	131	405
1.7	4	1428	17	38	6577	2047	48	22	73	69	120	100	11416	134	524
1.8	4	1487	23	39	7241	2507	71	38	77	71	151	102	13954	156	581
1.9	2	1542	18	38	7542	2600	52	36	75	76	149	91	15469	179	673
2	13	1593	18	49	8034	2644	95	55	92	74	160	118	15986	199	716
2.1	13	1602	14	40	8498	3038	82	51	79	71	188	109	17940	219	808
2.2	4	1433	21	49	7977	2797	61	54	94	69	151	81	16698	210	813
2.3	5	1334	19	52	7610	2496	85	43	79	64	101	88	15824	212	779
2.4	4	1552	26	57	8397	2994	93	46	108	73	154	105	17104	210	906
2.5	5	1534	24	34	9145	3397	146	52	101	72	184	68	20068	242	1008
2.6	6	1419	21	45	8893	3401	93	57	91	66	188	109	20184	248	927
2.7	5	1341	19	61	9042	3217	80	46	74	61	159	95	19668	243	939
2.8	11	1333	16	54	8754	3751	117	65	101	51	185	92	20556	249	950
2.9	7	1226	37	55	9217	3312	95	57	90	66	136	79	20039	214	948
3	9	1328	26	47	9725	3724	112	50	109	61	186	73	21538	240	988
3.1	4	1400	21	56	10276	3898	120	75	110	65	207	69	22739	252	1021

3.2	2	1374	10	40	10339	3903	86	54	103	67	196	90	23409	258	952
3.3	5	1414	35	62	10895	4210	115	64	76	69	218	84	24331	281	1000
3.4	16	1463	18	60	11967	4529	122	66	108	50	256	113	29176	295	1045
3.5	3	1428	34	58	11238	4424	103	64	119	66	225	109	25535	267	1017
3.6	4	1466	29	33	11560	4433	91	60	91	65	242	80	25372	273	1027
3.7	9	1322	25	48	11296	4458	110	71	121	58	267	98	26610	274	1020
3.8	7	1417	31	40	11121	4488	133	73	109	55	282	111	26835	273	1014
3.9	12	1336	24	43	10818	4325	153	61	104	53	243	92	25080	262	1050
4	6	1290	38	46	10730	4056	140	73	104	59	231	84	23566	282	1035
4.1	8	1275	33	51	10873	4011	107	72	95	54	207	109	24122	243	1030
4.2	16	1254	38	53	11394	4225	136	70	121	60	226	123	25134	284	1057
4.3	17	1258	32	52	10373	4017	97	79	108	42	214	77	23143	255	964
4.4	4	1196	29	47	10068	3910	102	56	96	56	231	80	22456	245	927
4.5	7	1166	21	43	9349	3873	111	60	120	46	254	78	21683	220	897
4.6	12	1142	30	42	9030	3952	79	53	78	52	235	69	21376	237	904
4.7	7	1216	35	59	10088	3907	123	59	93	48	204	75	23590	249	1000
4.8	12	1298	29	47	9916	4322	106	68	86	44	258	66	24167	241	915
4.9	7	1307	39	42	10072	4281	103	52	98	58	272	90	23711	242	952
5	17	1763	30	47	10801	4404	122	62	111	63	252	109	25088	268	957
5.1	10	1428	32	68	10800	4489	67	62	98	58	273	103	25663	274	1002
5.2	7	1531	42	58	11507	4902	126	77	137	61	286	76	26912	287	1036
5.3	17	1514	29	59	11549	4987	85	86	126	66	319	119	28115	274	1022
5.4	18	1244	26	47	9933	4227	127	58	89	53	266	81	22728	236	896
5.5	10	1238	24	63	10108	4174	93	69	108	53	249	87	23319	245	912
5.6	13	1301	29	51	9931	4188	88	66	104	54	242	68	23744	229	927
5.7	1	1326	25	33	9649	4057	101	48	95	47	252	82	22645	205	858
5.8	7	1258	33	40	9083	4066	90	31	87	49	269	77	22416	222	795
5.9	4	1275	25	43	9142	3875	71	51	82	53	271	75	21152	214	811
6	15	1173	30	48	8586	3671	82	60	101	51	240	87	20096	217	808
6.1	5	1112	32	50	8603	3612	104	68	94	40	242	98	20662	225	858
6.2	11	1264	30	51	9449	4025	88	63	118	46	249	107	22958	249	927
6.3	13	1266	29	39	9234	3959	90	59	97	48	241	114	22855	229	952
6.4	10	1143	28	49	8647	3641	88	43	75	39	204	128	21264	225	890
6.5	9	1156	23	56	9111	3865	119	59	125	39	216	101	21851	232	923
6.6	9	1065	34	52	9170	3565	98	71	102	42	249	90	20887	240	919
6.7	19	1177	28	47	10086	4142	55	74	108	43	279	103	22475	256	900
6.8	3	1111	30	48	9220	3827	74	61	95	41	256	63	20279	228	886
6.9	11	1015	28	48	8509	3582	78	49	78	45	224	80	20177	217	808
7	9	1169	28	49	9144	4023	135	60	94	44	260	76	21397	225	898
7.1	9	979	28	48	8706	3366	106	63	77	37	217	81	19163	206	839
7.2	6	1023	17	34	8274	3577	135	45	116	41	227	72	20432	217	914
7.3	7	1164	29	40	9258	3914	110	58	133	42	237	83	22297	219	976
7.4	7	1129	29	47	8973	3821	107	46	105	50	227	83	22105	221	875
7.5	8	1311	45	48	9998	4430	135	66	107	50	309	81	23434	255	974
7.6	24	1301	27	46	10341	4619	139	73	108	55	319	87	25320	259	1095
7.7	12	1393	19	53	10740	4912	141	70	106	53	303	84	26337	282	1077
7.8	4	1433	25	42	10469	4873	115	64	91	46	311	82	25553	274	1046

7.9	6	1247	31	42	10117	4428	143	64	120	45	291	103	24216	244	1007
8	7	1331	39	51	10388	4731	147	70	132	54	323	100	25128	267	1046
8.1	7	1365	25	36	10298	4808	119	75	132	44	310	82	25096	266	1079
8.2	8	1280	23	-22	10142	4579	117	57	133	55	321	84	24645	259	1014
8.3	13	1300	30	51	10047	4677	95	57	110	39	314	82	24587	257	984
8.4	4	1273	25	50	10129	4660	112	66	113	54	339	94	24666	250	970
8.5	9	1276	30	47	10060	4671	78	64	123	51	330	79	25799	240	988
8.6	18	1303	17	43	9930	4656	102	53	98	46	321	85	25327	239	1026
8.7	6	1205	22	43	9611	4124	110	53	117	55	284	99	22293	242	941
8.8	10	1294	27	61	10394	4516	156	64	103	54	319	92	25336	251	972
8.9	7	1277	24	58	9660	4339	111	62	104	53	284	92	23817	252	1002
9	10	1451	27	63	10940	4883	134	73	94	46	348	114	25628	275	1099
9.1	8	1342	34	54	11592	4725	103	63	102	61	350	100	26737	261	1014
9.2	12	1372	33	51	11106	4853	100	58	101	57	365	84	25485	267	984
9.3	5	1163	26	51	9831	4363	100	58	89	57	309	72	22479	228	905
9.4	11	985	29	31	8298	3659	99	60	81	40	254	82	19085	204	791
9.5	9	1096	36	48	8170	3914	85	47	83	39	259	75	19817	193	792
9.6	7	1107	26	41	8467	3854	80	61	110	38	254	73	21198	216	818
9.7	16	1108	26	56	9140	3989	105	59	83	38	274	82	21695	238	974
9.8	6	1030	26	42	8926	3674	111	53	94	37	231	75	20660	220	1003
9.9	4	1055	20	47	8684	3801	107	60	89	41	256	93	20248	217	906
10	7	900	25	42	7585	3249	74	44	77	34	200	61	17567	186	787
10.1	3	915	23	25	8061	3163	59	54	87	37	192	71	17539	176	739
10.2	5	933	22	51	7920	3463	72	55	69	24	192	71	19451	219	874
10.3	13	1072	27	42	8892	3871	100	63	110	34	237	86	21861	212	845
10.4	15	1025	29	56	8615	3671	116	54	101	34	217	74	21288	230	897
10.5	9	1148	32	35	8320	4114	101	44	123	35	235	101	21692	204	902
10.6	17	1296	32	37	9816	4852	121	58	96	38	283	69	25085	230	984
10.7	12	1255	31	49	9702	4522	140	67	123	46	275	100	26118	250	968
10.8	18	1319	38	47	10705	4916	119	64	86	44	321	78	26468	252	977
10.9	15	1471	32	66	11607	5312	145	76	127	42	323	119	29085	286	1129
11	15	1619	51	66	13544	5930	116	79	136	54	372	80	31776	298	1143
11.1	20	1557	38	47	11810	5293	144	74	106	56	333	91	28141	275	1076
11.2	10	1300	23	44	11032	4863	88	67	103	40	303	109	26200	266	997
11.3	15	1187	34	58	10294	4434	82	60	93	36	272	56	24359	249	895
11.4	5	1088	28	53	9562	4156	59	65	91	43	265	86	23102	225	887
11.5	9	1088	29	33	9316	4173	112	62	113	37	259	94	22284	224	880
11.6	17	1000	26	42	8516	3794	102	52	102	30	227	65	21292	213	817
11.7	8	1137	25	57	9468	4259	100	66	104	40	269	53	23454	225	890
11.8	22	1127	31	39	9257	4106	73	58	100	39	250	89	23115	232	890
11.9	6	1253	33	58	10230	4591	109	58	91	44	299	73	25204	243	985
12	16	1391	39	46	11003	5179	94	68	107	43	326	80	27932	281	1004
12.1	23	1355	36	44	10997	5208	121	67	103	55	341	71	27381	288	1020
12.2	18	1361	44	54	11412	5148	86	77	130	52	328	86	26322	279	978
12.3	17	1304	32	55	10930	4976	109	75	96	43	325	65	25620	270	986
12.4	11	1214	33	42	10491	4533	84	66	99	49	328	68	23903	246	941
12.5	9	1175	29	53	10655	4474	108	55	109	39	304	102	23691	254	912

12.6	6	1124	19	49	9633	4194	114	65	88	38	258	74	22540	237	877
12.7	13	1173	32	47	10011	4427	95	72	78	48	320	53	23849	242	939
12.8	3	1142	28	58	10251	4330	98	69	73	46	288	72	23765	251	949
12.9	7	1272	23	48	11382	4887	114	84	102	49	328	77	26702	282	1007
13	14	1265	31	47	10816	4646	104	66	98	40	306	82	24400	259	889
13.1	13	1554	26	39	10072	4276	86	60	101	39	276	79	23141	245	882
13.2	14	1130	37	40	9570	4304	91	59	75	35	264	69	22473	238	782
13.3	8	859	36	28	7360	3221	93	44	77	36	194	68	17373	178	658
13.4	20	738	33	34	6406	2610	48	40	57	33	181	53	14432	145	523
13.5	5	581	27	31	4559	2153	30	32	54	32	146	43	11205	111	407
13.6	5	696	27	37	5457	2456	34	32	37	27	169	59	13089	132	469
13.7	17	885	31	48	7026	3160	54	45	81	39	201	70	16539	172	614
13.8	7	980	49	42	8191	3755	82	54	69	33	249	55	19521	173	698
13.9	1	72	18	16	159	125	11	10	11	10	11	18	443	24	54
14	1	126	11274	24	169	117	17	30	56	99	12	17	490	35	60
14.1	3	213	17895	21	855	367	19	22	24	157	26	18	1831	57	97
14.2	2	339	18363	18	1239	622	22	17	22	158	37	19	3224	61	120
14.3	3	358	9496	20	1664	853	31	23	27	82	54	33	4037	51	145
14.4	8	557	7208	25	2505	1218	40	20	30	79	106	40	6199	78	222
14.5	5	890	687	38	4145	2033	68	36	63	36	182	57	10291	118	367
14.6	11	1391	42	54	7388	3601	92	66	73	60	337	74	20012	202	620
14.7	9	1401	53	37	7492	3729	109	51	84	70	332	86	19880	185	676
14.8	14	1719	56	51	8090	4082	103	63	91	72	371	87	20999	206	696
14.9	10	1773	64	47	8475	4273	98	56	101	83	423	66	21833	208	758
15	10	1441	56	41	9245	5059	96	50	90	73	450	75	25086	195	760
15.1	15	1551	54	61	8266	4518	122	57	109	67	384	212	22765	236	798
15.2	13	3594	57	67	8767	4560	107	60	78	76	432	396	24015	242	748
15.3	22	1454	53	52	8586	4541	127	42	101	74	420	100	23871	203	840
15.4	25	1657	47	50	9456	4806	159	61	95	84	424	97	25206	216	897
15.5	12	1428	60	54	9521	4704	148	51	112	74	430	94	24470	213	869
15.6	13	1338	47	56	9222	4738	146	59	86	62	409	101	25024	230	913
15.7	16	1450	68	57	9610	4953	177	62	102	72	424	91	25678	237	931
15.8	15	1383	45	52	9695	4758	151	54	107	75	401	94	24190	234	902
15.9	14	1395	43	64	10081	4783	155	57	104	75	395	94	25399	226	887
16	6	1495	69	54	9820	5480	145	45	101	73	439	78	27812	247	924
16.1	20	1476	65	58	9873	5807	144	63	104	74	474	85	27371	239	921
16.2	10	1412	67	51	9581	5173	140	64	104	70	441	84	27291	235	868
16.3	18	1325	64	52	9219	4939	123	53	102	66	403	75	25678	220	846
16.4	16	1433	56	62	9099	5393	124	73	80	72	422	95	26397	222	854
16.5	14	1528	61	42	9288	5294	145	51	100	79	435	99	26749	250	899
16.6	17	1347	63	90	9566	4849	137	62	76	74	404	96	27155	271	904
16.7	14	1319	52	55	9561	4931	123	77	115	65	394	87	26124	255	844
16.8	18	1386	58	60	9112	5033	164	63	83	70	405	89	26297	242	897
16.9	24	1354	58	54	9244	5077	154	60	110	74	409	74	26820	242	918
17	15	1398	43	48	9209	5253	155	64	119	64	430	97	26068	225	895
17.1	7	1428	49	60	9053	5026	95	69	100	63	434	54	26604	224	822
17.2	19	1390	53	63	9941	5019	102	67	92	67	433	69	28640	225	812

17.3	14	1384	49	61	9650	4864	128	71	82	67	435	88	27612	222	800
17.4	8	1513	58	52	9149	4881	127	54	102	65	408	88	25480	223	829
17.5	11	1396	62	59	8786	4870	145	62	91	80	385	127	25641	224	859
17.6	18	1563	82	63	9180	5067	141	60	119	72	411	98	27531	222	821
17.7	13	1514	59	62	9533	5063	114	40	91	84	403	96	25797	231	787
17.8	10	1863	78	54	9570	4767	111	68	86	82	388	110	26412	205	812
17.9	16	1416	68	59	8748	4878	130	57	95	71	391	86	24292	218	776
18	15	1379	91	63	8630	4594	139	52	82	72	356	99	24037	210	789
18.1	15	1318	77	41	8392	4478	103	55	91	75	356	85	23336	212	720
18.2	12	1364	90	53	7848	4117	142	52	95	78	346	74	21601	196	753
18.3	13	1315	91	48	8329	4304	121	68	103	73	333	86	22393	191	785
18.4	4	1542	85	57	9224	4834	135	63	97	71	356	87	25172	215	839
18.5	15	1545	83	70	9499	4743	130	70	80	82	357	90	24645	220	787
18.6	13	1558	65	53	9125	5014	115	59	91	72	390	73	25568	207	795
18.7	17	1455	62	51	8777	5055	125	56	75	72	368	60	24681	205	793
18.8	11	1276	61	51	8841	4510	147	53	99	73	356	93	23947	210	783
18.9	13	1323	68	67	8959	4638	120	54	91	82	364	67	26384	218	802
19	11	1364	67	64	8442	4623	135	52	101	92	358	107	24021	199	781
19.1	14	1337	55	36	7851	4189	119	60	96	91	330	88	22550	181	711
19.2	5	1471	54	73	7901	3989	116	78	82	74	327	67	21607	196	688
19.3	18	1290	67	59	8138	4331	112	54	91	81	339	95	23943	198	731
19.4	18	1162	42	40	8081	4346	107	68	97	61	366	89	22226	196	671
19.5	16	1044	58	33	7214	3744	93	46	63	64	305	55	18861	153	634
19.6	17	1038	56	51	6890	3674	90	40	91	54	288	72	18849	164	616
19.7	7	1054	39	41	7462	3653	82	49	95	52	295	68	18755	162	624
19.8	8	1081	45	51	6829	3537	91	51	51	50	272	70	17870	169	590
19.9	8	971	41	38	6848	3393	75	44	81	56	247	80	18432	168	563
20	14	906	39	55	7050	3360	105	53	51	49	250	55	17641	163	601
20.1	5	988	45	46	7915	3509	114	45	79	55	270	68	19657	171	685
20.2	18	1087	40	44	6810	3416	91	55	70	52	255	67	17224	166	604
20.3	9	1607	34	51	7279	3661	120	41	71	59	289	75	18985	183	675
20.4	5	1155	45	40	7362	4196	94	44	57	65	280	93	19530	177	661
20.5	9	1104	44	39	7174	3543	74	45	78	63	287	81	18447	184	643
20.6	12	918	35	46	7300	3535	102	59	99	61	302	82	19421	179	651
20.7	16	947	38	37	6973	3469	105	46	98	49	285	80	18957	174	629
20.8	15	1156	35	49	7417	3700	88	68	62	54	276	61	19624	177	620
20.9	11	1024	36	53	7264	3794	105	55	83	55	303	73	19902	179	667
21	4	1032	43	51	7288	3707	95	56	83	53	293	69	19576	182	670
21.1	9	1098	59	45	8739	4186	133	43	83	58	335	70	22767	202	715
21.2	8	1097	46	58	8976	4135	73	60	79	65	334	78	22254	215	756
21.3	9	990	54	48	7838	3712	87	50	69	58	268	72	20437	192	674
21.4	12	1035	49	44	7583	3725	106	51	76	57	269	68	20554	173	668
21.5	15	1010	36	51	7318	3714	83	57	67	42	281	52	20118	183	664
21.6	4	1119	36	48	7691	3878	99	54	70	55	301	80	20640	181	648
21.7	10	985	31	54	7455	3947	84	60	78	47	277	68	20117	188	655
21.8	5	997	29	56	8042	4141	83	51	81	45	313	80	20497	179	665
21.9	13	969	33	41	7683	3681	105	64	92	65	275	70	20210	178	666

22	12	1105	39	55	8341	4146	93	42	72	60	286	73	21705	201	647
22.1	11	930	49	43	7179	3521	91	52	66	54	252	73	19680	155	647
22.2	5	885	39	48	7060	3520	72	49	59	52	261	55	19208	159	585
22.3	12	1020	49	59	8093	3850	98	56	83	54	262	81	20465	190	636
22.4	12	1040	45	58	7829	3797	97	59	70	72	278	75	20702	194	666
22.5	8	907	54	44	6879	3418	113	53	69	51	235	83	18769	198	653
22.6	3	1102	34	42	8284	4014	107	51	87	60	286	96	21423	187	697
22.7	14	1105	36	37	8839	4206	104	51	79	66	295	88	21886	208	724
22.8	7	1127	51	47	8544	4178	101	59	86	62	298	60	23433	187	761
22.9	11	1071	36	19	7504	4253	122	50	71	51	304	79	21404	198	714
23	5	1002	55	41	7008	3632	106	48	97	61	244	76	18961	176	689
23.1	14	1021	58	48	7831	3852	130	46	90	56	272	86	20594	201	720
23.2	13	1112	65	54	8195	3993	107	56	65	59	281	84	22490	195	715
23.3	13	1056	58	53	8263	3814	104	57	89	50	239	89	20155	204	685
23.4	8	915	52	52	7051	3470	110	51	76	59	242	67	18817	165	609
23.5	5	1014	45	45	7151	3478	82	45	50	57	219	49	19501	156	595
23.6	6	983	42	56	7025	4166	102	45	89	54	234	94	20838	180	622
23.7	14	1062	65	51	7329	3897	82	46	63	61	262	77	21063	181	610
23.8	10	994	40	56	7119	3723	105	36	85	56	235	70	20179	185	680
23.9	11	926	39	56	7209	3537	112	61	55	46	232	67	19936	193	708
24	14	879	59	44	7470	3375	99	42	82	50	230	55	19520	176	711
24.1	5	845	56	36	6932	3258	116	50	62	47	196	61	17957	168	683
24.2	5	853	42	50	7268	3292	109	49	89	41	224	65	18740	187	716
24.3	10	867	52	51	7140	3295	110	40	61	48	224	66	19686	189	634
24.4	8	848	44	50	6828	3310	95	42	55	38	217	85	18312	159	626
24.5	11	820	57	53	7433	3478	101	57	68	45	220	60	18973	191	687
24.6	4	809	53	51	6488	3535	91	60	72	38	228	46	18357	169	597
24.7	5	737	59	56	6190	3113	89	48	65	36	213	59	17112	162	566
24.8	8	751	58	49	6242	3027	102	42	62	40	207	67	17300	156	610
24.9	6	767	56	52	6798	3200	72	47	73	42	218	89	18277	190	694
25	13	840	49	47	7413	3517	115	50	86	31	238	75	19932	170	739
25.1	2	976	63	66	8150	4017	93	63	87	52	261	58	21912	199	757
25.2	6	809	48	49	8203	3543	114	56	93	46	219	80	20998	196	788
25.3	8	950	55	62	9341	4095	128	56	89	53	271	105	23486	211	818
25.4	6	1003	63	68	8425	4113	141	59	93	46	260	83	23089	205	806
25.5	6	1047	72	51	8663	3888	146	61	102	61	263	100	22843	206	885
25.6	5	1180	70	69	8829	4434	140	60	90	59	302	88	24525	230	858
25.7	8	1175	67	62	8515	4974	133	64	94	50	328	82	24318	215	810
25.8	3	1034	72	53	8089	4730	122	47	60	60	371	86	23149	205	762
25.9	5	1038	57	46	7548	4000	102	59	57	57	328	55	21756	201	698
26	14	1107	56	46	7274	3957	80	52	77	56	311	69	20677	175	690
26.1	4	809	70	40	6536	3471	65	35	64	47	262	55	22477	173	587
26.2	14	706	54	50	5962	3041	82	49	60	33	237	45	16443	148	532
26.3	8	657	48	47	5353	2807	57	43	58	28	222	33	15291	134	536
26.4	2	555	36	39	5049	2412	64	36	57	29	180	57	14234	117	485
26.5	7	624	36	45	5603	2626	82	43	54	39	198	50	15762	141	532
26.6	13	697	36	55	6384	3154	62	53	63	39	238	53	18064	162	576

26.7	11	858	33	63	6706	3275	90	54	60	45	262	49	18010	174	604
26.8	8	776	35	39	7039	3293	89	46	68	41	257	57	19097	168	616
26.9	8	754	24	41	6992	3367	82	50	68	45	260	64	18893	165	634
27	9	697	23	41	6627	3102	91	42	82	39	232	68	17320	170	618
27.1	10	683	23	48	6313	3021	67	45	51	38	228	50	16060	149	523
27.2	4	548	25	46	5467	2649	60	35	46	34	195	48	14359	129	456
27.3	13	480	31	40	4140	2160	57	31	26	35	155	43	11851	98	365
27.4	3	284	21	33	2725	1437	42	23	22	23	105	25	6533	74	269
27.5	3	235	20	37	2367	1031	57	30	46	13	22	34	6721	71	294
27.6	1	1154	49	29	3402	1480	35	40	24	63	14	9	17071	82	347
27.7	1	128	21	0	315	283	0	8	28	11	9	9	1264	6	46
27.8	12	826	7	36	4187	1663	24	18	41	33	126	23	10442	84	321
27.9	19	1910	18	16	7783	5506	47	20	79	47	307	90	17429	166	552
28	1	1127	31	51	5855	1515	62	34	52	32	108	34	9865	160	405
28.1	5	1939	18	61	5957	2181	32	45	41	43	106	61	12086	157	344
28.2	5	1817	14	42	3964	1512	23	29	50	36	69	97	8602	125	312
28.3	6	1000	22	31	3646	1260	43	29	48	21	76	54	7064	103	342
28.4	8	782	12	32	3791	1405	33	18	44	26	94	68	10139	87	311
28.5	1	777	22	36	4192	1492	52	17	44	39	87	56	8652	102	310
28.6	2	857	12	48	4319	1569	33	39	51	28	83	63	9014	117	331
28.7	4	804	16	19	4558	1725	70	34	44	34	94	58	9839	110	379
28.8	2	847	21	43	4862	1754	45	34	82	42	75	87	10257	117	399
28.9	4	820	24	29	6079	2093	62	32	47	34	113	39	14246	148	512
29	7	966	29	33	7401	3143	69	45	77	37	148	86	18777	174	673
29.1	11	977	34	35	7670	3265	100	33	81	48	159	88	17833	191	701
29.2	1	984	32	50	7726	2902	97	61	66	36	128	105	17455	204	654
29.3	6	858	29	50	7192	2417	130	36	89	29	89	86	15107	194	672
29.4	6	1027	24	45	7309	3201	117	38	71	34	149	85	16381	183	701
29.5	2	920	33	52	7583	2923	86	43	86	42	156	53	17085	192	724
29.6	1	892	30	61	8944	3006	104	46	70	34	177	65	18499	237	720
29.7	10	910	36	48	8134	3039	101	26	82	30	167	65	18694	212	712
29.8	1	892	28	60	7618	3164	91	58	72	35	175	69	17890	192	749
29.9	17	793	10	42	7060	2962	85	54	47	29	152	70	15572	190	687
30	7	731	20	28	6426	2607	98	31	67	42	130	70	14753	142	693
30.1	3	1092	23	57	6603	2894	112	68	73	44	155	49	16791	187	756
30.2	4	973	33	47	7178	3196	117	62	77	37	152	90	17730	205	722
30.3	11	889	23	41	7102	3177	97	65	63	30	153	102	18070	194	688
30.4	1	828	21	43	7302	3076	87	48	81	31	161	53	17353	170	628
30.5	7	774	26	27	6771	3018	91	52	89	47	148	66	17123	178	673
30.6	2	1011	25	71	7235	3715	78	50	80	38	162	97	17742	203	705
30.7	6	715	22	41	5975	2985	89	54	75	31	142	49	14652	169	581
30.8	9	553	25	45	5468	2282	78	36	60	22	119	58	12597	167	570
30.9	1	608	15	27	6012	2510	96	38	80	30	136	86	14681	151	603
31	9	802	35	55	6621	2994	126	49	109	38	177	70	17488	170	736
31.1	5	765	25	41	7298	3048	102	54	81	36	188	89	18128	184	688
31.2	1	738	25	54	6982	3041	99	50	89	33	170	69	17381	192	676
31.3	8	618	16	59	5926	2379	55	56	58	21	114	45	14225	175	631

31.4	8	625	23	56	5818	2432	84	38	40	36	110	31	14394	136	568
31.5	7	678	20	38	5997	2559	67	43	66	34	136	64	14641	155	583
31.6	1	620	16	56	6041	2392	66	42	55	25	141	60	15342	191	643
31.7	5	554	23	31	5479	2057	96	40	73	22	100	59	11863	155	595
31.8	1	531	25	48	4659	1863	60	39	31	21	88	60	10767	131	490
31.9	2	557	23	37	5017	1859	78	55	47	30	93	87	10989	123	459
32	3	514	37	49	4484	1969	74	39	64	22	93	41	11413	125	470
32.1	2	682	33	40	6338	2461	100	47	64	29	130	51	14860	172	539
32.2	2	650	34	38	5561	2286	40	33	29	26	119	58	14261	138	482
32.3	4	662	19	50	5861	2431	71	41	37	31	134	71	14557	157	540
32.4	9	818	27	49	6906	2685	108	55	86	35	151	90	15338	179	590
32.5	3	706	21	37	6446	2662	-637	43	63	35	123	39	14400	162	581
32.6	11	614	21	46	5609	2409	89	41	53	34	114	55	13768	151	570
32.7	10	584	28	39	5188	2256	65	41	73	29	112	45	13615	160	607
32.8	4	567	27	58	4867	2216	70	34	53	38	135	61	12372	147	527
32.9	14	561	26	44	4719	2097	49	35	48	30	121	63	12151	131	506
33	1	744	29	58	5740	2888	60	34	52	42	172	37	15912	145	584
33.1	8	749	28	45	6261	2851	59	48	104	34	184	119	16903	172	712
33.2	14	811	24	49	6901	3291	129	57	56	43	188	36	18991	169	735
33.3	2	694	27	44	5415	2930	76	34	68	48	187	61	15503	142	637
33.4	3	712	23	74	5393	2882	113	35	48	21	198	54	16316	175	644
33.5	7	780	22	52	6664	3147	81	58	68	47	210	46	18006	156	607
33.6	3	650	16	31	5329	2423	45	31	72	39	162	35	13661	126	507
33.7	5	714	8	56	5875	2727	94	45	78	47	170	85	15607	149	627
33.8	11	746	22	54	6204	2988	90	53	100	34	214	66	17714	148	670
33.9	1	760	16	51	6692	3280	130	43	74	51	221	35	19313	186	717
34	1	778	19	60	6753	3175	136	62	83	39	166	62	18531	178	817
34.1	5	913	25	49	8233	3797	110	49	105	51	218	108	22537	216	895
34.2	19	869	32	52	8313	3627	124	44	104	49	187	59	22865	257	889
34.3	6	894	27	56	8275	3619	132	68	85	26	176	52	22649	207	857
34.4	9	859	17	67	8253	3598	98	67	116	40	177	85	22437	220	860
34.5	11	808	27	46	7391	3251	114	57	90	35	164	92	20570	196	796
34.6	1	796	38	53	7215	3329	137	44	80	42	191	51	20144	187	858
34.7	6	906	27	39	7807	3655	138	55	91	32	222	86	22080	200	868
34.8	11	927	40	46	8169	3834	142	44	137	56	226	91	22962	213	922
34.9	6	949	42	43	7947	3895	111	46	129	51	257	86	22546	201	881
35	1	1017	48	35	8306	4131	140	52	125	61	267	84	23453	222	892
35.1	17	932	34	66	7979	3821	179	52	87	46	237	68	22534	209	848
35.2	6	1066	45	47	7966	4050	123	56	96	46	262	105	22754	201	841
35.3	7	956	56	52	8611	4167	87	46	102	52	255	89	23715	218	819
35.4	10	929	37	52	7896	3741	114	58	80	45	236	86	20821	208	787
35.5	11	924	31	51	7766	3604	121	59	101	28	231	90	21225	192	804
35.6	19	887	24	30	7978	3482	118	50	108	33	203	96	21749	200	800
35.7	5	918	27	57	8354	3737	152	59	101	32	229	73	21729	197	812
35.8	5	938	20	53	7533	3443	135	53	88	51	218	68	19808	202	747
35.9	11	779	27	55	7305	3433	101	56	106	35	200	79	18849	171	762
36	12	744	23	34	6935	3281	110	34	87	33	209	71	19126	183	734

36.1	9	830	36	53	7573	3316	151	69	66	42	206	94	20897	202	784
36.2	8	907	31	66	7956	3701	75	72	113	40	213	134	22332	226	824
36.3	15	842	27	56	7685	3529	109	54	99	40	220	77	20667	213	796
36.4	15	946	24	37	7899	3817	125	44	118	34	246	107	21947	214	773
36.5	5	880	29	51	7695	3602	121	61	86	39	220	96	20329	201	778
36.6	4	858	30	57	7648	3450	118	61	88	48	226	96	19801	194	779
36.7	6	887	31	44	9193	3432	150	56	99	46	230	97	20018	203	833
36.8	6	839	34	46	7250	3271	115	41	81	41	210	76	19795	173	787
36.9	4	813	24	49	7597	3231	104	48	115	33	185	114	18827	186	802
37	3	816	29	45	8207	3280	134	44	100	38	180	125	20775	188	777
37.1	3	887	32	67	8554	3362	140	65	118	48	201	120	21211	207	819
37.2	3	807	44	37	7856	3322	114	59	73	48	183	82	20574	194	818
37.3	2	822	113	53	7623	3254	148	58	117	41	177	118	19960	186	822
37.4	5	825	38	46	7618	3370	141	58	96	34	189	94	20057	212	860
37.5	9	862	39	47	7693	3320	132	67	79	43	174	81	20477	213	817
37.6	8	878	37	47	8204	3299	132	47	122	43	160	109	20890	196	818
37.7	7	783	44	53	7496	3307	76	51	109	39	181	91	22954	195	735
37.8	9	848	48	65	8481	3547	75	66	85	44	203	103	25804	200	789
37.9	4	951	54	64	7968	3717	94	66	89	48	219	119	23224	199	813
38	4	956	34	46	8071	3867	123	57	73	46	216	89	23450	227	901
38.1	8	989	45	51	8797	4023	133	62	86	35	237	92	23426	219	916
38.2	9	1047	41	46	8909	4064	153	50	99	46	226	83	24160	228	929
38.3	10	902	32	45	8742	3801	145	65	137	49	210	105	22891	213	912
38.4	13	984	54	50	9334	4015	157	62	118	42	220	100	24243	225	983
38.5	6	869	41	52	8650	3879	162	56	103	44	191	96	21614	210	930
38.6	13	944	40	58	8811	4126	136	40	85	49	229	76	22957	223	934
38.7	3	954	29	58	9410	4146	130	52	108	44	219	60	23361	235	932
38.8	11	819	29	61	8542	3554	161	51	115	37	193	70	21132	211	883
38.9	5	865	24	49	7997	3354	135	48	95	47	182	66	19816	194	837
39	7	744	22	48	7991	3185	110	64	96	28	164	106	19158	198	821
39.1	6	705	31	49	7747	3025	108	46	87	41	156	75	17966	206	769
39.2	6	659	34	51	7383	2835	108	55	90	32	137	78	17079	204	808
39.3	10	676	29	45	8186	3078	140	60	80	26	149	83	19296	199	777
39.4	9	769	22	48	6875	2950	92	39	71	26	154	65	16187	176	714
39.5	4	787	27	45	7259	3210	113	50	83	36	182	73	17756	176	745
39.6	1	663	30	48	7151	2844	92	43	76	27	142	75	16322	186	679
39.7	9	625	28	39	6872	2628	69	57	71	33	148	64	15227	178	673
39.8	1	630	23	49	7095	2742	91	58	53	31	137	59	16356	190	681
39.9	4	611	18	45	6416	2715	73	52	46	32	152	39	15232	158	582
40	7	386	33	34	4026	1723	95	44	73	21	86	52	9856	127	536
40.1	5	500	23	42	6329	2279	117	38	74	29	127	59	15803	168	681
40.2	9	575	35	42	6105	2599	112	45	94	29	157	59	14801	161	671
40.3	1	539	14	43	6417	2282	108	49	87	25	129	84	13476	166	714
40.4	4	851	17	70	8947	3396	123	64	104	36	186	109	19792	231	871
40.5	9	660	23	32	7049	2864	74	42	107	41	159	79	14805	182	700
40.6	8	776	35	39	7039	3293	89	46	68	41	257	57	19097	168	616
40.7	8	754	24	41	6992	3367	82	50	68	45	260	64	18893	165	634

40.8	9	697	23	41	6627	3102	91	42	82	39	232	68	17320	170	618
40.9	10	683	23	48	6313	3021	67	45	51	38	228	50	16060	149	523
41	4	548	25	46	5467	2649	60	35	46	34	195	48	14359	129	456
41.1	13	480	31	40	4140	2160	57	31	26	35	155	43	11851	98	365
41.2	3	284	21	33	2725	1437	42	23	22	23	105	25	6533	74	269
41.3	3	235	20	37	2367	1031	57	30	46	13	22	34	6721	71	294
41.4	1	1154	49	29	3402	1480	35	40	24	63	14	9	17071	82	347
41.5	1	319	18	52	6644	643	87	88	186	1	1	112	6003	281	951
41.6	1	771	54	58	8055	2031	153	59	58	38	119	89	14618	259	917
41.7	2	1126	60	57	7684	3046	122	42	128	48	219	120	15209	229	812
41.8	1	1356	51	42	9369	3507	194	100	85	45	257	123	20248	244	990
41.9	4	1011	65	35	9263	3022	103	54	115	47	156	84	18610	251	869
42	4	876	42	51	7870	2369	109	49	119	30	114	129	14583	233	909
42.1	4	1110	42	43	8461	2590	137	47	134	39	112	112	17028	210	906
42.2	7	975	34	61	7172	2114	83	55	87	24	118	118	13786	211	696
42.3	3	1205	33	38	6847	2344	66	34	101	35	109	151	13795	158	617
42.4	2	1246	50	49	6932	2068	80	52	93	41	108	126	12444	169	638
42.5	7	1150	44	51	6718	2659	114	40	90	35	154	96	14407	191	743
42.6	6	1226	42	52	8672	3197	111	57	94	47	187	102	17869	231	847
42.7	5	1537	52	52	9214	3412	133	51	104	54	179	103	20644	236	850
42.8	14	1310	52	70	8193	3280	120	45	75	38	150	73	17615	217	751
42.9	3	1090	44	62	8297	3068	129	39	95	35	141	120	19057	246	857
43	3	1292	51	59	8848	3241	109	53	87	41	157	86	20545	218	831
43.1	5	1104	55	70	8923	3125	110	61	82	48	151	89	20040	229	831
43.2	3	947	46	54	8228	2986	143	40	108	32	138	106	18497	215	922
43.3	6	1030	63	55	8338	3437	140	61	75	39	187	82	20241	236	925
43.4	9	1218	40	42	8973	3574	175	51	105	45	178	97	21818	236	989
43.5	6	1035	56	56	8875	3752	154	60	101	41	225	88	22244	235	968
43.6	5	985	55	56	9416	3846	152	62	91	35	203	126	23037	244	1014
43.7	9	1027	49	55	9252	4201	178	58	119	38	239	128	23839	240	979
43.8	4	1029	66	57	9102	4213	151	60	95	44	233	104	23588	228	961
43.9	6	1257	62	40	8875	4150	146	54	104	45	222	110	23416	229	978
44	8	937	53	48	9221	4148	172	64	93	45	227	85	24038	237	1039
44.1	5	961	53	74	9205	4141	198	85	124	34	221	120	23647	257	1099
44.2	11	1107	56	53	9420	4384	190	64	119	41	220	86	24176	234	1085
44.3	6	1040	47	58	9155	4260	153	72	101	50	249	96	24712	248	1013
44.4	16	945	57	48	10292	4350	164	67	97	35	259	83	25177	268	1076
44.5	14	953	52	54	9962	4582	188	57	126	51	287	119	24167	267	1110
44.6	13	1102	55	52	10241	5163	191	69	116	45	340	93	25899	258	1146
44.7	16	1044	52	69	10147	4962	171	80	129	34	319	84	25782	269	1161
44.8	12	1065	51	67	11446	4928	176	73	119	39	328	78	27433	275	1067
44.9	15	1001	49	54	10430	4792	157	64	102	39	304	80	26233	262	1064
45	13	1139	41	60	9543	5031	206	74	112	39	325	85	25350	268	1118
45.1	10	1081	34	53	10756	5413	183	63	109	41	375	93	26253	263	1142
45.2	14	1092	50	46	10607	5455	209	66	113	47	363	108	27044	274	1143
45.3	19	1005	51	56	10461	5083	172	74	106	39	355	75	24985	246	1083
45.4	4	911	40	51	8745	4406	157	56	109	32	295	95	22573	226	966

45.5	17	961	46	34	9858	4695	195	66	120	34	301	95	24507	236	1085
45.6	11	953	52	46	9843	5008	174	60	121	36	295	75	25131	255	1151
45.7	8	1036	53	51	10711	5086	181	78	104	45	318	79	25759	270	1154
45.8	21	1099	46	58	10675	5050	172	77	115	39	311	122	25213	272	1136
45.9	5	1087	45	50	10401	5251	209	81	127	38	315	101	25254	284	1123
46	14	1274	46	51	10733	5267	203	62	104	43	343	67	26494	272	1130
46.1	9	1167	36	40	10508	5362	187	68	110	41	341	90	26019	281	1145
46.2	11	1128	36	57	11145	5459	196	64	121	42	341	78	26132	270	1171
46.3	10	977	43	65	11109	5051	193	63	101	36	323	103	25560	270	1128
46.4	12	985	29	51	10336	4869	185	76	112	38	315	95	23882	276	1111
46.5	12	804	39	44	8846	4279	188	70	125	31	262	86	20830	243	1062
46.6	11	1055	46	51	10648	5175	207	63	121	40	324	93	27056	276	1206
46.7	15	1108	50	55	10617	5648	212	78	129	47	379	87	27973	279	1251
46.8	17	1135	58	51	11116	6033	222	69	103	44	431	94	28515	303	1273
46.9	15	1103	63	51	10504	5740	209	62	130	43	400	109	26550	256	1208
47	16	1000	46	54	10512	5328	209	58	104	40	343	71	25602	262	1144
47.1	9	1023	40	47	9971	5085	186	69	129	40	303	82	24259	264	1098
47.2	7	946	43	51	10516	5072	195	73	120	42	331	116	24431	262	1179
47.3	18	1042	42	45	10712	5270	227	67	109	35	353	87	25414	270	1192
47.4	6	1147	51	52	10662	5487	182	72	125	35	386	158	27497	280	1168
47.5	9	1091	39	55	10844	5572	216	70	130	42	362	76	26754	283	1250
47.6	9	1120	41	46	11099	5566	225	84	113	40	362	102	26903	289	1255
47.7	8	1096	41	56	11308	5534	232	69	114	39	370	88	27056	281	1207
47.8	21	1130	49	48	10898	5568	201	66	130	38	397	85	27038	297	1152
47.9	9	900	33	52	9556	4600	182	54	103	33	301	70	24097	231	1021
48	6	862	40	42	8437	4220	201	56	92	35	280	83	21121	241	955
48.1	9	747	41	38	8577	4122	159	56	95	31	290	68	20753	240	999
48.2	7	900	43	49	9359	4749	155	59	84	31	308	76	21558	243	970
48.3	4	793	37	47	7953	4026	155	60	82	34	282	74	19477	205	826
48.4	5	778	30	52	7201	3693	146	50	94	31	235	88	16930	198	780
48.5	8	769	38	50	8424	4005	155	65	86	32	263	69	19020	208	867
48.6	18	760	37	37	8424	3966	112	51	92	32	257	68	19782	204	788
48.7	11	2055	14	36	3736	1780	10	58	48	60	161	102	9378	131	296
48.8	8	1229	28	43	2025	793	31	24	37	30	79	44	4011	93	187
48.9	1	694	22	38	3173	1499	67	24	29	28	117	66	6929	106	399
49	9	718	37	44	6258	2647	101	50	52	38	236	81	15049	159	703
49.1	12	827	38	46	7320	3605	132	47	70	40	311	94	18089	199	841
49.2	11	908	47	43	8087	4083	160	54	76	41	355	44	21360	194	800
49.3	11	777	55	51	7462	4209	162	58	69	50	346	67	20281	194	935
49.4	12	994	45	52	9196	4910	196	55	86	54	394	95	24271	227	1118
49.5	11	1104	61	75	10960	5867	228	75	109	62	442	100	28524	288	1303
49.6	15	1328	62	73	11072	5797	248	91	127	67	436	87	29506	277	1296
49.7	13	1255	46	70	11237	6067	240	74	113	56	458	106	29926	294	1343
49.8	9	1137	45	61	11712	6058	231	85	90	57	488	98	29472	297	1295
49.9	15	1352	55	61	12340	6509	259	85	86	52	501	109	30853	312	1356
50	18	1268	44	59	12504	6739	260	100	100	52	521	119	31646	302	1375
50.1	15	1284	51	67	12625	6856	242	88	103	61	520	114	31712	311	1337

50.2	20	1163	32	61	12238	6871	234	77	119	47	539	103	31708	291	1263
50.3	19	1023	33	63	14192	6402	211	91	108	49	536	96	33895	298	1231
50.4	10	1326	34	76	12805	6562	220	94	85	49	530	109	32552	313	1297
50.5	23	1237	36	67	12907	6571	209	93	94	51	559	98	32305	306	1290
50.6	9	1001	33	79	11761	6327	232	89	106	42	558	94	30809	310	1239
50.7	25	1082	39	69	12343	6293	216	75	106	60	512	104	30152	289	1217
50.8	13	1270	42	65	11883	6397	214	72	82	48	532	96	30637	309	1186
50.9	11	1019	32	61	11899	6248	209	80	66	43	535	95	29653	289	1166
51	12	1030	32	60	11028	5700	180	76	73	53	482	95	26570	284	1097
51.1	14	1187	31	63	11502	5578	174	83	79	44	501	105	28568	271	1085
51.2	23	1093	36	56	11445	5858	174	75	85	62	521	81	27571	268	1033
51.3	10	993	25	72	11675	5931	166	61	73	42	515	103	28591	278	1096
51.4	13	858	38	48	9661	5020	129	68	72	48	423	73	23966	240	918
51.5	13	769	25	52	8849	4584	145	69	64	46	385	74	22068	220	919
51.6	14	764	32	56	8986	4513	153	77	66	33	424	51	21786	225	874
51.7	18	808	26	48	7964	4452	154	61	64	46	375	67	20705	195	842
51.8	5	764	25	28	8086	4056	182	51	89	40	347	97	19281	208	998
51.9	26	1016	35	61	11363	5705	229	77	99	46	499	106	29004	286	1336
52	9	905	26	45	10478	5410	227	73	88	44	497	104	26488	257	1241
52.1	16	884	24	53	11690	5239	231	70	79	44	441	90	24923	282	1204
52.2	26	1065	36	63	11756	5757	218	76	98	47	513	114	29274	273	1221
52.3	14	948	36	55	11044	5069	197	69	77	39	444	84	25273	251	1180
52.4	12	1210	22	60	10309	5128	237	65	86	41	435	68	25089	255	1214
52.5	18	1089	33	89	11421	6078	235	91	107	48	503	97	29211	283	1262
52.6	12	1152	40	49	12102	6314	269	77	105	58	540	106	29967	294	1413
52.7	18	1111	36	68	12181	6698	263	87	78	53	538	62	31056	315	1342
52.8	17	1210	40	69	11792	6484	242	80	103	57	550	103	30838	297	1306
52.9	16	1078	55	58	11653	6339	195	77	99	53	525	90	29005	286	1271
53	17	1262	40	66	11565	6381	254	82	99	55	526	84	30970	280	1350
53.1	31	1098	40	63	11422	6434	226	80	101	55	539	127	29475	288	1275
53.2	15	1138	38	58	12125	6642	230	84	88	40	561	97	30477	306	1280
53.3	9	1085	41	74	12089	5876	217	87	110	50	525	114	29943	308	1272
53.4	27	1037	34	51	11962	6219	246	78	96	50	511	107	29623	277	1283
53.5	10	1212	40	65	12120	6569	234	77	114	52	518	119	30196	305	1318
53.6	17	1174	39	51	12734	7001	230	58	114	56	546	81	31346	318	1300
53.7	12	1181	35	62	13208	7016	221	89	106	52	592	91	32024	297	1250
53.8	8	1109	33	60	12143	6537	184	75	98	42	540	90	29724	279	1127
53.9	8	921	32	60	10522	5651	170	86	91	41	464	77	25820	275	1051
54	19	1164	32	46	11753	6611	174	75	101	42	549	69	29440	276	1135
54.1	12	1004	27	63	12090	6478	186	87	111	45	545	86	29338	295	1158
54.2	13	1023	33	58	11641	5878	182	82	88	50	483	102	27813	284	1093
54.3	15	1008	26	69	11954	6303	203	89	84	59	523	69	30954	290	1158
54.4	19	982	29	75	11599	6366	173	83	80	51	530	72	30826	291	1184
54.5	19	1070	28	69	11427	6655	202	66	101	49	552	89	29756	282	1172
54.6	24	1172	35	51	11960	6394	219	70	96	63	540	75	38148	287	1288
54.7	14	1071	28	70	12220	6747	207	74	94	57	583	71	31707	302	1171
54.8	17	1096	36	64	12621	6647	217	79	85	56	568	104	31085	291	1210

54.9	21	1050	34	58	12224	6663	200	62	96	56	544	92	31723	299	1225
55	11	1050	33	63	11884	6159	205	80	81	47	462	83	29626	293	1201
55.1	12	994	21	61	10945	5494	184	78	82	38	410	107	26425	261	1124
55.2	10	747	21	66	9356	4362	153	74	64	40	355	93	21572	243	962
55.3	11	725	18	64	9124	4126	159	64	81	40	300	70	20246	248	906
55.4	1	625	7	52	8402	3908	153	60	63	26	308	110	19066	209	896
55.5	1	2109	1	43	11861	7253	216	56	82	65	606	86	31414	278	1103
55.6	1	64	22	16	182	284	12	15	13	7	1	33	933	18	115
55.7	1	99	19	9	795	502	17	14	13	28	44	23	2379	54	416
55.8	1	169	14	15	1811	944	112	29	39	12	50	66	4943	59	575
55.9	1	311	21	50	3046	1370	90	37	29	25	69	70	8118	91	622
56	1	698	30	45	6977	3262	127	28	98	35	179	80	18285	215	950
56.1	4	942	40	39	8473	3891	158	47	106	61	255	119	21771	213	1103
56.2	14	826	41	61	8777	3707	220	63	88	44	235	83	21360	245	1086
56.3	4	889	34	53	8904	3887	147	45	92	56	239	123	20357	219	999
56.4	1	754	23	41	6822	3183	121	45	82	51	227	92	17308	166	821
56.5	5	922	31	53	8371	3885	136	42	102	43	251	95	20607	217	1015
56.6	9	993	44	72	8724	4056	160	63	97	56	267	119	21875	231	987
56.7	11	984	26	61	9209	4183	147	48	104	47	287	77	22274	218	989
56.8	12	1011	33	61	8682	4183	129	53	68	54	267	93	22451	218	899
56.9	9	969	32	55	8822	4278	130	64	112	50	284	97	22480	228	924
57	8	900	28	61	8679	4081	152	59	87	50	233	88	21729	223	1029
57.1	5	1054	44	58	9831	4654	155	61	89	60	286	78	24790	241	1089
57.2	9	1082	38	59	10273	4792	171	67	109	52	324	105	25691	239	1140
57.3	11	1230	45	60	9782	5450	156	57	111	51	332	81	25840	244	1107
57.4	15	1144	37	53	10517	5758	192	59	95	49	379	117	27820	274	1147
57.5	14	1215	43	62	11161	6075	174	80	120	46	396	95	28643	295	1205
57.6	21	1259	40	51	11534	6330	201	70	101	40	428	73	30591	294	1215
57.7	15	1295	35	58	11721	6190	193	78	109	55	449	81	30602	298	1228
57.8	10	1106	46	48	11257	5837	174	83	85	50	423	93	29391	277	1145
57.9	7	1267	35	63	11150	6201	183	73	100	41	424	81	29326	260	1212
58	28	1121	37	68	10883	5918	203	72	105	41	408	107	28033	269	1198
58.1	14	1169	40	59	12364	6225	177	72	95	22	429	90	30587	297	1194
58.2	17	1133	33	56	11763	5912	181	88	99	42	427	81	29791	318	1194
58.3	15	1666	30	66	10856	6163	200	-1469	97	40	458	92	29578	267	1209
58.4	21	1210	42	65	11381	6500	186	78	111	59	472	99	31121	292	1251
58.5	16	1238	33	69	12128	6485	196	75	113	48	479	75	30892	289	1214
58.6	36	1292	34	60	11566	6318	192	85	88	48	444	75	30923	291	1192
58.7	25	1125	39	57	11137	5896	168	73	109	47	411	78	28075	293	1201
58.8	11	1137	29	58	11046	6012	186	74	121	35	441	106	29899	268	1244
58.9	7	1103	29	55	11475	6002	156	86	103	45	431	108	30323	294	1196
59	16	1164	30	52	10769	5953	201	72	112	37	438	114	28878	262	1231
59.1	7	1118	31	62	11192	6055	201	76	57	42	430	123	29752	288	1186
59.2	13	1371	24	66	11412	5950	202	71	83	38	414	115	29454	276	1178
59.3	12	1145	32	40	10904	5742	187	74	103	47	407	107	28677	270	1180
59.4	20	1454	41	53	10590	5896	150	73	118	43	395	142	28930	277	1233
59.5	9	1130	52	64	10571	5968	173	61	105	47	403	110	28347	265	1158

59.6	21	1434	49	61	11273	6261	186	69	80	49	440	83	29976	269	1163
59.7	17	1152	52	56	11684	6224	186	76	113	49	463	77	30393	284	1191
59.8	8	1135	35	53	11008	6191	201	56	105	45	425	107	29330	274	1184
59.9	28	1180	34	53	10693	5978	174	62	101	48	413	93	28412	276	1185
60	14	1154	42	46	11126	5908	188	77	100	45	444	94	29404	256	1182
60.1	20	1241	36	56	12216	6093	199	78	79	42	450	90	29957	270	1205
60.2	28	1143	32	62	11944	6090	186	59	122	57	445	120	27671	289	1199
60.3	9	1134	26	64	12159	6188	186	70	106	61	453	85	30327	279	1174
60.4	21	1129	30	54	11991	5981	206	58	113	48	416	82	30364	293	1209
60.5	15	1044	32	60	10562	5642	202	71	99	45	394	102	27107	268	1152
60.6	10	1036	31	56	11312	5682	207	88	128	43	381	104	29552	269	1204
60.7	10	1129	28	58	11642	5754	206	69	101	40	413	93	31731	263	1241
60.8	14	1135	33	46	10500	5789	155	55	98	48	405	130	28036	271	1128
60.9	23	1151	31	74	10845	6352	215	82	123	46	423	106	28571	276	1223
61	11	1086	23	66	11354	5928	218	89	98	42	421	66	30018	280	1169
61.1	14	1180	35	157	11468	6287	165	226	97	48	484	58	31163	313	1197
61.2	19	1133	32	58	11990	6029	204	57	110	53	454	110	29596	295	1166
61.3	7	1059	36	55	11655	5869	194	75	97	51	451	108	30105	274	1158
61.4	13	1010	29	55	11579	5456	187	50	105	47	421	107	28103	262	1180
61.5	6	1164	22	53	10759	5953	182	76	92	40	429	72	27731	284	1141
61.6	15	1185	31	62	11604	6061	193	62	116	44	453	120	29687	298	1240
61.7	18	1183	33	59	11639	5928	172	77	88	47	462	83	28830	266	1165
61.8	17	1122	35	57	11625	5992	208	68	108	42	442	121	28458	298	1179
61.9	30	1065	43	53	11914	5648	184	83	91	52	441	100	27955	276	1109
62	16	1090	31	44	11552	5718	210	57	102	51	435	79	28673	286	1179
62.1	19	1068	35	54	11761	5431	198	68	96	45	413	111	27394	263	1178
62.2	18	1191	32	56	11920	6449	182	83	102	33	499	95	29656	286	1189
62.3	20	1227	46	57	12735	6752	198	88	116	41	539	125	32198	303	1244
62.4	14	1192	27	59	13562	6220	225	99	79	44	500	100	31940	311	1294
62.5	24	1120	31	56	13198	6146	236	93	113	37	506	100	32824	309	1285
62.6	21	1148	32	54	13563	6128	221	93	118	34	536	112	31703	304	1288
62.7	18	1075	27	44	13683	6029	194	92	96	46	526	81	30566	324	1276
62.8	17	963	20	48	11364	5202	196	77	100	38	434	116	26230	273	1158
62.9	17	841	20	40	10239	4528	159	58	64	34	380	77	24008	246	976
63	16	838	33	34	10400	4338	175	78	109	34	347	87	25639	245	1085
63.1	9	866	32	48	11118	4959	150	91	87	35	435	95	26039	260	1031
63.2	5	962	26	45	10761	4968	180	68	92	37	413	81	27680	269	1108
63.3	16	1042	36	49	11313	5560	169	82	71	40	430	70	28225	279	1082
63.4	9	924	26	42	11592	4949	171	77	90	30	383	90	23932	269	1049
63.5	8	900	32	36	10859	4413	148	64	80	33	338	86	23812	236	1059
63.6	7	902	35	49	8742	4090	134	72	97	36	304	100	20732	185	876
63.7	14	1156	33	55	10233	4628	171	76	88	32	317	106	21659	217	1042
63.8	9	954	41	47	12699	5214	174	80	85	32	390	70	27748	279	1141
63.9	17	891	38	50	11607	5076	176	82	89	29	348	88	25532	276	1032
64	8	1059	34	44	11119	5219	192	95	93	35	397	96	24978	271	1059
64.1	11	1280	35	45	12074	5762	173	83	90	31	403	115	26178	267	985
64.2	25	3195	34	33	11940	5852	176	85	91	40	445	160	28938	262	1071

64.3	9	1631	35	43	11539	5479	190	63	90	33	414	120	26650	276	1083
64.4	12	951	32	47	11204	5554	219	62	109	35	409	122	26502	259	1083
64.5	22	1345	34	59	12229	5968	235	82	87	40	473	146	30737	277	1152
64.6	20	1301	40	58	11056	6409	197	65	110	33	448	122	27936	263	1133
64.7	24	1245	26	62	11938	6035	203	79	104	36	395	93	30307	296	1149
64.8	18	1199	26	54	11903	5884	197	81	94	40	425	96	28492	280	1151
64.9	17	2336	32	50	11253	6201	181	79	112	41	440	331	26376	284	1084
65	17	1483	40	45	13786	5697	184	77	105	41	390	361	29037	316	1179
65.1	14	2929	35	53	13302	5566	200	84	119	34	389	109	27024	272	1150
65.2	13	1921	32	70	12393	6091	204	79	86	32	421	110	26610	274	1151
65.3	23	1279	36	85	10983	5694	191	94	122	34	397	88	27583	283	1063
65.4	6	1074	28	60	11040	5354	184	77	95	30	388	112	26136	264	1044
65.5	11	1101	37	53	15336	5790	184	91	88	30	441	74	27860	285	1144
65.6	7	1156	24	51	14881	5915	214	104	113	34	461	116	29879	309	1226
65.7	14	1074	28	44	12193	5796	174	69	92	35	428	91	26629	260	1067
65.8	18	1453	30	41	10571	5173	158	55	65	32	433	77	24847	245	922
65.9	21	1071	34	53	9531	4606	148	70	83	38	371	85	22478	225	820
66	18	2053	23	44	7929	3883	-579	61	90	27	318	88	18853	184	640
66.1	13	4330	23	20	5291	3299	46	36	40	29	290	64	12668	105	379
66.2	9	338	17	20	2593	1686	34	24	8	22	164	15	7286	68	187
66.3	2	80	28	15	297	197	22	14	17	13	20	21	864	17	55

Table A-28: XRF values from discrete samples from Lake Rutundu

	Chemical Elements (cps)																
Depth (cm)	**Al**	**Si**	**P**	**S**	**K**	**Ca**	**Ti**	**Mn**	**Fe**	**Ni**	**Cu**	**Zn**	**Rb**	**Sr**	**Zr**	**Nb**
4	21543	269562	4538	38594	2780733	938028	727700	256351	3576397	996	3078	56664	45090	18243	482845	88607
12	24677	267509	4060	36697	2974693	894896	787324	227996	2896214	861	3525	60095	46858	17732	571554	106727
21	22066	274728	3951	45108	2759583	902897	737450	256235	3483677	847	3755	54584	46410	17324	493408	92384
28	22404	281929	2712	36563	2909363	862119	758387	240509	3435037	1074	3496	56505	48231	16551	480374	92496
36	18197	266789	2479	39336	3016932	826593	779362	237889	2991947	1660	3585	58396	50647	15761	504999	93964
44	14750	288833	3269	36112	2872863	877932	743720	246490	3144757	1181	3581	53664	48454	18285	487060	93198
52	19234	285192	1650	28256	3220052	837183	781619	219437	2769660	580	3360	55400	52321	16832	571769	107093
60	22858	288244	3257	37218	3016945	843649	792412	237184	2994161	675	3528	52204	51403	16401	519518	100079
68	23168	287237	2294	39319	3062966	885389	766190	243685	2937379	1183	3309	57747	52311	18495	523787	97235
76	23466	290741	2526	31875	3127288	891640	748591	237053	2620297	1024	3683	55636	53195	16620	543510	101701
84	22518	295480	4193	40038	3025547	896415	713959	243968	2614862	982	3598	55622	52334	18678	520632	98329
92	16958	278630	5869	54924	2763027	851194	661355	265182	2253706	973	3983	60437	50926	16335	500676	90403